The Dissertation Committee for Jung Jae Lee Certifies that this is the approved version of the following dissertation:

Dynamic Characteristics of Municipal Solid Waste (MSW) in the Linear and Nonlinear Strain Ranges

Committee:

Kenneth H. Stokoe II, Supervisor

Ellen M. Rathje

Jorge G. Zornberg

John L. Tassoulas

Clark R. Wilson

Dynamic Characteristics of Municipal Solid Waste (MSW) in the Linear and Nonlinear Strain Ranges

by

Jung Jae Lee, B.S.; M.S.

Dissertation

Presented to the Faculty of the Graduate School of

The University of Texas at Austin

in Partial Fulfillment

of the Requirements

for the Degree of

DOCTOR OF PHILOSOPHY

The University of Texas at Austin

December 2007

Acknowledgements

I would like to express sincere gratitude to my supervisor Dr. Kenneth H. Stokoe II, for his guidance, support, and encouragement throughout this research. His endless passion and enthusiasm in his work has made me deeply impressed during this research and last four years. I would also appreciate to other dissertation committee members, Dr. Ellen M. Rathje, Dr. Jorge G. Zornberg, Dr. John L. Tassoulas, and Dr. Clark Wilson for their assistance to this research and review of this dissertation.

I would like to extend my thanks to Dr. Roy E. Olson, Dr. Stephen G. Wright, and Dr. Robert B. Gilbert for their lectures, which broadened my knowledge about the further understanding of geotechnical engineering.

I would like to express my thanks to Dr. Jeong-Yun Won, Songcheng Li, Jiabei Yuan, Yuannian Wang, Boo Hyun Nam, Sang Hyun Seo, Nam Hong Min, Sengyeol Jeon for their help for the preparation of MSW specimens.

I would appreciate to Songcheng Li and Young Jae Choi for conversations and discussions and I would like to express my thanks to Ian V.T. Johnson for his kind advices and corrections on my dissertation writing.

I would like to thank Teresa Tice-Boggs, Norma Gonzales, and Chris Trevino for their administrative support and I would also like to extend my thanks to Johnie Williams and Max Trevino for their technical support.

Finally, with all my heart, I would really appreciate to my wife, Sun Young Im, my parents, family, and my parents-in-law for their endless love, patience, help, and support.

Dynamic Characteristics of Municipal Solid Waste (MSW) in the Linear and Nonlinear Strain Ranges

Publication No._____

Jung Jae Lee, Ph.D.

The University of Texas at Austin, 2007

Supervisor: Kenneth H. Stokoe, II

A series of resonant column and torsional shear (RCTS) and large scale resonant column (LSRC) tests were performed to investigate the dynamic properties (shear modulus and material damping ratio) of municipal solid waste (MSW). the MSW materials were recovered from the Tri-Cities landfill adjacent to the San Francisco Bay in California. A total of 30 specimens 2.8-in. (71.1-mm) and 6.0-in. (152.4-mm) of old, fresh, and mixed MSW were reconstituted in accordance with established sample preparation procedures. Ten of specimens were small-diameter (2.8-in. (71.1-mm)) RCTS specimen and 20 specimens were larger (6.0-in. (152.4-mm)) LSRC specimens. Dynamic laboratory measurements were performed in the linear and nonlinear strain ranges. Test parameters affecting the dynamic properties in the linear range included: (1) duration of confinement, (2) isotropic total confining pressure, σ_o, (3) excitation frequency, f, and (4) specimen size. Other test parameters affecting dynamic properties in the nonlinear strain range were: (1) shearing strain amplitude, γ, (2) isotropic total confining pressure, (3) overconsolidation ratio, (4) number of loading cycles, and (5)

excitation frequency. In addition, the effects on dynamic properties of MSW specimens of material parameters such as (1) waste composition, (2) water content, (3) unit weight of waste, and (4) particle size were evaluated.

The total unit weights of old, fresh, and mixed MSW specimens were estimated during testing in the RCTS and LSRC devices. These estimated total unit weights in the laboratory were compared with those measured at other MSW landfills and were found to generally be less than the field measurements. At a given σ_o, G_{max} decreases with decreasing weight percentage of soil-size (passing the ¾-in. (19.1-mm) sieve) material. However, D_{min} increases slightly with decreasing weight percentage of soil-size material. Another relationship was developed between estimated total unit weight, γ_t, and confining pressure, including weigh percentage of soil-size material. The V_s profiles of old, fresh, and mixed MSW specimens obtained in the laboratory tests were compared with those measured at other MSW landfills in situ. The 62 to 76 % soil-size material groups are in good agreement with in-situ V_s profiles.

The variation in normalized shear modulus and material damping ratio curves were patterned after the Darendeli model (2001) for different weight percentages of soil-size material. An empirical relationship between normalized shear modulus (G/G_{max}) and modified material damping ratio ($D-D_{min}$) was developed in the nonlinear strain range. As part of collaborative research project, nonlinear shear modulus reduction and material damping curves generated by The University of Texas at Austin (UT) and The University of California at Berkeley (UCB) were compared according to different weight percentages of soil-size material. Furthermore, nonlinear shear modulus reduction and material damping ratio curves generated by UT were also compared with ones previously proposed by other researchers.

Table of Content

List of Figures xvii

List of Tables xlv

CHAPTER 1: INTRODUCTION 1

1.1 Motivation 1

1.2 Objectives of This Research 5

1.3 Organization of Dissertation 6

CHAPTER 2: LITERATURE REVIEW 10

2.1 Introduction 10

2.2 Dynamic Properties of MSW 11

2.2.1 Unit Weight 11

2.2.2 Shear Wave Velocity 15

2.2.3 Shear Modulus Reduction and Material Damping Curves 20

2.2.4 Poisson's Ratio 25

2.2.5 Dynamic Shear Strength 28

2.3 Seismic Performance of Waste Landfill in Earthquake Events 29

2.4 Summary 35

CHAPTER 3: LABORATORY TESTING EQUIPMENT 36

3.1 Introduction 36

3.2 Overview of RCTS and LSRC Test Equipment and Principles of Operation 40

3.2.1 History of RCTS Equipment at UT 40

3.2.2 History of Free-Free RC Equipment at UT 41

3.2.3 Basic Operational Testing at Resonance....41
3.3 Theoretical Framework of the RCTS Testing Technique....43
3.3.1 Fixed-Free Resonant Column (RC) Test....43
3.3.1.1 Shear Modulus....43
3.3.1.2 Shearing Strain....46
3.3.1.3 Half-Power Bandwidth Method....48
3.3.1.4 Free-Vibration Decay Method....52
3.3.2 Torsional Shear (TS) Test....55
3.3.2.1 Shear Modulus and Shearing Strain....55
3.3.2.2 Hysteretic Damping Ratio....58
3.3.3 Free-Free Resonant Column (RC) Test....59
3.3.3.1 Shear Modulus....60
3.3.3.2 Shearing Strain....61
3.3.3.3 Half-Power Bandwidth Method....64
3.3.3.4 Free-Vibration Decay Method....65
3.4 Organization of Fixed-Free RCTS Testing Equipment....66
3.4.1 Confinement System....67
3.4.2 Drive System....68
3.4.3 Height-Change Measurement System....70
3.4.4 Motion Monitoring System....71
3.4.4.1 Resonant Column (RC) Test....71
3.4.4.2 Torsional Shear Test....73
3.5 Organization of Free-Free RC Testing Equipment....74
3.5.1 Confinement System....75
3.5.2 Specimen Supporting System....75

3.5.3 Driving System 77
3.5.4 Height-Change Measurement System....78
3.5.5 Motion Monitoring System....80
3.6 Summary 82
CHAPTER 4: Material Properties of MSW....84
4.1 Introduction....84
4.2 In-Situ Characterization of MSW 86
4.2.1 State of Degradation and In-Situ Classification of Retrieved MSW 87
4.2.2 Variation in Temperature of MSW 89
4.2.3 Measurements of In-Situ Total Unit Weight 90
4.3 Material Properties of MSW Determined in the Laboratory 91
4.3.1 Water Content Measurements for A3 and C6 MSW Groups 91
4.3.2 Grain Size Distribution Analysis for A3 and C6 MSW Groups....93
4.3.3 Plasticity Index (PI) Measurement Old MSW 95
4.4 Summary 95
CHAPTER 5: Sample Preparation....97
5.1 Introduction....97
5.2 Identification of MSW Specimens Tested in Each Material Group with the RCTS and LSRC Devices....97
5.3 Preparation of Small-Diameter (2.8-in. (19.1-mm)) Specimens....100
5.3.1 Specimen Reconstitution with Soil-Sizes Material at the In-Situ Natural Condition....100
5.2.2 Hydration of Specimen 104
5.3 Preparation of Large-Diameter (6.0- in. (152.4-mm)) Specimen 107

5.3.1 Specimen Reconstitution with Soil-Size Material at Its Natural Condition....107

5.3.2 Specimen Reconstitution with Larger Particles at Its Natural Condition....111

5.5 Summary....117

CHAPTER 6: Small-Strain Dynamic Properties of Old MSW....119

6.1 Introduction....119

6.2 Test Procedures....120

6.2.1 Testing with the RCTS Device....120

6.2.2 Testing with the LSRC Device....123

6.3 Test Parameters Affecting G_{max} and D_{min} of Old Waste in the Small-Strain Range....125

6.3.1 Duration of Confinement at a Constant Pressure....125

6.3.1.1 Change in G_{max} with Confinement Time....126

6.3.1.2 Change in D_{min} with Confinement Time....130

6.3.2 Total Isotropic Confining Pressure....134

6.3.2.1 Log G_{max} - Log σ_o Relationship....134

6.3.2.2 Log D_{min} - Log σ_o Relationship....139

6.3.3 Excitation Frequency....143

6.3.4 Specimen Size....151

6.4 Estimation of Total Unit Weight of Old MSW Specimens During the RC Tests and Comparison with Previous Studies....155

6.4.1 Development of an Empirical Relationship of Estimated Total Unit Weight and Confining Pressure of Old MSW....162

6.5 Material Parameters Affecting G_{max} and D_{min} of Old Waste in the Small-Strain Range....163

6.5.1 Waste Composition 163
6.5.2 Water Content 169
6.5.3 Total Unit Weight Variation for the Same Material Group 173
6.5.4 Particle Size 176
6.6 Development of an Empirical Relationship between G_{max} and D_{min} for Old MSW 184
6.7 Comparison of Small-Strain Dynamic Properties of Old MSW and Loose Sand 187
6.8 Summary 189
CHAPTER 7: Small-Strain Dynamic Properties of Fresh MSW 191
7.1 Introduction 191
7.2 Test Procedures 191
7.2.1 Testing with the RCTS Device 191
7.2.2 Testing with the LSRC Device 193
7.3 Test Parameters Affecting G_{max} and D_{min} of Fresh Waste in the Small-Strain Range 196
7.3.1 Duration of Confinement at a Constant Pressure 196
7.3.1.1 Change in G_{max} with Confinement Time 196
7.3.1.2 Change in D_{min} with Confinement Time 198
7.3.2 Total Isotropic Confining Pressure 203
7.3.2.1 Log G_{max} - Log σ_o Relationship 203
7.3.2.2 Log D_{min} - Log σ_o Relationship 207
7.3.3 Excitation Frequency 209
7.3.4 Specimen Size 216
7.4 Estimation of Total Unit Weight of Fresh MSW Specimens During the RC Tests and Comparison with Previous Studies 221

7.4.1 Development of an Empirical Relationship of Estimated Total Unit Weight and Confining Pressure of Fresh MSW 226

7.5 Material Parameters Affecting G_{max} and D_{min} of Fresh Waste in the Small-Strain Range 228

7.5.1 Waste Composition 228

7.5.2 Water Content 232

7.5.3 Total Unit Weight Variation for the Same Material Group 236

7.5.4 Particle Size 238

7.6 Development of an Empirical Relationship between G_{max} and D_{min} for Fresh MSW 246

7.7 Comparison of Small-Strain Dynamic Properties of Fresh MSW and Loose Sand 249

7.8 Summary 251

CHAPTER 8: Comparison of Small-Strain Dynamic Properties of Old and Fresh MSW 253

8.1 Introduction 253

8.2 Effect of Confining Pressure on G_{max} and D_{min} 253

8.2.1 Log G_{max} - Log σ_o Relationships 253

8.2.2 Log D_{min}-Log σ_o Relationships 255

8.3 Effect of Excitation Frequency on G_{max} and D_{min} 260

8.3.1 Log G_{max}-Log f and Log $G_{max}/G_{max,\ f=1Hz}$ -Log f Relationships 260

8.3.2 Log D_{min}-Log f and Log $D_{min}/D_{min,\ f=1Hz}$ -Log f Relationships 264

8.4 Change in Estimated Total Unit Weight with Confining Pressure 267

8.5 Summary 269

CHAPTER 9: Comparison of Shear Wave Velocities from Laboratory and Field Measurements 271

9.1 Introduction 271

9.2 V_s Measurements in the Laboratory on MSW Specimens 271

9.3 Estimating the Field V_s Profiles form the Laboratory Log V_s – Log σ_o Relationships 276

9.4 In-Situ V_s Measurements in Tri-Cities Landfill Using the SASW Method 281

9.5 Comparison of V_s Profiles Obtained from Laboratory Tests with V_s Profiles Measured at the Tri-Cities Landfill 284

9.6 Comparison of V_s Profiles from Laboratory with Other Studies 286

9.7 Summary 293

CHAPTER 10: Nonlinear Behavior of Old MSW 294

10.1 Introduction 294

10.2 Test Procedures 295

10.2.1 Testing with the RCTS Device 295

10.2.2 Testing with the LSRC Device 299

10.3 Test Parameters Affecting G and D 301

10.3.1 Test Parameters Investigated 301

10.3.2 Shearing Strain Amplitude 302

10.3.3 Total Isotropic Confining Pressure 309

10.3.4 Overconsolidation Ratio 316

10.3.5 Number of Loading Cycles 319

10.3.6 Excitation Frequency 324

10.4 Material Parameters Affecting G and D 330

10.4.1 Material Parameters Investigated 330

10.4.2 Waste Composition 330
10.4.2 Water Content 334
10.4.3 Total Unit Weight Variation for the Same Material Type 337
10.4.4 Particle Size 339
10.5 Relationship Between Normalized Shear Modulus and Material Damping Ratio of Old MSW 346
10.6 Comparison of Nonlinear Dynamic Properties of Old MSW and Loose Sand 350
10.7 Summary 352
CHAPTER 11: Nonlinear Behavior of Fresh MSW 354
11.1 Introduction 354
11.2 Test Procedures 354
11.2.1 Testing with the RCTS Device 354
11.2.2 Testing with the LSRC Device 356
11.3 Test Parameters Affecting G and D 358
11.3.1 Test Parameters Investigated 358
11.3.2 Shearing Strain Amplitude 358
11.3.3 Total Isotropic Confining Pressure 364
11.3.4 Overconsolidation Ratio 368
11.3.5 Number of Loading Cycles 371
11.3.6 Excitation Frequency 375
11.4 Material Parameters Affecting G and D 380
11.4.1 Material Parameters Investigated 380
11.4.2 Waste Composition 381
11.4.3 Water Content 383

11.4.4 Total Unit Weight Variation for the Same Material Type.....386
11.4.5 Particle Size 388
11.5 Relationship Between Normalized Shear Modulus and Material Damping Ratio of Fresh MSW 391
11.6 Comparison of Nonlinear Dynamic Properties of Old MSW and Loose Sand 393
11.7 Summary 396
CHAPTER 12: Comparison of the Nonlinear Behavior of Old and Fresh MSW 398
12.1 Introduction 398
12.2 Variation in Shear Modulus, Normalized Shear Modulus, and Material Damping Ratio with Shearing Strain at a Given Confining Pressure 398
12.3 Variation in Shear Modulus, Normalized Shear Modulus, and Material Damping Ratio with Shearing Strain at a Given Excitation Frequency 401
12.4 Summary 406
CHAPTER 13: Comparison of Shear Modulus Reduction and Material Damping Ratio Curves with UCB and Other Studies.....407
13.1 Introduction 407
13.2 Data Fitting Using a Modified Hyperbolic Model.....407
13.2.1 G/G_{max} c log γ Relationships.....409
13.2.2 D – log γ Relationships 411
13.3 Comparison of Nonlinear Shear Modulus Reduction and Material Damping Ratio Curves Between UT and UCB 415
13.3.1 G_{max} Values.....415
13.3.2 G/G_{max} – log γ Relationships 418
13.3.3 D – log γ Relationships 420

13.4 Comparison of Nonlinear Shear Modulus Reduction and Material Damping Ratio Curves with Other Studies....423

13.4 Summary....426

CHAPTER 14: Summary, Conclusions, and Recommendations....427

14.1 Summary....427

14.2 Conclusions....429

14.2.1 Small-Strain Dynamic Behavior of Old and Fresh MSW....429

14.2.2 Nonlinear Dynamic Behavior of Old and Fresh MSW....433

14.2.3 Comparisons in G_{max} in the Small-Strain Range and G/G_{max} – log γ Curves and D – log γ Curves in the Nonlinear Strain Range between UT and UCB and Sands....436

14.3 Recommendations....437

References....438

Vita....446

List of Figures

Figure 1.1 Total Yearly Waste Generation in U.S.A between 1960 and 2003 (from U.S.EPA, 2003).....2

Figure 1.2 Percent Distribution of Constituents for Total Waste Generation in 2003 (from U.S.EPA, 2003) 2

Figure 2.1 Variation of Total Unit Weight of MSW with Depth (from Kavazanjian et al. 1995) 13

Figure 2.2 Profiles of the Measured and Proposed (dashed line) Total Unit Weight Profile at SS2 in OII Landfill (from Morochnik et al. 1998).....14

Figure 2.3 Distribution of Total Unit Weight of MSW with Depth at OII Landfill (from Matasovic et al. 1998).....14

Figure 2.4 The V_s Profiles from Different Testing Methods at Station SS2 in OII Landfill in California (from Metasocvic et al. 1995).....16

Figure 2.5 The V_s Profiles of Maximum, Minimum, Mean, and Mean ± One Standard Deviation Measured at Different Landfill Sites in Los Angeles (from Kavazanjian et al. 1996) 17

Figure 2.6 Variation in V_p and V_s Profiles with Depth at NWRLF in Arizona (from Houston et al. 1995).....19

Figure 2.7 Distribution of V_s Profiles from Different MSW Landfill Sites in Atlanta, Georgia (from Haker et al. 1997).....19

Figure 2.8 Normalized Shear Modulus and Material Damping Ratio with Cyclic Shear Strain for Refuse Material (from Singh and Murphy, 1990) 21

Figure 2.9 Normalized Shear Modulus (Top) and Equivalent Viscous Damping Ratio (Bottom) for Back-Calculation Analysis (from Kavazanjian et al. 1994) 22
Figure 2.10 Variation of (a) Normalized Shear Modulus and (b) Damping Ratio with Shearing Strain (from Idriss et al. 1994) 23
Figure 2.11 Variation of Shear Modulus (a) and Damping Ratio (b) with Cyclic Shear Strain (from Matasovic et al. 1998) 24
Figure 2.12 Variation of Shear Modulus (Top) and Material Damping (Bottom) with Different Weight Percentages of Soil-Size Material (from Zekkos, 2005) ..26
Figure 2.13 Variation of Poisson's Ratio with Depth Beneath the Top Recording Station at OII Landfill (from Metasovic et al. 1995) 28
Figure 2.15 Stress-Strain Behavior of Specimens at Different Strain Rates for Different Weight Percentages: (a) 100 %, (b) 62 %, and (c) 20 % (from Zekkos 2005) 30
Figure 2.16 Map of Location of the Waste Landfills Surveyed for Seismic Performance during Loma Prieta Earthquake (from Orr et al. 1990) 31
Figure 2.17 Location of Landfill Sites Surveyed for Seismic Performance during the Northridge Earthquake (from Metasovic et al. 1995) 33
Figure 3.1 Idealization of (a) Fixed-free RCTS and (b) Free-free LSRC Testing Equipments 37
Figure 3.2 Illustration of Combined RCTS Testing Device without Confining Chamber (from Kim, 1991) 38
Figure 3.3 Photograph of General Configuration of LSRC Testing Device with Confining Chamber (from Menq, 2003) 39
Figure 3.4 Variation of f_r/f_n with Material Damping Ratio, D 45

Figure 3.5 Simplified Drawing of Distribution of Deformation Induced in a Specimen during the Resonant Column Test (after Hwang, 1997) 47
Figure 3.6 Typical Illustration for the Material Damping Measurements using Half-Power Bandwidth Method (from Hwang, 1997) 50
Figure 3.7 Comparison of the Frequency Response Curves Obtained from Downgrade and Upgrade Sweep Processes (from Ni, 1987).....52
Figure 3.8 General Configuration of (a) Free-Vibration Decay Curve and (b) Example of Computation of Damping Ratio (from Hwang, 1997) 53
Figure 3.9 Illustration of measurements of Shear Modulus and Material Damping Ratio from Hysteresis Loop (from Kim, 1991) 56
Figure 3.10 Distributions of Displacement and Shearing Strain along the Length of Specimen with End Caps (from Menq, 2003) 62
Figure 3.11 Typical Frequency Response Curve Obtained from a LSRC Test on a Fresh MSW Specimen 65
Figure 3.12 Cross-Sectional View of Confinement System with Specimen and Confining Chamber (after Kim, 1991).....68
Figure 3.13 Simplified Configuration of Driving System in RCTS Tests (after Hwang, 1997).....69
Figure 3.14 Simplified Configuration of Height-Change Measurement System in RC Tests (after Hwang, 1997).....70
Figure 3.15 Simplified Configuration of Motion Monitoring System in RC Tests (after Hwang, 1997).....72
Figure 3.16 Simplified Configuration of Motion Monitoring System in TS Tests (after Hwang, 1997).....74
Figure 3.17 Simplified Configuration of Confinement System in the LSRC Tests.....76

Figure 3.18 General Configuration and Expanded Views of Each Part of the Supporting System (from Menq, 2003) 77
Figure 3.19 Configuration of Driving System in the LSRC Device (from Menq, 2003) 78
Figure 3.20 Simplified Diagram of Driving System in the LSRC Device 79
Figure 3.21 Simplified Diagram of Height-Change System in the LSRC Testing Device (after Menq, 2003) 80
Figure 3.22 Picture of Motion Monitoring System with Cable for the Accelerometer and Vacuum Lines in the LSRC Test Device 81
Figure 4.1 Location of Tri-Cities Waste Landfill in California 85
Figure 4.2 Plan View of the Tri-Cites Waste Landfill with Borehole Locations (Courtesy of GeoSyntec Constants, 2003) 86
Figure 4.3 Classification of Waste Materials into Components in Terms of Percentage Weight for A3 and C6 Groups (after Zekkos, 2005) 88
Figure 4.4 Variation in Temperature in the MSW from Two Boreholes in the Tri-Cities Landfill (after Zekkos, 2005) 90
Figure 4.5 Variation in Total Unit Weight in the Tri-Cities Landfill (after Zekkos, 2005) 92
Figure 4.6 Grain Size Distribution Curves for A3 and C6 Groups 94
Figure 5.1 Split Mold and Compaction Hammer for the Construction of 2.8-in. (71.1 mm) Diameter Specimen 102
Figure 5.2 Configuration of the Compaction Pattern of Each Layer 104
Figure 5.3 General Configuration for the Hydration of RCTS Specimens 105
Figure 5.4 Comparison of Soil-Sizes Materials Passing the (a) ¾-in. (19.1-mm) and (b) 3/8-in. (9.5-mm) Sieves Used for Specimen Construction 108

Figure 5.5 Split Mold and Compaction Hammer for Construction of Large-Diameter Specimens Used in the LSRC Tests.....109
Figure 5.6 Larger Particle Components Used for the Construction of Large-Diameter Specimens: (a) Wood, (b) Soft Plastic, (c) Paper, and (d) Gravel.....114
Figure 6.1 Stage Loading Sequence Showing the Variation in Isotropic Confining Pressure with Duration of Confinement in the RC Measurements.....122
Figure 6.2 Variation in Low-Amplitude Shear Modulus with Magnitude and Duration of Confinement for Specimen MSW2ONS1 (100 % Soil-Size Material).....127
Figure 6.3 Comparison of the Variation in Normalized Shear Modulus Increase with Different Weight Percentage of Old, MSW at Their Natural Water Content in the (a) OC and (b) NC States 131
Figure 6.4 Variation in Low-Amplitude Material Damping Ratio with Magnitude and Duration of Confinement for MSW2ONS1 (100 % Soil-Size Material).....132
Figure 6.5 Comparison of the Variation in Normalized Material Damping Ratio Increase with Different Weight Percentage of Old, MSW in the (a) OC and (b) NC States for Old MSW.....135
Figure 6.6 Variation in Low-Amplitude Shear Modulus with Isotropic Confining Pressure for 100 % Soil-Size Old MSW Specimens in the RCTS Device .137
Figure 6.7 Comparison of the Variation in the Values of Exponent in the (a) OC and (b) NC States with Different Weight Percentages of Soil-Size Old MSW 140

Figure 6.8 Variation in Low-Amplitude Material Damping Ratio with Isotropic Confining Pressure for 100 % Soil-Size Old MSW Specimens in the RCTS Device 141

Figure 6.9 Comparison of the Values of: (a) the Exponent, n_D, and (b) Material Damping Ratio at One Atmosphere, D_1, in the Loading Sequence of Different Weight Percentages of Soil-Size Old MSW Specimens 144

Figure 6.10 Variation in Shear Modulus with Excitation Frequency from RCTS and LSRC Tests for 100 % Soil-Size, Old MSW Specimens.....145

Figure 6.11 Variation in Normalized Shear Modulus with Excitation Frequency from the RCTS and LSRC Tests for 100 % Soil-Size Old MSW Specimens.....147

Figure 6.12 Variation in Normalized Shear Modulus with Excitation Frequency for All MSW Groups (A3, C6, and C3 Groups) Using a Cyclic Triaxial Device (from Zekkos, 2005).....147

Figure 6.13 Variation in Material Damping Ratio with Excitation Frequency from the RCTS and LSRC Tests for 100 % Soil-Size Old MSW Specimens.....149

Figure 6.14 Nonlinear Relationship Fit to the Variation in Normalized Material Damping Ratio with Excitation Frequency for 100 % Soil-Size Old MSW Specimens.....150

Figure 6.15 Comparison of the Variation in Low-Amplitude Shear Modulus with Isotropic Confining Pressure of Different Specimen Sizes Reconstituted with 100 % Soil-Size Old MSW Passing the 3/8-in. (9.5-mm) Sieve: (a) Uncorrected for f and γ_t and (b) Corrected for f and γ_t 152

Figure 6.16 Comparison of the Variation in Low-Amplitude Shear Modulus with Isotropic Confining Pressure of Different Specimen Sizes Reconstituted with 100 % Soil-Size Old MSW Passing the ¾-in. (19.1-mm) Sieve: (a) Uncorrected for f and γ_t and (b) Corrected for f and γ_t 154

Figure 6.17 Comparison of the Variation in Low-Amplitude Material Damping Ratio with Isotropic Confining Pressure of Different Specimen Sizes Reconstituted with 100 % Soil-Size Old MSW Passing the 3/8-in. (9.5-mm) Sieve: (a) Uncorrected for f and (b) Corrected for f.....156

Figure 6.18 Comparison of the Variation in Low-Amplitude Material Damping Ratio with Isotropic Confining Pressure of Different Specimen Sizes Reconstituted with 100 % Soil-Size Old MSW Passing the ¾-in. (19.1-mm) Sieve: (a) Uncorrected for f and (b) Corrected for f.....157

Figure 6.19 Variation in Estimated Total Unit Weight with Isotropic Confining Pressure from RC Tests for Old and Mixed MSW Specimens (All Groups) 159

Figure 6.20 Comparison of the Variation in Estimated Total Unit Weight of Old and Mixed MSW Specimens (All Groups) with Total Unit Weight Profiles Measured at MSW Landfills.....161

Figure 6.21 Variation in Normalized Total Unit Weight with Isotropic Confining Pressure for Old and Mixed MSW (All Groups).....163

Figure 6.22 Comparison of Predicted Total Unit Weight and Measured Total Unit Weight for Old and Mixed MSW (All Groups).....164

Figure 6.23 Variation in Low-Amplitude Shear Modulus with Isotropic Confining Pressure for Different Weight Percentages of Soil-Size Material for Old and Mixed MSW Specimens: (a) Uncorrected for f and γ_t and (b) Corrected for f and γ_t.....165

Figure 6.24 An Example of Adjusting Low-Amplitude Shear Modulus of One Specimen to Account for the Difference in Total Unit Weights Between Two Specimens; Both Specimens have the Same Confinement: (a) Adjustment of G_{max} at σ_o = 2.5 psi (17 kPa), and (b) Total Unit Weight of Both Specimens at σ_o = 2.5 psi (17 kPa) 167

Figure 6.25 Variation in Low-Amplitude Material Damping Ratio with Isotropic Confining Pressure for Different Weight Percentages of Soil Content for Old and Mixed MSW Specimens: (a) Uncorrected for f and (b) Corrected for f.....168

Figure 6.25 Comparison of the Variation in Low-Amplitude Shear Modulus with Isotropic Confining Pressure at its Natural and Hydrated Conditions for 100 % Soil-Size Old MSW Specimens: (a) Uncorrected for f and γ_t and (b) Corrected for f and γ_t.....170

Figure 6.26 Comparison of the Variation in Low-Amplitude Material Damping Ratio with Isotropic Confining Pressure at its Natural and Hydrated Conditions for 100 % Soil-Size Old MSW Specimens: (a) Uncorrected for f and (b) Corrected for f.....172

Figure 6.27 Comparison of the Variation in Low-Amplitude Shear Modulus with Estimated Total Unit Weight at Different Isotropic Confining Pressures for 100 % Soil-Size Old MSW Specimens: (a) Uncorrected for f and (b) Corrected for f.....175

Figure 6.28 Comparison of the Variation in Low-Amplitude Material Damping Ratio with Estimated Total Unit Weight at Different Isotropic Confining Pressures for 100 % Soil-Size Old, MSW Specimens: (a) Uncorrected for f and (b) Corrected for f 177

Figure 6.29 Comparison of the Variation in Low-Amplitude Shear Modulus with Isotropic Confining Pressure for Different Particle Sizes of the 100 % Soil-Size, Old MSW Material Tested in the RCTS Device: (a) Uncorrected for f and γ_t and (b) Corrected for f and γ_t 179

Figure 6.30 Comparison of the Variation in Low-Amplitude Shear Modulus with Isotropic Confining Pressure for Different Particle Sizes of the 100 % Soil-Size, Old MSW Material Tested in the LSRC Device: (a) Uncorrected for f and γ_t and (b) Corrected for f and γ_t 180

Figure 6.31 Comparison of the Variation in Low-Amplitude Material Damping Ratio with Isotropic Confining Pressure for 100 % Soil-Size, Old MSW Specimens with Different Maximum Particle Sizes: (a) Uncorrected for f and (b) Corrected for f 182

Figure 6.32 Comparison of the Variation in Low-Amplitude Material Damping Ratio with Isotropic Confining Pressure for 100 % Soil-Size Old MSW Specimens with Different Maximum Particle Sizes: (a) Uncorrected for f and (b) Corrected for f 183

Figure 6.33 Variation in Low-Amplitude Material Damping Ratio with Low-Amplitude Shear Modulus for Old and Mixed MSW Specimens (All Groups): (a) Uncorrected for f (b) Corrected for f.....185

Figure 6.34 Comparison of the Corrected and Predicted Values of D_{min} for Old and Mixed MSW Specimens (All Groups).....186

Figure 6.35 Plot of the Ratio of Corrected D_{min} to Predicted D_{min} with Isotropic Confining Pressure for Old and Mixed MSW Specimens (All Groups) 187

Figure 6.36 Comparison of the Variation in Low-Amplitude Shear Wave Velocity with Isotropic Confining Pressure for Old MSW (All Groups) and Loose Sand.....188

Figure 6.37 Comparison of the Variation in Low-Amplitude Shear Modulus with Isotropic Confining Pressure for Old MSW (All Groups) and Loose Sand.....188

Figure 6.38 Comparison of the Variation in Low-Amplitude Material Damping Ratio with Isotropic Confining Pressure for Old MSW (All Groups) and Loose Sand.....189

Figure 7.1 Variation in Low-Amplitude Shear Modulus with Magnitude and Duration of Confinement for 100 % Soil-Size Fresh MSW Specimen MSW2FNS2.....197

Figure 7.2 Comparison of the Variation in Normalized Shear Modulus Increase with Different Weight Percentages of Fresh, MSW at Their Natural Water Content in the: (a) OC and (b) NC States 199

Figure 7.3 Variation in Low-Amplitude Material Damping Ratio with Magnitude and Duration of Confinement for MSW2FNS2 (100 % Soil-Size Material).....200

Figure 7.4 Comparison of the Variation in Normalized Material Damping Ratio Increase with Different Weight Percentage of Fresh, MSW at Their Natural Water Content in the: (a) OC and (b) NC States 202

Figure 7.5 Variation in Low-Amplitude Shear Modulus with Isotropic Confining Pressure for 100 % Soil-Size Fresh MSW Specimens in the RCTS Device 204
Figure 7.6 Comparison of the Variation in the Values of Exponent in the (a) OC and (b) NC States with Different Weight Percentages of Soil-Size Fresh MSW 206
Figure 7.7 Variation in Low-Amplitude Material Damping Ratio with Isotropic Confining Pressure for 100 % Soil-Size Fresh Waste Specimens in the RCTS Device 207
Figure 7.8 Comparison of the Values of: (a) the Exponent, $n_{D,}$ and (b) Material Damping Ratio at One Atmosphere, D_1, in the Loading Sequence of Different Weight Percentages of Soil-Size Fresh MSW Specimens 210
Figure 7.9 Variation in Shear Modulus with Excitation Frequency from RCTS and LSRC Tests for 100 % Soil-Size, Fresh Waste Specimens 211
Figure 7.6 Variation in Normalized Shear Modulus with Excitation Frequency from the RCTS and LSRC Tests for 100 % Soil-Size Fresh Waste Specimens..212
Figure 7.7 Variation in Material Damping Ratio with Excitation Frequency from the RCTS and LSRC Tests for 100 % Soil-Size Fresh Waste Specimens..214
Figure 7.8 Nonlinear Relationship Fit to the Variation in Normalized Material Damping Ratio with Excitation Frequency for 100 % Soil-Size Fresh Waste Specimens 215
Figure 7.9 Comparison of the Variation in Low-Amplitude Shear Modulus with Isotropic Confining Pressure of Different Specimen Sizes Reconstituted with 100 % Soil-Size Fresh MSW Passing the 3/8-in. (9.5-mm) Sieve: (a) Uncorrected for f and γ_t and (b) Corrected for f and γ_t.....217

Figure 7.10 Comparison of the Variation in Low-Amplitude Shear Modulus with Isotropic Confining Pressure of Different Specimen Sizes Reconstituted with 100 % Soil-Size Fresh MSW Passing the ¾-in. (1915-mm) Sieve: (a) Uncorrected for f and γ_t and (b) Corrected for f and γ_t.....219

Figure 7.11 Comparison of the Variation in Low-Amplitude Material Damping Ratio with Isotropic Confining Pressure of Different Specimen Sizes Reconstituted with 100 % Soil-Size Fresh MSW Passing the 3/8-in. (9.5-mm) Sieve: (a) Uncorrected for f and (b) Corrected for f.....220

Figure 7.12 Comparison of the Variation in Low-Amplitude Material Damping Ratio with Isotropic Confining Pressure of Different Specimen Sizes Reconstituted with 100 % Soil-Size Fresh MSW Passing the ¾-in. (19.1-mm) Sieve: (a) Uncorrected for f and (b) Corrected for f.....222

Figure 7.13 Variation in Estimated Total Unit Weight with Isotropic Confining Pressure from RC Tests for Fresh and Mixed MSW Specimens (All Groups) 223

Figure 7.13 Comparison of the Variation in Estimated Total Unit Weight of Fresh and Mixed MSW Specimens with Total Unit Weight Profiles Measured at MSW Landfills.....225

Figure 7.11 Comparison of Predicted Total Unit Weight and Measured Total Unit Weight for Fresh and Mixed MSW Specimens 227

Figure 7.12 Comparison of Predicted Total Unit Weight and Measured Total Unit Weight for Fresh and Mixed MSW Specimens 227

Figure 7.13 Variation in Low-Amplitude Shear Modulus with Isotropic Confining Pressure upon Different Weight Percentages of Soil Contents for Fresh and Mixed MSW Specimens: (a) Uncorrected for f and γ_t and (b) Corrected for f and γ_t.....229

Figure 7.14 Variation in Low-Amplitude Material Damping Ratio with Isotropic Confining Pressure upon Different Weight Percentages of Soil Content for Fresh and Mixed MSW Specimens: (a) Uncorrected for f and (b) Corrected for f.....231

Figure 7.15 Comparison of the Variation in Low-Amplitude Shear Modulus with Isotropic Confining Pressure at its Natural and Hydrated Conditions for 100 % Soil-Size Fresh MSW Specimens: (a) Uncorrected for f and γ_t and (b) Corrected for f and γ_t.....233

Figure 7.16 Comparison of the Variation in Low-Amplitude Material Damping Ratio with Isotropic Confining Pressure at its Natural and Hydrated Conditions for 100 % Soil-Size Fresh MSW Specimens: (a) Uncorrected for f and (b) Corrected for f.....235

Figure 7.17 Comparison of the Variation in Low-Amplitude Shear Modulus with Estimated Total Unit Weight at Different Isotropic Confining Pressures for 100 % Soil-Size Fresh MSW Specimens: (a) Uncorrected for f and (b) Corrected for f.....237

Figure 7.18 Comparison of the Variation in Low-Amplitude Material Damping Ratio with Estimated Total Unit Weight at Different Isotropic Confining Pressures for 100 % Soil-Size Fresh, MSW Specimens: (a) Uncorrected for f and (b) Corrected for f.....239

Figure 7.19 Comparison of the Variation in Low-Amplitude Shear Modulus with Isotropic Confining Pressure for Different Particle Sizes of the 100 % Soil-Size, Fresh MSW Material Tested in the RCTS Device: (a) Uncorrected for f and γ_t and (b) Corrected for f and γ_t 240

Figure 7.20 Comparison of the Variation in Low-Amplitude Shear Modulus with Isotropic Confining Pressure for Different Particle Sizes of the 100 % Soil-Size, Fresh MSW Material Tested in the LSRC Device: (a) Uncorrected for f and γ_t and (b) Corrected for f and γ_t 242

Figure 7.21 Comparison of the Variation in Low-Amplitude Material Damping Ratio with Isotropic Confining Pressure upon Different Particle Size for 100 % Soil-Size, Small-Diameter Fresh MSW Specimens: (a) Uncorrected for f and (b) Corrected for f 244

Figure 7.22 Comparison of the Variation in Low-Amplitude Material Damping Ratio with Isotropic Confining Pressure upon Different Particle Size for 100 % Soil-Size, Large-Diameter Fresh MSW Specimens: (a) Uncorrected for f and (b) Corrected for f 245

Figure 7.23 Variation in Low-Amplitude Material Damping Ratio with Low-Amplitude Shear Modulus for Fresh and Mixed MSW Specimens (All Groups): (a) Uncorrected for f (b) Corrected for f.....247

Figure 7.24 Comparison of the Corrected and Predicted Values of D_{min} for Fresh and Mixed MSW Specimens (All Groups).....248

Figure 7.25 Plot of the Ratio of Corrected D_{min} to Predicted D_{min} with Isotropic Confining Pressure for Fresh and Mixed MSW Specimens (All Groups)..248

Figure 7.26 Comparison of the Variation in Low-Amplitude Shear Wave Velocity with Isotropic Confining Pressure for Fresh MSW (All Groups) and Loose Sand.....250
Figure 7.27 Comparison of the Variation in Low-Amplitude Shear Modulus with Isotropic Confining Pressure for Fresh MSW (All Groups) and Loose Sand.....250
Figure 7.28 Comparison of the Variation in Low-Amplitude Material Damping Ratio with Isotropic Confining Pressure for Fresh MSW (All Groups) and Loose Sand.....251
Figure 8.1 Variation in Low-Amplitude Shear Modulus with Isotropic Confining Pressure for 100% Soil-Size MSW: (a) Old Waste and (b) Fresh Waste...254
Figure 8.2 Variation in Low-Amplitude Shear Modulus with Isotropic Confining Pressure for 62-76 % Soil-Size MSW: (a) Old Waste and (b) Fresh Waste.....256
Figure 8.3 Variation in Low-Amplitude Material Damping Ratio with Isotropic Confining Pressure for 100% Soil-Size MSW: (a) Old Waste and (b) Fresh Waste.....257
Figure 8.4 Variation in Low-Amplitude Material Damping Ratio with Isotropic Confining Pressure for 62-76% Soil-Size MSW: (a) Old Waste and (b) Fresh Waste.....259
Figure 8.5 Variation in Shear Modulus with Excitation Frequency for 100 % Soil-Size MSW: (a) Old Waste and (b) Fresh Waste 261
Figure 8.6 Variation in Normalized Shear Modulus with Excitation Frequency for 100 % Soil-Size MSW: (a) Old Waste and (b) Fresh Waste 263

Figure 8.7 Variation in Material Damping Ratio with Excitation Frequency for 100 % Soil-Size MSW: (a) Old Waste and (b) Fresh Waste 265
Figure 8.8 Variation in Normalized Material Damping Ratio with Excitation Frequency for 100 % Soil-Size MSW: (a) Old Waste and (b) Fresh Waste.....266
Figure 8.9 Variation in Estimated Total Unit Weight with Isotropic Confining Pressure for 100 %, 62 to 76 % Soil-Sizes, and 14 % Soil-Size Mixed MSW: (a) Old and Mixed Wastes and (b) Fresh and Mixed Wastes.....268
Figure 9.1 Variation in Low-Amplitude Shear Wave Velocity with Isotropic Confining Pressure for Old and Mixed MSW (All Groups) Determined by RCTS and LSRC Tests 272
Figure 9.2 Variation in Low-Amplitude Shear Wave Velocity with Isotropic Confining Pressure for Fresh and Mixed MSW (All Groups) Determined by RCTS and LSRC Tests 273
Figure 9.3 Variation in (a) Coefficient of Lateral Earth Pressure at Rest, (b) Poisson's Ratio, and (c) Overconsolidation Ratio with Depth for the Conversion of Isotropic Confining Pressure in the Laboratory to Depth in the Field 278
Figure 9.4 Variation in Shear Wave Velocity with (a) Vertical Total Stress and (b) Depth for Old and Mixed MSW Specimens 279
Figure 9.5 Variation in Shear Wave Velocity with (a) Vertical Total Stress and (b) Depth for Fresh and Mixed MSW Specimens 280
Figure 9.6 Plan View and Locations of SASW Test Arrays in the Tri-Cites Landfill (Courtesy of GeoSyntec Constants, 2001).....282

Figure 9.7 The Variation in Vs Profiles Measured by SASW Testing Near Two Boreholes (BH-1 and BH-2) in the Tri-Cities Landfill (Lin et al., 2004)...283

Figure 9.8 Comparison of the Variations in V_s Profiles Measured at the Tri-Cities Landfill with Those Obtained from the Laboratory for (a) Old and Mixed and (b) Fresh and Mixed Specimens 285

Figure 9.7 Variations in Average V_s Profiles Measured at the Altamont, Redwood, and Tri-Cities Landfills by SASW Testing (after Lin et al., 2004) 287

Figure 9.8 Variations in Average V_s Profiles Measured at the OII, Azusa, and NWRLF Landfills and Mean V_s Profile Generated from Six Different Landfills in Southern California (after Kavazanjian et al., 1996, and Houston, 1995).....289

Figure 9.9 Comparison of the Variations in V_s Profiles of Old and Mixed Specimens Measured in the Laboratory with Those Obtained from (a) Altamont, Redwood, and Tri-Cities Landfills and (b) OII, Azusa, NWRLF, and Southern California Landfills.....291

Figure 9.10 Comparison of the Variations in V_s Profiles of Fresh and Mixed Specimens Measured in the Laboratory with Those Obtained from (a) Altamont, Redwood, and Tri-Cities Landfills and (b) OII, Azusa, NWRLF, and Southern California Landfills.....292

Figure 10.1 An Example Set of High-Amplitude RCTS Tests Procedure at One Confining Pressure in the RCTS Device 297

Figure 10.2 Typical Variation in Isotropic Confining Pressure with Duration of Confinement.....298

Figure 10.3 An Example Set of High-Amplitude RC Tests Procedure at One Confining Pressure in the LSRC Device 300

Figure 10.4 Comparison of the Variation in Shear Modulus with Shearing Strain for 100 % Soil-Size Old MSW Specimens Reconstituted with Material Passed the 3/8-in. (9.5-mm) Sieve in the RCTS and LSRC devices 303
Figure 10.5 Comparison of the Variation in Shear Modulus with Shearing Strain for 100 % Soil-Size Specimen MSW5ONS1 Obtained from RC and TS Tests in the RCTS Device.....304
Figure 10.6 Comparison of the Variation in Shear Modulus with Shearing Strain for 100 % Soil-Size Old MSW Specimens Reconstituted with Material Passed the ¾-in. (19.1-mm) Sieve in the RCTS and LSRC devices 305
Figure 10.7 Comparison of the Variation in Material Damping Ratio with Shearing Strain for 100 % Soil-Size Old MSW Specimens Reconstituted with Material Passed the 3/8-in. (9.5-mm) Sieve in the RCTS and LSRC devices.....306
Figure 10.8 Comparison of the Variation in Material Damping Ratio with Shearing Strain for 100 % Soil-Size Specimen MSW5ONS1 Obtained from RC and TS Tests in the RCTS Device 308
Figure 10.9 Comparison of the Variation in Material Damping Ratio with Shearing Strain for 100 % Soil-Size Old MSW Specimens Reconstituted with Material Passed the ¾-in. (19.1-mm) Sieve in the RCTS and LSRC devices.....309
Figure 10.10 Comparison of the Variation in Shear Modulus with Shearing Strain and Isotropic Confining Pressures from RC and TS Tests for MSW3ONS1 (100% Soil-Size Material) 311

Figure 10.11 Comparison of the Variation in Normalized Shear Modulus with Shearing Strain and Isotropic Confining Pressures from RC tests for MSW3ONS1 (100% Soil-Size Material).....312
Figure 10.12 Comparison of the Variation in Elastic Threshold Shearing Strain with Isotropic Confining Pressures from RC tests for 100 %, 76 %, 62 %, and 14 % Soil-Size Old and Mixed MSW Groups.....314
Figure 10.13 Comparison of the Variation in Material Damping Ratio with Shearing Strain and Isotropic Confining Pressures from RCTS tests for MSW3ONS1 (100% Soil-Size Material).....315
Figure 10.14 Comparison of the Variation in (a) Shear Modulus and (b) Normalized Shear Modulus with Shearing Strain upon Reloading and Unloading Sequences from RC tests for MSW3ONS1 (100% Soil-Size Material).....317
Figure 10.15 Comparison of the Variation in Material Damping Ratio with Shearing Strain upon Reloading and Unloading Sequences from RC tests for MSW3ONS1 (100% Soil-Size Material).....319
Figure 10.16 Comparison of the Variation in Shear Modulus with Shearing Strain from RCTS Tests for MSW3ONS1 (100% Soil-Size Material).....320
Figure 10.17 Comparison of the Variation in Normalized Shear Modulus with Shearing Strain from RCTS Tests for MSW3ONS1 (100% Soil-Size Material).....321
Figure 10.18 Variation in Normalized Shear Modulus, G/G_{1st}, with the Number of Loading Cycles from TS Tests for MSW3ONS1 (100% Soil-Size Material).....322
Figure 10.19 Comparison of the Variation in Material Damping Ratio with Shearing Strain from RCTS Tests for MSW3ONS1 (100 % Soil-Size Material) 323

Figure 10.20 Variation in Normalized Material Damping Ratio, D/D_{1st}, with the Number of Loading Cycles from TS tests for MSW3ONS1 (100 % Soil-Size Material).....325
Figure 10.21 Variation in Shear Modulus with Excitation Frequency from the RCTS and LSRC Tests for 100 % Soil-Size Old MSW in the nonlinear strain range.....325
Figure 10.22 Variation in Normalized Shear Modulus with Excitation Frequency from the RCTS and LSRC Tests for 100 % Soil-Size Old MSW in the nonlinear strain range.....327
Figure 10.23 Variation in Material Damping Ratio with Excitation Frequency from the RCTS and LSRC Tests for Old MSW in the nonlinear strain range 328
Figure 10.24 Variation in Normalized Material Damping Ratio with Excitation Frequency from the RCTS and LSRC Tests for 100 % Soil-Size Old MSW in the nonlinear strain range 329
Figure 10.25 Comparison of the Variation in (a) Shear Modulus and (b) Normalized Shear Modulus with Shearing Strain from LSRC Tests upon Different Weight Percentages of the Soil-Size Old and Mixed MSW Specimens.....332
Figure 10.26 Recommended Normalized Shear Modulus with Shearing Strain upon Different Weight Percentages of Soil-Size Material for Upper 66 ft (20 m) of a Landfill (from Zekkos, 2005).....333
Figure 10.27 Comparison of the Variation in Material Damping Ratio with Shearing Strain from LSRC Tests upon Different Weight Percentages of the Soil-Size Material, Old and Mixed MSW Specimens 334

Figure 10.28 Comparison of the Variation in (a) Shear Modulus and (b) Normalized Shear Modulus with Shearing Strain from RC Tests upon Specimens at Its Natural and Hydrated Conditions for 100 % Soil-Size Old MSW 335
Figure 10.29 Comparison of the Variation in Material Damping Ratio with Shearing Strain from RC Tests upon Specimens at Its Natural and Hydrated Conditions for 100 % Soil-Size Old MSW 337
Figure 10.30 Comparison of the Variation in (a) Shear Modulus and (b) Normalized Shear Modulus with Shearing Strain from RC Tests of Specimens with Different Total Unit Weights for 100 % Soil-Size Old Waste 338
Figure 10.31 Comparison of the Variation in Material Damping Ratio with Shearing Strain from RC Tests of 100 % Soil-Size Old MSW Specimens with Different Unit Weights 340
Figure 10.32 Comparison of the Variation in (a) Shear Modulus and (b) Normalized Shear Modulus with Shearing Strain from RC Tests of Specimens with Different Particle Sizes for 100 % Soil-Size Old MSW in the RCTS Device 341
Figure 10.33 Comparison of the Variation in Material Damping Ratio with Shearing Strain from RC Tests of Specimens with Different Particle Sizes for 100 % Soil-Size Old MSW in the RCTS Device.....343
Figure 10.34 Comparison of the Variation in (a) Shear Modulus and (b) Normalized Shear Modulus with Shearing Strain of Specimens with Different Particle Sizes for 100 % Soil-Size Old MSW in the LSRC Device 344
Figure 10.35 Comparison of the Variation in Material Damping Ratio with Shearing Strain from RC Tests of Specimens with Different Particle Sizes for 100 % Soil-Size Old MSW in the LSRC Device.....345

Figure 10.36 Plot of Normalized Shear Modulus with Modified Material Damping Ratio from RCTS and LSRC Tests for All Groups of Old and Mixed MSW 347

Figure 10.37 Comparison of the Values of Measured D-D_{min} and Predicted D-D_{min} from (a) RC Tests and (b) TS Tests for All Groups of Old MSW.....349

Figure 10.38 Comparison of the Variation in Shear Modulus with Shearing Strain at a Confining Pressure of 11 psi (76 kPa) for Old MSW and Loose Sand 351

Figure 10.39 Comparison of the Variation in Normalized Shear Modulus with Shearing Strain at a Confining Pressure of 11 psi (76 kPa) for Old MSW and Loose Sand.....351

Figure 10.40 Comparison of the Variation in Material Damping Ratio with Shearing Strain at a Confining Pressure of 11 psi (76 kPa) for Old MSW and Loose Sand.....352

Figure 11.1 Comparison of the Variation in Shear Modulus with Shearing Strain for 100 % Soil-Size Fresh MSW Specimens Reconstituted with Material Passed the 3/8-in. (9.5-mm) Sieve in the RCTS and LSRC devices 359

Figure 11.2 Comparison of the Variation in Shear Modulus with Shearing Strain for 100 % Soil-Size Specimen MSW3FNS1 Obtained from RC and TS Tests in the RCTS Device.....360

Figure 11.3 Comparison of the Variation in Shear Modulus with Shearing Strain for 100 % Soil-Size Fresh MSW Specimens Reconstituted with Material Passed the ¾-in. (19.1-mm) Sieve in the RCTS and LSRC devices 361

Figure 11.4 Comparison of the Variation in Material Damping Ratio with Shearing Strain for 100 % Soil-Size Fresh MSW Specimens Reconstituted with Material Passed the 3/8-in. (9.5-mm) Sieve in the RCTS and LSRC devices.....362
Figure 11.5 Comparison of the Variation in Material Damping Ratio with Shearing Strain for 100 % Soil-Size Specimen MSW3FNS1 Obtained from RC and TS Tests in the RCTS Device 363
Figure 11.6 Comparison of the Variation in Material Damping Ratio with Shearing Strain for 100 % Soil-Size Fresh MSW Specimens Reconstituted with Material Passed the ¾-in. (19.1-mm) Sieve in the RCTS and LSRC devices.....364
Figure 11.7 Comparison of the Variation in Shear Modulus with Shearing Strain and Isotropic Confining Pressures from RC tests for Specimen MSW2FNS2 Specimen (100 % Soil-Size Material).....365
Figure 11.8 Comparison of the Variation in Normalized Shear Modulus with Shearing Strain and Isotropic Confining Pressures from RC tests for Specimen MSW2FNS2 Specimen (100 % Soil-Size Material).....366
Figure 11.9 Comparison of the Variation in Elastic Threshold Shearing Strain with Isotropic Confining Pressures from RC tests for 100 %, 76 %, 62 %, and 14 % Soil-Size Fresh and Mixed MSW Groups 367
Figure 11.10 Comparison of the Variation in Material Damping Ratio with Shearing Strain and Isotropic Confining Pressures from RCTS tests for Specimen MSW2FNS2 (100 % Soil-Size Material) 369

Figure 11.11 Comparison of the Variation in (a) Shear Modulus and (b) Normalized Shear Modulus with Shearing Strain upon Loading and Unloading Sequences from RC tests for Specimen MSW4FNL3 (100 % Soil-Size Material).....370

Figure 11.12 Comparison of the Variation in Material Damping Ratio with Shearing Strain upon Loading and Unloading Sequences from RC tests for Specimen MSW4FNL3 (100 % Soil-Size Material) 372

Figure 11.13 Comparison of the Variation in Shear Modulus with Shearing Strain from RCTS tests for Specimen MSW1FNS1 (100 % Soil-Size Material) .372

Figure 11.14 Variation in Normalized Shear Modulus, G/G_{1st}, with the Number of Loading Cycles from TS tests for Specimen MSW1FNS1 (100 % Soil-Size Material).....373

Figure 11.15 Comparison of the Variation in Material Damping Ratio with Shearing Strain from RCTS tests for Specimen MSW1FNS1 (100 % Soil-Size Material).....374

Figure 11.16 Variation in Normalized Material Damping Ratio, D/D_{1st}, with the Number of Loading Cycles from TS tests for Specimen MSW1FNS1 (100 % Soil-Size Material) 375

Figure 11.17 Variation in Shear Modulus with Excitation Frequency from the RCTS and LSRC Tests for 100 % Soil-Size Fresh MSW in the nonlinear strain range.....376

Figure 11.18 Variation in Normalized Shear Modulus with Excitation Frequency from the RCTS and LSRC Tests for 100 % Soil-Size Fresh MSW in the nonlinear strain range.....377

Figure 11.19 Variation in Material Damping Ratio with Excitation Frequency from the RCTS and LSRC Tests for 100 % Soil-Size Fresh MSW in the nonlinear strain range.....378
Figure 11.20 Variation in Normalized Material Damping Ratio with Excitation Frequency from the RCTS and LSRC Tests for 100 % Soil-Size Fresh MSW in the nonlinear strain range 380
Figure 11.21 Comparison of the Variation in (a) Shear Modulus and (b) Normalized Shear Modulus with Shearing Strain from LSRC Tests upon Different Weight Percentages of Soil-Size Fresh and Mixed MSW Specimens.....382
Figure 11.22 Comparison of the Variation in Material Damping Ratio with Shearing Strain from LSRC Tests upon Different Weight Percentages of Soil-Size Fresh and Mixed MSW Specimens.....383
Figure 11.23 Comparison of the Variation in (a) Shear Modulus and (b) Normalized Shear Modulus with Shearing Strain from RC Tests of Specimens at Its Natural and Hydrated Conditions for Fresh MSW Specimens (100 % Soil-Size Material) 384
Figure 11.24 Comparison of the Variation in Material Damping Ratio with Shearing Strain from RC Tests upon Specimens at Its Natural and Hydrated Conditions for 100 % Soil-Size Fresh MSW Specimens.....385
Figure 11.25 Comparison of the Variation in (a) Shear Modulus and (b) Normalized Shear Modulus with Shearing Strain from RC Tests of Specimens with Different Total Unit Weights for 100 % Soil-Size Fresh MSW Specimens 387

Figure 11.26 Comparison of the Variation in Material Damping Ratio with Shearing Strain from RC Tests of Specimens with Different Total Unit Weights for 100 % Soil-Size Fresh MSW Specimens 388
Figure 11.27 Comparison of the Variation in (a) Shear Modulus and (b) Normalized Shear Modulus with Shearing Strain from RC Tests of Specimens with the Different Particle Size of Fresh MSW Specimens (100 % Soil-Size Material).....389
Figure 11.28 Comparison of the Variation in Material Damping Ratio with Shearing Strain from RC Tests upon Specimens with the Different Particle Size of Fresh MSW Specimens (100 % Soil-Size Material).....390
Figure 11.29 Plot of Normalized Shear Modulus with Modified Material Damping Ratio from RCTS and LSRC Tests for All Groups of Fresh and Mixed MSW Specimens.....392
Figure 11.30 Comparison of the Values of Measured D-D_{min} and Predicted D-D_{min} from (a) RC Tests and (b) TS Tests for Fresh MSW Specimens.....394
Figure 11.31 Comparison of the Variation in Shear Modulus with Shearing Strain at a Confining Pressure of 11 psi (76 kPa) for Fresh MSW and Loose Sand ...395
Figure 11.32 Comparison of the Variation in Normalized Shear Modulus with Shearing Strain at a Confining Pressure of 11 psi (76 kPa) for Fresh MSW and Loose Sand 395
Figure 11.33 Comparison of the Variation in Material Damping Ratio with Shearing Strain at a Confining Pressure of 11 psi (76 kPa) for Fresh MSW and Loose Sand.....396

Figure 12.1 Comparison of the Variation in (a) Shear Modulus and (b) Normalized Shear Modulus with Shearing Strain from RC Tests for Old and Fresh MSW Specimens (100 % Soil-Size Material) 399
Figure 12.2 Comparison of the Variation in Material Damping Ratio with Shearing Strain from RC tests for Old and Fresh MSW Specimens (100 % Soil-Size Material).....401
Figure 12.3 Comparison of the Variation in Normalized Shear Modulus with Shearing Strain from RC tests for (a) Old and (b) Fresh MSW Specimens (100 % Soil-Size Material).....402
Figure 12.4 Comparison of the Variation in Normalized Material Damping Ratio with Shearing Strain from RC tests for (a) Old and (b) Fresh MSW Specimens (100 % Soil-Size Material).....405
Figure 13.1 Comparison of the Fitted Relationships for the Variation in Normalized Shear Modulus with Shearing Strain from RC Tests in of Old, Fresh, and Mixed MSW Patterned After Darendeli's (2001) Model 410
Figure 13.2 Comparison of the Fitted Relationships for the Variation in Material Damping Ratio with Shearing Strain from RC Tests of Old, Fresh, and Mixed MSW Patterned After Darendeli's (2001) Model 412
Figure 13.3 Comparison of the Fitted Relationships for the Variation in Material Damping Ratio with Shearing Strain from RC Tests of Old, Fresh, and Mixed MSW Patterned After Darendeli (2001): (a), (b), and (c) Uncorrected for f and (d), (e), and (f) Corrected for f 413
Figure 13.4 Comparison of the Variation in Low-Amplitude Shear Modulus with Isotropic Confining Pressure from RC and Cyclic Triaxial Tests of 100 % and 62 to 76 % Soil-Size Old MSW: UT and UCB 416

Figure 13.5 Comparison of the Variation in Low-Amplitude Shear Modulus with Isotropic Confining Pressure from RC and Cyclic Triaxial Tests of 100 % and 62 to 76 % Soil-Size Fresh MSW: UT and UCB 418
Figure 13.6 Comparison of the Variation in Normalized Shear Modulus with Shearing Strain for Different Weight Percentages of Soil-Size Material between UT and UCB Measurements.....419
Figure 13.7 Comparison of the Variation in Material Damping Ratio with Shearing Strain upon Different Weight Percentages of Soil-Size Material between UT and UCB: (a) 100 %, (b) 62 to 76 %, and (c) 14% (8 to 25 %).....422
Figure 13.8 Comparison of the Variation in Normalized Shear Modulus with Shearing Strain with Other Studies.....424
Figure 13.9 Comparison of the Variation in Material Damping Ratio with Shearing Strain with Other Studies.....425

List of Tables

Table 2.1 Summary of Seismic Performance of Various Waste Landfill Sites during Northridge Earthquake Event (from Matasovic et al. 1995). 34

Table 5.1 Number of MSW Specimens Tested in Each Material Group with the RCTS and LSRC Devices (All Groups) 98

Table 5.2 Name of MSW Specimens Tested in Each Material Group with the RCTS and LSRC Devices (All Groups) 99

Table 5.3 Summary of the Initial Material Characteristics of Small-Diameter MSW Specimens for Fixed-Free (Fx-Fr) RCTS Tests for 100 % Soil-Size Material Group 101

Table 5.4 Summary of Initial Material Characteristics of Small-Diameter Hydrated MSW Specimens for Fixed-Free (Fx-Fr) RCTS Tests for 100 % Soil-Size Material Group 106

Table 5.5 Summary of the Initial Material Characteristics of Large-Diameter MSW Specimens for Free-Free (Fr-Fr) LSRC Tests for 100 % Soil-Size Material Group 110

Table 5.6 Weight Percentages of Each Constituent Used to Construct Specimens in the Different Percentage Groups 112

Table 5.7 Summary of the Initial Material Characteristics of Large-Diameter MSW Specimens Reconstituted with Larger Particles for Free-Free (Fr-Fr) LSRC Tests for 62 to 76 % Soil-Size Material Groups 115

Table 5.8 Number of Blows per Layer for the Large-Diameter Specimens Constructed with Larger Particles for Old, Fresh, and Mixed MSW Specimens for 62 to 76 % Soil-Size Material Groups 116
Table 6.1 Isotropic Confining Pressures Used in Low-Amplitude RC Tests of Small-Diameter, 100 % Soil-Size Old Waste Specimens in the RCTS Device 121
Table 6.2 Isotropic Confining Pressures Used in Low-Amplitude RC Tests of Large-Diameter, Soil-Size Old Waste Specimens in the LSRC Device.....124
Table 6.3 Isotropic Confining Pressures Used in Low-Amplitude RC Tests of Large-Diameter, Soil-Size Mixed Waste Specimens in the LSRC Device 125
Table 6.3 Summary of Coefficients of Shear Modulus Increase, I_G, and Values of a Normalized Shear Modulus Increase, N_G, for Specimen MSW2ONS1 (100 % Soil-Size Material) 129
Table 6.4 Summary of Values of Material Damping Ratio Increase, I_D, and Values of a Normalized Material Damping Ratio Increase, N_D, for Specimen MSW2ONS1 (100 % Soil-Size Material).....134
Table 6.5 A Set of Exponents (n_G) and Shear Moduli at One Atmosphere (G_1) of G_{max} upon Loading and Unloading Sequences for 100 % Soil-Size Old MSW Specimens in the RCTS Device 138
Table 6.5 A Set of Exponents (n_D) and Material Damping Ratio at One Atmosphere (D_1) of D_{min} upon Loading and Unloading Sequences for 100 % Soil-Size Old MSW Specimens in the RCTS Device 142
Table 7.1 Isotropic Confining Pressures Used in Low-Amplitude RC Tests for Small-Diameter, Soil-Size Fresh Waste Specimens in the RCTS Device..192

Table 7.2 Isotropic Confining Pressures Used in Low-Amplitude for Large-Diameter, Soil-Size Fresh Waste Specimens and Fresh Waste Specimens with Larger Particles in the LSRC Device.....195

Table 7.3 Summary of Coefficients of Shear Modulus Increase, I_G, and Values of A Normalized Shear Modulus Increase, N_G, for Specimen MSW2FNS2 (100 % Soil-Size Material) 198

Table 7.4 Summary of Values of Material Damping Ratio Increase, I_D, and Values of a Normalized Material Damping Ratio Increase, N_D, for Specimen MSW2FNS2 (100 % Soil-Size Material) 201

Table 7.5 A Set of the Values of n_G and G_1 upon Loading and Unloading Sequences for 100 % Soil-Size Fresh MSW Specimens in the RCTS Device 205

Table 7.6 A Set of the Values of Exponents (n_D) and Material Damping Ratio at One Atmosphere (D_1) upon Loading and Unloading Sequences for 100 % Soil-Size Fresh MSW Specimens in the RCTS Device 208

Table 9.1 Values of Exponents (n_S), Shear Wave Velocity at One Atmosphere (V_{s1}) of V_s, and Resultant Compaction Pressure, (σ_p), upon Loading Sequence for All Groups of Old, Fresh, and Mixed MSW Specimens in the RCTS and LSRC Devices.....275

Table 10.1 Isotropic Confining Pressures Used in High-Amplitude RCTS Tests for Small-Diameter 100% Soil-Size Old MSW Specimens in the RCTS Device 296

Table 10.2 Isotropic Confining Pressures Used in High-Amplitude RC Tests for Large-Diameter 100 %, 76 %, and 62 % Soil-Sizes Old MSW Specimens in the LSRC Device.....299

Table 10.3 Values of Elastic Threshold Shearing Strain (γ_t^e) for G with Confining Pressures for Specimen MSW3ONS1 (100 % Soil-Size Material) 313
Table 10.4 Values of Elastic Threshold Shearing Strain (γ_t^e) for D with Confining Pressures for MSW3ONS1 (100% Soil-Size Material) 316
Table 10.5 Values of Reference Strain, γ_r, and Curvature Coefficient, a, with Different Values of OCR for MSW3ONS1 (100% Soil-Size Material).....318
Table 11.1 Isotropic Confining Pressures Used in High-Amplitude RCTS Tests for Small-Diameter 100% Soil-Size Fresh MSW Specimens in the RCTS Device 355
Table 11.2 Isotropic Confining Pressures Used in High-Amplitude RC Tests for Large-Diameter 100 %, 76 %, and 62 % Soil-Sizes Fresh MSW Specimens in the LSRC Device 357
Table 11.3 Values of Elastic Threshold Shearing Strain (γ_t^e) for G with Confining Pressures for Specimen MSW2FNS2 (100 % Soil-Size Material) 367
Table 11.4 Values of Elastic Threshold Shearing Strain (γ_t^e) for D with Confining Pressures for Specimen MSW2FNS2 (100 % Soil-Size Material) 369
Table 13.1 Summary of the Values of Modified Hyperbolic Parameters used for the Best Fit of Each Group of Normalized Shear Modulus Curves Patterned After Darendeli's (2001) Model 410
Table 13.2 Summary of the Values of the Adjusted Masing Behavior Model Parameters Used for Best Fit of Each Group of Uncorrected Material Damping Ratio Curves for Frequency 414
Table 13.3 Summary of the Values of the Adjusted Masing Behavior Model Parameters Used for Best Fit of Each Group of Corrected Material Damping Ratio Curves for Frequency 415

Table 13.4 A Summary of the Values of Factors Used for Frequency Corrections for Material Damping Ratio Curves with Different Weight Percentages of Soil-Size Material 423

CHAPTER 1: INTRODUCTION

1.1 MOTIVATION

As residential areas in urban environments continue to expand, the amount of garbage and/or trash generated has been greatly increasing. The garbage and trash discharged from urban residential areas are referred to as a municipal solid waste (MSW). The increase in total yearly waste generation in the United States over the past 40 years is illustrated in Figure 1.1. As seen in the Figure 1.1, the yearly waste generation has been steadily increasing, even though a large portion of the waste is being recycled. Figure 1.2 shows the percent of waste generation with respect to each component for 2003. In this year, 236 million tons of MSW were generated. According to Figure 1.2, the majority of the MSW that was produced is composed of paper, yard trimmings, food, and plastics. Most of the waste is dumped into MSW landfills. Consequently, the size and height of MSW landfills have been steadily increasing.

If MSW landfills are constructed in seismic zones, the landfill can be damaged during earthquake shaking resulting in the potential release of contaminations in the environment. Seismic zones are defined herein as areas with a ten percent or greater probability that the maximum horizontal acceleration will exceed 0.1 g in 250 years (Repetto et al., 1993). One significant consideration is the seismic stability of landfill slopes. A thesis by Zekkos (2005) summarizes examples of five landfill slope failures in different locations around the world. These landfill slope failures are as follows: (1) on March 9, 1996, Rumpke Sanitary Landfill in Ohio, U.S.A, (2) on September 27, 1997, Dona Juanna Landfill in Columbia, (3) on July 10, 2000, Payatas Landfill in the Pilipppines, (4) on March, 2003, Ano Liosia Landfill in Greece, and (5) on

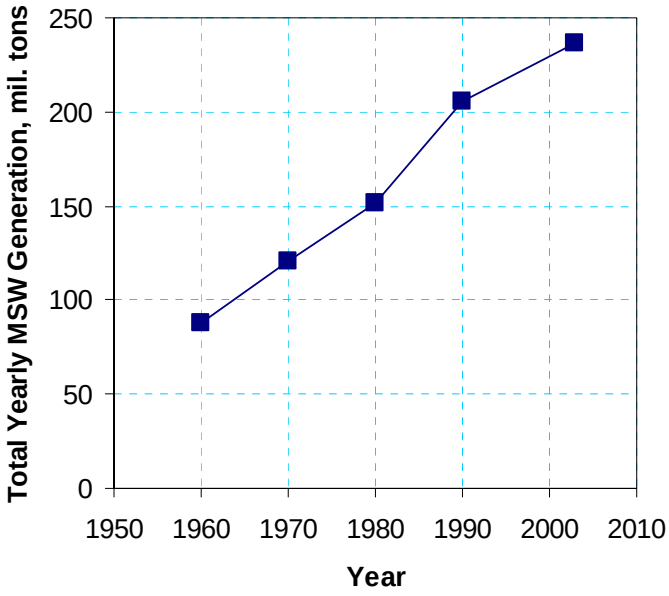

Figure 1.1 Total Yearly Waste Generation in U.S.A between 1960 and 2003 (from U.S.EPA, 2003)

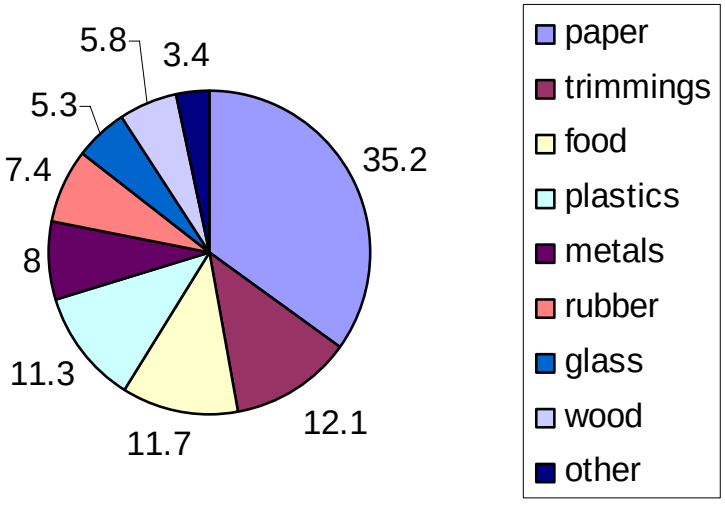

Figure 1.2 Percent Distribution of Constituents for Total Waste Generation in 2003 (from U.S.EPA, 2003)

February 21, 2005, Leuwigajah Landfill close to Bandung in the Western Java Province of Indonesian. In addition to slope failures, there are other types of damage to MSW landfill during earthquake shaking. This damage includes cracking of the soil cover(s), tears in the geosynthetic liner systems, and the temporary shutdown of the gas extraction systems. Augello et al. (1995) surveyed the seismic performance of waste landfills from six different waste landfills during the Northridge earthquake in 1994. They concluded that none of the waste landfills exhibited any sign of major damage, but the cracking was observed in most landfills.

During the past 15 years, MSW landfills have evolved into sophisticated engineered systems. In spite of this sophistication, our understanding of MSW landfills is still very elementary. A prerequisite to conducting an engineering analysis on the reliability of the seismic stability of landfills is an improved understanding of the mechanical behavior of MSW. Unfortunately, our engineering knowledge of MSW is limited due to the existence of significant uncertainties and difficulties in measuring the dynamic properties, i.e., shear modulus and material damping ratio. These uncertainties are increased by the heterogeneity of MSW and the fact that it can vary with time as it decomposes. In addition, it is difficult to quantify the relationship between MSW constituents. When using numerical methods for seismic or dynamic analysis, it has been identified that the input parameters such as the shear wave velocity (V_s) profile, material damping profile in shear, Poisson's ratio (υ), and nonlinearity in the shear modulus and material damping play important roles in the site response analysis. Thus, knowledge of the in-situ V_s profile, nonlinear shear modulus and material damping curves allow evaluation of the seismic stability of MSW landfills and prediction of ground motions within and at the top of MSW landfills. With a given V_s profile, the shear modulus can be estimated by simply multiplying the mass density with the square

of the shear wave velocity.

Over the past 40 years, numerous studies have been performed on the dynamic properties of both cohesive and cohesionless geotechnical materials (e.g., Hardin and Drevich, 1972, Ishihara, 1996). As a result, the dynamic behavior of these materials is well established and organized in the fields of soil dynamics and geotechnical earthquake engineering. For instance, measurements of the nonlinear shear modulus and material damping curves have been performed in many laboratories with a wide range of test equipment. (e.g., Seed and Idriss, 1970, Hardin and Drnevich, 1972, Anderson and Richart, 1976, Stokoe and Lodde, 1978, Darendeli, 2001, etc). For cohesionless soils, many researchers have measured and studied the shear modulus and material damping curves using laboratory testing equipment (Hardin and Black, 1966, Silver and Seed, 1970, Drnevich and Richart, 1970, Iwasaki et al., 1978, Ni, 1987, Ishihara, 1996, Menq, 2003, etc).

Compared with the numerous studies dealing with the dynamic properties of conventional geotechnical materials, research on MSW has been very limited until recently. In spite of the limited number of studies, there is, of course, useful information regarding the strain-dependent dynamic properties on the MSW. One of the available sources of information is back-calculated dynamic properties using recorded ground motions at the recording station at the Operating Industries, Incorporated (OII) MSW landfill during the Northridge earthquake in 1994. The back-calculated dynamic properties are expressed in terms of normalized shear modulus and material damping ratio curves with shearing strain. In addition, a series of large-diameter cyclic triaxial tests were carried out to find strain-dependent dynamic properties using MSW material retrieved from the Tri-Cities landfill in California (Zekkos, 2005). Finally, large-diameter free-free resonant column laboratory testing was performed to find the same

properties of a synthetic MSW which was a mixture of sand and shredded paper (Menq et al., 2001).

In conclusion, due to limited available resources dedicated to the understanding of the mechanical behavior of MSW and the demand for the enhancement of engineering analyses of MSW landfills design, it is necessary to study and investigate the dynamic characteristics of MSW.

1.2 OBJECTIVES OF THIS RESEARCH

The primary goal of this research is to investigate the dynamic properties of MSW using two different devices: (1) a combined resonant column (RC) and torsional shear (TS) device and (2) a large-scale, free-free resonant column device. Small (2.8-in. (71.1-mm)) and large (6.0-in. (152.4-mm)) diameter specimens were used for combined resonant column and torsional shear (RCTS) and large-scale free-free resonant column (LSRC) testing, respectively. The laboratory testing involved measurements in both the linear and nonlinear strain ranges. The test parameters affecting the dynamic properties at its natural and hydrated conditions in the linear strain range that were studied include: (1) duration of confinement at a constant pressure, (2), confining pressure, and (3) excitation frequency. Also, the test parameters which have an impact on the dynamic properties in the nonlinear strain range at its natural and hydrated conditions that were studied include: (1) strain amplitude, (2) confining pressure, (3) overconsolidation ratio, (4) number of loading cycles, and (5) excitation frequency.

The second objective of this research was to assess the influence of: (1) the waste composition, (2) the age of the waste, (3) the test specimen and particle sizes, (4) the unit weight of the waste, and (5) the water content of the specimen on the mechanical behavior of MSW. To achieve these goals, LSRC tests were conducted on MSW

specimens composed of various weight percentages of each component to evaluate the influence of these effects without the effect of hydration of the specimen.

The last objective of this research was to suggest representative nonlinear shear modulus and material damping curves with shearing strain for MSW. Important input parameters in performing a seismic response analysis of MSW landfills are the strain-dependent shear modulus reduction and material damping ratio curves. The representative curves were patterned after Darendeli's model (2001).

1.3 ORGANIZATION OF DISSERTATION

A literature review associated with the dynamic properties of MSW including unit weight, shear wave velocity, shear modulus reduction and material damping ratio curves, Poisson's ratio, and dynamic shear strength for site response analyses under seismic loadings is presented in Chapter Two. The dynamic properties were obtained either by measurements in the laboratory and field or back-calculation analyses from the recorded ground motions. The seismic performance of various MSW landfills during earthquakes is evaluated as well.

The RCTS and LSRC testing devices used in this study are explained in Chapter Three. The theoretical framework of the RCTS and LSRC testing techniques and the principal of computations of shear modulus, shearing strain, and half-power and free-vibration damping ratios are discussed. Detailed descriptions of the RCTS and LSRC testing device components such as the confinement system, driving system, height-change measurement system, and motion monitoring system are also described.

The characterization of MSW material retrieved from boreholes in the Tri- Cities landfill and material properties, for instance, in-situ total unit weight profile, variation in temperature with depth, water content measurements, and grain size distribution of

MSW, determined either in the field or laboratory is presented in Chapter Four.

The sample preparation method and procedure for small- and large-diameter specimens at their natural conditions are discussed in Chapter Five. In addition, the procedure for the hydration of specimens that have been tested in the RCTS device at their natural conditions is also described.

The test parameters affecting low-amplitude shear modulus, G_{max}, and low-amplitude material damping ratio, D_{min}, of **old** MSW in the linear strain range are investigated in Chapter Six. Those test parameters include: duration of confinement at a constant pressure, confining pressure, and excitation frequency. The estimated total unit weight obtained from RC tests is compared with those provided by both other researchers and measured in other waste landfills. In addition, the effects of waste composition, water content, unit weight, and specimen and particle sizes on the dynamic behavior of old MSW are studied in the linear strain range. An empirical relationship between estimated total unit weight and confining pressure, including the weight percentage of soil content, is developed. Also, an empirical relationship between G_{max} and D_{min} is provided to show how G_{max} and D_{min} are related to each other for **old** MSW.

The test parameters affecting G_{max} and D_{min} of **fresh** MSW in the linear strain range are investigated in Chapter Seven. These parameters include as follows: duration of confinement at a constant pressure, confining pressure, and excitation frequency. The estimated total unit weight obtained throughout RC tests is compared with those provided by both other researchers and measured in other waste landfills. In addition, the effects of waste composition, water content, unit weight, and specimen and particle sizes on the dynamic behavior of fresh MSW are studied in the linear strain range. An empirical relationship between estimated total unit weight and confining pressure, including the weight percentage of soil content, is developed. Also, an empirical

relationship between G_{max} and D_{min} is provided to show how G_{max} and D_{min} are related to each other for **fresh** MSW.

Comparison of the effects of confining pressure and excitation frequency on G_{max} and D_{min} of old and fresh MSW is made in Chapter Eight. Additionally, the change in estimated total unit weight of old and fresh MSW is compared.

Comparison of shear wave velocities measured during RC and LSRC laboratory tests is made with those measured in the Tri-Cities landfill, where the testing materials were retrieved for this study, is presented in Chapter Nine. The shear wave velocities and V_s profiles are compared with the V_s measurements presented in previous studies.

The test parameters affecting shear modulus, G, normalized shear modulus, G/G_{max}, and material damping ratio, D, of **old** MSW in the nonlinear strain range are investigated in Chapter Ten. These test parameters include the shearing strain amplitude, isotropic confining pressure, overconsolidation ratio, number of loading cycles, and excitation frequency. The effects of waste composition, water content, specimen and particle sizes, and unit weight of the specimens on dynamic nonlinear behavior for old MSW are discussed as well. An empirical relationship between G/G_{max} and $D\text{-}D_{min}$ is presented to demonstrate how shear modulus and material damping are correlated to each other for **old** MSW.

The parameters affecting the dynamic properties of **fresh** MSW in the nonlinear strain range are investigated in Chapter Eleven. These parameters include: strain amplitude, confining pressure, overconsolidation ratio, number of loading cycles, and excitation frequency. The effects of waste composition, water content, unit weight, and specimen and particle sizes on dynamic nonlinear behavior for old MSW are discussed as well. An empirical relationship between G/G_{max} and $D\text{-}D_{min}$ is presented to demonstrate how G and D are correlated to each other for **fresh** MSW.

The comparison of the variation in G, G/G_{max}, and D with shearing strain at a given confining pressure for old and fresh MSW in the nonlinear strain range is made in Chapter Twelve. The variation in G and D with excitation frequency at a given confining pressure in the nonlinear strain range is compared. Also, normalized shear modulus at a frequency of 1 Hz, $G/G_{f=1Hz}$, and normalized material damping ratio at a frequency of 1 Hz, $D/D_{f=1Hz}$, are compared.

Nonlinear shear modulus reduction and material damping ratio curves measured by The University of Texas at Austin (UT) are compared with those obtained by the University of California at Berkeley (UCB) regarding different weight percentages of soil content in Chapter Thirteen. Also, the nonlinear shear modulus reduction and material damping ratio curves measured by UT are compared with those proposed previously by other researchers.

Finally, the summary and conclusions drawn from this research are presented. Recommendations for future study are also discussed.

CHAPTER 2: LITERATURE REVIEW

2.1 INTRODUCTION

A review of the publications associated with the measurements or estimation of the dynamic properties of MSW and the seismic performance of MSW landfills when subjected to dynamic loadings such as blasting, machine vibrations, earthquakes, etc. is provided in this chapter. A limited number of studies have been performed to investigate the dynamic characteristics of MSW over the last decade. To characterize the dynamic properties of MSW, these studies have employed laboratory tests, in-situ seismic measurements, and the back-calculation analysis method.

Despite a lack of knowledge of the mechanical behavior of MSW and well documented case histories, one source of information is back-calculation of dynamic properties from the recorded ground motions at OII landfill during Northridge earthquake, which occurred on January 17, 1994. Using the recorded ground motions, the strain-dependent modulus reduction and material damping ratio curves were developed by some researchers (Kavazanjian et al. 1995, Idriss et al. 1995, Matasovic et al. 1995). The Whittier Narrows (1987), the Loma Prieta (1989), and the Northridge (1994) earthquakes provided a good opportunity to observe and evaluate the seismic performance of solid waste landfills during the seismic loading. One of the in-situ seismic testing techniques, spectral-analysis-of-surface waves (SASW) method was used to evaluate V_s profiles at different landfill sites by some researchers (Kavazanjian et al. 1996, Haker et al. 1997). The SASW testing method is considered to be more appropriate because no boreholes are required so that it is less sensitive to environmental problems beneath soil covers on landfills and it can be completed quickly.

The dynamic characteristics and seismic performance of solid waste landfills in earthquake events that have been estimated and observed by other researchers are presented and discussed in the following sections.

2.2 DYNAMIC PROPERTIES OF MSW

Material properties required for seismic or dynamic analysis of MSW landfills subjected to seismic loadings are unit weight, V_s profile, shear modulus reduction and material damping curves, Poisson's ratio, and dynamic shear strength. When performing the site-specific response analysis, the ground motions recorded at the surface of landfills can be significantly influenced by these parameters. Consequently, it is important to characterize and understand the dynamic properties properly to achieve more accurate predictions in the dynamic analysis.

2.2.1 Unit Weight

The unit weight of MSW is one of the input parameters for static and dynamic analysis of waste landfills. It can be reasonably assumed that the value of unit weight of MSW changes over a wide range depending upon the composition of waste, placement technique, age, depth, and environmental factors. The unit weight is required in the computation of shear modulus which is simply a product of mass density (unit weight divided by acceleration of gravity) and square of shear wave velocity. In addition to unit weight, which is used to calculate the shear modulus at representative points, the distribution of unit weight with depth is important as well. It is obvious that the site response analysis can be affected by the variation of unit weight. Realizing the important roll of unit weight in both static and dynamic analyses, values of unit weight which were measured in both laboratory and field studies have been reported by many researchers. However, there exists significant discrepancies and scattering in the values

due to the strongly heterogeneous and fibrous nature of solid wastes from site to site, even in the same landfill. The values of unit weight of MSW proposed by other researchers are presented below.

Landva et al. (1990) measured the unit weights of waste from different test pits across the Canada, varying in the range of 6.8 kN/m^3 to 16.2 kN/m^3 (43.3 to 103.1 pcf). They stated that the values greater than 14 kN/m^3 might have errors in measurements of weights and volumes as a result of inaccurate scales and irregular shapes of the test pits, respectively.

Sharma et al. (1990) estimated the unit weights of refuse fill located in the City of Richmond, California. The estimated unit weights from weights and volumes were determined indirectly from the weigh station and estimated volume for a given period was 7.2 kN/m^3 (46 pcf).

Kavazanjian et al. (1995) modified the total unit weight of waste landfill at the Puente Hills interpreted by Earth Technology (1988) and developed their own unit weight profile for seismic response analyses of waste landfills. The unit weight (represented by a solid line in Figure 2.1) at the surface of the MSW landfill was 6.5 kN/m^3 (41.4 pcf) and increased to 13 kN/m^3 (82.8 pcf) at of depth of about 90 m as shown in Figure 2.1. Inspection of Figure 2.1 reveals that the unit weight is changed dramatically to the depth of 50 m but beyond this depth remains mostly constant.

Morochnik et al. (1998) reported the distribution of unit weight underneath two stations at toe (SS1) and top (SS2) in OII landfill. The variation of unit weight at SS2 is shown in Figure 2.2. The unit weight was determined by three different ways: (1) the measured weight and cutting volume, (2) the percentage of soil in the sample, and (3) the weight and estimated volume. The proposed value of unit weight at SS2 was approximately 14.1 kN/m^3 (89.8 pcf), although there existed large scatter with depth as

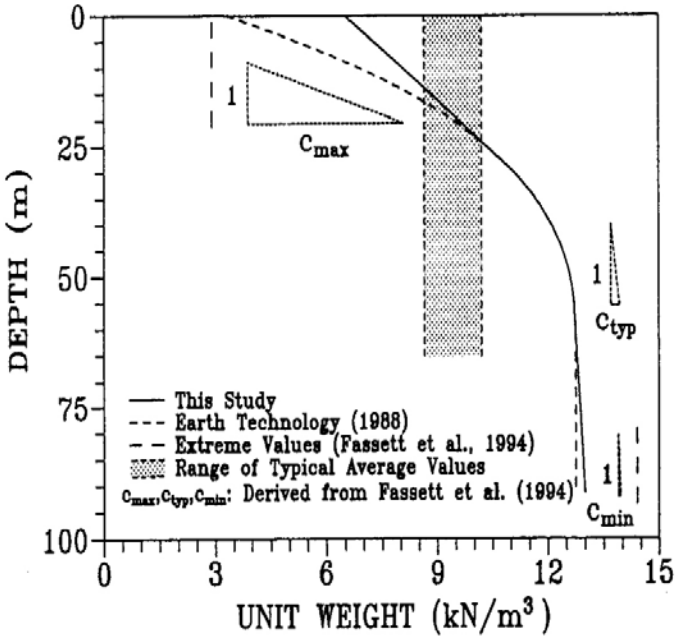

Figure 2.1 Variation of Total Unit Weight of MSW with Depth (from Kavazanjian et al. 1995)

illustrated in Figure 2.2. They suggested that the reason for the variation in values was resulted from employing different methods as mentioned above, which was attributed to the difficulty of sampling properly the highly heterogeneous waste material.

Matasovic et al. (1998) made measurements of in-situ total unit weight using the sand cone procedure in accordance with ASTM D 1556 at six different locations in the OII landfill. The distribution of measured unit weight is fairly scattered with depth varying from 12 kN/m^3 (76.4 pcf) to 21 kN/m^3 (133.7 pcf) as presented in Figure 2.3. Most values of unit weight fall into the ranges of 14 kN/m^3 (89.1 pcf) to 18 kN/m^3 114.6 pcf). Another measurement of in-situ total unit weight from a test trench at the shallow depth was equal to 16 kN/m^3 (101.8 pcf).

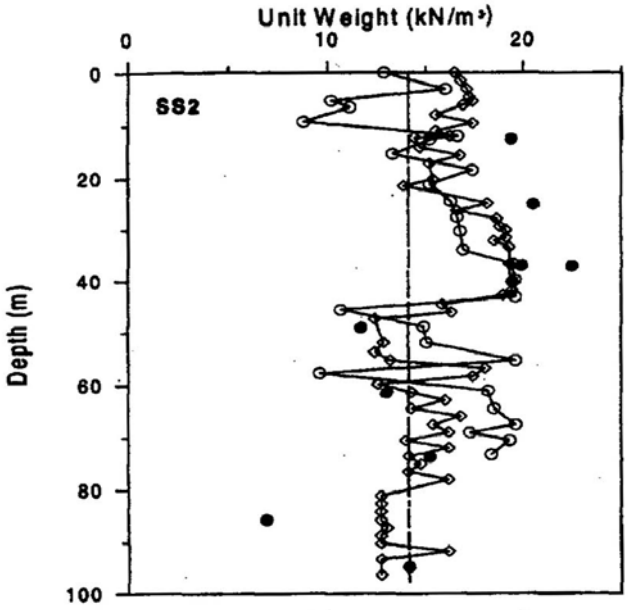

Figure 2.2 Profiles of the Measured and Proposed (dashed line) Total Unit Weight Profile at SS2 in OII Landfill (from Morochnik et al. 1998)

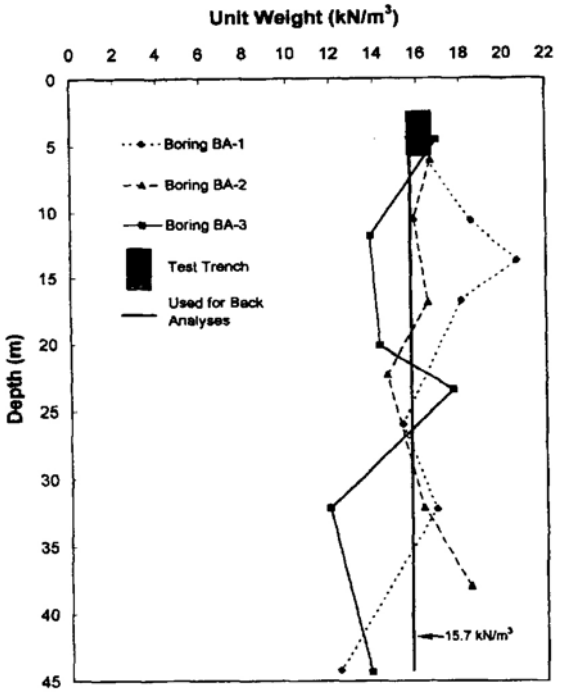

Figure 2.3 Distribution of Total Unit Weight of MSW with Depth at OII Landfill (from Matasovic et al. 1998)

2.2.2 Shear Wave Velocity

Besides the information about unit weight, performing conventional deformation and dynamic analyses require the V_s profiles with depth. It is evident that the selection of different V_s profiles leads to different results. Accordingly, attempts to accurately measureof shear wave velocity of MSW have been made by some researchers using seismic in-situ testing techniques such as downhole and SASW tests. These measurements are summarized in the following sections.

Sharma et al. (1990) conducted downhole tests at a landfill site that is located in the City of Richmond, California. The measured average value of V_s was 650 ft/sec (198 m/sec) for a depth of 0 ft to 50.2 ft (15.3 m).

Singh and Murphy (1990) summarized the average V_s of 274 m/sec (900 ft/sec) performed by Earth Technology, Inc. (1988) using crosshole and downhole tests. The shear wave velocities measured at West Richmond Fill by Redpath Geophysics and Redwood Refuse Fill by Portola Geophysics for EMCON were 213 m/sec (700 ft/sec) and 91 m/sec (300 ft/sec), respectively.

Anderson et al. (1992) carried out a two-dimensional, equivalent-linear, finite element analyses to model a landfill material using V_s of 244 m/sec (800 ft/sec).

Matasovic et al. (1995) reported a subsurface exploration program result regarding the V_s measurement performed by New Cure, Inc. at OII landfill by means of in-hole OYO suspension logging and downhole tests. The distribution of V_s measured in the top of the landfill is shown in Figure 2.4. The V_s profile from the OYO suspension logging test exhibits more scatter than that of the down-hole measurement. However, the general trend of increase in V_s with depth agrees well from both testing techniques.

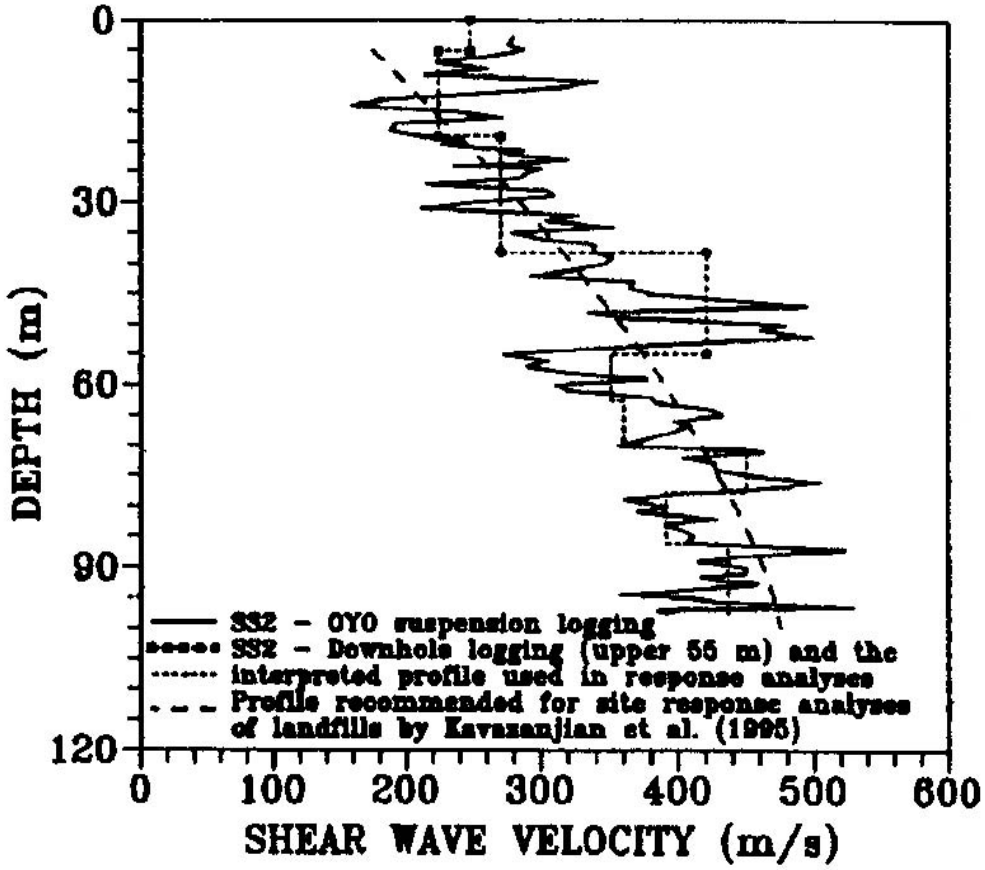

Figure 2.4 The V_s Profiles from Different Testing Methods at Station SS2 in OII Landfill in California (from Metasocvic et al. 1995)

In addition, Figure 2.4 indicates that the V_s measurements matched well with the profile developed by Kavazanjian et al. (1995).

Kavazanjian et al. (1996) measured shear wave velocities of MSW landfills at six different solid waste landfills in Los Angeles area using the SASW testing technique. The six landfills are: (1) Operating Industries, Inc (OII) landfill, (2) Azusa Land Reclamation Company landfill, (3) Sunshine Canyon landfill, (4) Lopez Canyon landfill, (5) Toyon Canyon landfill, and (6) unidentified landfill named as landfill A. They used a servo-hydraulic actuator as a source to generate long-period vibrations (low

frequencies) while a conventional impact source was used to reach shallow depths to produce high-frequency surface waves. The mean profile of all V_s profiles from the six landfills and profiles for the mean plus/minus one standard deviation are shown in Figure 2.5 with a recommended curve for site response analyses of landfills. They mentioned that the shear wave velocities measured at OII landfill were typically higher than those measured at other landfill sites because the OII landfill was most likely composed of more soil and soil-like material compared with the other waste constituents.

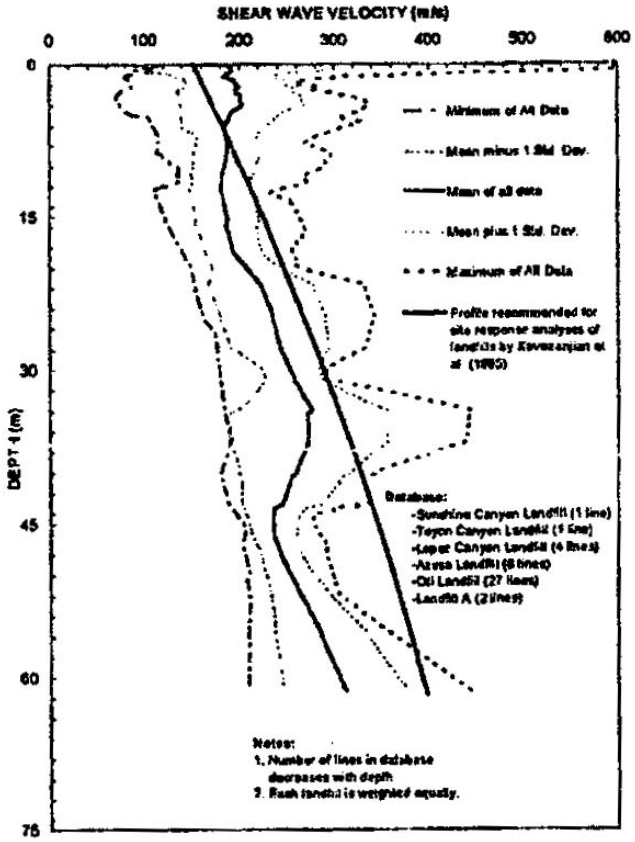

Figure 2.5 The V_s Profiles of Maximum, Minimum, Mean, and Mean ± One Standard Deviation Measured at Different Landfill Sites in Los Angeles (from Kavazanjian et al. 1996)

Houston et al. (1995) performed the downhole tests to produce the compressional wave (V_p) and shear wave profiles with depth at the Northwest Regional Landfill Facility (NWRLF) in Arizona. The V_p and V_s profiles measured by downhole tests are presented in Figure 2.6, varying from 235 m/sec (771 ft/sec) and 124 m/sec (407 ft/sec) at depth of 1.5 m (5 ft) to 346 m/sec (1135 ft/sec) and 229 m/sec (751 ft/sec) at dept of 10 m (33 ft). The discontinuity in compressional and shear wave velocities is clearly seen at the interface of cover soil and refuse. The resulting Poisson's ratio from the V_p and V_s measurements is 0.3 at the depth of 1.5 m (5 ft) and 0.11 at the depth of 10 m (33 ft). The calculation of Poisson's ratio is discussed in Section 2.2.4.

Haker et al. (1997) conducted SASW tests to measure the V_s and material damping ratio in shear at three different landfill sites in Atlanta, Georgia: Live Oak landfill, Sanifill Inc., and Bolton Road Sanitary landfill. The Bolton Road and Live Oak landfills were classified as "new waste" whereas the Sanifill landfill was classified as "old waste" according to the thickness of daily soil cover. The shear wave velocity is constant with depth at the Live Oak landfill but, for the other two landfills, the shear wave velocity increase with depth as illustrated in Figure 2.7. They remarked that the discrepancy in shear wave velocity might be attributed to waste type, density, confinement, age, placement technique, and soil content of MSW, resulting in a different dynamic properties from landfill to landfill.

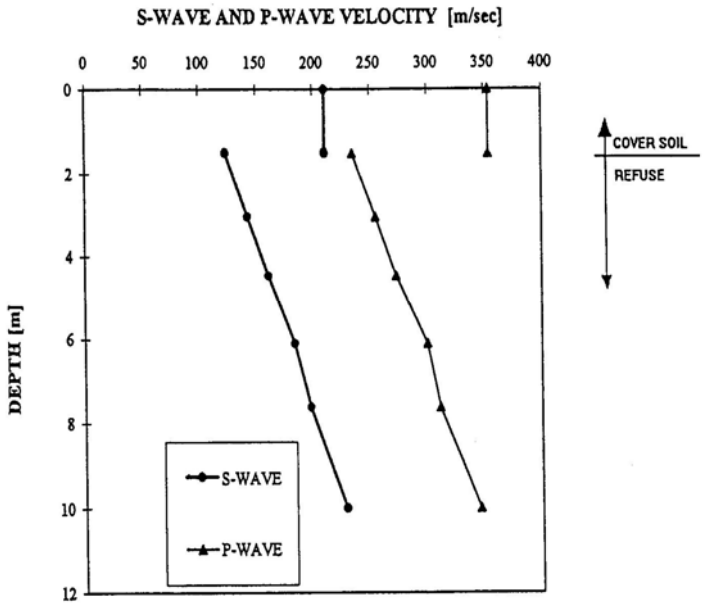

Figure 2.6 Variation in V_p and V_s Profiles with Depth at NWRLF in Arizona (from Houston et al. 1995)

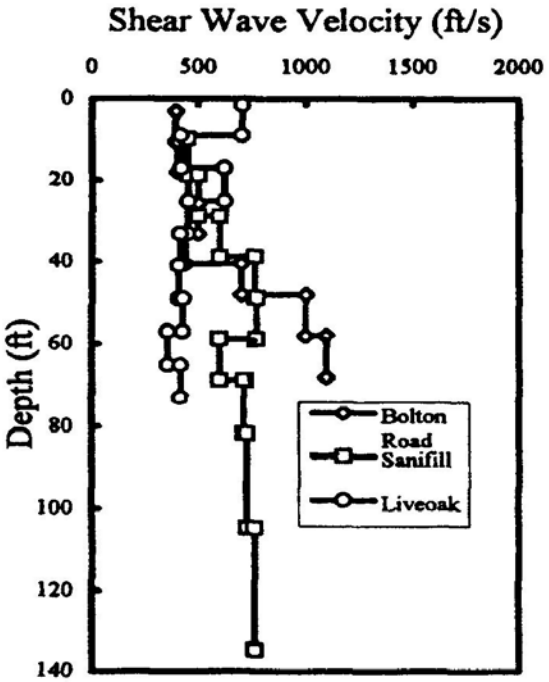

Figure 2.7 Distribution of V_s Profiles from Different MSW Landfill Sites in Atlanta, Georgia (from Haker et al. 1997)

2.2.3 Shear Modulus Reduction and Material Damping Curves

Other important input parameters for dynamic or seismic response analyses are a nonlinear shear modulus and material damping curves as a function of shearing strain. The selection of shear modulus reduction and material damping curves can significantly affect site response analyses. Therefore, choice of the appropriate curves representing the site conditions for dynamic analyses is much important than many other input parameters. Although the importance of these input parameters is realized, no studies have been performed until recently. Most proposed nonlinear shear modulus and material damping curves were derived by back-calculation analysis from recorded strong ground motions at the OII landfill. The proposed shear modulus reduction and material damping curves with shearing strain for dynamic analysis are summarized below.

Singh and Murphy (1990) developed strain-dependent modulus reduction and material damping curves for refuse material by taking the average of peat and clay curves based on the assumption that the material strength properties of refuse material were more cohesive than frictional. The synthesized shear modulus and damping curves are represented by solid lines in Figure 2.8.

Kavazanjian et al. (1995) developed shear modulus reduction and material damping curves for equivalent-linear and truly nonlinear, one-dimensional seismic response analysis by means of back-calculation analyses from recorded strong ground motions during the Northridge earthquake. The shear modulus reduction and material damping curves derived from back-calculation using modified Kondner and Zelasko model (MKZ) model parameters (Matasovic and Vucetic, 1993) are presented in Figure 2.9. The program SHAKE was adopted for one-dimensional equivalent-linear analyses and the computer program, which is called D-MOD developed by Matasovic (1993), was

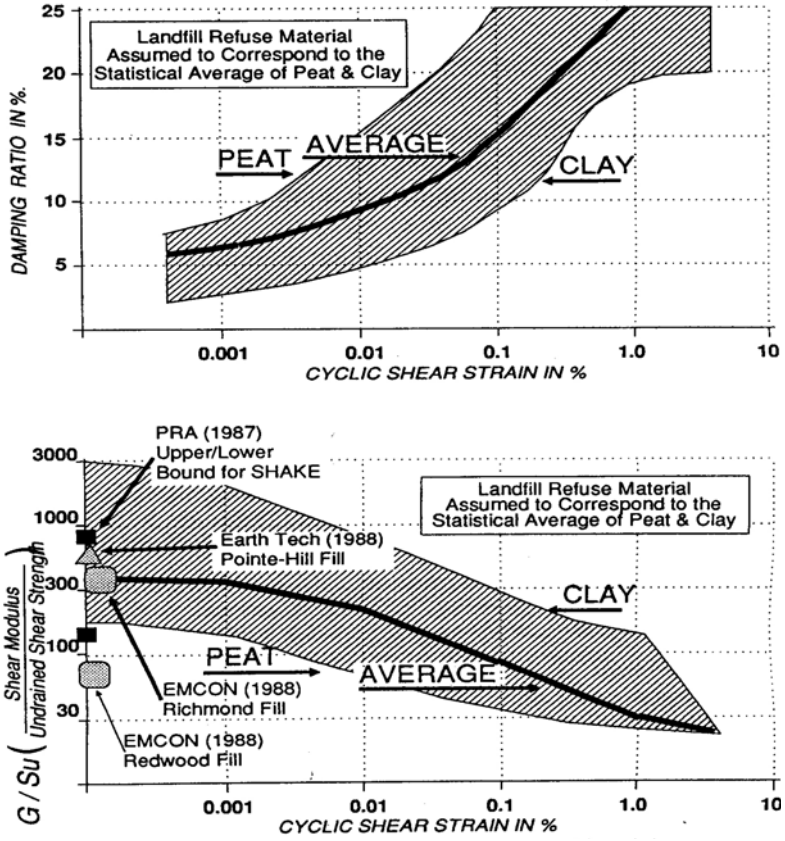

Figure 2.8 Normalized Shear Modulus and Material Damping Ratio with Cyclic Shear Strain for Refuse Material (from Singh and Murphy, 1990)

employed to perform the truly nonlinear analyses. The results from both equivalent-linear and nonlinear D-MOD analyses showed reasonably good agreement.

Idriss et al. (1995) derived shear modulus reduction and material damping curves of MSW material as a function of shear strain from one-, and two-dimensional seismic response analyses using recorded ground motions at the OII landfill. The derived shear modulus reduction and material damping curves are shown in Figure 2.10. They reported that the correlation between observed and calculated response showed good agreement when using the shear modulus reduction and material damping curves similar to that of high plasticity clays and that of sand or clay, respectively.

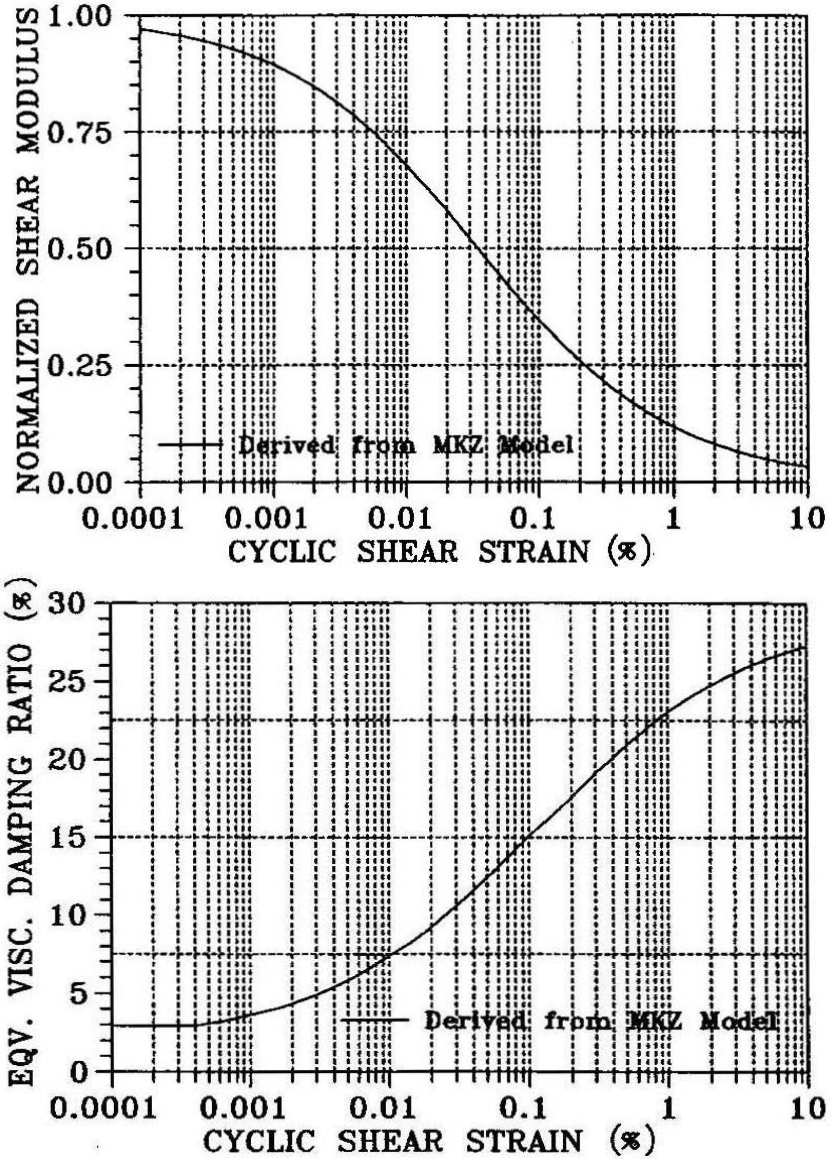

Figure 2.9 Normalized Shear Modulus (Top) and Equivalent Viscous Damping Ratio (Bottom) for Back-Calculation Analysis (from Kavazanjian et al. 1994)

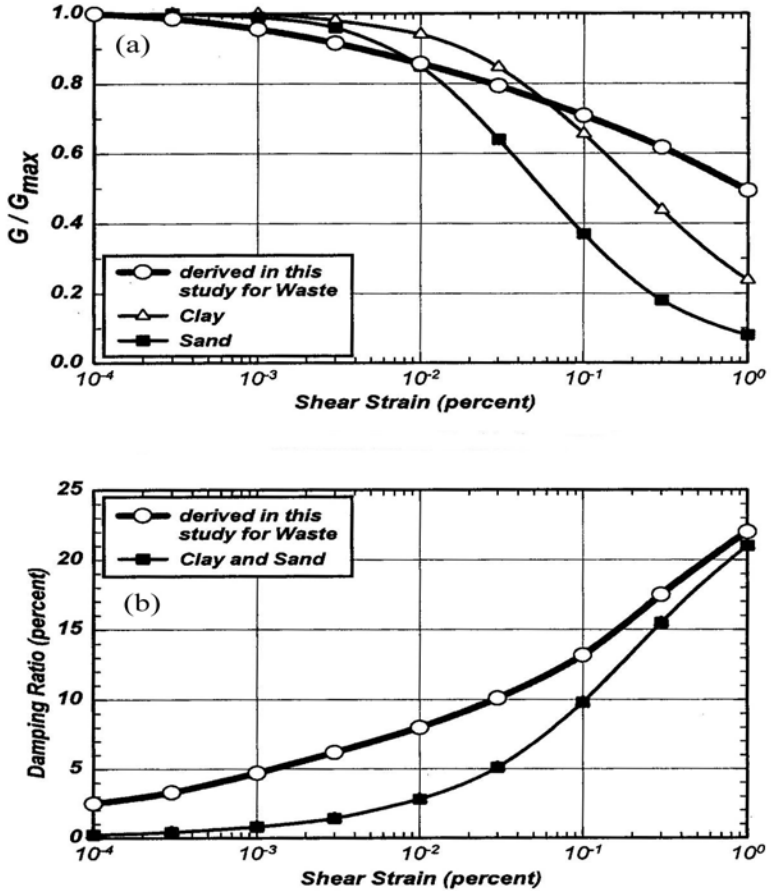

Figure 2.10 Variation of (a) Normalized Shear Modulus and (b) Damping Ratio with Shearing Strain (from Idriss et al. 1994)

Matasovic et al. (1998) proposed the family of "internally consistent" curves which were combined with back-calculation analysis from recorded ground motions at the OII landfill and data from cyclic direct simple shear tests. The group of these curves is presented in Figure 2.11. They recommend use of the upper bound and lower bound modulus reduction and material damping curves, respectively, because: (1) the upper bound modulus reduction curve showed a more consistent result with that obtained from the back-calculation analysis, (2) disturbance occurred during sampling and sample preparation, and (3) taking the upper-bound and lower-bound modulus reduction and

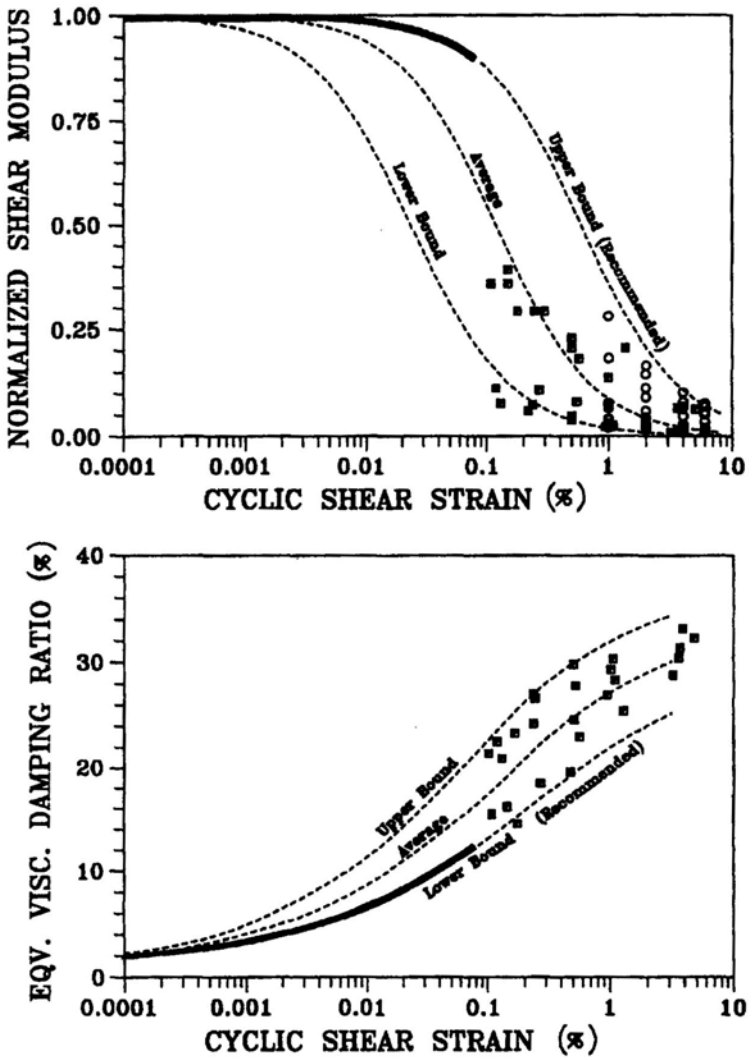

Figure 2.11 Variation of Shear Modulus (a) and Damping Ratio (b) with Cyclic Shear Strain (from Matasovic et al. 1998)

material damping curves was more conservative in terms of acceleration response at the landfill surface.

Zekkos (2005) generated the shear modulus reduction for given assumed Poisson's ratios (e.g., 0.3 for specimens constructed by soil-like material (defined on less than 20 mm in diameter) and 0.2 for specimens reconstituted by soil-size material plus

larger paticles) and material damping ratio curves directly using waste material retrieved from Tri-Cities landfill. He used 12.0 in. diameter cyclic triaxial tests to estimate the MSW. The proposed curves were divided in accordance with different weight percentages of soil-size material, i.e., 100 %, 62 to 76 %, and 8 to 25 %. The proposed curves of MSW corresponding to the depth of upper 65.6 ft (20.0 m) of a landfill are illustrated in Figure 2.12. He found that the waste composition was a very significant factor for both shear modulus reduction and material damping curves. He also found that the confining pressure also impacted the normalized shear modulus reduction curve but had a small influence on the material damping ratio curve. However, those curves were barely influenced by the state of degradation of wastes, i.e., age of the waste.

2.2.4 Poisson's Ratio

Measurements of Poisson's ratio of MSW have been attempted in the laboratory and in-situ waste landfill using one-dimensional compression or conventional triaxial testing devices and seismic testing methods during last decade. Based on the theory of elasticity, Poisson's ratio (υ) is defined as the ratio of lateral strain to axial strain. Poisson's ratio is used for the purpose of conversion of the elastic constants such as G, E, and M from any given two constants. Another way to compute Poisson's ratio is to use the V_p and V_s and these velocities are related with Poisson's ratio as follow:

$$\upsilon = \frac{0.5\left(\frac{V_p}{V_s}\right)^2 - 1}{\left(\frac{V_p}{V_s}\right)^2 - 1} \tag{2.1}$$

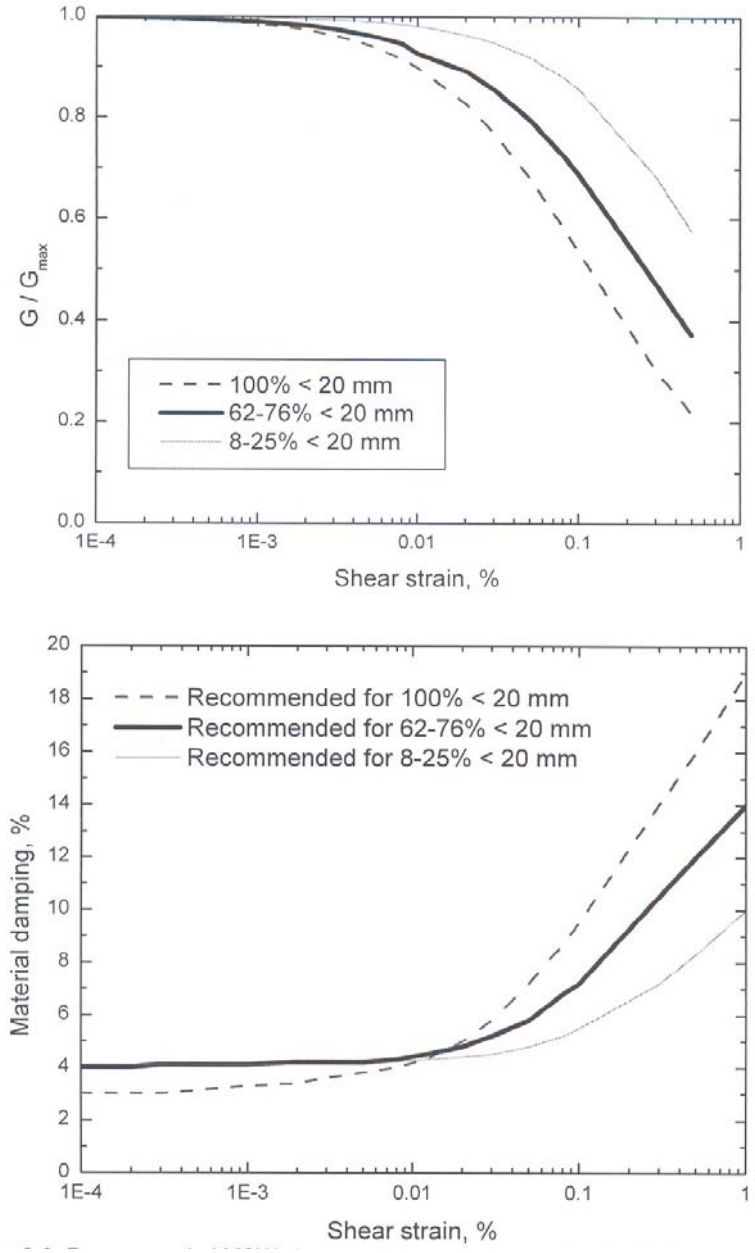

Figure 2.12 Variation of Shear Modulus (Top) and Material Damping (Bottom) with Different Weight Percentages of Soil-Size Material (from Zekkos, 2005)

Measurements of Poisson's ratio from the laboratory and in-situ tests are summarized below.

Sharma et al. (1990) conducted seismic downhole tests for the purpose of measuring the Poisson's ratio of refuse at a landfill site located in the City of Richmond, California. They reported that the Poisson's ratio calculated using the V_p and V_s measurements for refuse material was equal to 0.49.

Houston et al. (1995) evaluated the Poisson's ratio from V_p and V_s measured by the downhole tests in the landfill which was located in north western Maricopa County, Arizona. The values of V_p and V_s increased with depth beyond the cover soil. Poisson's ratio of cover soil was 0.23, thus Poisson's ratio for MSW ranged from 0.3 at a depth of 5.0 ft (1.52 m) to 0.11 at a depth of 32.8 ft (10.0 m).

Matasovic et al. (1995) developed the Poisson's ratio profile at OII landfill using the V_p and V_s profiles reported by Matasovic et al (1995) and Idriss et al (1995). The profiles of Poisson's ratio determined from the OYO suspension logging and downhole tests are presented in Figure 2.13. As seen in Figure 2.13, there is much scatter in the data but they suggested a Poisson's ratio of 0.33 as an approximated value for the OII landfill.

Zekkos (2005) estimated the Poisson's ratio directly by measuring the radial deformation using elastometer gauges and axial deformation using a linear variable differential transducer (LVDT) during cyclic triaxial tests on the materials retrieved from the Tri-Cities landfill. One thing he found was that the Poisson's ratio tended to be constant in the shearing strain range of 0.01 % to 1 %. Another thing was that at given mean confining pressures of 3.6 psi (25 kPa) to 13.1 psi (90 kPa), Poisson's ratio of the soil cover was 0.30 to 0.35 while for a soil-refuse mixture, Poisson's ratio reduced from 0.3 to nearly zero because of the small deformations in the radial direction due to large

voids

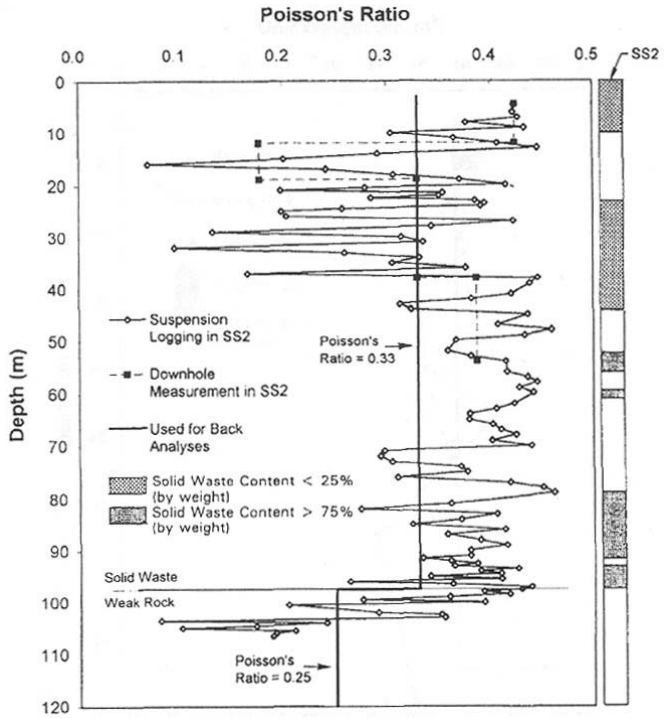

Figure 2.13 Variation of Poisson's Ratio with Depth Beneath the Top Recording Station at OII Landfill (from Metasovic et al. 1995)

between the particles. He finally remarked that the reason for such a large scatter might be attributed to (1) heterogeneous nature of waste material and (2) the way of deposition of refuse and soil-like materials.

2.2.5 Dynamic Shear Strength

Similar to static shear strength, the dynamic shear strength of waste material is also expressed in terms of Mohr-Coulomb strength parameters. It is now considered that the waste materials are composed of cohesive and frictional components from observations of stable vertical faces over various time periods (Eid et al., 2000). The dynamic shear strength of MSW has been assumed to be equal to the static shear strength

until the Northridge earthquake (1994). Several attempts have been made to evaluate the dynamic strength of waste material either by back-calculation analyses or by laboratory measurements. A summary of those attempts are listed below.

Augello et al. (1995) and Augello (1997) have made an effort to estimate the dynamic strength properties of waste fill material through pseudo-static stability analyses of MSW landfills. A conservative range of back-calculated dynamic friction angles for unlined landfills are 30° to 40° while the static friction angles were conservatively estimated to be on the order of 19° to 39° for a factor of safety of 1.2. They concluded that the dynamic friction angles are greater than the lower bound static friction angles obtained with a factor of safety of 1.2.

Zekkos (2005) performed the large-diameter (300 mm) triaxial tests to investigate the dynamic strength of MSW obtained from Tri-Cites landfill. The investigation was conducted by comparing the shear stresses in terms of axial strain with a different strain rates (e.g., 0.5 %/min, 5 %/min and 50 %/min) on test specimens having different weight percentages, i.e., 100 %, 62 %, and 20 % of soil-like material (material diameters smaller than 20 mm). The test result is illustrated in Figure 2.15. The figure indicates that the slope of shear stress versus shear strain relationship becomes larger with increasing strain rate. This effect is more evident with decreasing weight percentage of soil-like material. He concluded that the dynamic shear strength of MSW is larger than the static shear strength by 25 % to 30 % and suggested for a practical purpose that the dynamic strength is greater than the static strength approximately by a factor of 1.2.

2.3 SEISMIC PERFORMANCE OF WASTE LANDFILL IN EARTHQUAKE EVENTS

With the limited number of well-documented case histories and knowledge of the mechanical behavior during seismic loading of MSW landfills, the Whittier Narrows

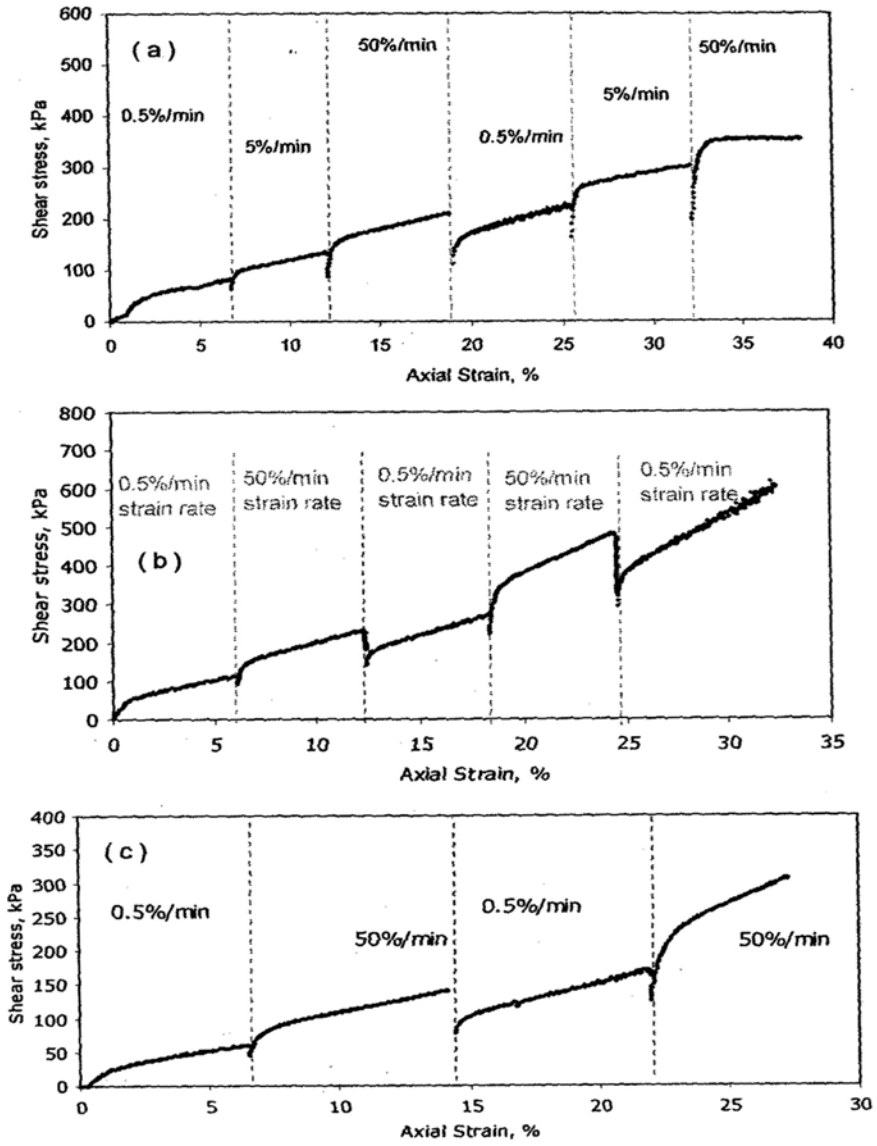

Figure 2.15 Stress-Strain Behavior of Specimens at Different Strain Rates for Different Weight Percentages: (a) 100 %, (b) 62 %, and (c) 20 % (from Zekkos 2005)

earthquake (moment magnitude, M_w = 6.0), which occurred in 1987 provided the first good opportunity to examine the seismic performance of waste landfills. No strong motion recording instruments were, however, installed in any other landfills in the United States. This lack of field recordings encourages installation of ground motion

monitoring equipment at the OII landfill to quantify the level of ground acceleration.

The seismic performance of landfills during the Loma Prieta earthquake, (M_w = 7.1) was evaluated by Orr and Finch (1990). They surveyed ten MSW landfills, which are designated by the initials of each landfill in Figure 2.16. These landfills were damaged by the Loma Prieta earthquake near the epicenter and San Francisco Bay Area, with estimated peak horizontal accelerations of 0.1 to 0.45 g. None of the landfills were instrumented or equipped with liners. The most common type of damage was only minor cracking in the landfill slope surface. Based on the limited surface damage, they drew a conclusion that the mass of the landfill functioned like an energy attenuator, in other words, the landfills could absorb energy propagating within the landfills generated by earthquakes, thus resulted in a reduction of earthquake effects at the surface.

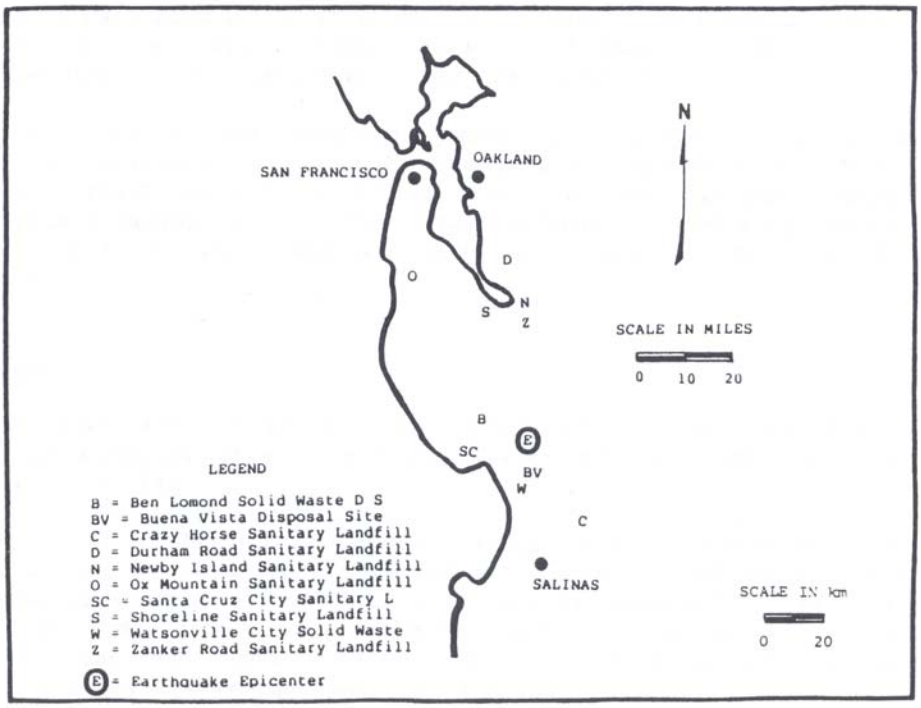

Figure 2.16 Map of Location of the Waste Landfills Surveyed for Seismic Performance during Loma Prieta Earthquake (from Orr et al. 1990)

The occurrence of the Northridge earthquake also provided a good chance to understand and characterize the seismic performance of MSW landfills, having a recorded maximum horizontal acceleration (MHA) of about 0.3 to 0.4 g (Augello et al. 1995).

A number of surveys of the seismic performance of MSW landfills from 22 different sites were performed after the Northridge earthquake. The location of each landfill surveyed is presented in Figure 2.17. The level of damage was categorized into 5 categories according to quantitatively defined damage in operation of the landfill.
The seismic performance of each landfill is described in Table 2.1. As indicated in Table 2.1, the most common damage was a cracking of cover soil which is consistent with the damage from the Loma Prieta earthquake. Cracking was found either at the waste fill and native ground contact or at the changes in geometry (Augello et al. 1995). The reasons causing cracking in the cover soil are: (1) difference in stiffness between cover soil and ductile waste, (2) difference in stiffness of waste fill and adjacent natural ground, (3) uneven waste fill settlement from earthquake shaking, (4) limited down-slope movement, and (5) cracking by rapid gas release due to shaking and/or temporary loss of gas extraction system (Augello et al. 1995).

As a result of damage observations from the various landfills, the following conclusion was drawn: “the solid waste landfill exhibited inherently moderate to strong energy absorption characteristics, which might be attributed to the existence of interlocking between the refuses, strain-hardening behavior, and light weight” (Singh et al. 1995)

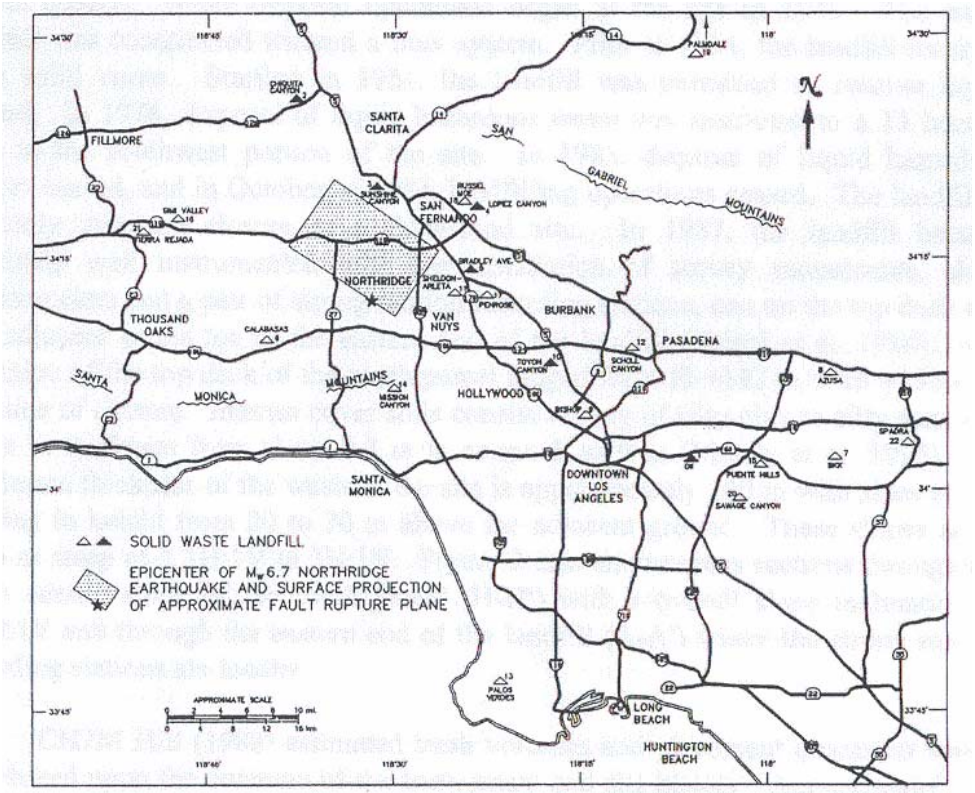

Figure 2.17 Location of Landfill Sites Surveyed for Seismic Performance during the Northridge Earthquake (from Metasovic et al. 1995)

Table 2.1 Summary of Seismic Performance of Various Waste Landfill Sites during Northridge Earthquake Event (from Matasovic et al. 1995).

SOLID WASTE LANDFILL	TYPE OF LANDFILL	ENGINEERED CONTAINMENT SYSTEM	DISTANCE FROM ZONE OF ENERGY RELEASE (km)	ESTIMATED ROCK PEAK HORIZONTAL ACCELERATION (g)	DAMAGE CATEGORY (I - V)	DAMAGED ELEMENT
1. Oil	Gravel Pit Fill	None	43	0.10 (0.24)	Minor Damage (II)	Cover Soil
2. Toyon Canyon	Canyon Fill	LCRS; Subsurface Barrier	22.2	0.21	Minor Damage (II)	Cover Soil; Gas Collection Header
3. Sunshine Canyon	Side Hill Fill	None	7	0.46	Moderate Damage (III	Cover Soil
4. Lopez Canyon	Canyon Fill	None (Disposal Areas A,B, AB+); Geosynthetic Liner System & LCRS (Disposal Area C)	8.4	0.42	Moderate Damage (III	Cover Soil; Gas System
5. Chiquita Canyon	Canyon Fill	None (Primary Landfill) Geosynthetic Liner System & LCRS (All other Canyons)	12.2	0.33	Significant Damage (IV)	Cover Soil; Geomembrane Tears
6. Bradley Avenue	Gravel Pit Fill	None (East); Clay Liner (West);Geosynthetic Liner System & LCRS (West Extension)	10.8	0.36	Moderate Damage (III	Cover Soil
7. Russel Moe	Canyon Fill	None	7.8	0.43	Moderate Damage (III	Cover Soil
8. Sheldon-Arleta	Gravel Pit Fill	None	10.7	0.36	Minor Damage (II)	Cover Soil; Gas Collection Headers
9. Penrose	Gravel Pit Fill	None	12.3	0.33		
10. Mission Canyon	Canyon Fill	None	18.4	0.25	No Damage (I)	None
11. Simi Valley	Canyon Fill	Geosynthetic Liner System & LCRS; Compacted Soil	22.3	0.21	Minor Damage (II)	Cover Soil; Gas System; Leachate Pump
12. Terra Rejada	Canyon Fill	None	22.4	0.21	Minor Damage (II)	Cover Soil
13. Calabasas	Canyon Fill	Geosynthetic Liner System & LCRS (Cell P)	23.1	0.20	Moderate Damage (III	Gas System; Cover Soil
14. Scholl Canyon	Canyon Fill	None	28.4	0.16	Moderate Damage (III	Cover Soil
15. Bishop Canyon	Canyon Fill	None	30.7	0.15	Little Damage (I)	Cover Soil
16. Palmdale	Area Fill	None	41.1	0.11	Minor Damage (II)	Cover Soil
17. Puente Hills	Side Hill Fill; Canyon Fill	Geosynthetic Liner System & LCRS (Canyon 9)	49.7	0.09	No Damage (I)	None
18. Palos Verdes	Canyon Fill	None	50.8	0.08	No Damage (I)	None
19. Azusa	Gravel Pit Fill	Geosynthetic Liner System & LCRS (Partial Coverage)	51.7	0.08	No Damage (I)	None
20. Savage Canyon	Canyon Fill	None	52.8	0.08	No Damage (I)	None
21. Spadra	Canyon Fill	Geosynthetic Liner System (Western Half) & LCRS	55.1	0.07	No Damage (I)	None
22. BKK	Canyon Fill	Compacted Soil (Haz. Waste Unit)	57.2	0.07	No Damage (I)	None

DAMAGE CATEGORY:		DESCRIPTION:
V.	Major Damage	General instability with significant deformations. Integrity of waste containment system jeopardized.
IV.	Significant Damage	Waste containment system impaired, but no release of contaminants. Damage cannot be repaired within 48 hours. Specialty contractor needed to repair the damage.
III.	Moderate Damage	Damage repaired by landfill staff within 48 hours. No compromise of the waste containment system integrity
II.	Minor Damage	Damage repaired without interruption to regular landfill operations
I.	Little or No Damage	No damage or slight damage but no immediate repair needed

2.4 SUMMARY

The material properties of MSW material required for dynamic analyses are briefly reviewed in this chapter. These properties included unit weight, shear wave velocity, shear modulus reduction and material damping curves, Poisson's ratio, and dynamic shear strength. The values of unit weight and Poisson's ratio measured at landfills, as discussed in Section 2.2.1 and Section 2.2.4, respectively, exhibit significant scatter which might be explained by the heterogeneous nature of waste materials. Shear wave velocity profiles and shear modulus reduction and material damping curves proposed or measured by various researchers have come from seismic field measurements (e.g., seismic crosshole, P-S logger, and SASW tests) and back-calculation analyses from recorded ground motions, as described in Section 2.2.2 and Section 2.2.3, respectively. Several attempts have been made to evaluate the dynamic shear strength of MSW either by pseudostatic back-analysis of landfill slopes or laboratory measurements.

The seismic performance of MSW landfills during earthquakes has been evaluated and the type of damage of landfills under seismic loading has been identified in Section 2.3. Among the damages created by earthquake events, the cracking at the cover soil and/or surface slope was the most common damages, which indicated that the waste landfills had an inherent energy absorption characteristic.

CHAPTER 3: LABORATORY TESTING EQUIPMENT

3.1 INTRODUCTION

Both RCTS and LSRC test equipment were used to measure the dynamic properties of MSW. The RCTS equipment has been developed and modified over the past three decades by Dr. Stokoe and several of his graduate students at UT (Isenhower, 1979, Lodde, 1982, Ni, 1987, Kim, 1991, Hwang, 1997, Darendeli, 2001). The RCTS equipment is appropriate for relatively small-diameter specimens, in the range of 1.5 to 3.0 inches. In addition, the LSRC device, which is able to test large-diameter specimens (6.0 in.), was developed by Dr. Stokoe and Dr. Menq (2003). It is also called a multi-mode device (MMD) because, besides shear modulus, this device can also be used to measure Young's modulus (E) and constrained modulus (M) at small strains by means of measuring the unconstrained compression wave velocity (V_c) and constrained compression wave velocity (V_p), respectively. This device has been designed to run on geotechnical materials with large particle size (maximum of 1 inch) like gravelly soils.

The RCTS apparatus has fixed-free (fx-fr) boundary conditions as shown in Figure 3.1(a). The bottom of the specimen is fixed to the base pedestal and the top of specimen is free to move in response to dynamic or cyclic torsional loading. Torsional motion is created by the coils and magnets at the top of specimen. In contrast to the RCTS device, both ends of specimen in the LSRC device have free-free (fr-fr) boundary conditions as illustrated in Figure 3.1(b). The specimen is supported in a vertical position by four springs. The torsional motion is applied to the bottom of the specimen using a coil-magnet driving system similar to the RCTS device. General testing configurations for both the RCTS and LSRC devices are presented in Figures 3.2 and 3.3,

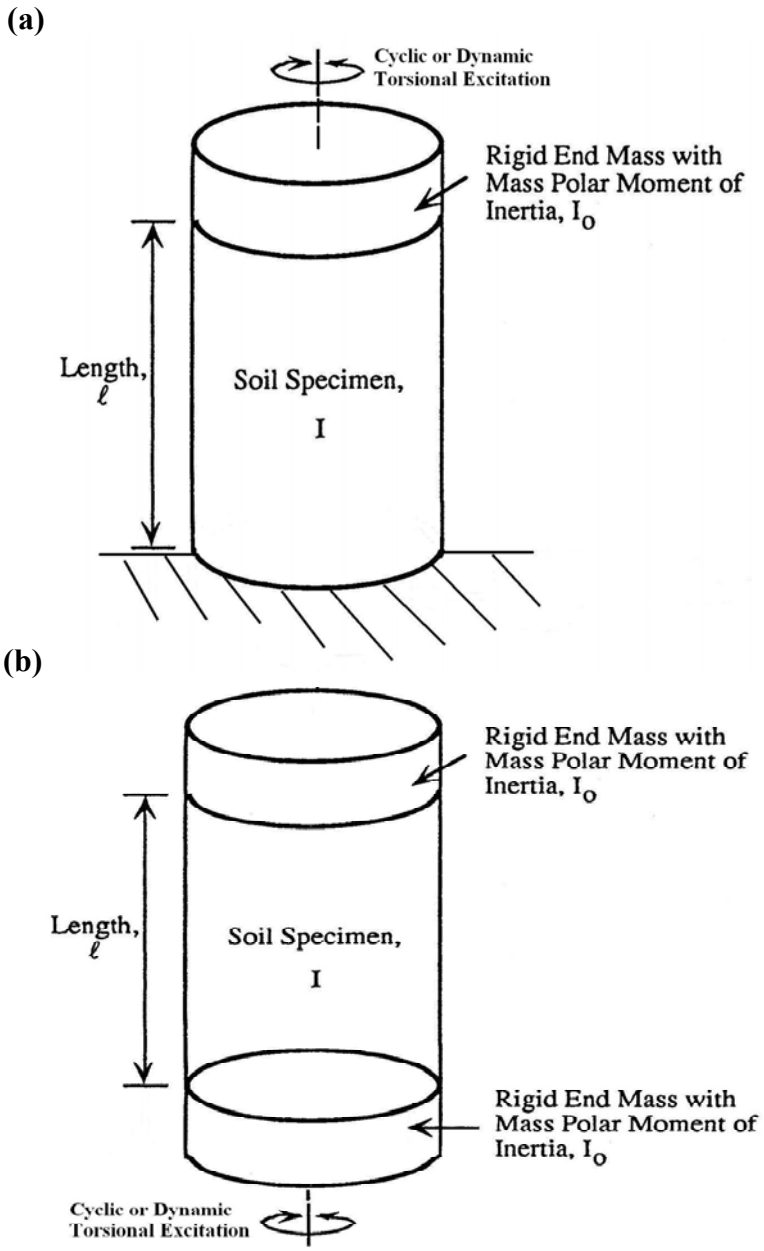

Figure 3.1 Idealization of (a) Fixed-free RCTS and (b) Free-free LSRC Testing Equipments

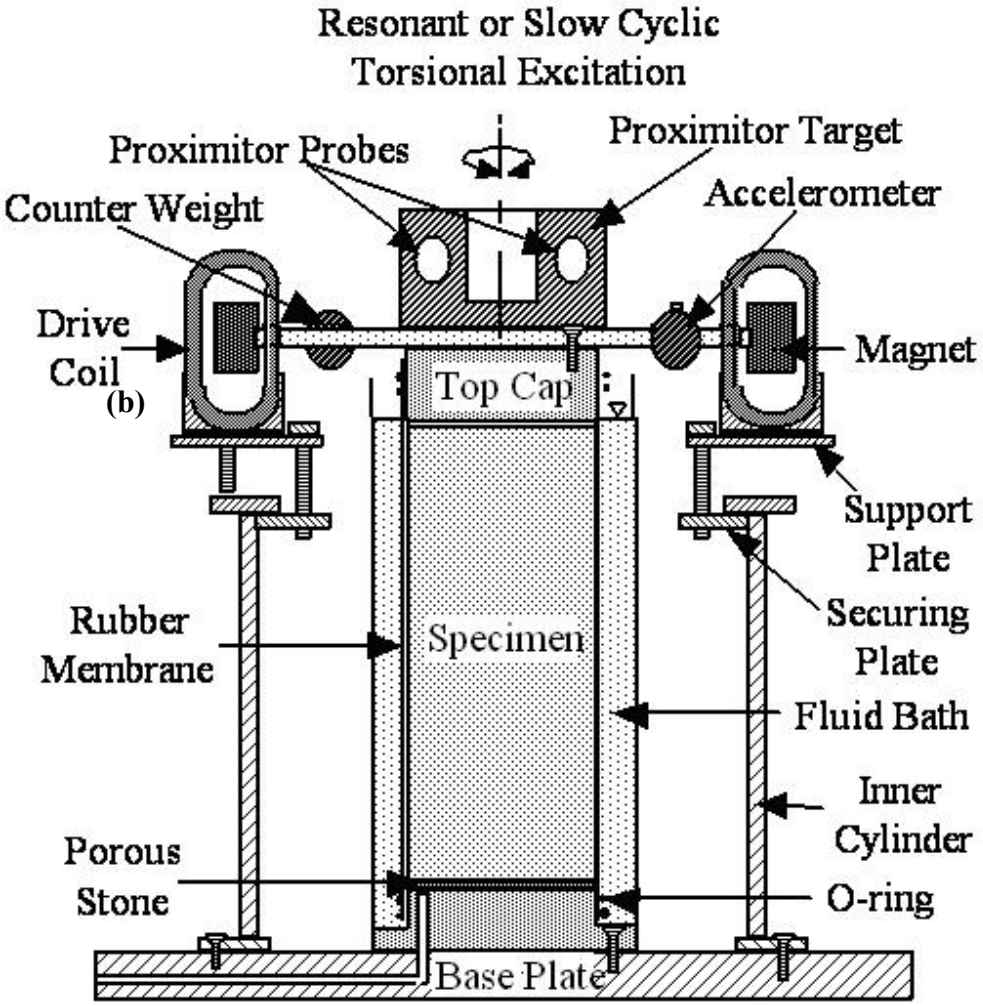

Figure 3.2 Illustration of Combined RCTS Testing Device without Confining Chamber (from Kim, 1991)

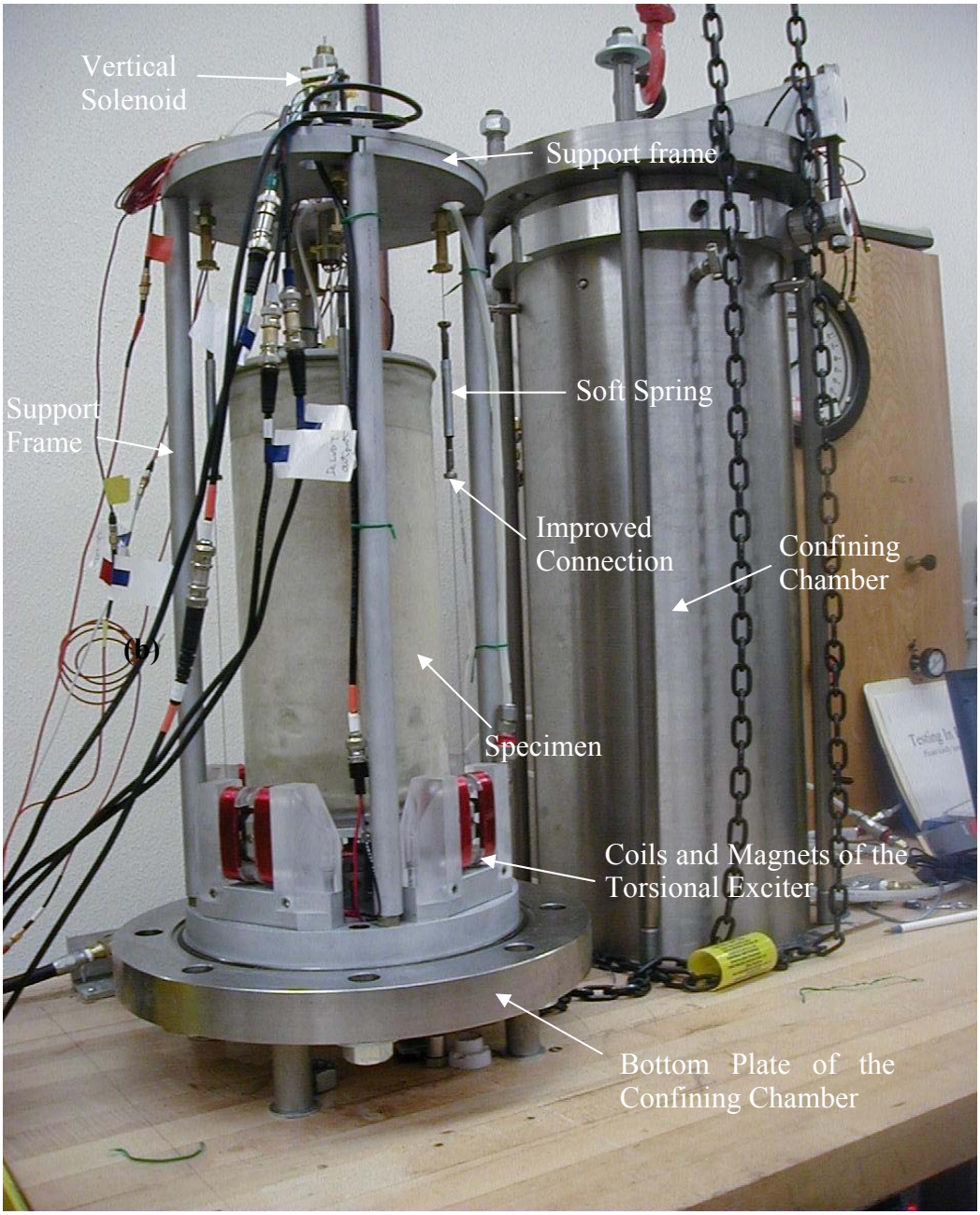

Figure 3.3 Photograph of General Configuration of LSRC Testing Device with Confining Chamber (from Menq, 2003)

respectively.

Detailed descriptions of the test equipment and theoretical backgrounds for both the RCTS and LSRC devices are discussed in the following sections.

3.2 OVERVIEW OF RCTS AND LSRC TEST EQUIPMENT AND PRINCIPLES OF OPERATION

3.2.1 History of RCTS Equipment at UT

The RCTS equipment is used at The University of Texas at Austin to measure the dynamic properties of various types of materials in the linear and nonlinear strain ranges. The original device was designed and constructed by Professor Stokoe in 1973-1974. Isenhower (1979) modified the original RC equipment to allow cyclic torsional shear (TS) to be applied. The device then became known as the combined RCTS device. The TS testing allowed the influence of excitation frequency and number of loading cycles on shear modulus and material damping ratio to be studied. Ni (1987) modified the equipment such that a true triaxial state of stress could be applied to a hollow specimen and introduced an automated computer system to perform the RCTS tests and data acquisition process. Kim (1991) improved the motion monitoring system to enhance the accuracy of measurements in the TS tests at small strain ranges (0.00001 % to 0.001 %) using micro-proximitors.

Hwang (1997) took system-generated damping into account to calculate true material damping values obtained either from the half-power bandwidth or free-vibration decay methods. He achieved true material damping values by linearly subtracting the system-generated damping from measured damping values. System-generated damping is referred to as a back-electromagnetic force (EMF) that is generated by the movement of magnets inside the drive coils.

3.2.2 History of Free-Free RC Equipment at UT

In the case of the free-free RC test device, Lewis (1990) evaluated three different moduli, i.e., M, E, and G of specimens under biaxial states of stress with a multi-moduli test device, or multi-mode test device. The biaxial states of stress were simulated as a result of the all-around cell pressure plus additional axial pressure with a double acting air piston. Vaghela (1995) measured the modulus and material damping of specimens that were positioned horizontally in a supporting frame. A vacuum pressure was applied to confine the specimens. Weston (1996) performed similar tests to measure the dynamic properties of specimens that were vertically oriented in a supporting frame. Menq (2003) developed that a new multi-mode device with a confining chamber and an internal torsional motor. He used this equipment to measure measure different moduli (M, E, and G) and material damping of specimens oriented vertically, as shown in Figure 3.3, with respect to longitudinal and torsional directions. Menq's device was the first production-level MMD device for laboratory testing of all of these devices. The device was renamed to the free-free large-scale resonant column (LSRC) device.

3.2.3 Basic Operational Testing at Resonance

The operational principle of RC testing is to vibrate a cylindrical specimen at its first-mode resonance. The reason for dynamic measurements at first-mode resonance is that it is much easier to obtain the first-mode shape and the most motion occurs in the first-mode. In addition, first-mode is the least complex deformational shape which permits equivalent strains (either shearing strain in torsion motion or longitudinal strain in axial motion) to be calculated.

Both solid and hollow specimens have been employed in the RCTS tests. Typically, the hollow specimens have been used to reduce the nonlinear effect even

though they have difficulties in the handling and trimming processes. It needs to be noted that the operational principle of fixed-free and free-free RC testing is identical. Only the boundary conditions are different between the two configurations. Therefore, the operational principle explained below uses fixed-free RC configuration in the example.

As illustrated in Figure 3.2, the specimen is placed on a fixed base pedestal with a free top cap. To increase the bonding between the specimen and top cap and base pedestal, the pedestal and top cap are machined with a rough surface. The base pedestal is fixed into the base plate to replicate a fixed boundary condition. The drive plate is tightened firmly with screws to the top cap. Constant amplitude of sinusoidal motion is supplied to the top of the specimen, generating torsional excitation in the specimen. By varying the excitation frequencies from high to low, the first-mode resonant frequency of the specimen is found. The first-mode frequency is identified as the highest accelerometer output in the frequency response curve.

Once the first-mode resonant frequency is determined, the shear modulus is computed in accordance with one-dimensional wave propagation. Material damping is evaluated either by the half-power bandwidth or free-vibration decay method.

Another testing technique to determine the shear modulus and material damping is the cyclic TS test. The cyclic TS test is different from the RC test in a sense that the excitation frequency is lower than the frequencies being used in RC test, generally below 5 Hertz (Hz). Cyclic properties in TS test are calculated from the hysteresis loop, which is caused by the time delay between excitation shear stress and induced shear strain. The shear modulus is the slope of the line passing through the end points of the hysteresis loop. Material damping is determined from the area of the hysteresis loop. The theoretical background for both the RC and TS tests is discussed below.

3.3 THEORETICAL FRAMEWORK OF THE RCTS TESTING TECHNIQUE

3.3.1 Fixed-Free Resonant Column (RC) Test

A one-dimensional wave propagation equation based on the theory of elasticity is the theoretical background of the fixed-free resonant column test. As recognized by its name, the specimen is fixed at the bottom and left free at the other end with an added mass (e.g., drive plate, accelerometer, top cap, and O-rings). With the constants of the system, dimensions, and weight of the specimen, the shear modulus is calculated from the first-mode resonant frequency. Material damping is measured either by the half-power bandwidth or free-vibration decay method. Detailed explanations on these measurements are discussed below.

3.3.1.1 Shear Modulus

The governing equation for resonant column test with fixed-free boundary conditions is expressed as follows:

$$\frac{\sum I}{I_o} = \frac{\omega_n \times \ell}{V_s} \times \tan\left(\frac{\omega_n \times \ell}{V_s}\right) \tag{3.1}$$

where, $\Sigma I = I_s + I_m$

I_s = mass moment of inertia of soil ($\frac{1}{2} m r_o^2$ for solid circular specimen),

I_m = mass moment of inertia of membrane ($\frac{1}{2} m(r_o^2 - r_i^2)$) for hollow circular specimen),

r_o = outside radius of solid or hollow specimen,

r_i = inside radius of a hollow specimen,

I_o = mass moment of inertia of end mass (top cap and drive plate),

ℓ = length of specimen,

V_s = shear wave velocity of specimen, and

ω_n = undamped natural circular frequency of system ($2\pi f_n$).

The value of I_o is obtained by calibration of the drive plate (see Hwang, 1997 for details) and dimensions of the top cap. In the same manner, the value of ΣI is acquired from the dimensions, weight of the specimen, membrane, and O-rings. After the first-mode resonant frequency is determined, the shear wave velocity is computed using Equation (3.1), by assuming that the resonant frequency, f_r, is equal to the natural frequency, f_n. The f_r is, however, not identical to the f_n with the exception of a theoretical system with zero damping. The f_r is related to f_n by:

$$f_r = f_n \times \sqrt{1 - 2D^2} \tag{3.2}$$

where, D = material damping of the system.

An examination of Equation (3.2) reveals that it is an equation of circle for the normalized frequency, f_r/f_n, versus material damping ratio with a radius of unity. The equation is depicted in Figure 3.4. As indicated in Figure 3.4, a typical material damping ratio in the small strains determined by the resonant column tests in this research was less than 6 percent (%) and the material damping ratio at larger strains was less than 10%. In addition, material damping ratio determined by RC tests at the highest shearing strain was about 18%. As a result, the maximum difference between f_r and f_n was about on the order of 3%. This difference is small and was ignored. Therefore, the quantities were considered equal throughout this work.

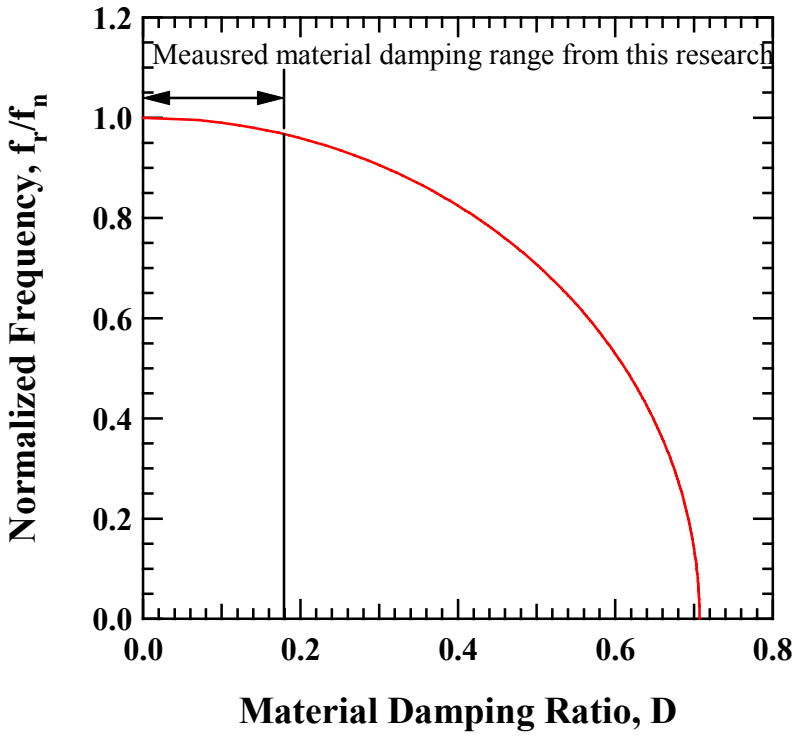

Figure 3.4 Variation of f_r/f_n with Material Damping Ratio, D

The shear wave velocity is determined by trial and error using Equation (3.1). The shear modulus is then computed from:

$$G = \rho \times V_S^2 = \frac{\gamma_t}{g} \times V_S^2 \tag{3.3}$$

where,

ρ = mass density of specimen,

γ_t = total unit weight of specimen, and

g = acceleration of gravity (32.2 ft/sec^2).

3.3.1.2 Shearing Strain

The shearing strain induced in the specimen during the resonant column test is presented in Figure 3.5. Inspection of Figure 3.5 shows that, with the added mass on the top, the distribution of deformation can be approximated to be linear along the length of the specimen, producing maximum deformation at the top and zero deformation at the fixed bottom (Drnevich et al., 1967). This deformation pattern along the length of the specimen at a given radial distance results in the shearing strain being approximately constant in longitudinal direction. The shearing strain, however, does vary linearly along the radial direction in the specimen, with zero shearing strain at the center of the specimen and maximum shearing strain at the edge of the specimen.

It is interesting to note that the distribution of the deformation of the specimen throughout the height without the mass added on top of specimen is curved, i.e., a quarter sine wave. Therefore, shearing strain also varies longitudinally for a fixed-free specimen with no mass added on top. The presence of the added mass makes the distribution of deformation along the specimen nearly linear because the mass lowers the resonant frequency and increases the wavelength, resulting in uniform shearing strain throughout the length of specimen (Ishihara, 1996).

Under this circumstance, the equivalent shearing strain, γ_{eq}, adopted throughout the research is given by:

$$\gamma_{eq} = \frac{r_{eq} \times \theta_{max}}{\ell} \tag{3.4}$$

where,

r_{eq} = equivalent radius,

θ_{max} = maximum rotation of specimen at the top, and

ℓ = length of specimen.

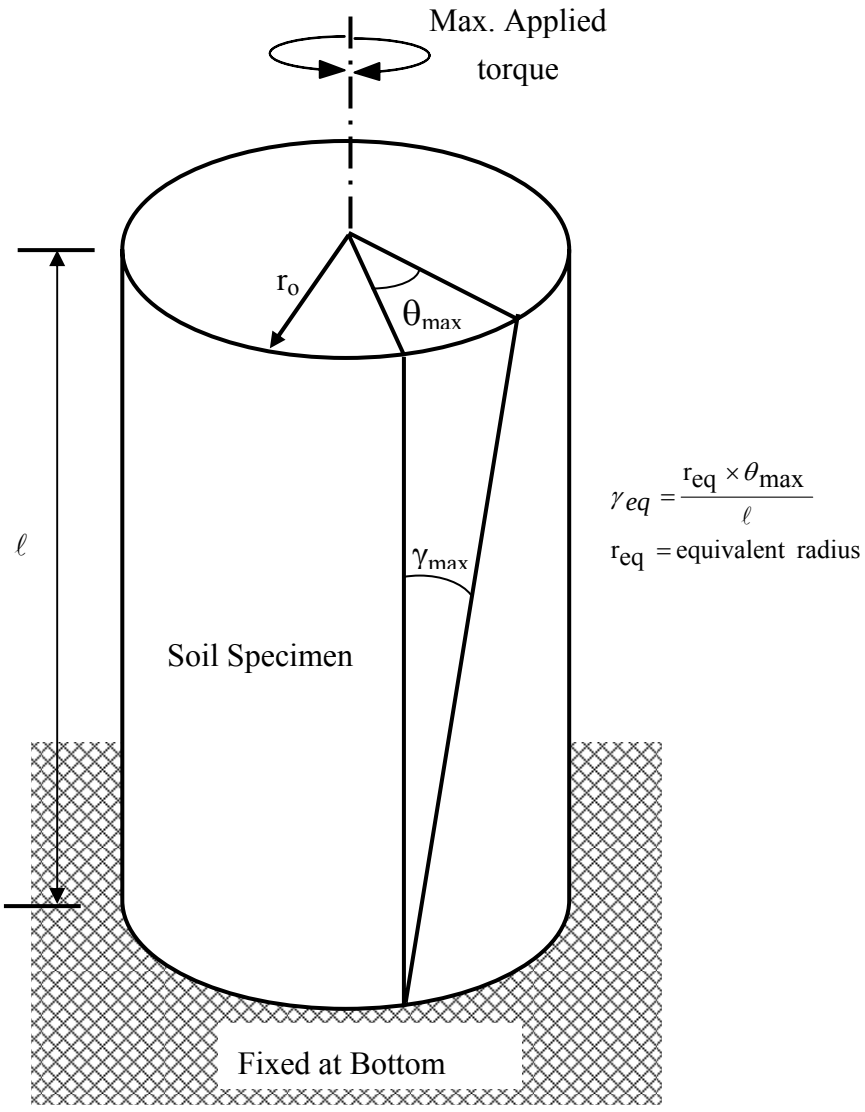

Figure 3.5 Simplified Drawing of Distribution of Deformation Induced in a Specimen during the Resonant Column Test (after Hwang, 1997)

Chen and Stokoe (1979) performed an analytical study of the radial distribution of shearing strain in a RC specimen to find an equivalent radius, r_{eq}, for the purpose of computing the equivalent shearing strain, γ_{eq}. They found that the value of r_{eq} varies

from $0.82 \times r_o$ at a peak shearing strain below 0.001% to $0.79 \times r_o$ at a peak shearing strain of 0.1% for a solid specimen. In the case of a hollow specimen (that is sometimes constructed to minimize the variation of shearing strain across the radius), they recommend using the average value of the inside and outside radii for r_{eq}.

In performing the RC test, the resonant period (T_r, seconds) and output voltage of the accelerometer (V_a, volts (RMS)) at resonance are measured. A measurement of accelerations is preferred in that it is easier to measure than displacements. Then, the output voltage from the accelerometer is transformed into the displacement by the accelerometer calibration factor (F_{ac}, volts (RMS)/in/sec^2). The displacement is divided by the distance (r_{ac}, inches) from the center of specimen to the location of accelerometer mounted on one of the arms of drive plate to compute the maximum rotation of specimen at the top (the value of r_{ac} is 2 in. (5.1 cm) in the UT RCTS equipment). As a result, the shearing strain is calculated by:

$$\gamma = r_{eq} \times \frac{V_a \times T_r^2}{4\pi^2 \times F_{ac}} \times \frac{1}{r_{ac}} \times \frac{1}{\ell} \tag{3.5}$$

3.3.1.3 Half-Power Bandwidth Method

One of the evaluations of material damping in the RC test is the use of the relative width of the frequency response curve around resonance by assuming the soil-equipment system is a linear single-degree-of-freedom system (Richart et al., 1970). A constant amplitude of the peak steady-state force (torque in this case) with different frequencies is provided from high to low frequencies. A function generator is used in this process to create a downgrade sweep. Resonance of a specimen is determined from this sweep. As a consequence, a frequency response curve is measured. This response curve is a plot of excitation frequency against the acceleration output. The frequency-acceleration

response curve is transformed into the frequency-displacement response curve by implementation of double integration. A typical frequency response curve from the half-power damping measurement is illustrated in Figure 3.6. An example of calculation of material damping ratio is shown in Figure 3.6. The half-power points in Figure 3.5 correspond to a -3 decibel (dB) drop from the peak point on a dB scale. For this reason, it is also called the 3-dB method. Using the quantities on the curve, the logarithmic decrement, δ, can be calculated from (Richart et al, 1970):

$$\delta = \frac{\pi}{2} \times \frac{f_2^2 - f_1^2}{f_r^2} \times \sqrt{\frac{A^2}{A_{max}^2 - A^2}} \times \sqrt{\frac{1 - 2D^2}{1 - D^2}} \tag{3.6}$$

where,

f_1 = frequency below the resonance where the strain amplitude is A,

f_2 = frequency above the resonance where the strain amplitude is A,

f_r = resonant frequency, and

D = material damping ratio.

Equation (3.6) contains the material damping ratio in the numerator and denominator, which should be solved by trial and error. If the material damping ratio is small (less than 20%), the last square root term can be approximated as equal to 1.0 and A chosen equal to $0.707A_{max}$, which is called the half-power point. Equation (3.6) can be rearranged as follows:

$$\delta \cong \pi \times \frac{f_2 - f_1}{f_r} \tag{3.7}$$

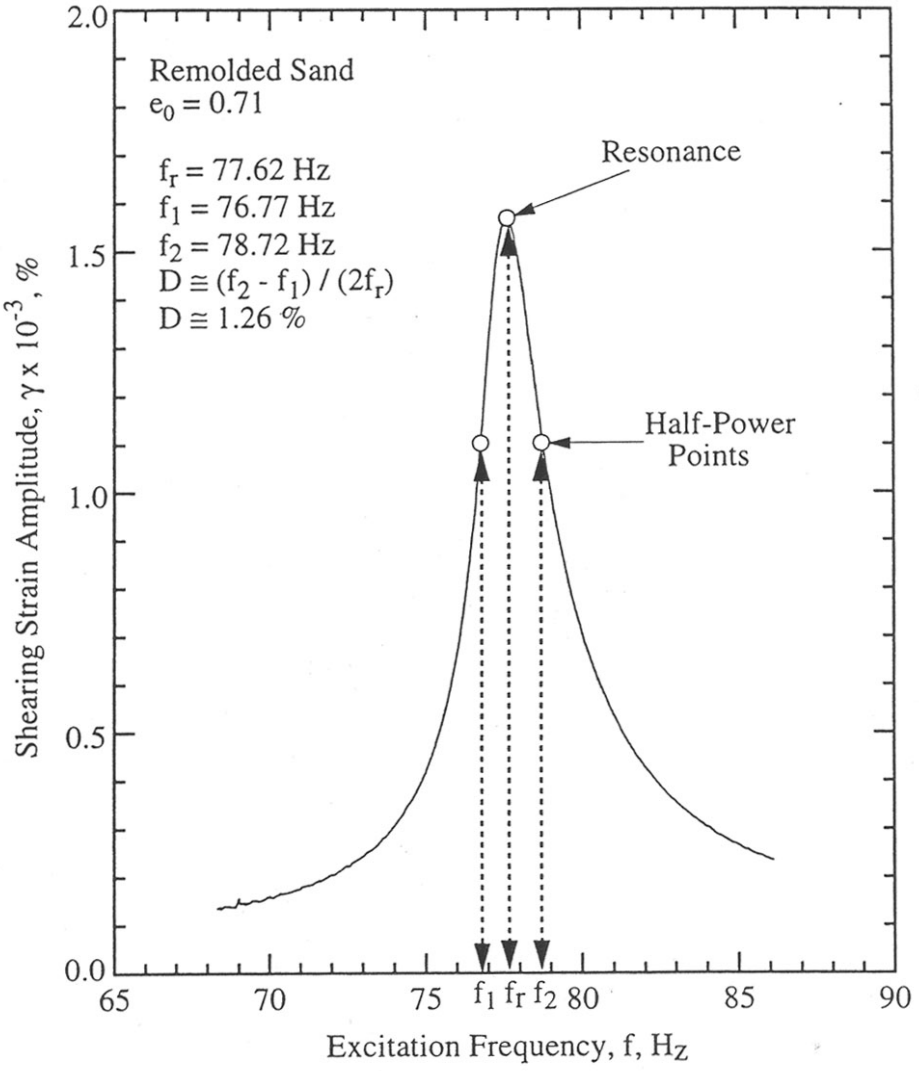

Figure 3.6 Typical Illustration for the Material Damping Measurements using Half-Power Bandwidth Method (from Hwang, 1997)

Consequently, the material damping ratio can be written as:

$$D \cong \frac{f_2 - f_1}{2f_r} \tag{3.8}$$

Compared with the free-vibration decay method, which is much more sensitive to background noise when measuring damping ratios at strains less than 0.001%, the half-power bandwidth method is able to measure material damping with relatively less influence from background noise. The reason is that, in the half-power bandwidth method, each data point on the frequency response curve is an average of approximately 10 cycles of excitation, but the free-vibration decay method uses the peaks determined with only one free-vibration test (Menq, 2003). Therefore, the half-power bandwidth method is more robust and considered to be a good method of measuring the material damping ratio at strains less than 0.001%. On the other hand, at larger strains, the shape of the response curve is distorted by even small nonlinearities such that a serious error can be introduced when measuring material damping from half-power bandwidth method (Ni, 1987).

Another problem caused by the non-symmetrical shape of the frequency response curve is obtaining different resonant frequencies from the downgrade and upgrade sweep processes. This problem can be introduced in the nonlinear strain ranges. Figure 3.7 shows a typical example of frequency response curves from the RC tests. As indicated in Figure 3.7, the resonant frequency from the upgrade sweep process is slightly larger than that obtained from the downgrade sweep process. It may seem reasonable to take an average of the resonant frequencies for the computation of shear wave velocity and shear modulus. However, in the case of softening material in the nonlinear strain range, a selection of resonant frequency from downgrade sweep process is more sensible

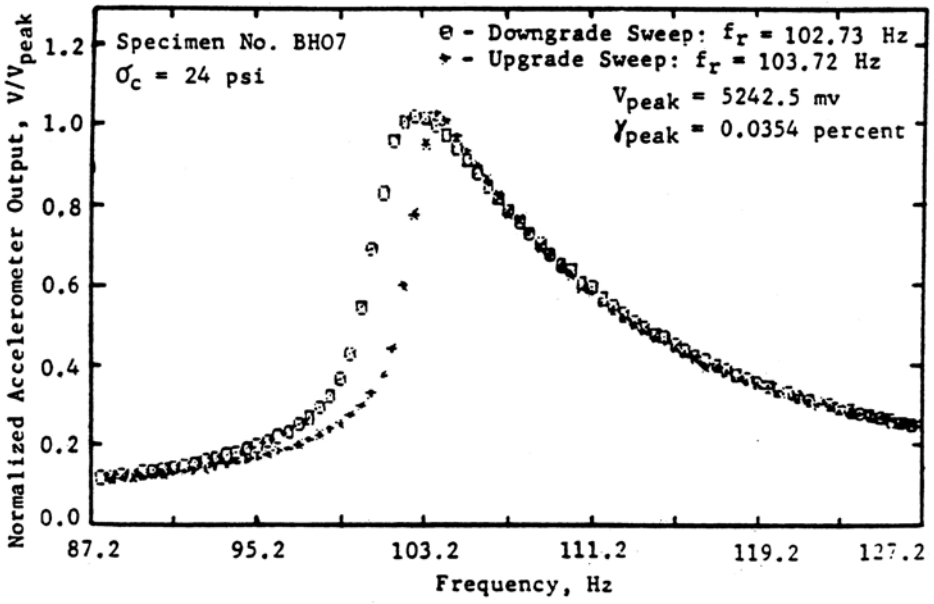

Figure 3.7 Comparison of the Frequency Response Curves Obtained from Downgrade and Upgrade Sweep Processes (from Ni, 1987)

than using the upgrade sweep process because the resonant frequency theoretically can "jump" to the higher resonant frequency due to high nonlinearity of softening material around resonance (Ni, 1987).

3.3.1.4 Free-Vibration Decay Method

Another way for measuring the material damping is the free-vibration decay method. After determining the resonant frequency, the specimen is excited with steady-state vibration at the resonant frequency for a few seconds. The current being supplied to the drive coils is then shut off, and the specimen is allowed to vibrate freely. The amplitude of vibration decreases, producing the free-vibration decay curve. The free-vibration decay curve displayed on the oscilloscope screen is transferred to the computer to calculate the damping ratio. A typical free-vibration decay curve is shown in Figure 3.8. As seen in Figure 3.8, the amplitude of vibration after steady-state vibration

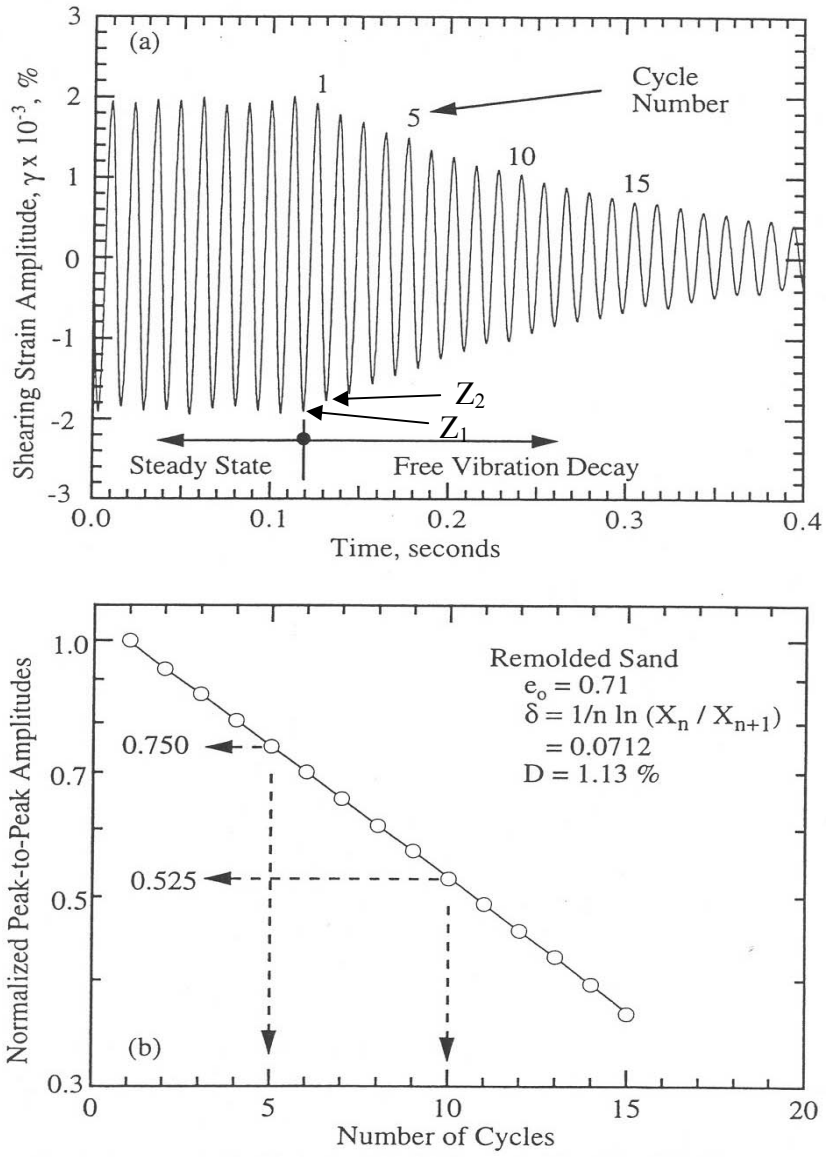

Figure 3.8 General Configuration of (a) Free-Vibration Decay Curve and (b) Example of Computation of Damping Ratio (from Hwang, 1997)

decreases with time. The ratio of the natural logarithm of two successive peaks of motion is referred to as logarithmic decrement, δ. The δ is expressed as:

$$\delta = \ln\left(\frac{Z_1}{Z_2}\right) = \frac{2\pi D}{\sqrt{1 - D^2}} \tag{3.9}$$

where,

Z_1 and Z_2 = two successive peak amplitudes, and

D = material damping ratio.

The material damping ratio is then computed by rearranging the Equation (3.9) and is given by:

$$D = \sqrt{\frac{\delta^2}{4\pi^2 + \delta^2}} \tag{3.10}$$

It is worth noting that the amplitude of free-vibration decreases, resulting in strain amplitudes decrease during the free-vibration decay as shown in Figure 3.8(a). It is difficult to tell which strain amplitude is a representative strain for the free-vibration damping measurements when computing the material damping ratio by Equation (3.10). It is evident, however, that the strain amplitude in the free-vibration state is less than during steady-state vibration. As an alternative, the representative strain amplitude is taken as an average of the first three cycles of free-vibration decay throughout this research.

It is also important to note that the free-vibration decay method is more correctly applied in the nonlinear strain range than the half-power bandwidth method. The primary assumption in the free-vibration decay method is the constant value of material damping ratio during the first three cycles. The measured material damping ratio at larger shearing strains (typically above 0.002%) was always determined with the free-vibration decay method.

3.3.2 Torsional Shear (TS) Test

The shear modulus and material damping can also be measured having the TS test in the same RCTS device. The primary difference between the RC and TS tests are the excitation frequency. Usually, the TS test uses excitation frequencies less than 5 Hz while the RC test uses excitation frequencies of about 20 to 300 Hz. Low-frequency measurements have an advantage because the hysteresis loop, which is a plot of applied shear stress versus induced shear strain, can be measured. Another benefit of the TS test is that the frequency of cyclic loading and the number of loading cycles are more similar to the seismic loading such as earthquakes.

Detailed descriptions of the shear modulus and material damping measurements in the TS test are discussed below.

3.3.2.1 Shear Modulus and Shearing Strain

The shear modulus is determined from the slope of a line passing through the end points of the hysteresis loop as shown in Figure 3.9. The hysteresis loop is made by plotting shearing stress and shearing strain. Therefore, it is necessary to study the shearing stress and shearing strain produced under the torsional motion. The formulas developed below are based on elasticity theory for circular bars of linearly elastic materials (Gere, 2001). The derivation of shearing stress and shearing strain is provided below.

Shearing Stress

Assuming pure torque, T, is applied to the top of specimen, T is obtained by integrating the incremental area at a given distance, r, over the entire area, which is expressed as:

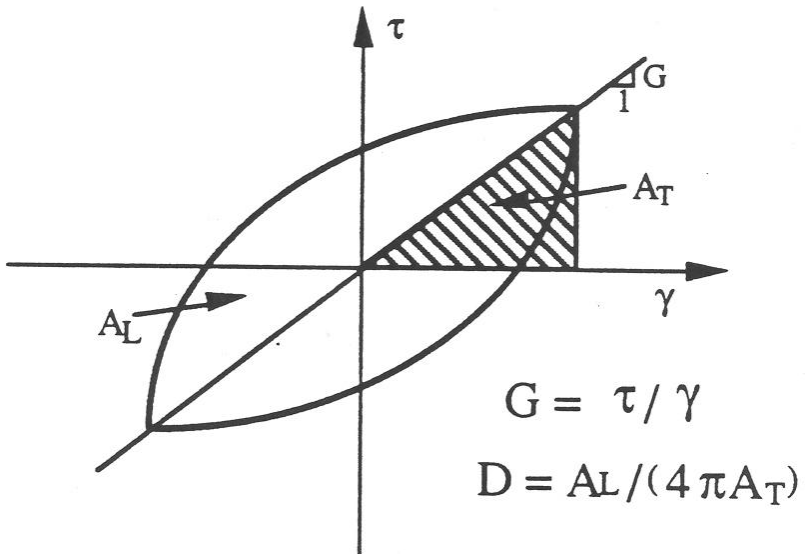

Figure 3.9 Illustration of measurements of Shear Modulus and Material Damping Ratio from Hysteresis Loop (from Kim, 1991)

$$T = \int_{r_i}^{r_o} \tau_r \, (2\pi r) \, r \, dr \tag{3.11}$$

where,

τ_r = shearing stress at a distance r from the center of the specimen, and

r_o and r_i = outside and inside radii, respectively.

However, shearing stress varies linearly from zero at the center to a maximum at the edge of the specimen. Using this relationship, shearing stress at an arbitrary location along the radius can be given by:

$$\tau_r = \tau_{max} \times \frac{r}{r_o} \tag{3.12}$$

where, τ_{max} = maximum shearing stress at $r = r_o$.

By substituting Equation (3.12) into Equation (3.11), the resulting equation for T is:

$$\begin{aligned} T &= \frac{\tau_{max}}{r_o} \times \frac{\pi}{2} \times (r_o^4 - r_i^4) \\ &= \frac{\tau_{max}}{r_o} \times J_P \end{aligned} \tag{3.13}$$

where, J_p = polar moment of inertia ($\frac{1}{2}\pi r^4$ for solid circular specimen).

By rearranging Equation (3.13), the maximum shearing stress is given by:

$$\tau_{max} = r_o \times \frac{T}{J_P} \tag{3.14}$$

As mentioned above, the shearing stress over the area is a linear function of the radius. Thus, the average shearing stress over the radius needs to be defined for use in plotting the hysteresis loop. The average shearing stress is then defined as:

$$\tau_{avg} = r_{eq} \times \frac{T}{J_P} \tag{3.15}$$

where, r_{eq} = equivalent radius.

The value of r_{eq} employs the same value as adopted in the RC test for the purpose of calculating shearing strain. Based on the formula developed above, the applied torsion at the top of specimen is calculated from the product of the input voltage, V_T (volts), and the torque calibration factor, K_T (torque/volts). Thus, the average shear stress, τ_{avg}, is:

$$\tau_{avg} = r_{eq} \times \frac{K_T}{J_P} \tag{3.16}$$

Shearing Strain

The procedure to calculate shearing strain in the TS test is identical to the procedure in the RC test. In the TS test, the displacement induced in the specimen is directly measured by using the low-frequency transducer, which is called a proximitor, such that the amount of rotation of the specimen at the top is easily obtained by the product of proximitor output voltage, V_P (volts), and calibration factor, K_P (rad/volt). The value of K_P is calibrated annually in the soil dynamics laboratory at the University of Texas at Austin (see Hwang (1997) for more detailed information about the calibration). As a result, the shearing strain, γ, is given by:

$$\gamma = r_{eq} \times \frac{K_P \times V_P}{\ell} \tag{3.17}$$

where,
r_{eq} = equivalent radius, and
ℓ = length of specimen.

3.3.2.2 Hysteretic Damping Ratio

Damping exists in all oscillatory materials or systems. Damping is defined as the energy dissipation of a material or system under cyclic loadings. For most soils, the material damping ratio exhibits frequency dependent behavior. However, at very small strains (less than 0.001%), damping in soil exhibits a frequency-independent characteristic in the limited frequency range of 0.1 Hz to 10 Hz (or even a smaller range, e.g., 0.5 to 2 Hz). In this range of frequencies, the material damping is regarded as a constant and this frequency-independent damping is called hysteretic or rate-independent damping (Shibuya et al., 1995, Rix et al., 2000). The result of cyclic loading yields a hysteresis loop as presented in Figure 3.9. Using the hysteresis loop, the material damping ratio can be obtained. The material damping ratio is defined as the ratio of the

total amount of energy dissipated during one cycle of sinusoidal loading, A_L, to the peak strain energy stored in the specimen during one loading cycle, A_T. The material damping ratio can be expressed as:

$$D = \frac{1}{4\pi} \times \frac{A_L}{A_T} \tag{3.18}$$

where,

A_L = area of hysteresis loop, and

A_T = area of triangle hatched area.

3.3.3 Free-Free Resonant Column (RC) Test

The theoretical background of the fr-fr RC test is explained by one-dimensional wave propagation based on the theory of elasticity. Unlike the fixed-free RC tests, both ends of the specimen in the free-free device are in the free boundary condition. In addition, both ends have added masses. Compared with the fixed-free RC test, one of the benefits of the free-free RC test is the capability of performing tests on larger diameter specimens (up to 6 in. in diameter using a 1-in. maximum particle size). The other advantage is that the point of fixidity in terms of zero displacement automatically occurs near the middle of the specimen. That is, the location of zero-displacement in the specimen, which is called the nodal point, occurs within the specimen and, for the case of a specimen with equal end masses, occurs mid-height of the specimen. On the other hand, the fixed-free RC test has a nodal point at the bottom of specimen so that the bottom of the specimen cannot be constrained to have zero displacement. As with the fixed-free RC test, given the constants of the system such as dimensions and weights of specimens, the shear modulus is calculated from the first-mode resonant frequency and material damping is measured by either the half-power bandwidth (at small strains) or

free-vibration decay (at larger strains) method.

Detailed explanations of the measurements of shear modulus and material damping ratio are given below.

3.3.3.1 Shear Modulus

The governing equation of the LSRC test with free-free boundary conditions is:

$$\tan\left(\frac{\omega_n \times \ell}{V_S}\right) = \frac{(R_1 + R_2) \times \frac{\omega_n \times \ell}{V_S}}{\left(R_1 \times R_2 \times \left(\frac{\omega_n \times \ell}{V_S}\right)^2 - 1\right)} \tag{3.19}$$

where,

$$R_1 = \frac{I_1}{I_S}, \tag{3.20}$$

$$R_2 = \frac{I_2}{I_S}, \tag{3.21}$$

I_1 = mass moment of inertia at one free end,

I_2 = mass moment of inertia at the other free end,

I_S = mass moment of inertia of the specimen ($\frac{1}{2} m r_o^2$ for solid circular specimen),

r_o = radius of the specimen,

ℓ = length of the specimen,

Vs = shear wave velocity of the specimen, and

ω_n = undamped natural circular frequency of system ($2\pi f_n$).

Looking inside Equation (3.19) reveals that if the value of either R_1 or R_2 approaches infinity (R_1 or $R_2 = \infty$), then the Equation (3.19) gives the same governing equation as a fixed-free RC test discussed in Section 3.3.1.1 (Weston, 1995).

The values of I_1 and I_2 are obtained easily from the calibration of the one end cap

plus drive plate and the other end cap, respectively (see Menq, 2003 for details in Appendix C). After the first-mode resonant frequency is determined from the frequency response curve, the shear wave velocity is computed from Equation (3.19) by assuming that the resonant frequency is equal to the natural frequency done in the fixed-free RC test.

After determining the shear wave velocity, the shear modulus is computed from:

$$G = \rho \times V_S^2 = \frac{\gamma_t}{g} \times V_S^2 \tag{3.22}$$

where,

ρ = mass density of specimen,

γ_t = total unit weight of specimen, and

g = acceleration of gravity (32.2 ft/sec^2).

3.3.3.2 Shearing Strain

The variation of displacement and shearing strain at the edge, γ_{edge}, along the length of a specimen that is excited in torsion is shown in Figure 3.10. The displacement, Z, at the edge with respect to sample height is given by:

$$Z = Z_O \times \cos\left(\frac{2\pi X}{\lambda}\right) \tag{3.23}$$

where, Z_o = displacement at the top of the top cap,

$$= \frac{Z_{top}}{\sin\left(\frac{\pi L}{\lambda}\right)} = Z_{acc} \times \frac{r_o}{r_{acc}} \times \frac{1}{\sin\left(\frac{\pi L}{\lambda}\right)}$$

Z_{top} = displacement on the boundary of specimen,

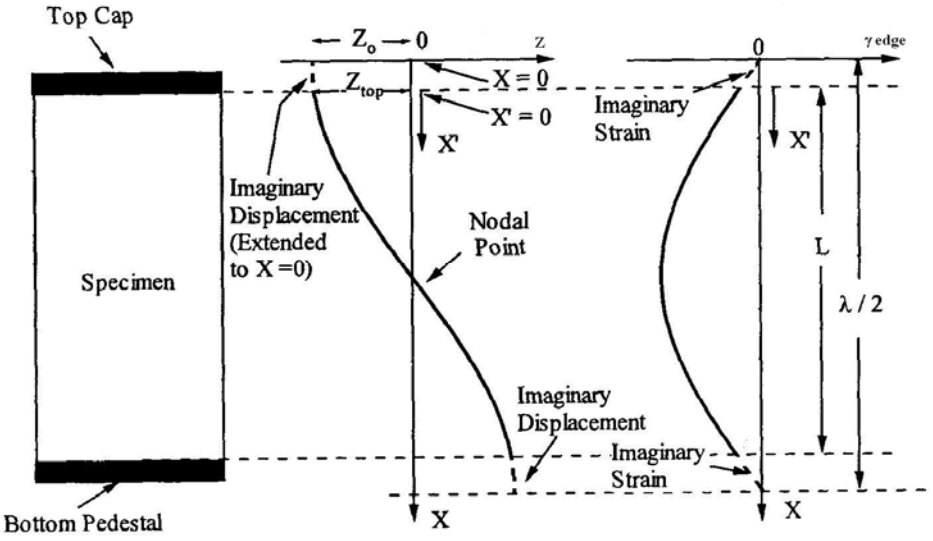

Figure 3.10 Distributions of Displacement and Shearing Strain along the Length of Specimen with End Caps (from Menq, 2003)

r_{acc} = radius to the mounted accelerometer,

r_o = radius of specimen,

Z_{acc} = displacement of accelerometer,

$$= \frac{1}{(2\pi f_r)^2} \times \frac{32.2 \times V_a}{F_{ac}}$$

f_r = resonant frequency,

V_a = accelerometer output,

F_{ac} = calibration factor for accelerometer,

λ = wavelength,

X = coordinate initiated from the top cap, and

L = specimen height.

The shearing strain induced at the edge of the specimen along the height is then defined by a derivative of Z with respect to X and yields:

$$\gamma = \frac{dZ}{dX} = -Z_O \frac{2\pi}{\lambda}\left[\sin(\frac{2\pi X}{\lambda})\right] \tag{3.24}$$

From Equation (3.24), the maximum shearing strain, γ_{max}, occurs at the mid-height of specimen (for the top and bottom caps having equal mass moments of inertia) and the corresponding absolute value is:

$$\gamma_{max} = Z_O \times \frac{2\pi}{\lambda} \tag{3.25}$$

As shown in Figure 3.10, the shearing strain varies longitudinally with a maximum shearing strain at the mid-height of the specimen and becomes zero at the top cap and bottom pedestal. A dashed line in the shearing strain distribution indicates an extended imaginary shearing strain induced by the top cap and bottom pedestal. In addition, the shearing strain also changes from zero at the center to maximum at the boundary of the specimen, r_o. For this reason, it is necessary to determine the equivalent shearing strain, γ_{eq}, which is calculated at the equivalent radius, r_{eq}, and the equivalent shearing strain is expressed as:

$$\gamma_{eq} = r_{eq} \times \gamma_{max} \tag{3.26}$$

where,

γ_{eq} = equivalent shearing strain,

r_{eq} = equivalent radius, and

γ_{max} = maximum shearing strain.

In a free-free RC test, the mass moment of inertia of top cap and bottom pedestal are smaller than that of testing specimen itself (e.g., the mass moments of inertia of top

cap and bottom pedestal and drive plate are equal to 0.001062 ft-lbs-sec^2 and 0.003795 ft-lbs-sec^2, respectively). Therefore, the correction of equivalent radius should be taken into account. Menq (2003) studied the determination of equivalent radius using a similar procedure suggested by Chen and Stokoe (1979) and provided an equivalent radius equal to $0.65 \times r_o$ (see Menq, 2003 for details in Appendix A).

By combining Equation (3.25) and Equation (3.26), the equivalent strain, γ_{eq}, is expressed as:

$$\gamma_{eq} = r_{eq} \times \frac{r_o}{r_{acc}} \times \frac{2\pi}{\lambda} \times \frac{1}{(2\pi f_r)^2} \times \frac{32.2 \times V_a}{F_{ac}} \times \frac{1}{\sin(\frac{\pi L}{\lambda})} \tag{3.27}$$

As a result, Equation (3.27) reduces to:

$$\gamma_{eq} = 79.5 \times \frac{V_a \times \beta}{f_r{}^2 \times F_{ac} \times L \times \sin(\frac{\beta}{2})} \tag{3.28}$$

where, $\beta = \frac{\omega_n \times L}{V_S} = \frac{2 \times \pi \times L}{\lambda}$

3.3.3.3 Half-Power Bandwidth Method

Like the RCTS test, the frequency response curve is generated by performing a downgrade sweep. A typical frequency response curve for a fresh waste material specimen in the LSRC test is presented in Figure 3.11. An example calculation of the half-power damping ratio is shown in the insert in the figure. It should be noted that system-generated damping in LSRC test can not be subtracted linearly from the measured damping value because the mass moment of inertia of the specimen is much larger than that of the added end masses (top cap and bottom pedestal). As an alternative, Menq

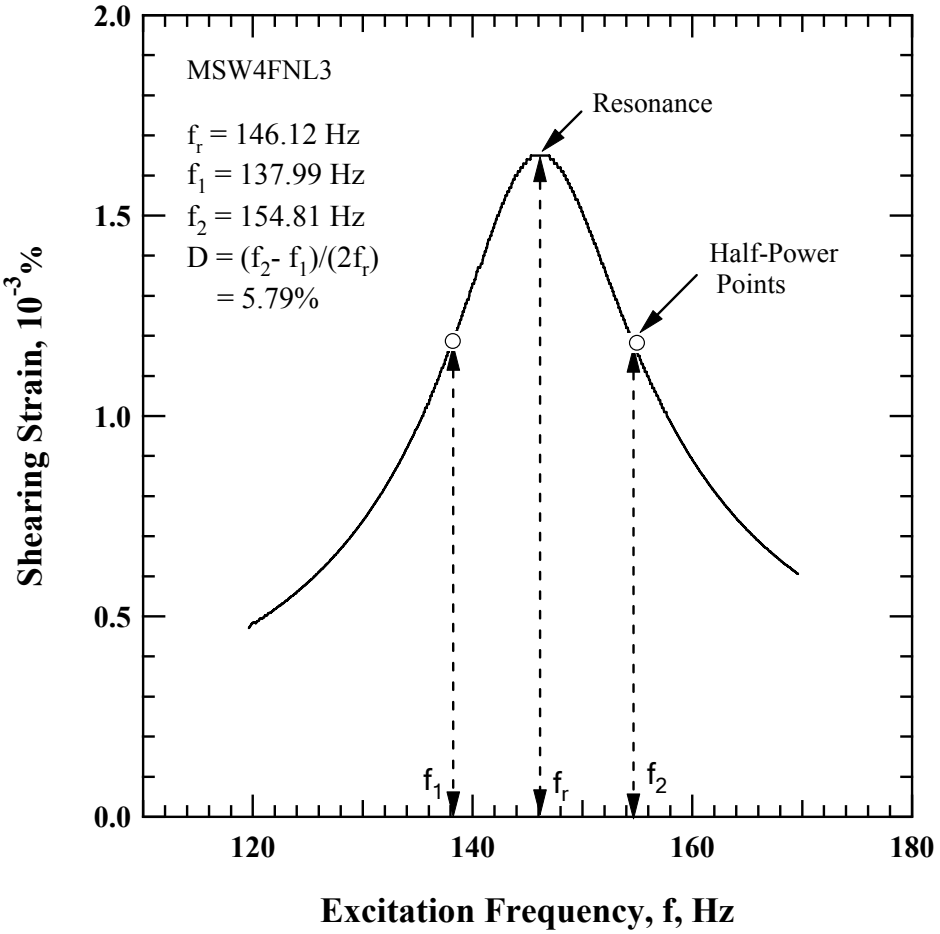

Figure 3.11 Typical Frequency Response Curve Obtained from a LSRC Test on a Fresh MSW Specimen

(2003) has investigated the method to compute the half-power damping ratio in the LSRC by changing the number of coils. He used an inter-chamber switch unit (ICS) to investigate this measurement (see Menq (2003) in Section 3.4 and Appendix B for more details).

3.3.3.4 Free-Vibration Decay Method

The free-vibration damping measurement in the LSRC test is somewhat different from this measurement in the fixed-free RC test for the following reason. The closed

pair of coils are opened simultaneously at the beginning of the free-vibration motion to eliminate system-generated damping produced by back electromagnetic force, commonly called back EMF. As a consequence, the specimen is allowed to vibrate freely, resulting in the elimination of system-generated damping (see Menq (2003) in Appendix B). As with the fixed-free RC test, the free-vibration decay curve is obtained as shown in Figure 3.8 and δ is computed with the amplitude of two successive peaks using Equation (3.9). Finally the material damping ratio is calculated using Equation (3.10).

It should be noted that the material damping ratio in the free-free RC test was obtained from a "best-fit" of the logarithmic decrement to the first three peaks with the assumption that material damping does not vary much within the first three cycles. The representative shearing strain corresponding to each free-vibration measurement was taken from the average of the first three cycles. Only the free-vibration damping ratios were used beyond the shearing strains of 0.01 % because of the fact that the half-power damping ratios were skewed due to nonlinearity in the MSW specimens.

3.4 ORGANIZATION OF FIXED-FREE RCTS TESTING EQUIPMENT

The fixed-free RCTS equipment was employed to measure the dynamic properties of MSW for small-diameter specimens (2.8-in. (71.1-mm) diameter) in this study. The RC tests were fully automated whereas the TS tests were semi-automated. The combined RCTS testing device used is composed of four specific functions as follows:

(1) Confinement System,

(2) Driving System,

(3) Height-Change Measurement System, and

(4) Motion Monitoring System.

3.4.1 Confinement System

The confinement system is composed of stainless hollow cylindrical chambers (thickness of 0.21 in. (5.3 mm)), circular or square cover plates (9.0-in by 9.0-in. (228.6-mm by 228.6-mm)), and four long connecting rods (20-in. long and 0.51-in. diameter (50.8-mm long and 12.9-mm in diameter)). A simplified illustration of the confinement system is presented in Figure 3.12. All confinement system components are made of stainless steel to eliminate the interaction with the RCTS device magnets. Rubber O-rings in the top and base plates are used to make sure that there is no air leakage between the confining chamber and those plates. The confining chamber has been designed to resist a maximum air pressure of 600 psi (4137 kPa). The sources of confinement on the specimens are supplied from either building pressure or industrial compressed nitrogen gas. The building pressure can provide up to 80 psi (552 kPa). The industrial compressed nitrogen gas is utilized for higher confining pressures to represent the condition of specimens at deeper depths.

The pneumatic pressure regulators (Fairchild Model 30) are used to control the air pressure from the building supply and to maintain a constant pressure at each testing stage. Another pneumatic pressure regulator (Tescom Model 44-2200) is used to control the industrial nitrogen gas at higher confining pressures.

After the specimen is placed onto the base pedestal with a surrounded rubber membrane sealed by O-rings and vacuum grease, a thin-wall cylinder is placed around the specimen. The vent line is connected to the bottom of the specimen, after passing through the base pedestal, is exposed to the atmosphere. Therefore, the RCTS testing represents a drained condition, but during torsional excitation with high frequencies, the undrained condition exists inside the specimen.

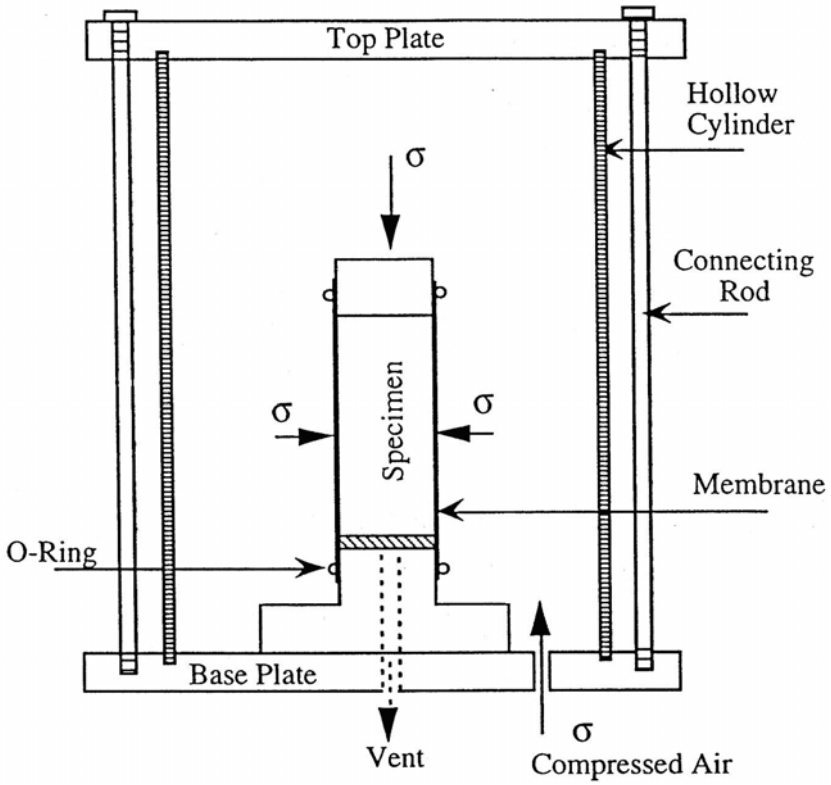

Figure 3.12 Cross-Sectional View of Confinement System with Specimen and Confining Chamber (after Kim, 1991)

3.4.2 Drive System

A coil-magnet drive system is used to vibrate the specimen in torsional motion at the top of specimen. The drive system consists of four pairs of closed loop coils and four rectangular permanent magnets (Alnico 8). These magnets are glued tightly to the end of the drive plate arm. The four pairs of closed loop coils are fixed to a support plate with drive-coil holders. There are two sets of four holes on the surface of drive plate to connect the top cap to the drive plate.

Torsional motion is generated on top of specimen by the interactive movement as a result of induced current when the alternating current passes through the coils.

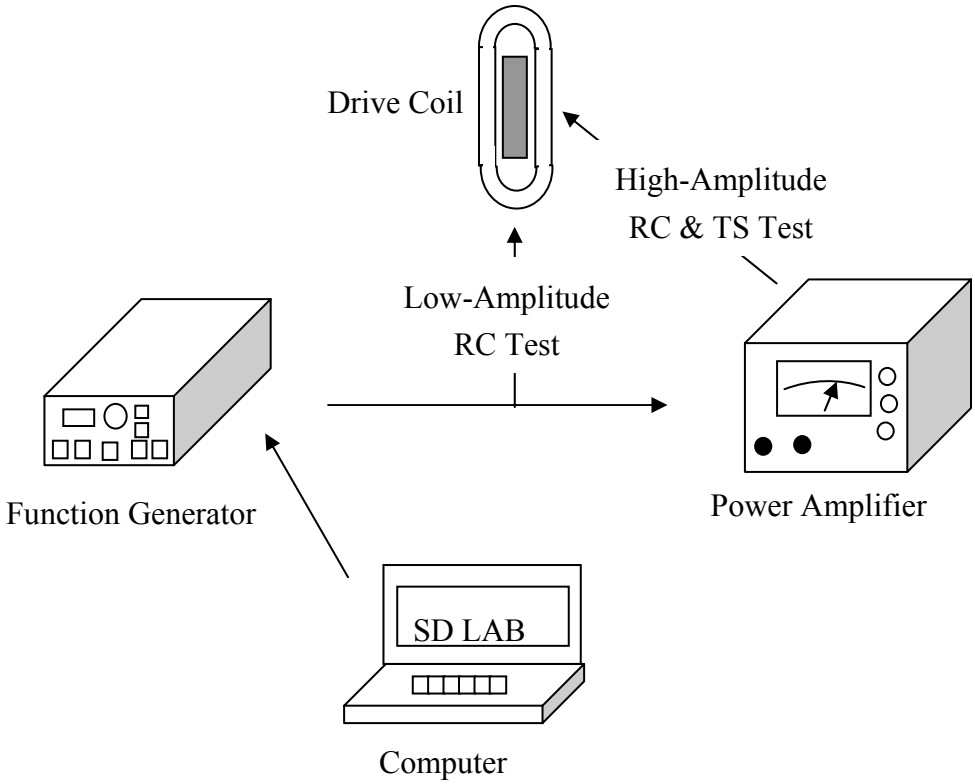

Figure 3.13 Simplified Configuration of Driving System in RCTS Tests (after Hwang, 1997)

The general configuration of driving system is illustrated in Figure 3.13. The arrows in the figure represent the flow of the operation. The power of the driving system is determined by the several factors: (1) strength of the permanent magnets, (2) number of coils, (3) number of winds in the coil, (4) diameter of wire in the coils, (5) capacity of the amplifier in terms of amperes, (6) gap between magnet and coil, and (7) arm length of drive plate from the center (after Hwang 1997). For high-amplitude RCTS tests, amplified excitation power is required to reach largest shearing strains, i.e., produce the most nonlinear behavior.

3.4.3 Height-Change Measurement System

A function generator (HP 3314A), a Linear Variable Differential Transducer (LVDT) (CRL Model SH-200-53R), and a digital multimeter (HP 3456A) comprise the height-change measurement system. The LVDT is used to measure the height change of the specimen during the entire test. A simplified configuration of the height-change measurement system is presented in Figure 3.14. As shown in Figure 3.14, the computer commands the Function Generator to send a signal with an amplitude of 4.77 root mean square (RMS) volts and frequency of 500 Hz to the LVDT. Then, the output from the LVDT is read by the multimeter and this value is transferred to the computer.

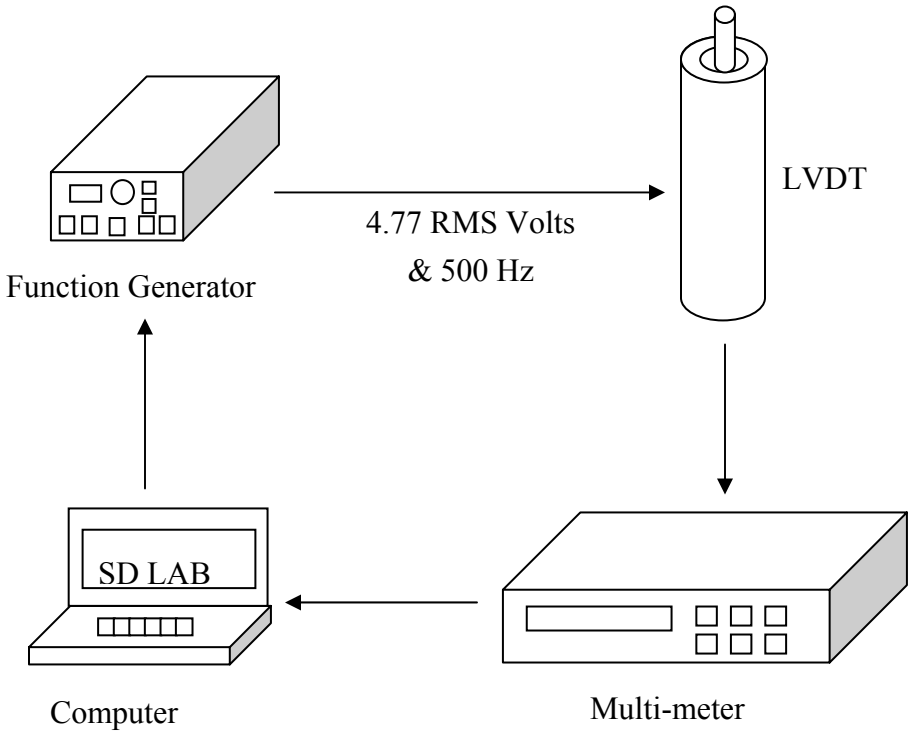

Figure 3.14 Simplified Configuration of Height-Change Measurement System in RC Tests (after Hwang, 1997)

The LVDT housing is connected to the supporting post and the core of the LVDT is secured in the middle of the U-shaped target. The core of the LVDT is not touched by the LVDT housing which allows the specimen to settle freely during tests. The LVDT reading is used to calculate the length of the specimen, estimate the diameter, and hence estimate the volume, and total density. It should be noted that the LVDT has an impact on computation of mass moment of inertia and total unit weight of the specimen which is directly associated with computation of shear wave velocity and shear modulus. Therefore, the LVDT readings are very important.

3.4.4 Motion Monitoring System

The primary difference between RC and TS tests is in their excitation frequency range. For this reason, different types of motion monitoring systems are required to measure the shear modulus and material damping ratio. Hence the RC tests use an accelerometer to monitor the acceleration response of specimen at high frequencies (above 20 Hz) while a low frequency transducer, called a proximitor, is used in TS tests to allow calculation a cyclic stress-strain response loop of the specimen in the low-frequency range (generally below 5 Hz).

3.4.4.1 Resonant Column (RC) Test

The purpose of the motion monitoring system in the RC test is to obtain the resonant frequency, the other two frequencies corresponding to the half-power points, shearing strain, free-vibration decay curve, and the shearing strain. This system is composed of an accelerometer (Columbia Research Lab. Model 3021), a charge amplifier (Columbia Research Lab. Model 4102M), a frequency counter (HP 5334A), a digital multimeter (HP 3458A), and a digital oscilloscope (Nicolet 2090-III). A simplified diagram of this system is shown in Figure 3.15.

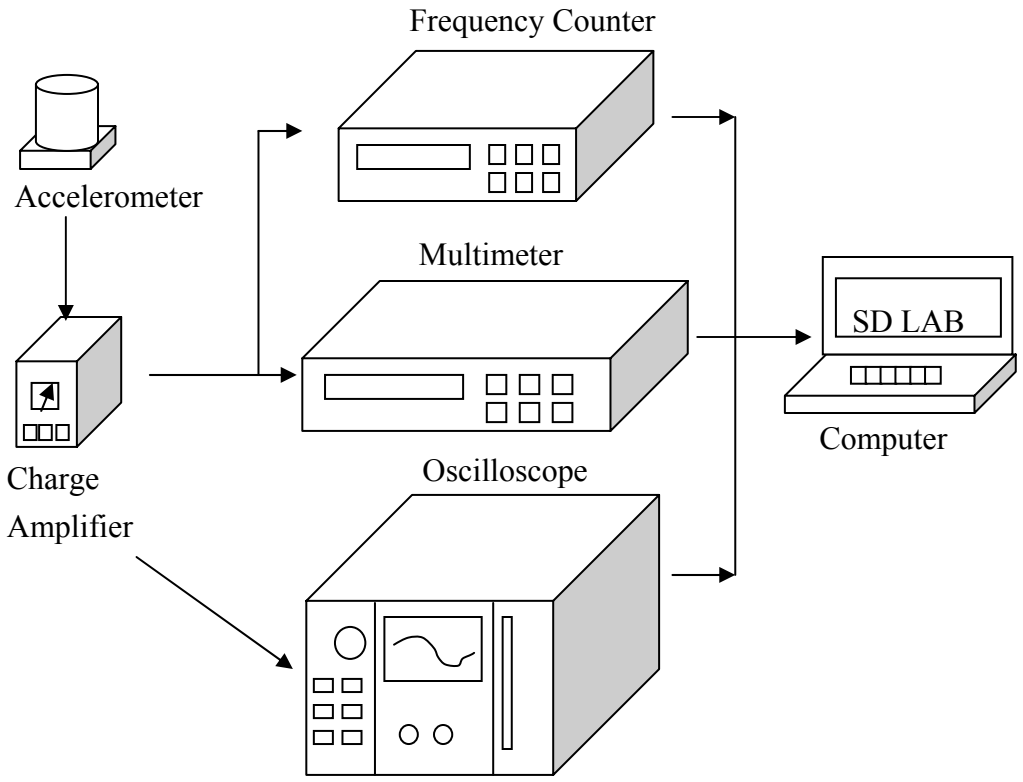

Figure 3.15 Simplified Configuration of Motion Monitoring System in RC Tests (after Hwang, 1997)

As illustrated in Figure 3.15, the dynamic response of specimen is captured by the accelerometer. The accelerometer mounted on one side of a drive plate arm (see Figure 3.2) is oriented to be sensitive to horizontal (torsional) motion. A counter weight is also attached in the opposite point on the drive plate to maintain the balance of the drive plate during torsional excitation. The charge amplifier is placed between the accelerometer and oscilloscope in order to acquire better signals. The output voltage of the accelerometer is read by the digital multimeter and the sweeping of frequencies are counted by using the period measurement in the frequency counter. The trace of accelerometer output versus frequency is referred to as the frequency response curve and the resonant frequency is selected after sweeping the swept frequencies by finding the

peak amplitude of the output voltage. Once the resonant frequency is determined, the specimen is vibrated with this frequency for a few seconds in steady state motion after which it is allowed to vibrate freely. The free-vibration decay curve is recorded by the digital oscilloscope and transferred to the computer.

3.4.4.2 Torsional Shear Test

The objective of the motion monitoring system in the TS test is to obtain the shearing strain in the hysteresis loop of specimen subjected to cyclic loading. The system consists of two proximitors (Bently Neveda M 20929-01), two proximitor probes (Bently Neveda M 300-00), an operational amplifier (Tektronix TM 504 with AM501), a DC power supply (Lambda M-11-902), a DC shifter (custom made in UT), a U-shape target, and a digital oscilloscope (Nicolet 2090-III). A schematic diagram of the motion monitoring system in the TS test is shown in Figure 3.16.

The purpose of the proximitor probes is to measure the air gap between U-shape target and tip of the proximitor probes. The signals from the two probes passed through the DC shifter and are sent to the operational amplifier so that the signals are combined together by subtracting one from the other. In dong so, any tilting of the specimen caused by forward or backward movements from the proximitor probes can be eliminated. The low-pass filter, as the name implies, eliminates the high-frequency noise and allows the specified low-pass frequencies (less than 5 Hz for TS tests at 0.5 Hz) be recorded. Defining the measurement of torque as a product of input voltage and torque calibration factor of the drive plate and the measurement of displacement as a product of output from the proximitor and proximitor constant of the drive plate, the torque-displacement hysteresis loop is obtained. Additional information is given in Hwang's dissertation (Hwang, 1997).

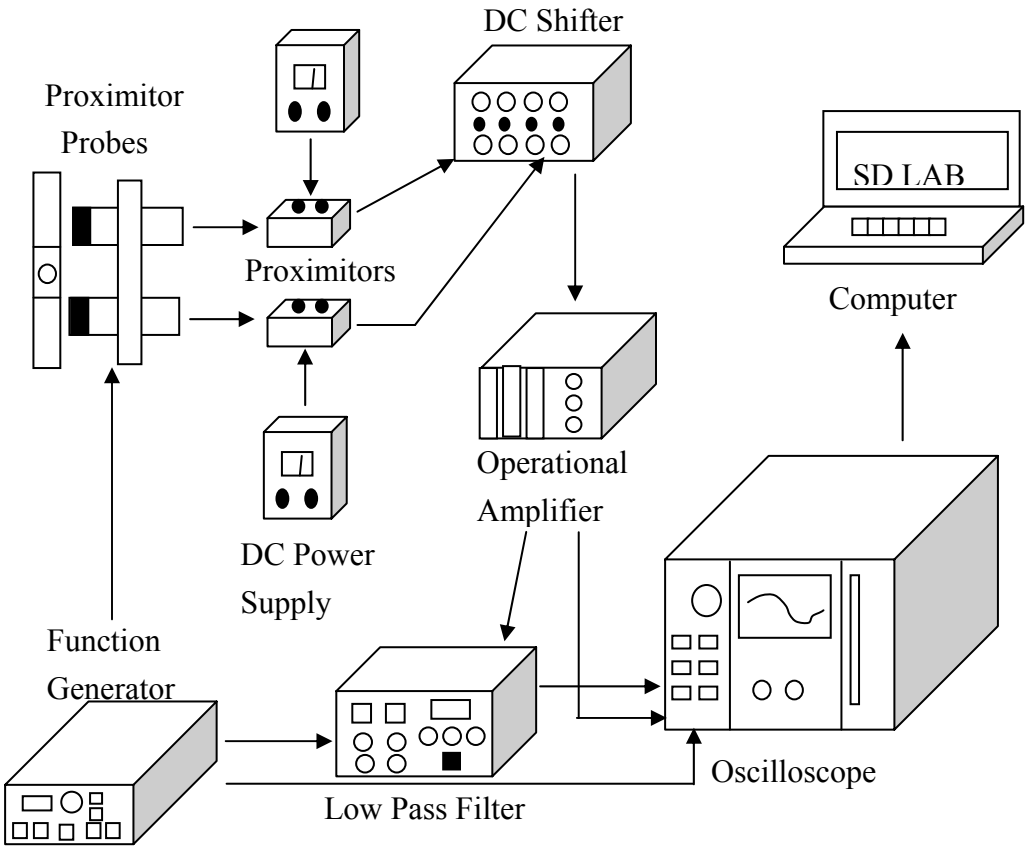

Figure 3.16 Simplified Configuration of Motion Monitoring System in TS Tests (after Hwang, 1997)

3.5 ORGANIZATION OF FREE-FREE RC TESTING EQUIPMENT

The LSRC testing device is used to measure the dynamic properties of the MSW for large-diameter (6.0-in. (152.4-mm)) specimens. As with the fixed-free RCTS device, the LSRC system is composed of five basic components:

(1) Confinement System,

(2) Specimen Support System,

(3) Driving System,

(4) Height-Change Measurement System, and

(5) Motion Monitoring System.

Detailed description and explanation for each system component is provided in the following sections. The LSRC system was designed and constructed by Menq (2003) and more details can be found in his dissertation.

3.5.1 Confinement System

The confinement system of the LSRC consists of a hollow circular cylinder (thickness of 0.4-in. (10.2-mm)), two circular end plates (7-in. (177.8-mm) diameter and 1.45-in. (36.8-mm) thickness), and four, long fixing rods (0.75-in. (19.1-mm) diameter and 32-in. (812.8-mm) length). Like the confinement system of the fixed-free RCTS equipment, all these components are made of stainless steel to minimize influencing the magnets in the device system of the LSRC. The base plate is somewhat elevated from the testing table to minimize background noise during measurements, resulting in good measurements at very small strains of material damping by the free-vibration decay method. The confining chamber has been designed to withstand to maximum confining pressure of 500 psi (3452 kPa). In addition, a lifting system shown in Figure 3.3 is required to handle the heavy weight of the confining chamber and end plate, weighing 200 pound (lb) (90718 g). The general configuration of confinement system with confining chamber is presented in Figure 3.17.

Similar to the fixed-free RCTS test, available pressure sources for confinement system are either building pressure or industrial nitrogen gas.

3.5.2 Specimen Supporting System

The specimen in the LSRC test is lifted by using fish wire to allow a free-free

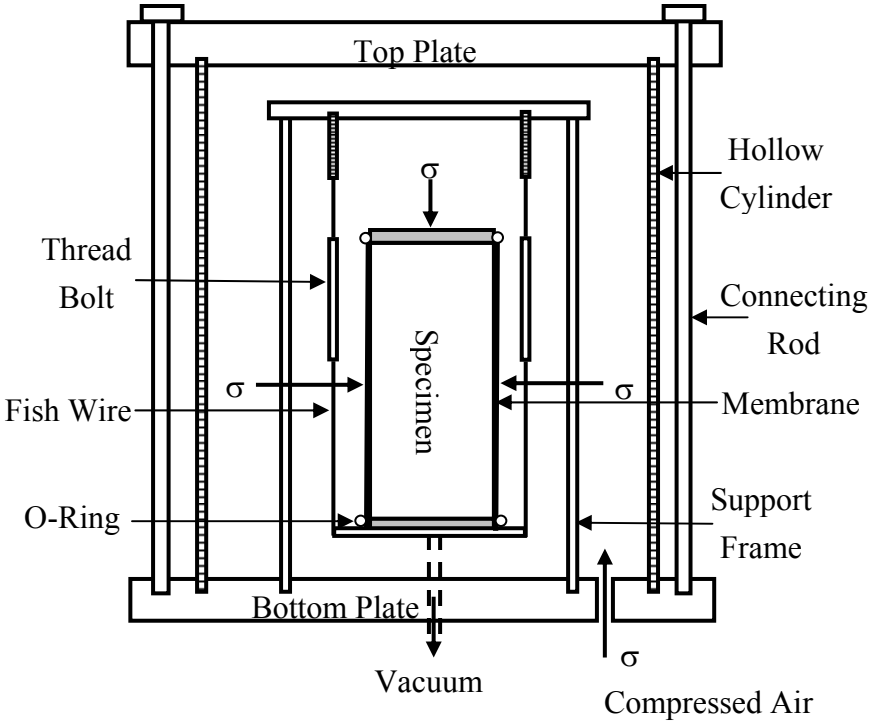

Figure 3.17 Simplified Configuration of Confinement System in the LSRC Tests

boundary of at the bottom of the specimen. The specimen supporting system is shown in Figure 3.18 with expanded views of each part. At the top and bottom expanded views, the supporting wires are secured by set screws firmly to eliminate the friction-induced damping. The stiffness of the supporting system, in terms of resonant frequencies in vertical, torsional, and rocking motions, should be small enough so that there is no effect on the dynamic measurements of the specimen being tested.

Menq (2003) found that the resonant frequencies of the supporting system acting like a rigid body in the longitudinal and torsional directions for granular materials were 18-20 Hz and 1-3 Hz, respectively. It is not that difficult to consider the resonant frequency of the supporting system with the MSW materials in longitudinal direction may be lower than with stiffer granular materials. The resonant frequencies obtained with the 6-in. (152.4 mm) diameter waste specimens in the longitudinal and torsional

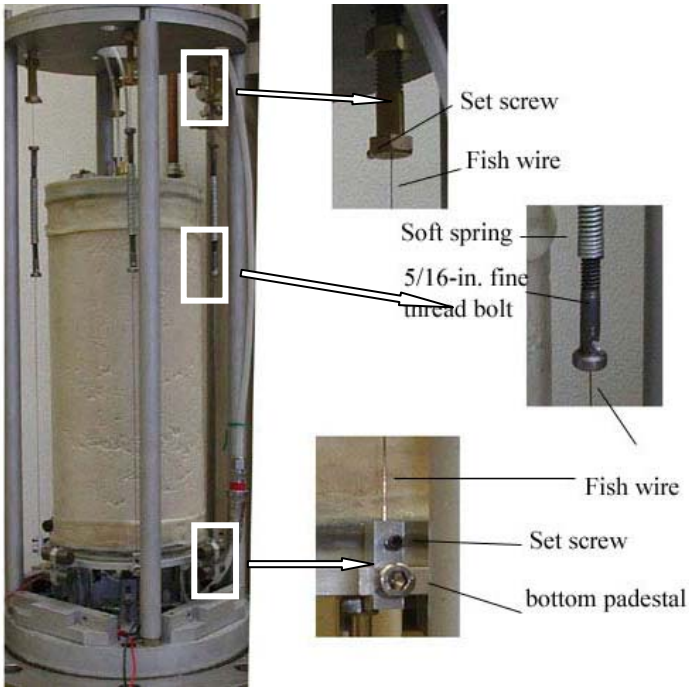

Figure 3.18 General Configuration and Expanded Views of Each Part of the Supporting System (from Menq, 2003)

directions were equal to 130-560 Hz and 100-360 Hz, respectively, in these tests. These resonant frequencies are higher than the system material frequencies by a factor of 10. Accordingly, the supporting system can be considered to represent the free-free boundary conditions.

3.5.3 Driving System

The driving system consists of eight Neodymium Iron Boron magnets and four pairs of electrical coils. A pair of magnets, with each magnet having a cylindrical shape, is attached to each end of the drive plate arm as shown in Figure 3.19. The magnet pair is stacked with two layers in the vertical direction. Each electrical coil is wounded in an elliptical shape. The holders supporting the coils are made of acrylic material is in an attempt to minimize the Eddy currents. The drive plate is connected to

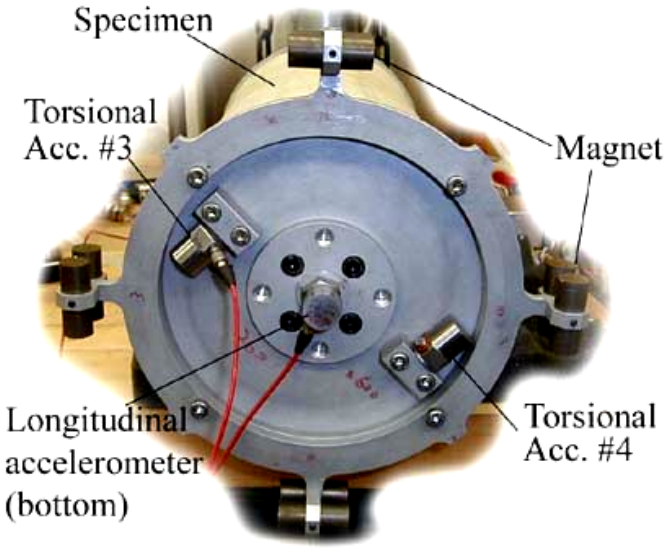

Figure 3.19 Configuration of Driving System in the LSRC Device (from Menq, 2003)

the bottom pedestal with four screw bolts.

The operational sequence in the RC tests is illustrated in Figure 3.20 and is represented by arrows in the figure. At first, the computer initiates a dynamic signal analyzer (HP 3562A) to send out a sinusoidal signal with constant amplitude.

The signal is sent directly to the drive coils for low-amplitude RC tests. However, in the case of high-amplitude RC testing, the signal from the dynamic signal analyzer is amplified by the power amplifier (MB Dynamics SS530) before being supplied to the drive coils. The amplification increases the current passing through the coils which leads to larger strains.

3.5.4 Height-Change Measurement System

The height-change measurement system is composed of: (1) a direct-current linear variable differential transducer, called DCLVDT, (Trans-Tek Model 243-0009), (2) a DC power supply (Agilent Model E3620A), (3) a switch control unit (HP 3488A), and (4)

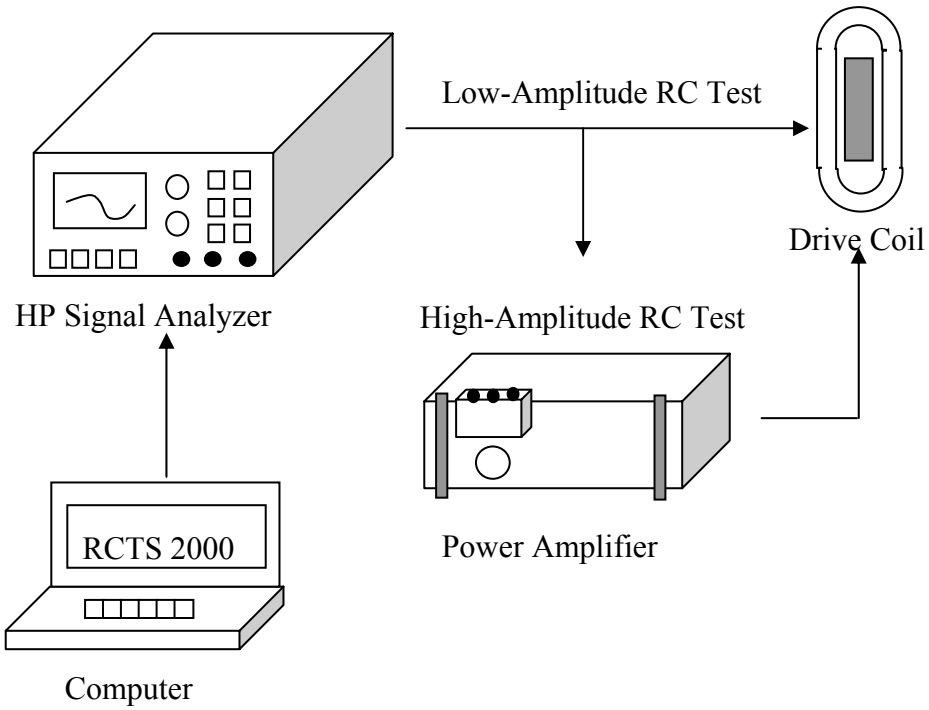

Figure 3.20 Simplified Diagram of Driving System in the LSRC Device

dynamic signal analyzer. A schematic diagram of the height-change measurement system is presented in Figure 3.21.

As seen in the figure, the DC power supply provides power to the DCLVDT. The output voltage of the DCLVDT is then read by dynamic signal analyzer and transferred to the computer. The DCLVDT is also employed as a dynamic source for the V_p and V_c measurements with the combination of a solenoid that is installed on top of the DCLVDT. Like the fixed-free RCTS device, the DCLVDT output values are important because the physical material properties are calculated using the weight and dimensions of the specimen and how these change with time and pressure. Therefore, continuous measurement of the specimen height by the DCLVDT output is very important. Obviously, incorrect values of specimen weight can induce errors in calculations on the shear wave velocity and shear modulus measurements.

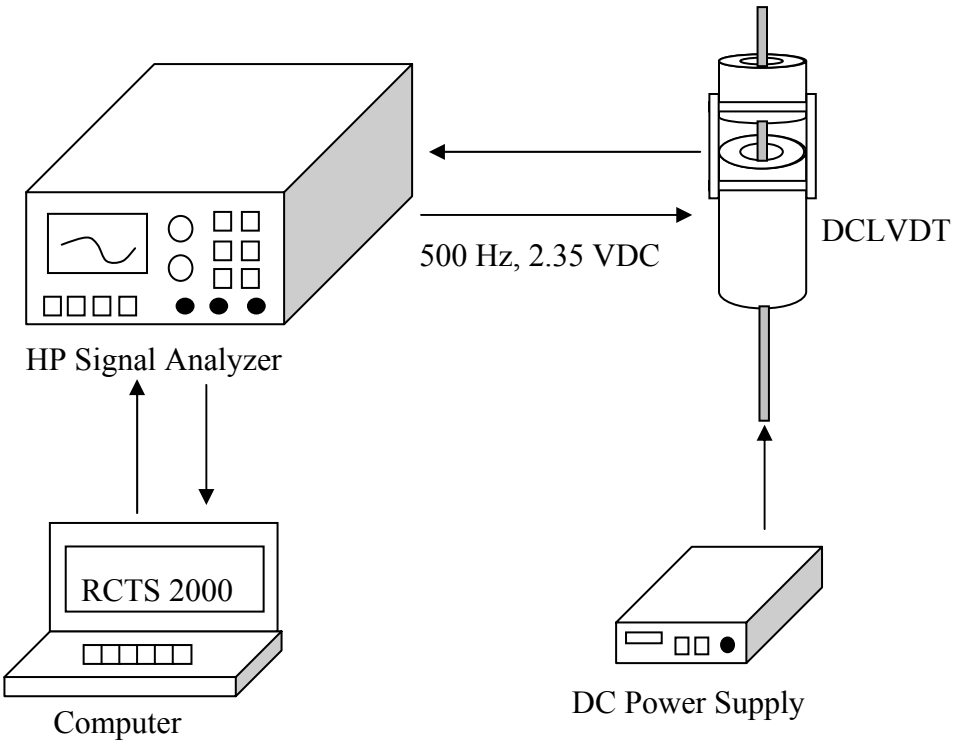

Figure 3.21 Simplified Diagram of Height-Change System in the LSRC Testing Device (after Menq, 2003)

3.5.5 Motion Monitoring System

The dynamic response of the specimen being excited in torsional motion is monitored by accelerometers (Columbia Research Lab. Model 3021) that are installed on top of the top cap. This motion monitoring system is presented in Figure 3.22.

As shown in the figure, a pair of accelerometers is placed parallel to each other. They are aligned on opposite side of the center of rotation to maintain the balance of top cap during torsional motion. One accelerometer is only chosen for motion monitoring for each measurement. The other accelerometer on the top is used for the case of the checking of pure torsion as needed.

In a same manner, there are two more accelerometers on the bottom pedestal.

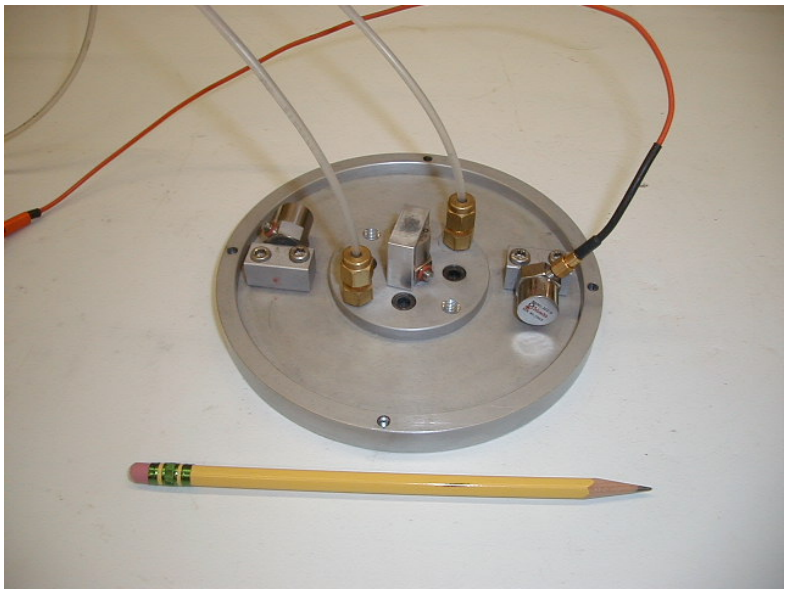

Figure 3.22 Picture of Motion Monitoring System with Cable for the Accelerometer and Vacuum Lines in the LSRC Test Device

These accelerometers are also used only for the purpose of checking the vibration of specimens in pure torsional motion if needed, and are not required to be used for torsional motion measurement.

This can be done by comparing the phase difference between the accelerometers being used on the top and bottom of the specimen (see Menq (2003) in Section 3.3.4.2 for more details). For instance, the phase difference between one used and the other one on top cap is zero degree because two accelerometers are moving in the same direction. On the other hand, the phase difference with ones on bottom pedestal is equal to 180 degree if two accelerometers are moving in the same direction, and is zero degree otherwise.

In addition, there are other accelerometers at the center of the top cap and bottom pedestal to capture the signals generated by longitudinal excitation in case of V_p and V_c measurements. The accelerometer on top is used as a trigger and the other one is used as a receiver. The V_p measurements are analyzed in the time domain by using time

difference between the two accelerometers with a given specimen length. The V_c measurements are analyzed in the frequency domain by implementing a Fast Fourier Transform (FFT) algorithm for the time domain signals of V_p measurements and determining the resonant frequency in longitudinal motion.

3.6 SUMMARY

A combined RCTS device and a LSRC device that were used to test MSW specimens are discussed in this chapter. The operational principle for both devices is to apply torsional excitation to the specimen either on the top or bottom of the specimen. The only difference between the two devices is in the boundary conditions, i.e., fixed-free and free-free conditions at the ends of the specimen. The different boundary conditions lead to different governing equations (Equation (3.1) and Equation (3.19)). However, in both cases the dynamic shear modulus (G) is determined.

The theoretical framework for RCTS and LSRC testing was provided in Section 3.3. This section covers the determination of shear modulus and material damping ratio. Once the resonant frequency is determined, the shear modulus is computed on the basis of one-dimensional wave propagation. The material damping ratios are determined either from the half-power bandwidth or free-vibration decay methods. However, in the TS tests, the hysteresis loop is generated, which is a plot of shear stress versus induced shear strain. The shear modulus is the slope of line passing through the end points of the loop while the material damping ratio is determined from the ratio of the area of loop relative to the stored strain energy.

The arrangement of the test equipment is presented in Sections 3.4 and 3.5 for the fixed-free RCTS and free-free RC testing equipments, respectively. The RCTS and LSRC test devices are mainly composed of: (1) a confinement system, (2) a drive system,

(3) a height-change measurement system, and (4) a motion monitoring system. Additionally a specimen supporting system is added to the LSRC device so that free boundary conditions can be achieved at both ends.

CHAPTER 4: Material Properties of MSW

4.1 INTRODUCTION

The MSW was recovered from the Tri-Cities Landfill which is located near Fremont, California, north of San Jose and east of the San Francisco Bay. The location of Tri-Cities Landfill is identified in Figure 4.1 with a star symbol. To retrieve the test samples, drilling operations were carried out by Big Iron Drilling Inc. using a 30-in. (762-mm) diameter bucket auger. Two different boreholes were drilled. The two boreholes, named BH-1 and BH-2, are shown in Figure 4.2 with their longitudinal and latitude coordinates. The retrieved waste materials from the two boreholes were collected and placed into 55-gallon High-Density Polyethylene (HDPE) drums. This work was part of a collaborative research project with The University of California at Berkeley, The University of Texas of Southern California and Geosyntec, Inc. and was sponsored by the National Science Foundation (NSF). Two, 55-gallon HDPE drums of the MSW were delivered from the University of California at Berkeley to the University of Texas at Austin to investigate the dynamic characteristics of the MSW using combined RCTS and LSRC laboratory test equipment.

The in-situ characteristics of the MSW as well as the measured material properties such as variation in temperature, total unit weight, and water content of the MSW in the field and laboratory are provided in the subsequent sections. These measurements were performed by Dr. Zekkos as part of his doctoral research. The grain size distribution analysis performed by UT is also provided.

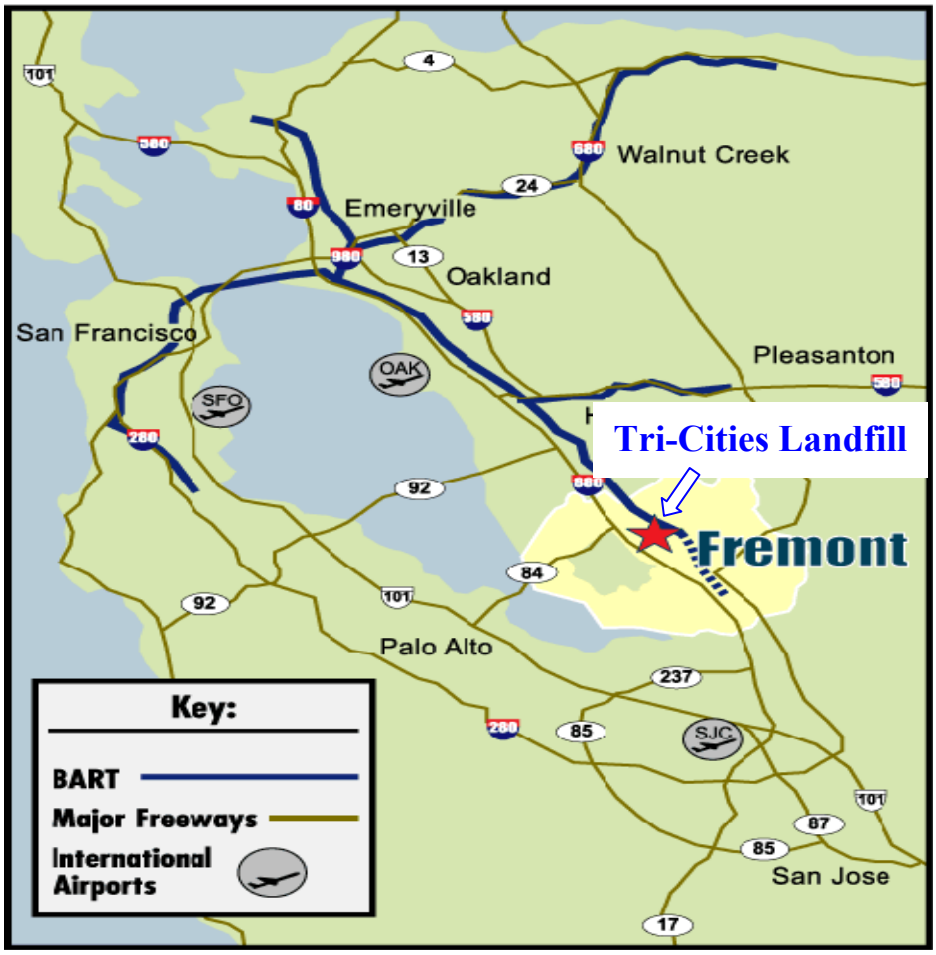

Figure 4.1 Location of Tri-Cities Waste Landfill in California

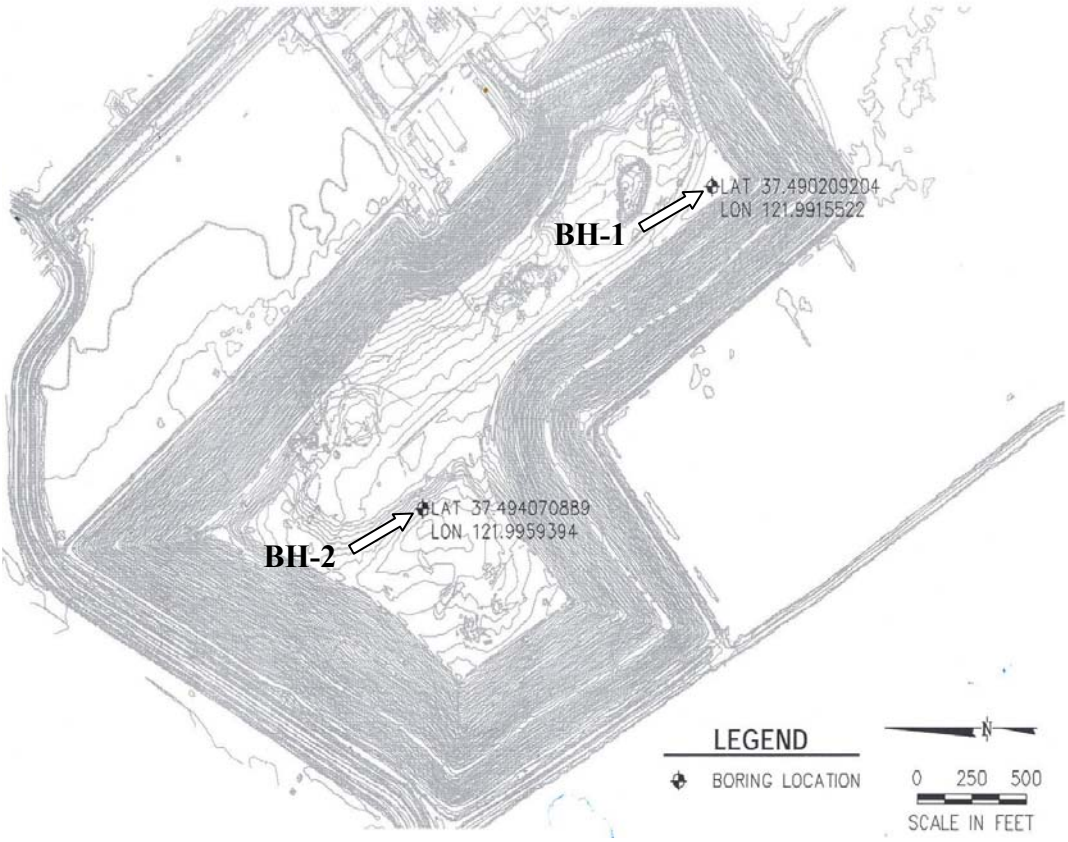

Figure 4.2 Plan View of the Tri-Cites Waste Landfill with Borehole Locations (Courtesy of GeoSyntec Constants, 2003)

4.2 IN-SITU CHARACTERIZATION OF MSW

In order to characterize the MSW, the boring processes were performed at the waste landfill in November 2002 and waste materials were retrieved. Borehole BH-1 was drilled to a depth of 31.5 ft (9.6 m) and Borehole BH-2, was drilled in the same manner to a depth of 106 ft (32.3 m). Fresh waste sample was collected from Borehole BH-1 and old waste samples were collected from Borehole BH-2. Throughout the boring process, the estimated height of the Tri-Cities waste landfill was about 106 ft (32.3 m). No presence of the ground water table was observed within the landfill during the

boring operations. Therefore, the ground water table was assumed to be located at a depth of approximately 120 ft (36.6 m) because of the fact that the Tri-Cities landfill is adjacent to San Francisco Bay.

The material properties of MSW were determined in the laboratory and characterized during the in-situ sampling process. These material properties and in-situ characterizations of the MSW are provided in the following sections.

4.2.1 State of Degradation and In-Situ Classification of Retrieved MSW

As presented in Figure 4.2, two boreholes were drilled into the waste landfill using the 30-in. (762-mm) diameter bucket auger. The waste materials recovered from Borehole BH-1 at a mean depth of 28.5 ft (8.7 m) were classified as fresh waste (C6 Group) (Zekkos, 2005). The age of the fresh waste that had been placed in the landfill was estimated to be less than 3 years old. In Borehole BH-2, at a mean depth of 85.0 ft (25.9 m), waste materials were also recovered and were classified as the old waste (A3 Group) with an estimated age of about 15 to 17 years old (Zekkos, 2005). One source of information conjecturing the age of the collected MSW was from dates specified on documents, newspapers and magazines, etc that were found in the waste. As an example, the dates found in newspapers for C6 and A3 groups were January, 2000 and June, 1987, respectively (Zekkos, 2005).

It is expected that the engineering properties and behavior of MSW would be influenced by the state of degradation and proportions of refuse to soil-like material. These factors are studied throughout the research in the small and large-stain ranges (< 0.002% and 0.01 to 0.3%, respectively) using the combined RCTS and LSRC testing devices, resulting in an enhanced and expanded understanding of MSW.

During the boring operations, each component, e.g., soft plastics, papers, woods

and gravels, etc could be approximated qualitatively by describing what kinds of materials composed the wastes. Visual inspections were made as well by Steve Chickey of Geosyntec Consultants and Dimitris Zekkos (Zekkos, 2005). The collected waste samples in turn were classified quantitatively in terms of the weight percentage of individual component for both A3 and C6 groups at the University of California at Berkeley by Zekkos (2005). The classification results are illustrated in Figure 4.3. As presented in Figure 4.3, a majority of waste components (about 60-75 % by weight) are soil and/or soil-like material which might be used for tentative soil covers.

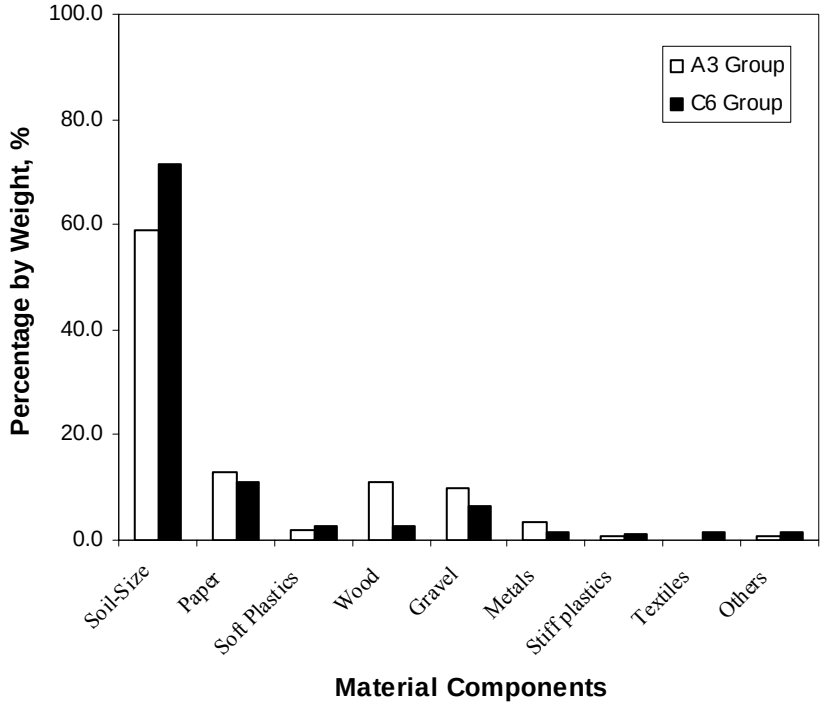

Figure 4.3 Classification of Waste Materials into Components in Terms of Percentage Weight for A3 and C6 Groups (after Zekkos, 2005)

Additional classification processes were conducted for other groups of waste

materials (A1, C1 and C3 Groups) recovered from different depths by Zekkos (2005). The A1 group was old waste whereas the C1 and C3 groups were classified as fresh waste (see Zekkos (2005) for more information). Except for the A1, C1 and C3 groups of materials that have been classified by UCB, only A3 and C6 groups of waste materials were delivered to UT and used to evaluate the dynamic characteristics of MSW using the combined RCTS and LSRC test devices.

4.2.2 Variation in Temperature of MSW

The temperature of the waste materials was measured right after placing the materials on the ground surface using a digital thermometer by Zekkos (2005). The variation in temperature with depth is given in Figure 4.4. It should be noted that the temperature measured from BH-2 has a large amount of variation and/or scatter after a depth of 30 ft (9.1 m). In the case of BH-1, however, the temperature was only measured up to about 30 ft (9.1 m) below the ground surface. Despite the large variation/scatter in the measurements, approximated trend lines representing the variations in temperature for BH-1 and BH-2 are expressed by dashed lines in the same figure. As seen in Figure 4.4, the temperatures increase rapidly at shallow depths (from the surface to 20 ft (6.1 m)) for both boreholes but appear to remain constant after a depth of 50 ft (15.2 m) for Borehole BH-2. The reason for this trend may be attributed to the fact that heat generated by biological degradation of organic materials would be dissipated differently with depth (Zekkos, 2005). That is, the shallow depths have a short heat dissipation path whereas the heat dissipation path becomes longer at deeper depths.

It is evident that the temperatures, shown in Figure 4.4, do not represent the actual temperature within the landfill being sampled because of the fact that the retrieved waste

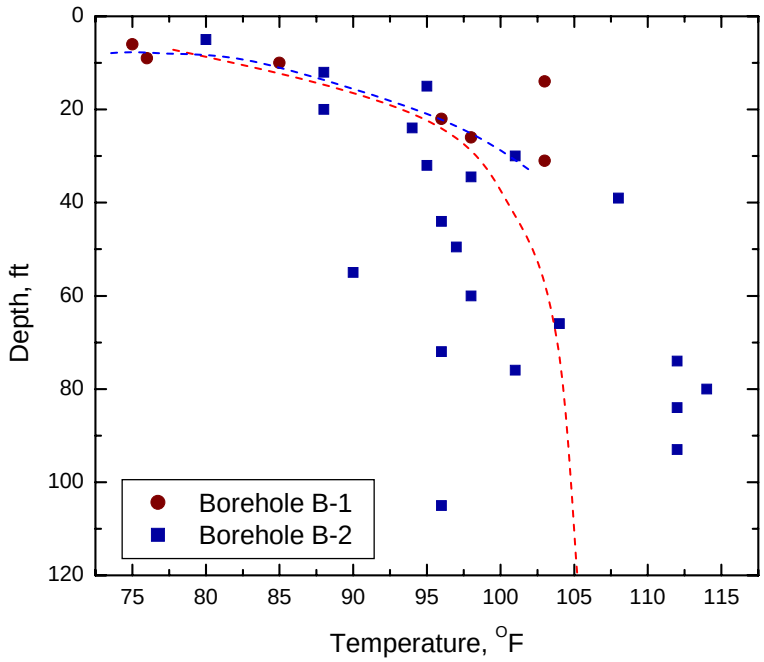

Figure 4.4 Variation in Temperature in the MSW from Two Boreholes in the Tri-Cities Landfill (after Zekkos, 2005)

materials were exposed to the air during their placement on the ground surface. Therefore, it is concluded that the actual temperature of the waste within the landfill is expected to be higher than the measured values.

4.2.3 Measurements of In-Situ Total Unit Weight

To reconstitute the specimens to their in-situ total unit weight in the laboratory to evaluate the dynamic properties of the MSW, the total unit weight, γ_t, of the MSW should be evaluated. The evaluation of the in-situ total unit weight was carried out by Big Iron Drilling Inc. under supervision of GeoSyntec Consultants and UCB. The field method was patterned after the ASTM D 5030-89 standard, "Density of Soil and Rock in Place by the Water Replacement Method in a Test Pit". Clean gravel was used for the determination of volume of boreholes over a give depth interval instead of water. The

unit weight of clean gravel is provided below. According to standard operation procedure for OII unit weight measurements prepared by GeoSyntec consultants (1995), the total unit weights for Tri-Cities landfill MSW were conducted similarly determined. The basic idea of total unit weight measurements for MSW is that a given weight of waste materials collected in a certain interval is divided by volume corresponding to that interval.

Clean gravel was used to determine the corresponding volume in the borehole over a given depth interval. Therefore, it was necessary to first determine the unit weight of clean gravel. The unit weight of clean gravel was calculated by means of the weight of 55-gallon HDPE drums filled with gravel divided by their volume. As a consequence, the average unit weight of the gravel was equal to 111.5 pcf (17.5 kN/m^3) with minimum and maximum boundaries of 103.4 pcf (16.2 kN/m^3) and 117.0 (18.4 kN/m^3), respectively. A total of eight measurements of in-situ total unit weight were conducted in the two boreholes. The measured in-situ total unit weight profile with depth is shown in Figure 4.5.

As seen in Figure 4.5, the unit weight increases with depth gradually to a depth of 40 ft (12.2 m) and appears to be constant with further increase in depth. The outliers indicated by the symbol (*) at depth of 40 to 50 ft (12.2 m to 15.2 m) result mainly from construction debris such as concrete blocks and steel reinforcement. To calculate vertical stresses, the distribution of measured unit weight was simplified by the dashed line in the figure.

4.3 MATERIAL PROPERTIES OF MSW DETERMINED IN THE LABORATORY

4.3.1 Water Content Measurements for A3 and C6 MSW Groups

The water content measurements on parent MSW materials were determined in

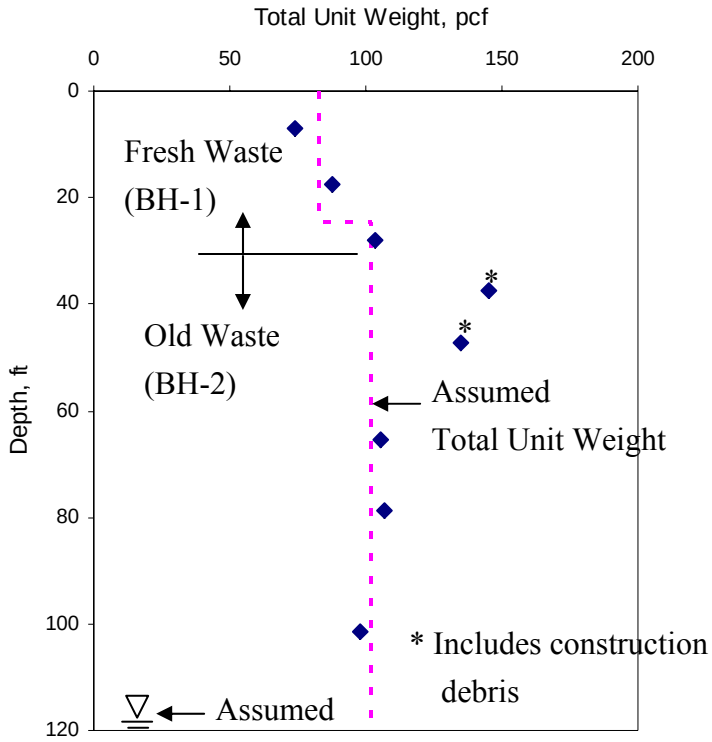

Figure 4.5 Variation in Total Unit Weight in the Tri-Cities Landfill (after Zekkos, 2005)

the Richmond Field Station at UCB by Zekkos (2005) following the procedure specified in ASTM D 2216, "Standard Method for Measuring the Moisture Content of Soil and Rock".

It should be noted that the water content measurements of waste materials are different to some extent from the measurements of conventional geotechnical materials (e.g., cohesive and cohesionless materials). The temperature in the dry-oven should be maintained as low as 50 to 60℃ to prevent ignition of organic materials in the MSW.

The MSW used for the water content measurements was a parent oil-sizes material which passed through the ¾-in. (19.1 mm) sieve opening for the A3 group. The measured average water content for the A3 group was approximately 12.0 %. In addition, the water content measurements conducted upon a parent soil-size material

which passed the ¾-in. (19.1-mm) sieve opening for the C6 group followed similar procedures to the A3 group and also turned out to be 12.0 %. It is noteworthy that the water contents of the parent soil-size material from both waste groups were equal regardless of the age of the waste.

However, according to values found in the literatures, Gabr et al. (1995) reported that the water content of municipal waste that was obtained in the Pioneer Crossing landfill in Pennsylvania tended to increase with depth, meaning that the water content of fresh waste was less than that of old waste. Contrary to this observation, Zornberg et al. (1999) did not observe a significant increase with depth in terms of gravimetric moisture content (defined as the ratio of the weight of water to the weight of solids). In summary, it seems that the difference in water content between fresh and old waste materials is not a unique characteristic and varies with the waste composition, the rate of biological decomposition and regional climate conditions.

4.3.2 Grain Size Distribution Analysis for A3 and C6 MSW Groups

To estimate the engineering characteristics of the MSW, the grain size distribution analysis for both A3 and C6 groups was performed at UT on the parent materials which passed the ¾-in. (19.1-mm) sieve opening according to ASTM standard D-2487, "Standard Method for Particle-Analysis of Soils". The parent soil-size material was air-dried in a high ratio of surface area to volume container. More than 3.5 lb (1.6 kg) of parent material for each group was prepared to satisfy the minimum requirement of 2.2 lb (1.0 kg), described in ASTM D-2487, Section 7. A series of sieves with different mesh sizes were stacked on top of one another, with the following sizes: ¾-in. (19.1-mm), 3/8-in. (9.5-mm), No. 4, No. 8, No. 16, No. 30, No. 150, No. 200 and the pan. The stacked sieves were transported onto the motorized sieve shaker (Gilson Company, INC Model

SS-8R). The lid was placed on top of the series of sieves to prevent the loss of waste material in the form of dust during shaking of the sieves. All sieves were pressurized by using a 2-way sieve clamping system and the shaking operation lasted for 5 minutes.

To determine the two engineering parameters, i.e., coefficient of uniformity (C_u) and coefficient of curvature (C_c), the weight of the remaining sample in each sieve was measured using an electrical scale (OHAUS) with an accuracy of 0.1 gram. Results of the grain size distribution analysis for the A3 and C6 groups are presented in Figure 4.6. The C_u and C_c values for the A3 group are 18 and 1.1, respectively, whereas the C_u and C_c values for the C6 group are 17 and 1.4, respectively.

It is interesting to see in Figure 4.6 that the shape of the grain size distribution for the old waste is similar to that of the fresh waste. The main difference is a slight

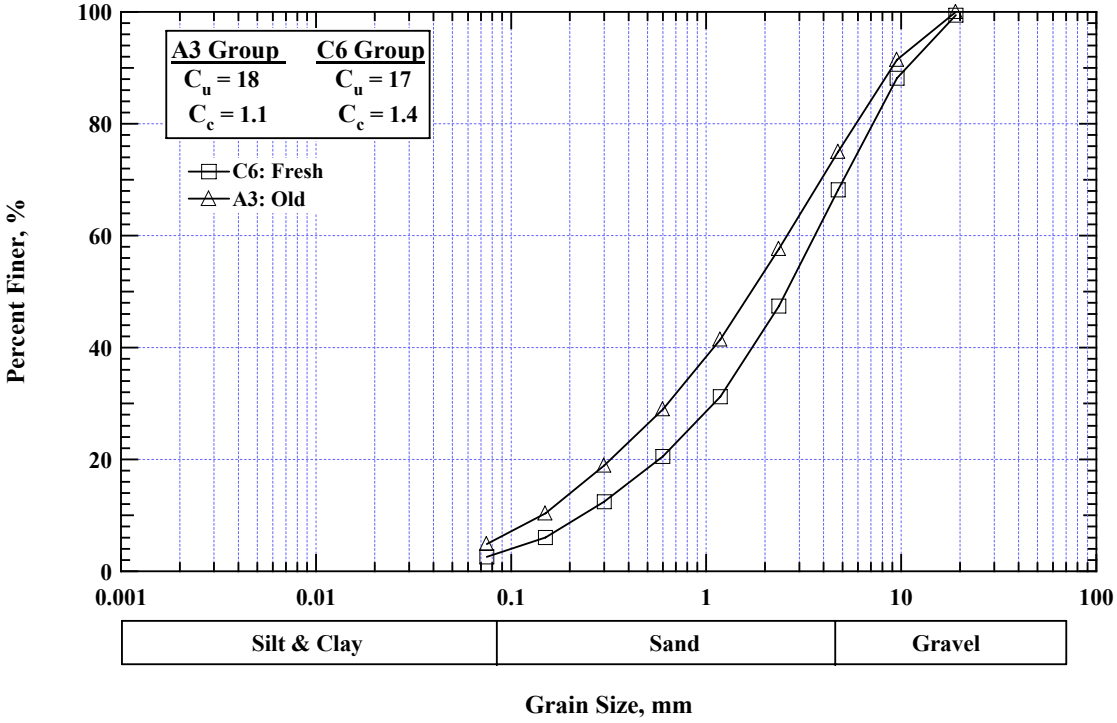

Figure 4.6 Grain Size Distribution Curves for A3 and C6 Groups

shifting in particle size in the grain size distribution curve when going old to fresh waste. This distribution indicates that the C6 group exhibits coarser grain distribution, namely, less percentage passing each sieve opening for the C6 group. The possible explanation for this is that the A3 group retained more fines than the C6 group by decomposition during the relatively long periods.

The median grain sizes (D_{50}) for both the A3 and C6 groups from the figure are equal to 0.069 in. (1.76 mm) and 0.102 in. (2.60 mm), respectively. Using the Unified Soil Classification System (USCS), both waste materials would be classified as well-graded sand (SW).

4.3.3 Plasticity Index (PI) Measurement Old MSW

The plastic index is defined as the range of water content over which a soil behaves plastically. It is numerically the difference between a liquid limit and plastic limit. The liquid limit and plastic limit tests were performed with material that passed Standard Sieve No. 40 (0.017-in. (0.425-mm)) of old MSW in accordance with ASTM D 4318, "Standard Test Method for Liquid Limit, Plastic Limit, and Plasticity Index of Soils". Average values of liquid limit and plastic limit for old MSW were about 35.4 % and 23.4 %, respectively. Therefore, the plastic index for old MSW is 12 %.

4.4 SUMMARY

The MSW materials were recovered from the Tri-Cities landfill near Fremont, California, which in north of San Jose and east of the San Francisco Bay. Two boreholes, BH-1 and BH-2, were drilled into the MSW landfill. Fresh waste was retrieved from BH-1 at shallow depths while the old waste was retrieved from BH-2 at deeper depths. As part of collaborative research project with The University of California at Berkeley, The University of Texas of Southern California and Geosyntec,

Inc. and was sponsored by the National Science Foundation (NSF), part of retrieved materials were delivered to UT to investigate the dynamic characteristics of MSW using the combined RCTS and LSRC testing devices.

Properties of the material that were characterized in the field by Zekkos (2005) were: (1) state of degradation and classification of MSW into constituents, (2) variation in temperature with depth and (3) total unit weight. The ages of the wastes were determined from dates written on newspapers and magazines found in the waste. The individual components of the MSW in terms of weight percentage are shown in Figure 4.3. Temperatures were measured with a digital thermometer immediately the waste was removed from the borehole and placed on the ground surface. Variation in temperatures with depth is presented in Figure 4.4. A rapid increase in temperature was observed at shallow depths and the temperature appeared to remain constant after some depth. This fact might be attributed to different heat dissipation paths (Zekkos, 2005). The total unit weights of MSW in place were determined using a gravel-replacement method and the results were shown in Figure 4.5. The variation of total unit weights was simplified for the calculation of vertical stress and was expressed with a dashed line in the same figure.

In the laboratory, water content measurements were performed by UCB on the parent materials and the average water content was equal to 12.0 % regardless of the age of the waste. The grain size distribution analyses were performed by UT on the parent material that passed the ¾-in. (19.1 mm) sieve. The test results are presented in Figure 4.6. The fresh waste showed a slightly coarser grain-size distribution curve than the old waste. This difference was attributed to the fact that the old waste was decomposed more than the fresh waste. On the basis of the USCS, both waste materials have a grain-size curve that would result in them being classified as well-graded sand (SW).

CHAPTER 5: Sample Preparation

5.1 INTRODUCTION

To study the dynamic characteristics of MSW, numerous specimens had to be reconstituted. As part of this collaborative research project, a sample preparation procedure was determined for static and dynamic laboratory tests under the agreement of the faculty members (Professors Bray, Kavazanjian, Rathje, and Stokoe) and professional engineer (Dr. Matasovic) who were involved with the project. According to the sample preparation procedure established by UCB, compaction hammers were built to achieve the same compaction energy per blow for both small- and large-diameter specimens. All specimens were reconstituted at their natural conditions in six layers with hammers and compacted with a specified pattern. A total of 30 specimens were constructed for the purpose of laboratory tests on MSW. Ten specimens were used for small-diameter RCTS tests and 20 specimens were used for large-diameter LSRC tests.

Detailed explanations of the sample preparation procedures of small- and large-diameter specimens for dynamic laboratory tests at their natural (and hydrated conditions) are discussed in this chapter.

5.2 IDENTIFICATION OF MSW SPECIMENS TESTED IN EACH MATERIAL GROUP WITH THE RCTS AND LSRC DEVICES

The number of MSW specimens that were reconstituted to investigate the dynamic properties of MSW in the RCTS and LSRC devices is presented in Table 5.1. This table summarizes the entire number of MSW specimens that have been tested for the RCTS and LSRC tests. In addition, the name of MSW specimens tested in the RCTS and LSRC devices is presented in Table 5.2.

Table 5.1 Number of MSW Specimens Tested in Each Material Group with the RCTS and LSRC Devices (All Groups)

Groups		Maximum Particle Size	RCTS			LSRC		
			Old	Fresh	Mixed	Old	Fresh	Mixed
100% (Soil-Size)		<3/8-in.*(9.5-mm)	4	2	-	1	1	-
		<¾-in. +(19.1-mm)	2	2	-	2	3	-
76%	76% Soil-Size	<¾-in. (19.1-mm)	-	-	-	2	2	-
	24% Larger Particle	<1.5-in.†(38.1-mm)						
62%	62% Soil-Size	<¾-in. (19.1-mm)	-	-	-	4	3	-
	38% Larger Particle	<1.5-in.(38.1-mm)						
14%	14% Soil-Size	<¾-in. (19.1-mm)	-	-	-	-	-	2
	86% Larger Particle	<1.5-in. (38.1-mm)						

Notes:

* "Soil-Size" means all components of the MSW that pass the 3/8-in. (9.5-mm) sieve.

+ "Soil-Size" means all components of the MSW that pass the ¾-in. (19.1-mm) sieve.

† Larger particles are made up of paper, soft plastic, wood, and gravel that have sizes between ¾-in. (19.1-mm) and 1.5-in. (38.1-mm).

Table 5.2 Name of MSW Specimens Tested in Each Material Group with the RCTS and LSRC Devices (All Groups)

<table>
<tr><th colspan="2" rowspan="2">Groups</th><th rowspan="2">Maximum Particle Size</th><th colspan="3">RCTS</th><th colspan="3">LSRC</th></tr>
<tr><th>Old</th><th>Fresh</th><th>Mixed</th><th>Old</th><th>Fresh</th><th>Mixed</th></tr>
<tr><td colspan="2" rowspan="6">100% (Soil-Size)</td><td rowspan="4"><3/8-in.*(9.5-mm)</td><td>1ONS1</td><td rowspan="2">1FNS1</td><td rowspan="4">-</td><td rowspan="4">4ONL1</td><td rowspan="4">9FNL1</td><td rowspan="4">-</td></tr>
<tr><td>2ONS1</td></tr>
<tr><td>3ONS1</td><td rowspan="2">3FNS1</td></tr>
<tr><td>5ONS1</td></tr>
<tr><td rowspan="2"><¾-in.+ (19.1-mm)</td><td>4ONS2</td><td>2FNS2</td><td rowspan="2">-</td><td>2ONL2</td><td>1FNL2</td><td rowspan="3">-</td></tr>
<tr><td>6ONS2</td><td>4FNS2</td><td>7ONL2</td><td>3FNL2</td></tr>
<tr><td rowspan="2">76%</td><td>76% (Soil-Size)</td><td><¾-in. (19.1-mm)</td><td rowspan="2">-</td><td rowspan="2">-</td><td rowspan="2">-</td><td>1ONL3</td><td>4FNL3</td><td rowspan="2">-</td></tr>
<tr><td>24% Larger Particles</td><td><1.5-in.†(38.1-mm)</td><td>9ONL3</td><td>7FNL3</td></tr>
<tr><td rowspan="4">62%</td><td rowspan="2">62% (Soil-Size)</td><td rowspan="2"><¾-in. (19.1-mm)</td><td rowspan="4">-</td><td rowspan="4">-</td><td rowspan="4">-</td><td>3ONL4</td><td>2FNL4</td><td rowspan="4">-</td></tr>
<tr><td>5ONL4</td><td>6FNL4</td></tr>
<tr><td rowspan="2">38% Larger Particles</td><td rowspan="2"><1.5-in.(38.1-mm)</td><td>6ONL4</td><td rowspan="2">8FNL4</td></tr>
<tr><td>8ONL4</td></tr>
<tr><td rowspan="2">14%</td><td>14% (Soil-Size)</td><td><¾-in. (19.1-mm)</td><td rowspan="2">-</td><td rowspan="2">-</td><td rowspan="2">-</td><td rowspan="2">-</td><td rowspan="2">-</td><td>1MNL4</td></tr>
<tr><td>86% Larger Particles</td><td><1.5-in.(38.1-mm)</td><td>2MNL4</td></tr>
</table>

Notes:

* "Soil-Size" means all components of the MSW that pass the 3/8-in. (9.5-mm) sieve

+ "Soil-Size" means all components of the MSW that pass the ¾-in. (19.1-mm) sieve

† Larger particles are made up of paper, soft plastic, wood, and gravel that have sizes between ¾-in. (19.1-mm) and 1.5-in. (38.1-mm)

5.3 PREPARATION OF SMALL-DIAMETER (2.8-IN. (19.1-MM)) SPECIMENS

5.3.1 Specimen Reconstitution with Soil-Sizes Material at the In-Situ Natural Condition

The parent material which passed through the 3/8-in.(9.5-mm) and ¾-in. (19.1-mm) sieves was prepared and reconstituted to its in-situ water content and total unit weight, which is on the order of 82.6 pcf (13 kN/m^3) for only soil-sizes material, for the series of RCTS tests. The parent material was stored in sealed plastic bags to maintain the in-situ water content. The material that remained after completion of the specimen reconstitution was put back into the plastic bags and stored in the HDPE drum. Some amount of water, however, was added after mixing the specimen material with the remaining material after completion of the RCTS tests to maintain the water content for subsequent specimen constructions. As discussed in Section 4.3.1, the water content of the in-situ material was about 12%, but the water content of the parent material was measured again to confirm the actual value of the specimen to be tested prior to the RCTS tests. To do this, the material was taken from three different spots in the plastic bag to obtain a representative value. As mentioned in Section 4.3.1, the material was dried the oven under the temperature of 50 to 60℃ to prevent ignition of organic materials in MSW.

The initial characteristics of the entire specimen group are summarized in Table 5.3. As denoted in Table 5.2, each specimen is named with a number at the end of the name, which indicates the material that was used to build. For example, MSW1ONS1 represents the first small-diameter (2.8-in. (71.1-mm)) specimen built with material that passed the 3/8-in. (9.5-mm) sieve at its natural condition for the old waste whereas MSW4ONS2 is the fourth small-diameter (2.8-in. (71.1-mm)) specimen built with

Table 5.3 Summary of the Initial Material Characteristics of Small-Diameter MSW Specimens for Fixed-Free (Fx-Fr) RCTS Tests for 100 % Soil-Size Material Group

Waste Type	RC Type	Specimen ID	Height, inch(cm)	Diameter, inch(cm)	Total Unit Weight, γ_t, pcf(kN/m^3)	Water Content, (%)
Old (A3)	Fx-Fr	MSW1ONS1	5.97(15.2)	2.84(7.2)	81.5(12.8)	13.3
		MSW2ONS1	5.97(15.2)	2.83(7.2)	83.3(13.1)	15.0
		MSW3ONS1	5.80(14.7)	2.78(7.1)	83.7(13.1)	13.6
		MSW3ONS1(2)◊	5.80(14.7)	2.78(7.1)	83.7(13.1)	13.6
		MSW4ONS2	5.94(15.1)	2.83(7.2)	82.3(12.9)	11.5
		MSW5ONS1†	5.75(14.6)	2.83(7.2)	61.3(9.6)	11.1
		MSW6ONS2†	5.83(14.8)	2.80(7.1)	62.4(9.8)	12.2
Fresh (C6)	Fx-Fr	MSW1FNS1	5.78(14.7)	2.84(7.2)	90.6(14.2)	13.0
		MSW2FNS2	5.78(14.7)	2.84(7.2)	86.0(13.5)	13.4
		MSW3FNS1†	5.31(13.5)	2.78(7.1)	66.5(10.4)	9.9
		MSW4FNS2†	6.10(15.4)	2.78(7.1)	62.9(9.9)	13.9

Notes: N in the specimen ID denotes natural water content

◊(2) at the end of the specimen ID denotes a re-testing of Specimen MSW3ONS1 but with a confinement time of 60 min. at each σ_o

† denotes specimens tested with a lower total unit weight

1 at the end of the specimen ID denotes a specimen reconstituted with material passed the 3/8-in. (9.5-mm) sieve

2 at the end of specimen ID denotes a specimen reconstituted with material passed the ¾-in. (19.1-mm) sieve

material which passed the ¾-in. (19.1-mm) sieve at its natural condition for old waste. MSW3ONS1(2) is different from MSW3ONS1 in that the MSW3ONS1(2) was tested with a duration of confinement time of 60 min. at each confining pressure after completion of tests on MSW3ONS1. The specimens designated with an added symbol (e.g., MSW5ONS1†, MSW6ONS2†, MSW3FNS1† and MSW4FNS2†) were made with a low unit weight to study the effect of the initial unit weight of the MSW.

To achieve the same compaction energy per hammer area (0.765 Joules/cm^2), a compaction hammer made of stainless steel was built. The compaction hammer and a split mold made of acrylic material are shown in Figure 5.1. The weight of the compaction hammer and drop height were 1.93 lb (0.88 kg) and 1.64 ft (0.5 m), respectively.

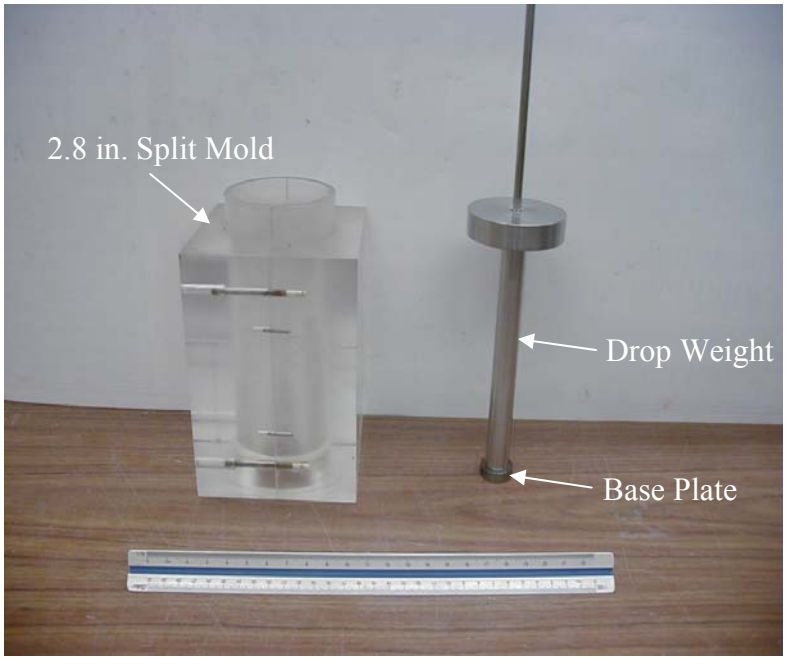

Figure 5.1 Split Mold and Compaction Hammer for the Construction of 2.8-in. (71.1 mm) Diameter Specimen

As seen in Figure 5.1, the base plate is designed slightly larger in diameter than the compaction hammer to prevent the damaging the membrane around the top of the split mold during the compaction process. All test specimens were reconstituted in six layers with a target thickness of 0.08 ft (0.025 m) after completion of compaction in each layer.

Each layer was compacted with the pattern illustrated in Figure 5.2. A total of 9 blows per layer were applied. It should be noted that achieving a uniform unit weight along the length of the specimen using the sample preparation technique described above was unlikely because the succeeding layers are further densified due to the subsequent compaction effort.

The surface of each layer was scarified with a thin, sharp steel rod after compaction with 9 blows. This process was done to enhance the interface connection between layers before the subsequent layer was placed. At the top layer, additional waste material was placed to make a level surface prior to placing the top cap. In addition, extra specimens having low total unit weight were constructed to study the effect of unit weight on the dynamic properties. These specimens were not compacted but constructed by simply placing the waste material that passed the 3/8-in. (9.5-mm) and ¾-in. (19.1 mm) sieves into the split mold.

Finally, each specimen was carried to the laboratory because the compaction process was performed in the basement of Cockerel Hall and was positioned on the base pedestal of the RCTS device. A seating pressure (about 1 psi (6.9 kPa)) was applied before measuring the dimensions of the specimen. An additional membrane was put on the specimen to ensure that no leakage would occur from any membrane punctures that might have been caused by the compaction effort.

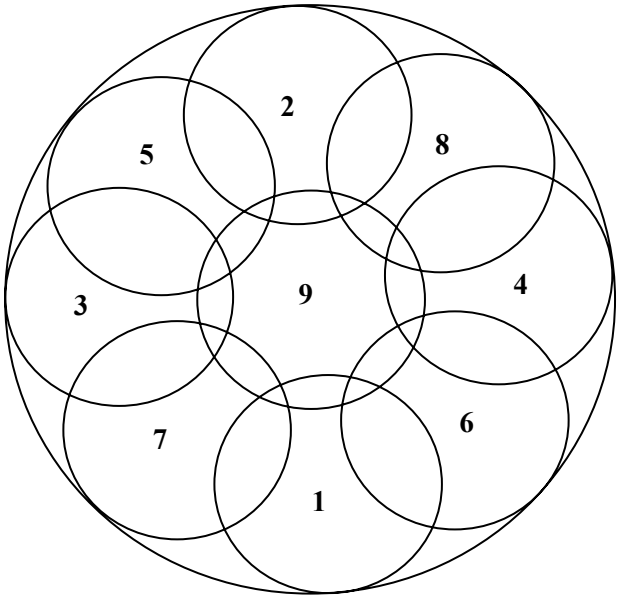

Figure 5.2 Configuration of the Compaction Pattern of Each Layer

5.2.2 Hydration of Specimen

After completion of the combined RCTS tests on each specimen at their natural condition, the RCTS device was dismantled for the purpose of hydrating the tested specimen. The split mold was reassembled around the specimen on the base plate before the water was added. The purpose of assembling the mold around the specimen was to provide resistance against the water pressure generated inside the specimen due to the watering. The entire configuration for hydrating the specimen is presented in Figure 5.3. As illustrated in Figure 5.3, a thin plastic bag was placed underneath the round stainless steel lid to minimize evaporation of water at the surface of the specimen. An experimental stand was placed next to the split mold and the drain line from the base plate was held to the guide rod with tape. Thus, it was easy to examine the increased elevation of the "water table" after pouring water in the specimen. It took some time for water to infiltrate the densified specimen.

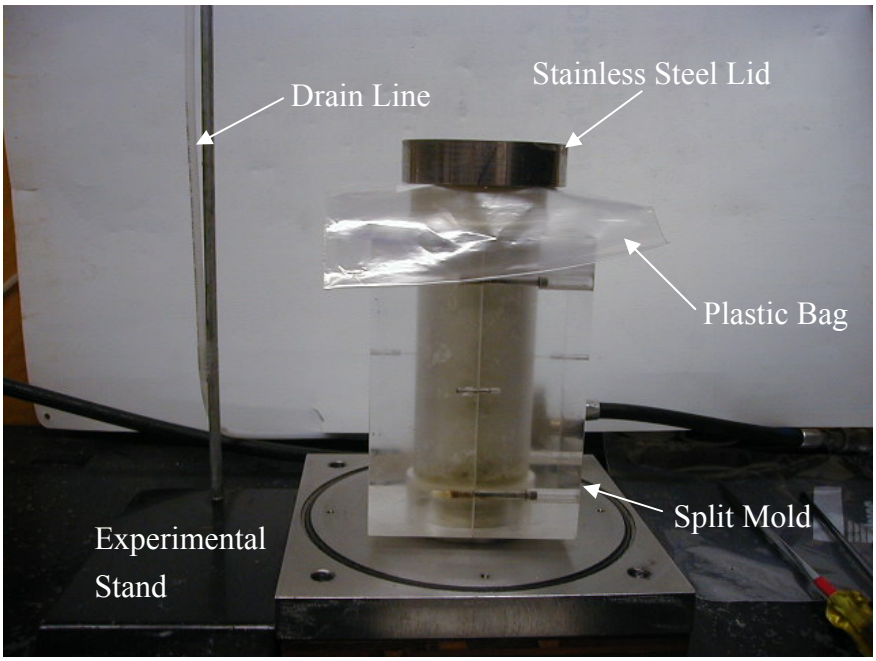

Figure 5.3 General Configuration for the Hydration of RCTS Specimens

The hydration process was repeated several times until the water was observed at the surface of the specimen. The initial characteristics of hydrated specimens are presented in Table 5.4. The weight of the added water was measured to calculate the new water content for the hydrated specimen. Once the specimen was hydrated, the name of the specimen, as given in Table 5.4, was denoted with an H in its name (e.g., MSW2ONS1 became MSW2OHS1). After hydration, the top cap was place on the top of the specimen and the split mold was detached carefully. The dimensions of the hydrated specimen under unconfined conditions (without vacuum pressure) were measured to calculate the new volume.

The purpose of hydration of the tested samples was to investigate the dynamic behavior of soil-sizes material such as daily cover soil for the case of hydration. The cover soil may be hydrated as a result of infiltrated precipitation and the inflow of surface water. The daily cover soil is commonly used in modern waste landfills. Thus, it is

Table 5.4 Summary of Initial Material Characteristics of Small-Diameter Hydrated MSW Specimens for Fixed-Free (Fx-Fr) RCTS Tests for 100 % Soil-Size Material Group

Waste Type	RC Type	Specimen ID	Height, inch(cm)	Diameter, inch(cm)	Total Unit Weight, γ_t, pcf(kN/m^3)	Water Content, (%)
Old (A3)	Fx-Fr	MSW1OHS1	5.80(14.7)	2.78(7.1)	100.4(15.8)	30.1
		MSW2OHS1	5.65(14.4)	2.77(7.0)	97.7(15.3)	27.0
		MSW3OHS1	5.54(14.1)	2.76(7.0)	103.5(16.3)	28.0
Fresh (C6)	Fx-Fr	MSW1FHS1	5.53(14.1)	2.84(7.2)	104.9(16.5)	26.5

Notes:

H in the specimen ID denotes a hydrated condition

1 at the end of specimen ID denotes specimen reconstituted with material passed the 3/8-in. (9.5-mm) sieve

expected that the presence of daily cover soil plays an important role in the seismic response analysis of landfills subjected to earthquake events. As a result, the RCTS tests performed on hydrated specimens would increase our knowledge and understanding of the mechanical behavior of soil-size material used at MSW landfills.

5.3 PREPARATION OF LARGE-DIAMETER (6.0- IN. (152.4-MM)) SPECIMEN

5.3.1 Specimen Reconstitution with Soil-Size Material at Its Natural Condition

A total of 7 specimens were reconstituted for dynamic measurements with the LSRC device of only soil-size materials of the A3 and C6 Groups that passed the 3/8-in. (9.5-mm) and ¾-in. (19.1-mm) sieves. The waste material (less than ¾-in. (19.1-mm)) used for large-diameter specimens contains more fibrous components, which included small pieces of soft plastics, woods, and gravels, than the small-diameter samples. For the purpose of comparison, the soil-size materials are shown together in Figure 5.4.

A 6.0-in. (152.4-mm) diameter split mold and hammer were built to produce the same energy per hammer area (0.765 Joules/cm^2) as need to compact the small-diameter specimens. The split mold and compaction hammer are made of stainless steel and are shown in Figure 5.5. For large-diameter specimens, the collar on top of the split mold was added to increase the stiffness at the opening the mold when using the larger compaction hammer. The weight of the compaction hammer and drop height were 7.30 lb (3.30 kg) and 1.97 ft (0.6 m), respectively. As shown in Figure 5.5, the base plate of drop weight was made larger than the compaction hammer to minimize membrane punctures during the compaction process. The compaction process was identical to the procedure previously described for the small-diameter specimens.

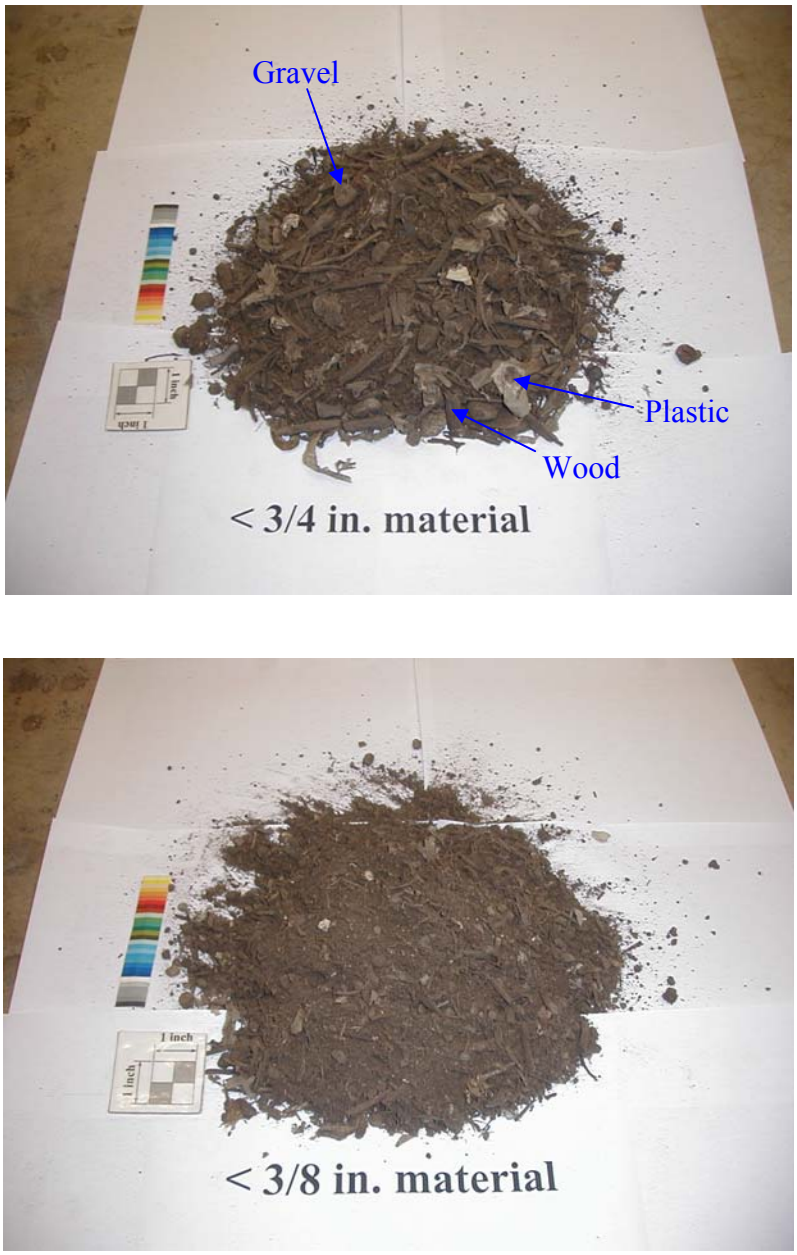

Figure 5.4 Comparison of Soil-Sizes Materials Passing the (a) ¾-in. (19.1-mm) and (b) 3/8-in. (9.5-mm) Sieves Used for Specimen Construction

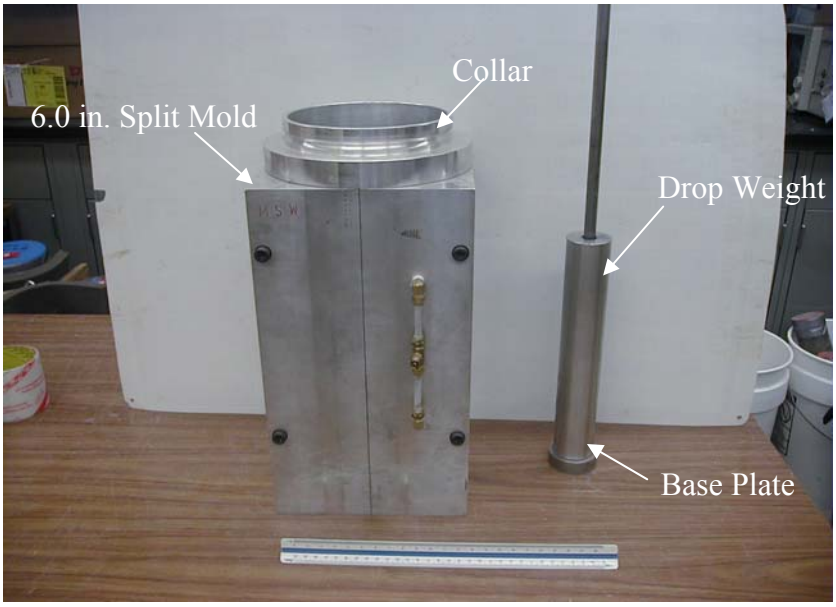

Figure 5.5 Split Mold and Compaction Hammer for Construction of Large-Diameter Specimens Used in the LSRC Tests

The waste material was taken from three different spots within the plastic bag containing the MSW material to obtain a representative water content. In some cases, water was added to maintain the in-situ water content for subsequent specimen constructions. The initial characteristics of reconstituted MSW specimens are summarized in Table 5.5. As shown in Table 5.5, each specimen is identified with a number at the end of its name. For instance, MSW2ONL2 refers to the second large-diameter specimen constructed with material that passed the ¾-in. (19.1-mm) sieve whereas MSW4ONL1 indicates the fourth large-diameter specimen with material that passed 3/8-in. (9.5-mm) sieve.

Each specimen was constructed with a target density of 82.6 pcf (13 kN/m^3) at their natural water content and compacted in six layers with the pattern shown in Figure 5.2, resulting in final height of each lift of 0.17 ft (0.051 m). A different compaction effort was made for fresh and old wastes specimens. Fresh waste specimens required 9

Table 5.5 Summary of the Initial Material Characteristics of Large-Diameter MSW Specimens for Free-Free (Fr-Fr) LSRC Tests for 100 % Soil-Size Material Group

Waste Type	RC Type	Specimen ID	Height, inch(cm)	Diameter, inch(cm)	Total Unit Weight, γ_t, pcf(kN/m^3)	Water Content, (%)
Old (A3)	Fr – Fr	MSW2ONL2	13.39(34.0)	6.07(15.4)	72.6(11.4)	14.4
		MSW4ONL1	11.84(30.1)	6.03(15.3)	84.1(13.2)	12.3
		MSW7ONL2	9.95(25.3)	5.54(14.1)	66.9(10.5)	15.3
Fresh (C6)	Fr – Fr	MSW1FNL2	11.63(29.5)	6.02(15.3)	86.4(13.6)	14.2
		MSW3FNL2	11.33(28.8)	5.93(15.1)	80.8(12.7)	13.0
		MSW5FNL2	12.14(30.8)	6.04(15.3)	84.5(13.3)	12.6
		MSW9FNL1	11.73(29.8)	6.06(15.4)	86.2(13.5)	14.4

Notes:

1 at the end of specimen ID denotes specimen reconstituted with material passed the 3/8-in. (9.5-mm) sieve

2 at the end of specimen ID denotes specimen reconstituted with material passed the ¾-in. (19.1-mm) sieve

blows per layer whereas MSW2ONL2 needed three sets of 9 blows per layer and MSW4ONL1 needed two sets of 9 blows per layer. The top of the layer was scarified with a thin, sharp steel rod to enhance the interface connection between layers before the next layer was placed. After completion of specimen reconstitution, the top of the specimen was made level by using additional material that passed the 3/8-in. (9.5-mm) sieve opening.

Finally, the specimen was carried to the laboratory because the compaction process was performed in the basement of Cockrell Hall and positioned on the testing table. The dimensions were measured before applying a vacuum pressure. Additional membranes were put onto the specimen to ensure that possible membrane punctures caused by the compaction effort would not affect the test.

5.3.2 Specimen Reconstitution with Larger Particles at Its Natural Condition

A total of 13 specimens were constructed using the old and fresh soil-size materials plus a mixture of larger particles. The larger particles included paper, soft plastic, wood, and gravel. The larger particles were cut into small pieces for the sample preparation. As described in American Standard Testing Materials (ASTM) D4015-92, the largest particle size should be smaller than one sixth of the specimen diameter for specimens having a diameter of 2.8-in. (71.1-mm) or larger. The diameter of the specimens to be tested was 6.0-in. (152.4-mm) such that a factor of eight was applied to the wood and gravel with a maximum particle size of 0.75-in. (19.1-mm) and a factor of four was applied to the soft plastic and paper with a maximum particle size of 1.5-in. (38.1-mm). It should be noted that the smaller factor for soft plastic and paper as compared to the wood and gravel was employed to take the more a fibrous aspect of soft plastic and paper into consideration. Four different ratios of soil-size material to large

particles (i.e., 100 %, 76 %, 62 %, and 14 %) were adopted to investigate the influence of the different weight percentages. These ratios were quantified in terms of percentage by weight of the soil-sizes material from samples retrieved in-situ. Table 5.6 shows the weight percentages of each component used in the sample construction for the different groups.

Table 5.6 Weight Percentages of Each Constituent Used to Construct Specimens in the Different Percentage Groups

Components	100 % Group	76 % Group	62 % Group	14 % Group
<¾-in. (19.1-mm)	100	75.9	62.1	13.7
Paper	0.0	12.9	14.0	56.3
Soft Plastic	0.0	3.7	2.7	5.0
Wood	0.0	7.4	11.2	13.1
Gravel	0.0	0.0	10.0	11.9

It should be noted that the measurements of water content for the specimens with larger particles is somewhat different than for 100 % soil-size MSW specimens. The water content measurements for specimens with larger particles consisted of two parts: (1) soil-size material and (2) larger particles. For water content measurements, a total of 6 containers were used. Three were for soil-size material and the others were for larger particles. Once the water content measurements of each part were obtained, average water content for the specimen were computed in accordance with the weight percentages as shown in Table 5.6. For example, Specimen MSW5ONL4 was made with the weight percentages of the soil-size material and larger particles equal to 62.1 % and 37.9 %,

respectively. Therefore, a factor of 0.621 was multiplied by the water content measurements for the soil-sizes material and a factor of 0.379 was assigned to the water content measurements for the larger particles, resulting in representative water content of 12.5 % (0.621×13.8 % + 0.379×10.3 % = 12.5 %).

Each larger component, e.g., paper, soft plastic, wood, and gravel, used for specimen construction is shown in Figure 5.6. The initial characteristics of the reconstituted specimens with larger particles are given in Table 5.7. Each specimen of 62 % and 76 % groups was constructed with a target density of 63.7 pcf (10 kN/m^3) at their natural conditions and compacted in six layers using the pattern shown in Figure 5.2. It should be noted that with a substantial amount of paper for the specimen of 14 % Group shown in Table 5.6, the larger particle, paper, of old and fresh waste were mixed together. Other lager particles such as soft plastic, wood, and gravel of old waste were used to construct the specimen. Since the specimen was mixed, the character "M" is present in the name of specimen ID in 14 % Group.

Each specimen, as shown in Table 5.7, is identified with a number at the end of its name. The number "3" at the end of the specimen ID represents that a specimen was made with the weight percentages, as shown in Table 5.6, in the 76 % Group. The number "4" at the end of the specimen ID indicates that a specimen was made with the weight percentages in the 62 % and 14 % Groups in Table 5.6. The difference between nomenclatures lies in the existence of gravel in the specimen; the number "3" does not include gravel, whereas the number "4" include gravel.

Compared to the density of the specimens reconstituted only with soil-size material whose density was equal to 82.8 pcf (13 kN/m^3), the target density with the larger-particle specimen for the 62 % and 76 % Groups was reduced to 63.7 pcf (10 kN/m^3). This reduced target density was used because paper and soft plastic occupies

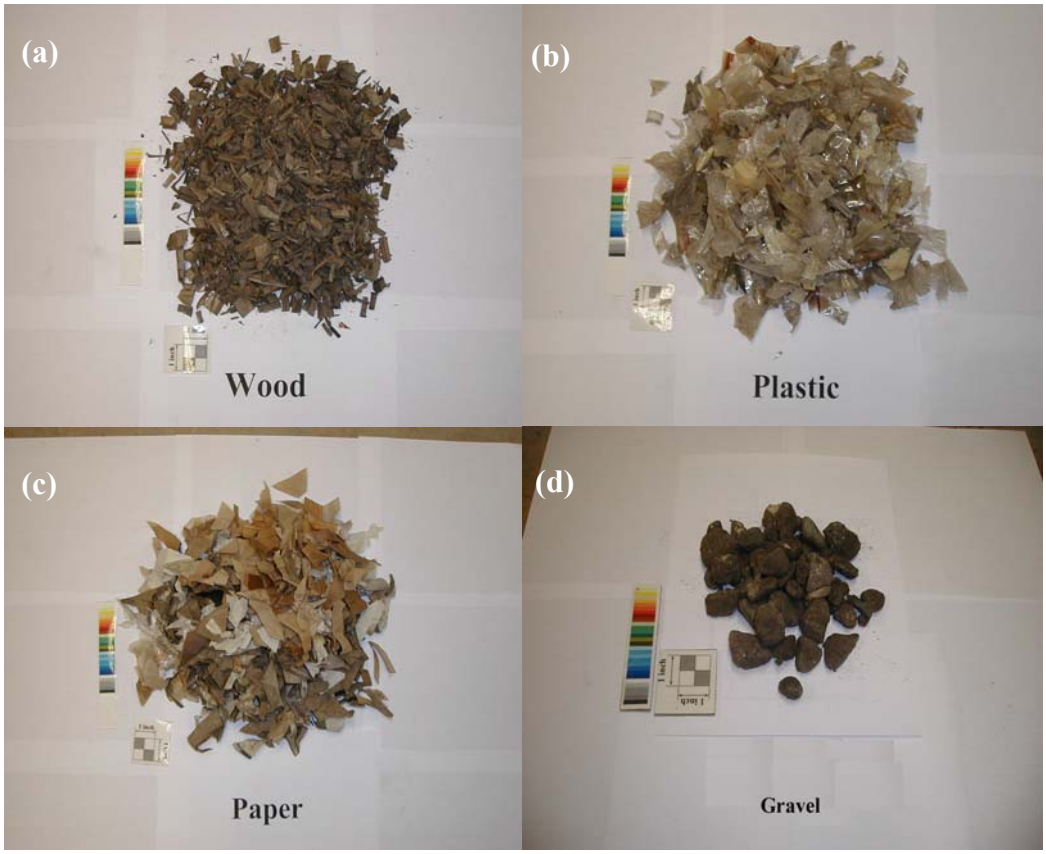

Figure 5.6 Larger Particle Components Used for the Construction of Large-Diameter Specimens: (a) Wood, (b) Soft Plastic, (c) Paper, and (d) Gravel

such a substantial volume in the specimen that it was difficult to reach the previous target density of 82.8 pcf (13 kN/m^3) despite an increase in compaction effort. Likewise, each specimen of 14 % Group was constructed with an even lower target density of 44.6 pcf (7 kN/m^3) at their natural conditions due to substantial amount of paper and compacted in six layers using the pattern shown in Figure 5.2.

Table 5.7 Summary of the Initial Material Characteristics of Large-Diameter MSW Specimens Reconstituted with Larger Particles for Free-Free (Fr-Fr) LSRC Tests for 62 to 76 % Soil-Size Material Groups

Waste Type	RC Type	Specimen ID	Height, inch(cm)	Diameter, inch(cm)	Total Unit Weight, γ_t, pcf(kN/m^3)	Water Content, (%)
Old (A3)	Fr-Fr	MSW1ONL3	13.47(34.2)	5.95(15.1)	58.4(9.2)	15.0
		MSW3ONL4	13.90(35.3)	6.05(15.4)	55.9(8.8)	7.38
		MSW5ONL4	13.18(33.5)	6.04(15.3)	58.9(9.3)	12.5
		MSW6ONL4	12.91(32.8)	6.05(15.4)	59.7(9.4)	12.8
		MSW8ONL4	13.10(33.3)	6.07(15.4)	59.1(9.3)	15.6
		MSW9ONL3	13.18(33.5)	6.11(15.5)	57.2(9.0)	14.3
Fresh (C6)	Fr-Fr	MSW2FNL4	12.18(30.9)	6.57(16.7)	53.2(8.4)	12.7
		MSW4FNL3	12.20(31.0)	6.12(15.5)	62.2(9.8)	12.7
		MSW6FNL4	12.28(31.2)	6.07(15.4)	62.8(9.9)	15.9
		MSW7FNL3	12.41(31.5)	6.06(15.4)	61.0(9.6)	12.0
		MSW8FNL4	12.30(31.2)	6.07(15.4)	62.2(9.8)	13.7
Mixed	Fr-Fr	MSW1MNL4	12.78(32.5)	6.08(15.5)	40.7(6.4)	10.7
		MSW2MNL4	12.60(32.0)	6.07(15.4)	43.0(6.8)	12.1

Notes:

3 in the specimen ID denotes a specimen reconstituted with paper, soft plastic, and wood

4 in the specimen ID denotes a specimen reconstituted with paper, soft plastic, wood, and gravel

The number of hammer blows per layer is tabulated in Table 5.8. This table indicates that the old waste specimens were reconstituted with much greater compaction efforts than fresh waste specimens for a single layer. This difference may be attributed to a different state of degradation of the old and fresh wastes.

After the specimen reconstitution was completed, the top of the specimen was made level using a soil-sizes material that passed the 3/8-in. (9.5-mm) sieve. A top cap, with vacuum grease along the side, was placed on the top of the specimen. Finally, the specimen was carried to the laboratory because the compaction process was performed in the basement of Cockrell Hall and was positioned on the testing table.

Table 5.8 Number of Blows per Layer for the Large-Diameter Specimens Constructed with Larger Particles for Old, Fresh, and Mixed MSW Specimens for 62 to 76 % Soil-Size Material Groups

Waste Type	Specimen ID	Number of Blows (per layer)	Remarks
Old (A3)	MSW1ONL3	270	
	MSW3ONL4	90	
	MSW5ONL4	135	
	MSW6ONL4	90	
	MSW8ONL4	45	
	MSW9ONL3	27	
Fresh (C6)	MSW2FNL4	45	1^{st} and 6^{th}: 90 blows
	MSW4FNL3	27	
	MSW6FNL4	27	
	MSW7FNL3	27	5^{th} and 6^{th}: 9 blows
	MSW8FNL3	27	5^{th} and 6^{th}:18 and 9 blows
Mixed	MSW1MNL4	27	
	MSW2MNL4	27	

The dimensions were measured before applying a vacuum pressure (about 6 psi

(41.4 kPa)). Additional membranes were placed around the specimen to ensure that possible membrane punctures caused by the compaction effort and protruding large particles would not cause leakage.

5.5 SUMMARY

A sample preparation procedure was determined for static and dynamic laboratory tests by the agreement of the faculty members and professional engineer involved in this project. On the basis of this established procedure, split molds and compaction hammers for specimen construction were built. The small- (2.8-in. (71.1-mm)) and large- (6.0-in. (152.4-mm)) diameter old and fresh waste specimens were reconstituted with the pattern as presented in Figure 5.2 for the laboratory tests using the combined RCTS and LSRC devices.

Most small-diameter specimens, which were constructed of materials that passed the 3/8-in. (9.5-mm) and ¾-in. (19.1-mm) sieves, were compacted at their natural conditions. The specimens, which have a lower unit weight, were also constructed by simply placing the material into the mold in order to investigate the effect of unit weight only for the 100 % group. Additional water was added to hydrate the specimens to examine the effect of water on the dynamic properties for 2.8-in. (71.1-mm) diameter soil-size specimen in RC tests (see Figure 5.3).

In the case of large-diameter specimens, the specimens were constructed at their natural conditions by two different procedures. The first was to reconstitute specimens with only soil-sizes material that passed the 3/8-in. (9.5-mm) and ¾-in. (19.1-mm) sieves as shown in Table 5.6 for the 100 % Group. The other reconstitute specimens were constructed with a mixture of materials (soil-size and refuse) which had different weight percentages of soil-size material as shown in Table 5.6 for the 76 %, 62 %, and 14 %

Groups. The water content measurements on the specimens reconstituted with larger particles was different in that the water contents obtained from the soil-size material plus larger particles was calculated by multiplying the factors of weigh percentages of soil-size material and remaining percentage from 100 % for the refuse materials.

CHAPTER 6: Small-Strain Dynamic Properties of Old MSW

6.1 INTRODUCTION

A series of RCTS and LSRC tests were performed on 2.8-in. (71.1-mm) and 6.0-in. (152.4-mm) diameter specimens to investigate the dynamic properties of old MSW in the small-strain range. The small-strain range is defined as shearing strains less than 0.002 %, which is typically called the linear range. The dynamic properties in the small-strain range are expressed in terms of low-amplitude shear modulus (G_{max}) and low-amplitude material damping ratio (D_{min}). The largest shearing strain at which the material being tested remains linear is called the elastic threshold shearing strain, γ_t^e. At shearing strains less than γ_t^e, the response of soil specimens, i.e., the stress-strain relationship, under cyclic and dynamic excitations is linear. However the response is elastic because a small amount of energy dissipates during each cycle of loading even at these small strain levels. As a result, the dynamic properties are constant and independent of strain amplitude but the damping ratio does not equal zero.

Test parameters affecting the dynamic properties of old waste in the small-strain range are investigated in this chapter. These parameters include: (1) duration of confinement, t, (2) total isotropic confining pressure, σ_o, (3) excitation frequency, f, and (4) specimen size. However, material parameters that affect the dynamic properties of old waste in the small-strain range are the main focus of this study. These parameters, which are also investigated in this chapter, are: (1) waste composition, (2) water content, (3) variation in total unit weight for the same material type, and (4) particle size. The test results from the measurements are discussed and compared below. In addition, the estimated total unit weights obtained throughout these tests for old and mixed waste are

compared with those determined in the field by other researchers.

6.2 TEST PROCEDURES

6.2.1 Testing with the RCTS Device

Low-amplitude RC tests (also denoted as LARC tests) were performed with small-diameter specimens at their natural water content (referred to natural condition) and at a hydrated condition. The hydrated condition was created by filling the specimen with water and then allowing drainage during testing. Testing was performed over a series of confining pressures, as given in Table 6.1. The level of shearing strain during the RC tests was kept less than 0.002 % to ensure small-strain measurements. Each specimen was confined under each specified confining pressure for at least one day and then advanced to the next confining pressure. In this way, stage loading was conducted as illustrated in Figure 6.1. At each confining pressure denoted by the symbol, *, only LARC tests were performed. At a given confining pressure represented by the symbol, **, both LARC and high-amplitude RCTS tests were performed. The test procedure for the high-amplitude RCTS test is discussed in Chapter 10. The confinement sequence was separated into two stages: loading and unloading stages. All measurements followed this loading pattern: first, the specimens were tested up to 40 psi (276 kPa) or 60 psi (414 kPa), and then testing was performed on an unloading sequence.

It should be noted that as part of the collaborative research project, a significant amount of testing was performed at a confining pressure of 11 psi (76 kPa) in order to compare test results obtained from the RCTS and LSRC devices with cyclic triaxial tests performed at UCB. In particular, Specimen MSW2OHS1 remained under a confining pressure of 40 psi (276 kPa) for a week to investigate the long-term time effect (Afifi and Woods, 1971, Stokoe and Lodde, 1978, Anderson and Stokoe, 1978). Three cycles of

Table 6.1 Isotropic Confining Pressures Used in Low-Amplitude RC Tests of Small-Diameter, 100 % Soil-Size Old Waste Specimens in the RCTS Device

Specimen ID	Isotropic Confining Pressure
	Low-Amplitude RC Tests, psi (kPa)
MSW1ONS1$^{\Delta}$	3.6, 7.5, 11, 15, 30, 60, 11*, 3.6* (25, 52, 76, 103, 207, 414, 76, 25)
MSW1OHS1	3.6, 7.5, 11, 15, 30, 60, 11*, 3.6* (25, 52, 76, 103, 207, 414, 76, 25)
MSW2ONS1	1.2, 2.5, 5, 11, 20, 40, 11*, 2.5* (8, 17, 34, 76, 138, 276, 76, 17)
MSW2OHS1	1.2, 2.5, 5, 11, 20, 40, 11*, 2.5*, 40†, 11*, 40†,80† , 11*, 2.5* (8, 17, 34, 76, 138, 276, 76, 17, 276, 76, 276, 552, 76, 17)
MSW3ONS1	1.2, 2.5, 5, 2.5*, 5†, 11†, 20†, 40†, 11*, 2.5*, 11†, 40†, 80†, 11*, 2.5* (8, 17, 34, 17, 34, 76, 138, 276, 76, 17, 76, 276, 552, 76, 17)
MSW3ONS1(2)$^{\Diamond}$	1.2†, 2.5†, 5†, 11†, 20†, 40†, 80†, 20*, 5*, 1.2*, 11† (8, 17, 34, 76, 138, 276, 552, 138, 34, 8, 76)
MSW3OHS1	1.2, 2.5, 5, 11, 20, 40, 80, 20*, 5*, 1.2*, 11† (8, 17, 34, 76, 138, 276, 552, 138, 34, 8, 76)
MSW4ONS2$^{\Delta}$	1.2, 2.5, 5, 11, 20, 40, 11*, 2.5* (8, 17, 34, 76, 138, 276, 76, 17)
MSW5ONS1	5, 11, 40 (34, 76, 276)
MSW6ONS2	2.5, 5, 11, 20, 40 (17, 34, 76, 138, 276)

Notes:

* denotes unloading stage

† denotes reloading stage

Δ1 at the end of the specimen ID denotes a specimen reconstituted with material passed the 3/8-in. (9.5-mm) sieve

⌂2 at the end of the specimen ID denotes a specimen reconstituted with material passed the ¾-in. (19.1-mm) sieve in the specimen ID

◊(2) at the end of the specimen ID denotes a re-testing of Specimen MSW3ONS1 but with a confinement time of 60 min. at each σ_o

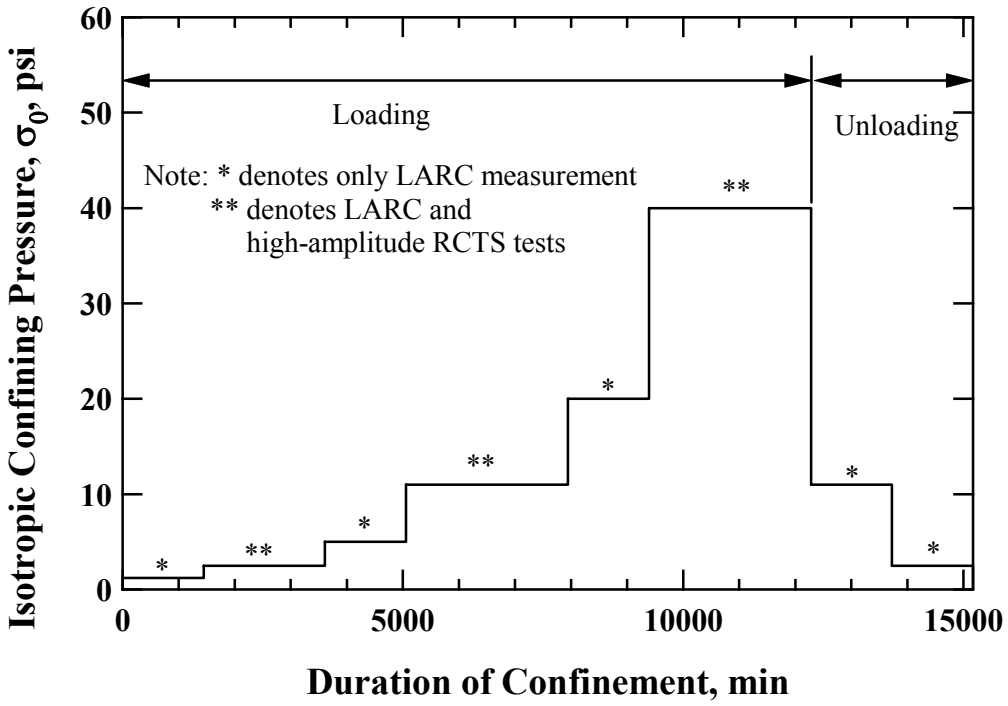

Figure 6.1 Stage Loading Sequence Showing the Variation in Isotropic Confining Pressure with Duration of Confinement in the RC Measurements

loading and unloading stages were repeated to examine the effects of stress history and overconsolidation on G_{max} and D_{min} with Specimen MSW3ONS1. To study the effect of unit weight for the same material type, Specimens MSW5ONS1 and MSW6ONS2 were prepared.

It should be noted that the RCTS device is employed to investigate the effect of test and material parameters with small-diameter specimens in the small-strain ranges. These test parameters include: (1) duration of confinement, (2) total isotropic confining pressure, (3) excitation frequency, and (4) specimen size. Material parameters investigated with the RCTS device are: (1) waste composition (only for 100 % soil-size MSW material), (2) water content, (3) total unit weight, and (4) particle size.

6.2.2 Testing with the LSRC Device

Similar to tests with the RCTS device, LARC tests were performed with large-diameter specimens reconstituted at their natural conditions. Testing was performed at multiple confining pressures, as specified in Table 6.2. The level of shearing strain during the RC tests was kept below 0.001 % to ensure small-strain measurements. Like the RCTS tests, each specimen was confined under each specified confining pressure for at least one day and then advanced to the next confining pressure, as illustrated in Figure 6.1.

The confinement sequences were separated into two stages: loading and unloading stages. All measurements followed this loading pattern: first, the specimens were tested up to 40 psi (276 kPa), and then testing was performed on an unloading sequence. As part of the collaborative research project, a significant amount of testing was performed at a confining pressure of 11 psi (76 kPa) in order to compare test results obtained from the RCTS and LSRC devices with the cyclic triaxial tests at UCB.

It should be noted that the hydration process was not possible in the LSRC device because the specimen and drive plate are hung by four soft springs. Therefore, it is difficult to assemble a 6.0-in. (152.4-mm) split mold around the specimen which could be needed during hydration. The effects of number of loading cycles and excitation frequency were not evaluated for the specimens with larger particles in the LSRC device since the LSRC device can not be used to perform TS tests.

It should also be noted that the LSRC was used to test larger particles than soil size. The specimens with 76 % soil-size material and 62 % soil-size material are noted in Table 6.2.

The LSRC device was employed to investigate the effect of test and material parameters with large-diameter specimens in the small-strain range. These test

Table 6.2 Isotropic Confining Pressures Used in Low-Amplitude RC Tests of Large-Diameter, Soil-Size Old Waste Specimens in the LSRC Device

Specimen ID	Weight Percentage of Soil-Size (%)	Isotropic Confining Pressure
		Low-Amplitude RC Tests, psi (kPa)
MSW1ONL3◊	76	1.2, 2.5, 5, 11, 20, 40, 11*, 2.5* (8, 17, 34, 76, 138, 276, 76, 17)
MSW2ONL2⌂	100	1.2, 2.5, 5, 11, 20, 40, 11*, 2.5* (8, 17, 34, 76, 138, 276, 76, 17)
MSW3ONL4□	62	1.2, 2.5, 5, 11, 20, 40, 11*, 2.5* (8, 17, 34, 76, 138, 276, 76, 17)
MSW4ONL1Δ	100	1.2, 2.5, 5, 11, 20, 40, 11*, 2.5* (8, 17, 34, 76, 138, 276, 76, 17)
MSW5ONL4	62	1.2, 2.5, 5, 11 (8, 17, 34, 76)
MSW6ONL4	62	1.2, 2.5, 5, 11, 20, 40, 11*, 2.5* (8, 17, 34, 76, 138, 276, 76, 17)
MSW7ONL2	100	1.2, 2.5, 5, 11, 20, 40 (8, 17, 34, 76, 138, 276)
MSW8ONL4	62	1.2, 2.5, 5, 11, 20, 40 (8, 17, 34, 76, 138, 276)
MSW9ONL3	76	2.5, 5, 11, 20, 40, 11*, 2.5* (17, 34, 76, 138, 276, 76, 17)

Notes:

* denotes unloading stage

Δ1 at the end of the specimen ID denotes a specimen reconstituted with material passed the 3/8-in. (9.5-mm) sieve

⌂2 at the end of the specimen ID denotes a specimen reconstituted with material passed the ¾-in. (19.1-mm) sieve

◊3 at the end of specimen ID denotes specimen reconstituted with paper, soft plastic, and wood

□4 at the end of specimen ID denotes specimen reconstituted with paper, soft plastic, wood, and gravel

parameters include: (1) duration of confinement, (2) total isotropic confining pressure, and (3) specimen size (in conjunction with the RCTS tests). Material parameters investigated are: (1) waste composition (all groups of the MSW material) and (2) particle size.

Finally, as discussed in Chapter 5, specimens were tested in the LSRC device with 14 % soil-size material MSW specimens. In this case, both old and fresh waste had to be mixed. These specimens are listed in Table 6.3.

Table 6.3 Isotropic Confining Pressures Used in Low-Amplitude RC Tests of Large-Diameter, Soil-Size Mixed Waste Specimens in the LSRC Device

Specimen ID	Weight Percentage of Soil-Size (%)	Isotropic Confining Pressure Low-Amplitude RC Tests, psi (kPa)
MSW1MNL4□	14	1.2, 2.5, 5, 11, 20, 40 (8, 17, 34, 76, 138, 276)
MSW2MNL4	14	1.2, 2.5, 5, 11, 20, 40 (8, 17, 34, 76, 138, 276)

Notes:

M denotes a mixed specimen

□4 denotes specimen reconstituted with paper, soft plastic, wood, and gravel in the specimen ID

6.3 TEST PARAMETERS AFFECTING G_{MAX} AND D_{MIN} OF OLD WASTE IN THE SMALL-STRAIN RANGE

6.3.1 Duration of Confinement at a Constant Pressure

To examine the effect of duration of confinement, a series of resonant column tests were conducted. The effect of duration of confinement is quite important in

laboratory RC measurements because the values of G_{max} and D_{min} normally change during confinement at a constant pressure. Since the dynamic properties vary with time of confinement, then the test results from different laboratory tests should be compared at the same confinement time under the same test conditions (e.g., drained or undrained conditions).

6.3.1.1 Change in G_{max} with Confinement Time

The effect of duration of confinement on G_{max} for Specimen MSW2ONS1 at natural water content is given in Figure 6.2. The loading sequence is represented by open symbols and the unloading sequence is denoted by solid symbols. It should be noted that the initial loading sequence can be divided into two states because of the compaction effort during specimen construction. These stages are: (1) the overconsolidated (OC) state, and (2) the normally consolidated (NC) state. Thus, the first three confining pressures (e.g., 1.2 psi (8 kPa), 2.5 psi (17 kPa), 5 psi (34 kPa)) represents the OC state and the rest of the confining pressures (e.g., 11 psi (76 kPa), 20 psi (138 kPa), 40 psi (276 kPa)) are in the NC state. It should be noted that for most cases, the change in the OC and NC states in the loading sequence is at the pressure level between 5 psi (34 kPa) and 11 psi (76 kPa). This change in stress states can be seen more easily in the log G_{max}-log σ_o relationship. A more detailed explanation is presented in Section 6.3.2.

As shown in Figure 6.2, G_{max} values increase with increasing duration of confinement as well as with increasing levels of confining pressure on the loading pressure sequence. The reason for the increase of G_{max} with duration of confinement can be considered as a combination of increasing total unit weight and continuous improvement of particle contacts under a constant state of confining pressure.

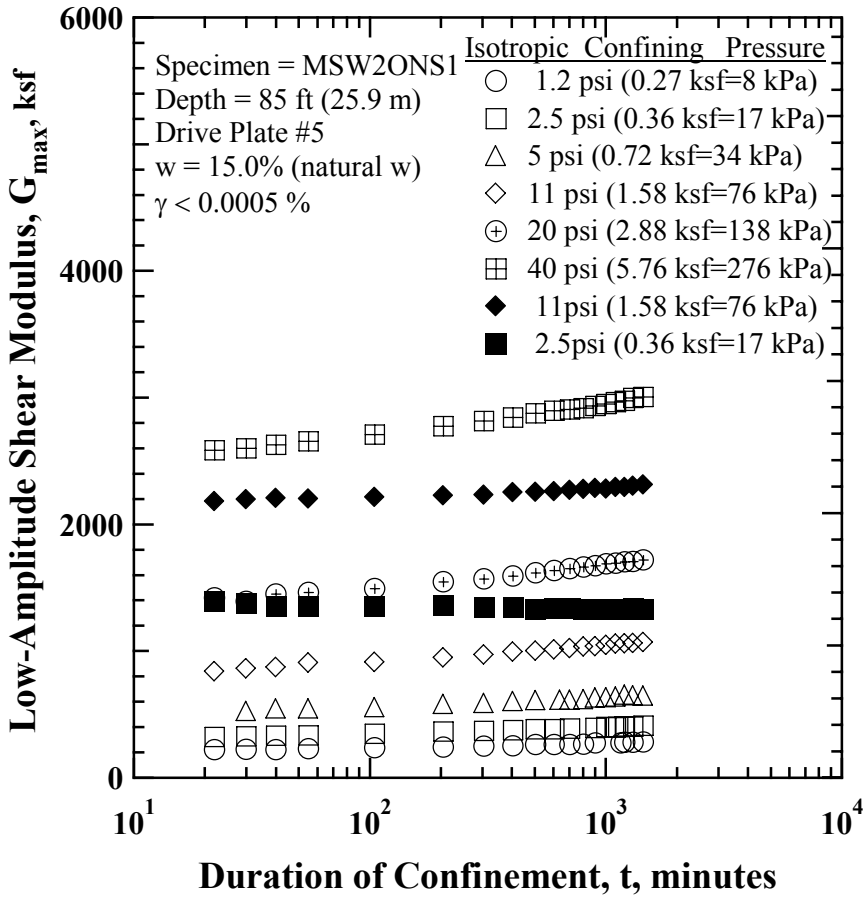

Figure 6.2 Variation in Low-Amplitude Shear Modulus with Magnitude and Duration of Confinement for Specimen MSW2ONS1 (100 % Soil-Size Material)

This increase in particle contacts is commonly referred to as creep behavior in geotechnical engineering. As the time of confinement increases under a constant pressure, the voids between the solid particles decrease and the inter-particle contacts between the solid particles increase. As a result, a specimen's resistance to shear deformation during the tests continuously increases.

Measurements of G_{max} and D_{min} of MSW during the unloading sequence are also an important feature throughout the research. Excavation of landfills is associated with stress release (similar to an unloading sequence). Thus, G_{max} measurements during the

unloading sequence are used to enhance our understanding of the response of MSW with respect to stress release. Higher G_{max} values during unloading than those during t loading at the same confining pressure show the effect of confinement time and overconsolidation. As revealed in Figure 6.2, G_{max} decreases slowly with increasing confinement time, which indicates that the specimen responds slowly to the release of confining pressures. Hence, a stress relaxation phenomenon is at work. Thus, a significant period of time is required before the specimen begins to exhibit increasing shear modulus with time at each unloading confining pressure. It is, however, expected that G_{max} values will again begin to increase with confinement of time under a constant confining pressure. However, it was not the intent of this research to confine specimens during unloading for several weeks at each unloading pressure to study the effect of time.

Stokoe and Lodde (1978) suggested two approaches to evaluate the long-term time effect in G_{max} measurements. One is a coefficient of shear modulus increase in absolute value, I_G, and is given by:

$$I_G = \frac{\Delta G}{\log_{10}(\frac{t_2}{t_1})} \tag{6.1}$$

where, ΔG represents the variation of shear modulus from time t_1 to t_2,

t_2 is longer than t_1, and

t_1 and t_2 are times after 1000 minutes (or times after primary consolidation in soils).

The other method is a normalized shear modulus increase in percent, N_G, and is expressed by:

$$N_G = \frac{I_G}{G_{1000}} \times 100\% \quad (6.2)$$

where, G_{1000} denotes the shear modulus at time of 1000 minutes.

It is worth noting that t_1 and t_2 can be any time after primary consolidation and G_{1000} can be G_{100} if primary consolidation is less than 100 minutes.

Values of the two parameters with confining pressure for Specimen MSW2ONS1 are presented in Table 6.3 (In this case, 1000 minutes was used). As shown, the values of I_G increase with increasing confining pressure, whereas the values of N_G are approximately the same regardless of confining pressure with the exception of N_G at lower confining pressures (1.2 psi (8 kPa) and 2.5 psi (17 kPa)).

Table 6.3 Summary of Coefficients of Shear Modulus Increase, I_G, and Values of a Normalized Shear Modulus Increase, N_G, for Specimen MSW2ONS1 (100 % Soil-Size Material)

Confining Pressure psi, (kPa)	I_G, ksf (MPa)	N_G, %
1.2 (8)	71.5 (3.4)	26.1
2.5 (17)	96.6 (4.6)	24.3
5 (34)	80.8 (3.9)	12.8
11 (76)	137.0 (6.6)	13.1
20 (138)	197.8 (9.5)	11.7
40 (276)	348.1 (16.7)	11.8

To investigate the long-term time effect of other groups of old MSW material, the values of N_G in the OC and NC states during the initial loading sequence were obtained using Equation (6.2). The variations in N_G with different weight percentages of soil-

size material in the OC and NC states upon loading are shown in Figures 6.3 (a) and (b), respectively.

As revealed in the figures, the values of N_G generally increase with increasing weight percentage of soil-size material in both the OC and NC states for old MSW. It is interesting to note that when comparing the values of N_G in the OC and NC states, the values of N_G in the OC state are smaller than in the NC state. Even though there appears to be considerable scatter in N_G in the NC state, for a given sample, the increase in G_{max} with duration of confinement time in the NC state is larger than in the OC state. This difference is attributed to the overconsolidation effect produced by the compaction effort. In other words, a larger change in inter-particle void space and particle contacts occurs in the NC state than in the OC state. The values of N_G generally appear to increase with increasing confining pressure regardless of material groups as well as the history of confining pressure i.e., OC and NC states, with some scatter.

For the comparison with sands and clays, typical values of N_G, suggested by Stokoe and Lodde (1978) and Ni (1987), are approximately 10 to 25 % for the San Francisco bay mud and 1 to 2 % for washed mortar sand, respectively.

6.3.1.2 Change in D_{min} with Confinement Time

Damping has been defined as a term to represent the energy dissipation of an inelastic material under cyclic loading and has been referred to as material or hysteretic damping. In general, material damping has been recognized collectively as the energy dissipation within the soil skeletal frame and water within the voids. Material damping in soils is much more complex than shear modulus. This complexity is strongly affected by the contribution to material damping of several mechanisms that one associated with energy dissipation during cyclic loading. Material damping in MSW will be studied in the same manner as done for soils.

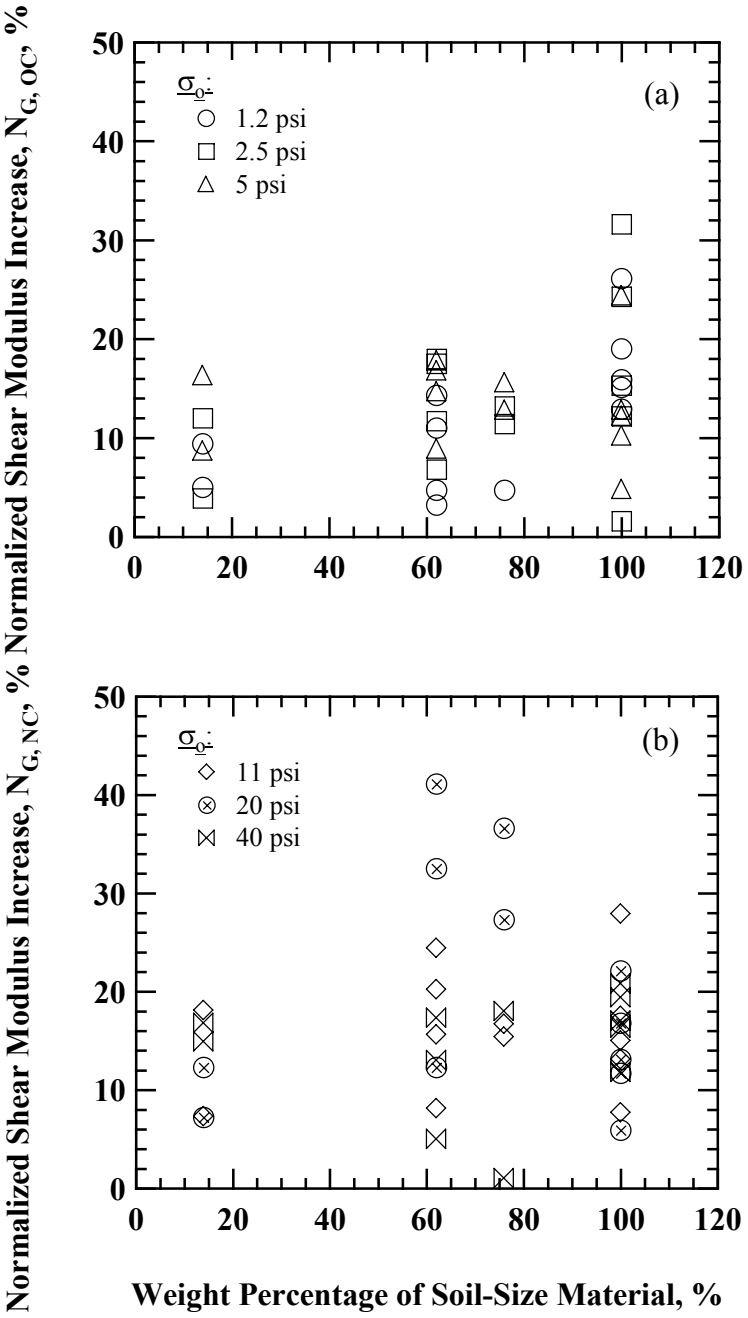

Figure 6.3 Comparison of the Variation in Normalized Shear Modulus Increase with Different Weight Percentage of Old, MSW at Their Natural Water Content in the (a) OC and (b) NC States

The effect of duration of confinement on D_{min} is presented in Figure 6.4 for Specimen MSW2ONS1 at natural water content. The values of material damping ratio were obtained using the half-power bandwidth method. In contrast to G_{max} shown in Figure 6.2, D_{min} generally decreases as duration of confinement increases. The fluctuation in D_{min} measurements might result to some extent from background noise during the damping measurements. Possible reasons for a decrease in D_{min} with duration of time may be structural changes in particle arrangement (Marcuson and Wahls, 1978) and or constrained relative movement of inter-particles (Stoll, 1989). However, the reasons have not been thoroughly researched.

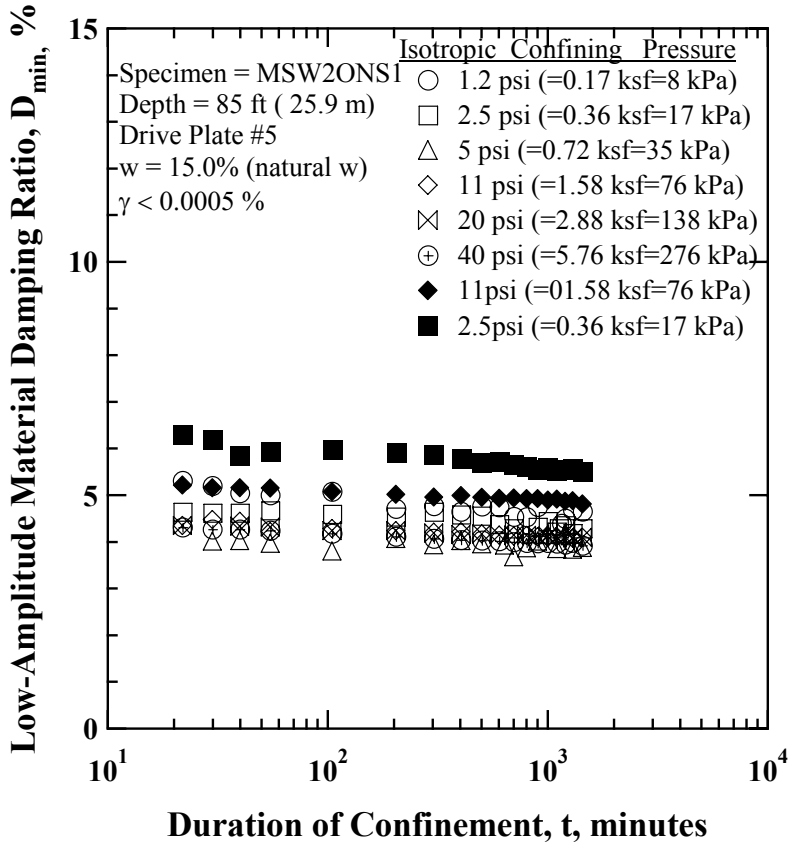

Figure 6.4 Variation in Low-Amplitude Material Damping Ratio with Magnitude and Duration of Confinement for MSW2ONS1 (100 % Soil-Size Material)

For unloading damping measurements, D_{min} increased with decreasing confining pressure. This difference may be somewhat explained by relatively more spaces for inter-particle movements during confining pressure release leading to an increase in D_{min}.

As with G_{max}, Ni (1987) suggested two approaches to evaluate the long-term time effect in the D_{min} measurements. One approach is a coefficient of material damping ratio increase in an absolute value, I_D, that is given by:

$$I_D = \frac{\Delta D}{\log_{10}(\frac{t_2}{t_1})} \tag{6.3}$$

where, ΔD represents the variation of material damping ratio from time of t_1 to t_2,

t_2 is longer than t_1, and

t_1 and t_2 are times after 1000 minutes (or times after primary consolidation in soils).

The other method is a normalized material damping ratio increase in percent, N_D, and is expressed by:

$$N_D = \frac{I_D}{D_{1000}} \times 100\% \tag{6.4}$$

where, D_{1000} denotes the material damping ratio at time of 1000 minutes.

Typical values of the two parameters, I_D and N_D, with confining pressure for Specimen MSW2ONS1 are tabulated in Table 6.4. As shown, the values of I_D show more scatter at lower confining pressures. However, at subsequent confining pressures in the NC state, the values of I_D decrease significantly (are large and become more negative). The values of N_D follow a similar trend.

Table 6.4 Summary of Values of Material Damping Ratio Increase, I_D, and Values of a Normalized Material Damping Ratio Increase, N_D, for Specimen MSW2ONS1 (100 % Soil-Size Material)

Confining Pressure psi, (kPa)	I_D, %	N_D, %
1.2 (8)	-0.56	-11.89
2.5 (17)	-0.48	-11.49
5 (34)	-0.13	-3.51
11 (76)	-0.02	-0.58
20 (138)	-0.14	-3.48
40 (276)	-0.32	-8.15

To examine the long-term time effect measured in all old MSW groups, the values of N_D were obtained using the Equation (6.4) at each confining pressure level in the loading sequence. The variations in N_D with respect to different MSW groups in the OC and NC states are shown in Figures 6.5 (a) and (b), respectively. As shown in the figures, the values of N_D show scatter, varying approximately from -20 % to 20 % in the OC state and approximately from 0 % to 20 % in the NC state. In addition, the values of N_D in the OC and NC states are approximately the same regardless of the different MSW groups. Unlike N_G, it is more difficult to find general trends of N_D with respect to confining pressure level.

For the comparison with sands, typical values of N_D, suggested by Ni (1987), vary from 5 to -10 % for washed mortar sands.

6.3.2 Total Isotropic Confining Pressure

6.3.2.1 Log G_{max} - Log σ_o Relationship

Confining pressure is a very important parameter affecting the dynamic properties of soil-

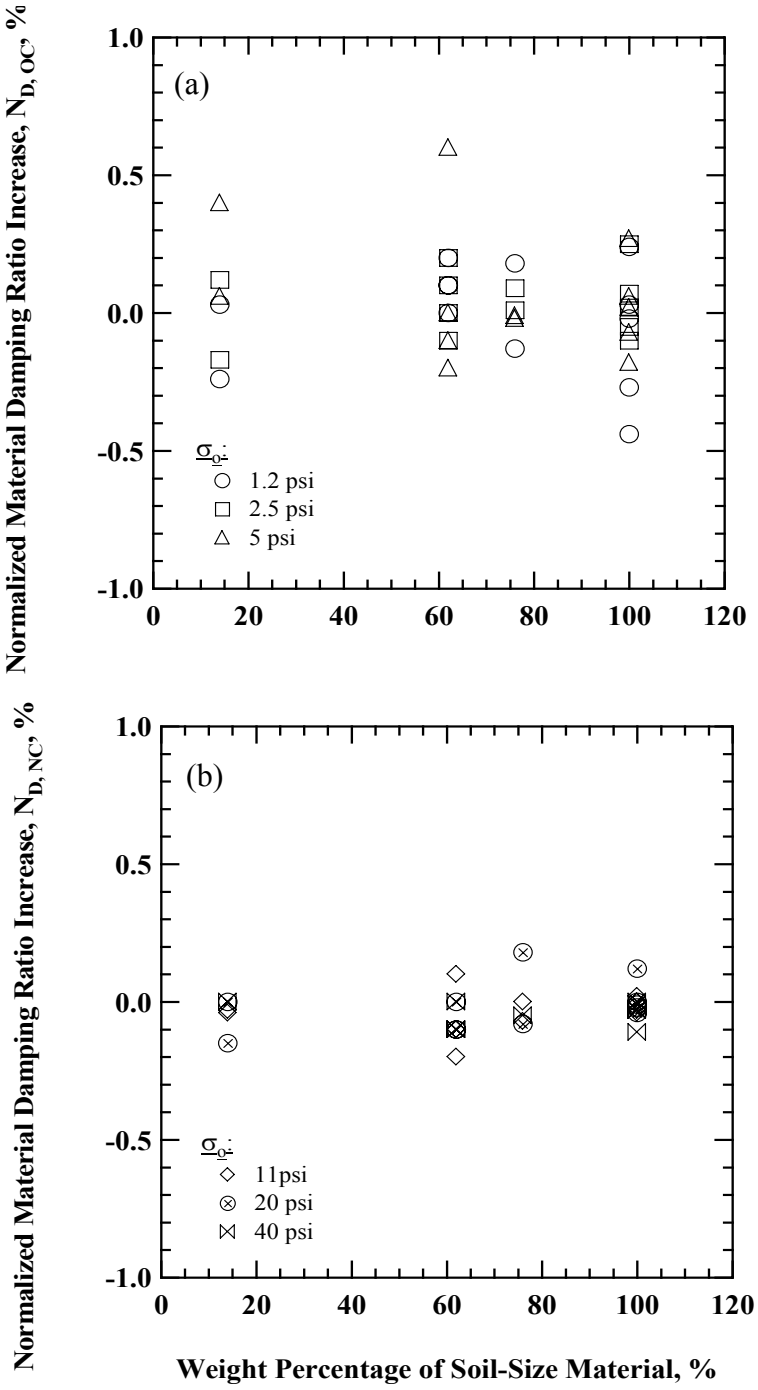

Figure 6.5 Comparison of the Variation in Normalized Material Damping Ratio Increase with Different Weight Percentage of Old, MSW in the (a) OC and (b) NC States for Old MSW

like materials in contrast to rock-like materials. MSW behaves like soil in many aspects as discussed below. The RC tests were performed at a series of total isotropic confining pressures for one day of confinement at each pressure so that the dynamic properties could be determined at a given time at each confining pressure upon loading and unloading. A typical variation in G_{max} with isotropic confining pressure for 100 % soil-size old MSW specimens is shown in Figure 6.6, with logarithmic scales for both G_{max} and σ_o. These values were obtained from the RCTS tests with 100 % soil-size MSW specimens. The loading sequence is shown by the open symbols whereas the unloading sequence is shown by the solid symbols of the same shape. Results are shown only for these waste tested at the natural water content found in the field ($w \approx 12.0$ %) (Zekkos, 2005).

As can be seen, the variations in G_{max} with isotropic confining pressure for MSW specimens are very similar in the RC measurements. At low confining pressures, that are less than about 1000 psf (48 kPa) in this material, the specimens are in the OC state due to the compaction process during reconstitution of the small-diameter specimens and vacuum pressure effect, which was used to install the specimen in the RCTS device. In addition, another OC state is observed in the unloading sequence produced by confining pressure release. The OC state is shown by the relative flat log G_{max} - log σ_o relationship. The resultant compaction pressure, σ_p, produced by compaction effort during specimen construction is provided in the figure and the σ_p is about 989 psf (47 kPa).

However, above about 1000 psf (48 kPa), the specimens become NC state as shown by the change in shape of the log G_{max}-log σ_o relationship. As illustrated in Figure 6.6, G_{max} increases significantly with increasing confining pressure because the increase in G_{max} resulted from a substantial change in inter-particle voids as well as from

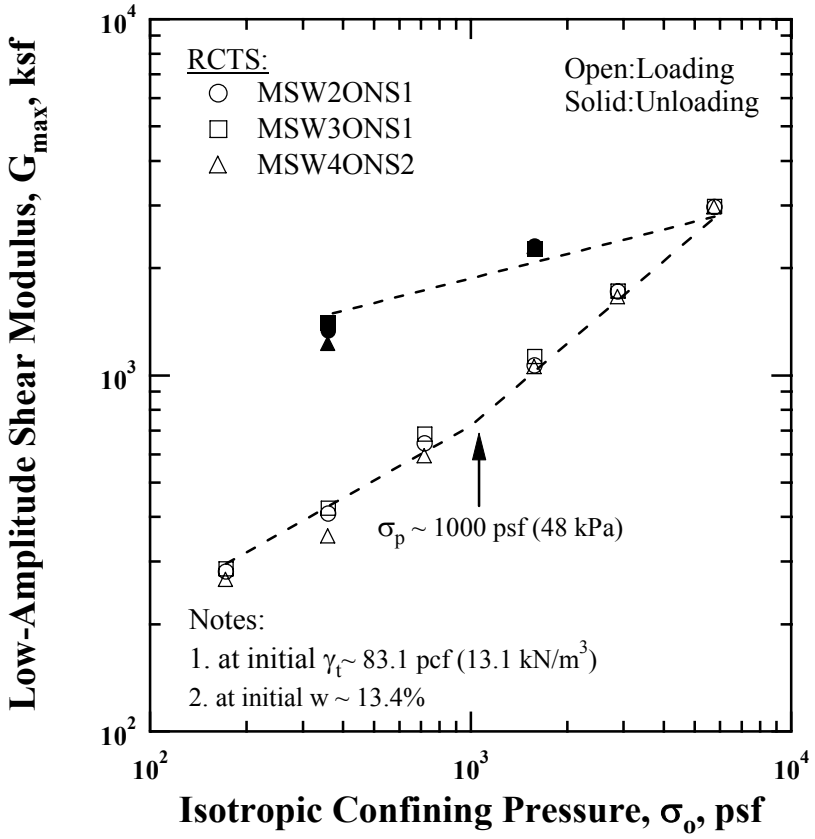

Figure 6.6 Variation in Low-Amplitude Shear Modulus with Isotropic Confining Pressure for 100 % Soil-Size Old MSW Specimens in the RCTS Device

an increase in confining pressure. It is interesting to observe that the initial slope in the OC state is larger than that of unloading sequence by a factor of an approximately two. This difference can be attributed to considerable change in voids spaces in the specimen during the initial loading sequence. Similarly, the variations in G_{max} with confining pressure measured with the LSRC device show the same trends, but more scatter exists.

The effect of confining pressure on G_{max} is expressed as a normalized confining pressure with an exponent of n_G and is given by:

$$G_{max} = G_1 \left(\frac{\sigma_O}{P_a}\right)^{n_G} \quad (6.5)$$

where, G_1 is a shear modulus corresponding to one atmosphere in psf,

σ_o is an isotropic confining pressure in the same unit as P_a,

P_a is one atmosphere (2116 psf or 100 kPa), and

n_G is a dimensionless exponent.

This equation was developed using the least-square method and was applied to the OC and NC states in the loading and unloading sequences separately. The fitted equations are presented by the dashed lines in Figure 6.6. A set of the values of G_1 and n_G generated from the above equation in the loading (OC and NC states) and unloading sequences are tabulated in Table 6.5.

To evaluate the effect of confining pressure on G_{max} of other old MSW Groups (e.g., 76%, 62%, and 14% soil-size material Groups), log G_{max} - log σ_o relationship of each group was fitted using the Equation (6.5) in the loading sequence.

Table 6.5 A Set of Exponents (n_G) and Shear Moduli at One Atmosphere (G_1) of G_{max} upon Loading and Unloading Sequences for 100 % Soil-Size Old MSW Specimens in the RCTS Device

Sequence		Exponent, n_G	Shear Modulus, G_1, ksf (MPa)
Loading	OC	0.58	1165 (56)
	NC	0.78	1350 (65)
Unloading		0.29	2305 (110)

As a result, the variation in the values of exponent, n_G, of the fitted equation in the OC and NC states is shown in Figures 6.7 (a) and 6.7 (b), respectively. As can be seen, it is hard to find general trend of the values of n_G with respect to different MSW groups. However, taking the scatter in the values of n_G into consideration, the values of n_G are approximately more constant in the OC state. This variation in the values of n_G can be attributed to the compaction effort and larger particle orientations during specimen construction. In the case of NC state, the values of n_G slightly decrease from the 100 % soil-size material Group to the 62 % soil-size material Group, but increase again at the 14 % soil-size material Group. Additionally, as shown in Figure 6.7 (b), all values of n_G are less than one, which is the exponent in the Mohr-Coulomb failure criterion for strength. In comparison with granular soils with a similar particle distribution (SW), values of n_G range around 0.50 (Hardin and Drenvich, 1972).

6.3.2.2 Log D_{min} - Log σ_o Relationship

A typical variation in D_{min} with isotropic confining pressure for the 100 % soil-size old MSW specimens is given in Figure 6.8 with logarithmic scales for both D_{min} and σ_o. These values were obtained using the RCTS devices for small-diameter specimens. Small-diameter specimens are indicated with an "S" in their name. The values of D_{min} from the RCTS device were determined by the half-power bandwidth method. The loading sequence is represented by open symbols, whereas the unloading sequence is represented by solid symbols, whose shapes are identical to loading sequence.

Figure 6.8 shows that D_{min} decreases with increasing confining pressure in the loading sequence, whereas D_{min} during the unloading sequence increases more than that determined at the identical confining pressures from the loading sequence. The reasons for change of material damping within soils have been postulated as follows: inelastic friction losses and fluid losses have been assumed to be a reasonable explanation for

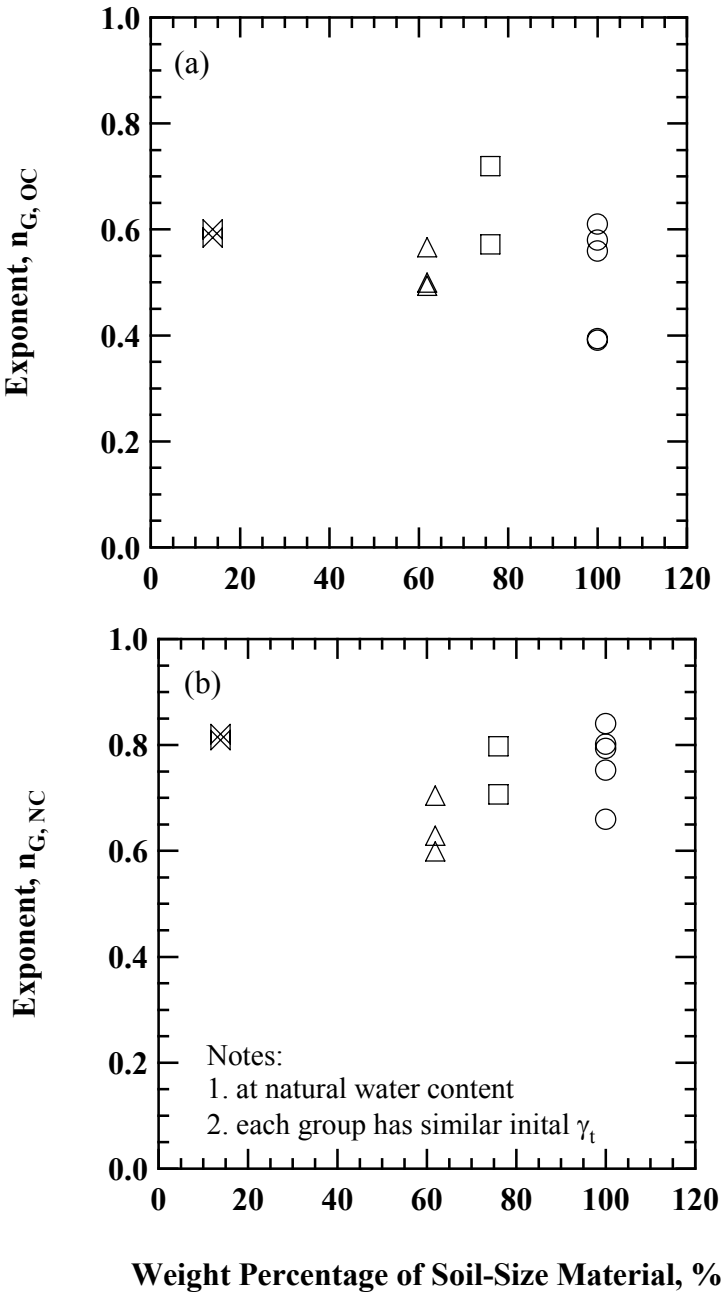

Figure 6.7 Comparison of the Variation in the Values of Exponent in the (a) OC and (b) NC States with Different Weight Percentages of Soil-Size Old MSW

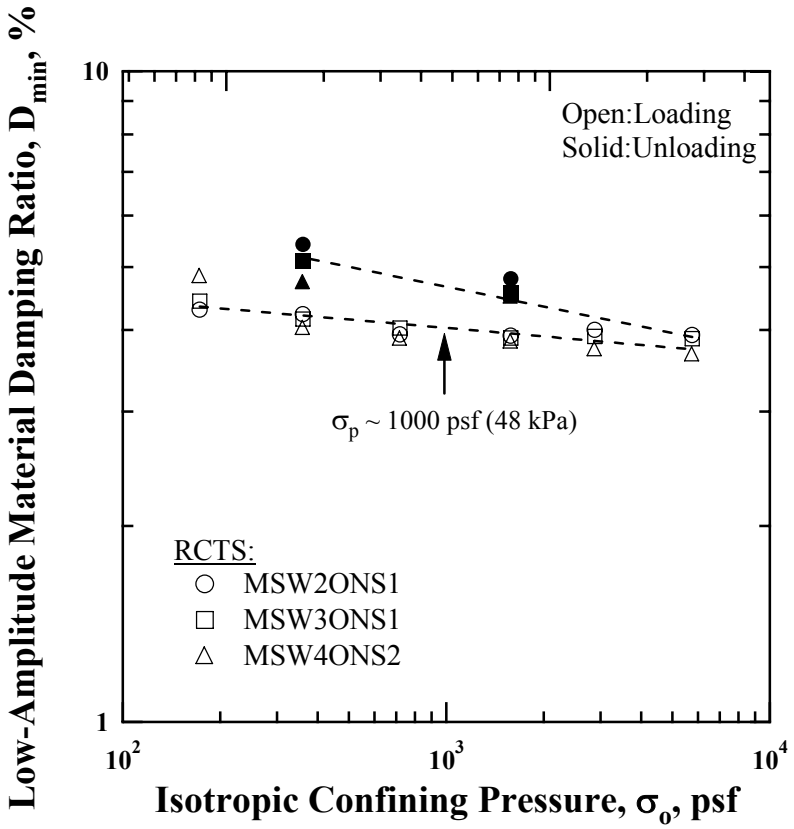

Figure 6.8 Variation in Low-Amplitude Material Damping Ratio with Isotropic Confining Pressure for 100 % Soil-Size Old MSW Specimens in the RCTS Device

material damping (White, 1983, Stoll, 1989). Inelastic friction losses are caused by a differential movement between individual soil particle and fluid flow losses are due to the relative movement between solid particles and water in the soil (Park, 1998).

Based on these assumptions, decrease in material damping in the MSW specimens can be explained as follow; as confining pressure increases, relative less movement between solid particles results in less friction losses at their contact areas so that less energy dissipation occurs, leading to a decrease in material damping in the MSW specimens. For unloading sequence, D_{min} increases with decreasing confining pressure.

Relative large movements between solid particles, produced by confining pressure release, contribute to an increase in energy dissipation in soil, producing a higher material damping. It is interesting to note that as shown in the figure, the effect of overconsolidation due to compaction effort tends to disappear in the variation in D_{min}.

The effect of confining pressure on D_{min} is expressed as a normalized confining pressure with an exponent of n_D and is given by:

$$D_{min} = D_1 \left(\frac{\sigma_O}{P_a}\right)^{n_D} \tag{6.6}$$

where, D_1 is a material damping ratio corresponding to one atmosphere in %,

σ_o is an isotropic confining pressure in the same unit as P_a,

Pa is one atmosphere (2116 psf or 100 kPa), and

n_D is a dimensionless exponent.

This equation was developed using the least-square method and applied to the loading and unloading sequences separately. The fitted equations are presented by dashed lines in Figure 6.8. A set of values of D_1 and n_D generated from the above equation in the loading and unloading sequences are tabulated in Table 6.5.

Table 6.5 A Set of Exponents (n_D) and Material Damping Ratio at One Atmosphere (D_1) of D_{min} upon Loading and Unloading Sequences for 100 % Soil-Size Old MSW Specimens in the RCTS Device

Sequence	Exponent, n_D	Material Damping Ratio, D_1, (%)
Loading	-0.04	3.90
Unloading	-0.10	4.32

To evaluate the effect of confining pressure on D_{min} of other MSW Groups (e.g., 76 %, 62 %, and 14 % soil-size material groups), log D_{min} - log σ_o relationships of each group were fitted using Equation (6.6) in the loading sequence. The variation in the values of exponent, n_D, and material damping ratio at one atmosphere, D_1, from the fitted data is shown in Figures 6.9 (a) and (b), respectively.

As shown in Figure 6.9 (a), although there is a scatter, the values of n_D generally increase with decreasing weight percentage of soil-size material of old MSW. In other words, the small-strain material damping ratio exhibits a smaller confining pressure dependency with decreasing weight percentage of soil-size material. Figure 6.9 (b) shows that the material damping ratio increases slightly when larger particles are added to the MSW specimens. As a consequence, the variation in D_{min} is less sensitive to confining pressure than G_{max}.

6.3.3 Excitation Frequency

To examine the excitation frequency effect, which is sometimes called a strain-rate effect, RC and TS tests were performed with 100 % soil-size old MSW specimens in the RCTS device. These specimens are MSW2ONS1, MSW3ONS1, MSW4ONS2, MSW5ONS1, and MSW6ONS2. The only RC tests performed with large-diameter specimens was Specimen MSW4ONL1 in the LSRC device. However, torsional shear testing can not be performed in the LSRC device. Therefore, the test results shown in this section only cover 100 % soil-size material old MSW that was tested in the RCTS device.

The variation of shear modulus with excitation frequency is shown in Figure 6.10, whose tests were performed at a confining pressure of 11 psi (76 kPa). The values of shear modulus were measured at shearing strain amplitudes of 0.0001 % and 0.001 %,

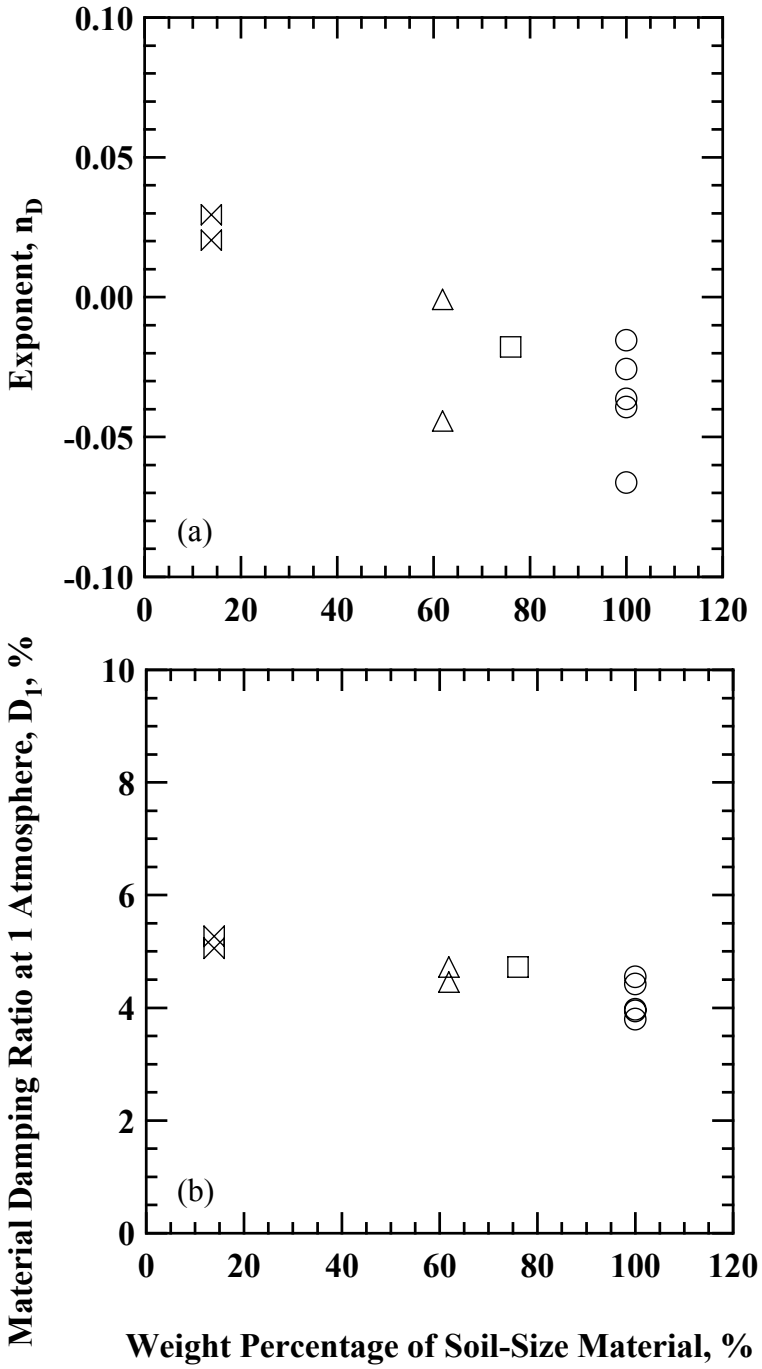

Figure 6.9 Comparison of the Values of: (a) the Exponent, n_D, and (b) Material Damping Ratio at One Atmosphere, D_1, in the Loading Sequence of Different Weight Percentages of Soil-Size Old MSW Specimens

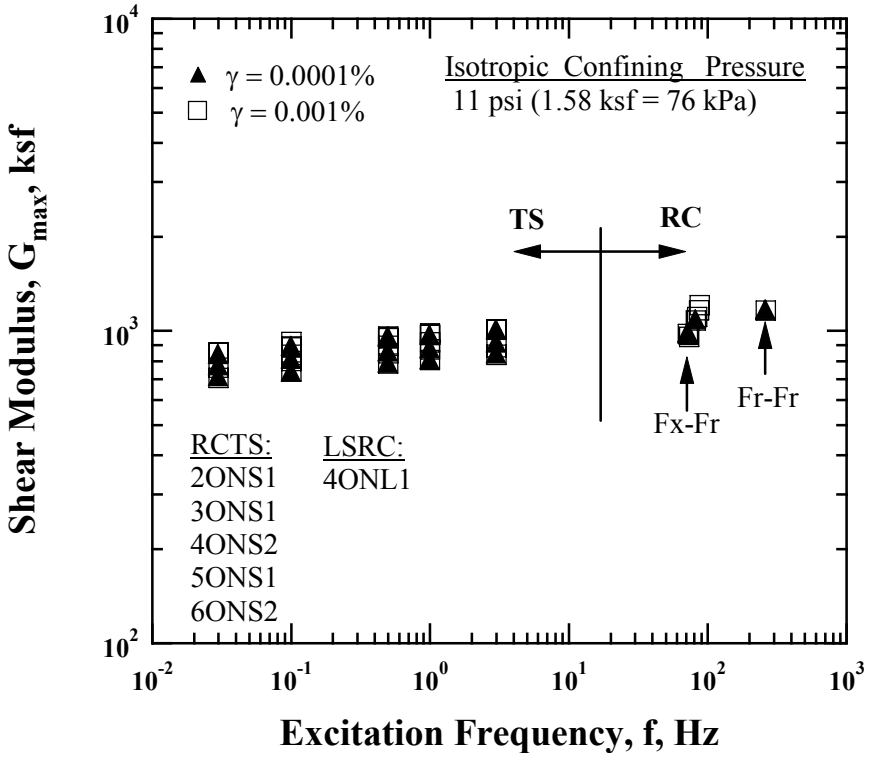

Figure 6.10 Variation in Shear Modulus with Excitation Frequency from RCTS and LSRC Tests for 100 % Soil-Size, Old MSW Specimens

in which shear modulus is equal to G_{max} and is independent of shearing strain amplitude. The values of G_{max} from the LSRC tests are shown in the figure and these are denoted by "Fr-Fr". The values of G_{max} from the RC tests obtained using the RCTS device are denoted by "Fx-Fr" in the figure.

It is obvious that the values of G_{max} increase linearly with respect to the log f of increasing excitation frequency. It is a well-known fact that a higher excitation frequency produces a larger stiffness and a higher strength for cohesive soils due to viscosity in the pores and soil skeleton system (Dobry and Vucetic, 1987, Lo Presti et al., 1996). As a result, G_{max} increases with increasing excitation frequency due to the viscosity of the MSW skeleton frame and moisture in the pore space.

To quantify the effect of excitation frequency on shear modulus at small strains, shear modulus was normalized with the shear modulus at a frequency of 1 Hz in the TS tests. This variation in normalized shear modulus, $G_{max}/G_{max,\ f=1Hz}$, is presented in Figure 6.11. The data shown in Figure 6.11 were fitted using the least-squares method and are plotted in the figure with a dashed line. This equation is expressed by:

$$\frac{G_{max}}{G_{max,\,f=1Hz}} = 0.09 \times \log(\text{Freq.}) + 1.0 \qquad (6.5)$$

where,

G_{max} is a shear modulus measured at small strains at a given frequencies, and

$G_{max,\ f=1Hz}$ is a shear modulus measured at small strains at a frequency of 1Hz

As noted earlier, the LSRC device can not be used to perform TS tests so that the shear modulus obtained from the LSRC test was normalized with the one averaged from the TS tests at a frequency of 1 Hz. Figure 6.11 indicates that normalized shear modulus increases linearly with the log f of excitation frequency. The increase in G_{max} is about 1.6 times $G_{max,\ f\ =\ 1\ Hz}$ when the excitation frequency increases by approximately four orders of magnitude, e.g., from 0.03 Hz to 260 Hz. Therefore, this is only a rather small effect of excitation frequency on shear modulus. In the collaborative research project, Zekkos (2005) performed a series of cyclic triaxial tests upon all MSW Groups (e.g., A3, C6, and C3 Groups) reconstituted with 100 % soil-size material and with soil-size material plus larger particles by changing the loading frequencies, e.g., 0.01 Hz, 0.1 Hz, 1 Hz, and 10 Hz. He obtained the same equation as UT and his test results are presented in Figure 6.12 (see Zekkos (2005) for more details). Therefore, the conclusion can be drawn that the effect of excitation frequency is the same for MSW specimens regardless

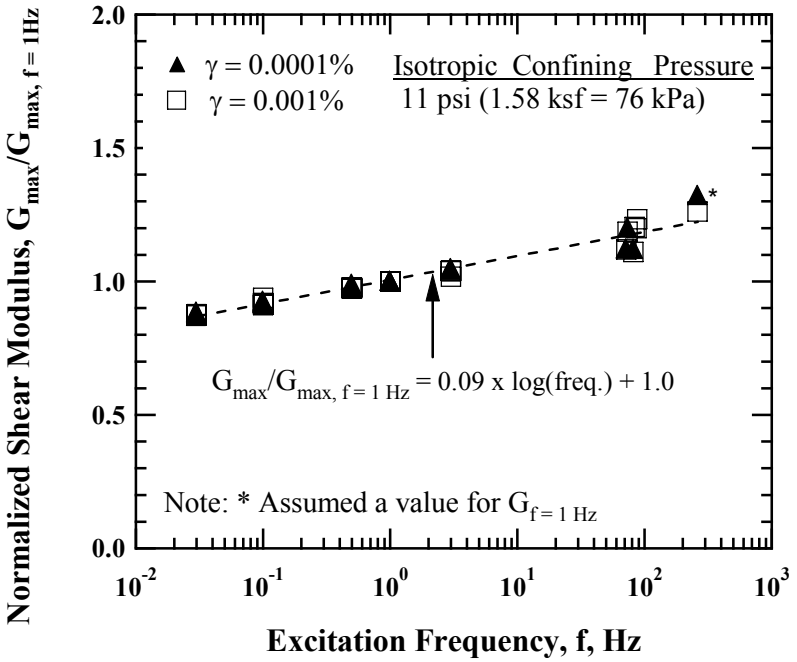

Figure 6.11 Variation in Normalized Shear Modulus with Excitation Frequency from the RCTS and LSRC Tests for 100 % Soil-Size Old MSW Specimens

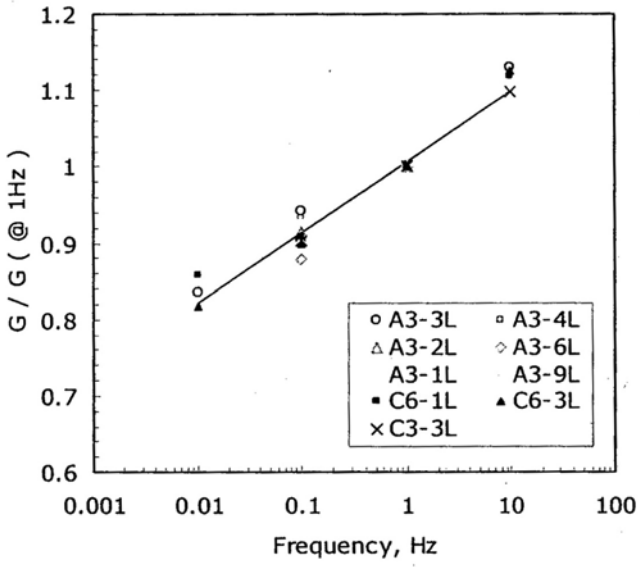

Figure 6.12 Variation in Normalized Shear Modulus with Excitation Frequency for All MSW Groups (A3, C6, and C3 Groups) Using a Cyclic Triaxial Device (from Zekkos, 2005)

of the specimen and particle sizes.

Taking the previous discussion into account, it should be pointed out that when someone wants to compare the measured shear modulus obtained from different laboratory testing devices, their operational frequencies should be taken into account, although this effect should on the order of 10 to 20 % (i.e., RC tests at 100 Hz vs. cyclic triaxial tests at 1 Hz).

As with G_{max}, material damping ratio was measured at a confining pressure of 11 psi (76 kPa) using the RCTS and LSRC devices on identical specimens listed earlier in Section 6.3.3. The variation in material damping ratio with excitation frequency is shown in Figure 6.13. Material damping measurements were made at a shearing strain amplitudes of 0.0001 % and 0.001 % so that the values of material damping ratio appear to be the same although they exhibit some scatter over the frequencies. The values of material damping ratio measured using the LSRC device are denoted by "Fr-Fr" in the figure and the values of material damping ratio measured using the RCTS device are denoted by "Fx-Fr" in the figure.

Figure 6.13 shows that the values of material damping ratio obtained at excitation frequencies below 0.5 Hz increase with decreasing excitation frequency due to creep. The explanation for this increase in material damping ratio is that the slower excitation frequency allows the sample to have more time to respond (strain) to the application of cyclic loading, resulting in larger hysteresis loops (Dobry and Vucetic, 1987). Shibuya et al. (1995) also mentioned this phenomenon, explaining that the increase in material damping ratio is a result of the shear-strain-rate-dependent nature of the stress-strain relationship.

For excitation frequencies of 0.5 Hz to 1 Hz, the material damping ratio appears to be reasonably constant as seen in Figure 6.13. This range is associated with a

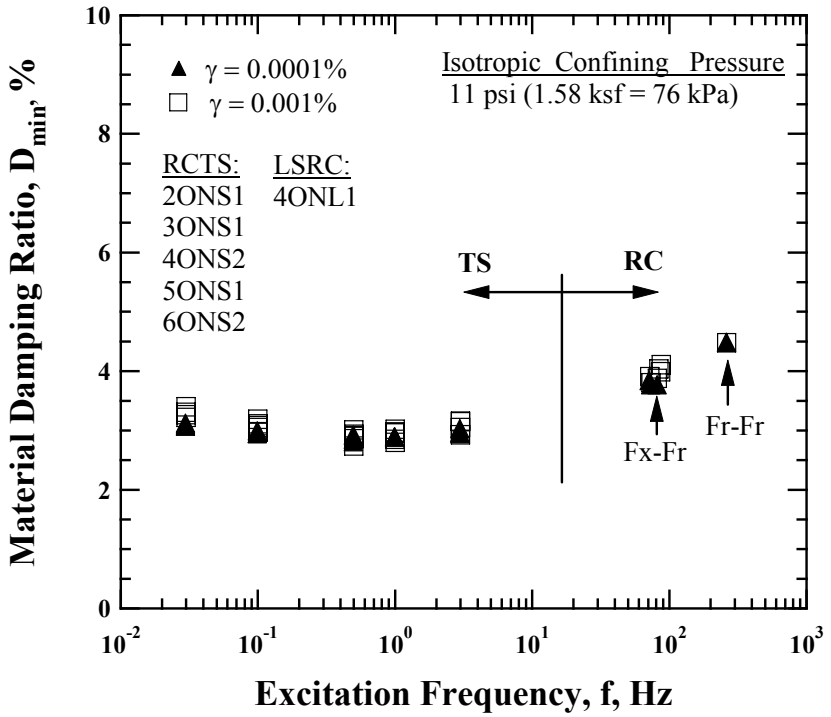

Figure 6.13 Variation in Material Damping Ratio with Excitation Frequency from the RCTS and LSRC Tests for 100 % Soil-Size Old MSW Specimens

hysteretic damping which has been generally recognized as independent of loading frequency. Shibuya et al. (1995) expanded the range of hysteretic damping from 0.1 Hz to 10 Hz, which correspond to frequencies typically created by seismic loadings. This range is acceptable for old MSW if changes less than about 10 % are ignored.

As seen in the Figure 6.13, the values of material damping ratios obtained at frequencies greater than 1 Hz continue to increase with excitation frequency. This increase can be attributed to an increased contribution of viscosity of the MSW skeleton and an increased relative movement between solid particles and water in the MSW skeleton frame by a faster application of loadings (Park, 1998, Shibuya et al., 1995).

Similar to shear modulus, the values of material damping ratio were normalized with values measured at a frequency of 1 Hz to quantify the amount of change in material

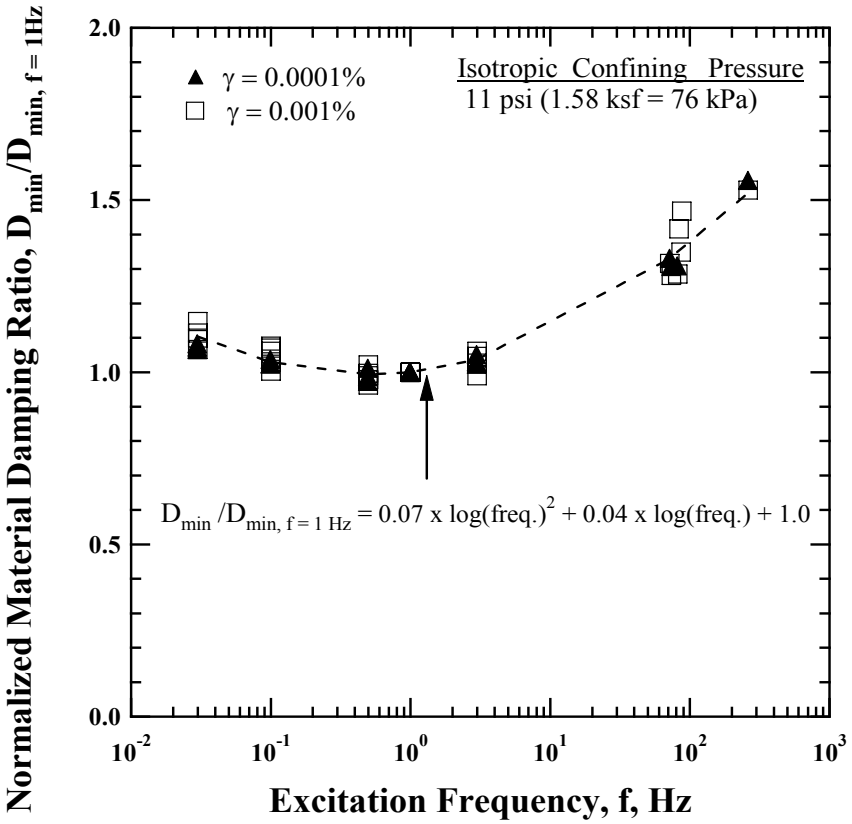

Figure 6.14 Nonlinear Relationship Fit to the Variation in Normalized Material Damping Ratio with Excitation Frequency for 100 % Soil-Size Old MSW Specimens

damping ratio with excitation frequency. Again, because the LSRC device can not be needed to perform TS tests, the values of material damping ratio were normalized with one averaged from TS tests in the RCTS device. The normalized material damping ratio, $D_{min}/D_{min, f=1Hz}$, with excitation frequency is plotted in Figure 6.14. The data were fitted as a form of the second-order of polynomial function using the least-squares method and the fitted equation is denoted by a dashed line. This equation is given by:

$$\frac{D_{min}}{D_{min, f=1Hz}} = 0.07 \times \log(Freq.)^2 + 0.04 \times \log(Freq.) + 1.0 \qquad (6.6)$$

where,

D_{min} is a material damping measured at small strains at a given frequency, and

$D_{min, f=1Hz}$ is a material damping measured at small strains at a frequency of 1 Hz.

Normalized material damping ratio increases as excitation frequency decreases below about 0.5 Hz due to creep, whereas normalized material damping increases as increasing excitation frequency greater than 1 Hz due to frequency effect. In the middle range, i.e., 0.5 Hz to 1 Hz, normalized material damping ratio is reasonably constant. The change in normalized material damping ratio from 1 Hz to the highest frequency (261 Hz) amounts to a factor of 1.5, whereas the change in normalized material damping ratio from 1 Hz to the lowest frequency of 0.03 Hz is about a factor of 1.1.

As a result, it can be concluded that the effect of excitation frequency is more pronounced on material damping than shear modulus for old MSW specimens. In the case of material damping, the effect of excitation frequency is much lager in the higher frequencies.

6.3.4 Specimen Size

To investigate the effect of specimen size on G_{max} and D_{min}, 2.8-in (71.1-mm) and 6.0-in. (152.4-mm) diameter MSW specimens were prepared. These specimens were constructed with 100 % soil-size MSW material that passed the 3/8-in. (9.5-mm) and the ¾-in. (19.1-mm) sieves. The RCTS and LSRC devices were used for small- and large-diameter MSW specimens to perform the RC tests, respectively.

The variations in G_{max} uncorrected and corrected for excitation frequency, f, and total unit weight, γ_t, with confining pressure for the Specimens MSW2ONS1, MSW3ONS1, and MSW4ONL1 are shown in Figures 6.15 (a) and (b), respectively.

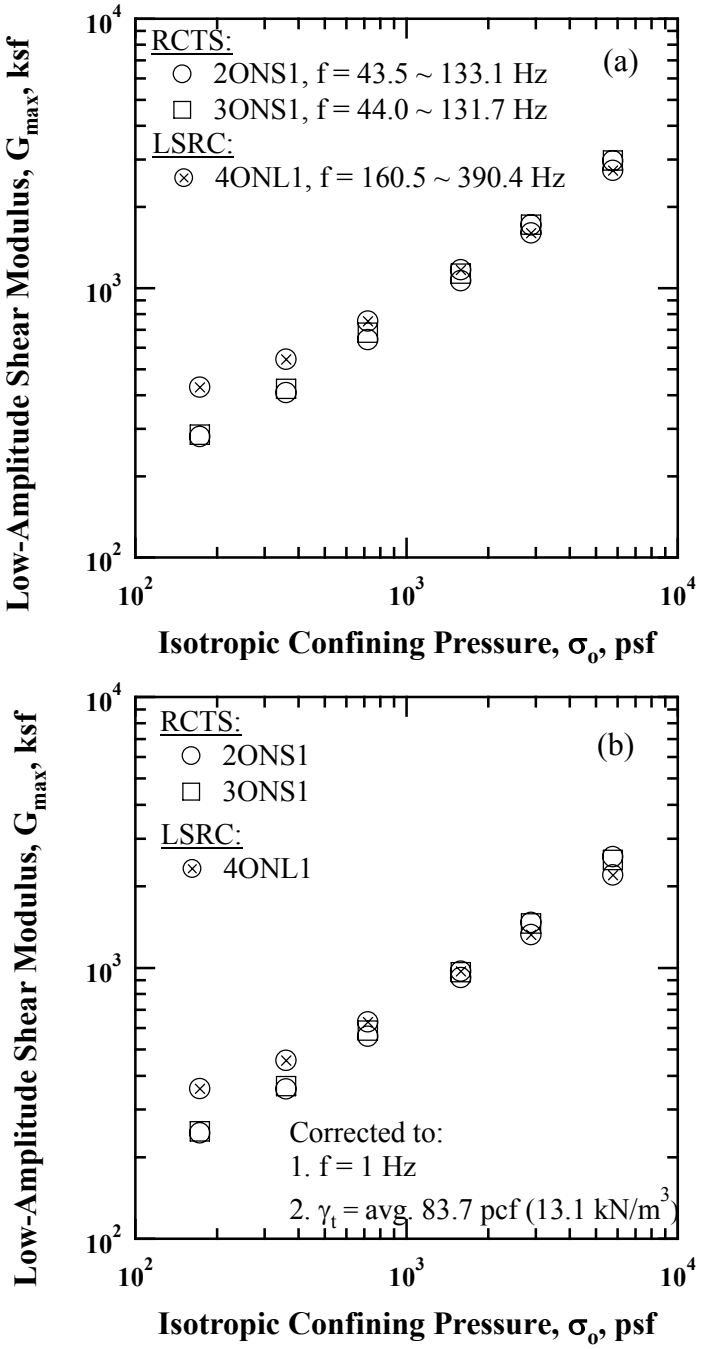

Figure 6.15 Comparison of the Variation in Low-Amplitude Shear Modulus with Isotropic Confining Pressure of Different Specimen Sizes Reconstituted with 100 % Soil-Size Old MSW Passing the 3/8-in. (9.5-mm) Sieve: (a) Uncorrected for f and γ_t and (b) Corrected for f and γ_t

These specimens were reconstituted with 100 % soil-size material passed the 3/8-in. (9.5-mm) sieve. Small-diameter specimens are represented by open symbols, whereas large-diameter specimen is represented by the open symbol with an "x" in the symbol. It should be noted that the values of G_{max} were corrected to f = 1 Hz using Equation (6.5) and the values of γ_t were adjusted to an average value of these specimens of 83.7 pcf (13.1 kN/m^3) to remove the effect of excitation frequency and total unit weight.

As can be seen in Figure 6.15 (a), the variations in G_{max} with confining pressure for small- and large-diameter specimens exhibit essentially the same behavior in the NC state. However, there is a difference in the OC state, with the LSRC test exhibits higher G_{max} which is assumed to be due mainly to an increased compaction being created during sample construction. In Figure 6.15 (b), the variation in G_{max} with confining pressure is slightly closer after correcting for excitation frequency and total unit weight. This comparison is needed to show that the effect of specimen size on G_{max} is small to negligible for old MSW specimens reconstituted with material passing the 3/8-in. (9.5-mm) sieve.

Another comparison of the variation in G_{max} (uncorrected and corrected for f and γ_t) with confining pressure is shown in Figures 6.16 (a) and (b) for the Specimens MSW4ONS2 and MSW2ONL2. These specimens were reconstituted with 100 % soil-size material that passed the ¾-in. (19.1-mm) sieve. As shown in Figure 6.16 (a), the variation in G_{max} with confining pressure for small- and large-diameter specimens exhibits very similar behavior in the NC state. After correcting for the excitation frequency and total unit weight of the specimens, the variations in G_{max} shown in Figure 6.16 (b) look nearly identical both in the OC and NC states. Thus, the effect of specimen size on G_{max} for old MSW specimens reconstituted with material passing the ¾-in. (19.1-mm) sieve is insignificant.

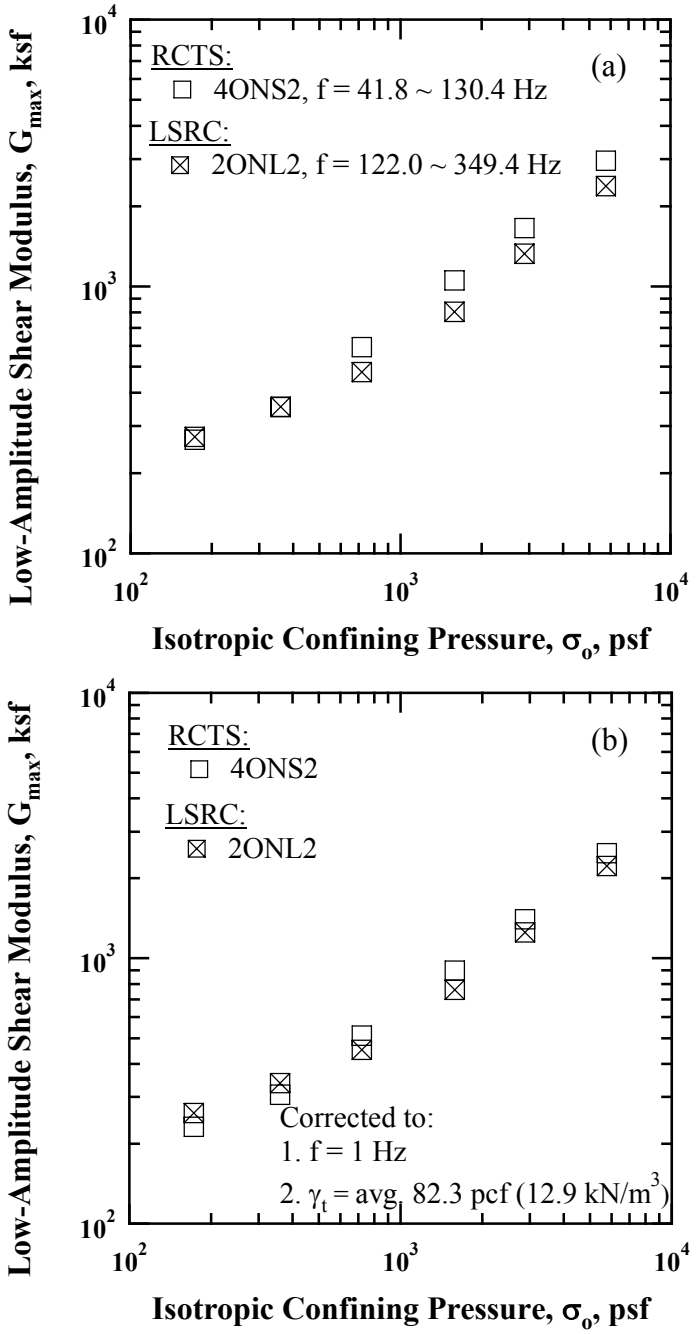

Figure 6.16 Comparison of the Variation in Low-Amplitude Shear Modulus with Isotropic Confining Pressure of Different Specimen Sizes Reconstituted with 100 % Soil-Size Old MSW Passing the ¾-in. (19.1-mm) Sieve: (a) Uncorrected for f and γ_t and (b) Corrected for f and γ_t

The variations in D_{min} (uncorrected and corrected for excitation frequency) with confining pressure for the Specimens MSW2ONS1, MSW3ONS1, and MSW4ONL1 are shown in Figures 6.17 (a) and (b), respectively. As shown in Figure 6.17 (a), the values of D_{min} measured in the LSRC device are somewhat higher than those measured in the RCTS device due to different excitation frequencies. Unlike G_{max}, only excitation frequency could be corrected for because of the limited knowledge on how to correct for total unit weight. After removing the effect of excitation frequency (corrected to f = 1 Hz using Equation (6.6)), the variation in D_{min} is nearly identical regardless of the specimen size. Therefore, the effect of specimen size on D_{min} for MSW specimens reconstituted with material passing the 3/8-in. (9.5-mm) is negligible.

Another variation in D_{min} (uncorrected and corrected for excitation frequency) with confining pressure for the Specimens MSW4ONS2 and MSW2ONL2 is shown in Figures 6.18 (a) and 6.18 (b), respectively. Similar to the observation from the MSW specimens reconstituted with material passing the 3/8-in. (9.5-mm) sieve, the values of D_{min} measured in the LSRC test are, to some extent, higher than those measured in the RCTS test. This difference in D_{min} is mainly due to excitation frequency. To remove the effect of excitation frequency on D_{min}, the values of D_{min} were normalized with using Equation (6.6), as shown in Figure 6.18 (b). As can be seen, the variation in D_{min} for the MSW specimens reconstituted with material passing the ¾-in. (19.1-mm) sieve is approximately the same. Thus, the effect of specimen size on D_{min} reconstituted with material passed the ¾-in. (19.1-mm) is also negligible.

6.4 ESTIMATION OF TOTAL UNIT WEIGHT OF OLD MSW SPECIMENS DURING THE RC TESTS AND COMPARISON WITH PREVIOUS STUDIES

Total unit weight of old and mixed MSW specimens is estimated during the RC tests in the RCTS and LSRC devices with an assumption that the MSW specimens are

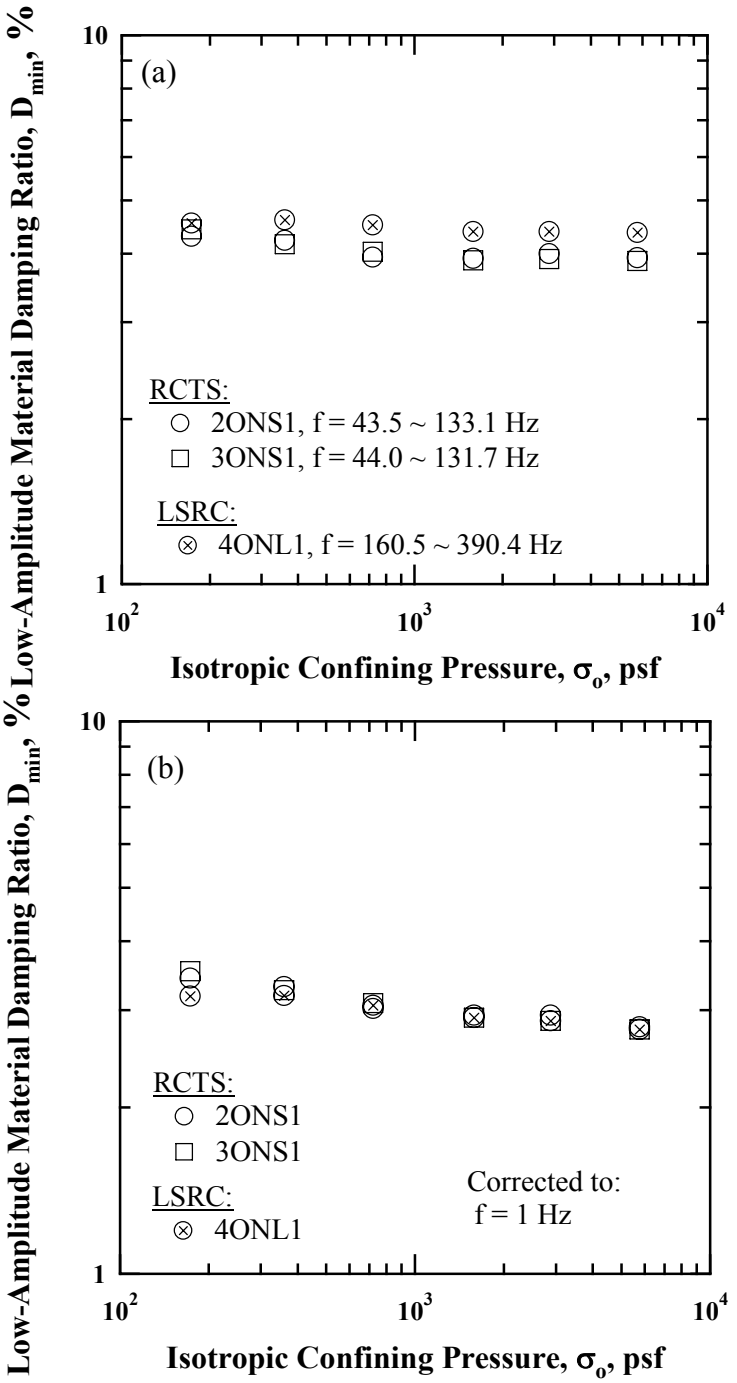

Figure 6.17 Comparison of the Variation in Low-Amplitude Material Damping Ratio with Isotropic Confining Pressure of Different Specimen Sizes Reconstituted with 100 % Soil-Size Old MSW Passing the 3/8-in. (9.5-mm) Sieve: (a) Uncorrected for f and (b) Corrected for f

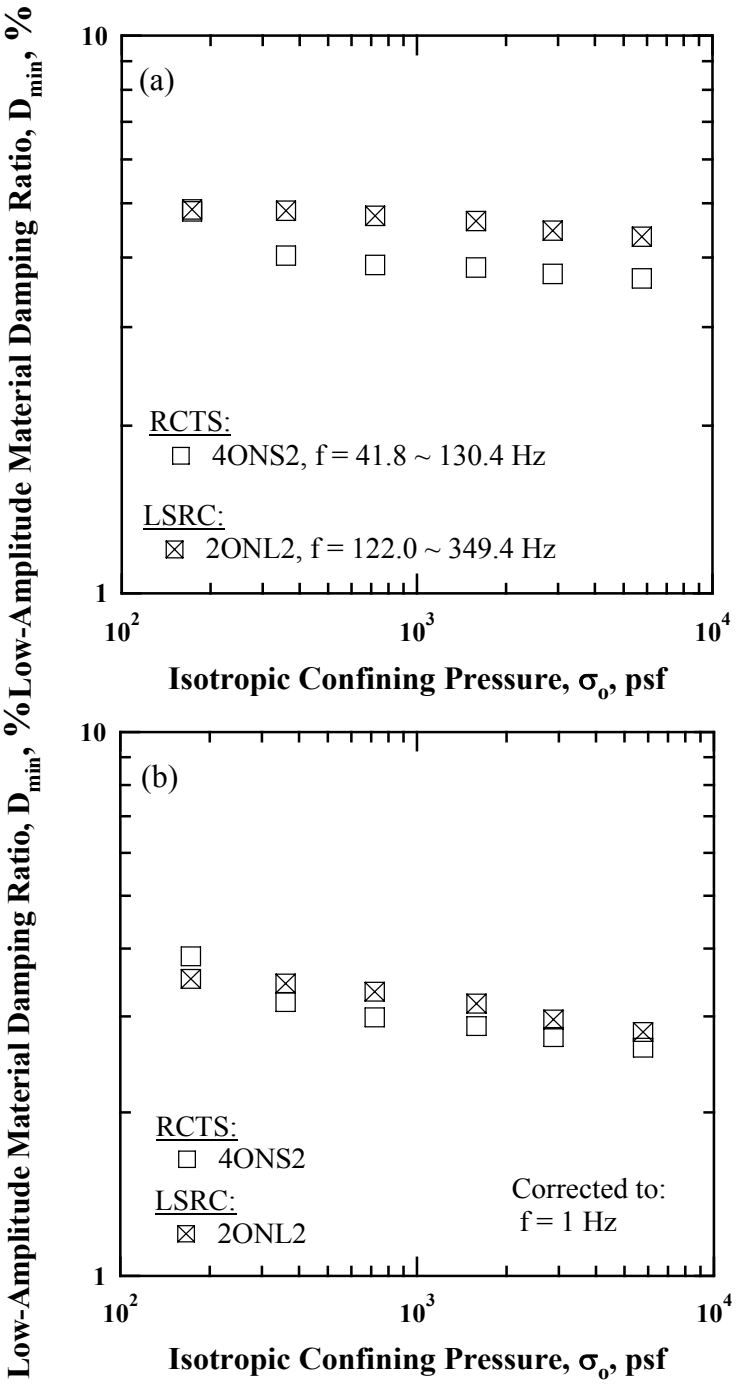

Figure 6.18 Comparison of the Variation in Low-Amplitude Material Damping Ratio with Isotropic Confining Pressure of Different Specimen Sizes Reconstituted with 100 % Soil-Size Old MSW Passing the ¾-in. (19.1-mm) Sieve: (a) Uncorrected for f and (b) Corrected for f

compressed with the same strain in the longitudinal and radial directions because the confinement is isotropic. The calculations of estimated total unit weight are based on the LVDT readings so that the LVDT readings during the RC tests in the RCTS and LSRC devices need to be accurate. The variations in estimated total unit weight with confining pressure for old and mixed MSW specimens (specimens with 14 % soil-size particles) in the loading sequence are shown in Figure 6.19. The initial total unit weights of the specimens shown in the figure are provided in Tables 5.3, 5.5, and 5.7. The MSW specimens with the 100 % soil-size material are represented by open symbols, whereas the MSW specimens with the 62 to 76 % soil-size material are represented by solid symbols. The 14 % soil-size material MSW specimens are represented by open symbols with an "x" in the symbol.

As shown in Figure 6.19, the estimated total unit weight increases with increasing confining pressure. As previously discussed in Section 6.3.2, the loading sequence can be divided into the OC and NC states due to the compaction effort. In general, the preconsolidation pressures, σ_p, are approximately around 1000 psf (48 kPa). Therefore, the increase in estimated total unit weight in the OC state is smaller than in the NC state due to overconsolidation. The increase in estimated total unit weight for the MSW specimens reconstituted with 100 % soil-size material is about 11% over two orders of magnitude of confining pressure (from 10^2 psf (5 kPa) to 10^4 psf (479 kPa)). The average increase in estimated total unit weight of the 62 to 76 % soil-size material MSW specimens is about 17 %. In addition, the average increase in estimated total unit weight for the 14 % soil-size material MSW specimens is about 42 %. As a result, it is worthwhile to note that the amount of increase in estimated total unit weight is generally dependent of its initial total unit weight and weight of percentage of soil-size material. The lower the percentage of soil-size material the lower the initial total unit weight of

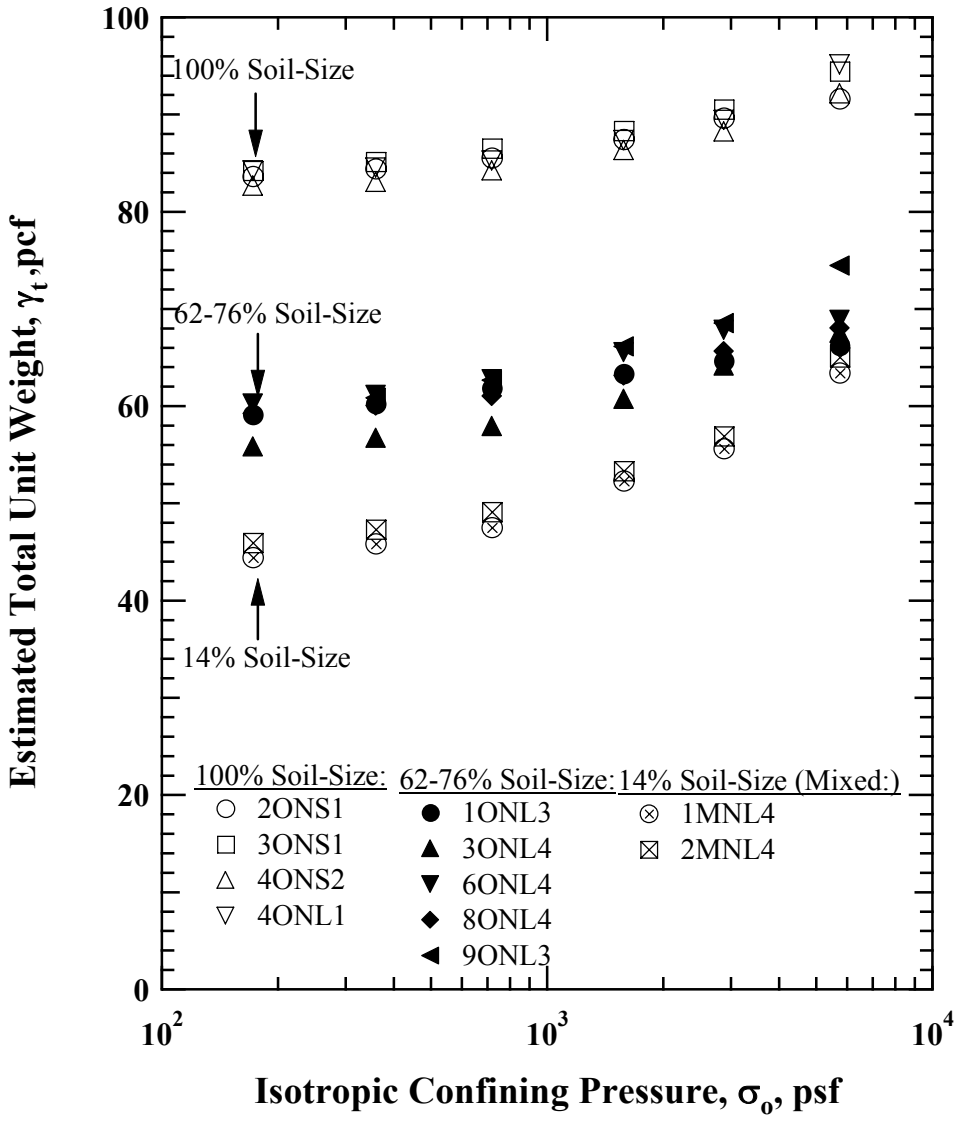

Figure 6.19 Variation in Estimated Total Unit Weight with Isotropic Confining Pressure from RC Tests for Old and Mixed MSW Specimens (All Groups)

the MSW specimen, and the larger the change in γ_t during the increasing pressure loading sequence.

The estimated total unit weight measured during the RC tests in the RCTS and LSRC devices of the old and mixed MSW specimens is compared with other total unit

weight profiles obtained from other MSW landfills in Figure 6.20. The coefficient of lateral earth pressure at rest, K_o, is required to convert the mean isotropic confining pressure in the laboratory into an equivalent depth in situ. Zekkos (2005) estimated Poisson's ratio of MSW specimen that was retrieved in the Tri-Cities landfill by directly measuring the radial deformation using elastomer gauges in the cyclic triaxial tests. He reported a more representative Poisson's ratio of about 0.3 to 0.35 for the 100 % soil-size material and Poisson's ratio varying from about zero to 0.3 for lower-weight percentages of soil-size material (see Zekkos (2005) for more information).

Therefore, as part of collaborative research project, the values of Poisson's ratio of 0.3 and 0.25 were used for 100 % soil-size material and the other groups (e.g., 76 %, 62 %, and 14 % Groups), respectively. Corresponding values of K_o are equal to 0.43 and 0.33, respectively.

The reference total unit weight profiles measured at MSW landfills used for the purpose of comparing with the estimated total unit weight profiles produced in the laboratory measurements were: Tri-cities landfill near San Francisco Bay area in California, OII landfill near Los Angeles in California, Azusa landfill near Los Angeles, California, and Cherry Island landfill, Delaware (Zekkos, 2005). Additionally, the average total unit weight profile suggested by Kavazanjian et al. (1995) is added to the figure by a dashed line. The variation in estimated total unit weight of specimens is divided into three groups in this case, i.e., 100 %, 62 to 76 %, and 14 % soil-size material Groups. As shown in Figure 6.20, the dashed line proposed by Kavazanjian et al. almost forms a lower bound of total unit weight variation measured MSW landfills.

The estimated total unit weight of the 100 % soil-size material MSW specimens agrees well with total unit weight profiles measured in situ. However, the estimated total unit weight of the 62 to 76 % soil-size material MSW specimens appears to

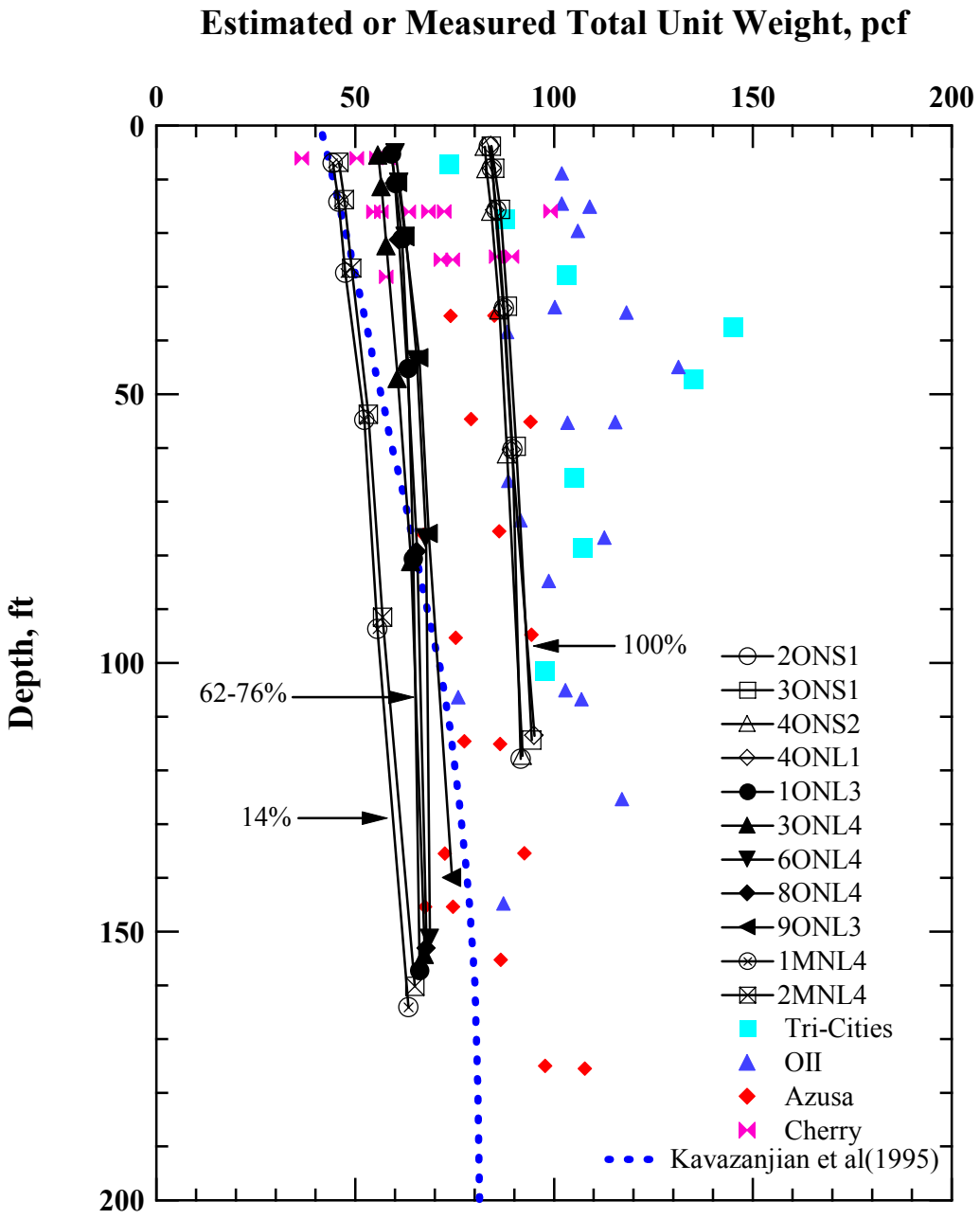

Figure 6.20 Comparison of the Variation in Estimated Total Unit Weight of Old and Mixed MSW Specimens (All Groups) with Total Unit Weight Profiles Measured at MSW Landfills

underestimate the in-situ total unit weights below a depth of about 80 ft (24 m). Additionally, the estimated total unit weights of the 14 % soil-size material MSW specimens are quite low after a depth of about 30 ft (9 m) compared with the in-situ total unit weight profiles. It is interesting to observe the, from either the estimated total unit weight profiles in the laboratory or the measured in-situ total unit weight profiles, the variation in total unit weight of the MSW does not change dramatically with depth.

6.4.1 Development of an Empirical Relationship of Estimated Total Unit Weight and Confining Pressure of Old MSW

To develop an empirical relationship between estimated total unit weight and confining pressure for the old and mixed MSW, the values of estimated total unit weight measured in the RCTS and LSRC devices at each confining pressure were normalized with the initial total unit weight of each specimen. The variation in normalized total unit weight with confining pressure is presented in Figure 6.21. The 100 %, 62 to 76 %, and 14 % of soil-size material specimens are represented by open circles, triangles, and squares, respectively. As shown in Figure 6.21, the amount of normalized total unit weight increases with decreasing weight percentage of soil-size material. The data were fitted using the least-squares method separately and the fitted equations were generalized with respect to the weight percentage of soil-size material. This equation is expressed by:

$$\frac{\gamma_t}{\gamma_{t,initial}} = -0.05 \times \left[(\ln(\%) - 5.24) \times (\ln(\sigma_o) - 4.74)\right] + 0.97 \qquad (6.7)$$

where, γ_t is an estimated total unit weight for a given confining pressure in pcf,

$\gamma_{t,initial}$ is an initial total unit weight of a given specimen,

% is a weight percentage of soil-size material, and

σ_o is a confining pressure in psf.

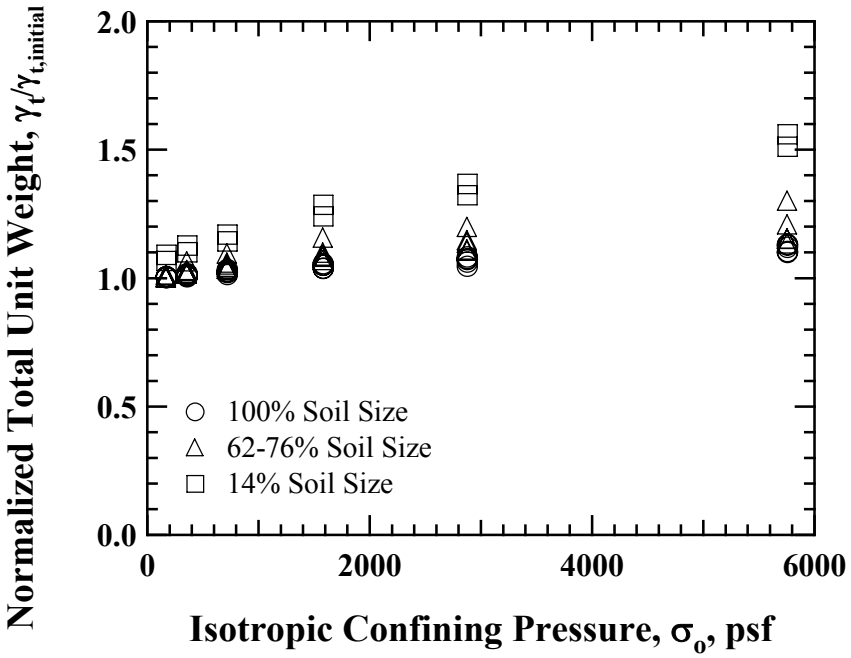

Figure 6.21 Variation in Normalized Total Unit Weight with Isotropic Confining Pressure for Old and Mixed MSW (All Groups)

To verify Equation (6.7), the values of predicted total unit weight were compared with those of measured total unit weight. The comparison is shown in Figure 6.22. As indicated in Figure 6.22, the values predicted by Equation (6.7) give a fairly good agreement with measured values.

6.5 MATERIAL PARAMETERS AFFECTING G_{MAX} AND D_{MIN} OF OLD WASTE IN THE SMALL-STRAIN RANGE

6.5.1 Waste Composition

MSW is, by its very nature, an extremely heterogeneous material composed of various types of organic materials (e.g., paper, food waste, plastic, textiles, and wood, etc) and inorganic materials (e.g., metals, glass, soil, concrete, and ceramics, etc). As a result, it is obvious that the dynamic behavior of MSW will be strongly affected by waste

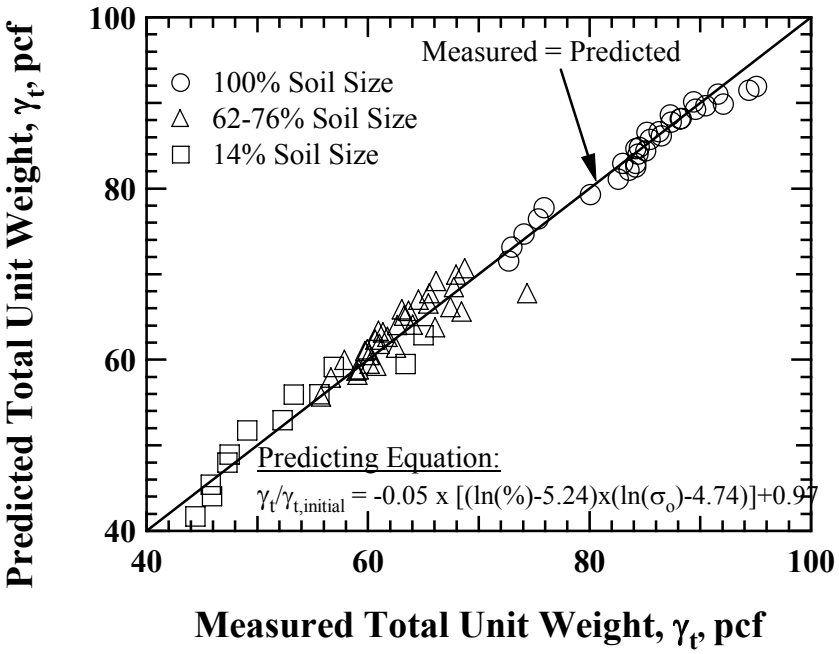

Figure 6.22 Comparison of Predicted Total Unit Weight and Measured Total Unit Weight for Old and Mixed MSW (All Groups)

composition, which is one of the key parameters in this study. Therefore, to investigate the effect of waste composition on G_{max} and D_{min}, large-diameter MSW specimens composed of different weight percentages of soil-size material were reconstituted in accordance with the procedures described in Section 5.3.2. The LSRC device was employed to achieve this purpose in the investigation.

The variation in G_{max} uncorrected and corrected for excitation frequency, f, and total unit weight, γ_t, with confining pressure with respect to different weight percentages, i.e., 100 %, 76 %, 62 %, and 14 % of soil-size material, is shown in Figures 6.23 (a) and (b), respectively. All specimens were confined at a constant confining pressure for at least one day and the values of G_{max} were taken from measurements at the end of the one-day confinement period. The data from the 76 % and 62 % soil-size material groups were combined together for the data fitting. Each group of data was fitted using the

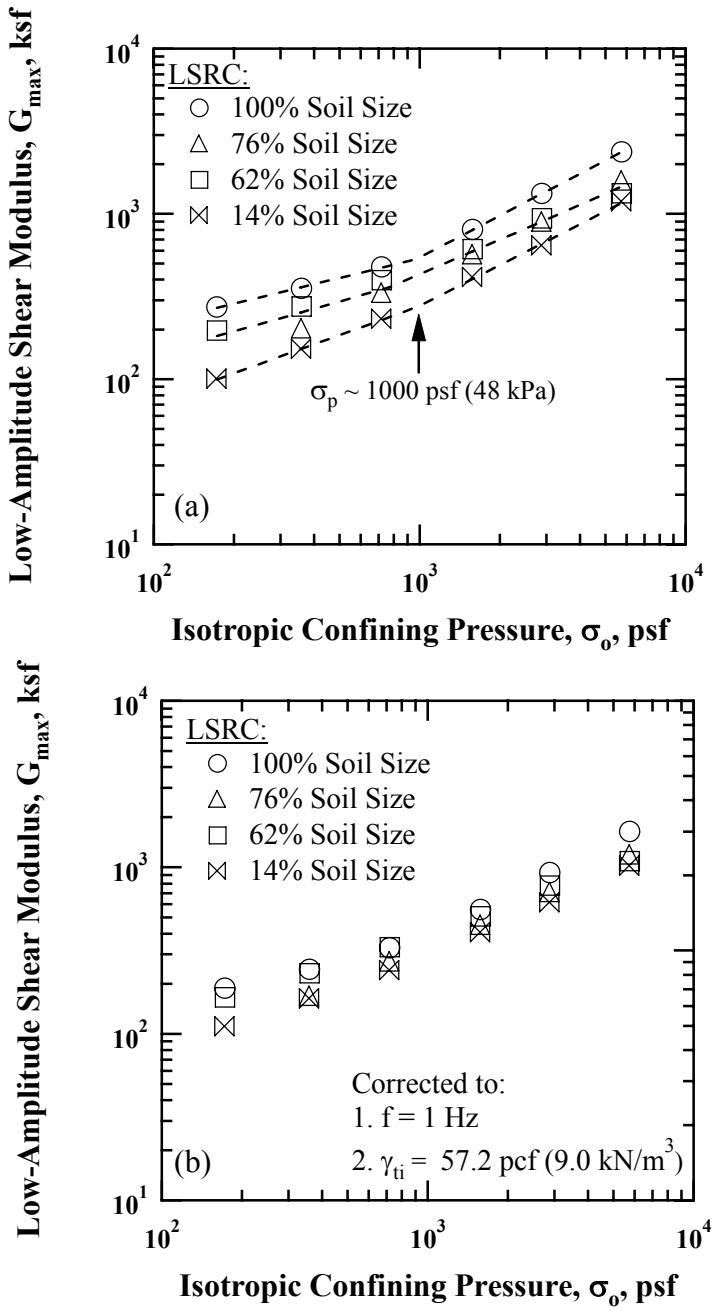

Figure 6.23 Variation in Low-Amplitude Shear Modulus with Isotropic Confining Pressure for Different Weight Percentages of Soil-Size Material for Old and Mixed MSW Specimens: (a) Uncorrected for f and γ_t and (b) Corrected for f and γ_t

least-squares method and is represented by dashed lines. As seen in Figure 6.23 (a), G_{max} increases with increasing confining pressure regardless of weight percentages of soil-size material, with a slightly flatter log G_{max} – log σ_o relationship in the OC state than in the NC state. It is important to point out that the values of G_{max} at each confining pressure in both OC and NC states depends on the weight percentage of soil-size material, indicating that the G_{max} of MSW is dependent on the waste composition, with G_{max} decreasing as the percentage of soil-size material decreases. In Figure 6.23 (b), each data was corrected to f = 1 Hz using Equation (6.5). The values of G_{max} were also adjusted to a value of 57.2 pcf (9.0 kN/m^3) (initial γ_t of 62 % soil-size material specimen) by multiply G_{max} to the values of ratio between the variation in estimated γ_t with σ_o other groups of specimens, as shown in Figures 6.24 (a) and (b). After correcting for excitation frequency and total unit weight shown in Figure 6.23 (b), G_{max} increases with increasing confining pressure regardless of weight percentages of soil-size material and the values of G_{max} become closer. However, as mentioned earlier, the values of G_{max} of MSW is dependent on the waste composition, with G_{max} decreasing as the percentage of soil-size material decreases.

The variation in D_{min} uncorrected and corrected for excitation frequency, f, with confining pressure for the different weight percentages of soil-size material is presented in Figures 6.25 (a) and (b), respectively. Similar to the G_{max}, the values of D_{min} shown in the figure were measured after one day of confinement at each pressure. These values are determined using the free-vibration decay method in the LSRC device.

Figure 6.25 (a) indicates that D_{min} decreases only slightly with confining pressure regardless of the weight percentage of soil-size material. The exception is the 14 % soil-size material specimen, where D_{min} exhibits a slight increase with confining pressure. Additionally, the behavior of D_{min} with confining pressure appears to be similar

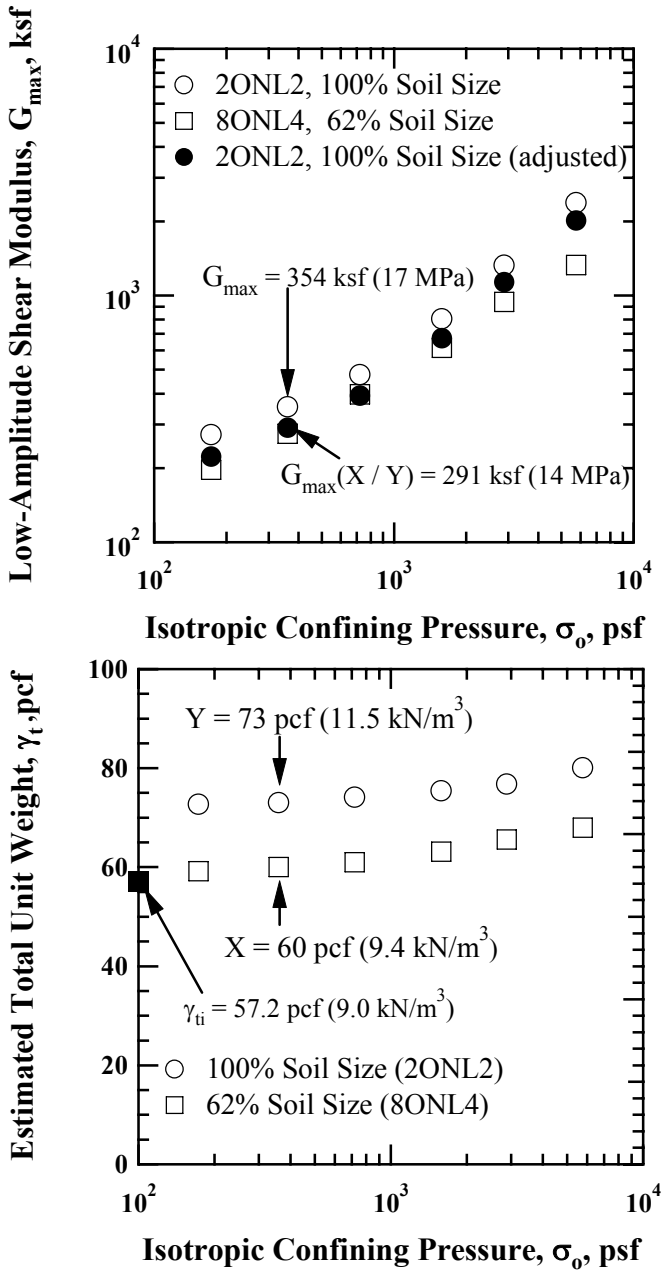

Figure 6.24 An Example of Adjusting Low-Amplitude Shear Modulus of One Specimen to Account for the Difference in Total Unit Weights Between Two Specimens; Both Specimens have the Same Confinement: (a) Adjustment of G_{max} at σ_o = 2.5 psi (17 kPa), and (b) Total Unit Weight of Both Specimens at σ_o = 2.5 psi (17 kPa)

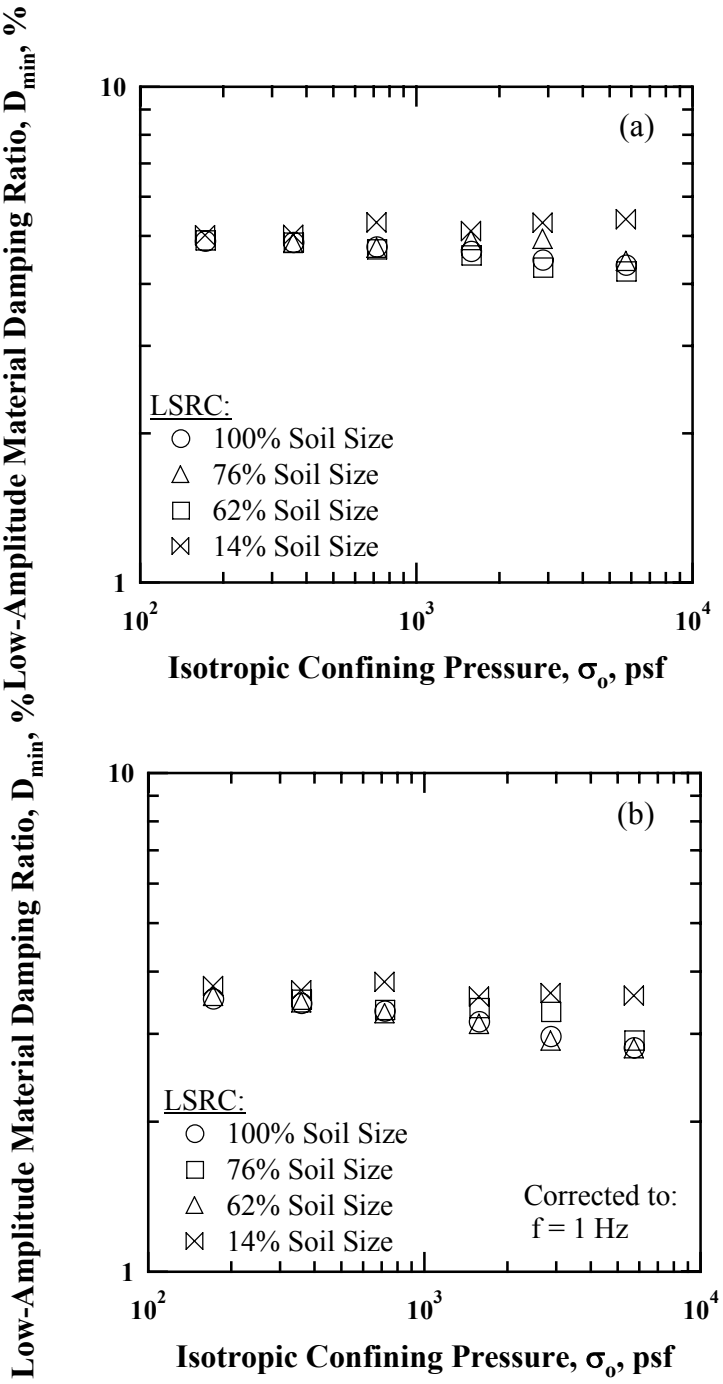

Figure 6.25 Variation in Low-Amplitude Material Damping Ratio with Isotropic Confining Pressure for Different Weight Percentages of Soil Content for Old and Mixed MSW Specimens: (a) Uncorrected for f and (b) Corrected for f

regardless of weight percentage of soil-size material, with an exception for the 14 % soil-size material. The data shown in Figure6.24 (b) were corrected for f using Equation (6.6). After removing the effect of excitation frequency, D_{min} exhibits similar trends. As a result, the effect of waste composition is small on D_{min}.

6.5.2 Water Content

In modern landfill operations, daily cover soil is used to retain the MSW that has been placed each day. The daily cover soil can be hydrated by the infiltration of precipitation. Thus, it can be considered that the presence of daily cover soil may play a role in the response of MSW landfills subjected to seismic loadings. However, there is a limited understanding of the dynamic behavior of hydrated landfill materials. For this reason, additional water was added to some of the MSW specimens to study the effect of water content on the dynamic properties. This investigation was performed on only the 100 % soil-size material specimens using the RCTS device because this is the only device with which hydration could be done.

The variation in G_{max} uncorrected and corrected for excitation frequency, f, and total unit weight, γ_t, with confining pressure at the natural and hydrated conditions for one specimen (i.e., MSW2ONS1) is shown in Figures 6.25 (a) and (b), respectively. The variation in G_{max} at the natural condition is denoted by the open symbols and the variation in G_{max} at hydrated condition is denoted by the solid symbols. The values of the initial total unit weight and water content for Specimen MSW2ONS1 were 83.3 pcf (13.1 kN/m^3) and 15.0 %, respectively. After completion of hydration process, total unit weight and water content of the hydrated specimen before performing the RCTS tests were 97.7 pcf (15.3 kN/m^3) and 27.0 %, respectively. As seen in Figure 6.25 (a), the variation in G_{max} with confining pressure after the hydration process is quite similar to

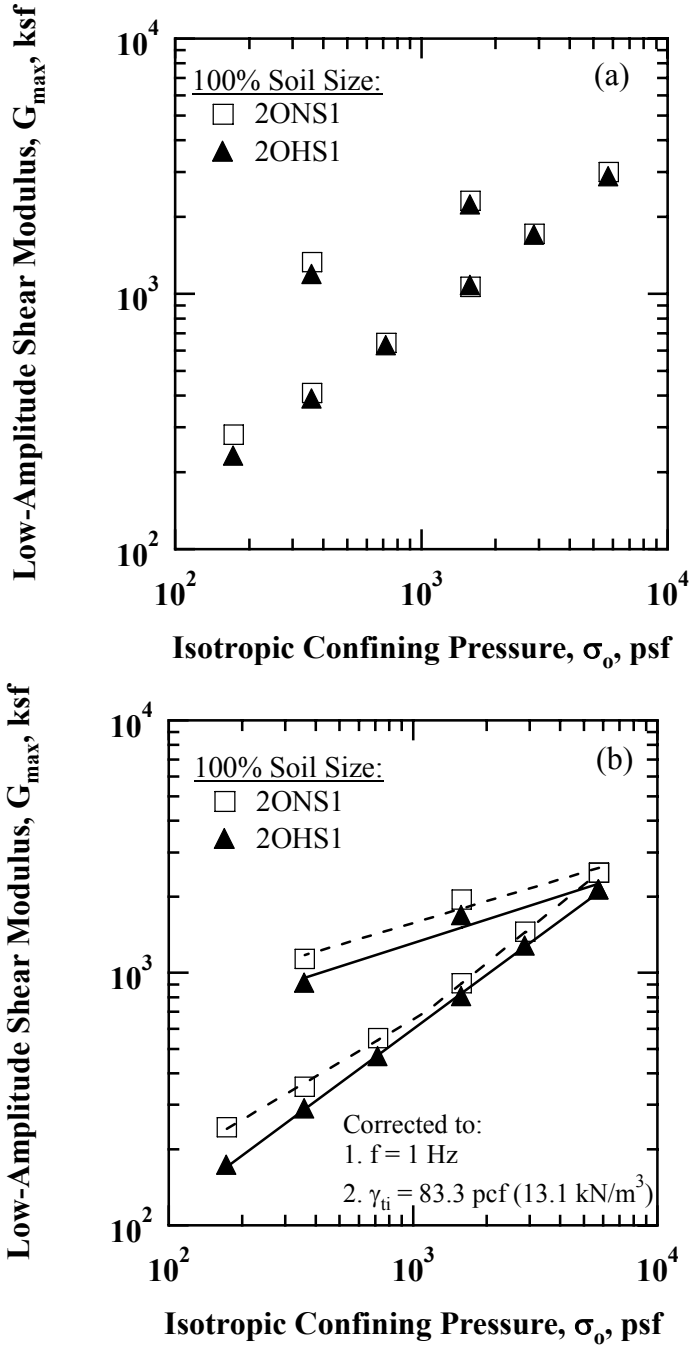

Figure 6.25 Comparison of the Variation in Low-Amplitude Shear Modulus with Isotropic Confining Pressure at its Natural and Hydrated Conditions for 100 % Soil-Size Old MSW Specimens: (a) Uncorrected for f and γ_t and (b) Corrected for f and γ_t

that at its natural condition, but as mentioned above, the values of γ_t are different. Therefore, when adjusted to a common total unit weight at each σ_o, the difference is seen in Figure 6.26 (b). The RC test was performed for hydrated specimen under a drained condition; that is, the drain line connected to the bottom pedestal was open during the tests. To eliminate the effect of excitation frequency and total unit weight, the values of G_{max} were corrected to f = 1 Hz and total unit weight of 83.3 pcf (13.1 kN/m^3). After correcting the excitation frequency and total unit weight, the difference in G_{max} became larger prior to correcting the f and γ_t. However, this difference decreases with increasing confining pressure, varying from about 40 % at the lowest pressure to about 17 % at the highest pressure. According to this observation, it can be concluded that hydrated specimen regains its stiffness rapidly under the circumstance of drained conditions.

Another important thing to point out is that hydrating a specimen initially eliminates the overconsolidation effect that appeared in a given specimen in its natural condition by unloading process. The overconsolidation effect reappears in hydrated specimen when it is unloaded (Lee et al., 2004).

As with G_{max}, the impact on D_{min} of an increase in water content in the MSW needs to be evaluated. The variation in D_{min} uncorrected and corrected for excitation frequency, f, with confining pressure at its natural and hydrated conditions is given in Figures 6.26 (a) and (b), respectively. As shown in Figure 6.26 (a), D_{min} increases somewhat after hydration process over the confining pressure, showing an increase in D_{min} of about 20 %. Similar to the natural condition, D_{min} measured in the hydrated condition also decreases with increasing confining pressure.

As previously discussed in Section 6.3.2, two mechanisms, i.e., inelastic friction losses and fluid flow losses, have been postulated as possible reasons for explaining the

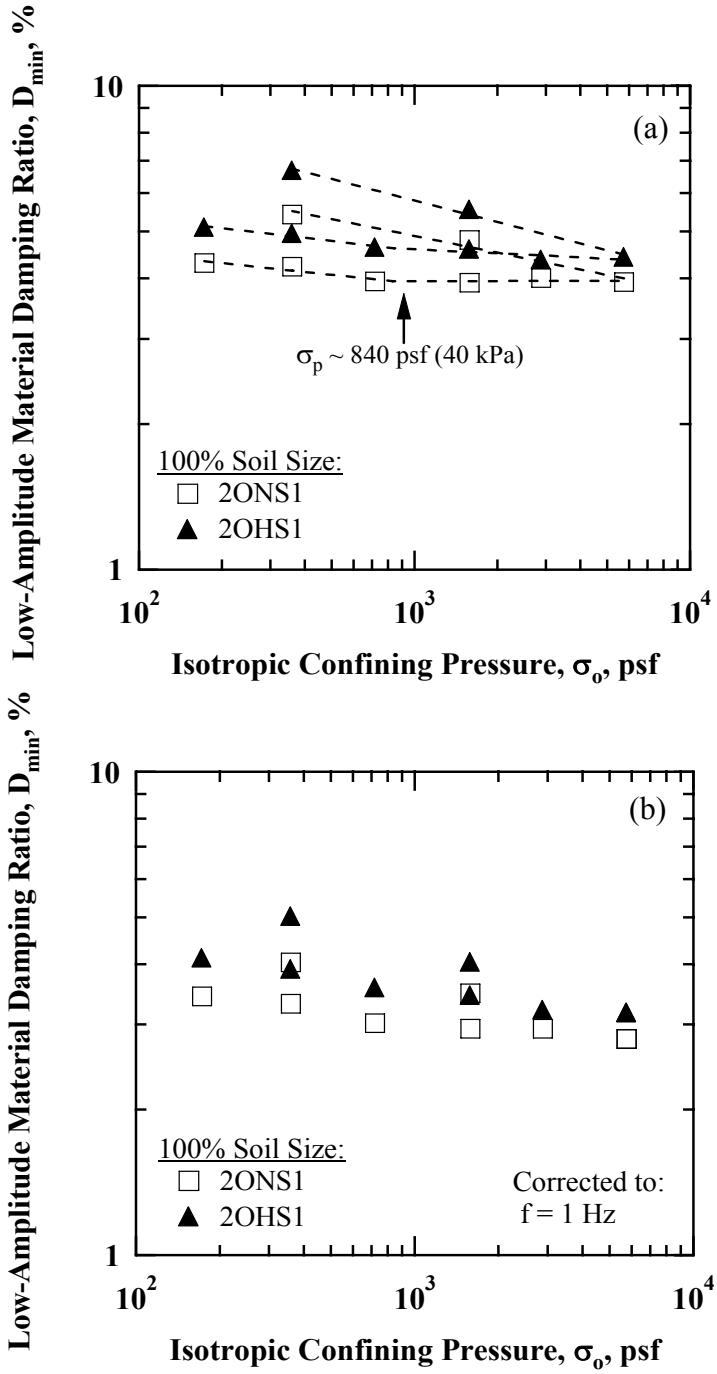

Figure 6.26 Comparison of the Variation in Low-Amplitude Material Damping Ratio with Isotropic Confining Pressure at its Natural and Hydrated Conditions for 100 % Soil-Size Old MSW Specimens: (a) Uncorrected for f and (b) Corrected for f

material damping in soils (White, 1983, Stoll, 1989). This postulation is supported by the increase in D_{min} measured after hydration which is mainly due to energy dissipation caused by relative movements between solid particles and water in the MSW specimen. The increase in D_{min} induced by interaction between solid particles and water would likely be even larger if added water was not drained.

The values of D_{min} measured in the natural and hydrated conditions were corrected for f = 1 Hz, as shown in Figure 6.26 (b). After removing the effect of excitation frequency, the values of D_{min} also show similar trends; D_{min} decreases with increasing confining pressure.

Similar to the G_{max}, hydrating the specimen initially eliminated the overconsolidation effect that appeared in the specimen in its natural condition. The overconsolidation effect reappeared in hydrated specimen when it was unloaded (Lee et al., 2004). For the unloading sequence, the increase in D_{min} becomes relatively larger as confining pressure decreases.

6.5.3 Total Unit Weight Variation for the Same Material Group

As discussed in Section 6.4, total unit weight of the MSW specimens estimated during the RC tests in the RCTS and LSRC devices increases with increasing confining pressure in all MSW groups. Other tests were conducted in an effort to investigate the effect of total unit weight on G_{max} and D_{min} for a given material group (e.g., 100 % soil-size material group). For this study, a pair of small-diameter specimens with a lower total unit weight was constructed: Specimens MSW5ONS1 and MSW6ONS2. Target unit weights for the lower unit weight specimens were initially 50.9 pcf (8 kN/m^3). These specimens were reconstituted in four layers and were constructed by simply placing by hand the 100 % soil-size material, passing the 3/8-in. (9.5-mm) and ¾-in.

(19.1-mm) sieves for the two specimens, into the mold. These specimens were not compacted with the compaction hammer.

A typical variation in G_{max} uncorrected and corrected for excitation frequency, f, with estimated total unit weight at different confining pressure levels for the 100 % soil-size material specimens is shown in Figures 6.27 (a) and (b), respectively. The specimens with the higher total unit weights are indicated by open symbols and the two specimens with the lower total unit weight are indicated by open symbols with an "x" in the symbol. G_{max} measurements failed at the first confining pressure level, 1.2 psi (8 kPa), for Specimen MSW6ONS2 (lower total unit weight), due to background noise. Therefore, levels of confining pressure shown in the figures are 2.5 psi (17 kPa), 5 psi (17 kPa), 11 psi (76 kPa), 20 psi (138 kPa), and 40 psi (238 kPa). However, for Specimen MSW5ONS1, the initial confining pressure was 5 psi (34 kPa), followed by two more measurements at 11 psi (76 kPa) and 40 psi (276 kPa).

As shown in Figure 6.27 (a), G_{max} increases with increasing estimated total unit weight. The change in estimated total unit weight for the lower and higher total unit weight specimens is approximately 30 % and 10 % over confining pressures (2.5 psi (17 kPa)) to 40 psi (276 kPa)), respectively. It should be noted that the difference in G_{max} below a confining pressure of 11 psi (76 kPa) is also affected by the compaction process; the lower total unit weight specimens were constructed without any compaction process. The difference in estimated total unit weight diminishes as confining pressure increases, making the difference in the absolute value of G_{max} with confining pressure become smaller.

To remove the effect of excitation frequency, the values of G_{max} were corrected for f = 1 Hz using Equation (6.5), as shown in Figure 6.27 (b). After correcting the excitation frequency, the variation in G_{max} follows similar trends. Therefore, although

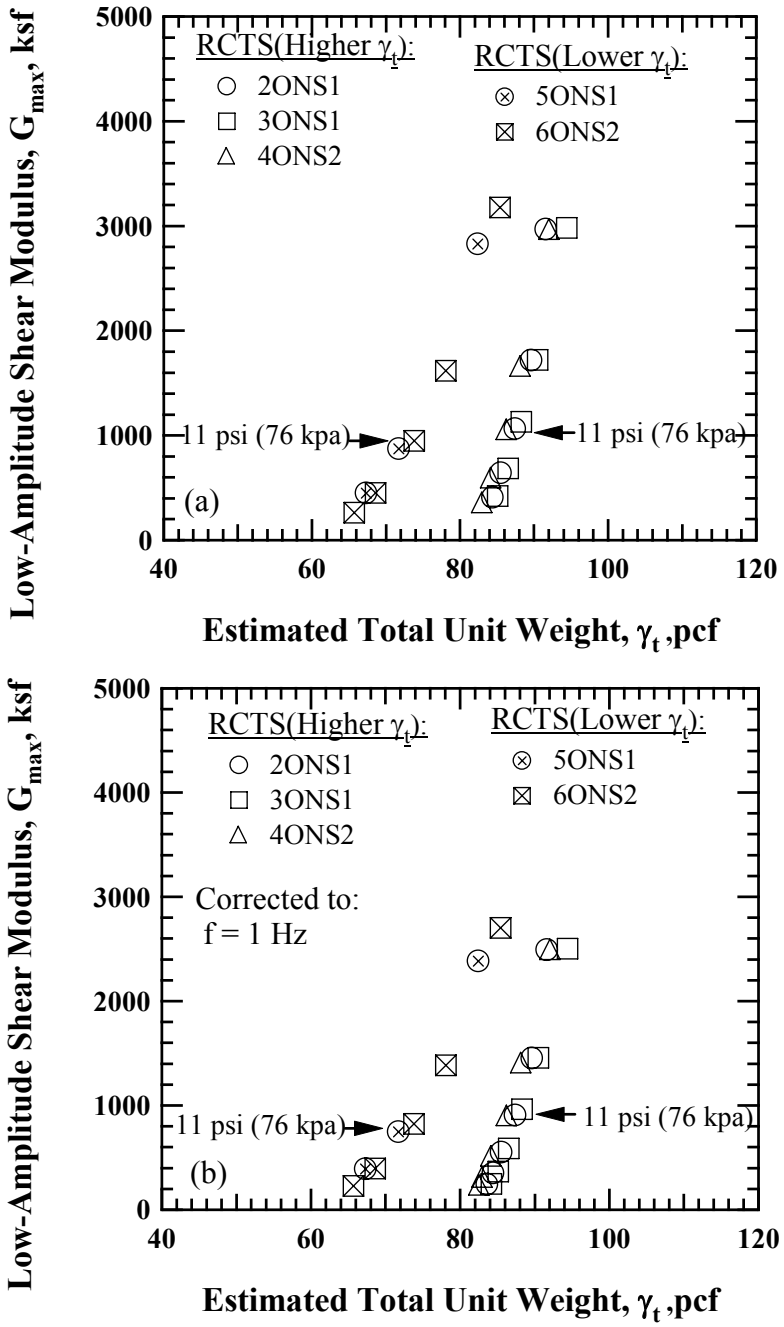

Figure 6.27 Comparison of the Variation in Low-Amplitude Shear Modulus with Estimated Total Unit Weight at Different Isotropic Confining Pressures for 100 % Soil-Size Old MSW Specimens: (a) Uncorrected for f and (b) Corrected for f

its initial unit weight is somewhat low, the increase in G_{max} with confining pressure appears to be accelerated because of a specimen's increased compressibility, explaining that the effect of variation in total unit weight is relatively small on G_{max} for the 100 % soil-size specimens.

The variation in D_{min} uncorrected and corrected for excitation frequency, f, with estimated total unit weight at different confining pressures is shown in Figures 6.28 (a) and (b), respectively. As shown in Figure 6.28 (a), D_{min} generally decreases with increasing estimated total unit weight. The pattern of variation in D_{min} is quite similar between higher and lower total unit weight specimens. In other words, D_{min} tends to decrease rapidly at the beginning, but it remains almost the same after some measurements regardless of its initial total unit weight.

To eliminate the effect of excitation frequency, the values of D_{min} were corrected to f = 1 Hz using Equation (6.6), as shown in Figure 6.28 (b). After correcting the effect of excitation frequency, the variation in D_{min} exhibit similar trends. Therefore, it can be concluded that the variation of total unit weight has a small impact on D_{min} for the 100 % soil-size material MSW specimen.

6.5.4 Particle Size

A pair of small- and large-diameter specimens was prepared to investigate the effect of particle size on G_{max} and D_{min} for 100 % soil-size old MSW. As recognized, the maximum particle size for a specimen construction should be less than one sixth of the specimen diameter as specified in ASTM D4015-92. Therefore, the largest particle size should not exceed 0.47-in. (11.9-mm) and 1.0-in. (25.4-mm) for the small- and large-diameter specimens, respectively.

According to this criterion, 100 % soil-size old MSW material that passed the 3/8-

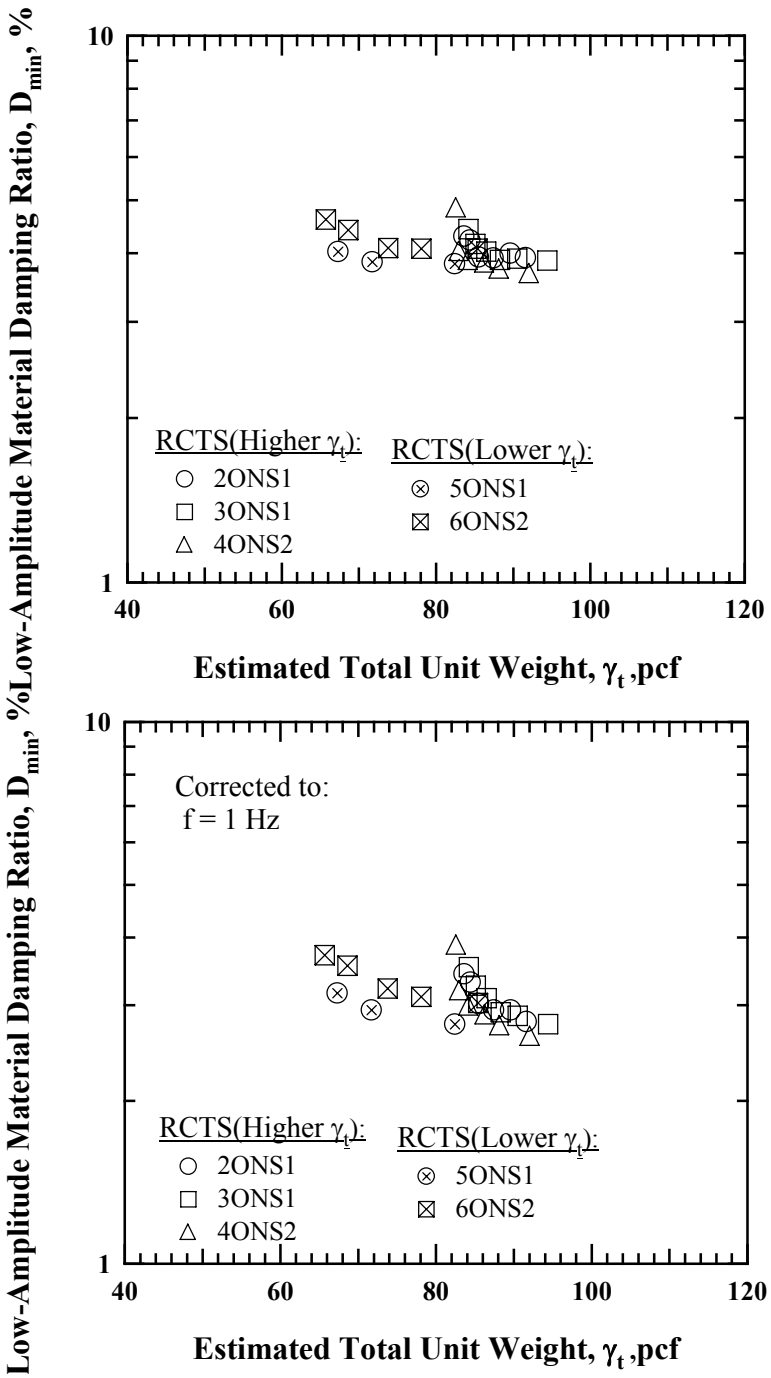

Figure 6.28 Comparison of the Variation in Low-Amplitude Material Damping Ratio with Estimated Total Unit Weight at Different Isotropic Confining Pressures for 100 % Soil-Size Old, MSW Specimens: (a) Uncorrected for f and (b) Corrected for f

in. (9.5-mm) and ¾-in. (19.1-mm) sieves was used for the construction of 2.8-in. (71.1-mm) and 6.0-in. (152.4-mm) diameter specimens. The RCTS and LSRC devices were used to perform the RC tests on the small- and large-diameter specimens, respectively. The variations in G_{max} uncorrected and corrected for excitation frequency, f, and total unit weight, γ_t, with confining pressure for Specimens 3ONS1 and 4ONS2 is shown in Figures 6.29 (a) and (b), respectively.

Initial total unit weights of these specimens are 83.7 pcf (13.1 kN/m^3) and 82.3 pcf (12.9 kN/m^3) for Specimens 3ONS1 and 4ONS2, respectively. Excitation frequency of these specimens varies from 44.0 Hz to 131.7 Hz for Specimen 3ONS1 and from 41.8 Hz to 130.4 Hz for Specimen 4ONS2. To eliminate the effects of excitation frequency and total unit weight, the excitation frequency was corrected to f = 1 Hz and the total unit weight was normalized with Specimen 3ONS1. As shown in Figure 6.29 (b), the variation in G_{max} with confining pressure is nearly the same regardless of particle size of the old MSW specimens after excitation and total unit weight corrections. (in fact, the corrections are very minor for these two specimens) with these tests, the effect of particle size on the small-diameter old MSW specimens reconstituted with material passing the 3/8-in. (9.5-mm) and ¾-in. (19.1-mm) sieves is negligible.

Variations in G_{max} uncorrected and corrected for f and γ_t with confining pressure for Specimens 4ONL1 and 2ONL2 is shown in Figures 6.30 (a) and (b), respectively. Initial total unit weights of these specimens are 84.1 pcf (13.2 kN/m^3) for the Specimen 4ONL1 and 72.6 pcf (11.4 2 kN/m^3) for the Specimen 2ONL2. Excitation frequency of these specimens varies from 160.5 Hz to 390.4 Hz for the Specimen 4ONL1 and from 122.0 Hz to 349.4 Hz for the Specimen 2ONL2. The G_{max} measurements of these specimens were corrected for f and γ_t to remove the effect of excitation frequency and total unit weight. As can be seen in Figure 6.30 (b), the variation in G_{max} in the NC state

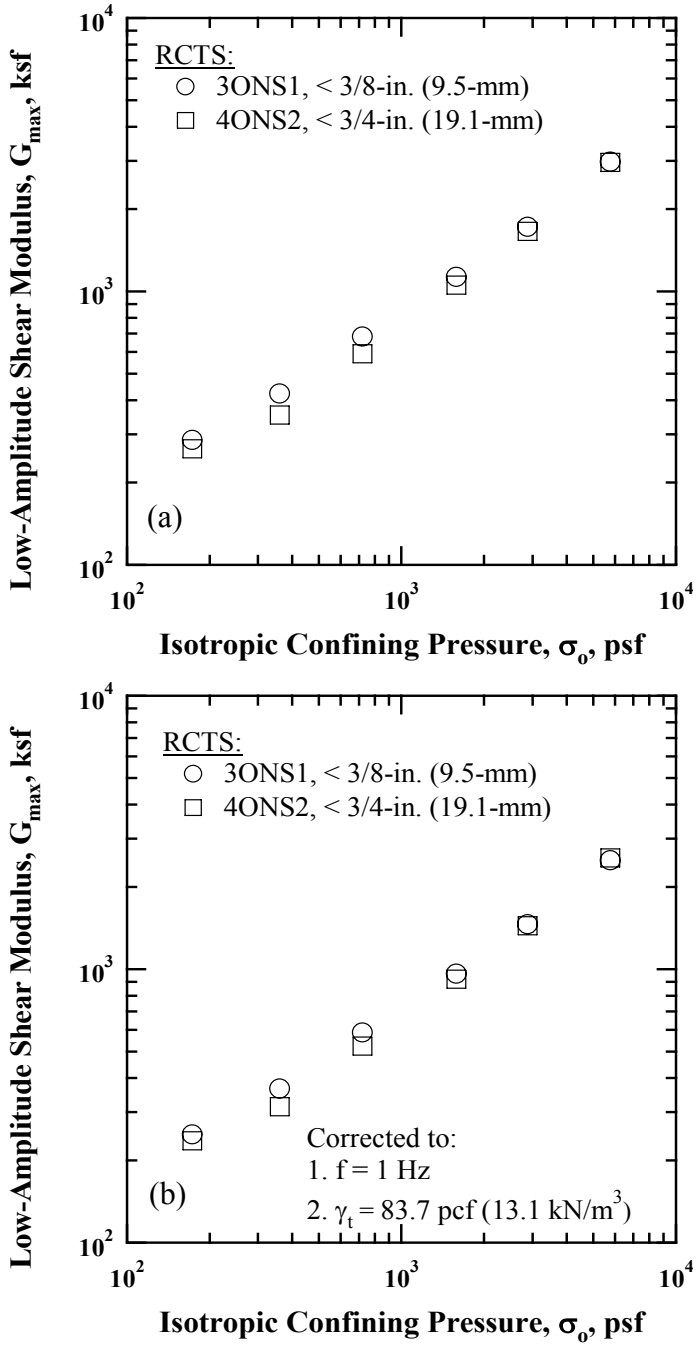

Figure 6.29 Comparison of the Variation in Low-Amplitude Shear Modulus with Isotropic Confining Pressure for Different Particle Sizes of the 100 % Soil-Size, Old MSW Material Tested in the RCTS Device: (a) Uncorrected for f and γ_t and (b) Corrected for f and γ_t

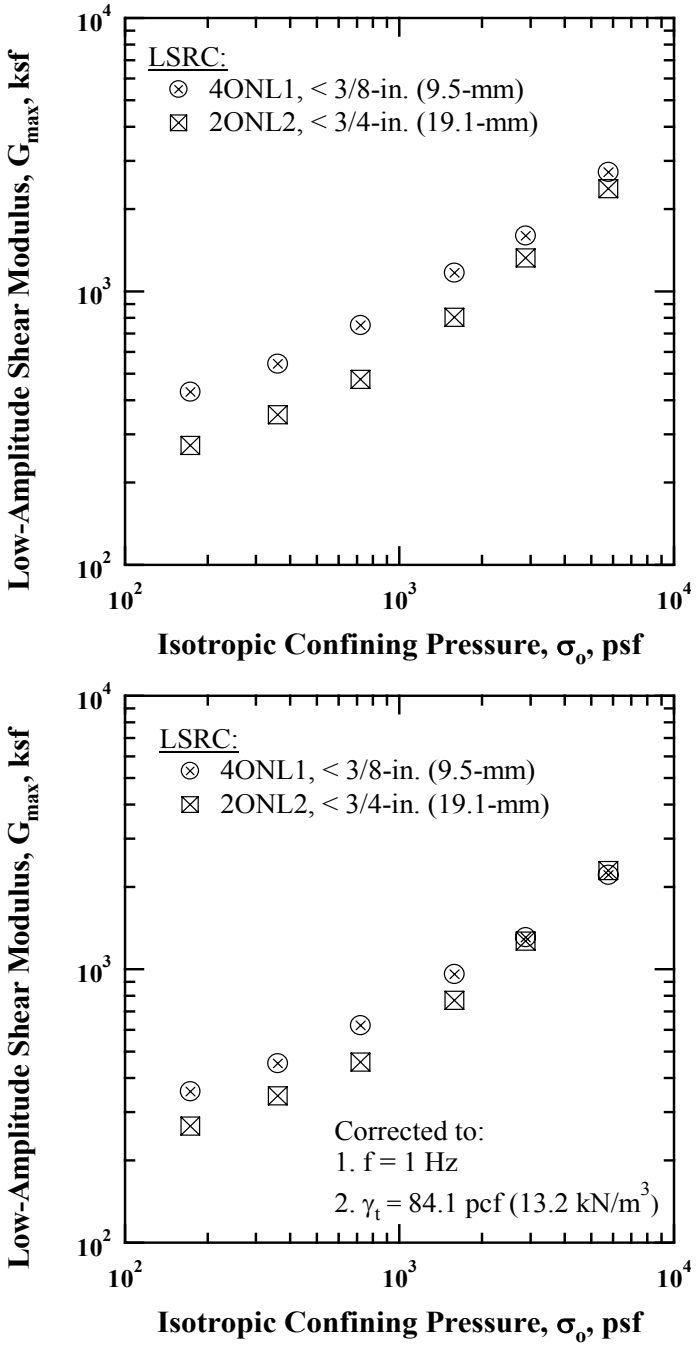

Figure 6.30 Comparison of the Variation in Low-Amplitude Shear Modulus with Isotropic Confining Pressure for Different Particle Sizes of the 100 % Soil-Size, Old MSW Material Tested in the LSRC Device: (a) Uncorrected for f and γ_t and (b) Corrected for f and γ_t

is approximately the same. However, there is a difference in G_{max} in the OC state. This difference is believed to be due to the compaction process and the larger particles which resulted in the lower γ_t for Specimen MSW2ONL2.

The variation in D_{min} with confining pressure for the Specimens 3ONS1 and 4ONS2 is shown in Figure 6.31. Figure 6.31 (a) shows D_{min} uncorrected for f and Figure 6.31 (b) show D_{min} corrected for f. Unlike G_{max}, the values of D_{min} were corrected only for excitation frequency using Equation (6.6) due to the lack of knowledge on how to correct D_{min} for total unit weight. As shown in Figure 6.31 (b), the values of D_{min} at each confining pressure are essentially the same regardless of the maximum particle size in these small-diameter RCTS tests. Therefore, the effect of particle size on small-diameter old MSW specimens is negligible as long as the particles all pass the ¾-in. (19.1-mm) sieve.

For the case of the large-diameter specimens, like small-diameter specimens, the values of D_{min} were also corrected to f = 1 Hz to eliminate the effect of excitation frequency. The variation in D_{min} (uncorrected and corrected for f)with confining pressure for Specimens 4ONL1 and 2ONL2 is shown in Figures 6.32 (a) and (b), respectively. As shown in Figure 6.32 (b), although there is a slight difference after correcting for excitation frequency (less than 10%), the values of D_{min} vary with confining pressure in the same manner regardless of the maximum particle size. Therefore, the effect of particle size for large-diameter old MSW specimens is negligible for these 100 % soil-size particles.

It is also important to note that the log D_{min} – log σ_o relationships after correcting D_{min} for f from the different test devices give nearly the same relationships.

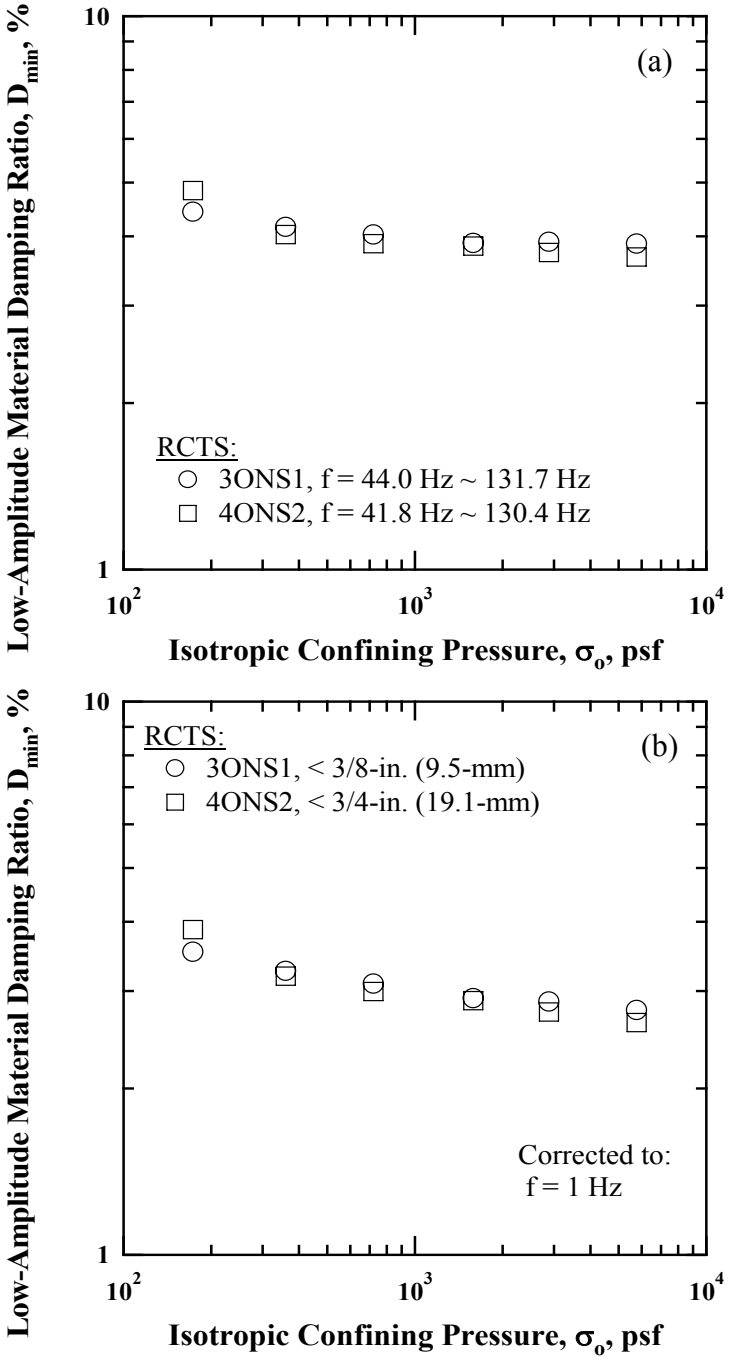

Figure 6.31 Comparison of the Variation in Low-Amplitude Material Damping Ratio with Isotropic Confining Pressure for 100 % Soil-Size, Old MSW Specimens with Different Maximum Particle Sizes: (a) Uncorrected for f and (b) Corrected for f

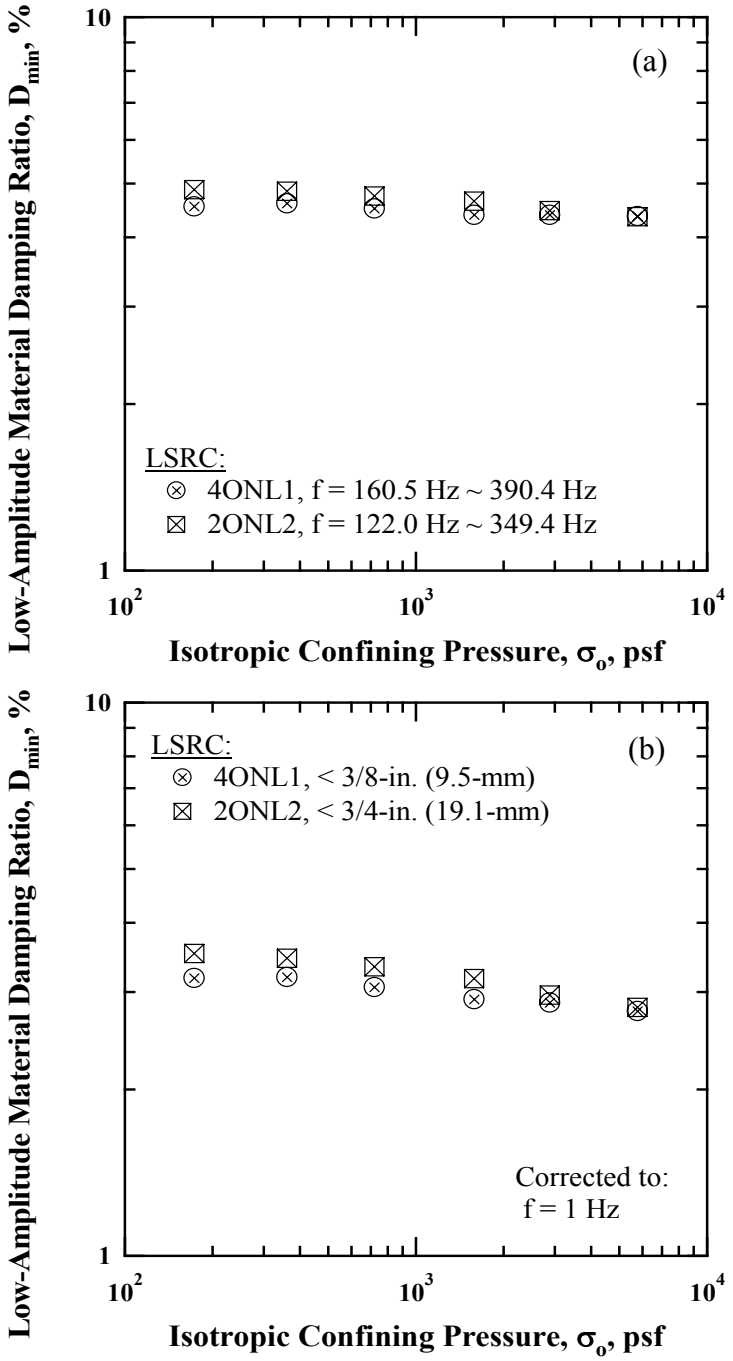

Figure 6.32 Comparison of the Variation in Low-Amplitude Material Damping Ratio with Isotropic Confining Pressure for 100 % Soil-Size Old MSW Specimens with Different Maximum Particle Sizes: (a) Uncorrected for f and (b) Corrected for f

6.6 DEVELOPMENT OF AN EMPIRICAL RELATIONSHIP BETWEEN G_{MAX} AND D_{MIN} FOR OLD MSW

Using the RC data measured from 100 %, 76 %, 62 %, and 14 % soil-size old and mixed MSW specimens in the RCTS and LSRC devices, an attempt was made to develop an empirical equation to predict values of D_{min} at in-situ MSW landfills. Prediction of the values of D_{min} is important in performing site response analyses in the MSW landfills subjected to earthquake loadings. Such site response analyses require the dynamic material property profiles of the MSW, e.g, V_s profile, unit weight profile, the values of D_{min}, and shear modulus reduction and material damping curves. The V_s profile (from which G_{max} is determined) can be determined by employing various seismic methods, one of these is the noninvasive SASW method used in this study.

However, compared with the V_s measurements, D_{min} measurements are rarely attempted using in-situ seismic testing techniques. Hence, the derivation of an empirical equation for MSW gives insight into the estimation of D_{min} either in the laboratory or in the field.

The variation in D_{min} with respect to G_{max} is plotted in Figures 6.33 (a) and (b). Figure 6.33 (a) shows the variation in D_{min} with G_{max} uncorrected both for excitation frequency, whereas Figure 6.33 (b) show the variation in D_{min} with G_{max} corrected for excitation frequency, respectively. The values of G_{max} and D_{min} were corrected for excitation frequency using Equations (6.5) and (6.6). The data shown in the figure were fitted using a form of a power function as expressed by:

$$D_{min} = 0.55 + 5.23 \times G_{max}^{-0.11} \tag{6.8}$$

where, D_{min} is the small-strain material damping ratio, and

G_{max} is the small-strain shear modulus.

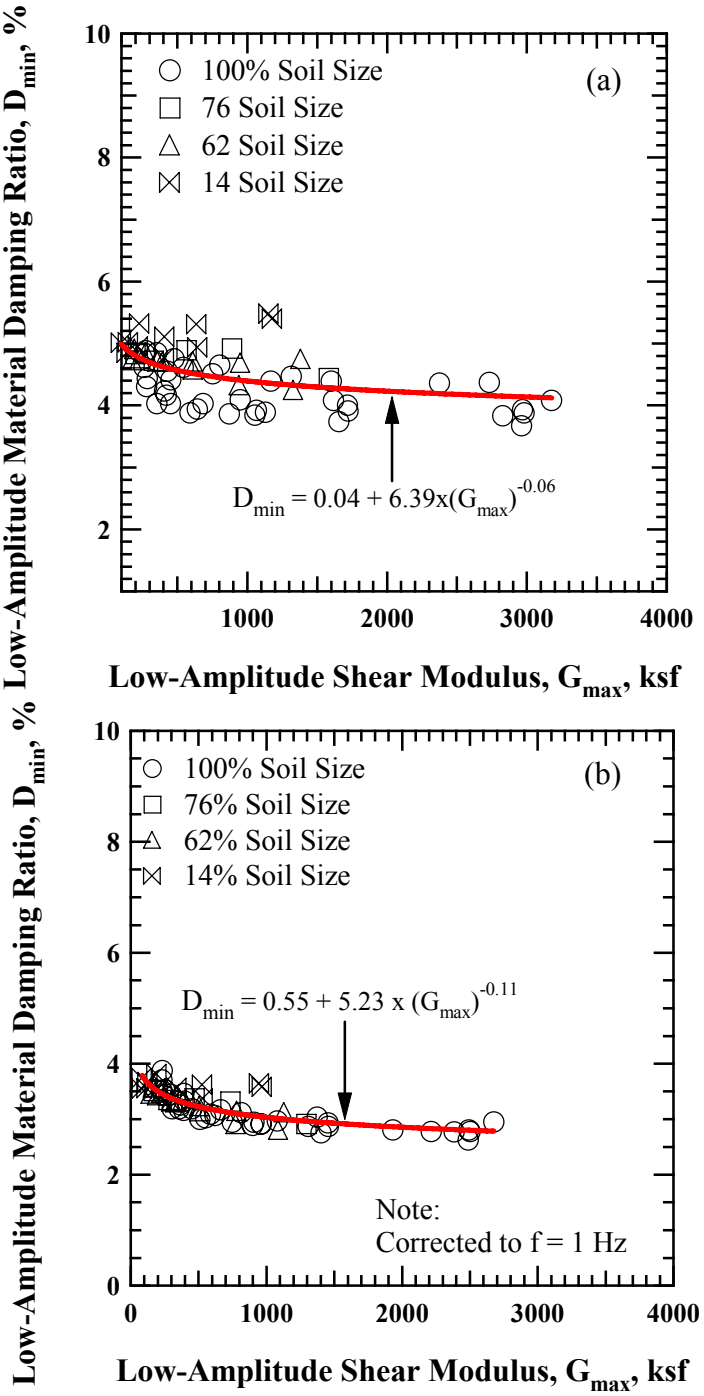

Figure 6.33 Variation in Low-Amplitude Material Damping Ratio with Low-Amplitude Shear Modulus for Old and Mixed MSW Specimens (All Groups): (a) Uncorrected for f (b) Corrected for f

The fitted line is shown by the solid line in Figure 6.33. As can be seen, D_{min} tends to decrease slightly with increasing G_{max}. However, the variation of D_{min} is quite small, less than about 10 % over the range in G_{max} values. The values of predicted material damping ratio computed using the Equation (6.8) are compared with corrected values is given in Figure 6.34.

As shown in the figure, the data distribute around the equality line with a scatter about ± 10 %. The maximum and minimum differences between corrected and predicted D_{min} values are about 21 % and 6 %, respectively. The ratio of corrected D_{min} to predicted D_{min} at corresponding confining pressures with mean and standard deviation lines is presented in Figure 6.35. This plot indicates how well the corrected D_{min} is related to the predicted D_{min} at each confining pressure. The mean value of the ratio of corrected D_{min} to predicted D_{min} is equal to 1.00 and the standard deviation, σ, is 0.05.

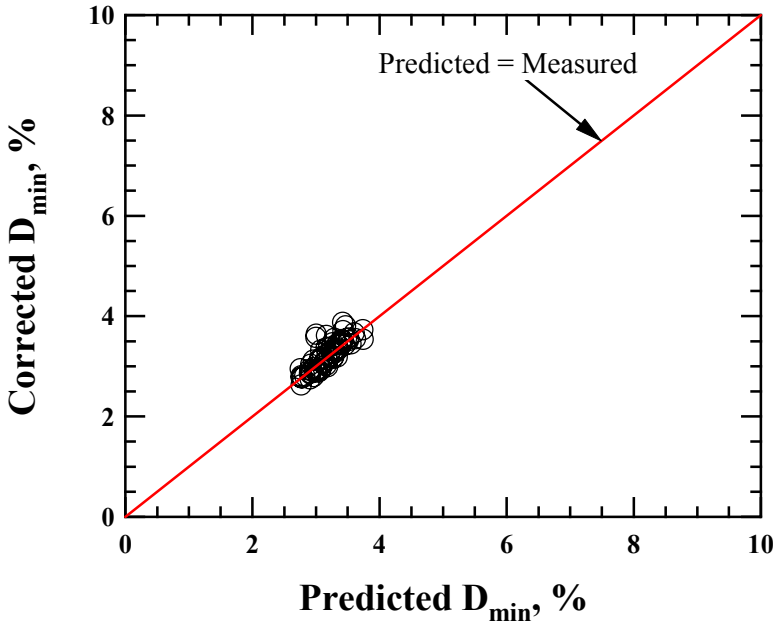

Figure 6.34 Comparison of the Corrected and Predicted Values of D_{min} for Old and Mixed MSW Specimens (All Groups)

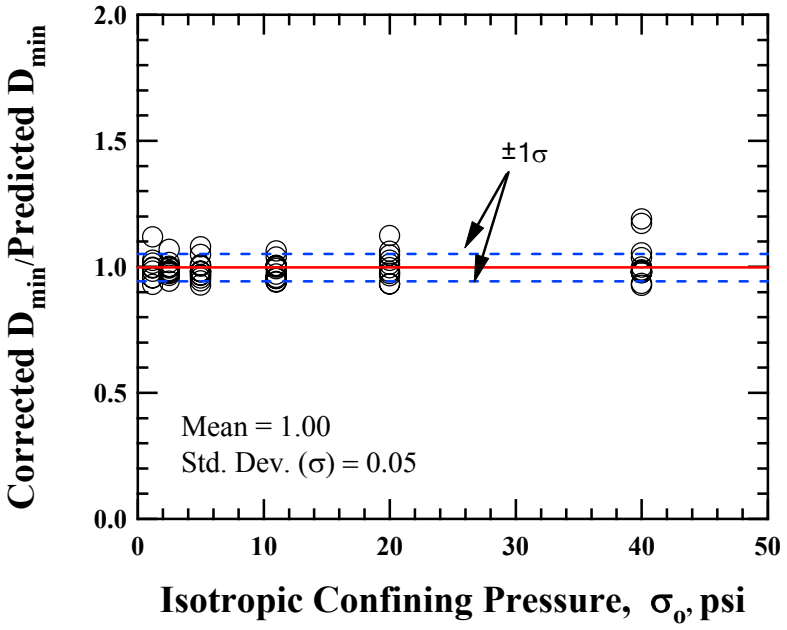

Figure 6.35 Plot of the Ratio of Corrected D_{min} to Predicted D_{min} with Isotropic Confining Pressure for Old and Mixed MSW Specimens (All Groups)

6.7 COMPARISON OF SMALL-STRAIN DYNAMIC PROPERTIES OF OLD MSW AND LOOSE SAND

The log G_{max} – log σ_o, log V_s – log σ_o, and log D_{min} – log σ_o relationships for old MSW are compared with these of loose sand in Figures 6.35, 6.36, and 6.37, respectively. Initial dry unit weight for loose sand is 118 pcf (18.5 kN/m^3). In addition, uniformity coefficient, C_u, and void ratio, e, for loose sand are 18 and 0.4, respectively. This loose sand is classified as well-graded sand (SW). Entire values of the old MSW were corrected for excitation frequency to f = 1 Hz using Equations (6.5) and (6.6). As seen in Figures 6.35, 6.36, and 6.37, σ_o has the same general influence on the small-strain dynamic properties of MSW as it does on sands; that is, as σ_o increases, G_{max} and V_s increase and D_{min} decreases slightly. However, there is a large difference between the values for the old MSW and sands. For instance, at σ_o = 11 psi (76 kPa), the difference

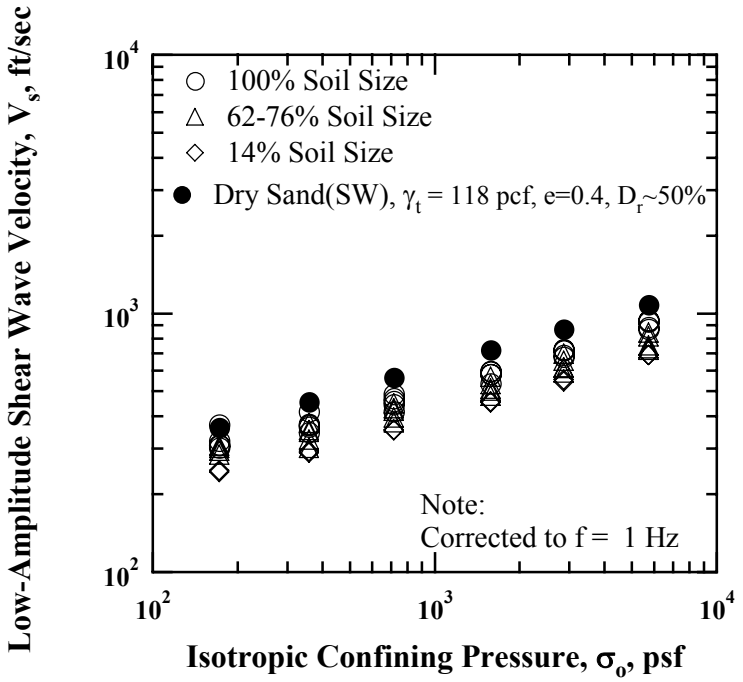

Figure 6.36 Comparison of the Variation in Low-Amplitude Shear Wave Velocity with Isotropic Confining Pressure for Old MSW (All Groups) and Loose Sand

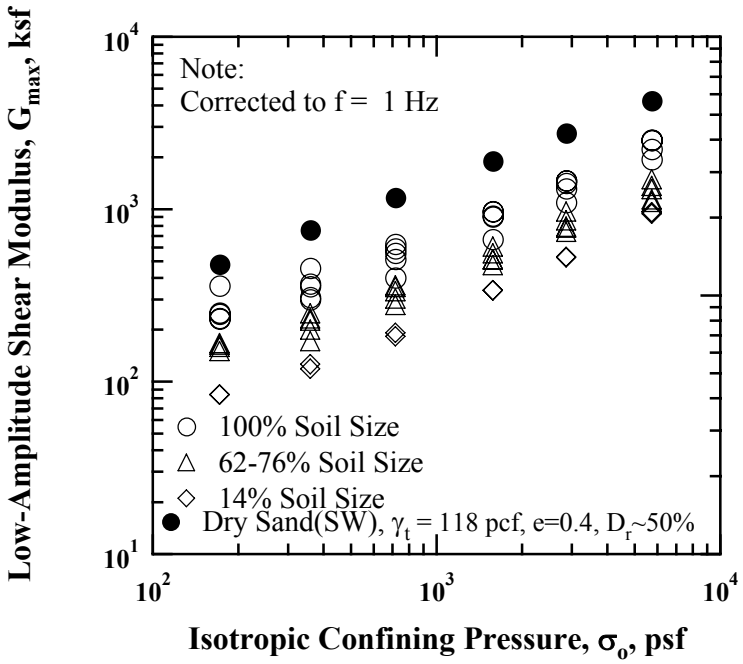

Figure 6.37 Comparison of the Variation in Low-Amplitude Shear Modulus with Isotropic Confining Pressure for Old MSW (All Groups) and Loose Sand

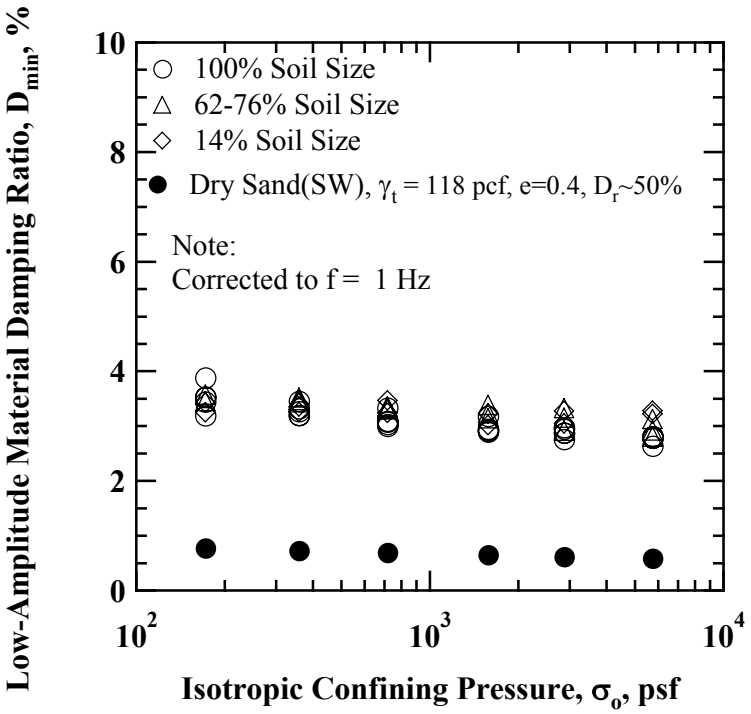

Figure 6.38 Comparison of the Variation in Low-Amplitude Material Damping Ratio with Isotropic Confining Pressure for Old MSW (All Groups) and Loose Sand

in G_{max} is approximately by a factor of two for 100 % soil-size material and the difference in V_s is about 20 % for 100 % soil-size material. For D_{min}, the difference is about a factor of 4.6.

6.8 SUMMARY

Test parameters affecting G_{max} and D_{min} of old MSW are investigated in this chapter. These test parameters include: (1) duration of confinement at a constant pressure, (2) total isotropic confining pressure, (3) excitation frequency, and (4) specimen size. The effects of duration of confinement, isotropic confining pressure, and specimen size were investigated using the RCTS and LSRC device. However, only the RCTS device was used for the study of the effect of excitation frequency since the LSRC device

can not be used to perform TS tests. Total unit weight of old MSW specimens were estimated during the RC tests in the RCTS and LSRC devices. Among these test parameters, the effects of duration of confinement and total isotropic confining pressure are very important. In addition, the excitation frequency has some impact on D_{min}. Other test parameters have small impact on G_{max} and D_{min}.

Also, total unit weight of mixed MSW specimen was estimated in the LSRC device. These values are compared with total unit weight profiles measured at other MSW landfills.

An empirical relationship between estimated total unit weight and confining pressure, including weight percentage of soil-size material, was developed. Values of total unit weight predicted by Equation (6.7) were compared with values measured in the RCTS and LSRC devices.

Along with the test parameters, the effects of material parameters were studied. These material parameters are: (1) waste composition, (2) water content, (3) total unit weight, and (4) particle size. The effects of water content, total unit weight, and particle size of the MSW specimens were studied using the RCTS device, whereas the LSRC device was used to investigate the effect of waste composition. The effects of waste composition, water content, and total unit weight have small impact on G_{max} and D_{min}. The effect of particle size is insignificant on G_{max} and D_{min}.

An empirical relationship between G_{max} and D_{min} was developed using the data of old and mixed MSW specimens measured in the RCTS and LSRC devices. This relationship can provide an insight into the prediction of values of D_{min} at in-situ MSW landfills with shear modulus measurements. The comparison between corrected D_{min} and predicted D_{min} is given in Figure 6.34.

Small-strain dynamic properties of old MSW were compared with this loose sand.

As a result, there is a large difference in G_{max}, V_s, and D_{min}.

CHAPTER 7: Small-Strain Dynamic Properties of Fresh MSW

7.1 INTRODUCTION

Similar to old MSW, a series of RC tests in the RCTS and LSRC devices were performed on 2.8-in. (71.1-mm) and 6.0-in. (152.4-mm) diameter specimens to investigate the dynamic properties of the fresh MSW in the small-strain range (γ<0.002 %). The values of G_{max} and D_{min} were measured in this strain ranges. Test parameters affecting G_{max} and D_{min} of fresh waste are investigated in this chapter. These parameters are: (1) duration of confinement, t, (2) isotropic confining pressure, σ_o, and (3) excitation frequency, f, and (4) specimen size.

The influence of material parameters affecting G_{max} and D_{min} is also investigated. These material parameters include: (1) waste composition, (2) water content, (3) variation of total unit weight for the same material type, and (4) particle size. The test results measured in the RCTS and LSRC devices are analyzed and compared below.

In addition, the variation in estimated total unit weights of fresh MSW specimens during the RC tests in the RCTS and LSRC devices are compared with profiles measured at other MSW landfills.

7.2 TEST PROCEDURES

7.2.1 Testing with the RCTS Device

LARC tests were performed on small-diameter specimens at their natural and

hydrated conditions. Testing was performed at a multiple confining pressures, as given in Table 7.1. The amplitude of shearing strain during the RC tests was kept less than 0.002 % to ensure small-strain measurements. Each specimen was confined under each specified confining pressure for at least one day and then advanced to the next confining

Table 7.1 Isotropic Confining Pressures Used in Low-Amplitude RC Tests for Small-Diameter, Soil-Size Fresh Waste Specimens in the RCTS Device

Specimen ID	Isotropic Confining Pressure
	Low-Amplitude RC Tests, psi (kPa)
MSW1FNS1$^{\Delta}$	1.2, 2.5, 5, 11, 20, 40, 11*, 2.5* (8, 17, 34, 76, 138, 276, 76, 17)
MSW1FHS1	1.2, 2.5, 5, 11 (8, 17, 34, 76)
MSW2FNS2$^{\triangle}$	1.2, 2.5, 5, 11, 20, 40, 11*, 2.5* (8, 17, 34, 76, 138, 276, 76, 17)
MSW3FNS1	2.5, 5, 11 (17, 34, 76)
MSW4FNS2	2.5, 5, 11, 20, 40 (17, 34, 76, 138, 276)

Notes:

* represents unloading stage

Δ1 at the end of specimen ID represents a specimen reconstituted with material passed the 3/8-in. (9.5-mm) sieve

⌂2 at the end of specimen ID represents a specimen reconstituted with material passed the ¾-in. (19.1-mm) sieve

pressure. The confinement sequence was separated into two stages: loading and unloading stages. All measurements followed this loading pattern: first, the specimens were tested up to 40 psi (276 kPa), and then testing was performed on an unloading

sequence. In a similar manner to old MSW, a pair of fresh MSW specimens, Specimen MSW 3ONS1 and MSW4ONS2, was constructed to study the effect of unit weight for the same material type.

It should be noted that the RCTS device is employed to investigate the effect of test and material parameters with small-diameter specimens in the small-strain ranges. These test parameters include: (1) duration of confinement, (2) total isotropic confining pressure, (3) excitation frequency, and (4) specimen size. Material parameters investigated with the RCTS device are: (1) waste composition (only for 100 % soil-size MSW material), (2) water content, (3) total unit weight, and (4) particle size.

7.2.2 Testing with the LSRC Device

LARC tests were performed with large-diameter specimens at their natural conditions. Testing was performed at a series of confining pressures, as shown in Table 7.2. Similar to with the RCTS tests, shearing strain amplitude kept less than 0.001 % to ensure small-strain measurements. Each specimen was confined under each specified confining pressure for at least one day and then advanced to the next confining pressure.

The confinement sequence was separated into two stages: loading and unloading stages. All measurements followed this loading pattern: first, the specimens were tested up to 40 psi (276 kPa), and then testing was performed on an unloading sequence.

As mentioned in Section 6.2.2, no investigation on the effect of water content with the LSRC device was done because it was difficult to assemble 6.0-in. (152.4-mm) split mold around the specimen. Furthermore, since the LSRC device could not perform the TS tests, a study on the effects of the number of loading cycles and excitation frequency on large-diameter specimens was not conducted.

Using the LSRC device, the influence of test and material parameters were

investigated upon large-diameter specimens reconstituted with 100 % soil-size material or soil-size material plus larger particles in the small-strain ranges. These test parameters are: (1) duration of confinement, (2) total isotropic confining pressure, and (3) specimen size (in conjunction with the RCTS tests). Material parameters investigated

Table 7.2 Isotropic Confining Pressures Used in Low-Amplitude for Large-Diameter, Soil-Size Fresh Waste Specimens and Fresh Waste Specimens with Larger Particles in the LSRC Device

Specimen ID	Weight Percentage of Soil-Size, (%)	Isotropic Confining Pressure
		Low-Amplitude RC Tests, psi (kPa)
MSW1FNL2$^{\triangle}$	100	1.2, 2.5, 5, 11, 20, 40, 11*, 2.5* (8, 17, 34, 76, 138, 276, 76, 17)
MSW2FNL4$^{\square}$	62	1.2, 2.5, 5, 11, 20, 40 (8, 17, 34, 76, 138, 276)
MSW3FNL2	100	1.2, 2.5, 5, 11, 20, 40, 11*, 2.5* (8, 17, 34, 76, 138, 276, 76, 17)
MSW4FNL3$^{\lozenge}$	76	1.2, 2.5, 5, 11, 20, 40, 11*, 2.5* (8, 17, 34, 76, 138, 276, 76, 17)
MSW5FNL2	100	1.2, 2.5, 5, 11, 20, 40, 11*, 2.5* (8, 17, 34, 76, 138, 276, 76, 17)
MSW6FNL4	62	2.5, 5, 11, 20, 40 (8, 17, 34, 76, 138, 276)
MSW7FNL3	76	1.2, 2.5, 5, 11, 20, 40 (8, 17, 34, 76, 138, 276)
MSW8FNL4	62	1.2, 2.5, 5, 11, 20, 40 (8, 17, 34, 76, 138, 276)
MSW9FNL1$^{\Delta}$	100	1.2, 2.5, 5, 11, 20, 40 (8, 17, 34, 76, 138, 276)

Notes:

* denotes unloading stage

Δ1 at the end of specimen ID denotes a specimen reconstituted with material passed the 3/8-in. (9.5-mm) sieve

⌂2 at the end of specimen ID denotes a specimen reconstituted with material passed the ¾-in. (19.1-mm) sieve

◊3 at the end of denotes a specimen reconstituted with paper, soft plastic, and wood

□4 at the end of specimen ID denotes specimen reconstituted with paper, soft plastic, wood, and gravel.

with the LSRC device are: (1) waste composition (all groups of MSW material) and (2) particle and specimen sizes.

7.3 TEST PARAMETERS AFFECTING G_{MAX} AND D_{MIN} OF FRESH WASTE IN THE SMALL-STRAIN RANGE

7.3.1 Duration of Confinement at a Constant Pressure

As already discussed in Chapter 6, the effect of duration of confinement is quite important in laboratory RC measurements, considering that the dynamic properties change with the duration of confinement at a constant confining pressure. Therefore, for given MSW specimens, comparison should be made at the same confinement time and under the same test conditions.

7.3.1.1 Change in G_{max} with Confinement Time

A typical example of the effect of duration of confinement on G_{max} at its natural condition is shown in Figure 7.1 for Specimen MSW1FNS1. Loading sequence is represented by open symbols and unloading sequence is represented by solid symbols. As mentioned in Section 6.3.1.1, the initial loading sequence can be divided into the OC and NC states. As shown in the figure, the values of G_{max} increase with increasing duration of confinement and magnitudes of confining pressure. Same explanation can be applied to an increase in G_{max}, as explained in Section 6.3.1.1. During unloading sequence, the values of G_{max} are somewhat higher than those measured at the initial loading sequence at the same confining pressures due to introduced by the effect of confinement time and overconsolidation. As can be seen, G_{max} decreases slightly with increasing confinement time, and then G_{max} begins to increase with confinement of time under a constant confining pressure.

Using Equations (6.1) and (6.2), proposed by Stokoe and Lodde (1978), long-

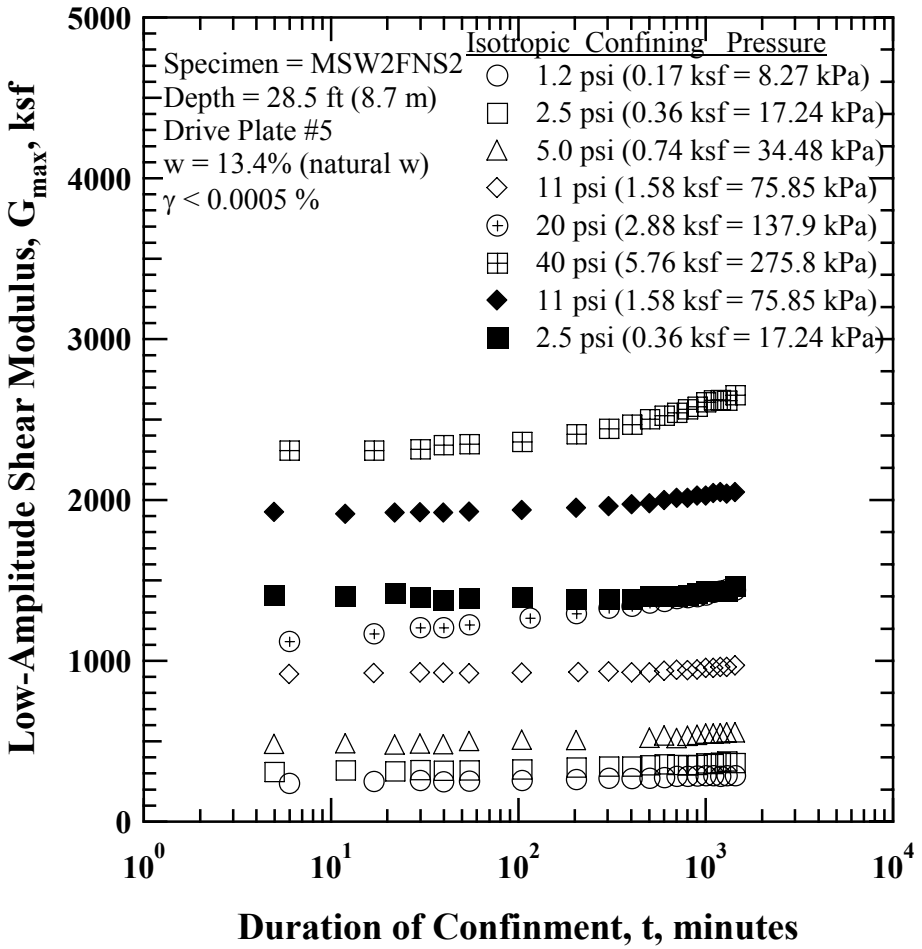

Figure 7.1 Variation in Low-Amplitude Shear Modulus with Magnitude and Duration of Confinement for 100 % Soil-Size Fresh MSW Specimen MSW2FNS2

term time effect in G_{max} measurements in terms of the values of I_G and N_G was evaluated typically for Specimen MSW2FNS2. These values of I_G and N_G are tabulated in Table 7.3. As indicated, the values of I_G increase with confining pressure, whereas the values of N_G are approximately constant, with some scatter at the confining pressures of 1.2 psi (8 kPa) and 2.5 psi (17 kPa).

To investigate the long-term time effect of other groups of fresh MSW, values of N_G in the OC and NC states during the initial loading sequence were obtained using

Table 7.3 Summary of Coefficients of Shear Modulus Increase, I_G, and Values of A Normalized Shear Modulus Increase, N_G, for Specimen MSW2FNS2 (100 % Soil-Size Material)

Confining Pressure psi, (kPa)	I_G, ksf (MPa)	N_G, %
1.2 (8)	2.3 (0.1)	0.8
2.5 (17)	11.9 (0.6)	3.3
5 (34)	58.2 (2.8)	10.7
11 (76)	97.9 (4.7)	10.3
20 (138)	184.0 (8.8)	13.1
40 (276)	287.9 (13.8)	11.0

the Equation (6.2). The variations in N_G with different weight percentages of soil-size material in the OC and NC states are shown in Figures 7.2 (a) and (b), respectively. As can be seen, the values of N_G generally increase with increasing weight percentage of soil-size material both in the OC and NC states for the fresh MSW. The values of N_G is are somewhat smaller in the OC state than in the NC state due to overconsolidation created by compaction effort. That is, a larger change in inter-particle void space and particle contacts occurs in the NC state than in the OC state. It is hard to find general trends of change in the values of N_G with confining pressure both in the OC and NC states, as shown in the figures.

7.3.1.2 Change in D_{min} with Confinement Time

A typical example of the variation in D_{min} with duration of confinement at its natural condition is presented in Figure 7.3 for Specimen MSW2FNS2. The values of D_{min} shown in the figure were determined using the half-power bandwidth method in the RCTS device. In contrast to G_{max} shown in Figure 7.3, D_{min} generally decreases with

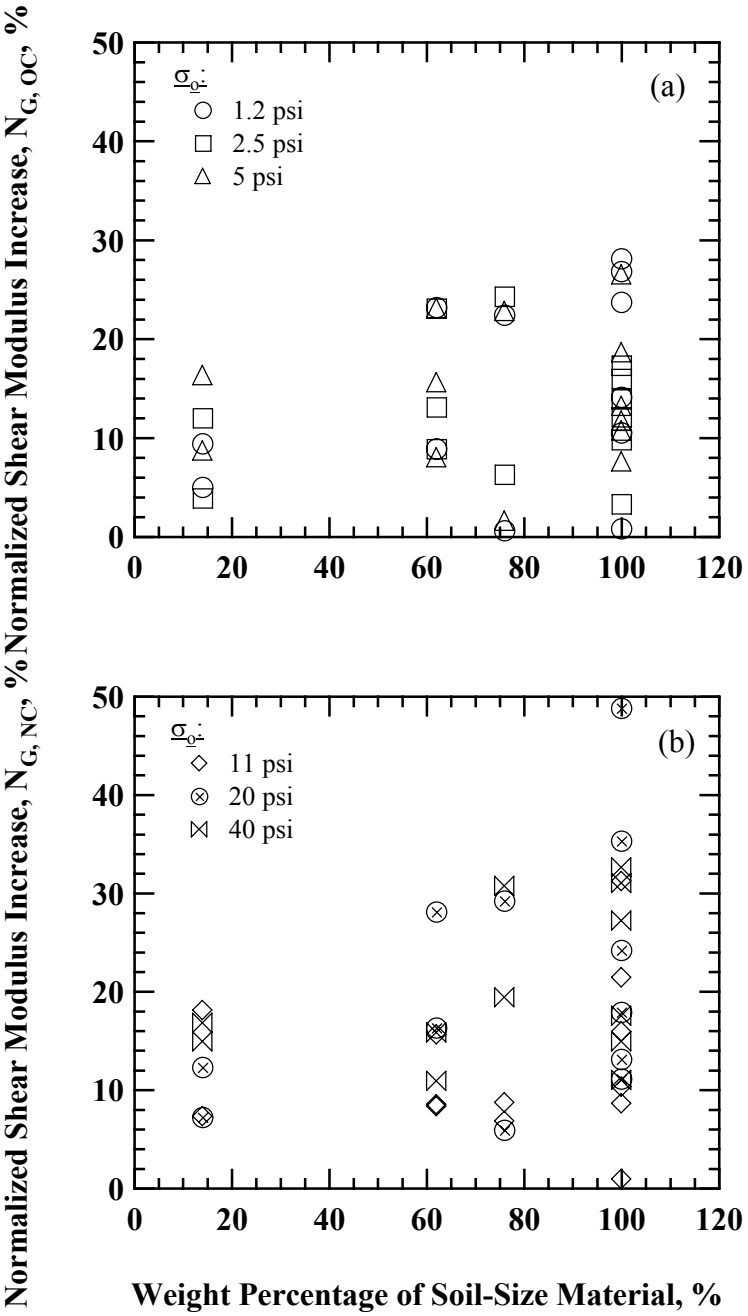

Figure 7.2 Comparison of the Variation in Normalized Shear Modulus Increase with Different Weight Percentages of Fresh, MSW at Their Natural Water Content in the: (a) OC and (b) NC States

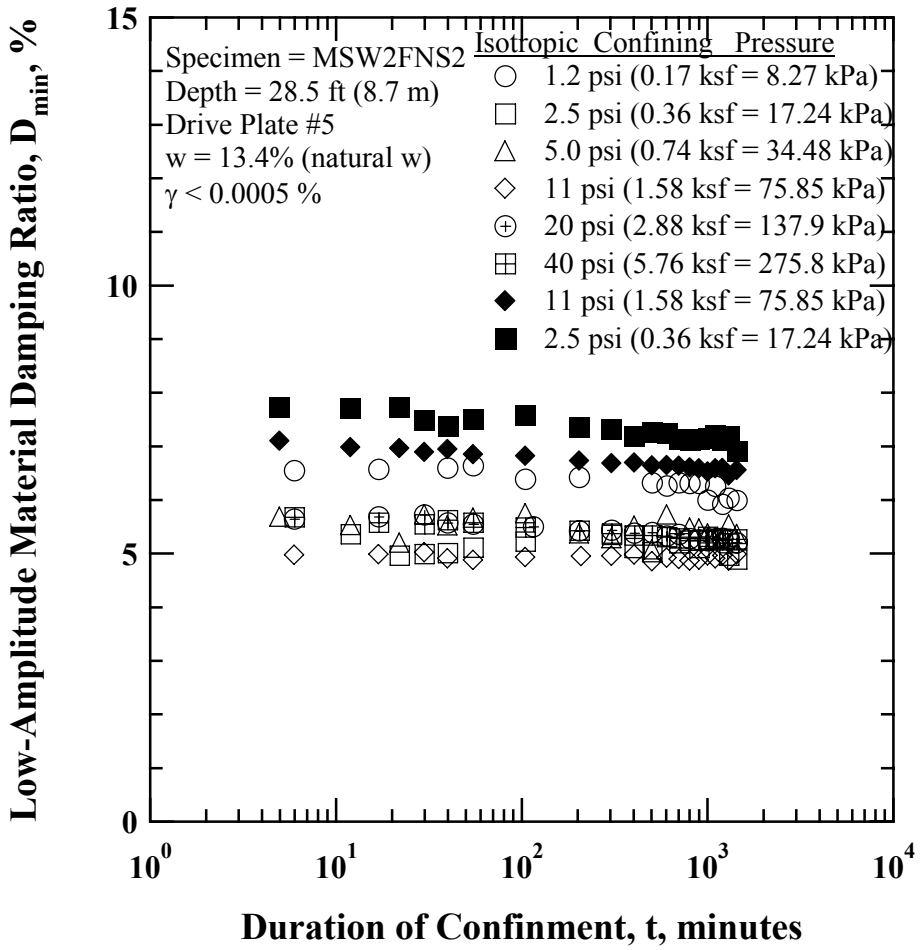

Figure 7.3 Variation in Low-Amplitude Material Damping Ratio with Magnitude and Duration of Confinement for MSW2FNS2 (100 % Soil-Size Material)

increasing duration of confinement. The fluctuation in D_{min} measurements might result to some extent from background noise during the damping measurements.

As explained in Section 6.3.1.2, either structural changes in particle arrangement (Marcuson and Wahls, 1978) or constrained relative movement of inter-particles (Stoll, 1989) may contribute to a decrease in D_{min} with increasing duration of confinement.

During the unloading sequence, the values of D_{min} are somewhat higher than those measured in the initial loading sequence at the same confining pressures. This

difference may be somewhat be explained by relatively more spaces in the inter-particle movements during confining pressure release leading to an increase in D_{min}.

As with G_{max}, using the Equations (6.3) and (6.4), long-term time effect in the D_{min} measurements was evaluated in terms of the values of I_D and N_D. Typical values of I_D and N_D with confining pressure for Specimen MSW2FNS2 are given in Table 7.4. As indicated, the values of I_D exhibit more scatter at lower confining pressures. However, at subsequent confining pressures in the NC state, the values of I_D generally decrease (are small and become more negative). The values of N_D follow a similar trend.

Table 7.4 Summary of Values of Material Damping Ratio Increase, I_D, and Values of a Normalized Material Damping Ratio Increase, N_D, for Specimen MSW2FNS2 (100 % Soil-Size Material)

Confining Pressure psi, (kPa)	I_D, %	N_D, %
1.2 (8)	-0.02	-0.38
2.5 (17)	0.79	14.61
5 (34)	-0.07	-1.39
11 (76)	0.17	3.37
20 (138)	-0.22	-4.29
40 (276)	-0.29	-5.54

To investigate the long-term time effect measured in all fresh MSW Groups, the values of N_D were calculated using the Equation (6.4) at each confining pressure level in the loading sequence. The variations in N_D with different MSW groups in the OC and NC states are shown in Figures 7.4 (a) and (b), respectively. As shown in the figures, the values of N_D show somewhat scatter both in the OC and NC states. The values of

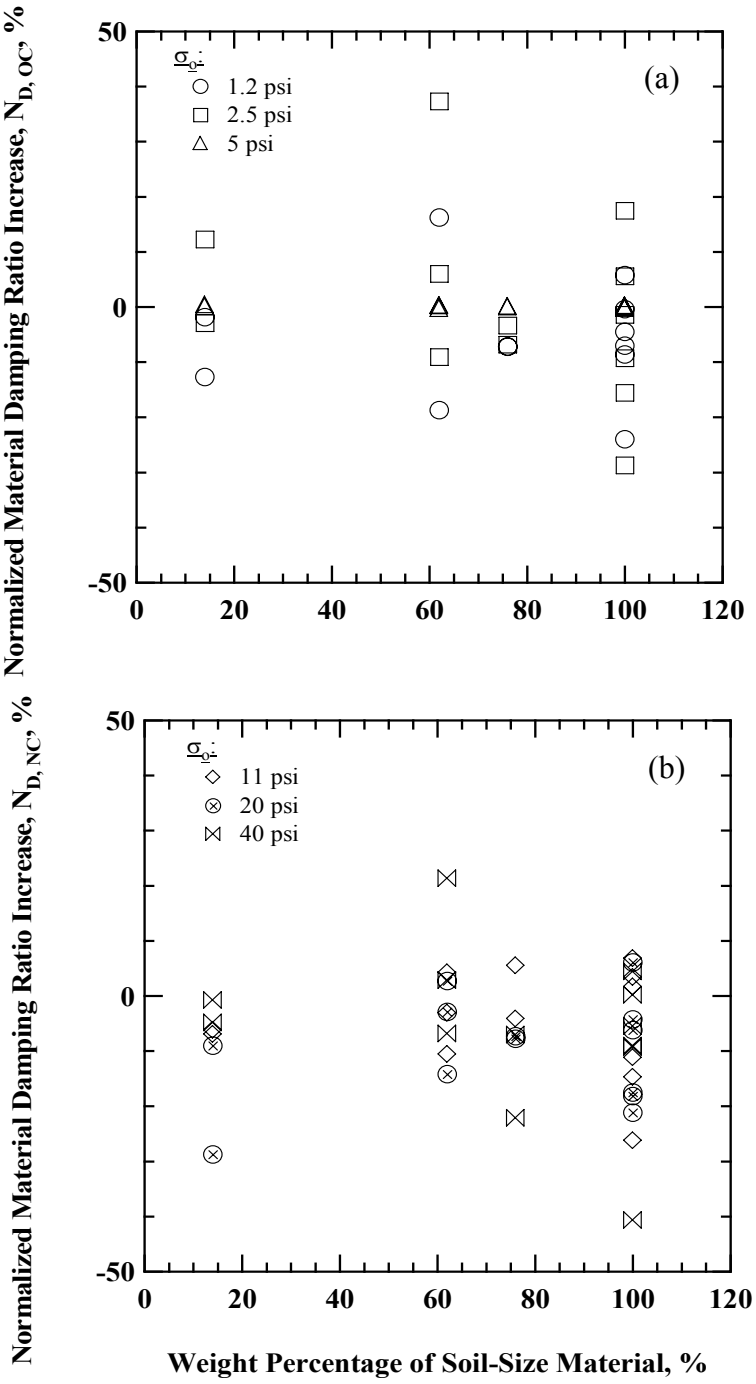

Figure 7.4 Comparison of the Variation in Normalized Material Damping Ratio Increase with Different Weight Percentage of Fresh, MSW at Their Natural Water Content in the: (a) OC and (b) NC States

N_D in the OC and NC states are approximately the same regardless of the different MSW groups. It is relatively more complex to find general trends of N_D with respect to confining pressure level. It is interesting to observe that the values of N_D in the NC state are located approximately below zero.

7.3.2 Total Isotropic Confining Pressure

7.3.2.1 Log G_{max} - Log σ_o Relationship

Along with the duration of confinement, confining pressure is one of the key test parameters that have a significant impact on G_{max} and D_{min} measurements. A series of RC tests were performed on fresh MSW specimens at multiple confining pressures for one day of confinement at each pressure upon loading and unloading.

A typical variation in G_{max} with isotropic confining pressure for the 100% soil-size fresh MSW specimens is plotted in Figure 7.5 with logarithmic scales for both G_{max} and σ_o. These values are obtained from the RCTS tests with 100 % soil-size MSW specimens. The loading sequence is represented by open symbols, whereas the unloading sequence is represented by solid symbols of the same shape. Results are shown only for waste tested at the natural water content found in the field ($w \approx 12.0$ %) (Zekkos, 2005). Initial total unit weights of the specimens are 90.6 pcf (14.2 kN/m^3) and 86.0 pcf (13.5 kN/m^3) for Specimens MSW1FNS1 and MSW2FNS2, respectively, showing a difference of about 5 %. Water contents are 13.0 % and 13.4 %, respectively. As shown in Figure 7.5, the variations in G_{max} with isotropic confining pressure for given MSW specimens are very similar in the RC measurements in the NC state, with a variation in the OC state. The overconsolidation behavior is presented in the initial loading sequence created by compaction effort and during the unloading sequence due to confining pressure release. This over consolidation in the initial loading sequence is

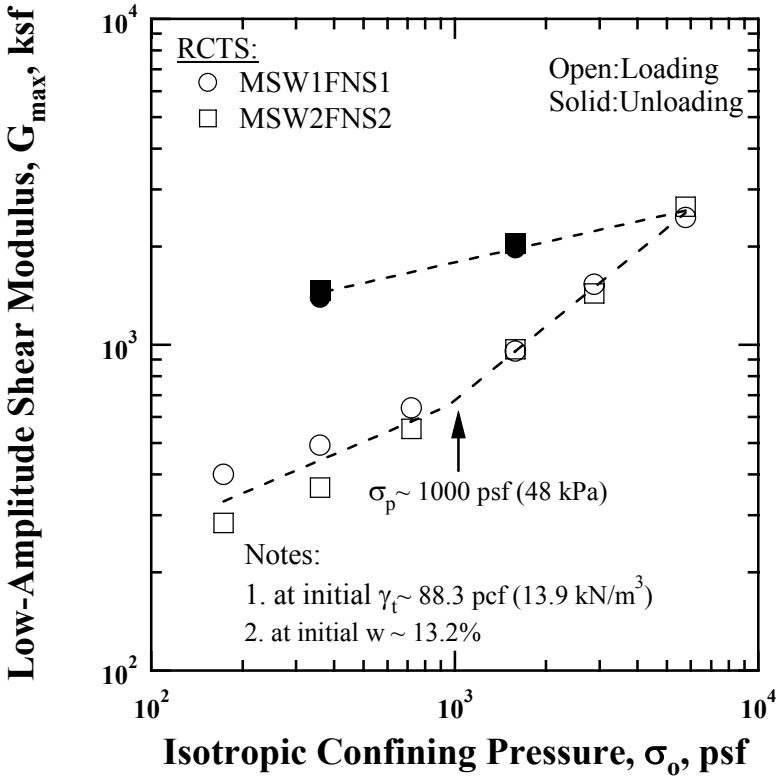

Figure 7.5 Variation in Low-Amplitude Shear Modulus with Isotropic Confining Pressure for 100 % Soil-Size Fresh MSW Specimens in the RCTS Device

divided into the OC and NC states. The value of σ_p produced by compaction effort was about 1085 psf (52 kPa). As shown in the figure, the OC state is shown by relative flat log G_{max}-log σ_o relationship.

However, above about 1000 psf (48 kPa), specimens become NC state, changing in shape of the log G_{max}-log σ_o relationship. This increase in G_{max} was largely due to a substantial change in inter-particle voids spaces and due to an increase in confining pressure. It is interesting to observe that the initial log G_{max}-log σ_o relationship in the OC state is larger than that of unloading sequence by a factor of about two. This difference can be attributed to considerable change in voids spaces in the specimen during the initial loading sequence.

The effect of confining pressure on G_{max} was evaluated using the Equation (6.5) in the loading and unloading sequences separately. The fitted equations are presented by the dashed lines in Figure 7.5. A set of the values of n_G and G_1 are given in Table 7.5.

Table 7.5 A Set of the Values of n_G and G_1 upon Loading and Unloading Sequences for 100 % Soil-Size Fresh MSW Specimens in the RCTS Device

Sequence		Exponent, n_G	Shear Modulus, G_1, ksf (MPa)
Loading	OC	0.40	891 (43)
	NC	0.76	1190 (57)
Unloading		0.21	2093 (100)

To evaluate the effect of confining pressure on G_{max} of other fresh MSW Groups (e.g., 76 %, 62 %, and 14 % soil-size material Groups), log G_{max}-log σ_o relationship of each group was fitted using the Equation (6.5) in the loading sequence. The variations in the values of n_G of the fitted equation in the OC and NC states with other MSW groups are shown in Figures 7.6 (a) and (b), respectively. As can be seen in the figures, the variation in the values of n_G in the OC state is relatively larger than in the NC states. Considering the scatter in the values, the values of n_G generally decrease with increasing weight percentage of soil-size material in the OC state. However, in the NC state, showing a relatively narrower variation, the values of n_G are approximately the same regardless of the weight percentage of soil-size material of the fresh MSW. Again, like the old MSW specimens, the values of n_G are less than one, which is an exponent in the Mohr-Coulomb failure criterion relationship.

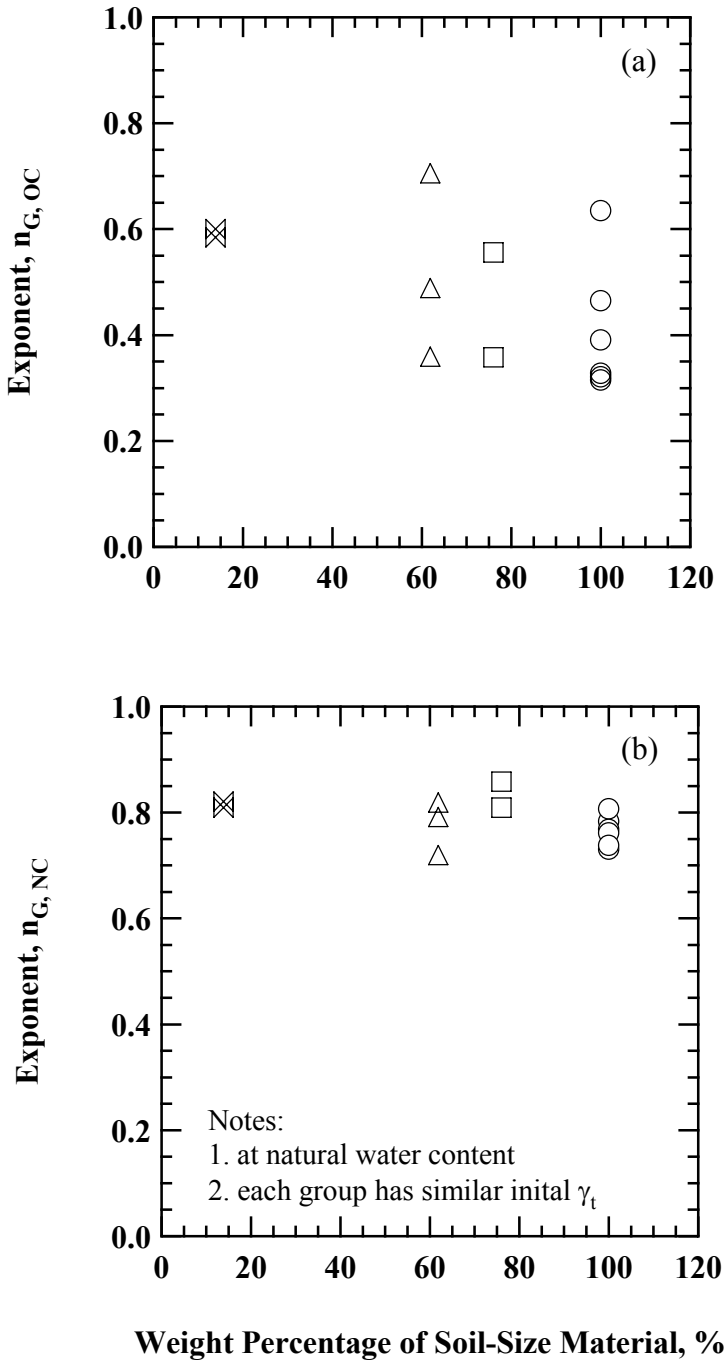

Figure 7.6 Comparison of the Variation in the Values of Exponent in the (a) OC and (b) NC States with Different Weight Percentages of Soil-Size Fresh MSW

7.3.2.2 Log D_{min} - Log σ_o Relationship

A typical variation in D_{min} with isotropic confining pressure is shown in Figure 7.7 for 100 % soil-size fresh MSW specimens with logarithmic scales for both D_{min} and σ_o. The loading sequence is represented by open symbols, whereas the unloading sequence is represented by solid symbols of the same shape. The values of D_{min} shown in the figure were determined by the half-power bandwidth and were selected at least at the end of one day confinement at each pressure. Like G_{max}, results are shown only for waste tested at the natural water content found in the field (w ≈ 12.0 %) (Zekkos, 2005).

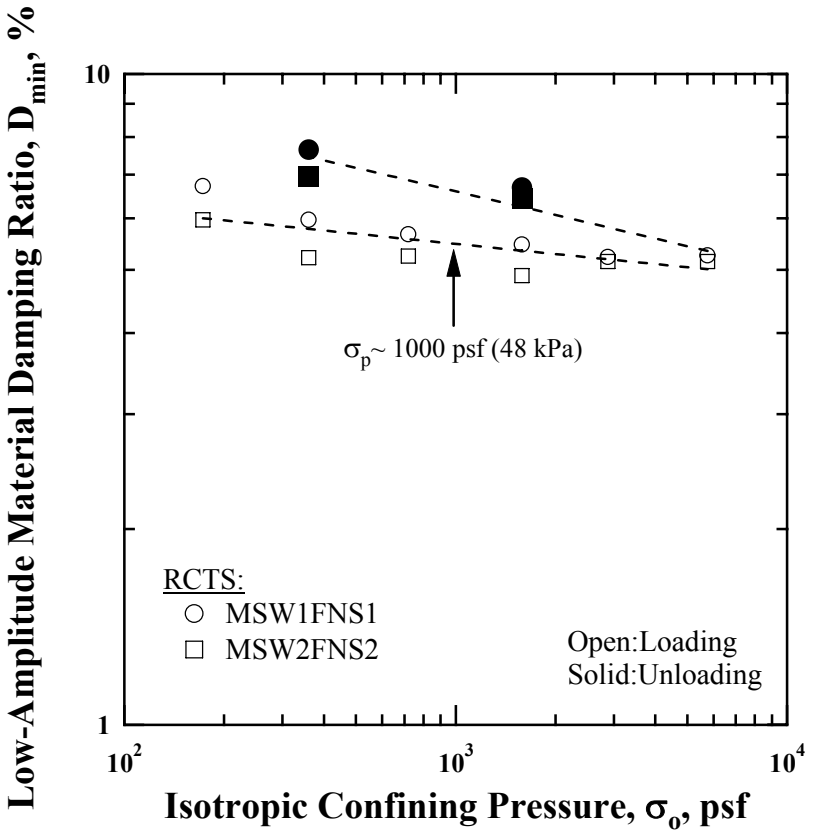

Figure 7.7 Variation in Low-Amplitude Material Damping Ratio with Isotropic Confining Pressure for 100 % Soil-Size Fresh Waste Specimens in the RCTS Device

As can be seen, D_{min} decreases with increasing confining pressure in the loading sequence, whereas D_{min} during the unloading sequence increases more than that determined at the identical confining pressures from the loading sequence. It is interesting to see that the effect of overconsolidation created by compaction effort, which was observed in log G_{max}-log σ_o relationship during the initial loading sequence, does not appear in the D_{min} measurements in the loading sequence. As discussed in Section 6.3.2.3, possible reasons for a decrease in D_{min} with increasing confining pressure is due to relatively less movements between inter-particles, resulting in less friction losses at their contact areas, thus, energy dissipation within the MSW specimens becomes smaller.

For the unloading sequence, opposite behavior in the D_{min} measurements is observed; D_{min} values increase with decreasing confining pressure. This difference may be explained by relatively more spaces for inter-particle movements during confining pressure release, resulting in an increase in D_{min}.

The effect of confining pressure on D_{min} was evaluated using the Equation (6.6) in the loading and unloading sequences separately. The fitted equations are shown by dashed lines in the figure. The values of exponent, n_D, and material damping ratio at one atmosphere, D_1, are tabulated in Table 7.6.

Table 7.6 A Set of the Values of Exponents (n_D) and Material Damping Ratio at One Atmosphere (D_1) upon Loading and Unloading Sequences for 100 % Soil-Size Fresh MSW Specimens in the RCTS Device

Sequence	Exponent, n_D	Material Damping Ratio, D_1, (%)
Loading	-0.05	5.28
Unloading	-0.12	6.03

When compared with the old MSW specimens, the values of n_D in the loading and unloading sequences are approximately the same, implying that the response of MSW specimens are similar regardless of age of the waste. Only difference in the D_{min} measurements exist in the absolute value over confining pressure; fresh MSW specimens exhibits slightly higher values in D_{min} than old MSW specimens.

To evaluate the effect of confining pressure on D_{min} of other fresh MSW Groups (e.g., 76 %, 62 %, and 14 % soil-size material Groups), log D_{min}-log σ_o relationship of each group was fitted using the Equation (6.6) in the loading sequence. As a result, the variation in the values of n_D and D_1 of the fitted equation in the loading sequence is given in Figures 7.8 (a) and (b), respectively.

As shown in Figure 7.8 (a), the values of n_D generally increase with decreasing weight percentage of soil-size material, indicating that material damping ratio of the fresh MSW specimens show a less sensitive response to an increase in confining pressure. Unlike old MSW specimens, the values of D_1 of the fresh MSW specimens are approximately the same regardless of the MSW groups.

7.3.3 Excitation Frequency

To investigate of the effect of excitation frequency of the fresh MSW, a series of RC and TS tests were performed with 100 % soil-size fresh MSW specimens in the RCTS device. These specimens are MSW1FNS1, MSW2FNS2, MSW3FNS1, and MSW4FNS2. The only RC tests performed with large-diameter specimens was Specimen MSW3FNL2, MSW5FNL2, and MSW9FNL1 in the LSRC device. However, TS testing can not be performed in the LSRC device. Thus, the effect of excitation frequency was investigated only with 100 % soil-size fresh MSW that was tested in the RCTS device. The variation in shear modulus with excitation frequency at a confining

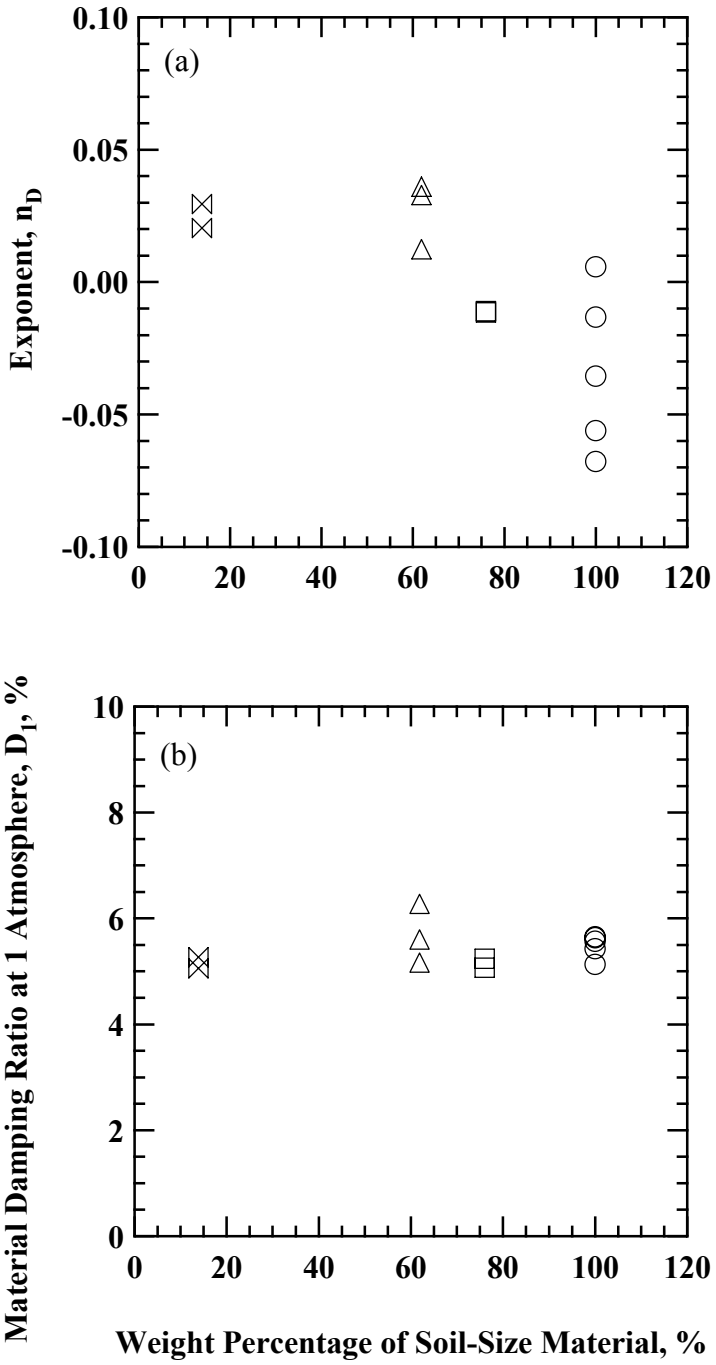

Figure 7.8 Comparison of the Values of: (a) the Exponent, n_D, and (b) Material Damping Ratio at One Atmosphere, D_1, in the Loading Sequence of Different Weight Percentages of Soil-Size Fresh MSW Specimens

pressure of 11 psi (76 kPa) is shown in Figure 7.9. The RC and TS tests were performed at shearing strain amplitudes of 0.0001 % and 0.001 %, in which shear modulus is equal to G_{max} and it is independent of shearing strain amplitude. The values of G_{max} from the RCTS tests are denoted by "Fx-Fr" and the values of G_{max} from the LSRC tests are denoted by "Fr-Fr" in the figure. As shown in the figure, the values of G_{max} increase linearly with respect to log f of increasing excitation frequency. As explained in Section 6.3.3, G_{max} increases with increasing excitation frequency due to the viscosity of the MSW skeleton frame and moisture in the pore space.

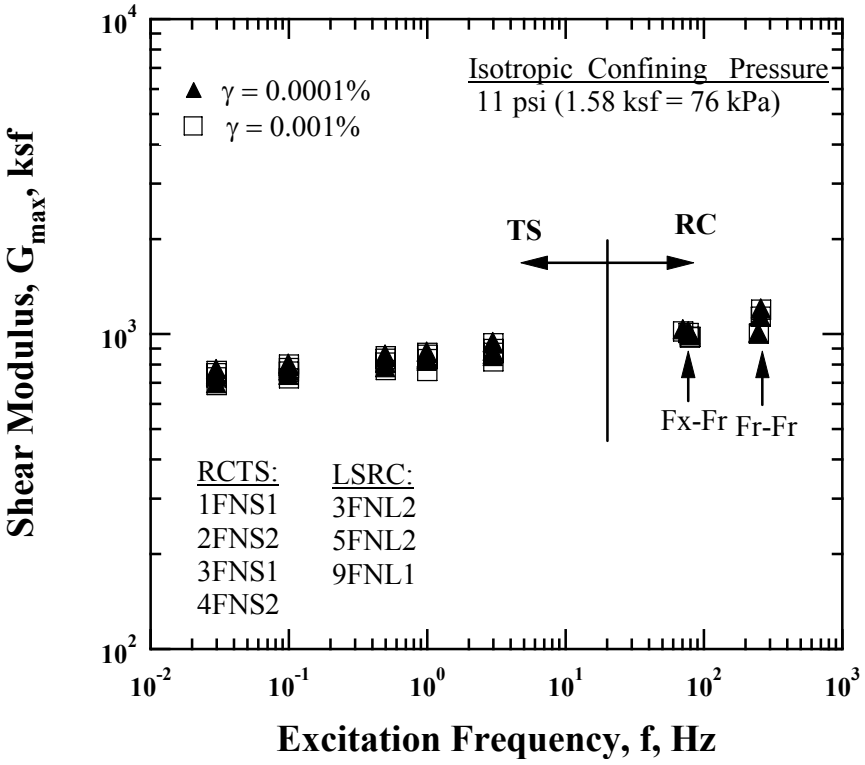

Figure 7.9 Variation in Shear Modulus with Excitation Frequency from RCTS and LSRC Tests for 100 % Soil-Size, Fresh Waste Specimens

To quantify the effect of excitation frequency on shear modulus at small strains, the values of G_{max} were normalized with the G_{max} measured at a frequency of 1Hz in the TS tests. The normalized shear modulus, $G_{max}/G_{max,\ f=1Hz}$, with excitation frequency is shown in Figure 7.6. These values were fitted using the least-squares method and the fitted line is given in the figure with a dashed line. The fitted equation is expressed by:

$$\frac{G_{max}}{G_{max,\ f=1Hz}} = 0.11 \times \log(\text{Freq.}) + 1.0 \qquad (7.1)$$

where,

G_{max} is a shear modulus measured at small strains at a given frequencies, and

$G_{max,\ f=1Hz}$ is a shear modulus measured at a frequency of 1Hz

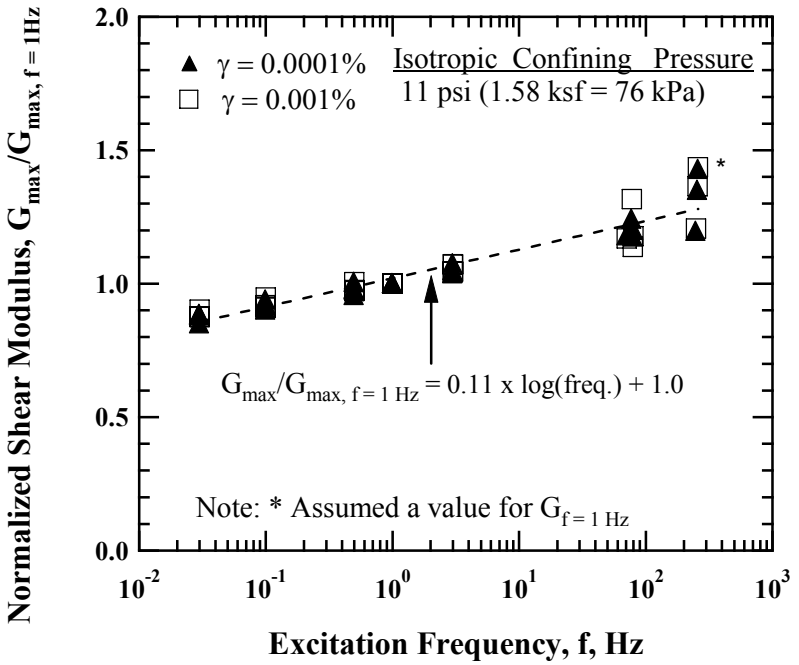

Figure 7.6 Variation in Normalized Shear Modulus with Excitation Frequency from the RCTS and LSRC Tests for 100 % Soil-Size Fresh Waste Specimens

As noted earlier, the LSRC device can not be need to perform torsional shear tests so that the shear modulus obtained from the LSRC tests was normalized with the one averaged from the TS tests at a frequency of 1 Hz. As can be seen in Figure 7.6, normalized shear modulus also increases linearly with the log f of increasing excitation frequency. The increases in G_{max} is about 1.6 times $G_{max,\ f = 1\ Hz}$ when the excitation frequency varies by approximately four orders of magnitude, e.g., from 0.03 Hz to 257 Hz. Thus, there is only a rather small effect of excitation frequency on G_{max}.

Material damping ratio was measured at a confining pressure of 11 psi (76 kPa) using the RCTS and LSRC devices on identical specimens listed earlier in 7.3.3. The variation in material damping ratio with excitation frequency is given in Figure 7.7. Material damping ratio measurements were made at a shearing strain amplitudes of 0.0001 % and 0.001 % so that the values of material damping ratio are approximately the same with some variation. The values of material damping ratio measured using the RCTS tests are indicated by "Fx-Fr" and the values of material damping ratio measured using the LSRC tests are indicated by "Fr-Fr" in the figure.

As shown in Figure 7.7, the values of D_{min} increase with decreasing excitation frequency below 0.5 Hz due to creep. Lager material damping ratio at lower excitation frequency is attributed to resultant larger hysteresis loops, resulting from a delayed response (strain) of MSW specimens to slower application of cyclic loading (Dobry and Vucetic, 1987). Frequency ranges from 0.5 Hz to 1 Hz are approximately constant.

On the other hand, the values of material damping ratio above the excitation frequency of 3 Hz increase dramatically with increasing excitation frequencies. This increase can result from an increased contribution of viscosity of MSW skeleton and an increased relative movement between solid particle and water in the MSW skeleton frame by a higher excitation frequency (Park, 1998, Shibuya et al., 1995).

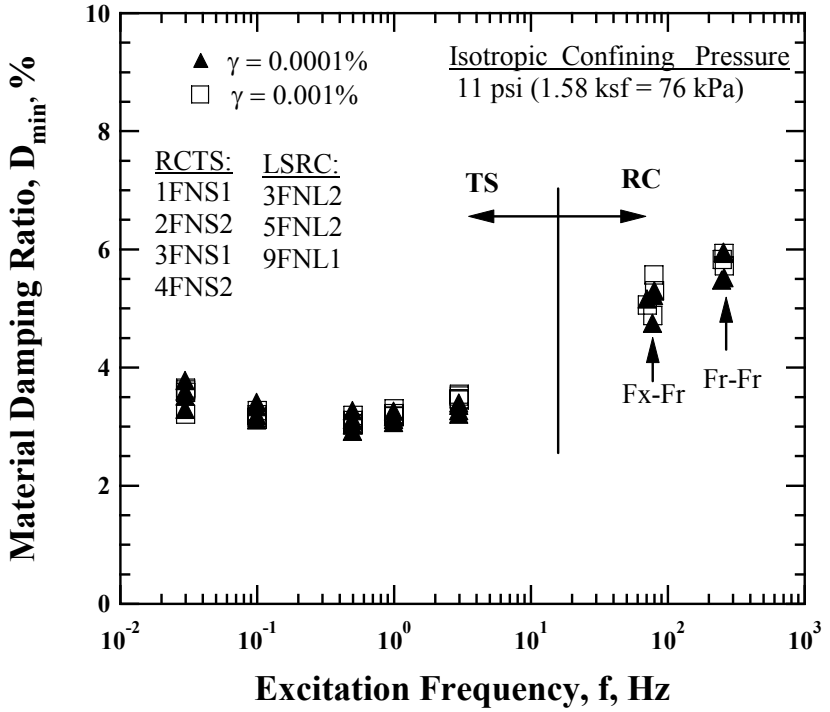

Figure 7.7 Variation in Material Damping Ratio with Excitation Frequency from the RCTS and LSRC Tests for 100 % Soil-Size Fresh Waste Specimens

To quantify the effect of excitation frequency, the values of material damping ratio were normalized with the material damping ratio measured at a frequency of 1 Hz in the TS tests. Normalized material damping ratio with excitation frequency is shown in Figure 7.8. Again, like shear modulus, the values of material damping ratio measured with the LSRC device were normalized with values measured at a frequency of 1 Hz in the TS tests. The data were fitted as a form of second-order of polynomial function using the least-squares method and the fitted equation is denoted by a dashed line. The fitted equation is given by:

$$\frac{D_{min}}{D_{min,\,f=1Hz}} = 0.11\times \log(\text{Freq.})^2 + 0.1\times \log(\text{Freq.}) + 1.0 \qquad (7.2)$$

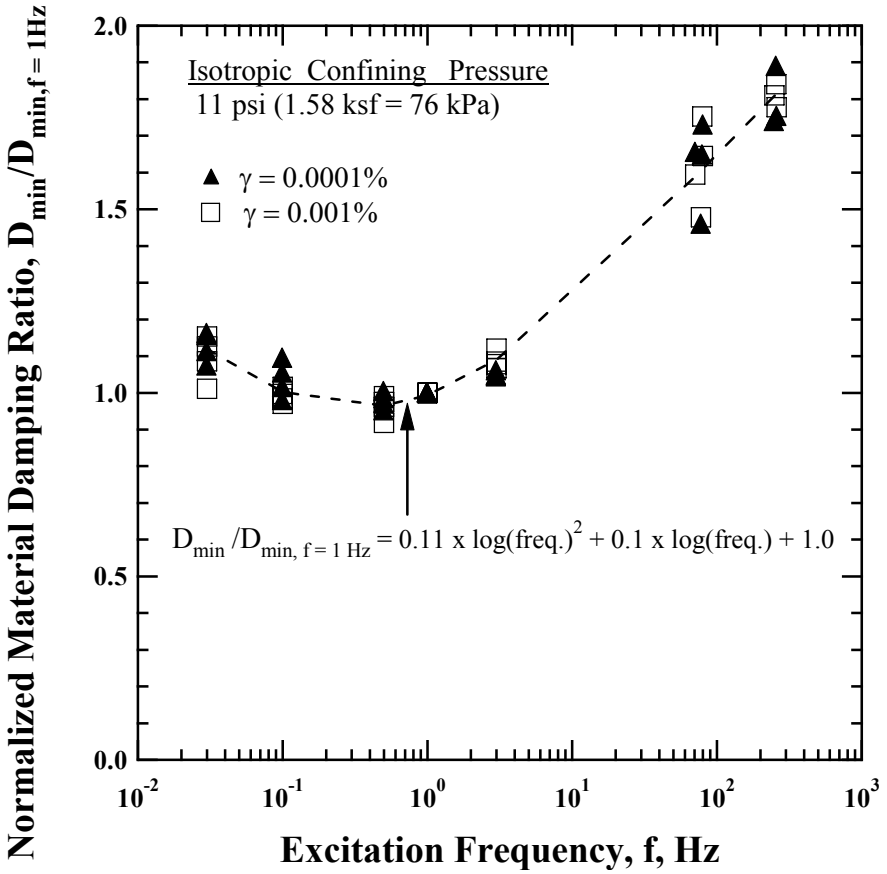

Figure 7.8 Nonlinear Relationship Fit to the Variation in Normalized Material Damping Ratio with Excitation Frequency for 100 % Soil-Size Fresh Waste Specimens

where,

D_{min} is a material damping ratio at small strains at a given frequencies, and

$D_{min, f=1Hz}$ is a material damping ratio measured at a frequency of 1 Hz.

As shown in Figure 7.8, normalized material damping ratio increases with decreasing excitation frequency below 0.5 Hz due to creep, whereas above the frequency of 0.5 Hz, material damping ratio increases with increasing excitation frequency due to frequency effect. The change in normalized material damping ratio from 0.03 Hz to 1

Hz amounts a factor of about 1.1 in average, whereas the change in normalized material damping ratio from 1 Hz to the highest frequency (257 Hz) amounts a factor of about 1.8 in average. On the basis of this observation, the effect of excitation frequency on material damping is significant at higher frequencies.

7.3.4 Specimen Size

To investigate the effect of specimen size on G_{max} and D_{min}, 2.8-in. (71.1-mm) and 6.0-in. (152.4-mm) diameter MSW specimens were prepared. These specimens were reconstituted with 100 % soil-size MSW material that passed the 3/8-in. (9.5-mm) and ¾-in. (19.1-mm) sieves. The RCTS and LSRC devices were employed to perform the RC tests for small- and large-diameter MSW specimens, respectively.

The variations in G_{max} uncorrected and corrected for excitation frequency, f, and total unit weight, γ_t, with confining pressure for the Specimens MSW1FNS1, MSW9FNL1 are shown in Figures 7.9 (a) and (b), respectively. These specimens were reconstituted with 100 % soil-size material passed the 3/8-in. (9.5-mm) sieve. Small-diameter specimen is represented by open symbol, whereas large-diameter specimen is represented by the open symbol with an "x" in the symbol. Like old MSW specimens, the values of G_{max} were corrected to f = 1 Hz using Equation (7.1) and the values of γ_t were normalized with a value of Specimen MSW1FNS1 of 90.6 pcf (14.2 kN/m^3) to eliminate the effects of excitation frequency and total unit weight.

As shown in Figure 7.9 (a), the variations of G_{max} with confining pressure for small- and large-diameter specimens are essentially the same behavior in the OC and NC states. In Figure7.9 (b), the variation in G_{max} with confining pressure is nearly the same as the Figure 7.9 (a) after correcting for excitation frequency and total unit weight. This comparison implies that the effect of specimen size on G_{max} is small to negligible for

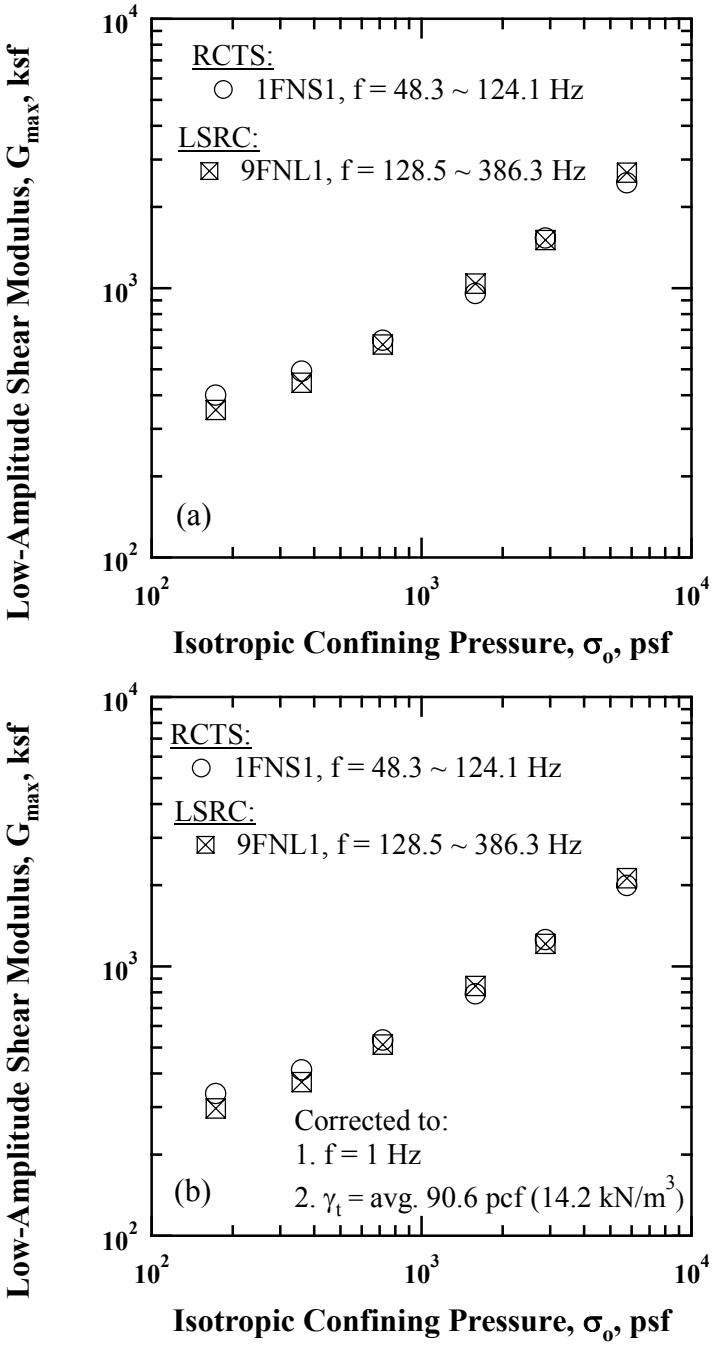

Figure 7.9 Comparison of the Variation in Low-Amplitude Shear Modulus with Isotropic Confining Pressure of Different Specimen Sizes Reconstituted with 100 % Soil-Size Fresh MSW Passing the 3/8-in. (9.5-mm) Sieve: (a) Uncorrected for f and γ_t and (b) Corrected for f and γ_t

fresh MSW specimens reconstituted with material passing the 3.8-in. (9.5-mm) sieve.

Another comparison of the variation in G_{max} (uncorrected and corrected for excitation frequency, f, and total unit weight, γ_t) with confining pressure is shown in Figures 7.10 (a) and (b) for Specimen MSW2FNS2 and MSW5FNL2. These specimens were reconstituted with material that passed the ¾-in. (19.1-mm) sieve. As shown in Figure 7.10 (a), the variations in G_{max} with confining pressure for small- and large-diameter specimens exhibit basically the same in the NC state. However, there is a difference in the OC state, with the LSRC tests exhibits higher G_{max} that is assumed to be due mainly to an increased compaction being created during sample construction.

In Figure 7.10 (b), the variation in G_{max} with confining pressure is slightly closer after correcting for excitation frequency and total unit weight. This comparison indicates that the effect of specimen size on G_{max} is small to negligible for fresh MSW specimens reconstituted with material passing the ¾-in. (19.1-mm) sieve. Based on these observations, the effect of specimen size on G_{max} for fresh MSW specimens reconstituted with material passing the 3/8-in. (9.5-mm) and ¾-in. (19.1-mm) sieves is unimportant.

The variations in D_{min} (uncorrected and corrected for excitation frequency) with confining pressure for the Specimens MSW1FNS1 and MSW9FNL1 are shown in Figures 7.11 (a) and (b), respectively. As shown in Figure 7.11 (a), the values of D_{min} measured in the RCTS and LSRC devices are almost the same with exceptions at the first and last D_{min} measurements. Unlike G_{max}, only excitation frequency could be corrected for because of the limited knowledge on how to correct for total unit weight. After removing the effect of excitation frequency (corrected to f = 1 Hz using Equation (7.2)), the values of D_{min} from the LSRC tests become smaller over confining pressures. Therefore, the effect of specimen size on D_{min} for MSW specimens reconstituted with

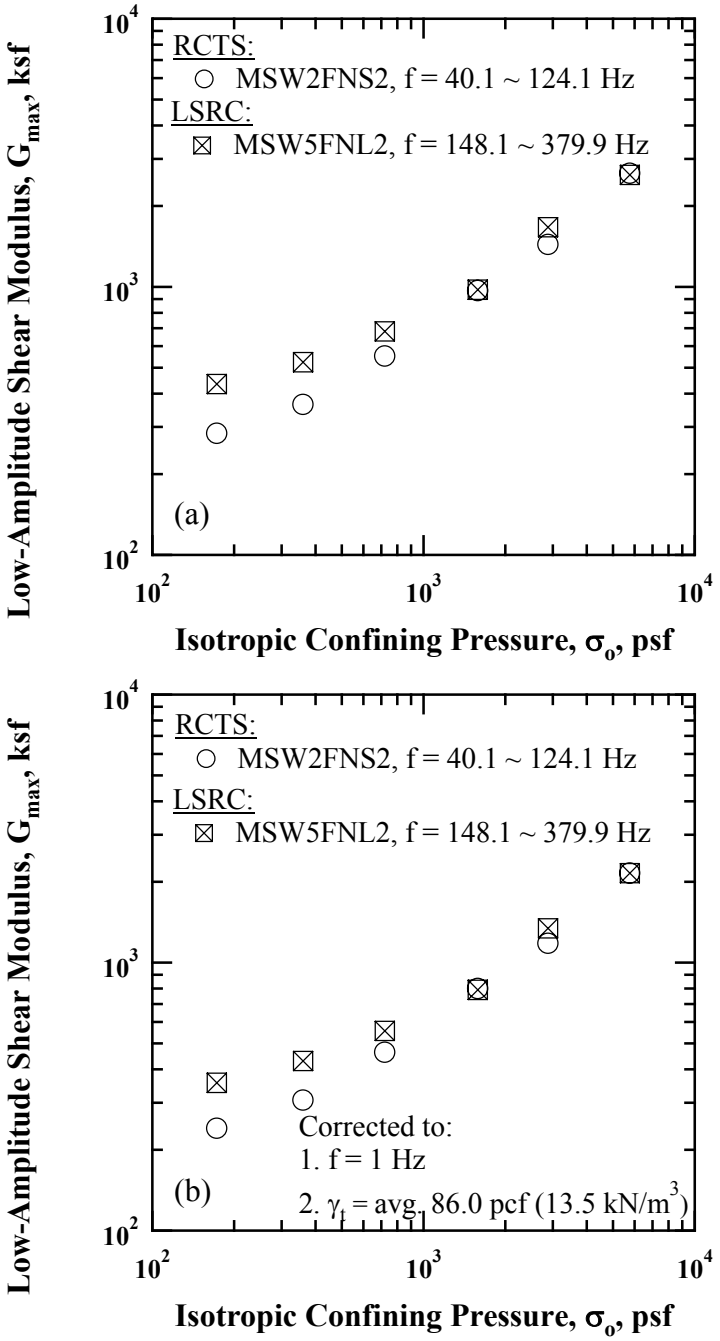

Figure 7.10 Comparison of the Variation in Low-Amplitude Shear Modulus with Isotropic Confining Pressure of Different Specimen Sizes Reconstituted with 100 % Soil-Size Fresh MSW Passing the ¾-in. (1915-mm) Sieve: (a) Uncorrected for f and γ_t and (b) Corrected for f and γ_t

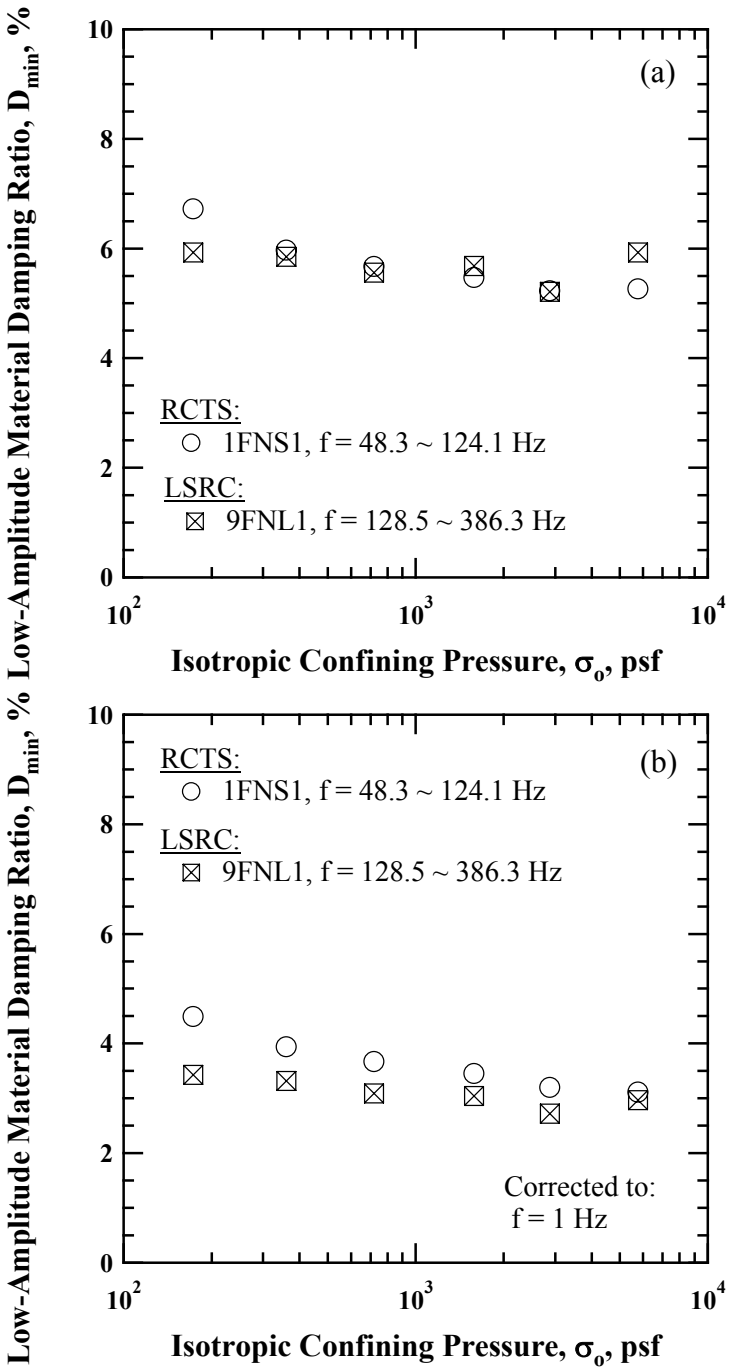

Figure 7.11 Comparison of the Variation in Low-Amplitude Material Damping Ratio with Isotropic Confining Pressure of Different Specimen Sizes Reconstituted with 100 % Soil-Size Fresh MSW Passing the 3/8-in. (9.5-mm) Sieve: (a) Uncorrected for f and (b) Corrected for f

material passing the 3/8-in. (9.5-mm) is negligible with some scatter.

Another variation in D_{min} (uncorrected and corrected for excitation frequency) with confining pressure for the Specimens MSW2FNS2 and MSW5FNL2 is shown in Figures 7.12 (a) and 7.12 (b), respectively. The values of D_{min} measured in the LSRC test are, to some extent, higher than those measured in the RCTS test. This difference in D_{min} is mainly due to excitation frequency. To remove the effect of excitation frequency on D_{min}, the values of D_{min} were normalized with using Equation (7.2). As can be seen, the variation in D_{min} for the MSW specimens reconstituted with material passing the ¾-in. (19.1-mm) sieve is essentially the same. Thus, the effect of specimen size on D_{min} reconstituted with material passed the ¾-in. (19.1-mm) is insignificant.

7.4 ESTIMATION OF TOTAL UNIT WEIGHT OF FRESH MSW SPECIMENS DURING THE RC TESTS AND COMPARISON WITH PREVIOUS STUDIES

As mentioned in Section 6.4, total unit weight of fresh and mixed MSW specimens is estimated during the RC tests in the RCTS and LSRC devices by assuming that a change in strain in the longitudinal and radial directions is the same due to isotropic confinement. The variations in estimated total unit weight with confining pressure for fresh and mixed MSW specimens in the loading sequence are given in Figure 7.13. The initial total unit weights of the specimens are listed in Tables 5.3, 5.5, and 5.7. The MSW specimens with the 100 % soil-size material are represented by open symbols, whereas the MSW specimens with the 62 to 76 % soil-size material are represented by solid symbols. The 14 % soil-size material MSW specimens are represented by open symbols with an “x” in the symbol.

Figure 7.13 shows that the estimated total unit weight increases with increasing confining pressure. The increase in the estimated total unit weight for the MSW specimens reconstituted with 100 % soil-size material is about 11 % over two orders of

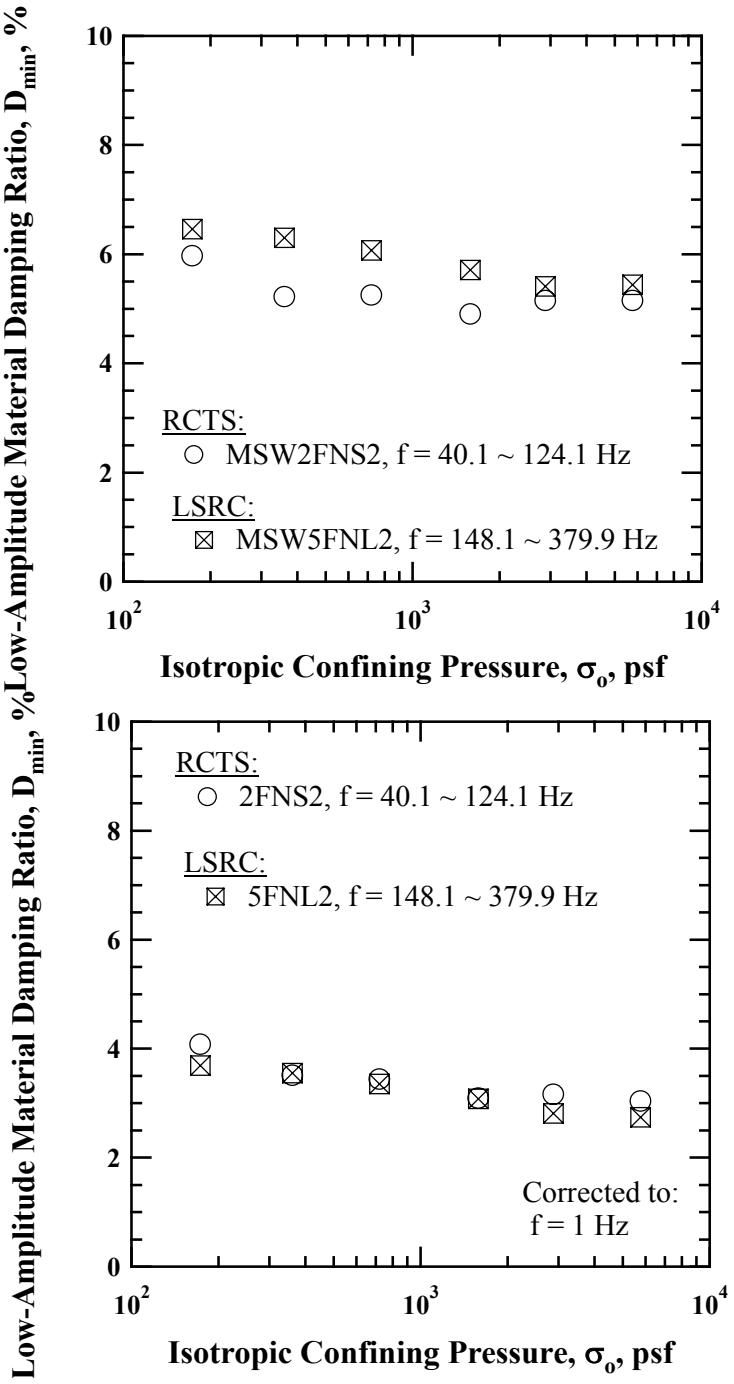

Figure 7.12 Comparison of the Variation in Low-Amplitude Material Damping Ratio with Isotropic Confining Pressure of Different Specimen Sizes Reconstituted with 100 % Soil-Size Fresh MSW Passing the ¾-in. (19.1-mm) Sieve: (a) Uncorrected for f and (b) Corrected for f

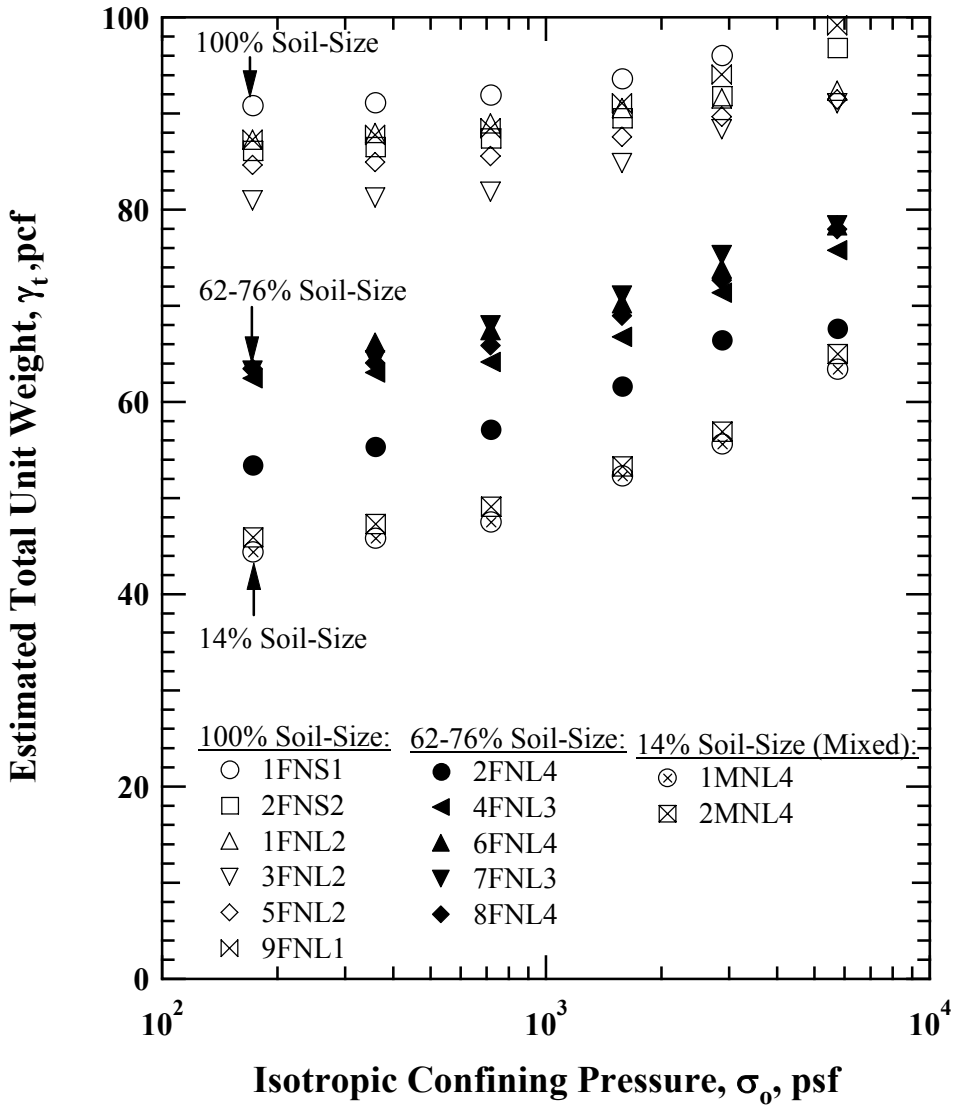

Figure 7.13 Variation in Estimated Total Unit Weight with Isotropic Confining Pressure from RC Tests for Fresh and Mixed MSW Specimens (All Groups)

magnitude of confining pressure (from 10^2 psf (5 kPa) to 10^4 psf (479 kPa)). The average increase in estimated total unit weight of the 62 to 76 % soil-size material MSW specimens is approximately 24 %. Finally, the average increase in estimated total unit weights for the 14% soil-size material MSW specimens is about 42 %. From the

observation of the change in estimated total unit weight of the fresh and mixed MSW specimens, it can be noted that the increase in total unit weight is a function of its initial unit weight and weight of percentage of soil-size material. The lower the percentage of soil-size the lower the initial total unit weight of the MSW specimen, and the larger the change in γ_t during the increasing pressure loading sequence.

The estimated total unit weight measured during the RC tests in the RCTS and LSRC devices is compared with other total unit weight profiles obtained from other MSW landfills. The comparison is shown in Figure 7.14. As discussed in Section 6.4, the values of 0.3 and 0.25 of Poisson's ratio were used for the 100 % soil-size material and for lower-weight percentages of soil-size material, respectively. Corresponding values of K_o are equal to 0.43 and 0.33, which are used for the conversion of mean isotropic confining pressure in the laboratory into an equivalent depth in situ.

The reference total unit weight profiles measured at MSW landfills used for the comparison with the estimated total unit weight profiles produced in the laboratory measurements were: (1) OII landfill, CA, (2) Azusa landfill, CA, (3) Cherry landfill, DW (Zekkos, 2005). Another average total unit weight profile suggested by Kavazanjian et al. (1995) was added to the figure by a dashed line. The variation of estimated total unit weight of specimens is classified into the 100 %, 62 to 76 %, and 14 % soil-size material Groups.

As shown in Figure 7.13, dashed line proposed by Kavazanjian et al. forms almost the lower bound of total unit weight variation measured at MSW landfills. The estimated total unit weight profile of the 100 % soil-size material MSW specimens agrees well with total unit weight profiles measured in situ. However, the estimated total unit weight profile of the 62 to 76 % soil-size material MSW specimens appears to follow the lower bound of the in-situ total unit weights below a depth of 100 ft (30 m).

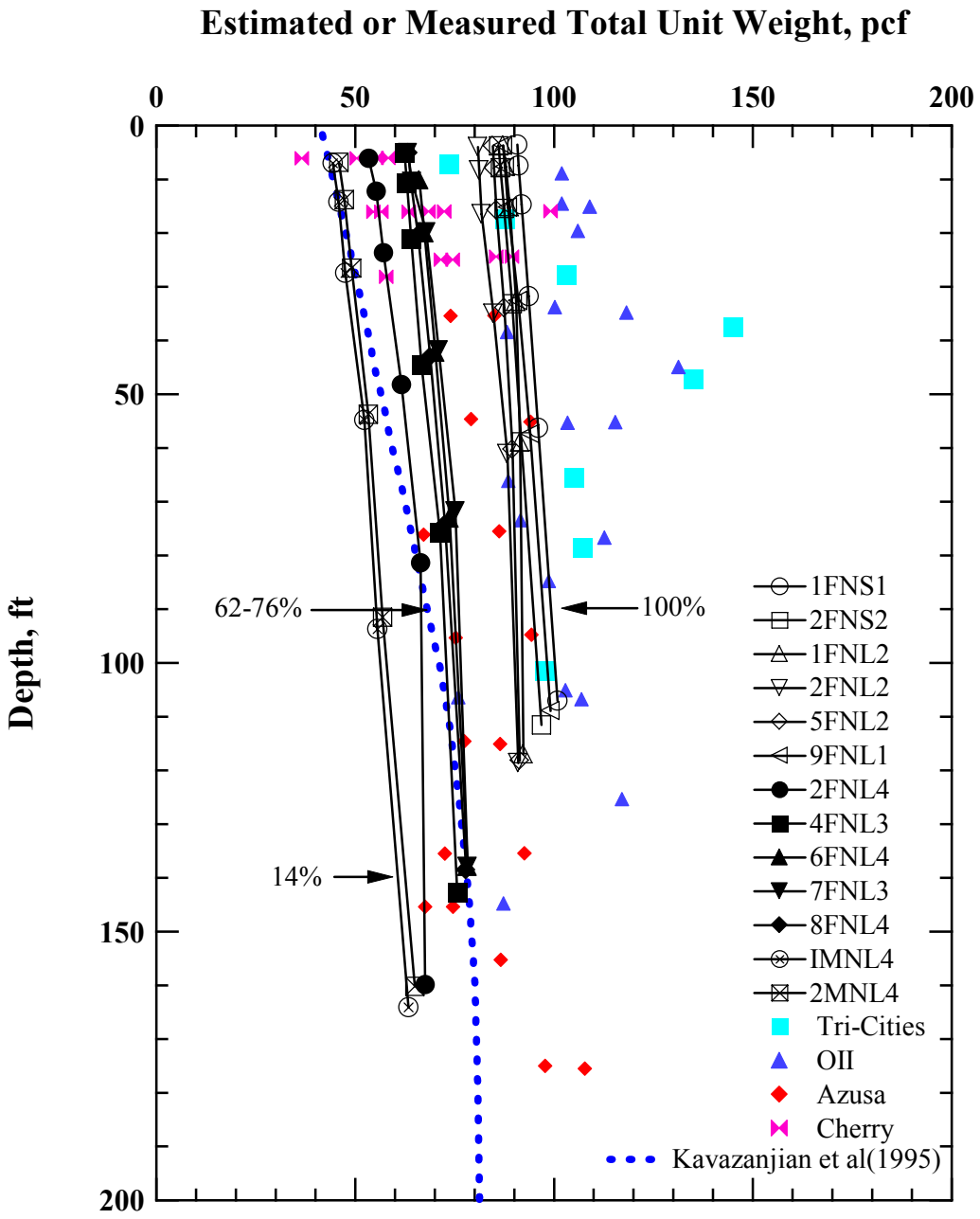

Figure 7.13 Comparison of the Variation in Estimated Total Unit Weight of Fresh and Mixed MSW Specimens with Total Unit Weight Profiles Measured at MSW Landfills

The estimated total unit weights of the 14 % soil-size material MSW specimens are quite low after a depth of 30 ft (9 m) compared with the in-situ total unit weight profiles. Like old MSW, it is interesting to observe that, from either the estimated total unit weight profiles in the laboratory or the measured in-site total unit weight profiles, the variation in total unit weight of the MSW does not change dramatically with depth.

7.4.1 Development of an Empirical Relationship of Estimated Total Unit Weight and Confining Pressure of Fresh MSW

To develop an empirical relationship between estimated total unit weight and confining pressure for the fresh MSW, the values of estimated total unit weight at a given confining pressure were normalized with the initial total unit weight of a given specimen. The variation of normalized total unit weight with confining pressure is shown in Figure 7.14. The 100 %, 62 to 76 %, and 14 % soil-size material specimens are represented by open circle, triangle, and square symbols, respectively. As shown in Figure 7.14, the amount of normalized total unit weight increases with decreasing weight percentage of soil-size material. The data were fitted using the least-squares method separately and the fitted equations were generalized with respect to the weight percentage of soil-size material. This equation is expressed by:

$$\frac{\gamma_t}{\gamma_{t,initial}} = -0.05 \times \left[(\ln(\%) - 5.44) \times (\ln(\sigma_o) - 4.70)\right] + 0.97 \qquad (7.3)$$

where,

γt is an estimated total unit weight for a given confining pressure in pcf,

$\gamma_{t,initial}$ is an initial total unit weight of a given specimen,

% is a weight percentage of soil-size material, and

σ_o is a confining pressure in psf.

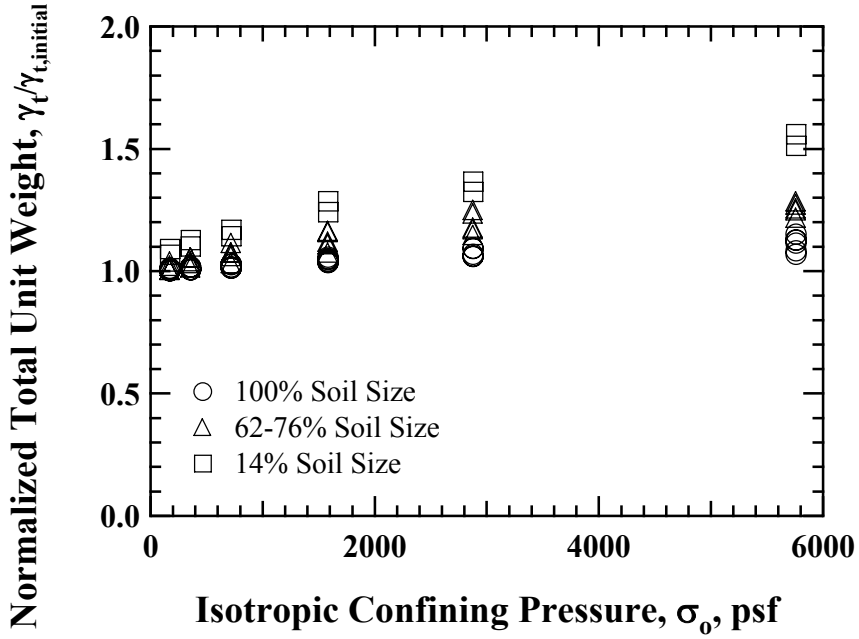

Figure 7.11 Comparison of Predicted Total Unit Weight and Measured Total Unit Weight for Fresh and Mixed MSW Specimens

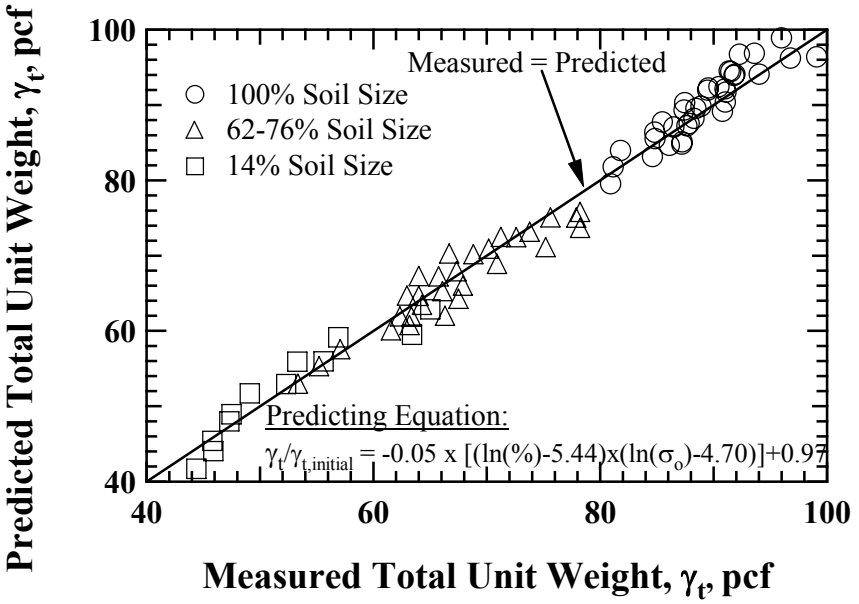

Figure 7.12 Comparison of Predicted Total Unit Weight and Measured Total Unit Weight for Fresh and Mixed MSW Specimens

To verify Equation (7.3), the values of predicted total unit weight were compared with the measured total unit weights. The comparison is presented in Figure 7.15. As shown in Figure 7.15, predicted values exhibit good agreement with measured values.

7.5 MATERIAL PARAMETERS AFFECTING G_{MAX} AND D_{MIN} OF FRESH WASTE IN THE SMALL-STRAIN RANGE

7.5.1 Waste Composition

Considering the nature of MSW composed of various types of materials, waste composition is an important factor in the behavior of MSW. To investigate the effect of the waste composition on G_{max} and D_{min} measurements, large-diameter specimens were prepared according to the procedures as described in Section 5.3.2. The LSRC device was used to perform the RC tests.

The variation in G_{max} uncorrected and corrected for excitation frequency, f, and total unit weight, γ_t, with confining pressure for the different weight percentages of soil-size material is shown in Figures 7.13 (a) and (b), respectively. The data plotted in the figure were chosen from measurements at the end of the one-day confinement period. The data from the 76 % and 62 % soil-size material groups were combined together to fit the data. Each group of data were fitted using the least-squares method and is represented by dashed lines in the figure.

As seen in Figure 7.13 (a), G_{max} increases regardless of weight percentages of soil-size material as confining pressure increases. There is a slightly flatter log G_{max} – log σ_o relationship in the OC state than in the NC state. It is important to note that the values of G_{max} at each confining pressure in both the OC and NC states depends on the weight percentage of soil-size material, implying that G_{max} of MSW is dependent on the waste composition, resulting in a decrease in G_{max} as the weight percentage of soil-size

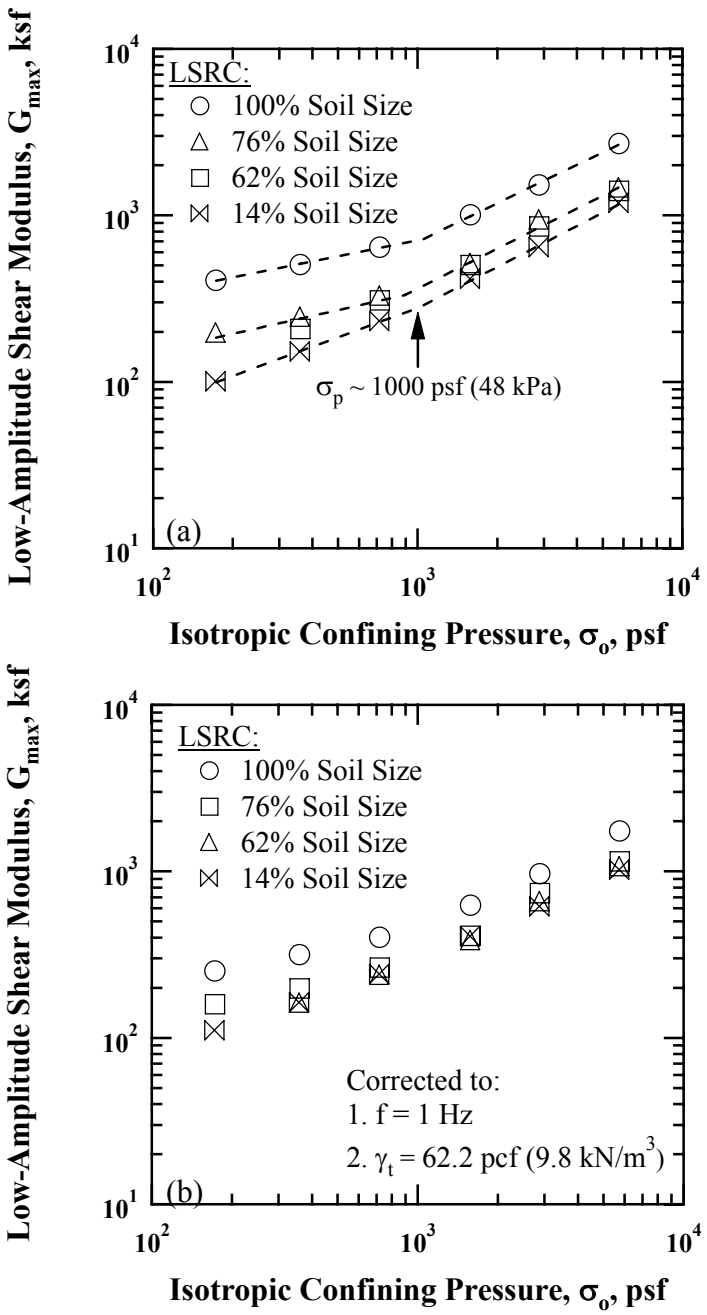

Figure 7.13 Variation in Low-Amplitude Shear Modulus with Isotropic Confining Pressure upon Different Weight Percentages of Soil Contents for Fresh and Mixed MSW Specimens: (a) Uncorrected for f and γ_t and (b) Corrected for f and γ_t

material decreases.

To remove the effect of excitation frequency and total unit weight, the values of G_{max} were corrected to f = 1 Hz using Equation (6.5) and the values G_{max} were normalized with the value of 62.2 pcf (9.8 kN/m^3) (75 % soil-size material specimen). As can be seen in Figure 7.13 (b), after correcting for the excitation frequency and total unit weight, the values of G_{max} become closer and G_{max} increases with increasing confining pressure regardless of weight percentage of soil-size material.

The variation in D_{min} uncorrected and corrected for excitation frequency, f, with confining pressure for the different weight percentages of soil-size material is shown in Figures 7.14 (a) and (b), respectively. The values of D_{min} shown in the figure were selected after one day of confinement at each confining pressure and were determined by the free-vibration decay method. As seen in Figure 7.14 (a), D_{min} exhibit nearly the same with increasing confining pressure regardless of the weight percentages of soil-size material; a very flatter log D_{min} – log σ_o relationship. The values of D_{min} for the 100 % soil-size material specimen are slightly higher than the values of D_{min} for the other groups. Lower weight percentages of soil-size material specimens behave similarly with confining pressure

The values of D_{min} were corrected to f = 1Hz using Equation (7.2) to remove the effect of excitation frequency, as show in Figure 7.14 (b). After correcting for the excitation frequency, the difference between the values of D_{min} of different weight percentages of soil-size material specimens become relatively larger. In addition, the values of D_{min} begin to decrease from the fourth D_{min} measurement, with approximately constant values in D_{min} up to the third measurements. As a result, the effect of waste composition is small on D_{min}.

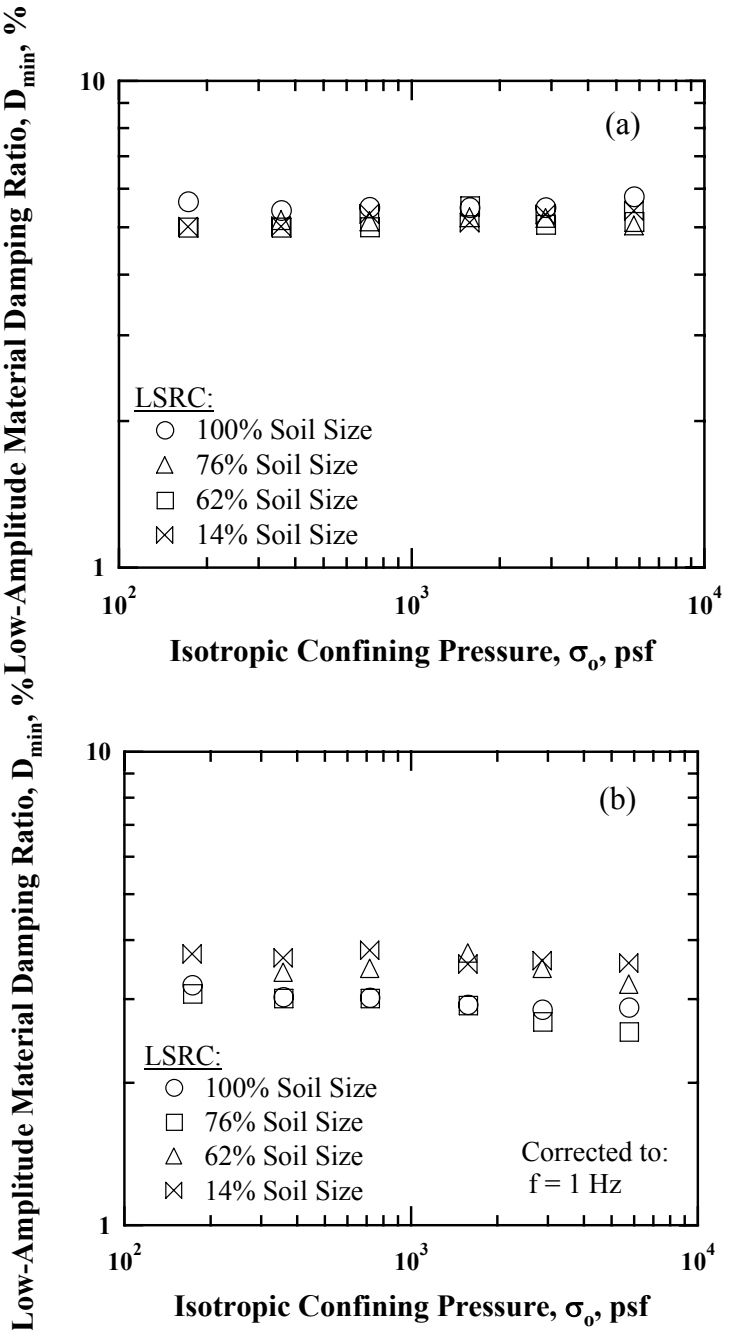

Figure 7.14 Variation in Low-Amplitude Material Damping Ratio with Isotropic Confining Pressure upon Different Weight Percentages of Soil Content for Fresh and Mixed MSW Specimens: (a) Uncorrected for f and (b) Corrected for f

7.5.2 Water Content

As discussed earlier in Section 6.5.2, dynamic properties of MSW will be affected by the presence of water within MSW landfills including daily cover soil. Therefore, additional water was added to investigate the effect of water content on the dynamic properties of fresh MSW.

The variation in G_{max} uncorrected and corrected for excitation frequency, f, and total unit weight, γ_t, with confining pressure at the natural and hydrated conditions is shown in Figures 7.15 (a) and (b), respectively. The variation in G_{max} at the natural condition is represented by open symbols and the variation in G_{max} at hydrated condition is represented by the solid symbols. The values of the initial total unit weight and water content for Specimen MSW1FNS1 were 90.6 pcf (14.2 kN/m^3) and 13.0 %, respectively. After hydration process was completed, the total unit weight and water content became 104.9 pcf (16.5 kN/m^3) and 26.5 %. It should be noted that RC measurements for Specimen MSW1FHS1 were terminated because the specimen was damaged after high-amplitude RC test at a confining pressure of 11 psi (76 kPa).

As seen in Figure 7.15 (a), difference in the absolute values in G_{max} before and after hydration process are considerable, resulting from the fact that RC tests on the hydrated specimen was performed in about two days after hydration process. Thus, this period of time was enough for the specimen to be fully hydrated. During the RC tests, the drain line was open, leading a drained condition. To remove the effect of excitation frequency and total unit weight, the values of G_{max} were corrected to f = 1 Hz and total unit weight of 90.6 pcf (14.2 kN/m^3). After correcting the excitation frequency and total unit weight, the difference in G_{max} increased slightly. However, this difference decreases with increasing confining pressure, varying from about 14 % at the lowest pressure to about 11 % at a confining pressure of 11 psi (76 kPa). Similar to old MSW,

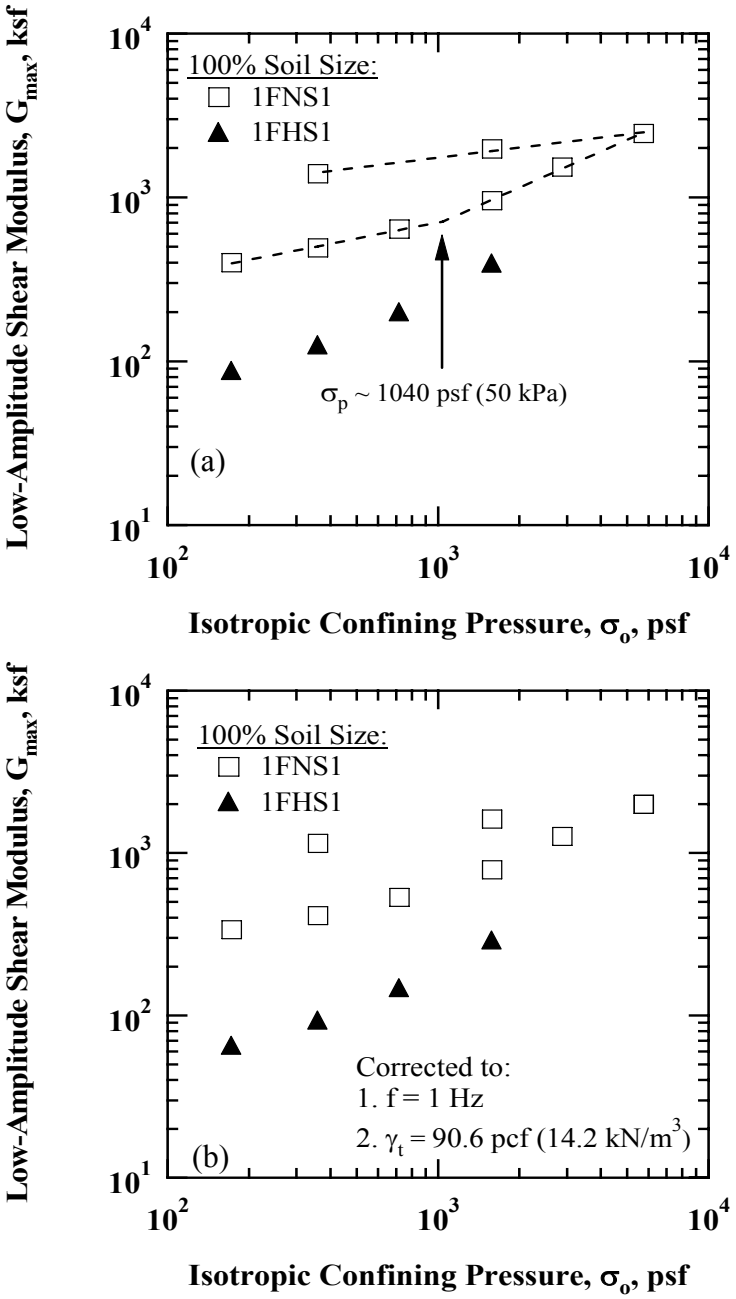

Figure 7.15 Comparison of the Variation in Low-Amplitude Shear Modulus with Isotropic Confining Pressure at its Natural and Hydrated Conditions for 100 % Soil-Size Fresh MSW Specimens: (a) Uncorrected for f and γ_t and (b) Corrected for f and γ_t

Hydrating a specimen eliminates the overconsolidation effect that appeared in a given specimen in its natural condition by unloading process.

The variation in D_{min} uncorrected and corrected for excitation frequency, f, with confining pressure at its natural and hydrated conditions is shown in Figures 7.16 (a) and (b), respectively. After hydration, D_{min} increases about 26% at the initial confining pressure and this increase becomes smaller with increasing confining pressure. For example, the difference at a confining pressure of 11 psi (76 kPa) is about 14 %. As with the D_{min} at the natural condition, the values of D_{min} decrease with increasing confining pressure. as discussed in Section 6.5.2, relative movements between solid particles and water in the MSW specimen are contribute to this increase in D_{min}.

The values of D_{min} measured in the natural and hydrated conditions were corrected for f = 1 Hz, as shown in Figure 7.16 (b). As seen in the figure, after eliminating the effect of frequency, the values of D_{min} also follow the similar trends. For the unloading sequence, the increase in D_{min} becomes relatively larger as confining pressure decreases.

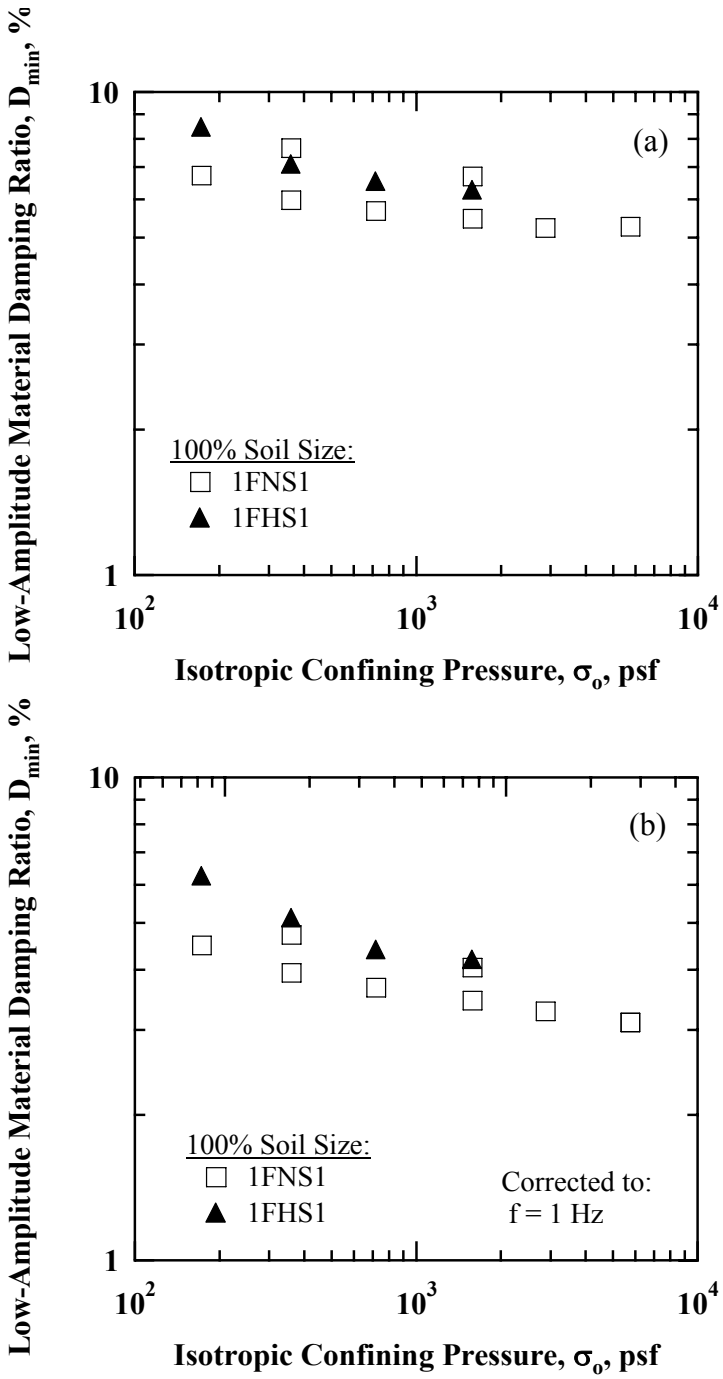

Figure 7.16 Comparison of the Variation in Low-Amplitude Material Damping Ratio with Isotropic Confining Pressure at its Natural and Hydrated Conditions for 100 % Soil-Size Fresh MSW Specimens: (a) Uncorrected for f and (b) Corrected for f

7.5.3 Total Unit Weight Variation for the Same Material Group

Similar to the old waste, to investigate the effect of total unit weight on G_{max} and D_{min} for a given material group, a pair of lower unit weight of specimens was constructed: Specimen MSW3FNS1 and MSW4FNS2. These specimens were reconstituted in four layers and were constructed by simply placing by hand the 100 % soil-size material, passing the 3/8-in. (9.5-mm) and ¾-in. (19.1-mm) sieves for the two specimens, into the mold. The initial target unit weight for these specimens was 57.3 pcf (9 kN/m^3). The variation in G_{max} uncorrected and corrected for excitation frequency, f, with estimated total unit weight at different confining pressures for the 100 % soil-size material specimens is presented in Figures 7.17 (a) and (b), respectively. The specimens with higher total unit weights are represented by open symbols and the specimens with lower total unit weight are represented by open symbols with an "x" in the symbol.

As can be seen in Figure 7.17 (a), G_{max} increases with increasing total unit weight. The change in estimated total unit weight for the lower and higher total unit weight specimens is approximately 30 % to 11 % over confining pressures (2.5 psi (17 kPa)) to 40 psi (276 kPa)), respectively. Below a confining pressure of 11 psi (76 kPa), the values of G_{max} with the higher total unit weight specimens are higher than lower total unit weight specimens due to compaction process. After a confining pressure of 11 psi (76 kPa), on the other hand, it is interesting to observe that an increase in G_{max} is accelerating for the lower unit weight specimens. This increase results probably from randomly-oriented particles in the specimens during the placement of 100 % soil-size material into the mold. In general, the effect of variation in total unit weight is small on G_{max}.

To remove the effect of excitation frequency, the values of G_{max} were corrected for f = 1 Hz, as shown in Figure 7.17 (b). After correcting the excitation frequency, the

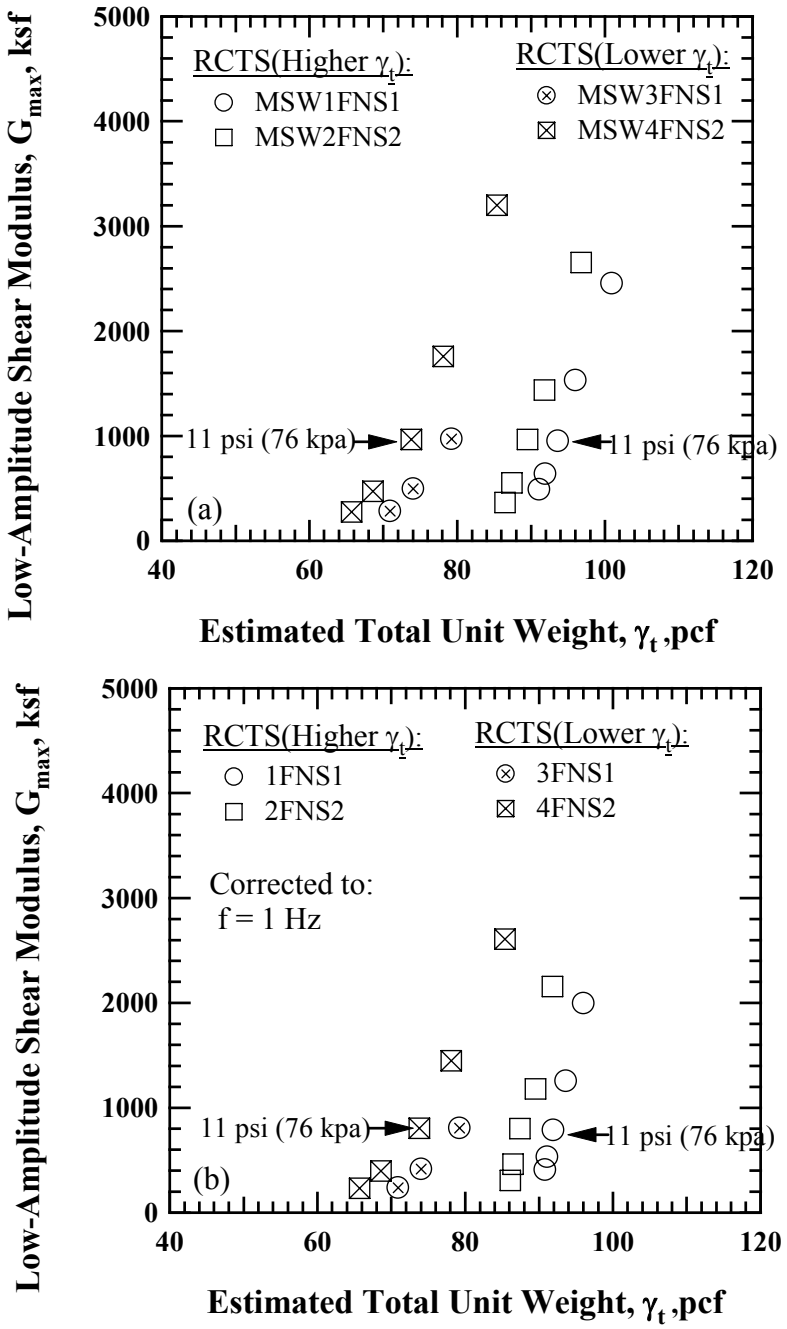

Figure 7.17 Comparison of the Variation in Low-Amplitude Shear Modulus with Estimated Total Unit Weight at Different Isotropic Confining Pressures for 100 % Soil-Size Fresh MSW Specimens: (a) Uncorrected for f and (b) Corrected for f

variation in G_{max} shows similar trends.

The variation in D_{min} uncorrected and corrected for excitation frequency, f, with estimated total unit weight is shown in Figures 7.18 (a) and (b), respectively. As seen in Figure 7.18 (a), D_{min} generally decreases with increasing estimated total unit weight. The pattern of variation in D_{min} is very similar between the higher and lower total unit weight specimens. That is, considerable change in D_{min} at the beginning, but it remains almost the same after some measurements regardless of its initial total unit weight.

To remove the effect of excitation frequency, the values of D_{min} were corrected to f = 1 Hz, as shown in Figure 7.18 (b). After correcting the effect of excitation frequency, the variation in D_{min} shows similar trends. Therefore, it can be drawn a conclusion that the values of D_{min} are not affected much by the variation of total unit weight.

7.5.4 Particle Size

A pair of small- and large-diameter specimens was prepared to investigate the effect of particle size on G_{max} and D_{min} for 100 % soil-size fresh MSW. As mentioned earlier in Section 6.5.4, the largest particle size should not exceed 0.47-in. (11.9-mm) and 1.0-in. (25.4-mm) for small- and large-diameter specimens, respectively. The 100 % soil-size material that passed the 3/8-in. (9.5-mm) and the ¾-in. (19.1-mm) sieves was used for the specimen construction. Like old MSW, the RCTS and LSRC devices were used to perform the RC tests.

The variation in G_{max} uncorrected and corrected for excitation frequency, f, and total unit weight, γ_t, with confining pressure for Specimens 1FNS1 and 2FNS2 is shown in Figures 7.19 (a) and (b), respectively. Initial total unit weights of these specimens are 90.6 pcf (14.2 kN/m^3) and 86.0 pcf (13.5 kN/m^3) for Specimen 1FNS1 and 2FNS2,

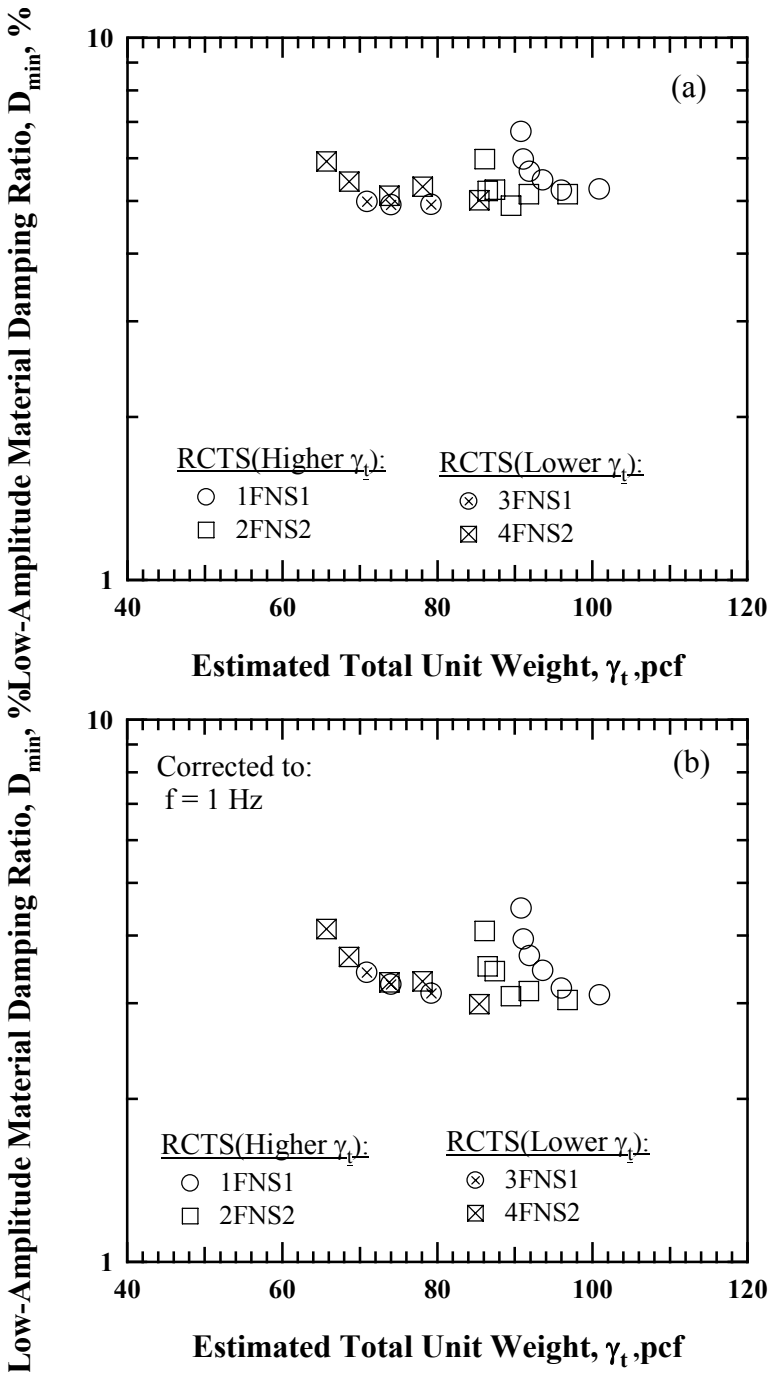

Figure 7.18 Comparison of the Variation in Low-Amplitude Material Damping Ratio with Estimated Total Unit Weight at Different Isotropic Confining Pressures for 100 % Soil-Size Fresh, MSW Specimens: (a) Uncorrected for f and (b) Corrected for f

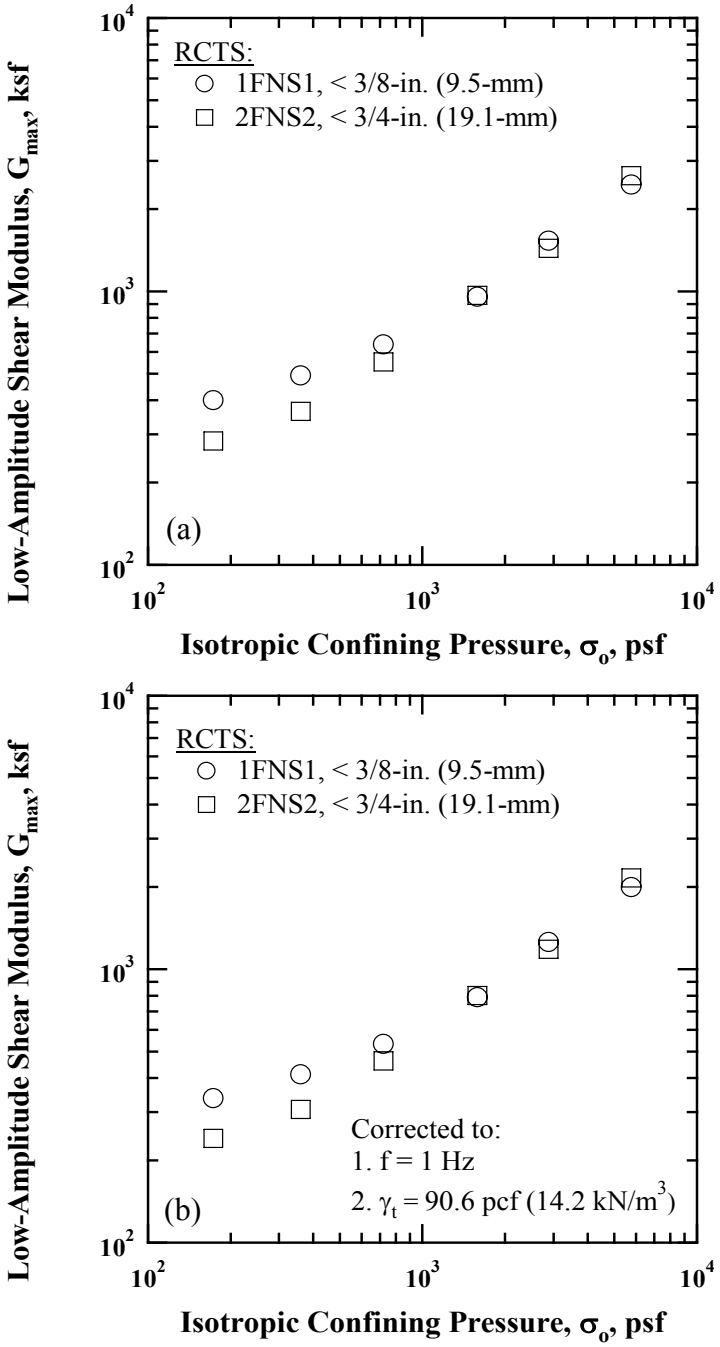

Figure 7.19 Comparison of the Variation in Low-Amplitude Shear Modulus with Isotropic Confining Pressure for Different Particle Sizes of the 100 % Soil-Size, Fresh MSW Material Tested in the RCTS Device: (a) Uncorrected for f and γ_t and (b) Corrected for f and γ_t

respectively. Excitation frequency of these specimens changes from 48.3 Hz to 124.1 Hz for Specimen 1FNS1 and from 40.1 Hz to 124.1 Hz for Specimen 2FNS2.

To remove the effect of excitation frequency and total unit weight, the excitation frequency was corrected to f = 1 Hz using Equation (7.1) and total unit weight was normalized with Specimen 1FNS1. As shown in Figure 7.19 (b), the variation in G_{max} with confining pressure in the NC state is essentially the same regardless of particle size of the fresh MSW specimens. However, in the OC state, there is somewhat difference in variation in G_{max}, resulting from a difference in its initial total unit weight between the specimens. Based on these tests, the effect of particle size on the small-diameter fresh MSW specimens reconstituted with material passing the 3/8-in. (9.5-mm) sieve is negligible in the NC state, but some effect exist in the OC state.

The variation in G_{max} uncorrected and corrected for excitation frequency and total unit weight with confining pressure for Specimens 9FNL1 and 5FNL2 is given in Figure 7.20 (a) and (b), respectively. Initial total unit weights of these specimens are 84.5 pcf (13.3 kN/m^3) for Specimen 9FNL1 and 86.2 pcf (13.5 kN/m^3) for Specimen 5FNL2. Excitation frequency of these specimens varies from 128.5 Hz to 386.3 Hz for Specimen 9FNL1 and from 148.1 Hz to 380.0 Hz for Specimen 5FNL2, respectively. The values of G_{max} were corrected for f and γ_t to remove the effect of excitation frequency and total unit weight.

As seen in Figure 7.20 (b), the variation in G_{max} is nearly the same in the NC state, with a small difference in the OC state. This difference is believed to be due to the compaction process and the larger particles.

With these tests, the effect of particle size on the large-diameter fresh MSW specimens reconstituted with material passing the 3/8-in. (9.5-mm) and ¾-in. (19.1-mm) sieves is neglgible.

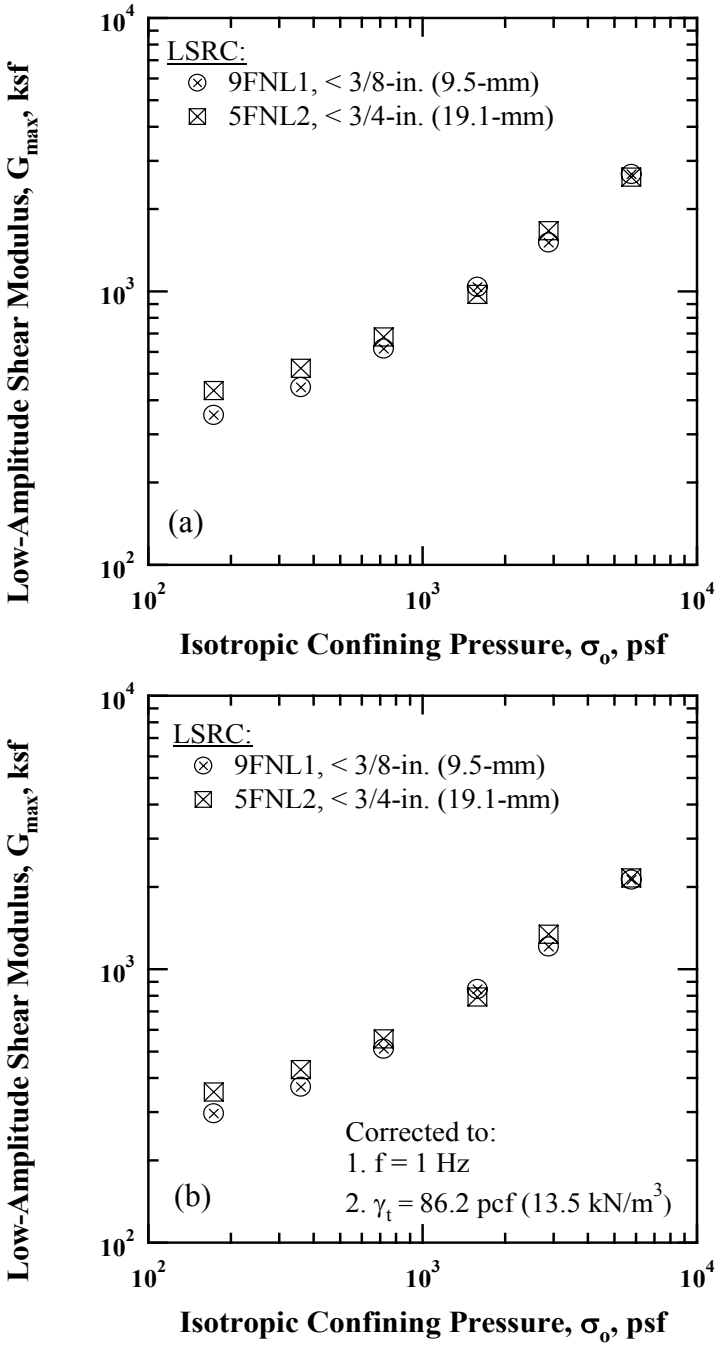

Figure 7.20 Comparison of the Variation in Low-Amplitude Shear Modulus with Isotropic Confining Pressure for Different Particle Sizes of the 100 % Soil-Size, Fresh MSW Material Tested in the LSRC Device: (a) Uncorrected for f and γ_t and (b) Corrected for f and γ_t

The variation in D_{min} uncorrected and corrected for excitation frequency with confining pressure for the Specimens 1FNS1 and 2FNS2 is shown in Figures 7.21 (a) and (b), respectively. The values of D_{min} decrease with increasing confining pressure regardless of particle sizes, as shown in Figure 7.21 (a). The values of D_{min} were corrected to f = 1 Hz using Equation (7.2). After correcting for the excitation frequency, the values of D_{min} are slightly closer with increasing confining pressure. With these observations, the effect of particle size for small-diameter fresh MSW specimens is insignificant.

For the large-diameter specimens, the values of D_{min} were corrected to f = 1 Hz using Equation (7.2) to remove the effect of excitation frequency. The variation in D_{min} uncorrected and corrected for the excitation frequency with confining pressure is shown in Figures 7.22 (a) and (b), respectively. As can be seen, D_{min} decreases with increasing confining pressure regardless of particle sizes. After correcting the excitation frequency, the values of D_{min} become slightly closer shown in Figure 7.22 (b), resulting in approximately the same. Therefore, the effect of particle size for large-diameter fresh MSW specimens is negligible.

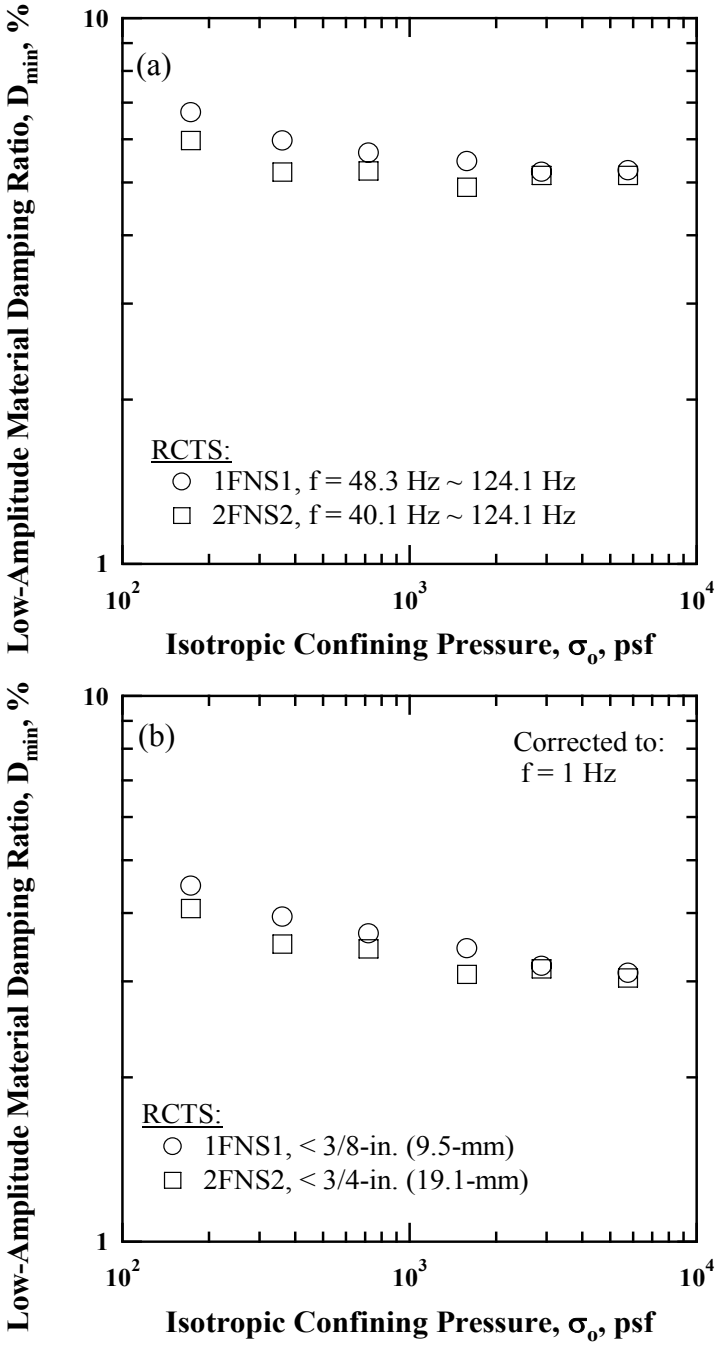

Figure 7.21 Comparison of the Variation in Low-Amplitude Material Damping Ratio with Isotropic Confining Pressure upon Different Particle Size for 100 % Soil-Size, Small-Diameter Fresh MSW Specimens: (a) Uncorrected for f and (b) Corrected for f

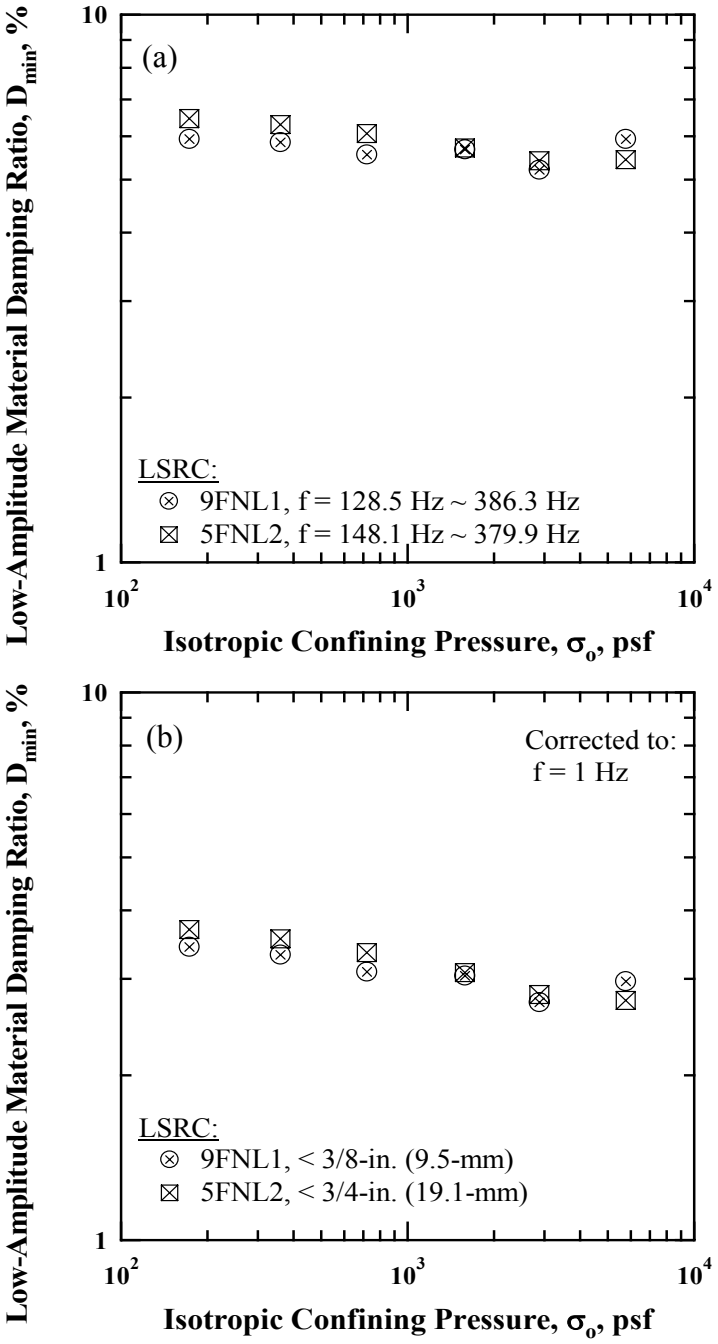

Figure 7.22 Comparison of the Variation in Low-Amplitude Material Damping Ratio with Isotropic Confining Pressure upon Different Particle Size for 100 % Soil-Size, Large-Diameter Fresh MSW Specimens: (a) Uncorrected for f and (b) Corrected for f

7.6 DEVELOPMENT OF AN EMPIRICAL RELATIONSHIP BETWEEN G_{MAX} AND D_{MIN} FOR FRESH MSW

Using the RC data of fresh and mixed waste measured from 100 %, 76 %, 62 %, and 14 % soil-size fresh and mixed MSW specimens in the RCTS and LSRC devices, an empirical relationship between G_{max} and D_{min} was derived for the purpose of predicting D_{min} at a given G_{max}. The variations in D_{min} with respect to G_{max} uncorrected and corrected for f = 1 Hz are shown in Figures 7.23 (a) and (b), respectively. The values of G_{max} and D_{min} were corrected using Equations (7.1) and (7.2). The data shown in Figure 7.23 (b) are fitted using a form of a power function as given by:

$$D_{min} = 3.60 - 0.02 \times G_{max}^{0.46} \tag{7.3}$$

where,

D_{min} is the small-strain material damping ratio, and

G_{max} is the small-strain shear modulus.

The fitted line is shown by the line in Figure 7.23. As can be seen, the variation in D_{min} appears to decrease slightly with increasing G_{max}. However, the variation in D_{min} is quite small, less than about 28 % over the range in G_{max} values. The values of corrected D_{min} and predicted D_{min} obtained using Equation (7.3) are compared in Figure 7.24. As shown in the figure, the data distribute around the equality line with a scatter of about ± 20 %. The maximum and minimum difference between corrected and predicted D_{min} values are equal to about 23 % and 17 %, respectively,

Another plot for the ratio of corrected D_{min} to predicted D_{min} is presented with respect to confining pressure with mean and standard deviation lines in Figure 7.25. The mean value of the ratio of measured D_{min} to predicted D_{min} is unity and the standard

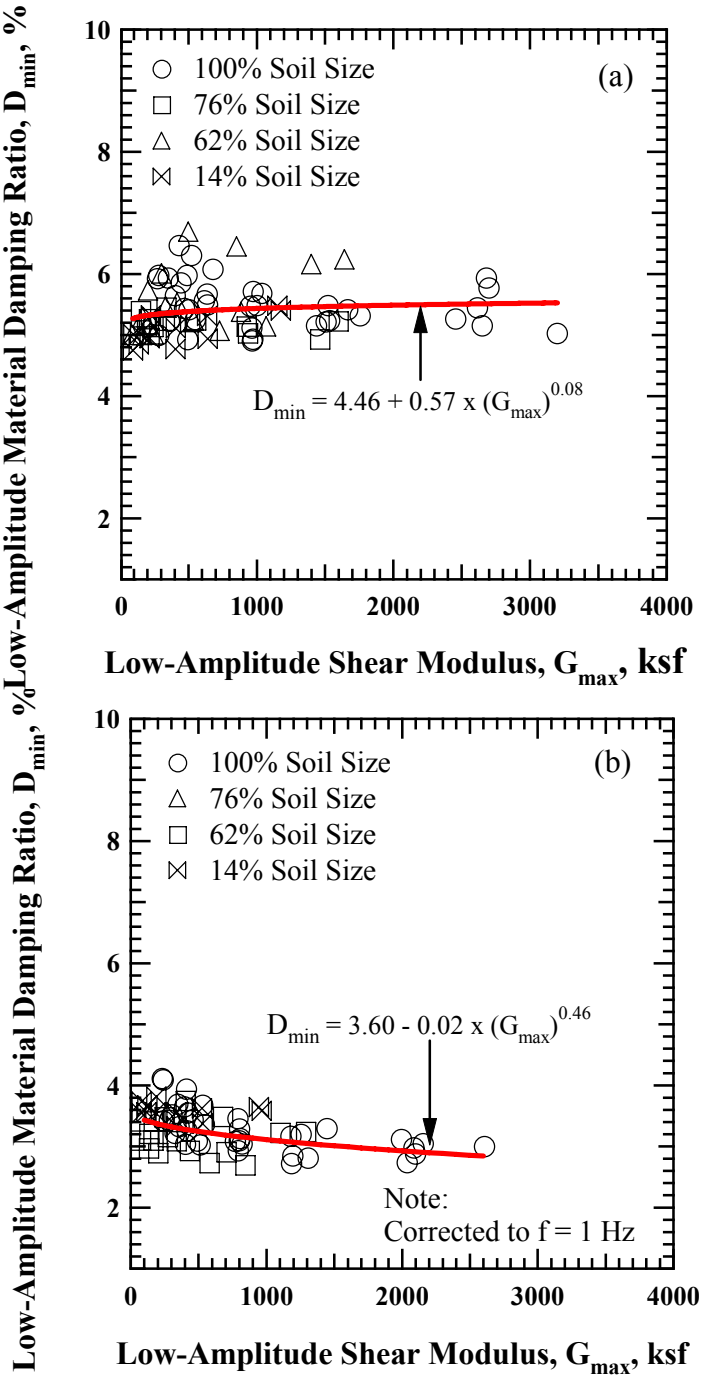

Figure 7.23 Variation in Low-Amplitude Material Damping Ratio with Low-Amplitude Shear Modulus for Fresh and Mixed MSW Specimens (All Groups): (a) Uncorrected for f (b) Corrected for f

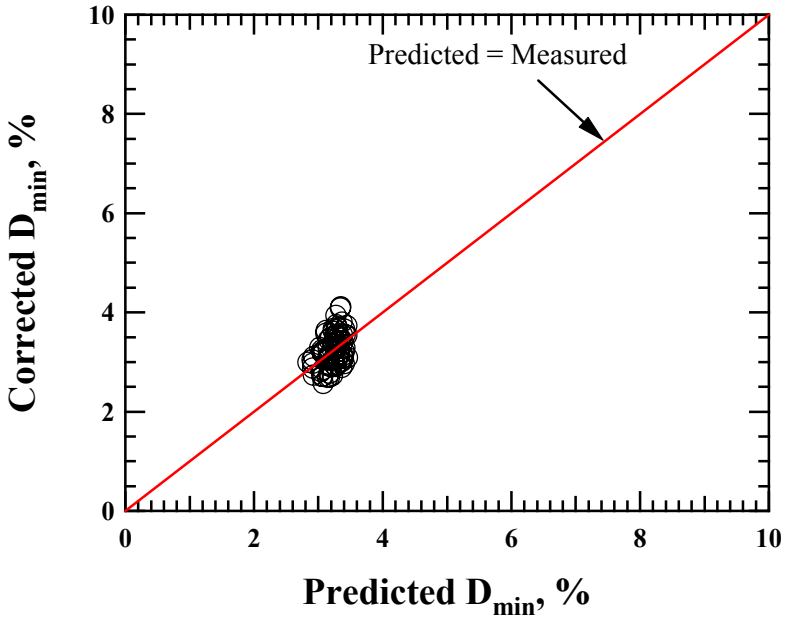

Figure 7.24 Comparison of the Corrected and Predicted Values of D_{min} for Fresh and Mixed MSW Specimens (All Groups)

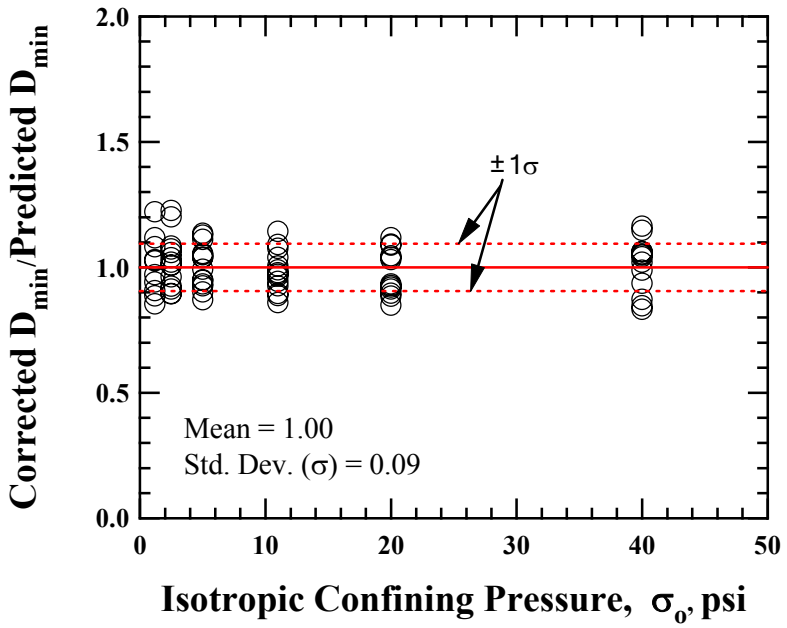

Figure 7.25 Plot of the Ratio of Corrected D_{min} to Predicted D_{min} with Isotropic Confining Pressure for Fresh and Mixed MSW Specimens (All Groups)

deviation, σ, turns out to be 0.09.

7.7 COMPARISON OF SMALL-STRAIN DYNAMIC PROPERTIES OF FRESH MSW AND LOOSE SAND

The log G_{max} – log σ_o, log V_s – log σ_o, and log D_{min} – log σ_o relationships for fresh MSW are compared with these of loose sand in Figures 7.25, 7.26, and 7.27, respectively. Initial dry unit weight for loose sand is 118 pcf (18.5 kN/m^3). In addition, uniformity coefficient, C_u, and void ratio, e, for loose sand are 18 and 0.4, respectively. This loose sand is classified as well-graded sand (SW). Entire values of the fresh MSW were corrected for excitation frequency to f = 1 Hz using Equations (7.1) and (7.2). As seen in Figures 7.25, 7.26, and 7.27, σ_o has the same general influence on the small-strain dynamic properties of MSW as it does on sands; that is, as σ_o increases, G_{max} and V_s increase and D_{min} decreases slightly. However, there is a large difference between the values for the old MSW and sands. For instance, at σ_o = 11 psi (76 kPa), the difference in G_{max} is approximately by a factor of 2.4 for 100 % soil-size material and the difference in V_s is about 31 % for 100 % soil-size material. For D_{min}, the difference is about a factor of 4.9.

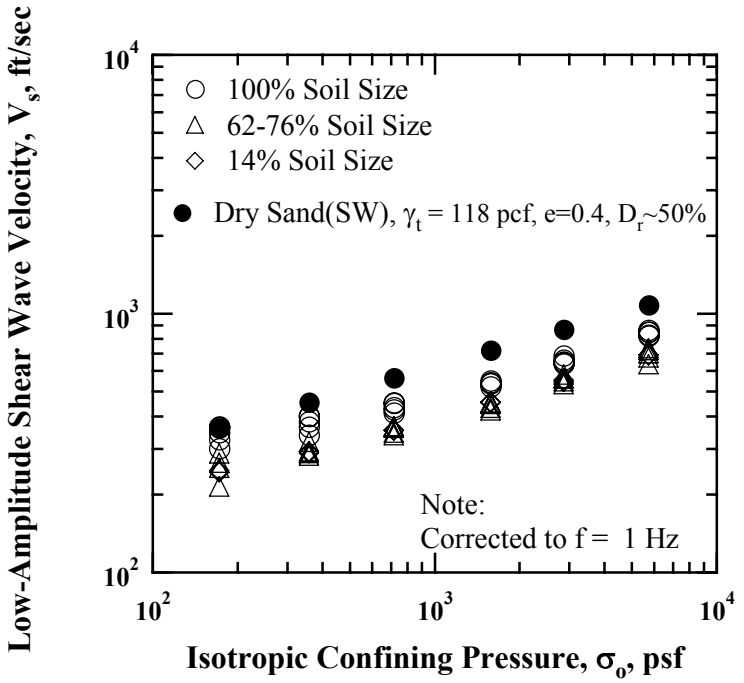

Figure 7.26 Comparison of the Variation in Low-Amplitude Shear Wave Velocity with Isotropic Confining Pressure for Fresh MSW (All Groups) and Loose Sand

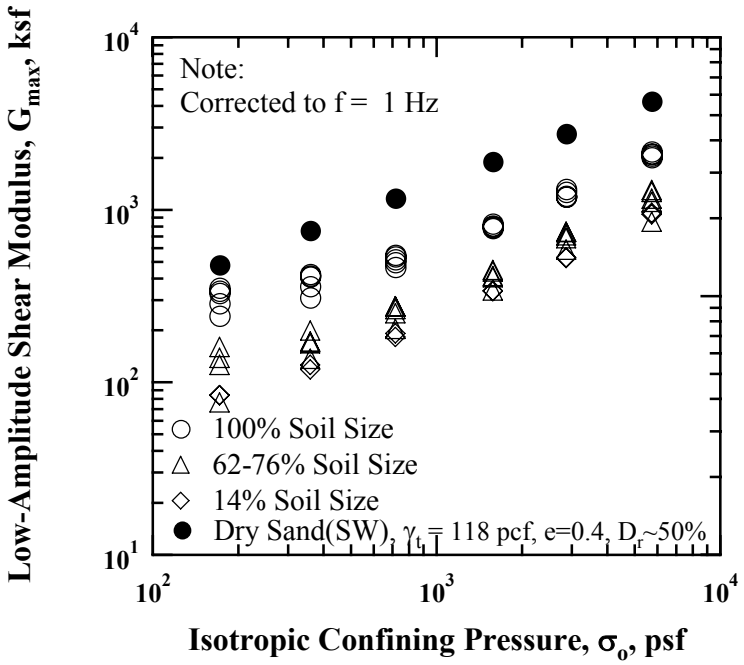

Figure 7.27 Comparison of the Variation in Low-Amplitude Shear Modulus with Isotropic Confining Pressure for Fresh MSW (All Groups) and Loose Sand

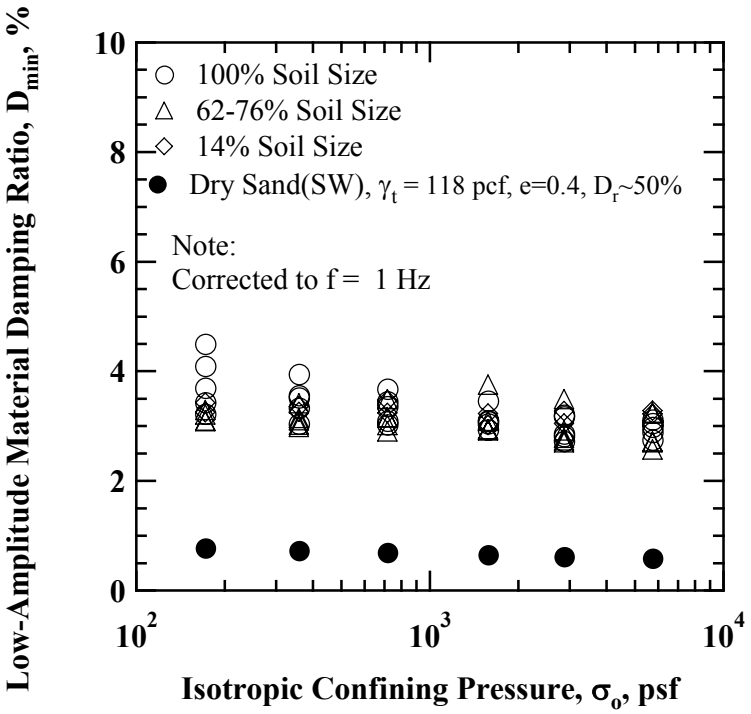

Figure 7.28 Comparison of the Variation in Low-Amplitude Material Damping Ratio with Isotropic Confining Pressure for Fresh MSW (All Groups) and Loose Sand

7.8 SUMMARY

Test parameters affecting G_{max} and D_{min} in the small-strain ranges for fresh MSW are studied in this chapter. These test parameters included: (1), duration of confinement at a constant confining pressure, (2) isotropic total confining pressure, (3) excitation frequency, and (4) specimen size. Test parameters listed above, except the excitation frequency, were investigated using the RCTS and LSRC devices. Only the RCTS device was employed to study the effect of excitation frequency on small-diameter MSW specimens. In addition, total unit weights of fresh MSW specimens were estimated during the RC tests in the RCTS and LSRC devices. Total unit weight of mixed waste specimens was also estimated in the LSRC device. These estimated total unit weights

were compared with total unit weight profiles measured at other MSW landfills.

An empirical relationship between estimated total unit weight and confining pressure, including weight percentage of soil-size material, was developed using the measured RC data.

The effects of material parameters were also investigated individually. These material parameters are: (1) waste composition, (2) water content, (3) total unit weight, and (4) particle size. The effects of water content, total unit weight, and particle size of the MSW specimens were studied using the RCTS device, while the effect of waste composition was investigated by the LSRC device.

An empirical relationship between estimated total unit weight and confining pressure including weight percentage of soil-size material was developed using the data of fresh and mixed MSW specimens measured in the RCTS and LSRC devices. Also, an empirical relationship between G_{max} and D_{min} was derived using the data measured from the RC tests of the fresh and mixed MSW specimens. The comparison between measured D_{min} and predicted D_{min} is given in Figure 7.24.

CHAPTER 8: Comparison of Small-Strain Dynamic Properties of Old and Fresh MSW

8.1 INTRODUCTION

Small-strain dynamic properties, G_{max} and D_{min}, of old and fresh MSW are compared in this chapter on the basis of the results presented in Chapters Six and Seven. The comparisons of G_{max} and D_{min} for old and fresh MSW are made only in the loading sequence. The comparisons are done in terms of the test parameters: (1) total isotropic confining pressure, σ_o, and (2) excitation frequency, f. Additionally, changes in the estimated total unit weight, γ_t, with confining pressure of old and fresh MSW are compared.

8.2 EFFECT OF CONFINING PRESSURE ON G_{MAX} AND D_{MIN}

8.2.1 Log G_{max} - Log σ_o Relationships

The variations in G_{max} with confining pressure of old and fresh MSW are compared in Figures 8.1 (a) and 8.1 (b), respectively. The specimens were reconstituted with 100% soil-size material that passed the 3/8-in. (9.5-mm) and ¾-in. (19.1-mm) sieves. The data were fitted using the least-squares method and the fitted lines are represented by the dashed lines in the figure. As shown in Figures 8.1 (a) and 8.1 (b), the behavior of old and fresh MSW with confining pressure is very similar in the normally consolidated (NC) range, with values of G_1 of 1282 ksf (61 MPa) and 1224 ksf, (59 MPa) respectively. This slightly higher value of G_1 of the old 100 % soil-size Group shows that the old 100 % soil-size Group is slightly stiffer. The values of n_G of the old and fresh MSW show that the respond is the same to σ_o. In the overconsolidated (OC) range, the old MSW has a somewhat higher G_1 and higher n_G than the fresh MSW.

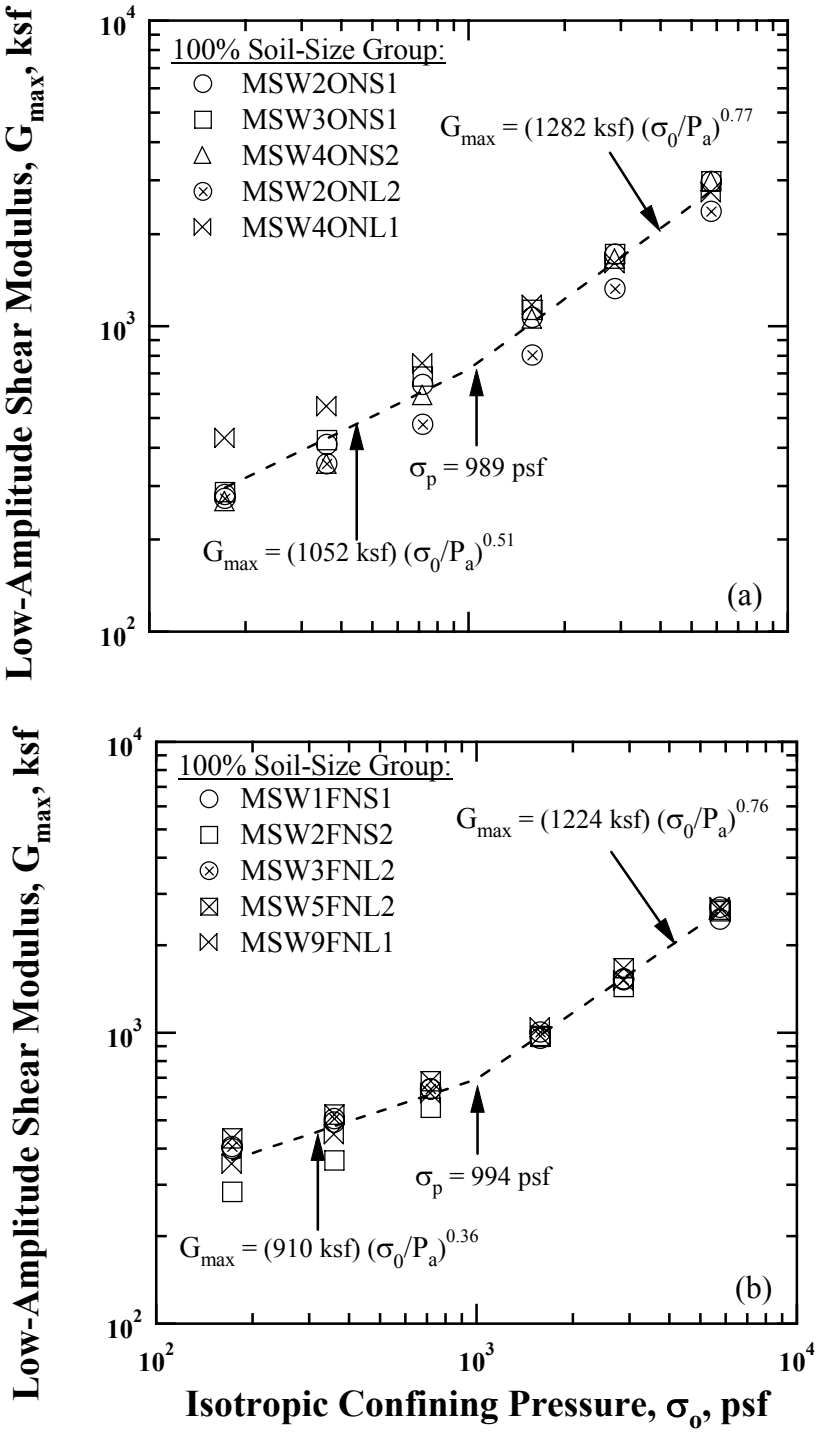

Figure 8.1 Variation in Low-Amplitude Shear Modulus with Isotropic Confining Pressure for 100% Soil-Size MSW: (a) Old Waste and (b) Fresh Waste

This difference is most likely due to difference in how the old and fresh wastes react under the compaction effort that created the overconsolidated state in the initial loading sequence. When compared with other conventional geotechnical materials such as sands and clays, it should be noted that the n_G values in the NC state are somewhat higher than n_G values obtained from sands and clays; they are usually in the range of 0.45 to 0.6. The reason for this higher n_G values is the relatively large change in γ_t that occurs in the NC range for the MSW waste. As a reference, the values of G_{max} of MSW specimens are about half of the G_{max} of loose sand.

The variation in G_{max} with a smaller percentage of soil-size material, hence the 62 and 76% Groups, is plotted in Figures 8.2 (a) and 8.2 (b), respectively. This variation in G_{max} with σ_o can be considered as more representative of field conditions. For reference, the representative weight percentage of soil-size material in the Tri-Cities landfill is about 50 to 75% (Zekkos, 2005). Figures 8.2 (a) and 8.2 (b) shows that: (1) the values of G_{max} of fresh MSW are lower at confining pressures in the NC state, ranging from 8% to 24% lower and (2) the variation in G_{max} with confining pressure of fresh MSW exhibits more pressure dependent than the old MSW, with a somewhat higher exponent in the NC state. Therefore, on the basis of these observations, it can be drawn a conclusion that the behavior of fresh MSW with confining pressure is softer and more pressure dependent than old MSW.

8.2.2 Log D_{min}-Log σ_o Relationships

The variations in D_{min} with confining pressure for 100% soil-size of the old and fresh MSW are illustrated in Figures 8.3 (a) and 8.3 (b), respectively. It should be noted that the values of σ_p shown in the figures were obtained in the log G_{max} – log σ_o relationships of 100 % soil-size old and fresh MSW specimens. As can be seen, D_{min}

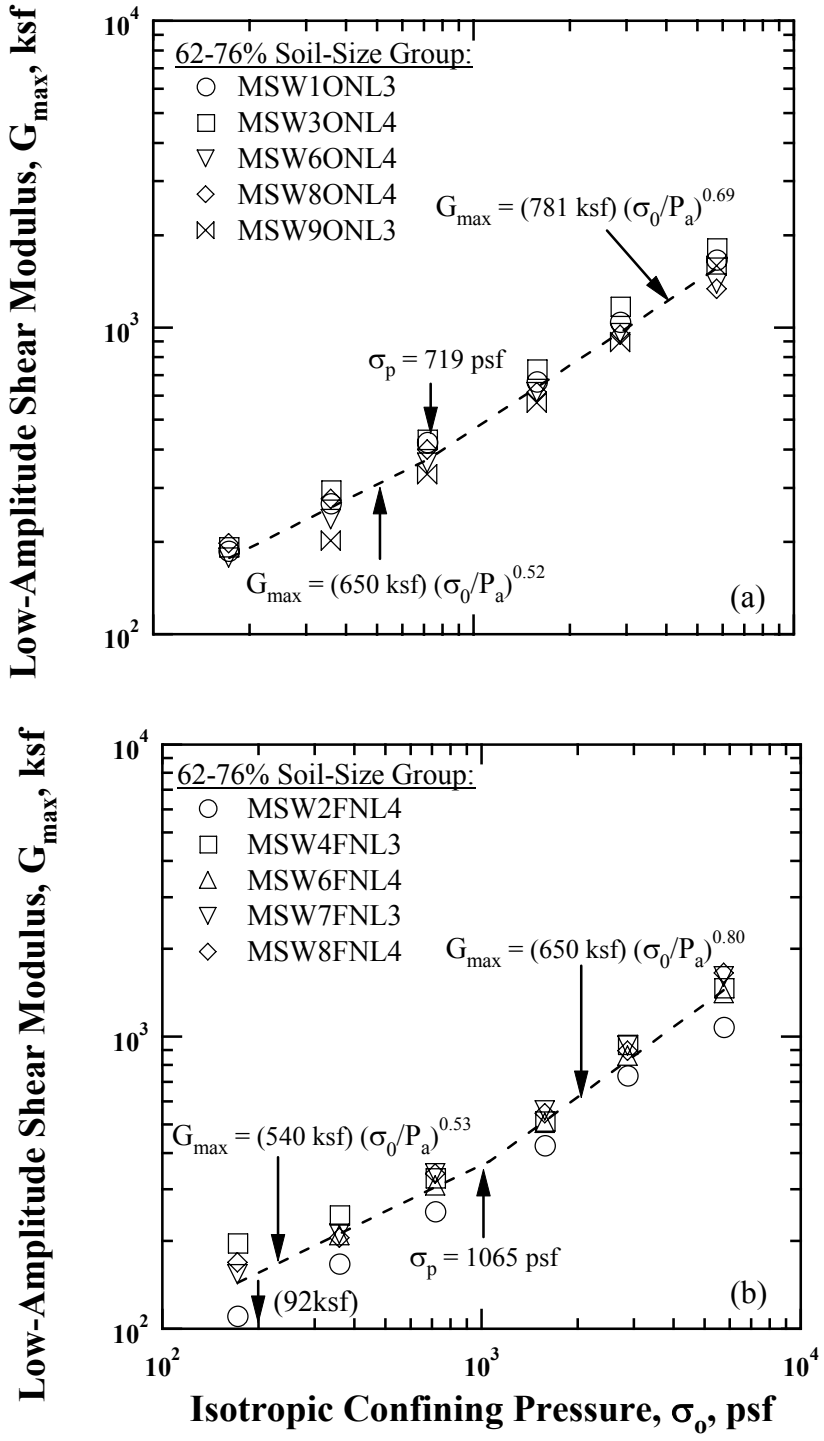

Figure 8.2 Variation in Low-Amplitude Shear Modulus with Isotropic Confining Pressure for 62-76 % Soil-Size MSW: (a) Old Waste and (b) Fresh Waste

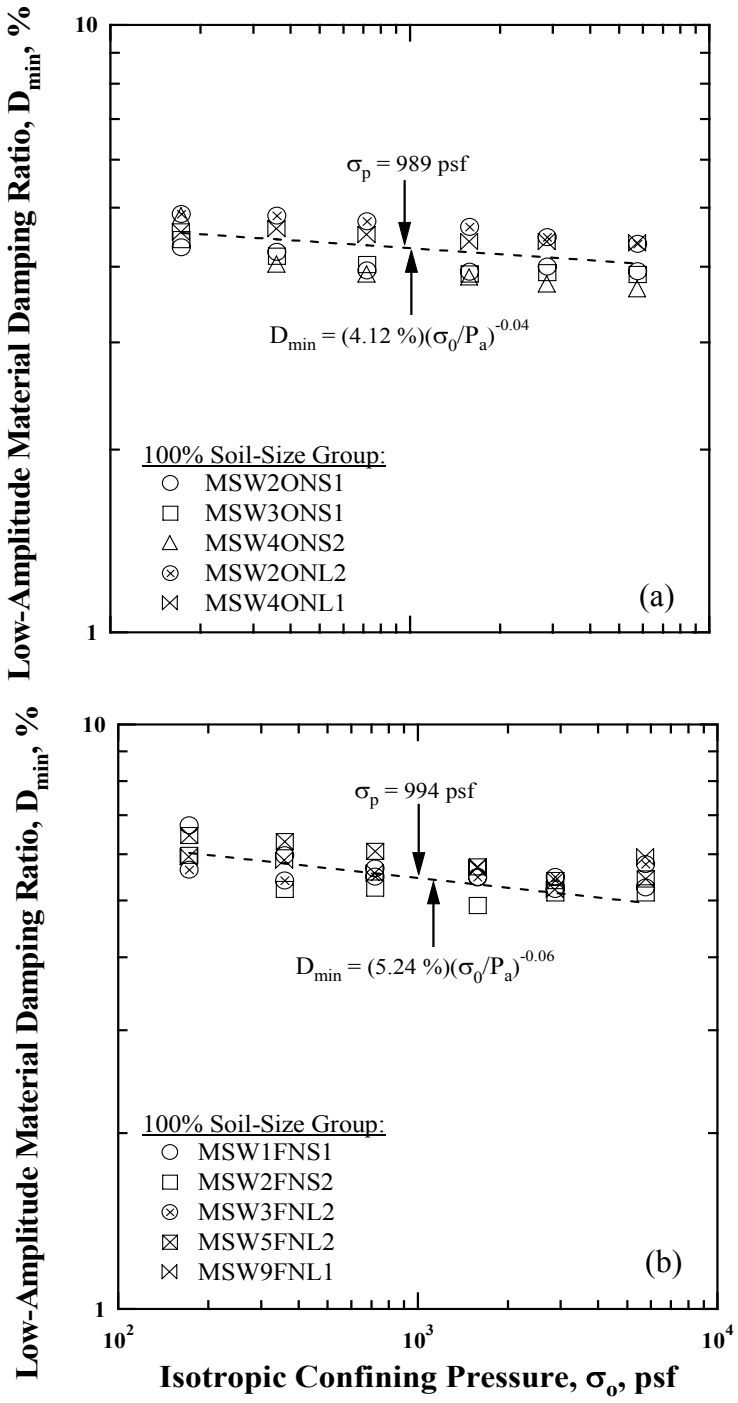

Figure 8.3 Variation in Low-Amplitude Material Damping Ratio with Isotropic Confining Pressure for 100% Soil-Size MSW: (a) Old Waste and (b) Fresh Waste

decreases slowly with an increase in confining pressure for the old and fresh MSW. However, the value of n_D of fresh MSW is slightly more negative than that of old MSW, indicating that the responses of old and fresh MSW to confining pressure are basically the same. The values of D_{min} for the fresh MSW are higher than those from the old MSW. The possible reason for this is that the sticky nature of soil-size material in the MSW weakens due to the time period of degradation process. Hence, induced-energy dissipation caused by the viscosity of soil-sizes material in the old MSW is less than that in the fresh MSW, making the material damping lower. When comparing the representative material damping ratio of the MSW with sands and clays, whose material damping ratios generally vary from 0.5 to 1.5 % and from 1 to 3 %, respectively, the values of D_{min} for the old and fresh MSW are significantly larger. These values typically range from 4 % to 6 %.

It is interesting to note from Figure 8.3 (a) that the values of D_{min} of soil-size material of the old MSW specimens clearly exhibit two distinct sets of data. The values of D_{min} of the large-diameter specimens are slightly higher over confining pressure than those of small-diameter specimens due to its different excitation frequency. This difference was equal to about 0.5% over confining pressure. Another important thing from Figure 8.3 (a) is that even though Specimen MSW2ONL2, whose initial total unit weight (72.6 pcf (11.4 kN/m^3)) is less than the other small-diameter specimens, D_{min} is still higher than that from the small-diameter specimens. Therefore, it seems that material damping of the old MSW is essentially independent of the initial total unit weight, and mainly depends on the excitation frequency.

On the other hand, material damping ratio of the fresh MSW does not show this pattern of behavior, as shown in Figure 8.3 (b). The values of D_{min} do not appear to be separated according to the specimen size and its excitation frequency.

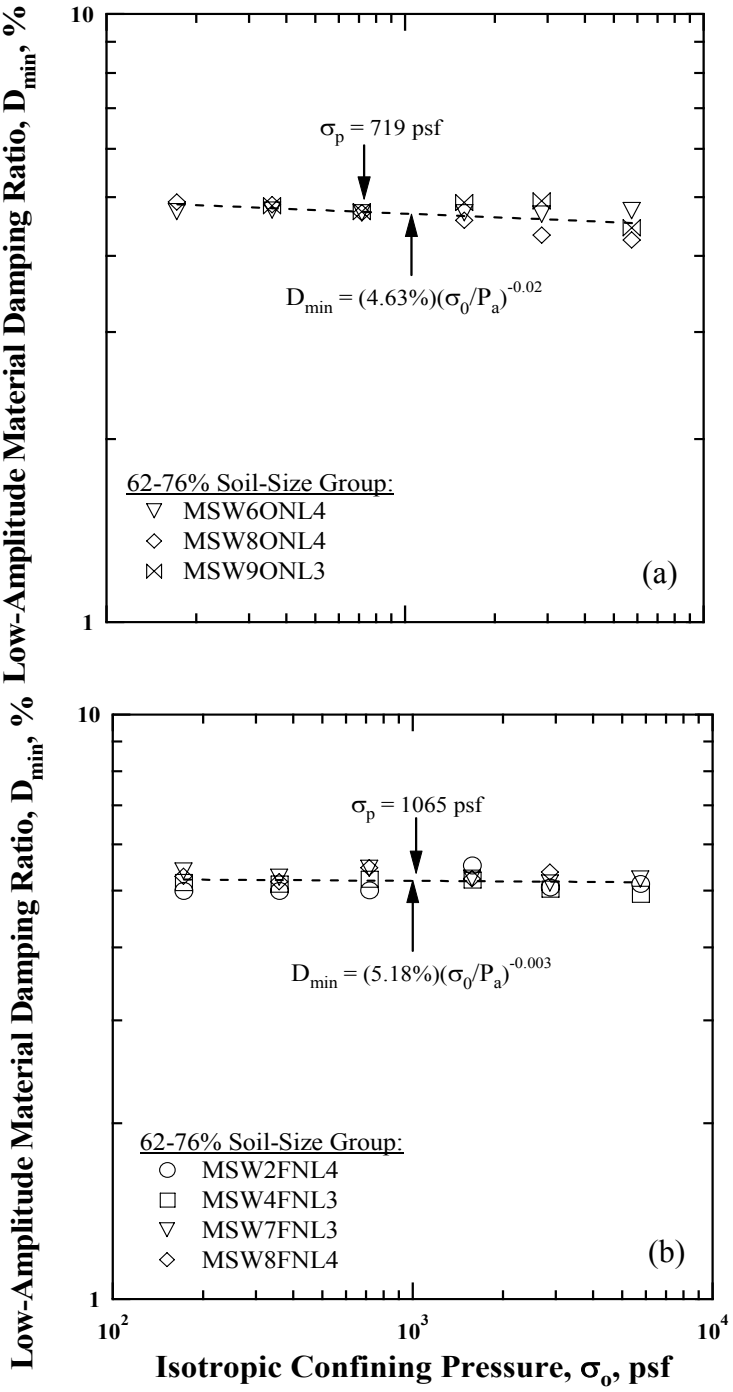

Figure 8.4 Variation in Low-Amplitude Material Damping Ratio with Isotropic Confining Pressure for 62-76% Soil-Size MSW: (a) Old Waste and (b) Fresh Waste

In addition, the variations in D_{min} with confining pressure for the old and fresh MSW with larger particles are plotted in Figures 8.4 (a) and 8.4 (b), respectively. It should be noted that the values of σ_p shown in the figures were obtained in the log G_{max} – log σ_o relationships of the old and fresh MSW specimens with larger particles. Similar to D_{min} for the 100% soil-size material, D_{min} decreases slightly with increasing confining pressure for the old and fresh MSW. It is interesting to note that after adding the larger particles, the values of n_D for the old and fresh MSW become slightly less negative than the values of n_D for the 100 % soil-size old and fresh MSW, indicating that D_{min} exhibits a less confining pressure dependency. For example, the value of n_D for the old MSW with larger particles was twice of that for the 100 % soil-size MSW, whereas the value of n_D for the fresh MSW with larger particles decreased dramatically by a factor of 20. Material damping ratio of the old MSW slightly increases with adding the larger particles. This increase is approximately 0.5 % over confining pressure. However, material damping ratio for the fresh MSW is nearly the same for adding larger particles.

In summary, D_{min} decreases slowly with increasing confining pressure for the old and fresh MSW and lower weight percentage of soil-sizes MSW exhibits slightly higher D_{min} values for the old MSW and while D_{min} of the fresh MSW exhibits lower values.

8.3 EFFECT OF EXCITATION FREQUENCY ON G_{MAX} AND D_{MIN}

8.3.1 Log G_{max}-Log f and Log $G_{max}/G_{max, f=1Hz}$ -Log f Relationships

The variations in G_{max} with excitation frequency for the old and fresh MSW are compared in Figures 8.5 (a) and 8.5 (b), respectively. These values were measured in the RCTS and LSRC tests for the old and fresh MSW specimens. The old MSW specimens include: MSW2ONS1, MSW3ONS1, MSW4ONS2, MSW5ONS1, MSW6ONS2, and MSW4ONL1. For the case of fresh MSW, Specimens MSW1FNS1,

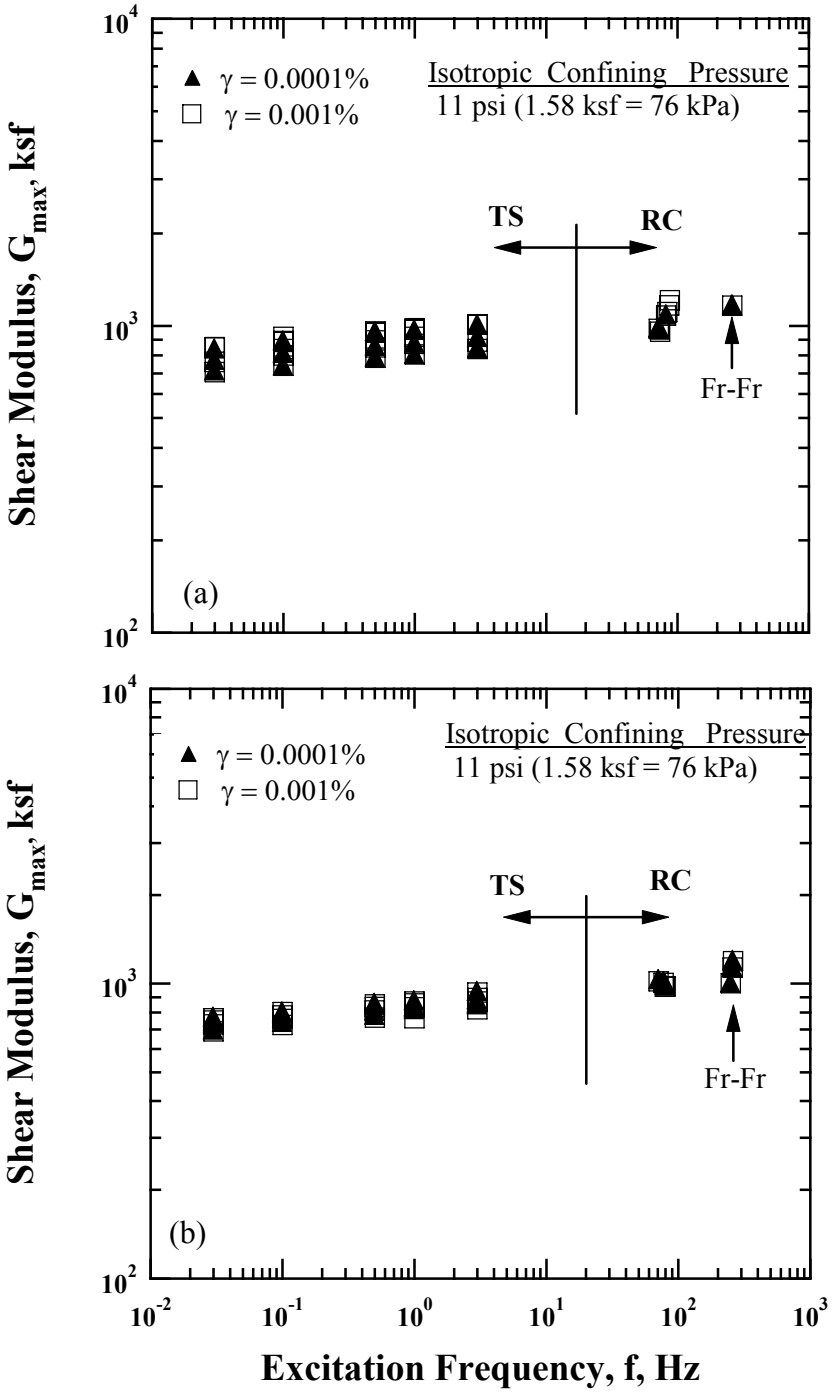

Figure 8.5 Variation in Shear Modulus with Excitation Frequency for 100 % Soil-Size MSW: (a) Old Waste and (b) Fresh Waste

MSW2FNS2, MSW3FNS1, MSW4FNS2, MSW3FNL2, MSW5FNL2, MSW9FNL1 were used. The comparison is made at the amplitudes of shearing strain of 0.0001 % and 0.001 % and is made at the confining pressure of 11 psi (76 kPa). Fr-Fr in the figures denotes the values from the LSRC tests in the figures. As shown in figures, the values of G_{max} increase with increasing excitation frequency for the old and fresh MSW due to frequency effect; a faster application of excitation loading produces a higher value of G_{max}. The values of G_{max} obtained at the amplitudes of shearing strain of 0.001 % and 0.001 % are almost the same, implying a strain amplitude-independent behavior of G_{max} in these strains.

To quantify the effect of excitation frequency, another comparison is made in terms of normalized shear modulus, $G_{max}/G_{max,f=1Hz}$, with excitation frequency. The values of G_{max} were normalized with those obtained from the TS tests at a frequency of 1 Hz. The variations in normalized shear modulus with excitation frequency for the old and fresh MSW are given in Figures 8.6 (a) and (b), respectively. As seen in the figures, the normalized shear modulus increases linearly with increasing excitation frequency for the old and fresh MSW.

The normalized shear modulus was fitted using the least-square method and the fitted equations are shown in the Figures 8.6 (a) and (b). Slope of the fitted equation of the fresh MSW is slightly higher than that of the old MSW. The change in G_{max} with excitation frequency of the old MSW amounts to a factor of about 1.47 when the excitation frequency increases by approximately four orders of magnitude, e.g., from 0.03 Hz to 260 Hz. Similarly, the change in G_{max} with excitation frequency of the fresh MSW amounts to a factor of about 1.59 when the excitation frequency increases by approximately four orders of magnitude, e.g., from 0.03 Hz to 257 Hz. Therefore, the response of the old and fresh MSW to the excitation frequency in terms of G_{max} is

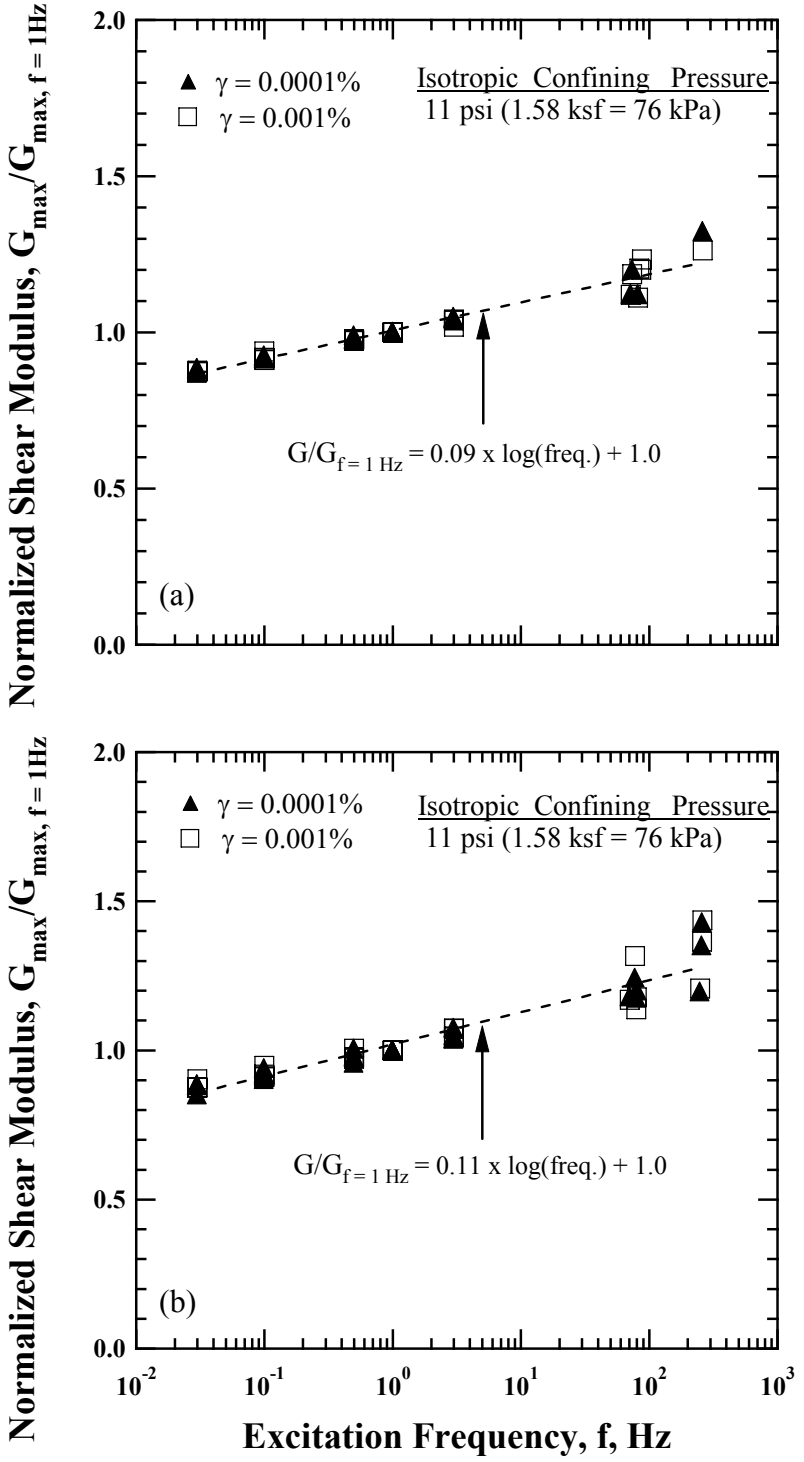

Figure 8.6 Variation in Normalized Shear Modulus with Excitation Frequency for 100 % Soil-Size MSW: (a) Old Waste and (b) Fresh Waste

approximately the same regardless of the age of waste.

8.3.2 Log D_{min}-Log f and Log $D_{min}/D_{min,\ f=1Hz}$ -Log f Relationships

The variations in D_{min} with excitation frequency are shown in Figures 8.7 (a) and (b) for the old and fresh MSW, respectively. As shown in the figures, the values of D_{min} increase with decreasing excitation frequency due to creep behavior below 1 Hz. On the other hand, values of D_{min} increase with increasing excitation frequency due to the frequency effect at frequencies larger than 1 Hz regardless of the age of MSW. As can be seen, the values of D_{min} obtained from the amplitudes of shearing strain of 0.001 % and 0.001 % are nearly the same, implying a strain amplitude-independent behavior of D_{min} at these strains.

To quantify the effect of excitation frequency, another comparison is made in terms of the variation of normalized material damping ratio, $D_{min}/D_{min,f=1Hz}$, with excitation frequency. The values of D_{min} were normalized with those obtained from the TS tests at a frequency of 1 Hz. The variations in normalized material damping ratio with excitation frequency for the old and fresh MSW are presented in Figures 8.8 (a) and (b), respectively. The normalized material damping ratio was fitted using the least-squares method and the fitted equations are given in the figures. The change in D_{min} with excitation frequency for the old MSW amounts to a factor of about 1.53 when the excitation frequency increases by approximately two and a half orders of magnitude, from 1 Hz to 260 Hz. For fresh MSW, however, the change in D_{min} is more significant at higher frequencies. For instance, the change in D_{min} amounts to a factor of 1.81 when the excitation frequency increases by approximately two and a half orders of magnitude, from1 Hz to 257 Hz.

At frequencies less than 1 Hz, the change in D_{min} is a factor of about 1.12 for both

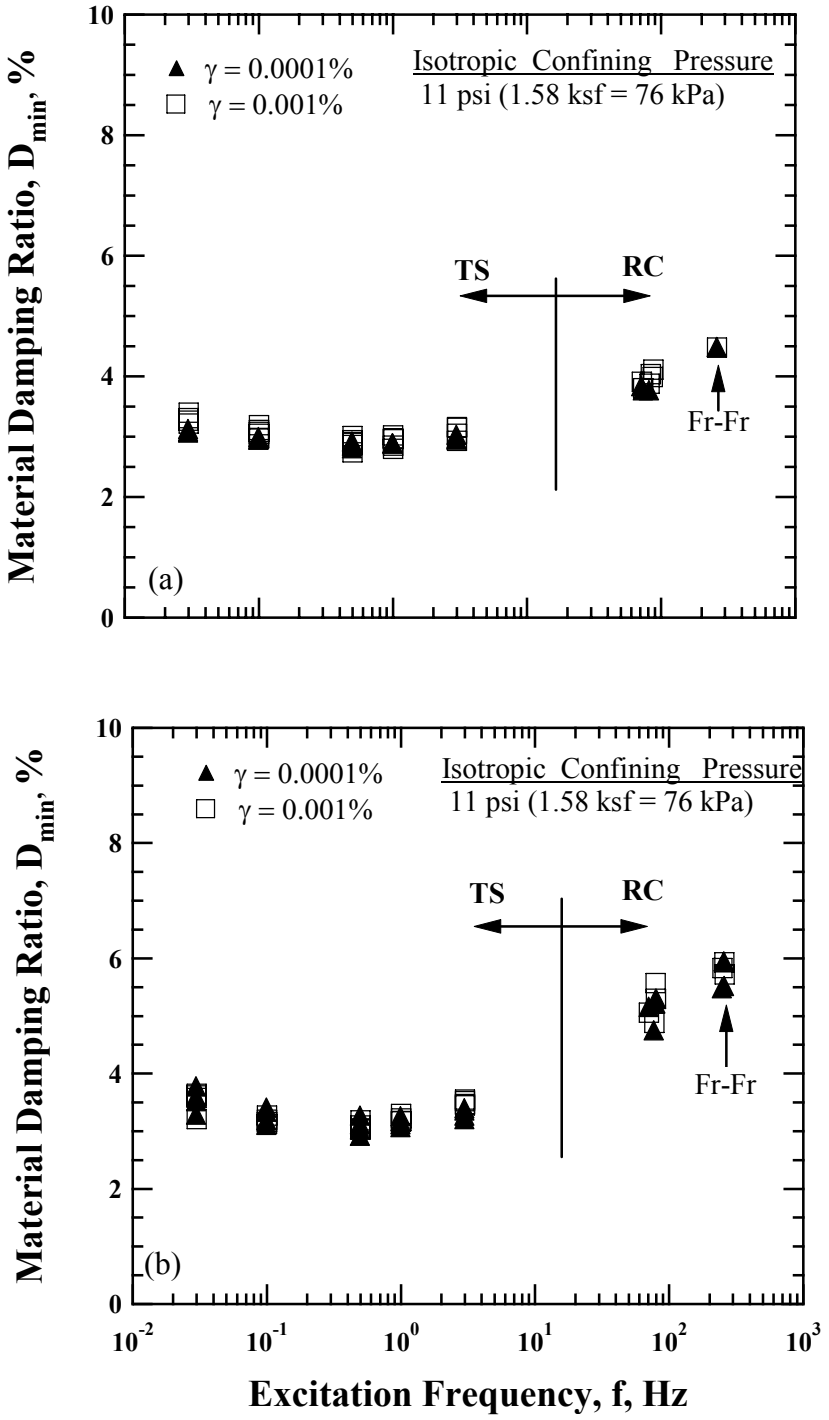

Figure 8.7 Variation in Material Damping Ratio with Excitation Frequency for 100 % Soil-Size MSW: (a) Old Waste and (b) Fresh Waste

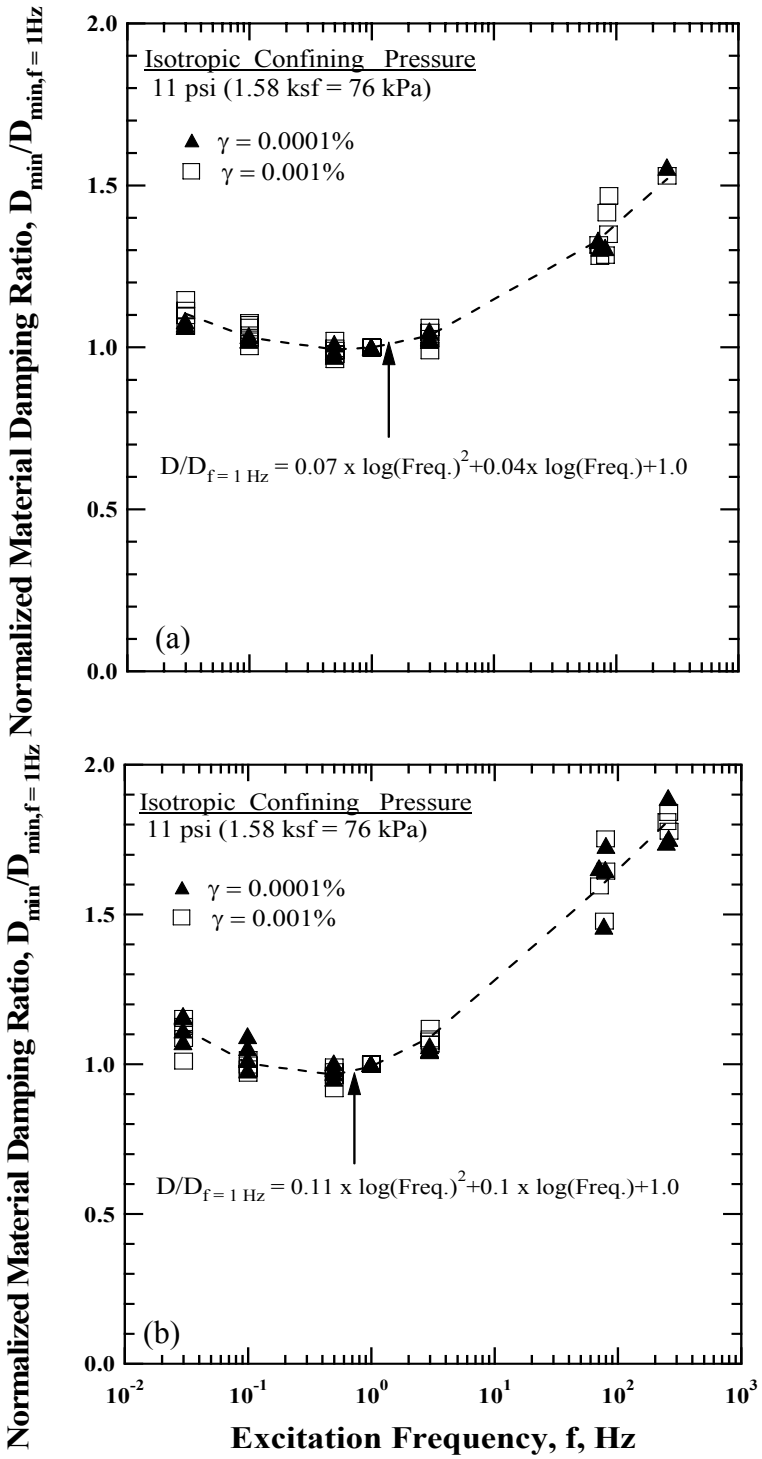

Figure 8.8 Variation in Normalized Material Damping Ratio with Excitation Frequency for 100 % Soil-Size MSW: (a) Old Waste and (b) Fresh Waste

old and fresh MSW when excitation frequency decreases by approximately one and a half orders of magnitude, from 1 Hz to 0.03 Hz.

As a result, D_{min} increases with decreasing excitation frequencies, less than 1 Hz, due to creep behavior, whereas D_{min} increases with increasing excitation frequencies, larger than 1 Hz, due to the frequency effect regardless of the age of waste. However, the increase in D_{min} at higher frequencies is slightly larger for fresh MSW.

8.4 CHANGE IN ESTIMATED TOTAL UNIT WEIGHT WITH CONFINING PRESSURE

The total unit weight of the old and fresh MSW specimens were estimated during the RCTS and LSRC tests. The changes in length and diameter of the old and fresh MSW specimens were computed using the vertical height change from the LVDT readings combined with an assumption that the MSW specimens are compressed at the same axial strains in the longitudinal and radial directions due to the isotropic confinement. The variations in estimated total unit weight for the old and fresh MSW are presented in Figures 8.9 (a) and 8.9 (b), respectively. For reference, the variation in estimated total unit weight of the mixed MSW is added to the old and fresh MSW plots. Specimens of the 100 % soil-size MSW are represented by open symbols, Specimens of the 62 to 76 % soil-size MSW are represented by solid symbols, and Specimens of the 14% mixed MSW are represented by open symbols with an "x" in the symbols.

As shown in the figures, estimated total unit weight increases with increasing confining pressure for the old, fresh, and mixed MSW. For the 100 % soil-size MSW specimens, the change in estimated γ_t is approximately 11 % on average (83.7 pcf (13.1 kN/m^3) to 93.3 pcf (14.7 kN/m^3) over confining pressures of 172.8 psf (8 kPa) to 5760 psf (276 kPa)) for the old and fresh MSW. The change in estimated γ_t is 17 % on average (59.0 pcf (9.3 kN/m^3) to 69.0 pcf (10.8 kN/m^3) over confining pressures of 172.8

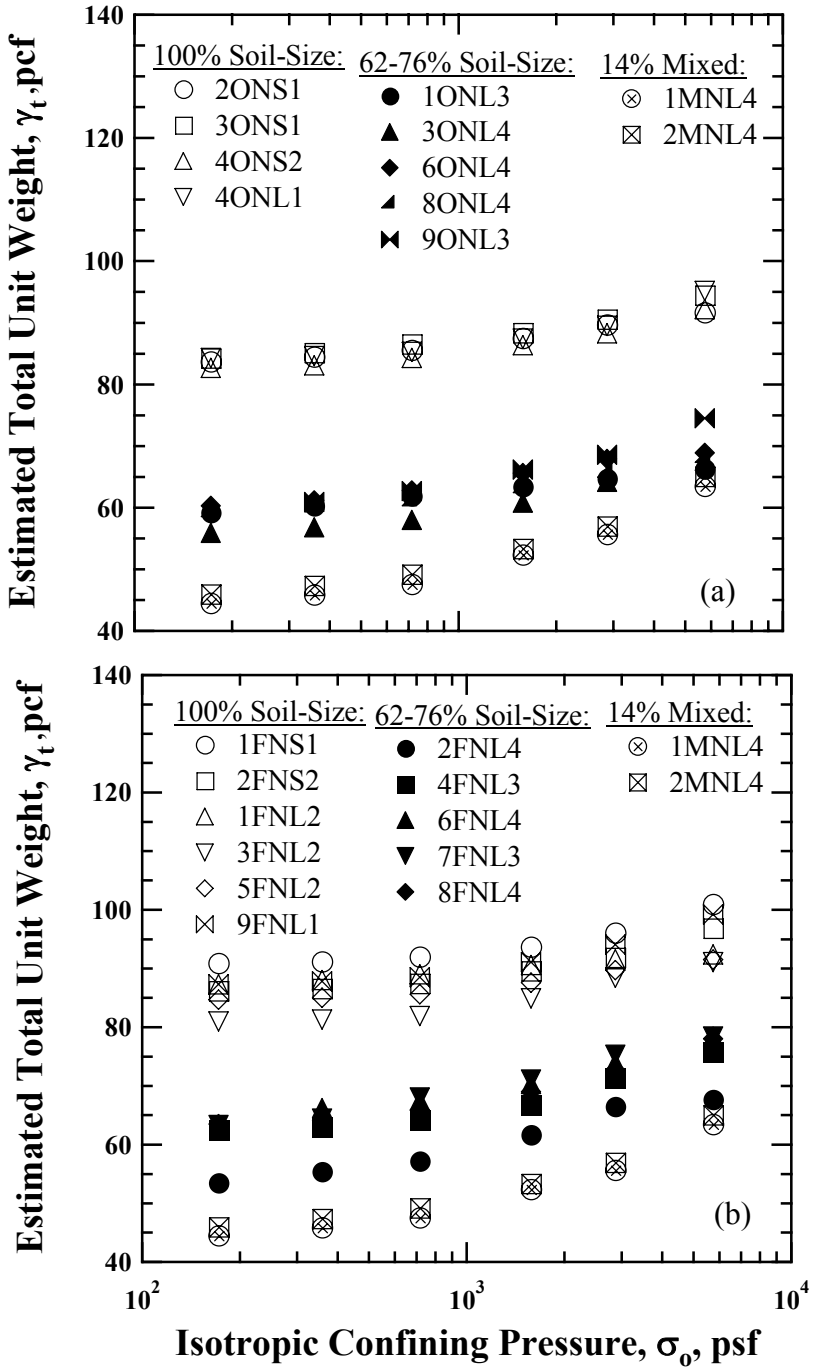

Figure 8.9 Variation in Estimated Total Unit Weight with Isotropic Confining Pressure for 100 %, 62 to 76 % Soil-Sizes, and 14 % Soil-Size Mixed MSW: (a) Old and Mixed Wastes and (b) Fresh and Mixed Wastes

psf (8 kPa) to 5760 psf (276 kPa)) for the 62 to 76 % soil-size old MSW specimens and 23% on average (61.7 pcf (9.7 kN/m^3) to 75.6 pcf (11.9 kN/m^3) over confining pressures of 172.8 psf (8 kPa) to 5760 psf (276 kPa)) of the 62 to 76 % soil-size fresh MSW specimens. Additionally the variation in estimated total unit weight of the 14 % mixed MSW specimens is added in the figures for reference. The change in estimated total unit weight of the 14 % mixed MSW is 42 % on average from 45.2 pcf (7.1 kN/m^3) to 64.2 pcf (10.1 kN/m^3) over confining pressure of 172.8 psf (8 kPa) to 5760 psf (276 kPa).

As shown in the figures, the variation in estimated total unit weight of MSW becomes lager as the weight percentage of soil-size material in the specimen decreases. This phenomenon is largely due to the lower initial total unit weight and due to the more increasing weight percentage of larger particles within the MSW specimens. Therefore, it can be concluded that the pattern of increase in total unit weight of MSW specimens with confining pressure is a function of the weight percentage of soil-size material, indicating that the change in total unit weight is dominantly controlled by their initial total unit weight.

8.5 SUMMARY

Small-strain dynamic properties, G_{max} and D_{min}, of the old and fresh MSW are compared in this chapter. The comparisons are made in terms of test parameters: (1) isotropic confining pressure and (2) excitation frequency. The variations in G_{max} and D_{min} of the 100 % and 62 to 76 % soil-size old and fresh MSW are compared in Sections 8.2.1 and 8.2.2. The response of MSW with confining pressure was approximately similar in the NC state regardless of the age and composition of waste. The effect of confining pressure was more pronounced on G_{max} than it was on D_{min}.

In terms of excitation frequency, the old and fresh MSW exhibit approximately

the same behavior in terms of G_{max}. G_{max} increases linearly with increasing excitation frequency in log f – G_{max} relationship, resulting from the viscosity effect of the 100 % soil-size MSW specimens. In the case of D_{min}, similar behavior with respect to excitation frequency, less than 1 Hz, is observed for the old and fresh MSW, however, the excitation frequencies larger than 1 Hz, the effect of excitation frequency becomes a significant for the old and fresh MSW. This effect is somewhat larger for the fresh MSW than old MSW.

Estimated total unit weights of the old and fresh MSW were measured during the RCTS and LSRC tests and are compared in Section 8.4. The estimated total unit weight increases with increasing confining pressure regardless of the age and composition of the MSW. Lower weight percentage of soil-size material MSW specimens result in much increase with confining pressure largely due to their lower initial total unit weight.

CHAPTER 9: Comparison of Shear Wave Velocities from Laboratory and Field Measurements

9.1 INTRODUCTION

Shear wave velocities measured in the laboratory from the RCTS and LSRC devices are compared with the shear wave velocities from field measurements at the Tri-Cities landfill in this chapter. In addition, the in-situ V_s profiles measured at the OII, Azusa, Southern California, NWRLF, Altamont, and Redwood landfills are also compared with the laboratory values. The in-situ V_s measurements were generally performed using the SASW method by UT personnel. The SASW method is well suited for measurements at MSW landfills in the sense that the method is non-invasive so no boreholes are drilled in the environmentally sensitive materials.

A brief explanation of the V_s laboratory measurements is given and the comparison between laboratory and in-situ V_s measurements in Tri-Cities landfill is presented first. Then, the laboratory Vs measurements are compared with values from previous studies in the following sections.

9.2 V_S MEASUREMENTS IN THE LABORATORY ON MSW SPECIMENS

As part of determining the dynamic properties of MSW with the RCTS and LSRC devices, V_s measurements are performed. For a given resonant frequency, the dimensions of the specimen and the system constant of the RC device, V_s is calculated by solving Equation (3.1) for the RCTS test. The same is true in the LSRC and V_s is determining by solving Equation (3.19). The variation of V_s with isotropic confining pressure from these tests is shown in Figures 9.1 and 9.2 for old and mixed wastes and fresh and mixed wastes, respectively. The specimens that were reconstituted with only

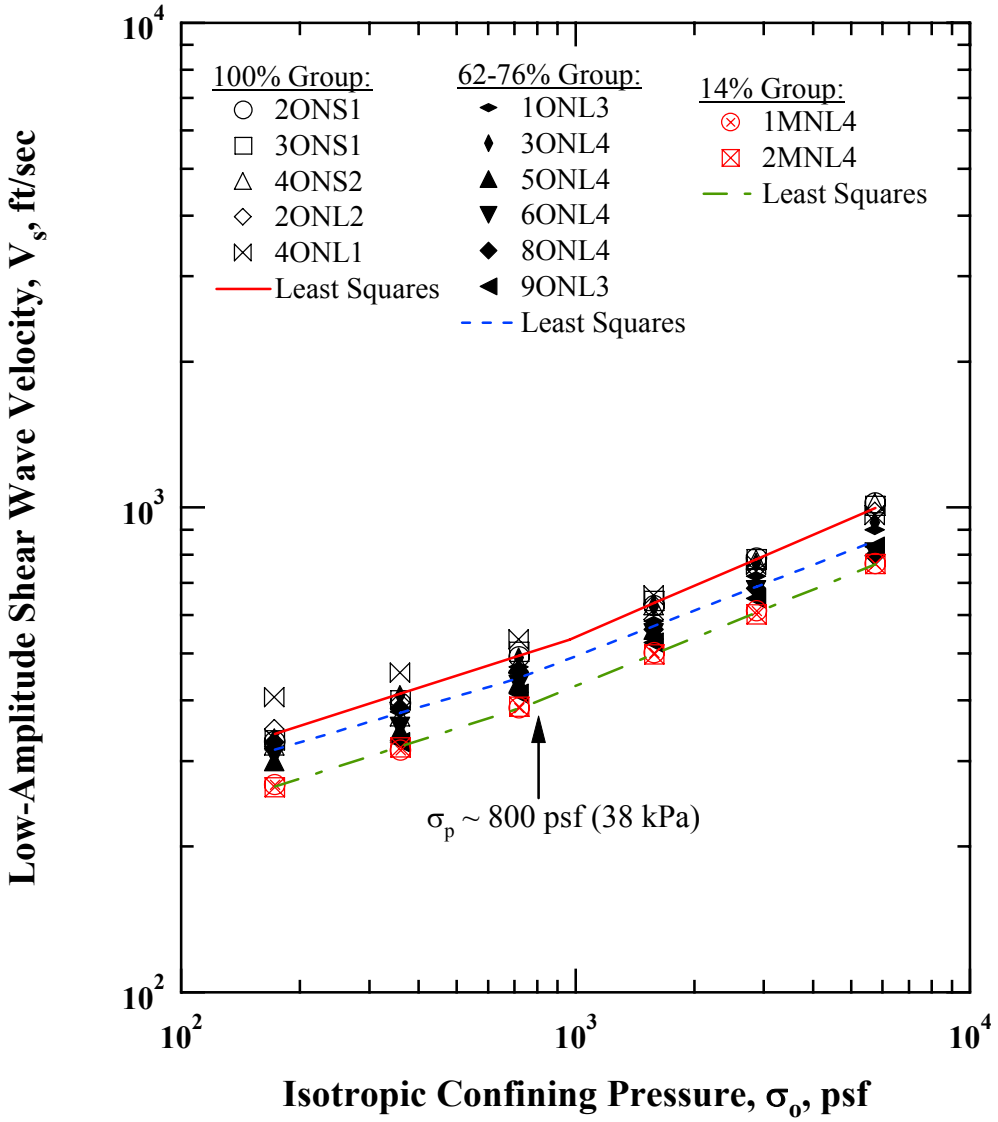

Figure 9.1 Variation in Low-Amplitude Shear Wave Velocity with Isotropic Confining Pressure for Old and Mixed MSW (All Groups) Determined by RCTS and LSRC Tests

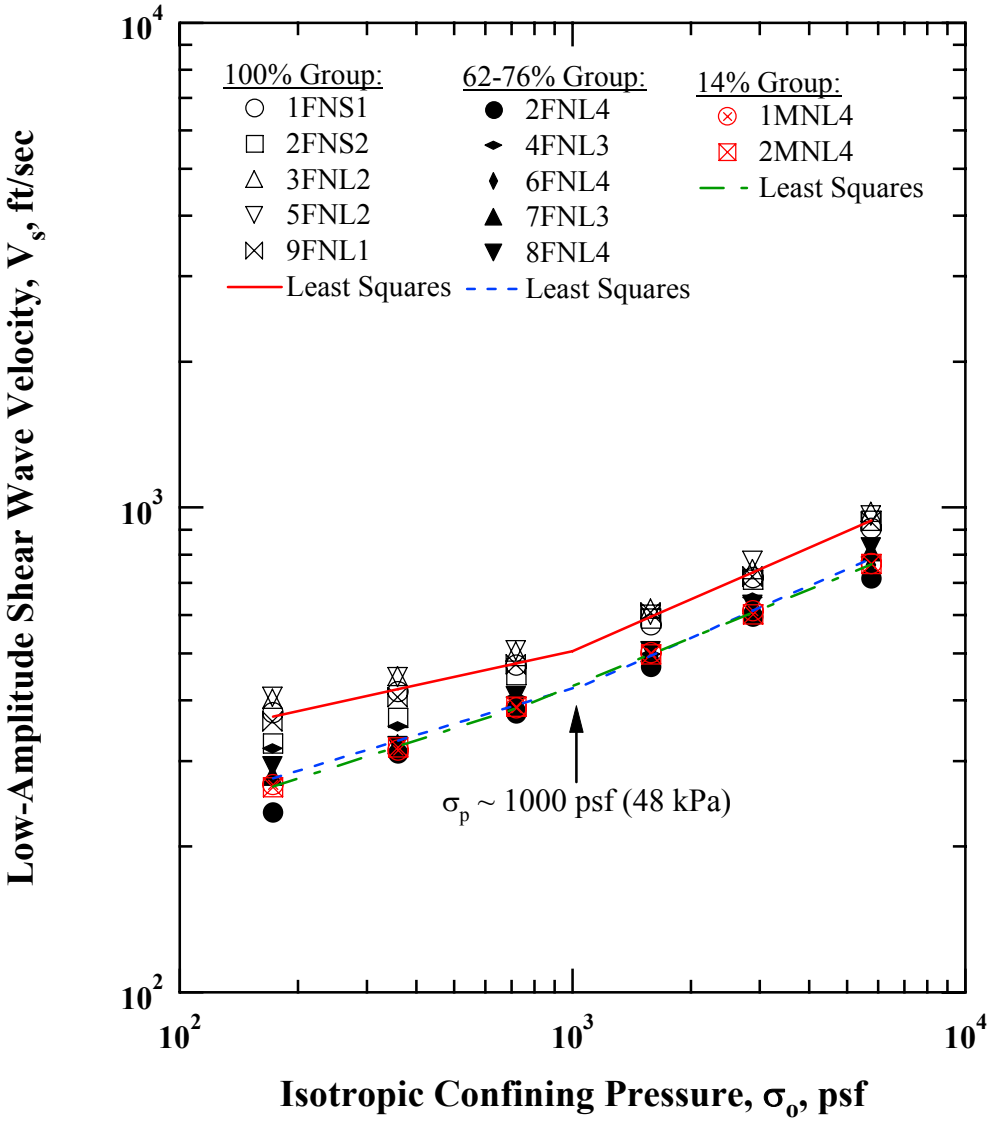

Figure 9.2 Variation in Low-Amplitude Shear Wave Velocity with Isotropic Confining Pressure for Fresh and Mixed MSW (All Groups) Determined by RCTS and LSRC Tests

soil-size material (passing the 3/4-in. (19.1-mm) sieve) are shown with the open symbols whereas specimens that were reconstituted with 62 to 76 % of soil-size material are shown with solid symbols. Also included in both figures are the V_s values from the mixed waste with 14% soil-size material and these specimens are represented by open symbols with an "x" in the symbol.

As seen in Figures 9.1 and 9.2, V_s increases with increasing confining pressure both old and mixed wastes and fresh and mixed wastes. Each group of specimens was fitted using the least-squares method and the fitted lines are shown with solid and dashed lines in the figures. The log Vs – log σ_o relationship that was fitted by:

$$V_s = V_{s1}\left(\frac{\sigma_O}{P_a}\right)^{n_S} \tag{9.1}$$

where,

V_{s1} is a shear wave velocity corresponding to one atmosphere in fps,

σ_o is an isotropic confining pressure in the same unit as P_a,

P_a is one atmosphere (2116 psf or 100 kPa), and

n_S is a dimensionless exponent.

This relationship was fitted separately to the overconsolidated (OC) range and the normally consolidated (NC) range. The values of parameters of old, fresh, and mixed MSW specimens are presented in Table 9.1. Additionally, the values of σ_p created by compaction effort of each group of specimens are given in the table.

Close examination of Figures 9.1 and 9.2 reveals that there is a change in slope of Vs between 720 psf (34 kPa) and 1584 psf (76 kPa) as a result of the compaction effort during sample preparation.

Table 9.1 Values of Exponents (n_S), Shear Wave Velocity at One Atmosphere (V_{s1}) of V_s, and Resultant Compaction Pressure, (σ_p), upon Loading Sequence for All Groups of Old, Fresh, and Mixed MSW Specimens in the RCTS and LSRC Devices

Sequence	Waste Type	% Soil-Size	Exponent, n_G		Shear Wave Velocity, V_{s1}, fps (m/sec)		σ_p psf(kPa)
			OC	NC	OC	NC	
Loading	Old & Mixed	100 %	0.26	0.35	655(200)	703(214)	966(46)
		62-76 %	0.24	0.31	576(176)	624(190)	719(34)
		14 %	0.26	0.33	510(155)	549(167)	738(35)
Loading	Fresh & Mixed	100 %	0.18	0.35	578(176)	660(201)	1000(48)
		62-76 %	0.24	0.36	508(155)	549(167)	1080(52)
		14 %	0.26	0.33	510(155)	549(167)	738(35)

It is interesting to compare the log Vs – log σ_o relationship in terms of absolute values of V_s at given confining pressure. In the NC state, the old and fresh wastes with 100 % soil-size particles have nearly the same values. In the OC state, compaction had a slightly larger effect on the fresh waste, resulting in the V_s values being slightly higher for the fresh waste. For the 62-76 % group, in the NC state, the values of V_s for the old waste exhibit slightly higher than fresh waste. However, fresh waste shows more pressure dependency. In the OC state, compaction had a slightly larger effect on the old waste resulting in slightly higher values of V_s for the old waste. Of course, the mixed waste group is the same in both figures and this group shows the lowest V_s values.

To correct for excitation frequency of V_s measurements in the laboratory, square

root of Equations (6.5) and (7.1) was taken for old and fresh MSW, respectively. It should be noted that when corrected for excitation frequency of V_s measurements in the laboratory to about 30 Hz, which would be typical frequency of in-situ seismic tests, frequency corrections were done by taking the ratio of shear modulus at a given excitation frequency to shear modulus at a excitation frequency of 30 Hz. As a result, this ratio turned out to be less than 5 %. Therefore, the correction for excitation frequency on V_s measurements was ignored.

9.3 ESTIMATING THE FIELD V_S PROFILES FORM THE LABORATORY LOG V_S – LOG σ_O RELATIONSHIPS

To convert mean total confining pressure in the laboratory tests to equivalent depth in the field, it is necessary to assume the coefficient of lateral earth pressure at rest, K_o, and total unit weight profiles. As part of the collaborative research project, Zekkos (2005) studied the variation of K_o regarding different weight percentages of soil-size material (e.g., 100 % and 62 to 76 % soil-size Groups) and suggested that Poisson's ratio, υ, for the 100% soil-size Group is about 0.3 to 0.35 and a value of υ for the 62 to 76 % soil-size Group varies from nearly 0 to 0.3. Therefore, this study used a value of υ of 0.3 for the 100 % soil-size Group and 0.25 for the 62 to 76 % soil-size Group. In addition, assumed Poisson's ratio of the 14 % soil-size Group is 0.25. The value of υ can be converted using:

$$K_o = \frac{\upsilon}{1-\upsilon} \tag{9.2}$$

Thus, equivalent values of K_o corresponding to assumed values of Poisson's ratio for the 100 % and 62 to 76 % and 14 % soil-size Groups are 0.43 and 0.33, respectively.

The variations in K_o, υ, and overconsolidation ratio (OCR) with depth are presented in Figure 9.3. As shown in the figures, the variations of these values near the top of surface (about 5 ft (1.5 m)) show higher values due to overconsolidation produced by heavy compaction vehicles in the MSW landfills. The OCR was simply assumed to be 4 and to be acting over the top 5 ft (1.5 m). Using these profiles, mean total confining pressure in the laboratory was turned into vertical total stress. This equation is expressed by:

$$\sigma_o = \frac{1+2K_o}{3}\sigma_v \tag{9.3}$$

where,

σ_o is the mean total confining pressure in the laboratory,

σ_v is the vertical total stress ($\sigma_v = \gamma_t$ x z) in the field,

γ_t is the total unit weight, and

z is the depth.

With given values of γ_t measured in the laboratory during the RCTS and LSRC tests and assumed K_o profiles, vertical total stress could be used to determine an equivalent depth in the field. The variations in V_s profiles with vertical total stress and equivalent depth of the old and mixed MSW are shown in Figure 9.4. In the same manner, the variations in V_s profiles with vertical total stress and equivalent depth of the fresh and mixed MSW are shown in Figure 9.5.

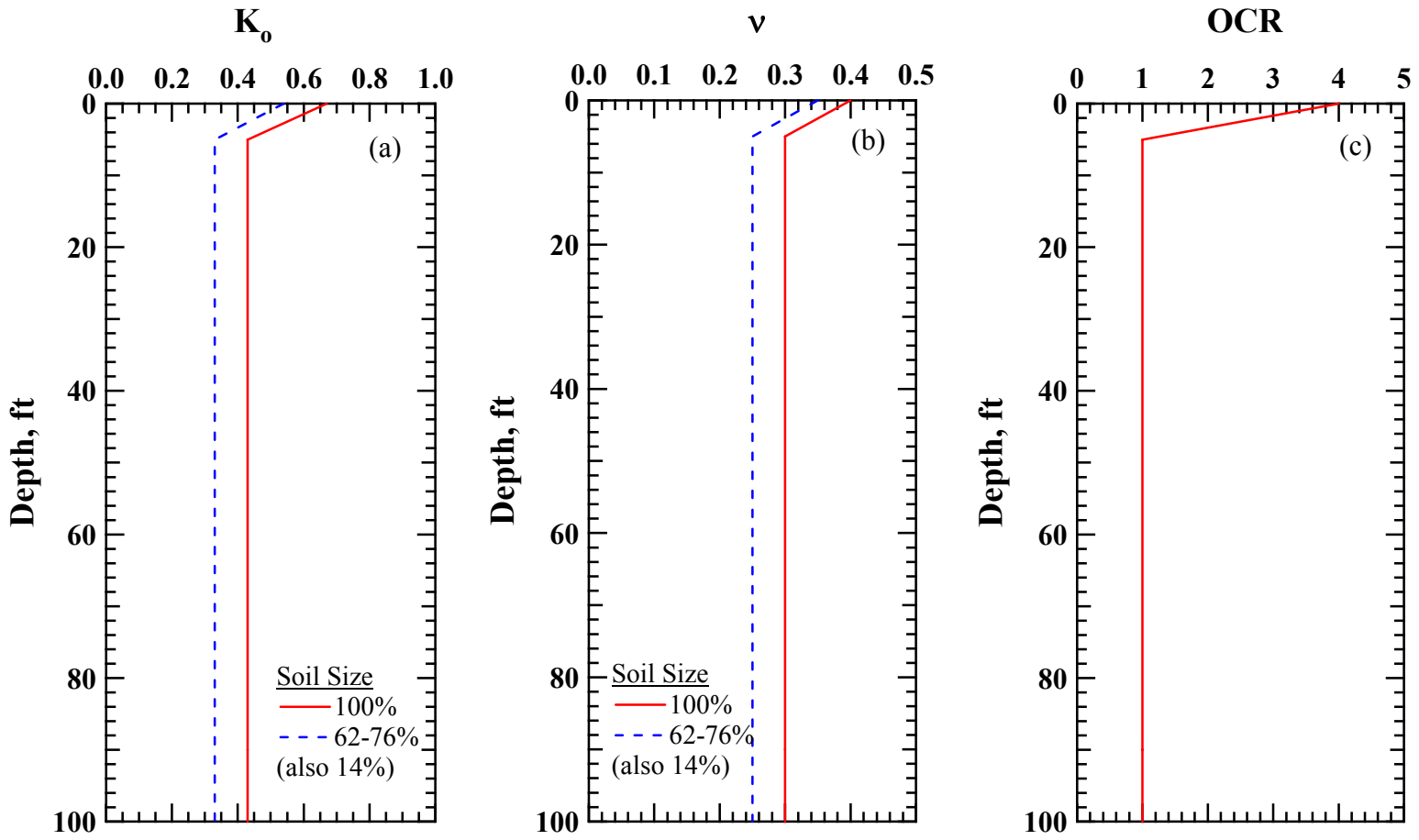

Figure 9.3 Variation in (a) Coefficient of Lateral Earth Pressure at Rest, (b) Poisson's Ratio, and (c) Overconsolidation Ratio with Depth for the Conversion of Isotropic Confining Pressure in the Laboratory to Depth in the Field

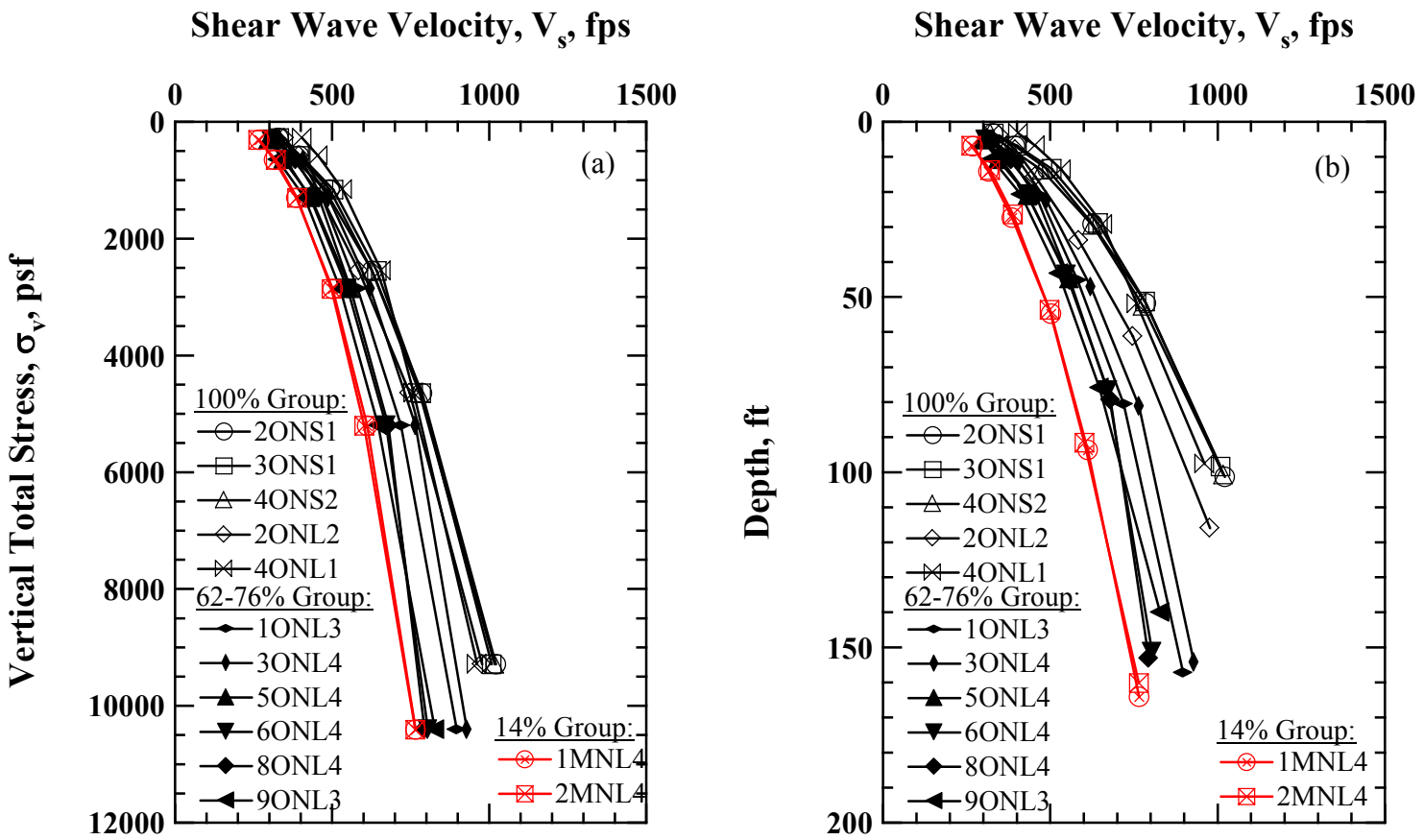

Figure 9.4 Variation in Shear Wave Velocity with (a) Vertical Total Stress and (b) Depth for Old and Mixed MSW Specimens

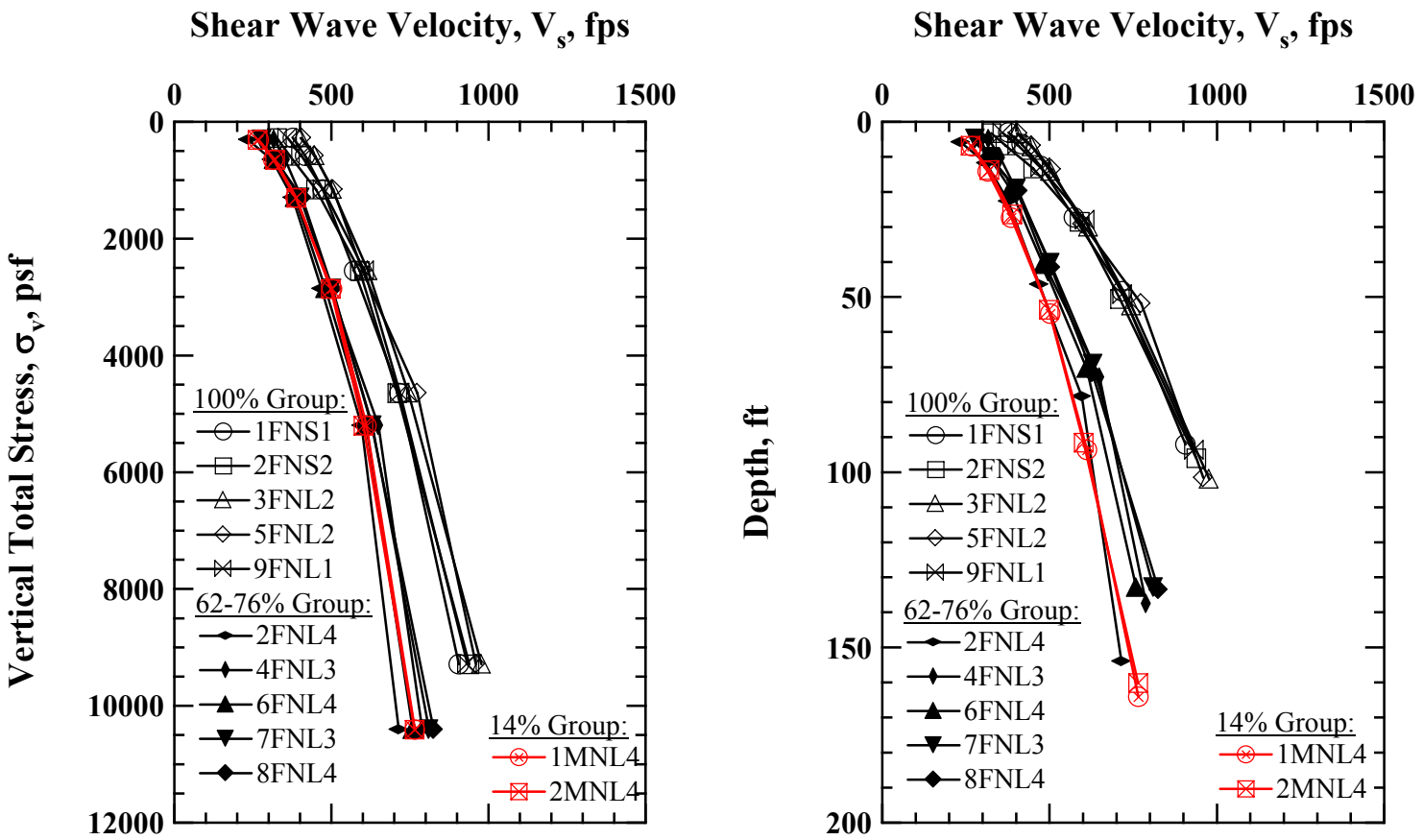

Figure 9.5 Variation in Shear Wave Velocity with (a) Vertical Total Stress and (b) Depth for Fresh and Mixed MSW Specimens

9.4 IN-SITU V_S MEASUREMENTS IN TRI-CITIES LANDFILL USING THE SASW METHOD

In-situ V_s measurements were conducted by UT personnel under the supervision of Dr. Stokoe using the SASW method at the Tri-Cities Landfill as well as at the Redwood and Altamont Landfills (Lin et al., 2004). The SASW test locations at the Tri-Cities Landfill are presented in Figure 9.6. The SASW tests included: four SASW arrays (indicated by T1 through T4) on the top surface, two SASW arrays along the side slope (indicated by S1 and S2), and one SASW array along the perimeter road at the base (indicated by R1). The boreholes where the old and fresh MSW materials were retrieved are shown in Figure 4.2. By comparing Figures 4.2 and 9.6, one can see that SASW location T1 corresponds to BH-1 (fresh waste) and SASW location T2 corresponds to BH-2 (old waste). The measured V_s profiles near these two boreholes in the Tri-Cities landfill are presented in Figure 9.7. In addition, sampling depths for the old and fresh wastes with a given interval (typically 10 ft (3.0 m)) are indicated in the figures. Mean sampling depths for the old and fresh wastes were 85 ft (25.9 m) and 28.5 ft (8.7 m)), respectively.

The field V_s profiles were generated by assuming different values for Poisson's ratio, i.e., 0.1, 0.2, and 0.4. The values of 0.30 and 0.25 for the 100 % soil-size waste and 62 to 76 % and 14 % soil-size wastes, respectively, were estimated from the UBC laboratory measurements. However, a value of 0.2 appears to be representative of Poisson's ratio of landfill material when compared with the values reported in the literature (e.g., Landva et al., 2000). As seen in Figure 9.7, the V_s profiles shift to lower V_s values at a given depth with increasing Poisson's ratios and the measurement depth (sampling depth) generally increases. It is interesting to observe in Figure 9.7 that V_s

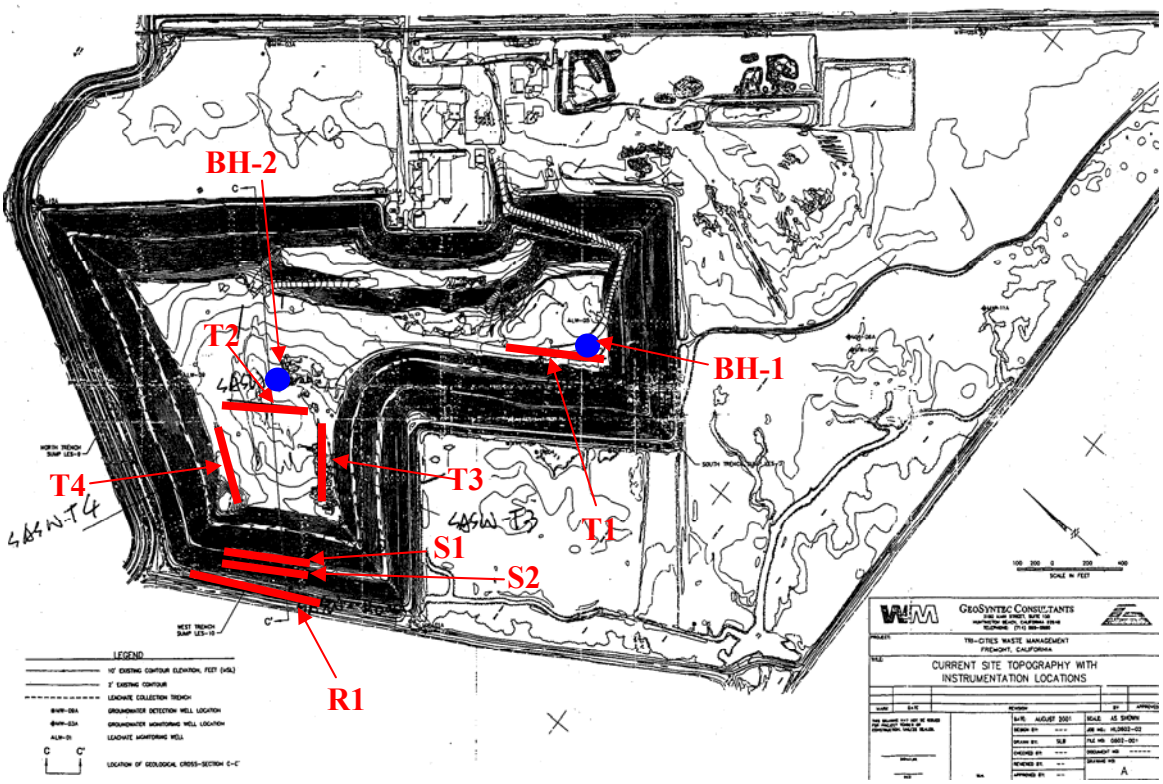

Figure 9.6 Plan View and Locations of SASW Test Arrays in the Tri-Cites Landfill (Courtesy of GeoSyntec Constants, 2001)

near the surface exhibits higher values, resulting from overconsolidation due to the vehicles that placed and compacted the waste in the landfill as well as an undetermined thickness of cover soil. it is also interesting to note that: (1) the values of Vs from the shallow depth of the fresh waste (23 to 33 ft (7 to 10 m) in Figure 9.7 (a)) are changed very little by the value of ν, and (2) the values of the vary by less than 10 % in the old waste for ν varying from 0.20 to 0.30 at depth (Figure 9.7 (b)).

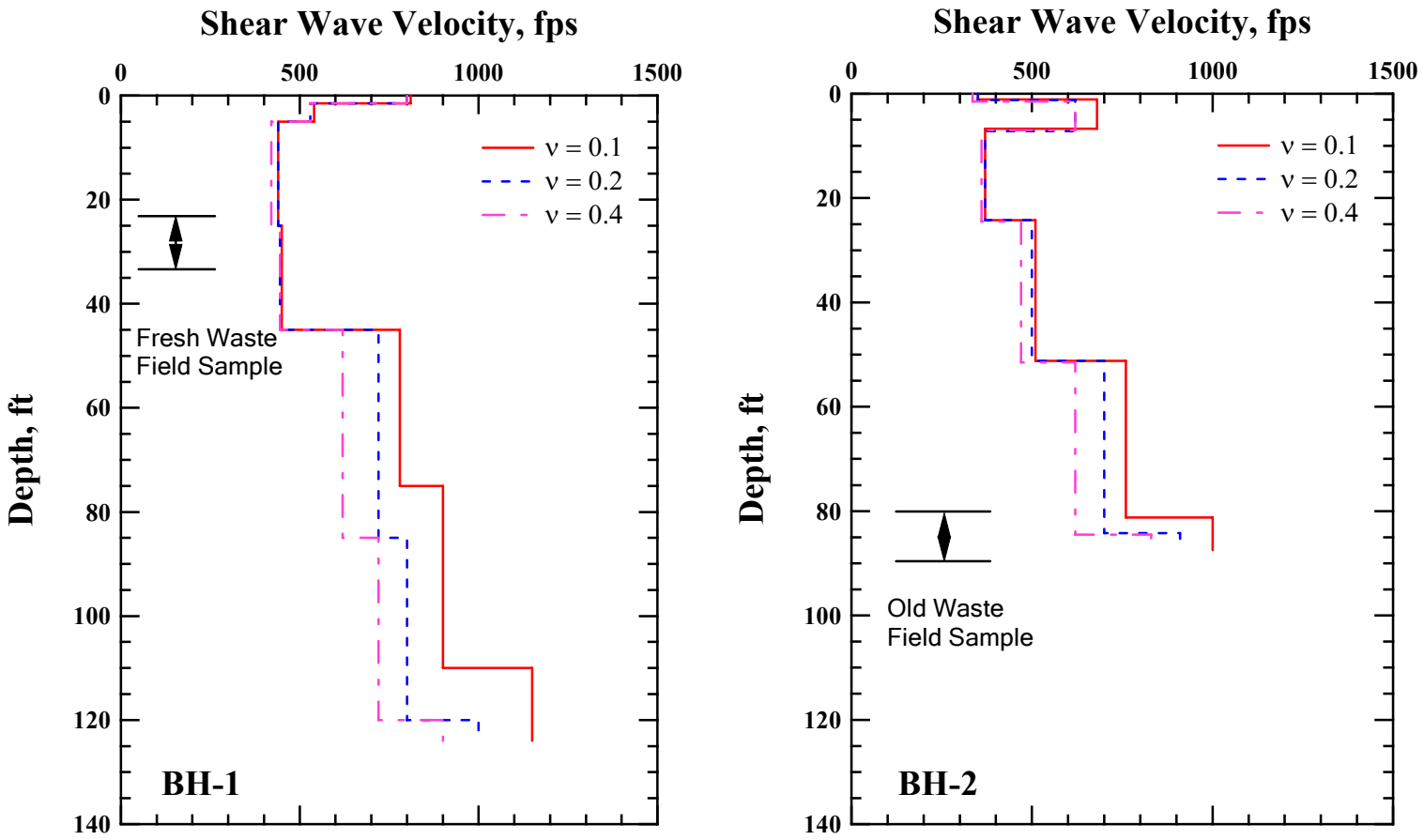

Figure 9.7 The Variation in Vs Profiles Measured by SASW Testing Near Two Boreholes (BH-1 and BH-2) in the Tri-Cities Landfill (Lin et al., 2004)

9.5 COMPARISON OF V_S PROFILES OBTAINED FROM LABORATORY TESTS WITH V_S PROFILES MEASURED AT THE TRI-CITIES LANDFILL

As discussed above, the field V_s profile that was generated by assuming Poisson's ratio of 0.2 was chosen for the purpose of comparing the field and laboratory measurements simply because this was close to the waste value (0.25) and resulted in almost not change at the shallow depth in V_s of the fresh waste. Comparison of the field and laboratory V_s profiles is given in Figure 9.8. It should be noted that the V_s profile near Borehole BH-1 (SASW array T1) was compared with the laboratory results measured with the fresh waste specimens, while the V_s profile near Borehole BH-2 (SASW array T2)and the V_s profiles from the SASW arrays of T3 and T4 was compared with measured with the old waste specimens. (The T2, T3, and T4 profiles were used simply to represent better the variation around Borehole BH-2.) This comparison is done this way because the fresh waste material was retrieved from a shallower depth (28.5 ft (8.7 m)) at Borehole BH-1 and the old waste material was retrieved from a deeper depth (85 ft (25.9 m)) at Borehole BH-2. The V_s profiles are represented by open symbols for 100 % soil-size specimens and are indicated as solid symbols for 62 to 76% soil-sizes specimens. The V_s profiles for 14 % soil-sizes specimens are denoted as open symbols with an "x" in the symbol.

As illustrated in Figure 9.8, laboratory shear wave velocities measured for the 100% soil-size old and fresh waste specimens exhibit higher values than the field V_s values at depth below about 10 to 15 ft (3 to 5 m). Considering a little higher values of V_s created by compaction effort in the V_s measurements at the first three confining pressure stages for the old and fresh waste specimens, shear wave velocities measured from the 62 to 76 % soil-size old waste specimens exhibit values slightly less than or

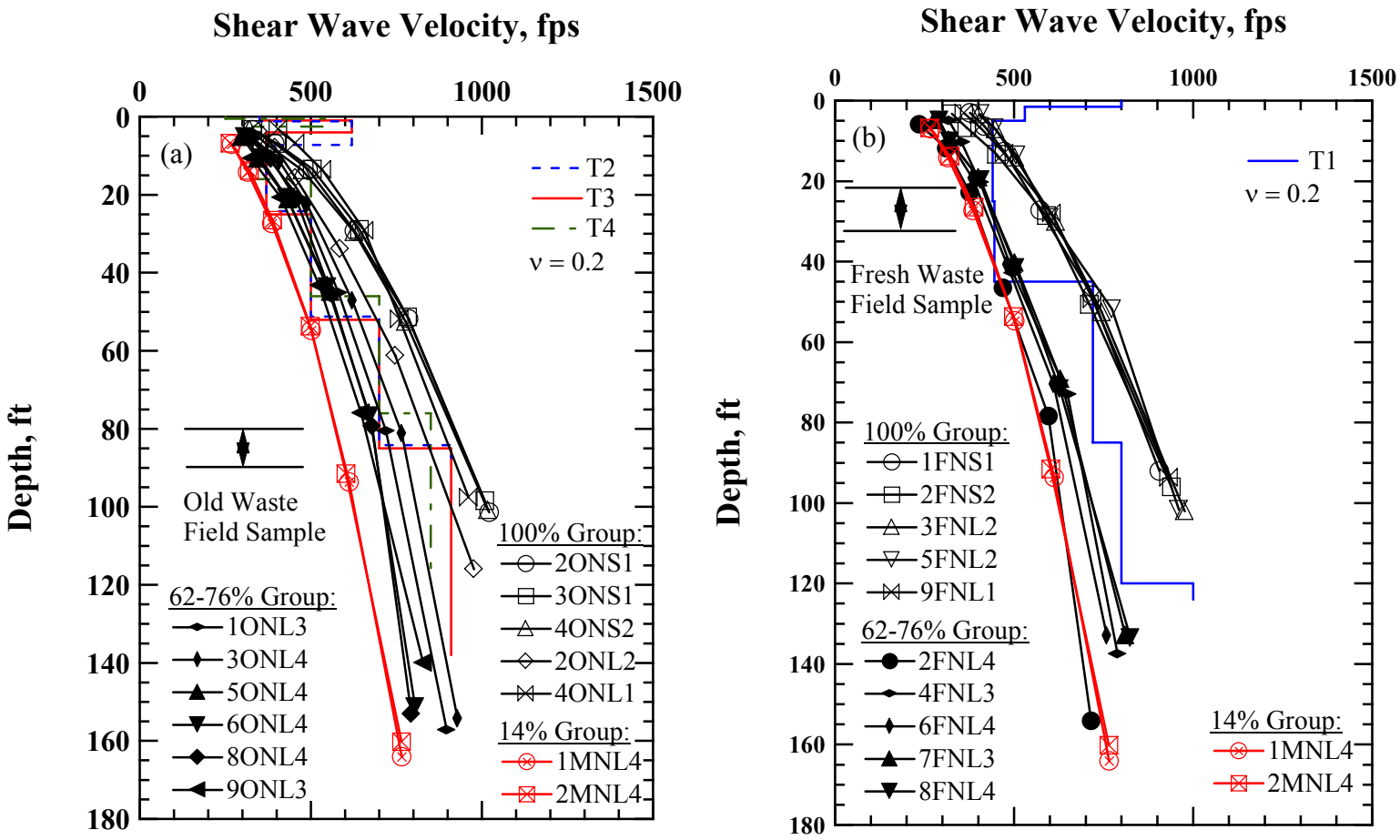

Figure 9.8 Comparison of the Variations in V_s Profiles Measured at the Tri-Cities Landfill with Those Obtained from the Laboratory for (a) Old and Mixed and (b) Fresh and Mixed Specimens

equal to the V_s profiles measured near Borehole BH-2 and other SASW arrays (T3 and T4). Similarly, shear wave velocities measured from the 62 to 76 % soil-size fresh waste specimens are somewhat less than the V_s profile measured near Borehole BH-1.

Taking a representative weight percentage of soil-size material (about 60 to 75 %) of the Tri-Cities landfill into account, this difference appears to be reasonable in the sense that the duration of confinement of the laboratory specimens is much shorter than that of the in-situ waste material. Other factors such as degradation during aging and bonding effect between waste components may contribute to the difference in shear wave velocity. In the case of the 14% soil-size material specimens, the values of V_s form the lower bound of V_s profile with depth regardless of the age of waste.

9.6 COMPARISON OF V_S PROFILES FROM LABORATORY WITH OTHER STUDIES

The measured V_s values were also used to make a comparison with previous V_s profiles measured at different landfills by UT and other researchers. Those landfills include the Altamont and Redwood Landfills in southern California which are in "wetter" areas (as is the Tri-Cities Landfill). OII Landfill, Northwest Regional Landfill Facility (NWRLF), AZ, and Azusa Landfill are used individually. Another V_s profile is a mean profile from V_s measurements of six Southern California waste landfills (Kavazanjian et al., 1996) ("drier" areas). These waste landfills included: (1) OII, (2) Azusa, (3) Toyon Canyon, (4) Sunshine Canyon, (5) Lopez Canyon, and (6) Landfill A (unidentified landfill). Also, V_s profiles from the most V_s profiles were measured using the SASW method and UT personnel were involved. The exception is the profile measured at the NWRF landfill, in which the seismic downhole method was employed.

The variation in V_s profiles measured at the Altamont, Redwood, and Tri-Cities landfills is shown in Figure 9.7. These V_s profiles are expressed in terms of average

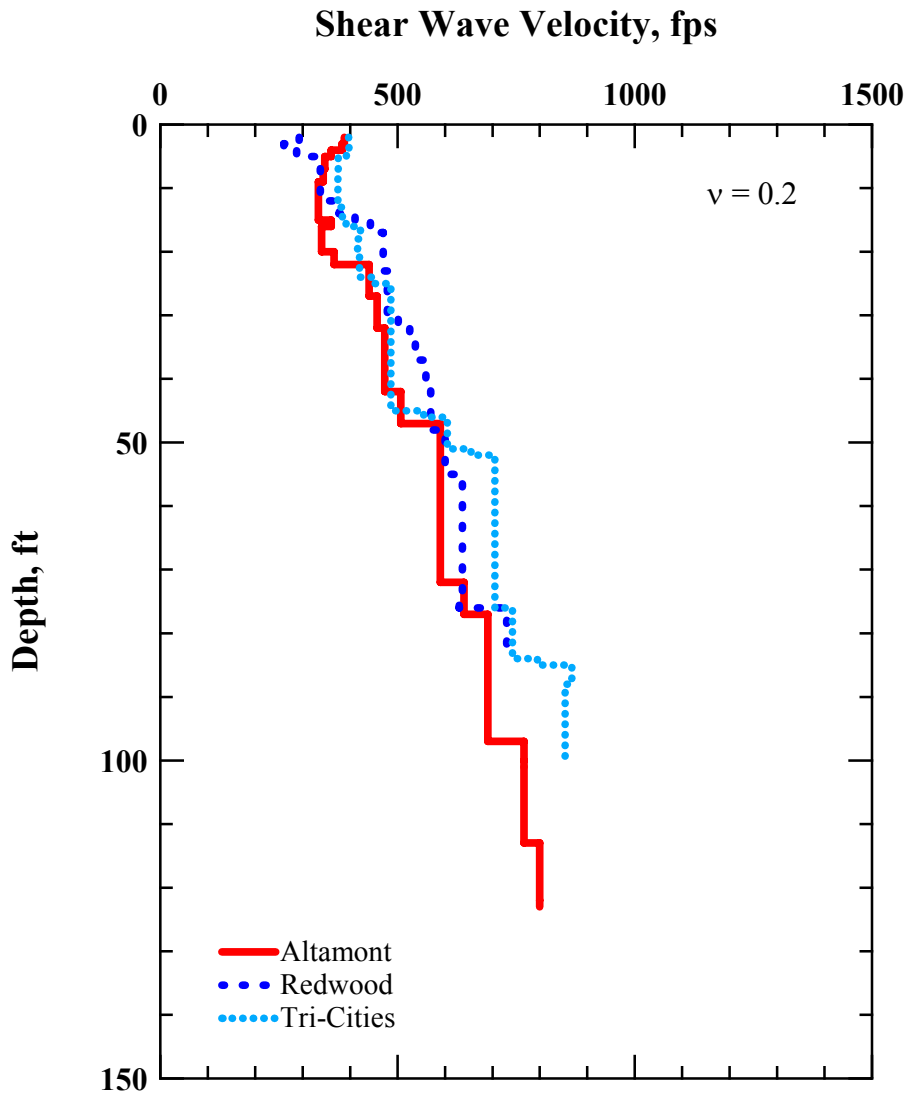

Figure 9.7 Variations in Average V_s Profiles Measured at the Altamont, Redwood, and Tri-Cities Landfills by SASW Testing (after Lin et al., 2004)

values (Lin et al., 2004). These profiles were generated with a value of Poisson's ratio of 0.2. As presented in the figure, V_s generally increases with depth, showing a small variation between the landfills. It is interesting to observe that V_s values at shallower depths become higher at these landfills largely due to the overconsolidation produced by

the compaction process and the soil cover upon which the measurements were performed.

The variation in V_s profiles measured at the OII, Azusa, and NWRLF landfills are shown in Figure 9.8. In addition, the mean V_s profile generated from six different landfills in Southern California is shown in Figure 9.8 (It should be noted that the OII and Azusa Landfills are also included in the mean V_s profiles of the six landfills.). It should be noted that V_s measurements in the LWRLF landfill have performed only up to 30 ft (9 m), which is relatively shallower than other V_s measurements.

As shown in the figure, V_s generally increases with depth in all profiles. It is interesting to note that the values of V_s measured in the OII, Azusa, NWRLF, and Southern California landfills, which are in drier weather conditions, are normally higher than those measured in the Altamont, Redwood, and Tri-Cities landfills to a depth of about 110 ft (33.5 m). Higher V_s values, even at shallower depths, in the OII landfill result from a very high ratio of soil-size material to solid waste at this site (Kavazanjian et al., 1996)

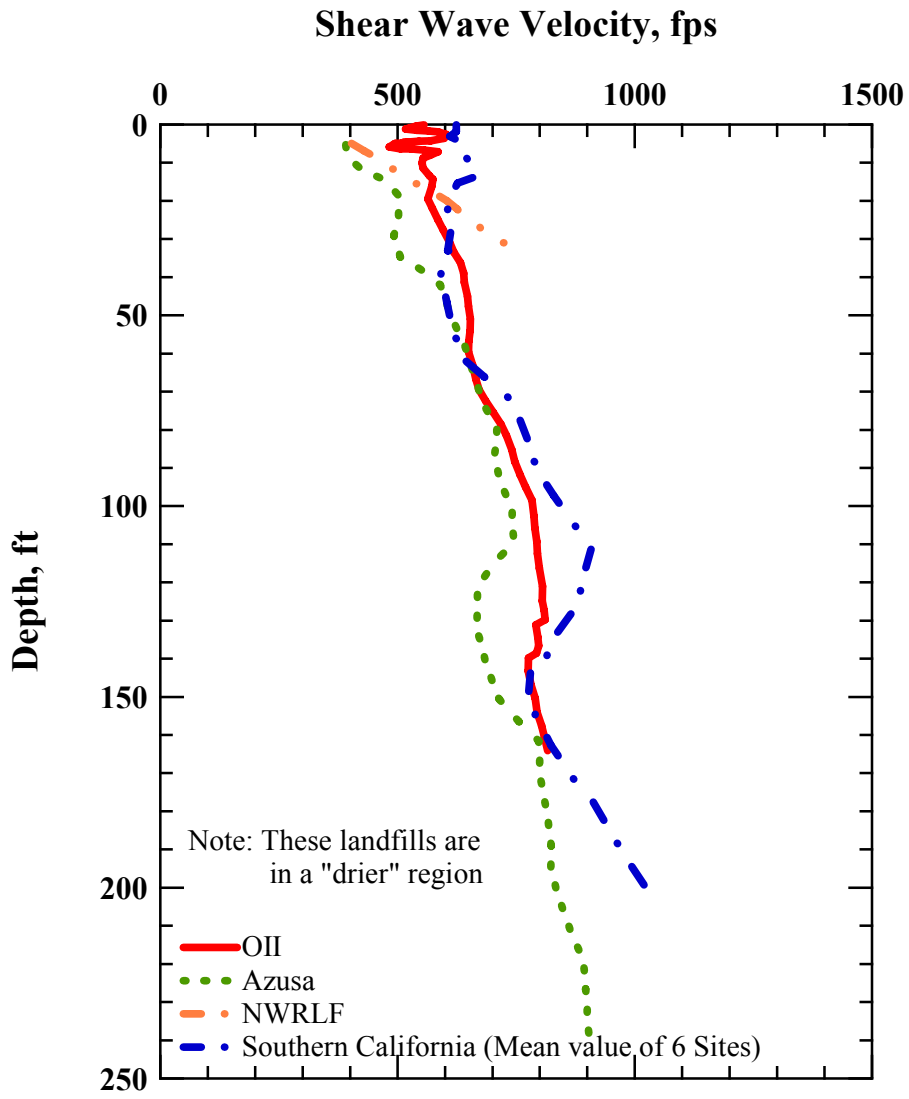

Figure 9.8 Variations in Average V_s Profiles Measured at the OII, Azusa, and NWRLF Landfills and Mean V_s Profile Generated from Six Different Landfills in Southern California (after Kavazanjian et al., 1996, and Houston, 1995)

The comparison of average V_s profiles of the old and mixed wastes measured in the laboratory with other landfills is presented in Figures 9.9 (a) and (b). Open symbols represent the V_s profiles measured from the 100 % soil-size material specimens and solid

symbols represent the V_s profiles measured from the 62 to 76 % soil-size material specimens. Open symbols with an "x" in the symbol represent the V_s profiles measure from the 14 % soil-size material specimens.

As shown in Figure 9.9, V_s values measured from the 100 % soil-size material specimens generally exhibit somewhat higher values than the in-situ V_s measurements except at the shallower depths (depths less than 20 ft (6 m)) in the OII and Southern California landfills. However, V_s values for the 62 to 76 % soil-size material specimens show good agreement with other in-situ V_s measurements. V_s values for the 14 % soil-size material specimens form a lower bound along depth.

In-situ V_s profiles are also compared with the laboratory measurements of fresh and mixed waste specimens and the variation in V_s profiles is shown in Figure 9.10. Again, the 100 % soil-size material specimens overestimate the V_s values whereas the 14% soil-size material specimens underestimate the V_s values along the depths. However, the 62 to 76 % soil-size material specimens give a quit good agreement with in-situ V_s measurements in other landfills.

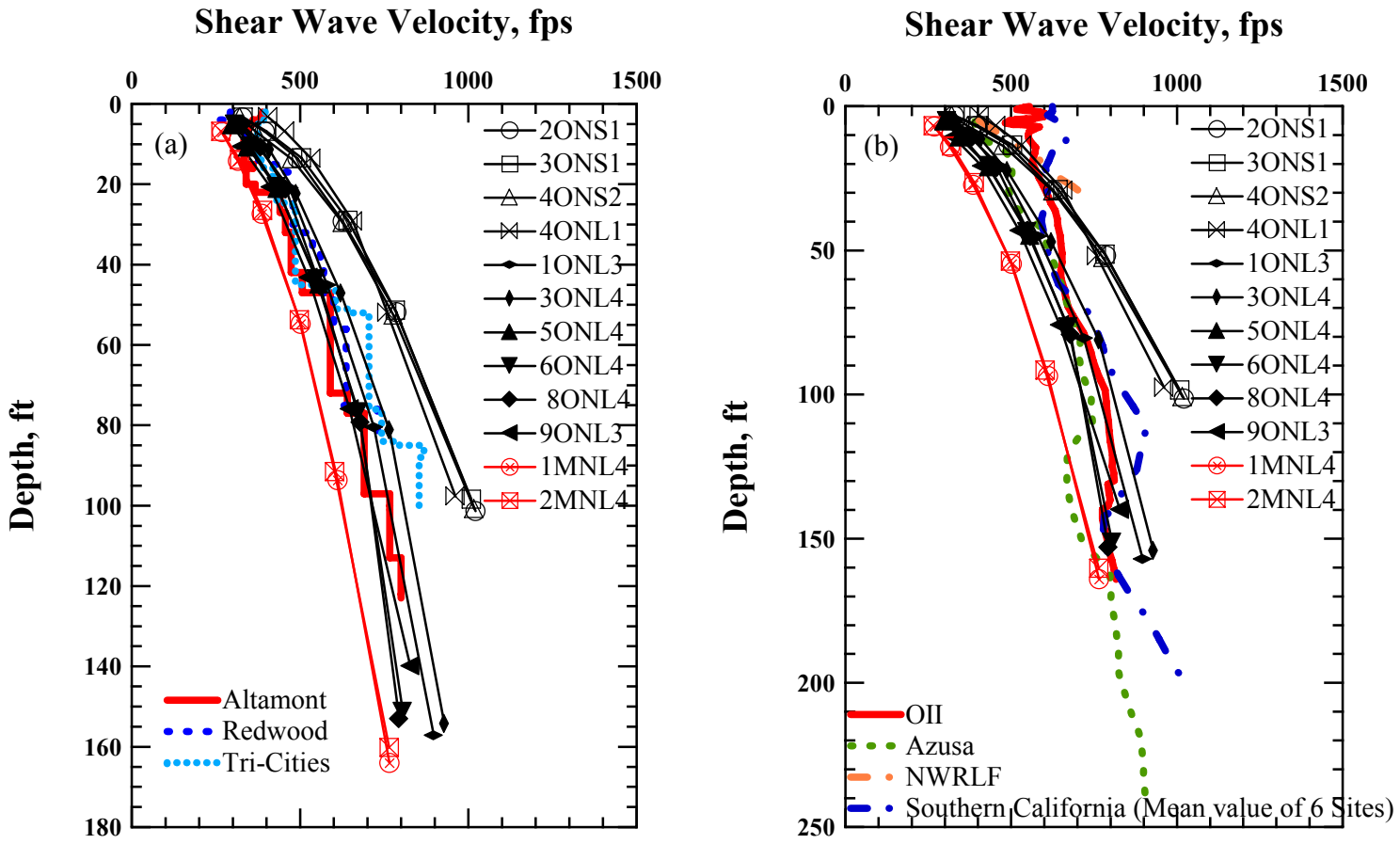

Figure 9.9 Comparison of the Variations in V_s Profiles of Old and Mixed Specimens Measured in the Laboratory with Those Obtained from (a) Altamont, Redwood, and Tri-Cities Landfills and (b) OII, Azusa, NWRLF, and Southern California Landfills

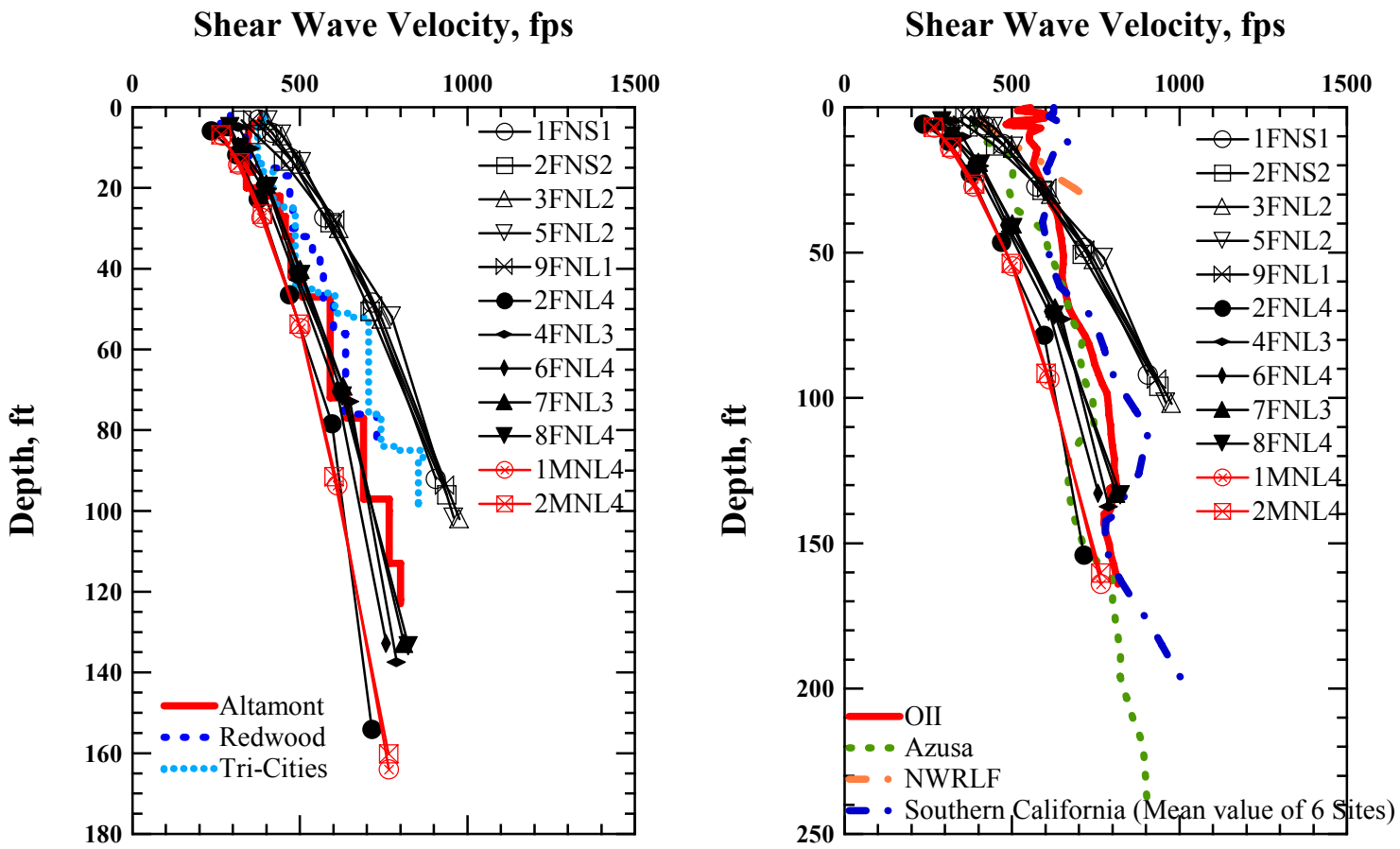

Figure 9.10 Comparison of the Variations in V_s Profiles of Fresh and Mixed Specimens Measured in the Laboratory with Those Obtained from (a) Altamont, Redwood, and Tri-Cities Landfills and (b) OII, Azusa, NWRLF, and Southern California Landfills

9.7 SUMMARY

Shear wave velocities were measured for MSW specimens with different weight percentages of soil-size material during the RCTS and LSRC tests in the laboratory. These values were compared with in-situ V_s profiles measured in the Tri-Cities landfill as well as other MSW landfills in this chapter. UT personnel performed a series of the SASW tests under supervision of Dr. Stokoe at the Tri-Cities landfill at the locations shown in Figure 9.6. The V_s profiles were generated for the arrays (T1 and T2) and these are shown in Figure 9.7 with the different values of Poisson's ratio, e.g., 0.1, 0.2, and 0.4.

The MSW bulk sample for the fresh waste was taken from the Borehole BH-1 and the bulk sample for the old waste taken from Borehole BH-2. Therefore, the V_s profile, generated with Poisson's ratio of 0.2, measured at SASW T1 near Borehole BH-1 is compared with the values of V_s of fresh MSW specimens. The V_s profiles measured from T2, T3, and T4 are compared with the values of V_s measured from old MSW specimens. Shear wave velocities of the 100 % soil-size material specimens are generally higher than those measured in the field whereas shear wave velocities of 62 to 76 % soil-size material specimens show generally good agreement or values slightly less than in-situ V_s measurements. The V_s profiles from the 14 % soil-size MSW specimens forms lower boundary.

The values of V_s measured in the laboratory are also compared with those measured in other landfills. The comparisons of V_s profiles are presented in Figures 9.9 and 9.10. As shown in the figures, V_s profiles from the 62 to 76 % soil-size material specimens show generally good agreement with those measured in other landfills.

CHAPTER 10: Nonlinear Behavior of Old MSW

10.1 INTRODUCTION

Evaluation of shear modulus (G) and material damping ratio (D) in the nonlinear strain range is important to understanding the dynamic properties of MSW. Selection of the nonlinear dynamic properties of MSW has a significant impact on the site response analyses of landfills. Despite the importance of nonlinear dynamic properties in site response analyses, many researches during previous decades have focused on estimating nonlinear dynamic properties of MSW by means of back-calculation analyses based on recorded ground motions at the OII landfill.

The nonlinear strain ranges were defined, herein, as the strain ranges beyond linear cyclic threshold shearing strain, γ_t^e, of 0.002 %, as mentioned in Chapter six. These nonlinear strain ranges were specifically divided into two regions; the nonlinear elastic range and the nonlinear range. The strain range between the γ_t^e and γ_t^c, which is called a volumetric or cyclic threshold shear strain, allows a significant permanent volume change or a permanent pore water pressure change to occur in the soil, and is defined as the nonlinear elastic range. The upper limits of the γ_t^c are 0.005 % for gravels, 0.01 % for sand, and 0.1 % for normally consolidated, high plasticity clays (Bellotti et al. 1989, Lo Presti, 1989, Vucetic and Dobry, 1991). The nonlinear properties do not change dramatically with increasing shearing strain and are stable with respect to number of cycles.

Strains greater than γ_t^c, are said to be occurring in the nonlinear range. The material in this range behaves nonlinearly, resulting in shear modulus degradation and in increase in material damping in clays, pore pressure generation in saturated sands, and

hardening behavior in dry sands. Instantaneous energy dissipation and energy losses occur with the number of loading cycles due to irrecoverable micro-structural change (Vucetic, 1994).

The test parameters affecting the dynamic properties of MSW in the nonlinear strain ranges are investigated in this chapter. Those parameters include: (1) shearing strain amplitude, γ, (2) total isotropic confining pressure, σ_o, (3) overconsolidation ratio (OCR), (4) number of loading cycles, N, (5) excitation frequency, f, and (6) specimen size. Other material parameters that influence the dynamic properties in the nonlinear strain range are to be studied as well. Those material parameters are: (1) water content, (2) waste composition, (3) total unit weight, and (4) particle size. The test results and observations from the measurements are discussed and compared in the subsequent sections.

10.2 TEST PROCEDURES

10.2.1 Testing with the RCTS Device

High-amplitude RC (HARC) tests and high-amplitude TS (HATS) tests were performed with small-diameter specimens at their natural condition and at a hydrated condition. These tests were performed at multiple confining pressures and the confining pressure levels are given in Table 10.1. An example set of RCTS tests at one confining pressure is presented in Figure 10.1. As shown in the figure, at first, low-amplitude RC (LARC) tests were performed to establish the baseline measurements of G_{max} and D_{min} for the purpose of comparison of those values after high-amplitude RCTS tests had been performed. Then, TS tests were performed with increasing shearing strain at a given frequency (typically 0.5 Hz). Another LARC tests were performed immediately after completion of HATS test to monitor any changes in the MSW skeleton induced by the

Table 10.1 Isotropic Confining Pressures Used in High-Amplitude RCTS Tests for Small-Diameter 100% Soil-Size Old MSW Specimens in the RCTS Device

Specimen ID	Isotropic Confining Pressure	
	High-Amplitude RC Tests, psi (kPa)	High-Amplitude TS Tests, psi (kPa)
MSW1ONS1$^{\Delta}$	11, 60 (76, 414)	11, 60 (76, 414)
MSW1OHS1	11, 60 (76, 414)	11, 60 (76, 414)
MSW2ONS1	2.5, 11, 40 (17, 76, 276)	2.5, 11, 40 (17, 76, 276)
MSW2OHS1	2.5, 11, 40, 40**, 11* (17, 76, 276, 276, 76)	2.5, 11, 40, 40**, 11* (17, 76, 276, 276, 76)
MSW3ONS1	2.5, 11†, 40†, 11*, 11†, 40†, 11* (17, 76, 276, 76, 76, 276, 76)	2.5, 11†, 40†, 11*, 11†, 40†, 11† (17, 76, 276, 76, 76, 276, 76)
MSW3ONS1(2)	11† (76)	11† (76)
MSW3OHS1	11† (76)	11† (76)
MSW4ONS2$^{\triangle}$	11, 40, 2.5* (17, 76, 276)	11, 40, 2.5* (17, 76, 276)
MSW5ONS1	11 (76)	11, 40 (76, 276)
MSW6ONS2	11, 40 (76, 276)	11, 40 (76, 276)

Notes:

* denotes unloading stage.

† denotes reloading stage.

Δ1 denotes specimen reconstituted with material passed the 3/8-in. (9.5-mm) sieve

⌂2 denotes specimen reconstituted with material passed the ¾-in. (19.1-mm) sieve in the specimen ID.

MSW3ONS1(2) indicates a specimen used for RCTS tests with a duration of confinement time of 60 minutes after completion of RCTS tests of MSW3ONS1

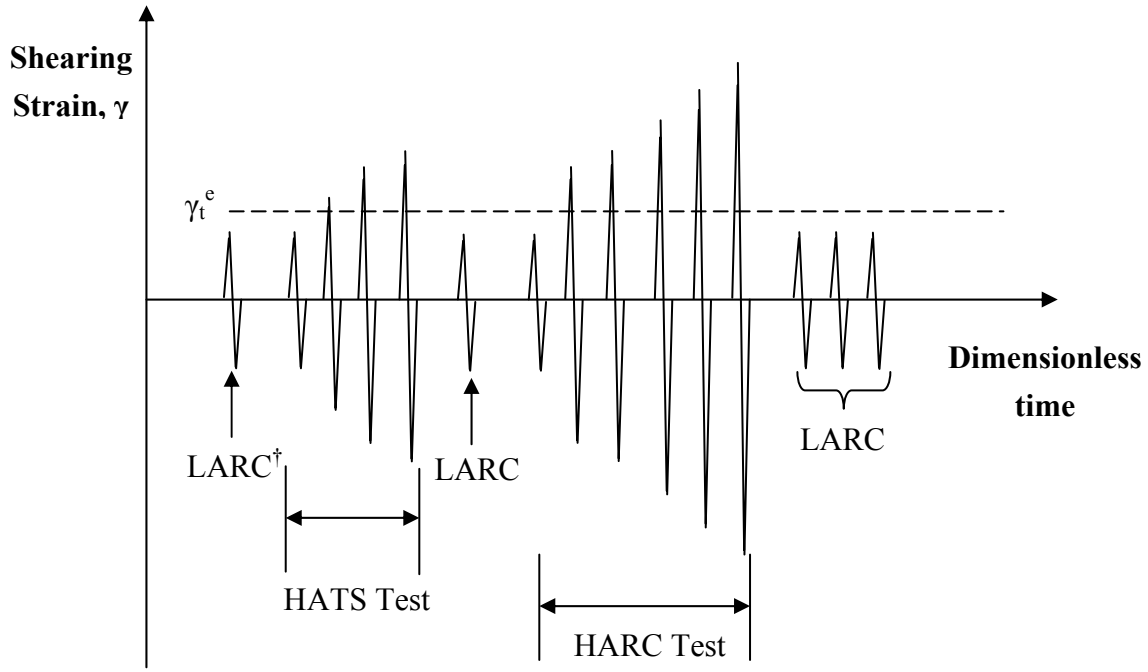

Notes: γ_t^e is an elastic threshold strain.

LARC is a resonant column test at low-amplitude strain.

LARC† is a resonant column test at low-amplitude strain after one day confinement prior to HATS test.

HARC is a resonant column test at high-amplitude strain.

HATS is a torsional shear test at high-amplitude strain.

Figure 10.1 An Example Set of High-Amplitude RCTS Tests Procedure at One Confining Pressure in the RCTS Device

HATS tests. After the HATS tests, each specimen was confined at the same confining pressure for an additional twelve to 24-hours in an attempt to allow the specimen regain its original state in terms of G_{max} and D_{min}.

HARC tests were performed after the specimens had regained their original states that were checked by LARC tests in terms of G_{max} and D_{min}. At the completion of the HARC tests, in the same manner, LARC tests were also performed immediately to

evaluate any changes. As with HATS tests, the specimens required a resting period of either a half day to a full day to regain their original state before advancing to the next pressure level.

Once the LARC, HATS, and HARC tests are completed at a given confining pressure, then RCTS tests continue to advance to next confining pressure, as shown in Figure 10.2.

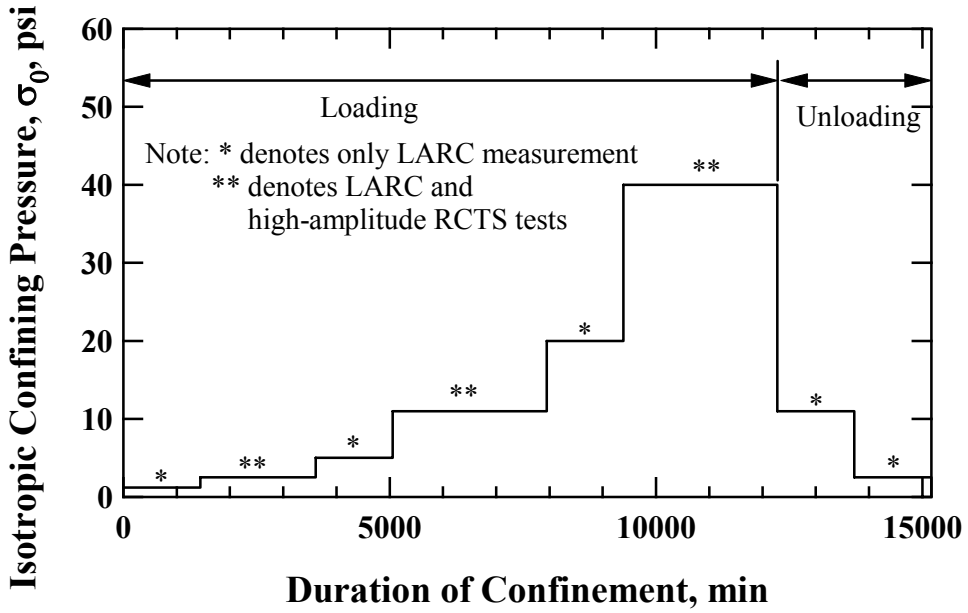

Figure 10.2 Typical Variation in Isotropic Confining Pressure with Duration of Confinement

It should be noted that the RCTS device was employed to investigate the test and material parameters with small-diameter specimens in the nonlinear strain ranges. These test parameters include: (1) shearing strain amplitude, (2) total isotropic confining pressure, (3) overconsolidation ratio, (4) number of loading cycles, and (5) excitation frequency. Material parameters investigated with the RCTS device are: (1) waste composition (only for 100% soil-size MSW material), (2) water content, (3) total unit

weight, and (4) particle size.

10.2.2 Testing with the LSRC Device

High-amplitude RC tests were performed with large-diameter specimens at their natural conditions. These tests were performed at multiple confining pressures and the confining pressure levels are given in Table 10.2.

Table 10.2 Isotropic Confining Pressures Used in High-Amplitude RC Tests for Large-Diameter 100 %, 76 %, and 62 % Soil-Sizes Old MSW Specimens in the LSRC Device

Specimen ID	Isotropic Confining Pressure
	High-Amplitude RC Tests, psi (kPa)
MSW1ONL3◊	2.5, 11, 40, 11*, 2.5* (17, 76, 276, 76, 17)
MSW2ONL2⌂	2.5, 11, 40, 11*, 2.5* (17, 76, 276, 76, 17)
MSW3ONL4□	2.5, 11, 40, 11*, 2.5* (17, 76, 276, 76, 17)
MSW4ONL1Δ	2.5, 11, 40, 11*, 2.5* (17, 76, 276, 76, 17)
MSW5ONL4	2.5, 11 (17, 76)
MSW6ONL4	2.5, 11, 40, 11*, 2.5* (17, 76, 276, 76, 17)
MSW7ONL2	11 (76)
MSW8ONL4	2.5, 11, 40 (17, 76, 276)
MSW9ONL3	2.5, 11, 40, 11*, 2.5* (17, 76, 276, 76, 17)

Notes: * denotes unloading stage.

Δ1 denotes specimen reconstituted with material passed the 3/8-in. (9.5-mm) sieve.

⌂2 denotes specimen reconstituted with material passed the ¾-in. (19.1-mm) sieve.

◊3 denotes specimen reconstituted with paper, soft plastic, and wood.

□4 denotes specimen reconstituted with paper, soft plastic, wood, and gravel in the specimen ID.

Unlike the RCTS device, no high-amplitude torsional shear tests are available in the LSRC device. Thus, HARC tests are performed subsequently after the LARC tests. An example set of LSRC tests at one confining pressure is shown in Figure 10.3. Similar to the RCTS tests, LARC tests are performed to establish the baseline measurements of G_{max} and D_{min} for the comparison of those values after the HARC tests have been conducted.

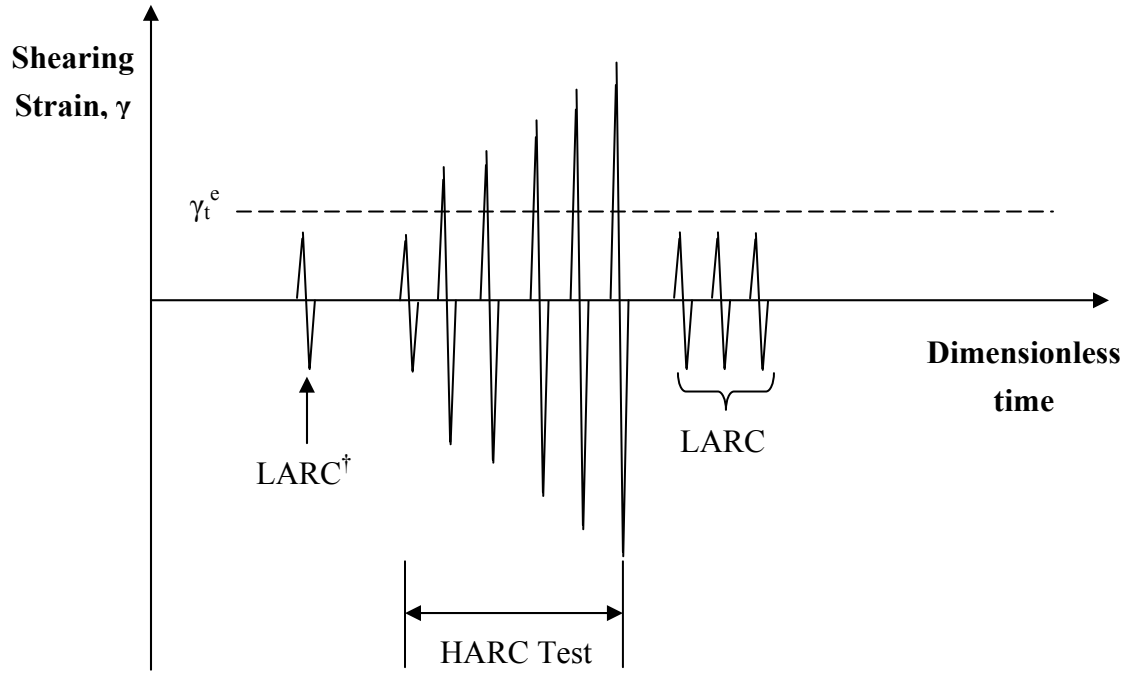

Notes: γ_t^e is an elastic threshold strain.

LARC is a resonant column test at low-amplitude strain.

LARC† is a resonant column test at low-amplitude strain after one day confinement prior to HARC test.

HARC is a resonant column test at high-amplitude strain.

Figure 10.3 An Example Set of High-Amplitude RC Tests Procedure at One Confining Pressure in the LSRC Device

HARC tests are conducted with increasing shearing strains and LARC tests are also performed immediately to check how much change in the MSW skeleton was induced due to the HARC tests. After the HARC tests, each specimen was confined at the same confining pressure for an additional twelve to 24-hours in an attempt to allow the specimen regain its original state in terms of G_{max} and D_{min}. Once the LARC and HARC tests are completed at a given confining pressure, then RC tests continue to go to next confining pressure, as shown in Figure 10.2.

It should be noted that hydration process was not available in the LSRC device because the specimen and drive plate was hung by four soft springs. It was difficult to assemble 6.0-in. (152.4-mm) split mold around the specimen. Another thing is that the effects of number of loading cycles and excitation frequency were not evaluated for the specimens with larger particles in the LSRC device since the LSRC device could not perform the TS tests.

The LSRC device was employed to investigate the test and material parameters with large-diameter specimens in the nonlinear strain ranges. These test parameters include: (1) shearing strain amplitude, (2) total isotropic confining pressure, and (3) overconsolidation ratio. Material parameters investigated with the LSRC device are: (1) waste composition (all groups of MSW material) and (2) particle size.

10.3 TEST PARAMETERS AFFECTING G AND D

10.3.1 Test Parameters Investigated

To investigate the effect of test parameters affecting G and D of MSW specimens in the nonlinear strains, both the RCTS and LSRC devices were employed. Test parameters investigated in the RCTS device include: (1) shearing strain amplitude, (2) total isotropic confining pressure, (3) overconsolidation ratio, (4) number of loading

cycles, and (5) excitation frequency. However, in the LSRC device, test parameters investigated were: (1) shearing strain amplitude, (2) total isotropic confining pressure, and (3) overconsolidation ratio.

10.3.2 Shearing Strain Amplitude

As previously discussed, after the strain amplitude exceeds γ_t^e, the value of G begins to decrease and the value of D begins to increase, as shearing strain amplitude increases. This nonlinear behavior of MSW has a significant impact on site response analyses of soil deposits. Thus, shearing strain amplitude is a key parameter in the investigation of the nonlinear behavior of MSW.

The variation in G with shearing strain upon small- and large-diameter specimens for old MSW measured in the RCTS and LSRC devices is plotted in Figure 10.4. This figure shows a typical variation in G with shearing strain for 100 % soil-size specimens that were reconstituted with material passed the 3/8-in. (9.5-mm) sieve measured in the RCTS and LSRC devices. Small-diameter specimens are represented by open symbols, whereas large-diameter specimen is represented by open symbol with an "x" in the symbol. The measurements were performed at a confining pressure of 11 psi (76 kPa).

As discussed in Section 10.3.3, the amplitude of γ_t^e for G is defined as a shearing strain corresponding to G/G_{max} equal to 0.98 in this study. It is assumed to be linear variation in G between data points around the G/G_{max} equal to 0.98. As a result, the values of γ_t^e for Specimens 2ONS1, 3ONS1, and 4ONL1 are 0.002 %, 0.0026 %, and 0.0032 %, respectively.

As seen in Figure 10.4, for all specimens, shearing strain less than about 0.002 %, G is constant and equal to G_{max},; G is independent of strain amplitude, implying that MSW exhibits linear behavior within these ranges, whereas after the shearing strain

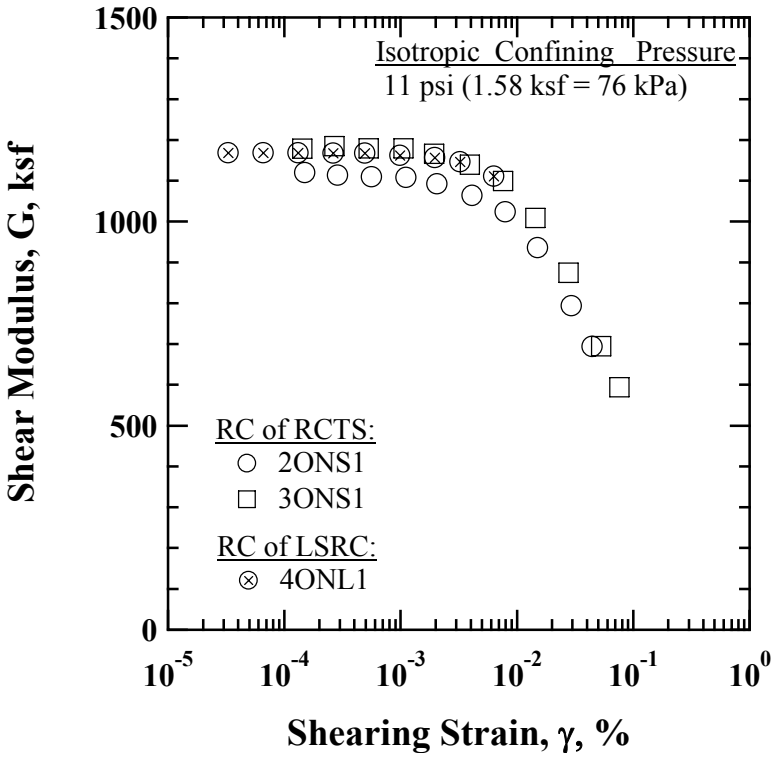

Figure 10.4 Comparison of the Variation in Shear Modulus with Shearing Strain for 100 % Soil-Size Old MSW Specimens Reconstituted with Material Passed the 3/8-in. (9.5-mm) Sieve in the RCTS and LSRC devices

reaches 0.002 %, G begin to decreases with an increase in shearing strain.

The variation in G with shearing strain for Specimen 5ONS1 obtained from RC and TS tests in the RCTS device is shown in Figure 10.5. RC data are represented by open symbol and TS data are represented by solid triangular symbols. The measurements were performed at a confining pressure of 11 psi (76 kPa).

The values of γ_t^e for Specimen MSW5ONS1 of RC and TS tests are 0.002 % and 0.003 %, respectively. As can be seen, G is constant less than about 0.002 % for RC test and is constant less than about 0.003 % for TS test. However, once shearing strain exceeds 0.002 % and 0.003 %, G begins to decrease with increasing shearing strain.

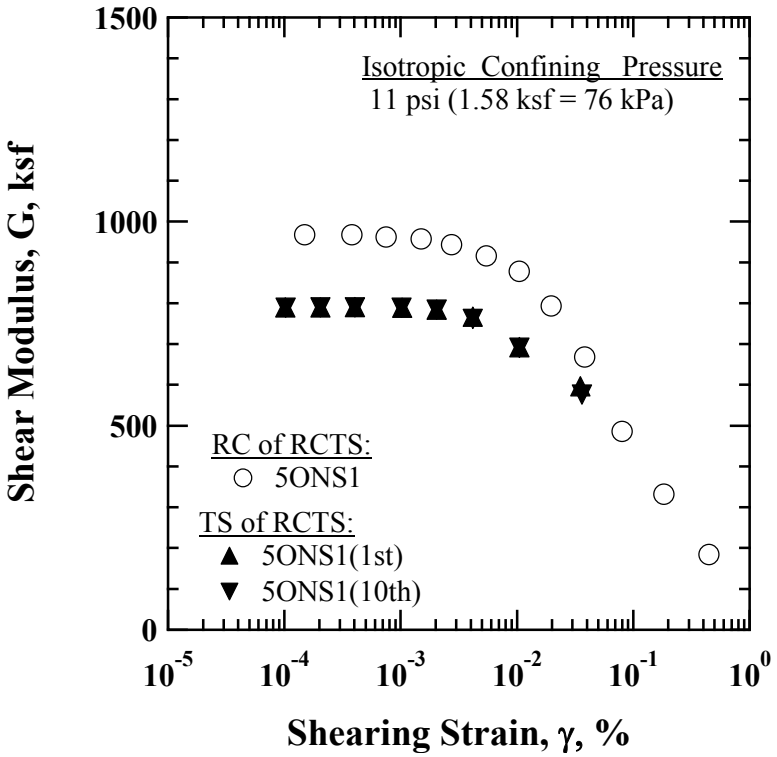

Figure 10.5 Comparison of the Variation in Shear Modulus with Shearing Strain for 100 % Soil-Size Specimen MSW5ONS1 Obtained from RC and TS Tests in the RCTS Device

There is a difference between the absolute values of G_{max} in the small-strain range obtained from RC and TS tests. This is mainly due to excitation frequency. In other word, the excitation frequency for RC test is relatively high, varying from 32.2 Hz to 73.9 Hz, whereas the excitation frequency for TS test is typically 0.5 Hz. It is interesting to see that the difference between RC and TS tests decreases with increasing shearing strain, implying that this frequency effect becomes smaller with increasing shearing strain; mainly effect of number of cycles.

The variation in G with shearing strain upon small- and large-diameter specimens for old MSW measured in the RCTS and LSRC devices is presented in Figure 10.6.

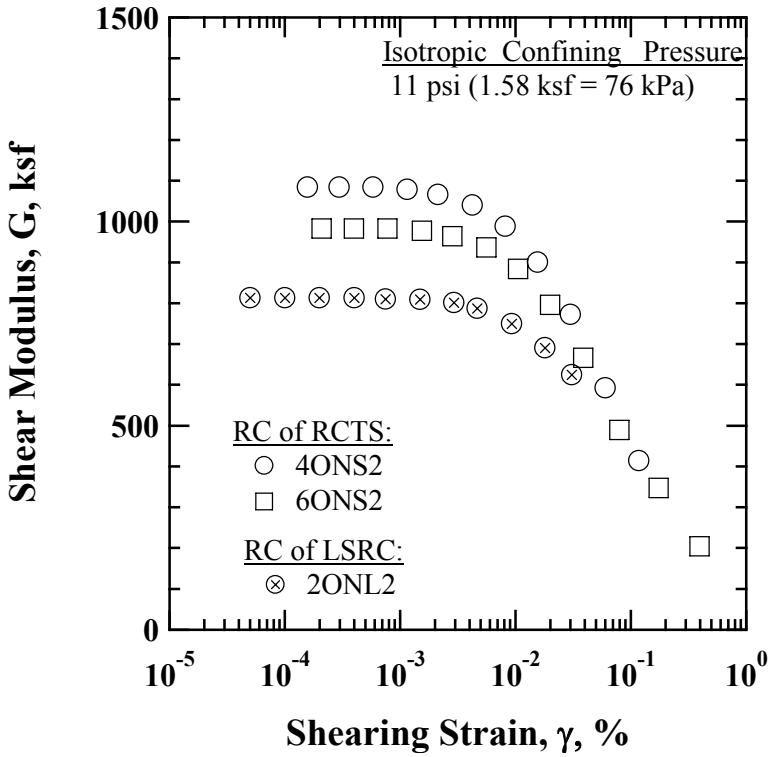

Figure 10.6 Comparison of the Variation in Shear Modulus with Shearing Strain for 100 % Soil-Size Old MSW Specimens Reconstituted with Material Passed the ¾-in. (19.1-mm) Sieve in the RCTS and LSRC devices

This figure shows a typical variation in G with shearing strain for 100 % soil-size specimens that were reconstituted with material passed the ¾-in. (19.1-mm) sieve measured in the RCTS and LSRC devices. The measurements were performed at a confining pressure of 11 psi (76 kPa).

The values of γ_t^e for Specimens MSW4ONS2, MSW6ONS2, and MSW2ONL2 are 0.003 %, 0.003 %, and 0.004 %, respectively. As seen in the figure, G is constant in the shearing strains less than about 0.003 % and 0.004 % and equal to G_{max}. Beyond the shearing strains of 0.003 % and 0.004 %, G begins to decrease with increasing shearing strain.

A typical variation in D with shearing strain upon small- and large-diameter specimens for 100 % soil-size old MSW measured in the RCTS and LSRC devices is shown in Figure 10.7. Small- and large-diameter specimens were reconstituted with material passed the 3/8-in. (9.5-mm) sieve. Small-diameter specimens are represented by open symbols, whereas large-diameter specimen is represented by open symbol with an "x" in the symbol. The measurements were performed at a confining pressure of 11 psi (76 kPa).

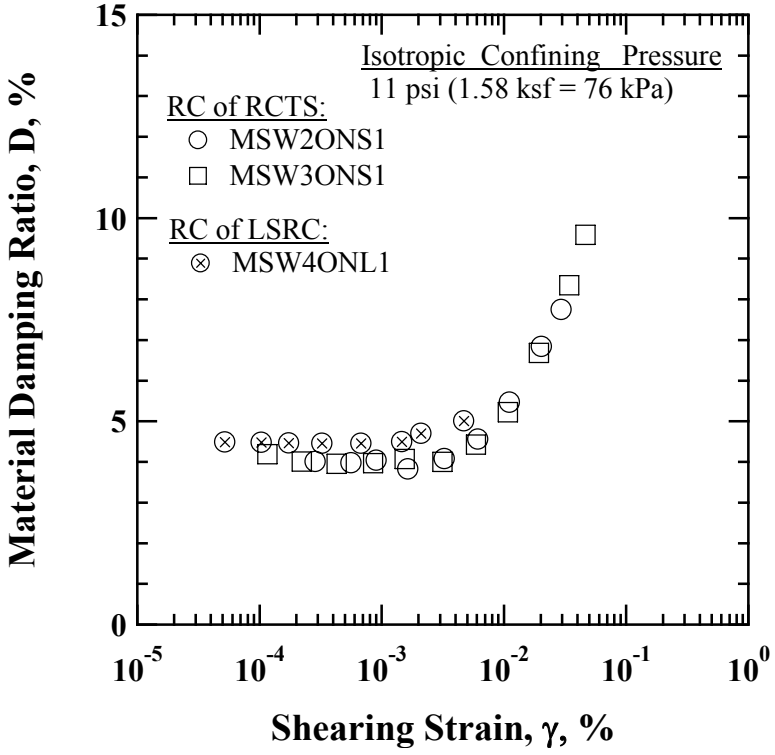

Figure 10.7 Comparison of the Variation in Material Damping Ratio with Shearing Strain for 100 % Soil-Size Old MSW Specimens Reconstituted with Material Passed the 3/8-in. (9.5-mm) Sieve in the RCTS and LSRC devices

As discussed in Section 10.3.3, the amplitude of γ_t^e for D is defined as a shearing strain corresponding to D/D_{min} equal to 1.05 in this study. It is assumed to be linear

variation in D between data points around the D/D_{min} equal to 1.05. As a result, the values of γ_t^e for Specimens MSW2ONS1, MSW3ONS1, and MSW4ONL1 are 0.004 %, 0.004 %, and 0.002 %, respectively.

Similar to the variation of G, D is constant and equal to D_{min} in the shearing strains less than about 0.002 % and 0.004 %; D exhibits a strain-independent behavior. However, beyond the shearing strains of 0.002 % and 0.004 %, D starts to increase with an increase in shearing strain. As can be seen, there is a difference in D of small- and large-diameter specimens in the small-strain ranges due to excitation frequency. As discussed in Section 6.3.4, after removing this excitation frequency effect, the values of D are essentially the same.

The variation in D with shearing strain for 100 % soil-size old MSW Specimen MSW5ONS1 obtained from RC and TS tests in the RCTS device is shown in Figure 10.8. The data from RC test are represented by open symbol, whereas the data from TS test are represented by solid triangular symbols. The measurements were performed at a confining pressure of 11 psi (76 kPa).

The values of γ_t^e for Specimen MSW5ONS1 of RC and TS tests are 0.003 % and 0.002 %, respectively. D is constant less than shearing strains of 0.002 % and 0.003 % and equal to D_{min}. Once the shearing strain exceeds these values, D starts to increase with increasing shearing strain. As shown in the figure, like G, there is a difference in the values of D in the small-strain ranges because of the aforementioned frequency effect. In addition, the difference in the values of D between RC and TS tests created by frequency effect becomes smaller as shearing strain increases; mainly effect of number of cycles.

The variation in D with shearing strain for Specimens MSW4ONS2, MSW6ONS2, and MSW2ONL2 measured in the RCTS and LSRC devices is shown in

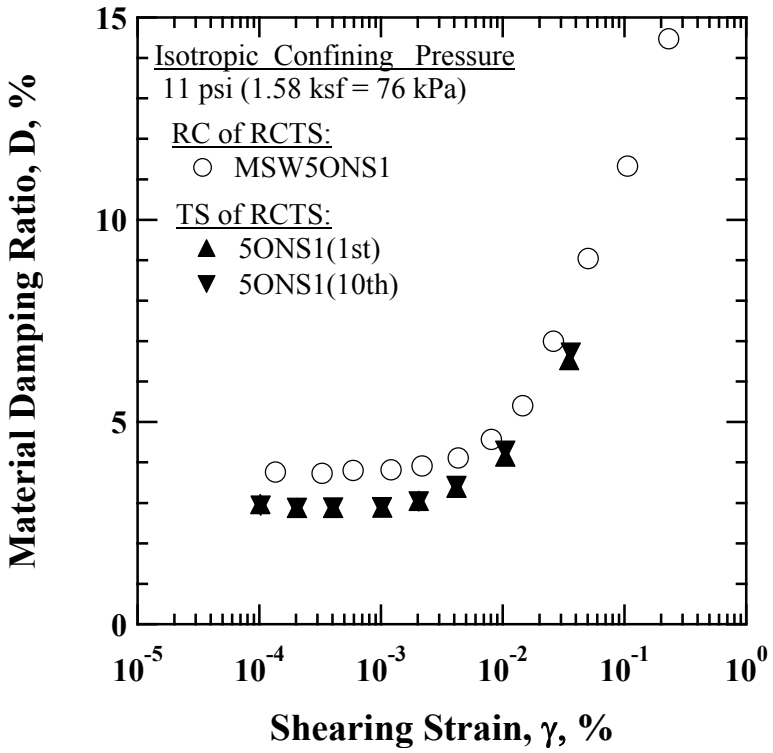

Figure 10.8 Comparison of the Variation in Material Damping Ratio with Shearing Strain for 100 % Soil-Size Specimen MSW5ONS1 Obtained from RC and TS Tests in the RCTS Device

Figure 10.9. These specimens were constructed with 100 % soil-size material passed the ¾-in. (19.1-mm) sieve. Small-diameter specimens are represented by open symbols, whereas large-diameter specimen is represented by open symbol with an "x" in the symbol. The measurements were performed at a confining pressure of 11 psi (76 kPa).

The values of γ_t^e for Specimens MSW4ONS2, MSW6ONS2, and MSW2ONL2 are 0.002 %, 0.005 %, 0.002 %, respectively. As seen in the figure, D is constant less than shearing strains of 0.002 % and 0.005 %. However, beyond these values, D begins to increases with increasing shearing strain. Small-diameter specimens exhibit a very similar behavior, whereas large-diameter specimen has higher material damping ratio in

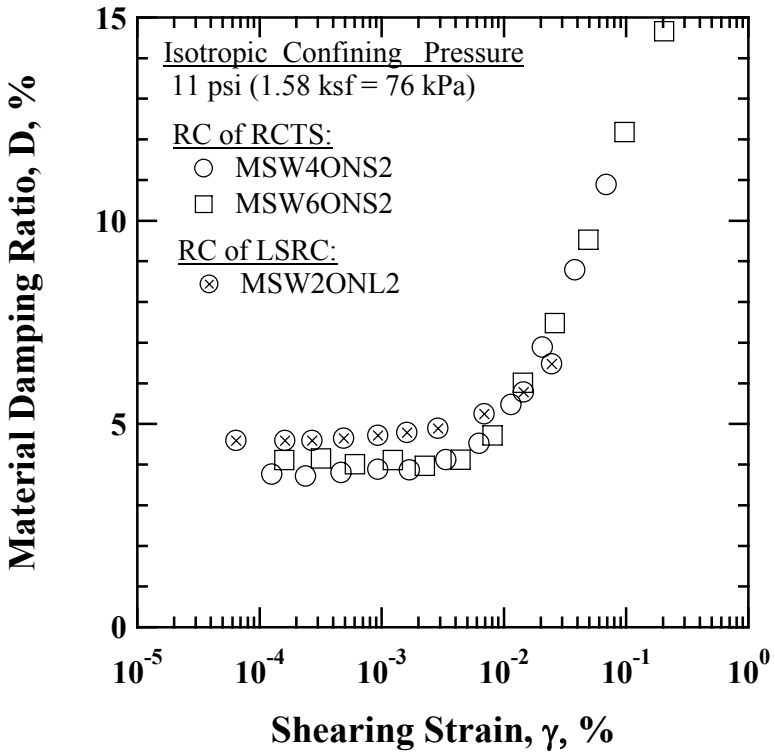

Figure 10.9 Comparison of the Variation in Material Damping Ratio with Shearing Strain for 100 % Soil-Size Old MSW Specimens Reconstituted with Material Passed the ¾-in. (19.1-mm) Sieve in the RCTS and LSRC devices

the small-strain ranges due to excitation frequency. As discussed in Section 6.3.4, although removing the effect of excitation frequency, the values of D for large-diameter specimen are slightly higher. It is interesting to observe that the values of D for large-diameter specimen become smaller beyond the shearing strains 0.01 %.

10.3.3 Total Isotropic Confining Pressure

Along with shearing strain amplitude, confining pressure is another important parameter affecting shear modulus reduction and material damping curves in the nonlinear range. It is well-known that for soils, shear modulus reduction curves shift to higher strains and the material damping curves move downward as confining pressure

increases (Seed and Idriss, 1970, Hardin and Drnevich, 1974, Stokoe et al., 1994, Stokoe et al., 1999, etc). In addition to confining pressure, nonlinear shear modulus and material damping curves of soils are affected by other fundamental soil parameters such as plastic index (PI), void ratio (e), etc.

A typical variation in G obtained from RCTS tests with shearing strain at given confining pressures (e.g., 2.5 psi (7 kPa), 11 psi (76 kPa), and 40 psi (276 kPa)) for 100 % soil-size Specimen MSW3ONS1 is shown in Figure 10.10. At each confining pressure, the data obtained from the RC tests are represented by open symbols, whereas the data obtained from the TS tests are represented by solid symbols. The TS data consist of pair of values at each strain amplitude that were measured at the first and tenth cycles.

As can be seen in Figure 10.10, the nonlinear values of G measured in the RCTS tests increase considerably as confining pressure increases. There are once again differences in absolute values between RC and TS tests because of the excitation frequency and number of loading cycles, as mentioned earlier. The differences in G between RC and TS tests are nearly the same regardless of confining pressure and are on the order of approximately 27 %. It should be noted that the difference between RC and TS measurements produced by the effects of excitation frequency and number of loading cycles tend to disappear with increasing shearing strain.

The values of γ_t^e, when nonlinear behavior begins to occur, increase with increasing confining pressure. In this study, the amplitude of γ_t^e is defined as a shearing strain, γ, corresponding to G/G_{max} equal to 0.98. The value of 0.98 was used to take the fluctuation of the measurements of shear modulus in small-strain ranges into consideration. It should be noted that the values of γ_t^e for G corresponding to each confining pressure were interpolated with an assumption that the variation between data

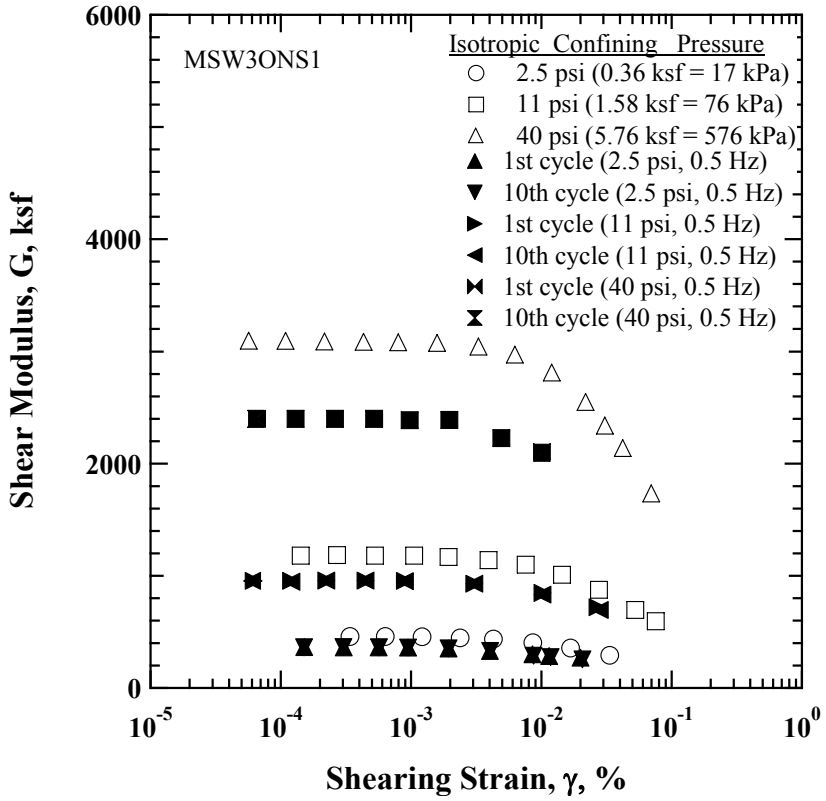

Figure 10.10 Comparison of the Variation in Shear Modulus with Shearing Strain and Isotropic Confining Pressures from RC and TS Tests for MSW3ONS1 (100% Soil-Size Material)

points around the G/G_{max} equal to 0.98 is linear. For reference, the value of 0.99 was used by Vucetic (1994), whereas Ni (1987) and Kim (1991) used the value of 0.98 for the amplitude of γ_t^e. As will be seen, this can be identified more clearly in the plot of normalized shear modulus with shearing strain, as discussed below. .

Another way to examine the effect of confining pressure is a plot of the variation of G in terms of normalized shear modulus, G/G_{max}. The variation in G/G_{max} with confining pressures is presented in Figure 10.11. The G/G_{max} – log γ curves shift slightly to higher strains with increasing shearing strain, indicating that nonlinear

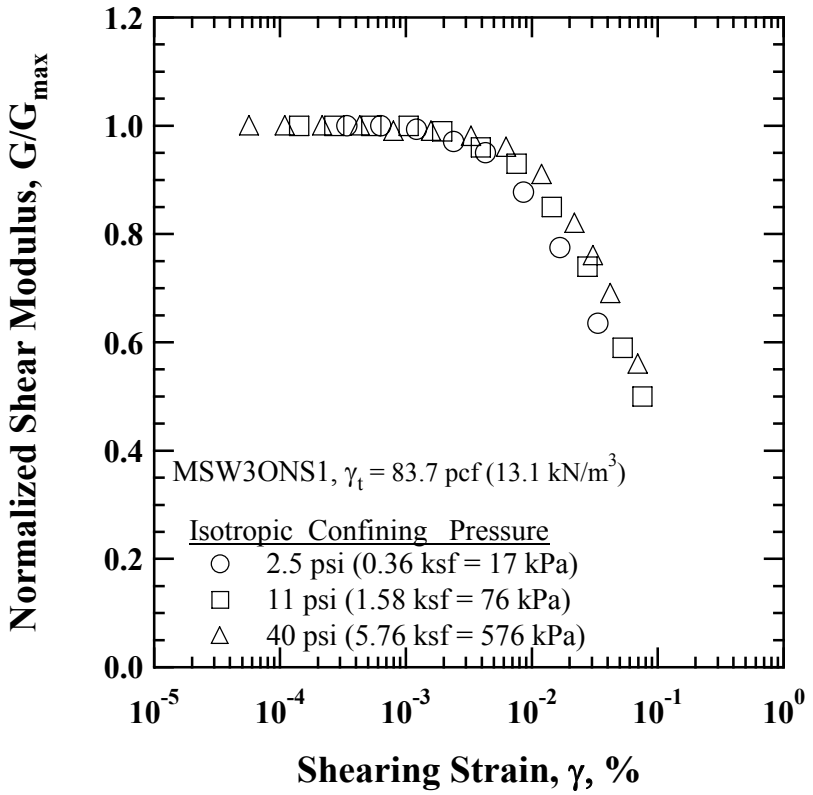

Figure 10.11 Comparison of the Variation in Normalized Shear Modulus with Shearing Strain and Isotropic Confining Pressures from RC tests for MSW3ONS1 (100% Soil-Size Material)

behavior of old MSW becomes slightly more linear with an increase in confining pressure. In other words, shear modulus reduction at a given shearing strain diminishes slightly with increasing confining pressure. The reason for this transition from nonlinear to linear may be attributed to the fact that as confining pressure increases; the movements between particles are constrained increasingly, resulting in a less energy dissipation within MSW. As shown in Figure 10.11, the values of γ_t^e continue to increase with increasing confining pressure and these values are given in Table 10.3.

Table 10.3 Values of Elastic Threshold Shearing Strain (γ_t^e) for G with Confining Pressures for Specimen MSW3ONS1 (100 % Soil-Size Material)

Confining Pressure, psi (kPa)	γ_t^e (%)
2.5 (17)	0.0019
11 (76)	0.0026
40 (276)	0.0038

To investigate the effect of total isotropic confining pressure of other old MSW Groups (e.g., 100 %, 76 %, 62 %, and 14 % Groups), the values of elastic threshold shearing strain were calculated in terms of the normalized shear modulus at which the HARC tests were performed. The variation in elastic threshold shearing strain with confining pressure of each group is shown in Figure 10.12. As can be seen, the amplitude elastic threshold shearing strain increases with increasing confining pressure as well as decreasing the weight percentage of soil-size material. This means that normalized shear modulus exhibits more elastic behavior as confining pressure increases and weight percentage of soil-size material decreases.

The variation in D obtained from RCTS tests with shearing strain at given confining pressures is compared in Figure 10.13. The data obtained from the RC tests are represented by open symbols and those obtained from the TS tests are indicated by solid symbols. The TS data consist of pairs of values at each strain amplitude that were measured at the first and tenth cycles. The values of D_{min} vary only slightly with the variation of confining pressure. After the shearing strain larger than 0.005 %, D values are influenced slightly by confining pressures, moving downward as confining pressure increases. Likewise, same mechanism for decrease in D with confining pressure can be

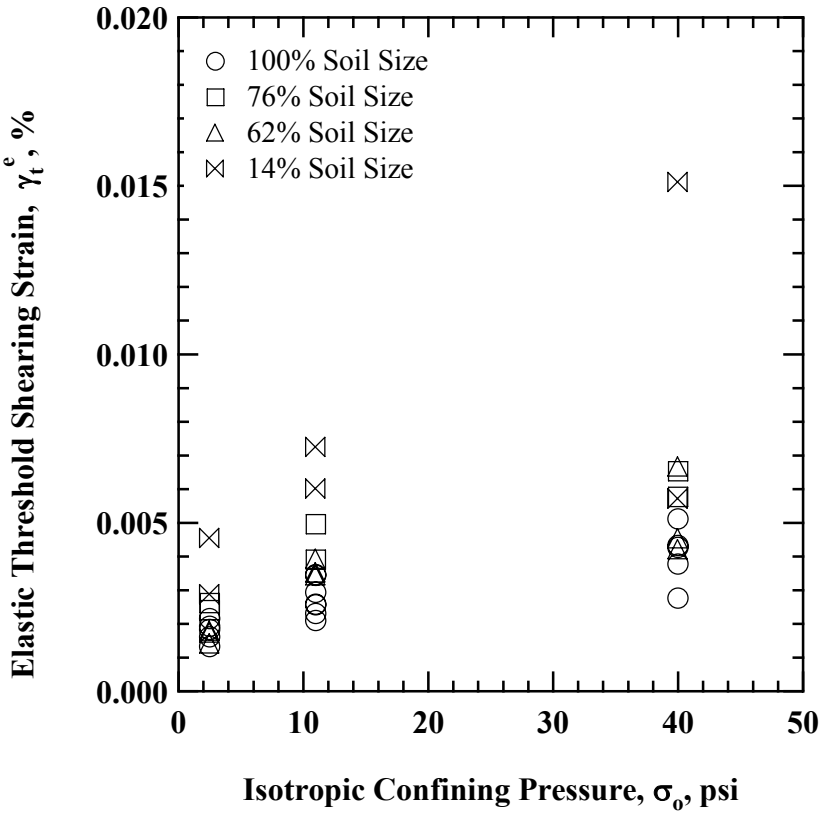

Figure 10.12 Comparison of the Variation in Elastic Threshold Shearing Strain with Isotropic Confining Pressures from RC tests for 100 %, 76 %, 62 %, and 14 % Soil-Size Old and Mixed MSW Groups

applied.

It is interesting to note that there is a small shift in the values of D_{min} with confining pressure at small-strain ranges in the RC than TS measurements. Like G – log γ curves, the difference between RC and TS measurements produced by the frequency effect and number of loading cycles tends to be smaller as shearing strain increases. In the TS tests at confining pressures of 2.5 psi (17 kPa) and 11 psi (76 kPa), it is obvious that the values of D obtained from the first and tenth cycles are different due to the number of loading cycles, at which the shearing strains exceed the cyclic threshold

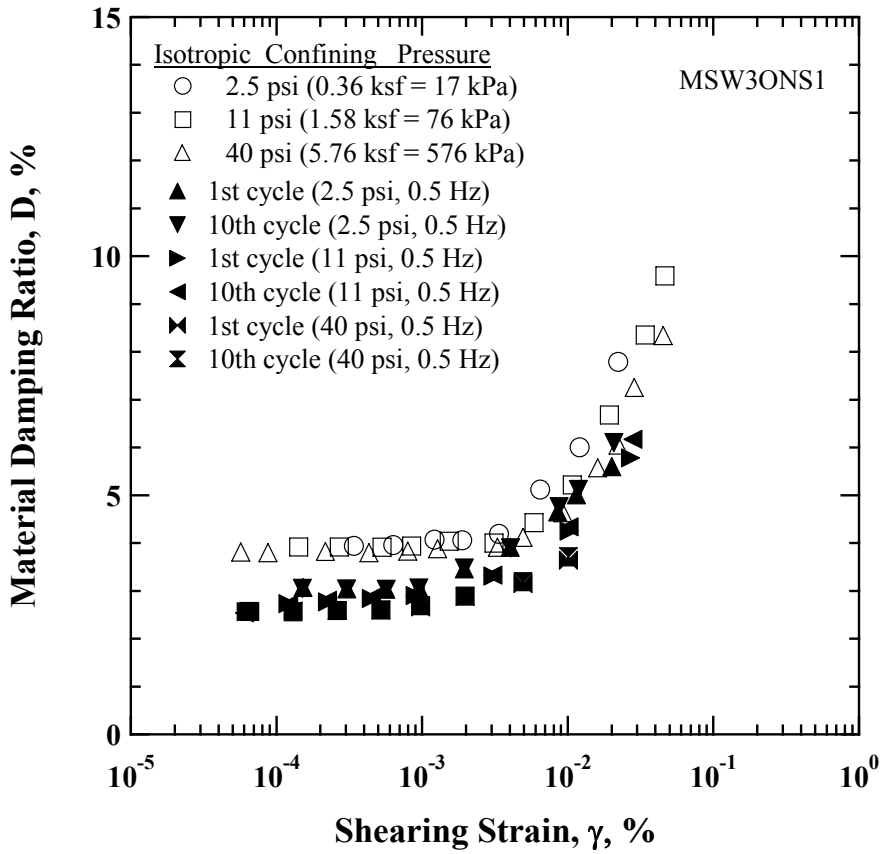

Figure 10.13 Comparison of the Variation in Material Damping Ratio with Shearing Strain and Isotropic Confining Pressures from RCTS tests for MSW3ONS1 (100% Soil-Size Material)

shearing strain, γ_t^c, as discussed in Section 10.3.5.

Not much attention has been paid to the definition of the amplitude of γ_t^e for material damping during last decades. One of the available sources is that Laird (1994) used two methods to define the γ_t^e; percentage change from its D_{min} and increase of D from D_{min}. In this study, the first method was adopted and γ_t^e was defined as the strain amplitude at which D is 5 % greater than D_{min}, i.e., D/D_{min} is equal to 1.05. It should be noted that the values of γ_t^e for D corresponding to each confining pressure were interpolated with an assumption that the variation between data points around the D/D_{min}

equal to 1.05 is a linear. The values of γ_t^e for D at each confining pressure were computed based on this definition and these values are tabulated in Table 10.4. As shown in Table 10.4, the values of γ_t^e continue to increase with increasing confining pressure. Compared with the values for G, these values are slightly larger.

Table 10.4 Values of Elastic Threshold Shearing Strain (γ_t^e) for D with Confining Pressures for MSW3ONS1 (100% Soil-Size Material)

Confining Pressure, psi (kPa)	γ_t^e (%)
2.5 (17)	0.0029
11 (76)	0.0039
40 (276)	0.0041

10.3.4 Overconsolidation Ratio

To evaluate the effect of overconsolidation ratio (OCR) on the dynamic properties of MSW, a series of RC tests were accomplished with a repetition of loading, unloading, and reloading sequences for a given specimen to attain different magnitudes of OCR, varying from 1 to about 7.

A typical variation in G with shearing strain upon the loading, unloading, and reloading sequences at a confining pressure of 11 psi (76 kPa) for 100 % soil-size material Specimen MSW3ONS1 is compared in Figure 10.14 (a). It is obvious from the figure that the shear modulus increases with increasing OCR. This trend is consistent with test results on clayey soils (Darendeli, 2001). The values of G obtained at small-strain ranges from the second unloading sequence increased significantly compared with those on the first reloading sequence. The difference in G at small strains is approximately a factor of two. It is noted that substantial decrease in voids spaces may contribute to the significant increase of shear modulus. The change in estimated total unit weight from

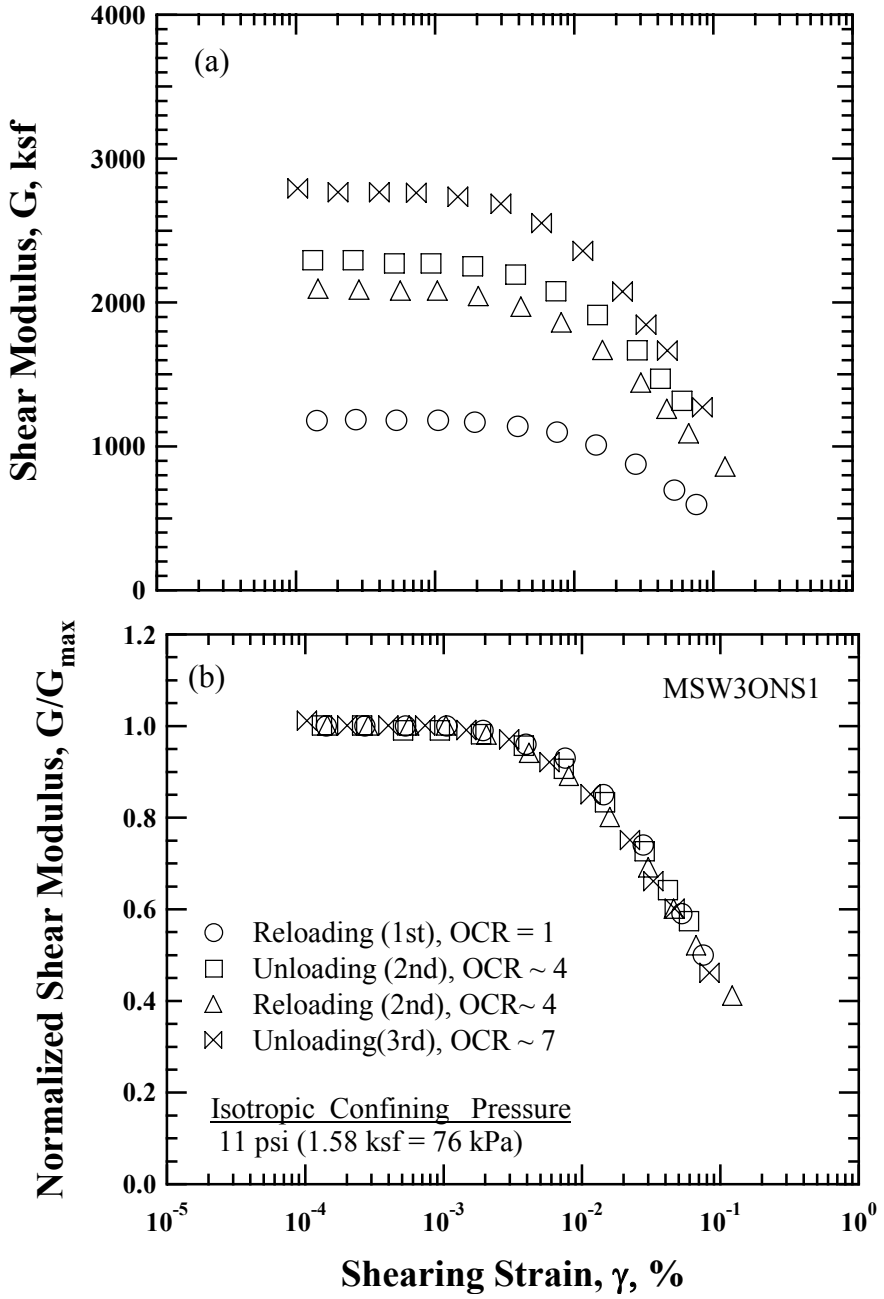

Figure 10.14 Comparison of the Variation in (a) Shear Modulus and (b) Normalized Shear Modulus with Shearing Strain upon Reloading and Unloading Sequences from RC tests for MSW3ONS1 (100% Soil-Size Material)

the first reloading sequence to second unloading sequence was from 88.3 pcf (13.9 kN/m^3) to94.2 pcf (14.8 kN/m^3), respectively. As a result, an increase in estimated total unit weight was equal to about 6.7 %.

Additionally, the effect of OCR on G was evaluated in terms of G/G_{max}. The variation of normalized shear modulus with shearing strain is shown in Figure 10.14 (b). Figure 10.14 (b) indicates that the effect of OCR has almost no impact on G/G_{max} regardless of the magnitudes of OCR for old MSW. The values of reference strain, γ_r, and curvature coefficient, a, are given in Table 10.5. These values of γ_r and a were patterned after Darendeli's modified hyperbolic model (2001). This modified hyperbolic model is discussed in Chapter 13. As shown in Table 10.5, the values of γ_r are approximately the same regardless of the magnitudes of OCR, whereas the values of a decrease with increasing OCR.

Table 10.5 Values of Reference Strain, γ_r, and Curvature Coefficient, a, with Different Values of OCR for MSW3ONS1 (100% Soil-Size Material)

Sequence (OCR)	Reference Strain, γ_r, %	Curvature Coefficient, a
Reloading (1st), OCR = 1	0.075	1.04
Unloading (2nd), OCR ~ 4	0.08	1.02
Reloading (2nd), OCR ~ 4	0.07	0.95
Unloading (3rd), OCR ~ 7	0.08	0.91

Kokusho et al. (1982) found the same trend of the effect of OCR on G/G_{max} from natural soft clays using a cyclic triaxial device that the G is not much affect by different consolidation histories, i.e., different magnitudes of OCR. They also made a comment that this tendency is very helpful to estimate the in-situ large strain shear modulus using

empirical correlations between laboratory and seismic in-situ measurements.

A typical variation in D with shearing strain upon the reloading and unloading sequences is presented in Figure 10.15. As seen in the figure, the material damping ratio curve moves slightly upward over the shearing strain ranges with increasing magnitude of OCR, indicating that OCR has a minor effect on D. The values of D obtained from the second unloading and reloading sequences are nearly the same. The effect of OCR is larger at small strains than larger strains.

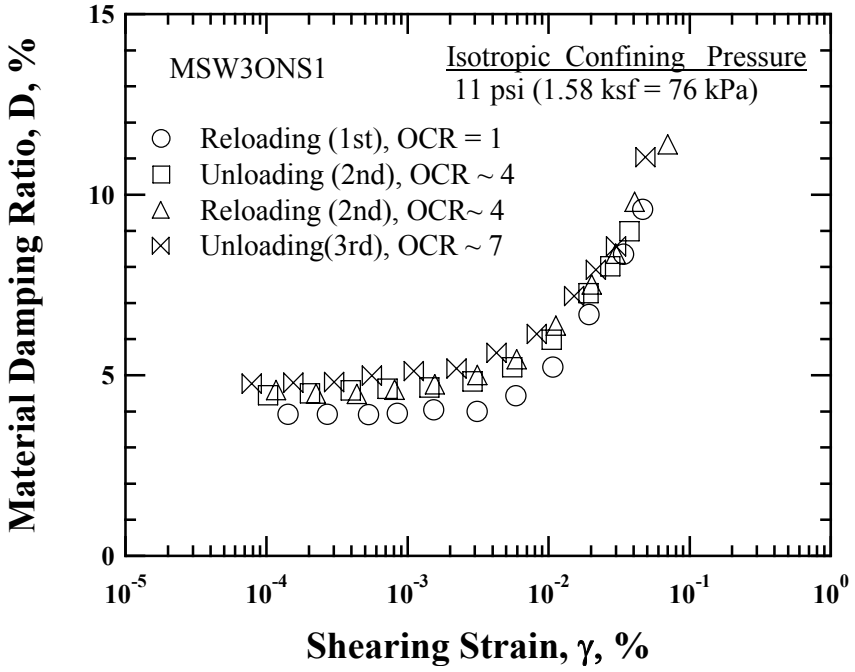

Figure 10.15 Comparison of the Variation in Material Damping Ratio with Shearing Strain upon Reloading and Unloading Sequences from RC tests for MSW3ONS1 (100% Soil-Size Material)

10.3.5 Number of Loading Cycles

Typical variations in G for 100 % soil-size material Specimen MSW3ONS1 with

shearing strain amplitude and number of loading cycles from RCTS tests are shown in Figure 10.16. The data measured in the RC test are represented by open circles and the data measured in the TS test are represented by open and solid triangles. It should be noted that the open triangle indicates G on 1st cycle and solid triangle shows G on 10th cycle. Figure 10.16 illustrates that in the shearing strain ranges less than 0.001 %, the values of G measured from RCTS tests are constant and those are not affected by the number of loading cycles. This supports a fact that the dynamic properties exhibit linear behavior in this small-strain range. The difference, as shown in Figure 10.16, between RC and TS tests is due to the frequency effect as discussed in Section 10.3.6.

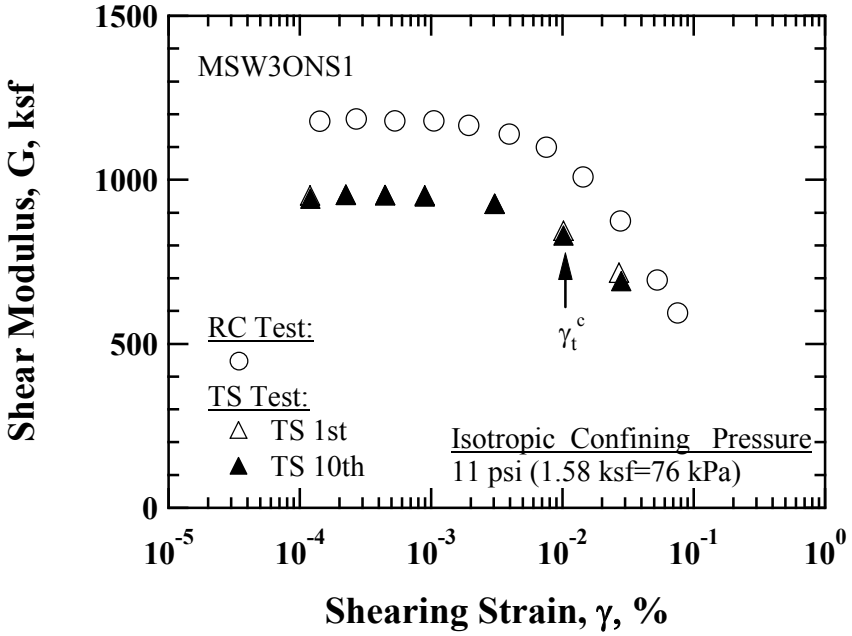

Figure 10.16 Comparison of the Variation in Shear Modulus with Shearing Strain from RCTS Tests for MSW3ONS1 (100% Soil-Size Material)

The variations in G/G_{max} for 100 % soil-size material Specimen MSW3ONS1 with shearing strain amplitude and number of loading cycles from RCTS tests are shown

in Figure 10.17. As can be seen, normalized shear modulus from the RC and TS tests with shearing strain is almost identical.

From the TS test result shown in Figure 10.16, the effect of the number of loading cycles appears to begin at strain is about on the order of 0.01 %. That is, after this amplitude of shearing strain, the values of G from the tenth cycle in TS test are at least 2 % less than those from the first cycle; cyclic degradation occurred in shear modulus. The amount of degradation caused by the number of loading cycles increase as shearing strain increases beyond shearing strain of 0.01 %. This amplitude of shearing strain is defined as the cyclic threshold shearing strain, γ_t^c, in which shear modulus from the tenth cycle equals to 98 % of shear modulus from the first cycle (Kim, 1991, Laird, 1994). γ_t^c for MSW3ONS1 is also indicated in Figure 10.16.

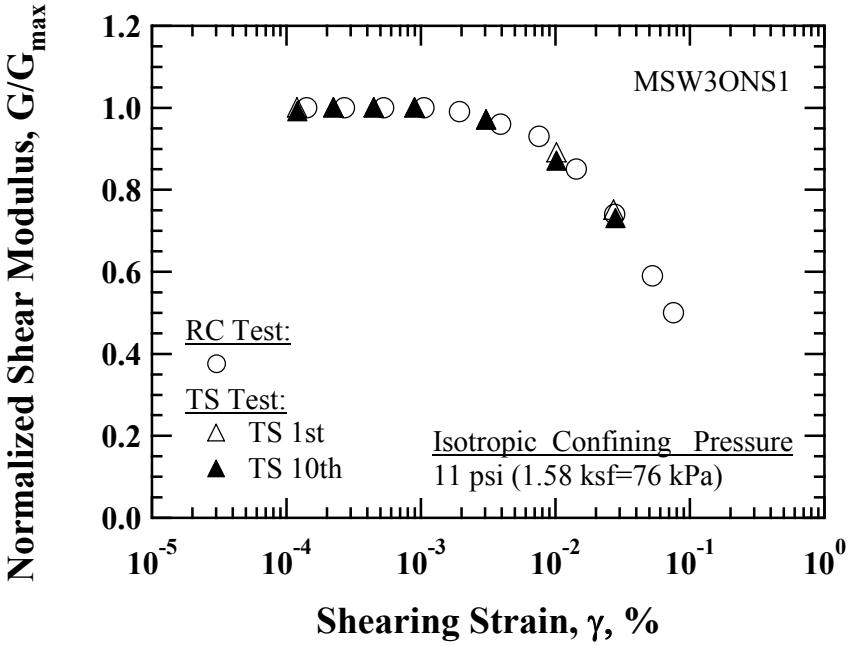

Figure 10.17 Comparison of the Variation in Normalized Shear Modulus with Shearing Strain from RCTS Tests for MSW3ONS1 (100% Soil-Size Material)

To quantify the effect of the number of loading cycles on G, the values of G at given loading cycles were normalized with that from the first cycle. The variation in normalized shear modulus, G/G_{1st}, with the number of loading cycles at different magnitudes of shearing strain from TS tests is shown in Figure 10.18. The measurement was made at a confining pressure of 11 psi (76 kPa).

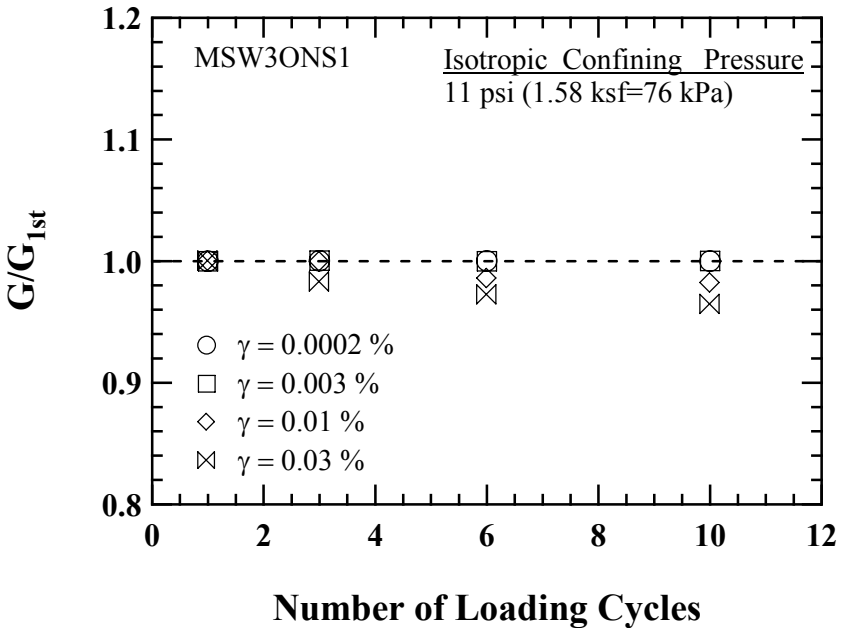

Figure 10.18 Variation in Normalized Shear Modulus, G/G_{1st}, with the Number of Loading Cycles from TS Tests for MSW3ONS1 (100% Soil-Size Material)

As indicated, G/G_{1st} remains constant until shearing strain amplitude reaches 0.003 %, however, after shearing strain of 0.01 %, G/G_{1st} decreases as the number of loading cycles increases. Furthermore, the amount of the decrease is dependent on strain amplitude, resulting in a decrease in G/G_{1st} as strain amplitude increases. The effect of the number of loading cycles begins to mobilize at a small number of cycles as shearing strain amplitude increases and it is negligible in the small-strain ranges less than

0.003 %, as expected (Lee et al., 2004).

A typical variation in D for 100 % soil-size material Specimen MSW3ONS1 with shearing strain and number of loading cycles from RCTS is presented in Figure 10.19. Open circles represent RC measurements and open and solid triangles represent TS measurements. Likewise, the open triangle indicates G on 1st cycle and solid triangle shows G on 10th cycle. In shearing strain ranges less than 0.003 %, the values of D from RC test are constant. Additionally, the values of D from TS test, less than about 0.001 %, are also constant and those are independent of number of loading cycles. Frequency effect results in a difference in small-strain material damping ratio in strain ranges less than 0.001 %.

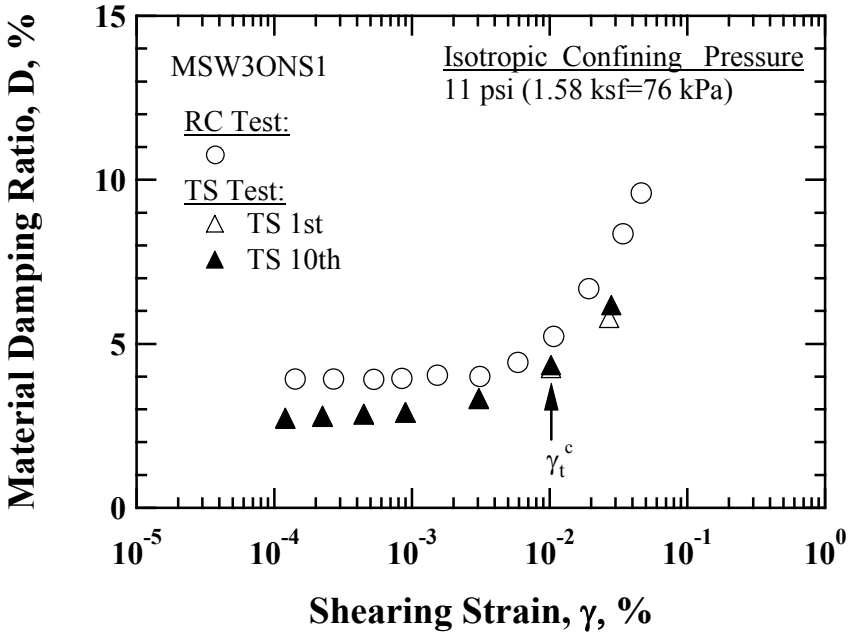

Figure 10.19 Comparison of the Variation in Material Damping Ratio with Shearing Strain from RCTS Tests for MSW3ONS1 (100 % Soil-Size Material)

The amplitude of γ_t^c was, herein, defined as a shearing strain in which the material damping ratio from the first cycle equals to 98 % of material damping ratio from the tenth

cycle (Kim, 1991, Laird, 1994) and it is denoted in Figure 10.19. As shown in Figure 10.19, an increase in D from TS test produced by the number of loading cycles is observed beyond the strain amplitude of 0.01 %. This increment increases as shearing strain increases, as shown in Figure 10.19.

The value of D at given loading cycles was normalized with one from the first cycle to determine the effect of number of loading cycles on D. The variation in normalized material damping ratio, D/D_{1st}, with number of loading cycles at different magnitudes of shearing strain from TS tests is shown in Figure 10.20. D/D_{1st} increases as the number of loading cycles increase. In addition, D/D_{1st} increases with an increase in the amplitudes of shearing strain. As shown in Figure 10.20, the effect of number of loading cycles is negligible in the strain ranges less than 0.003 % and it begins to mobilize at a small number of cycles as shearing strain increases (Lee et al., 2004).

10.3.6 Excitation Frequency

To evaluate the effect of excitation frequency on G and D in the nonlinear strain range, a series of the RC and TS tests were conducted on small-diameter specimens, MSW2ONS1, MSW3ONS1, MSW4ONS2, MSW5ONS1, and MSW6ONS2. These specimens are reconstituted with 100% soil-size MSW material. The only RC tests performed for large-diameter specimens were on MSW4ONL1. Frequency variation tests were accomplished at a confining pressure of 11 psi (76 kPa).

The variation in G with excitation frequency is shown in Figure 10.21. The value of G from LSRC test is shown and denoted as “Fr-Fr” in Figure 10.21. The data shown in the figure were chosen at the shearing strain amplitudes of 0.01 % and 0.04 %

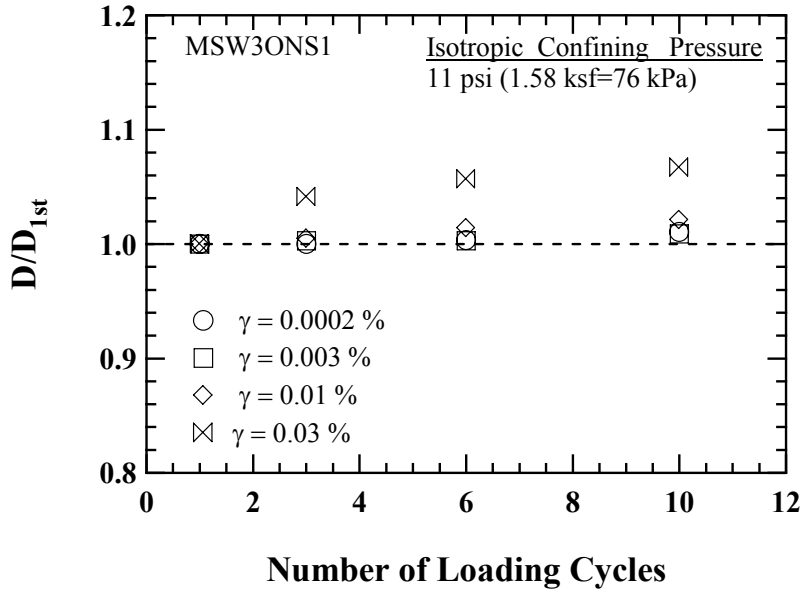

Figure 10.20 Variation in Normalized Material Damping Ratio, D/D_{1st}, with the Number of Loading Cycles from TS tests for MSW3ONS1 (100 % Soil-Size Material)

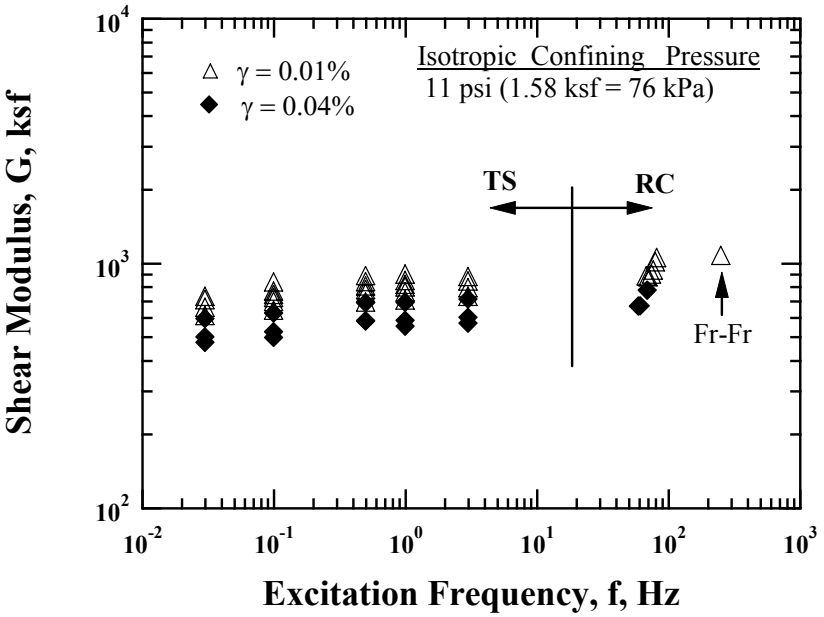

Figure 10.21 Variation in Shear Modulus with Excitation Frequency from the RCTS and LSRC Tests for 100 % Soil-Size Old MSW in the nonlinear strain range

from RCTS tests in the RCTS device and RC test in the LSRC device. It should be noted that only one data point from the Fr-Fr measurement at shearing strain amplitude of 0.01 % is presented because the RC test could not perform at shearing strain of 0.04 % in the LSRC device. As seen in the figure, G decreases with increasing shearing strain amplitude. It is an apparent evidence to show the nonlinearity of soil-sizes MSW material with shearing strain. Furthermore, it is evident to see that G increases linearly with an increase in excitation frequency due to frequency effect. As mentioned in Section 6.3.3, increase in G with increasing excitation frequency is attributed to the viscosity of the MSW skeleton frame.

To quantify the effect of excitation frequency on G, the values of G were normalized with G at a frequency of 1 Hz. The variation in normalized shear modulus, $G/G_{f=1Hz}$, is shown in Figure 10.22. The data were fitted using least-squares method and plotted together in the same figure as a dashed line. The equation is given by:

$$\frac{G}{G_{f=1Hz}} = 0.09 \times \log(\text{Frequency}) + 1.0 \qquad (10.1)$$

where,

G is a shear modulus measured over the varying frequencies, and

$G_{f=1Hz}$ is a shear modulus measured at a frequency of 1Hz.

Compared the effect of excitation frequency in small-strain range, as discussed in Section 6.3.3, with that in nonlinear strain range, the slopes of curve-fitted lines were identical, implying that the variation of G with excitation frequency shows a shearing strain independent behavior.

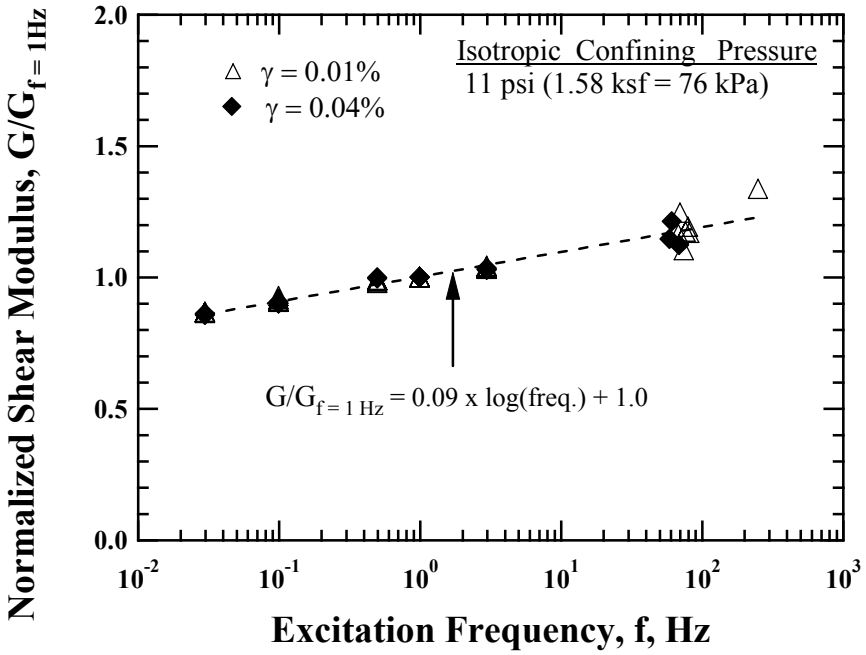

Figure 10.22 Variation in Normalized Shear Modulus with Excitation Frequency from the RCTS and LSRC Tests for 100 % Soil-Size Old MSW in the nonlinear strain range

It should be mentioned that TS testing could not be performed with the LSRC device so that G obtained from the LSRC test was normalized with the averaged value of G from the TS tests at a frequency of 1 Hz. As seen in Figure 10.22, G increases linearly with increasing excitation frequency and the variation in $G/G_{f=1Hz}$ amounts to a value of about 0.86 and 1.33 when the excitation frequency changes by approximately 10 and 100 times orders of magnitude such as from 0.03 Hz to 251 Hz, therefore indicating only a small effect of excitation frequency upon shear modulus.

The variation in D with excitation frequency is shown in Figure 10.23. The value of D from LSRC test is presented and is denoted as "Fr-Fr" in Figure 10.23. As revealed, values of D increase with decreasing excitation frequency below 1 Hz due to creep, while values of D increase with increasing excitation frequency due to the

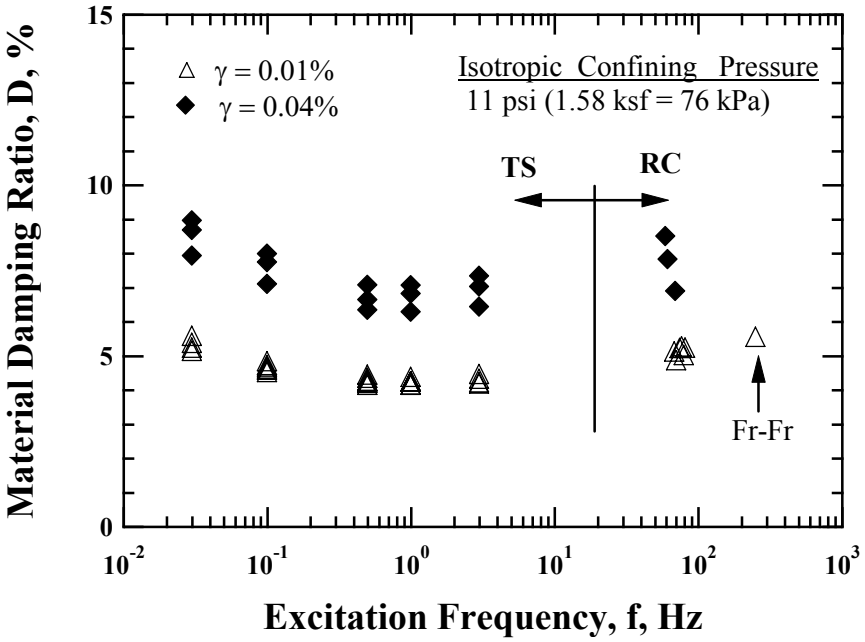

Figure 10.23 Variation in Material Damping Ratio with Excitation Frequency from the RCTS and LSRC Tests for Old MSW in the nonlinear strain range

frequency effect. It is interesting to note that the increase in D at excitation frequencies below 1 Hz due to creep behavior is slightly more pronounced as shearing strain increases and it is slightly more pronounced than the increase in D about 1 Hz.

To quantify the effect of excitation frequency on D, the values of D at given excitation frequencies were normalized with the value of D at a frequency of 1Hz. The variation in normalized material damping ratio, $D/D_{f=1Hz}$, is illustrated in Figure 10.24. The data were fitted as a form of a second-order of polynomial function using the least-squares method. The fitted line is given as a dashed line in Figure 10.24. The equation is expressed by:

$$\frac{D}{D_{f=1Hz}} = 0.08 \times \log(\text{Frequency})^2 - 0.04 \times \log(\text{Frequency}) + 1.0 \qquad (10.2)$$

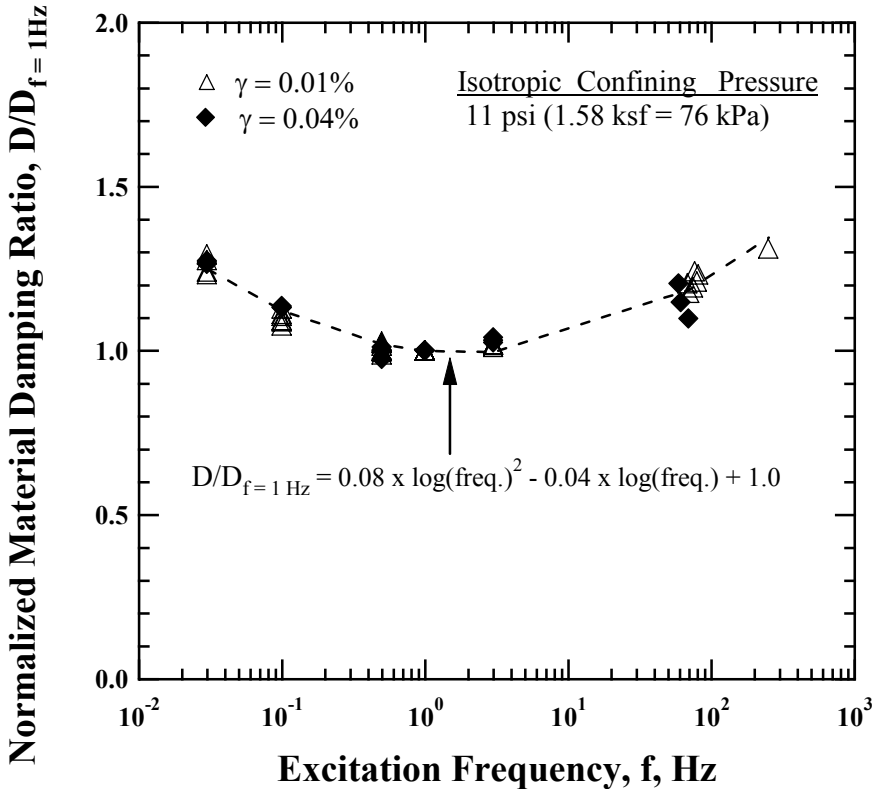

Figure 10.24 Variation in Normalized Material Damping Ratio with Excitation Frequency from the RCTS and LSRC Tests for 100 % Soil-Size Old MSW in the nonlinear strain range

where,

D is a material damping ratio measured at a given frequencies, and

$D_{f=1Hz}$ is a material damping ratio measured at a frequency of 1Hz.

As shown in Figure 10.24, the values of normalized material damping ratio increase with decreasing excitation frequency in the strain range less than 1 Hz, with a factor of 1.25 at the lowest frequency of 0.03 Hz. On the other hand, the values of $D/D_{f=1Hz}$, increase with increasing excitation frequency, with a factor of 1.31 at the highest frequency (251 Hz). It is interesting to compare the behavior of normalized

material damping ratio with excitation frequency in the nonlinear strain range with that in the small-strain range.

The increase in $D/D_{f=1Hz}$ at lower frequencies, less than 1 Hz, becomes slightly larger, whereas the increase in D with increasing excitation frequency becomes smaller as shearing strain increases.

10.4 MATERIAL PARAMETERS AFFECTING G AND D

10.4.1 Material Parameters Investigated

To investigate the effect of material parameters affecting G and D of MSW specimens in the nonlinear strains, both the RCTS and LSRC devices were employed. Material parameters investigated in the RCTS device include: (1) water content, (2) total unit weight, and (3) particle size. However, in the LSRC device, material parameters investigated were waste composition.

10.4.2 Waste Composition

As previously mentioned, MSW is a composite material of organic and inorganic materials, with a very heterogeneous nature. Therefore, it is reasonable to expect that waste composition may have a significant impact on the nonlinear dynamic behavior of MSW subjected to earthquake loading. Therefore, large-diameter old MSW specimens were reconstituted according to the procedures specified in Section 5.3.2 to examine the effect of waste composition. Of course, the "large-diameter" specimens are only 6-in. (152.4-mm) in diameter. It would have been better to have much larger specimens, say, 3 ft (0.9 m) in diameter. This portion of the project is covered by Prof. Kavazanjian at Arizona State University.

The variations in G and G/G_{max} with shearing strain for different weight

percentages of soil-size material are illustrated in Figures 10.25 (a) and (b), respectively. It should be noted that Specimen MSW2MNL4 was reconstituted with a mixture of papers of old and fresh wastes. Thus, the name of specimen was denoted with an M in the middle of its name rather than either O or F. All shear modulus measurements shown in Figure 10.25 (a) were performed at the same confining pressure of 11 psi (76 kPa). The differences in the values of G result from different initial unit weights for each specimen. The initial material properties of these specimens are given in Table 5.5 and Table 5.7. As shown in Figure 10.25 (a), G is constant and equal to G_{max} in the small-strain range, $\gamma < \gamma_t^e$, in which the amplitude of γ_t^e becomes larger with an increase in waste composition. On the other hand, G decreases with increasing shearing strain exceeding the amplitude of γ_t^e. The values of γ_t^e are indicated by arrows for each specimen in the figure.

Figure 10.25 (b) illustrates that G/G_{max} – log γ curves shift to higher strains as waste composition decreases, implying that specimens with lower weight percentages of soil-size material (< ¾-in (19.1-mm)) exhibit more linear behavior. For example, MSW2MNL4 has the lowest weight percentage of soil-size material (14 % soil-size material) and shows the most linear behavior. Therefore, γ_t^e is largest. The reason for this tendency is that the higher relative percentage of papers, soft plastics, and woods of which the specimen is comprised lead to more linear ("elastic") response. (This behavior is also shown in damping.) It is interesting to observe that the shift of G/G_{max} – log γ curves to higher strains appears to be accelerated as the weight percentage of soil-size material decreases. As will be discussed in Chapter 13, each group of curves is fitted using a modified hyperbolic model suggested by Darendeli (2001). As a collaborative research project, the variations in G/G_{max} – log γ curves in terms of different waste compositions are consistent with those measured by Zekkos (2005) using cyclic

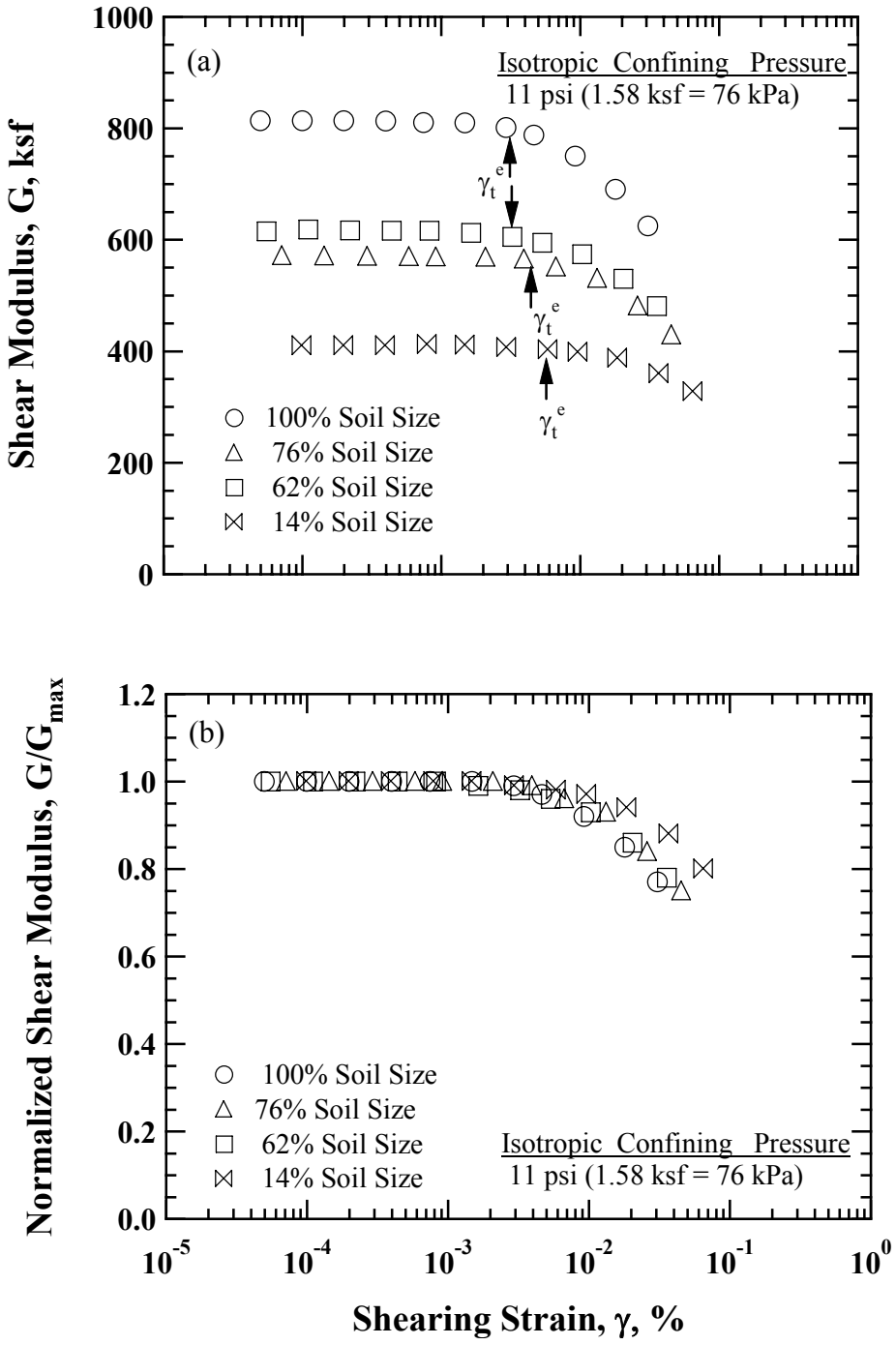

Figure 10.25 Comparison of the Variation in (a) Shear Modulus and (b) Normalized Shear Modulus with Shearing Strain from LSRC Tests upon Different Weight Percentages of the Soil-Size Old and Mixed MSW Specimens

triaxial tests, as shown in Figure 10.26.

The variation in D with shearing strain upon different weight percentages of soil-size material is shown in Figure 10.27. As can be seen, D is comparatively less dependent on the weight percentage of soil-size material, when compared with normalized shear modulus. Figure 10.27 shows that the values of D at small-strain ranges ($\gamma < 0.003$ %, i.e., D_{min}) increases slightly with decreasing the weight percentage of soil-size material, but the trend of increase in D with decreasing the weight percentage of soil-size material appears to be reversed after strain amplitude of about 0.03 %. With limited data in material damping ratio measurements from intermediate to high shearing strains, it can be concluded that material damping ratio is quite insensitive to waste composition and the influence of waste composition is less pronounced on material damping ratio than it is on G or G/G_{max}.

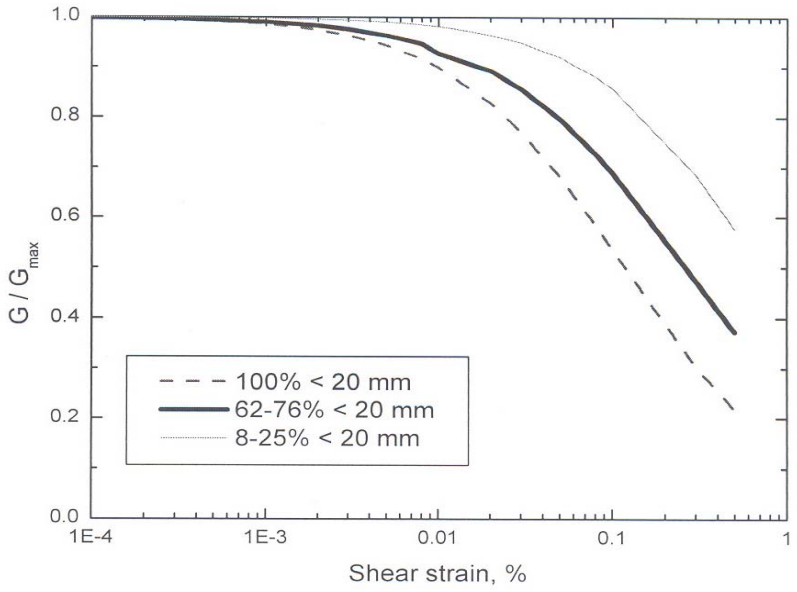

Figure 10.26 Recommended Normalized Shear Modulus with Shearing Strain upon Different Weight Percentages of Soil-Size Material for Upper 66 ft (20 m) of a Landfill (from Zekkos, 2005)

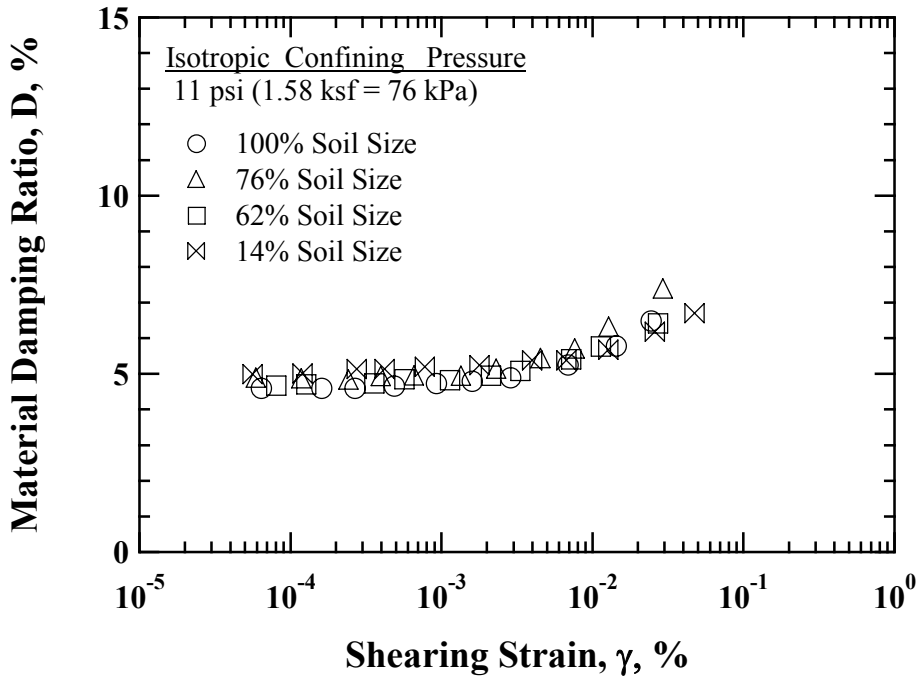

Figure 10.27 Comparison of the Variation in Material Damping Ratio with Shearing Strain from LSRC Tests upon Different Weight Percentages of the Soil-Size Material, Old and Mixed MSW Specimens

10.4.2 Water Content

High-amplitude RC tests were performed for 100 % soil-size material Specimens MSW2ONS1 and MSW2OHS1 to investigate the effect of water content on the nonlinear dynamic behavior of old MSW. High-amplitude RC tests were conducted at its natural and hydrated conditions. RC tests on the specimen at its natural condition precede the RC test on the specimen at the hydrated condition. Typical variations in G and G/G_{max} – log γ curves are compared in Figures 10.28 (a) and (b), respectively. The measurements at the natural condition are presented as open square symbols and the measurements at the hydrated condition are presented as solid triangular symbols. All high-amplitude RC tests were performed at a confining pressure of 11 psi (76 kPa).

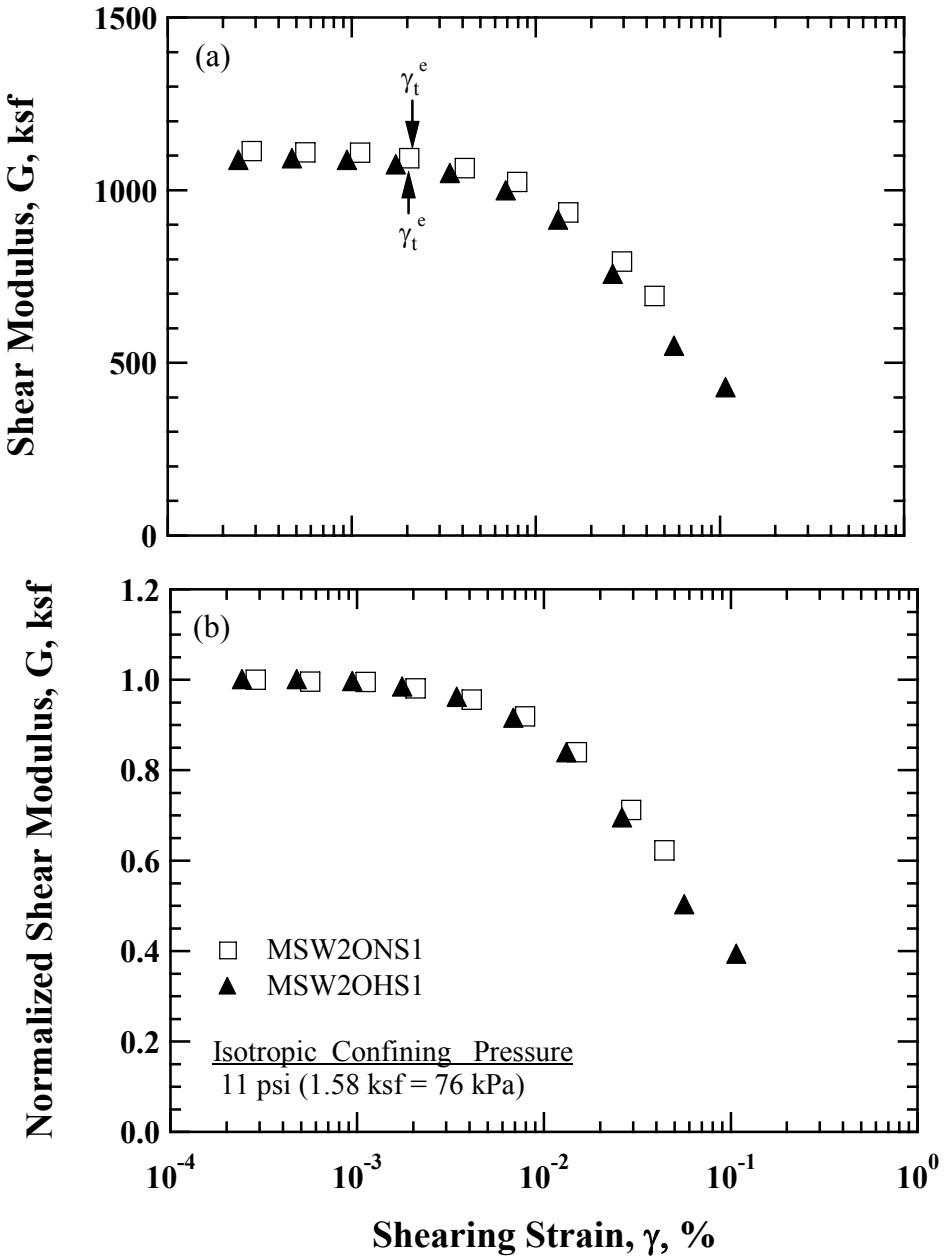

Figure 10.28 Comparison of the Variation in (a) Shear Modulus and (b) Normalized Shear Modulus with Shearing Strain from RC Tests upon Specimens at Its Natural and Hydrated Conditions for 100 % Soil-Size Old MSW

As seen in Figure 10.28 (a), there is a slight difference in the values of G with shearing strains, indicating that hydration for a given specimen appears to have little effect on the fundamental linear and nonlinear responses. It is of interest to mention that the values of G over shearing strain ranges are slightly different, showing that the stiffness of hydrated specimen increases rapidly with confining pressure. The shearing strain for hydrated specimen reaches further higher strains.

As indicated in Figure 10.28 (a), the value of γ_t^e of Specimens MSW2ONS1 and MSW2OHS1 is approximately 0.002 %, showing that the value of γ_t^e is not affected by the change in water content. However, it is important to point out that the values of γ_t^e for small-diameter specimens are slightly less than the value of γ_t^e for large-diameter specimen (e.g., 100 % soil-size specimen in Figure 10.25 (a), whose γ_t^e was 0.003 %). This means that the value of γ_t^e is affected by the specimen size. This pattern was observed throughout this study in comparison between other small- and large-diameter specimens.

In terms of G/G_{max}, the curve for hydrated specimen shifts slightly to lower strains, as shown in Figure 10.28 (b). However, the general trend of modulus reduction with respect to shearing strain is similar to that obtained from natural condition. As discussed at previous section, hydration for a given specimen has a small impact upon shear modulus reduction. For specimens tested at the natural and hydrated conditions, reference strains, γ_r, which is the amplitude of shearing strain at normalized shear modulus equal to 0.5, turned out to be 0.08 % and 0.06 %, respectively.

The D – log γ curves for Specimen MSW2ONS1 and 2OHS1 are illustrated in Figure 10.29. The values of D of the hydrated specimen are slightly higher than those from specimen at its natural condition over entire shearing strain ranges. As already discussed in Section 6.5.2, the reason for the increase of D may be largely due to energy

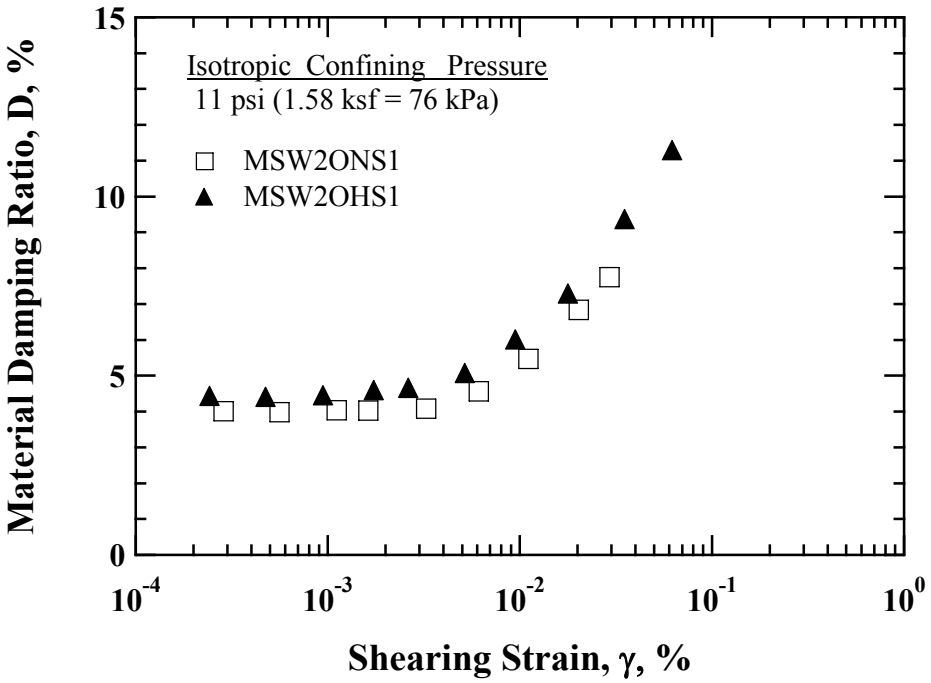

Figure 10.29 Comparison of the Variation in Material Damping Ratio with Shearing Strain from RC Tests upon Specimens at Its Natural and Hydrated Conditions for 100 % Soil-Size Old MSW

dissipation caused by relative movements between solid particles and added water and some effect from inelastic friction losses. As a result, the influence of water content on the nonlinear dynamic behavior of old MSW turned out to be small.

10.4.3 Total Unit Weight Variation for the Same Material Type

The variations in G and G/G_{max} with shearing strain for 100 % soil-size MSW specimens are presented in Figures 10.30 (a) and (b), respectively. The comparison was made regarding the variation in G and G/G_{max} measurements at a confining pressure of 11 psi (76 kPa). The specimens were reconstituted with 100 % soil-size material that was passed ¾-in. (19.1-mm) sieve. Higher unit weight specimen (82.3 pcf (12.9 kN/m^3)) MSW4ONS2, is denoted as open square symbol and lower unit weight specimen (62.4

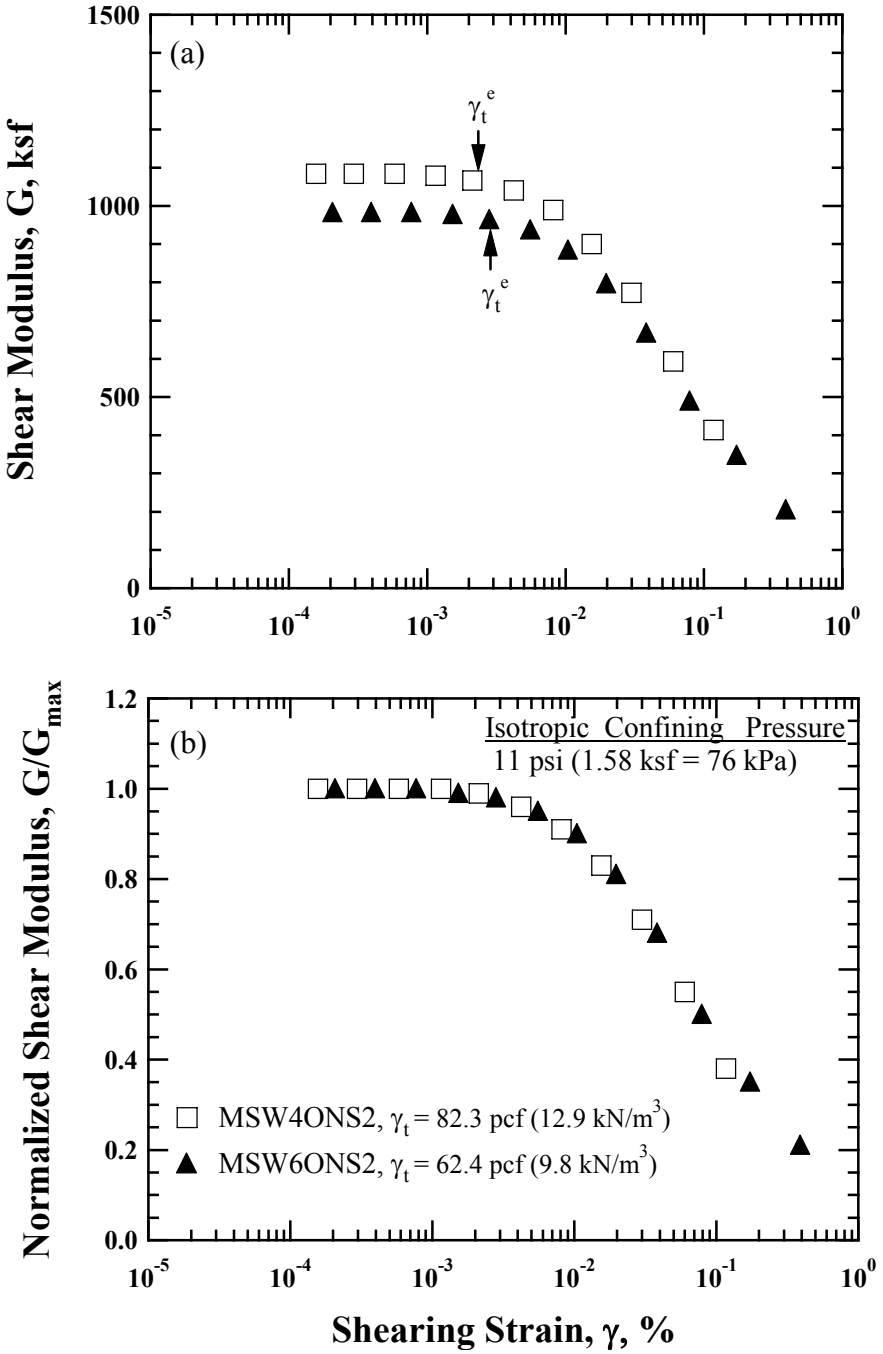

Figure 10.30 Comparison of the Variation in (a) Shear Modulus and (b) Normalized Shear Modulus with Shearing Strain from RC Tests of Specimens with Different Total Unit Weights for 100 % Soil-Size Old Waste

pcf (9.8 kN/m^3)), MSW6ONS2, is denoted as solid triangular symbol.

As shown in Figure 10.30 (a), for both specimens, the values of G are constant and equal to G_{max} in the strain ranges less than about 0.003 %. However, beyond 0.003 %, the values of G decrease with increasing shearing strain. The values of γ_t^e for Specimens MSW4ONS2 and MSW6ONS2 are equal to 0.0025 % and 0.0029 %, respectively. Lower unit weight specimen exhibits slightly higher value of γ_t^e. The difference in the values of G, which is about 10 % ($\gamma < 0.003$ %), is largely caused by different excitation frequency and total unit weight of the specimens.

The variations in G/G_{max} - log γ curves with shearing strain are depicted in Figure 10.30 (b). Figure 10.30 (b) demonstrates that G/G_{max} – log γ curves are nearly identical between specimens, indicating that the nonlinear behavior of MSW is almost not affected by the variation of total unit weight. Reference strains were equal to about 0.075 % and 0.080 % for Specimen MSW4ONS2 and MSW6ONS2, respectively; lower unit weight specimen exhibits barely higher value.

For material damping ratio, the D – log γ curves are almost identical as shown in Figure 10.31. It is of interest to note that in contrast to G, the values of D in the small-strain ranges ($\gamma < 0.002$ %) are not affected by the difference in unit weights of the specimens. Figure 10.31 indicates that the effect of unit weight of specimen has nearly no impact on D. In conclusion, only G – log γ curves are dominated by the variation of unit weight. However, there is approximately no effect on the variation in unit weight for G/G_{max} – log γ and D – log γ curves.

10.4.4 Particle Size

The variations in G and G/G_{max} with shearing strain are compared in Figures 10.32 (a) and (b), respectively. To evaluate the effect of particle, the nonlinear moduli

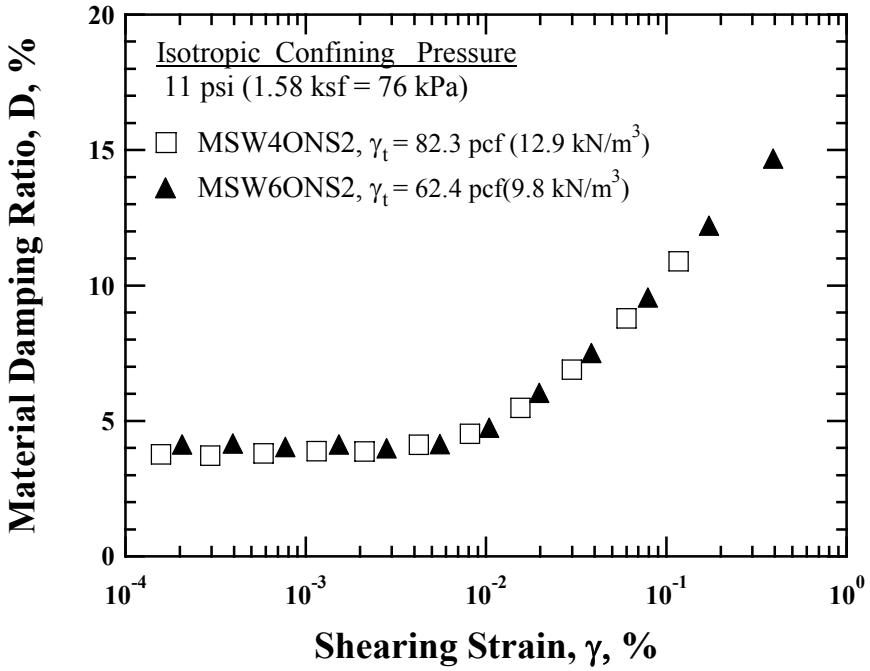

Figure 10.31 Comparison of the Variation in Material Damping Ratio with Shearing Strain from RC Tests of 100 % Soil-Size Old MSW Specimens with Different Unit Weights

Specimens MSW3ONS1 and MSW4ONS2 were used. The MSW3ONS1 were prepared with 100 % soil-size material passing the 3/8-in. (9.5-mm) sieve and is represented by open symbols. On the other hand, MSW4ONS2 was prepared with 100 % soil-size material passing the ¾-in. (19.1-mm) sieve and is represented by solid triangular symbols. As previously illustrated in Figure 5.4, 100 % soil-size material that passed the ¾-in. (19.1-mm) sieve included small-size of refuse, e.g., soft plastic, wood, paper, and gravel. Nonlinear measurements were made at a confining pressure of 11 psi (76 kPa) and the initial material properties of the specimens are given in Table 5.3.

As seen in Figure 10.32 (a), the values of G are constant and equal to G_{max} in the small-strain ranges (about $\gamma < 0.0025$ %). However, after shearing strains greater than 0.0025 %, the values of G begin to decrease with increasing shearing strain.

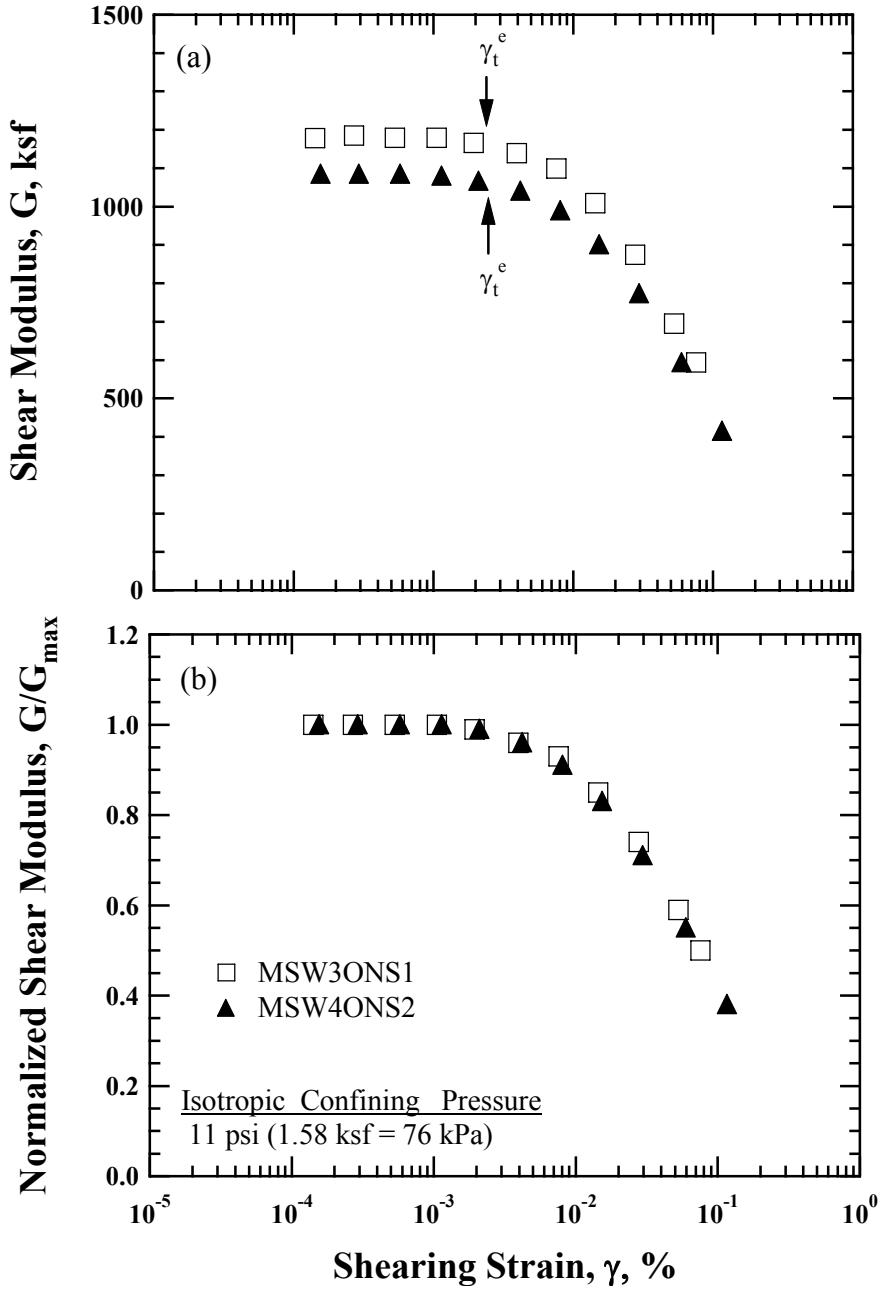

Figure 10.32 Comparison of the Variation in (a) Shear Modulus and (b) Normalized Shear Modulus with Shearing Strain from RC Tests of Specimens with Different Particle Sizes for 100 % Soil-Size Old MSW in the RCTS Device

The absolute difference of G in the shearing strain ranges, ($\gamma < 0.0025$ %), results mainly from differences in their initial material properties and excitation frequencies. The values of estimated total unit weight for Specimen MSW3ONS1 and MSW4ONS2 at a confining pressure of 11 psi (76 kPa) are equal to 88.3 pcf (13.9 kN/m^3) and 86.3 pcf (13.6 kN/m^3), respectively. The values of excitation frequency are 61.3 Hz to 86.4 Hz and 50.7 Hz to 81.7 Hz for Specimens MSW3ONS1 and MSW4ONS2.

The variation in G/G_{max} with shearing strain for Specimens MSW3ONS1 and MSW4ONS2 is shown in Figure 10.32 (b). Interestingly, normalized shear modulus with strain for both specimens exhibits nearly the same behavior, showing that the nonlinear behavior for the same material type is not affected by the particle size of specimen. As shown in the figure, reference strains turned out to be approximately 0.075 % and 0.070 % for Specimen MSW3ONS1 and MSW4ONS2, respectively.

The variation in D with shearing strain for Specimens MSW3ONS1 and MSW4ONS2 is presented in Figure 10.33. Similar to normalized shear modulus, the values of D exhibit the same behavior with shearing strain regardless of the particle size of the specimens. In case of the D, the difference produced by a different its initial unit weight and excitation frequency for G disappears in small-strain ranges, implying that the values of D are not very sensitive to its initial conditions. Finally, it can be drawn conclusions that the effect of particle size on the specimen passing the 3/8-in. (9.5-mm) sieve has some effect on the G – log γ curves, while the G/G_{max} – log γ curves are not nearly affected by the particle size of the specimen

To investigate the effect of particle size of large-diameter specimens in the LSRC device, Specimens MSW2ONL2 and MSW4ONL1 were used. The MSW2ONS2 was constructed with material passing the ¾-in. (19.1-mm) sieve, whereas the MSW4ONL1 was constructed with material passing the 3/8-in. (9.5-mm) sieve.

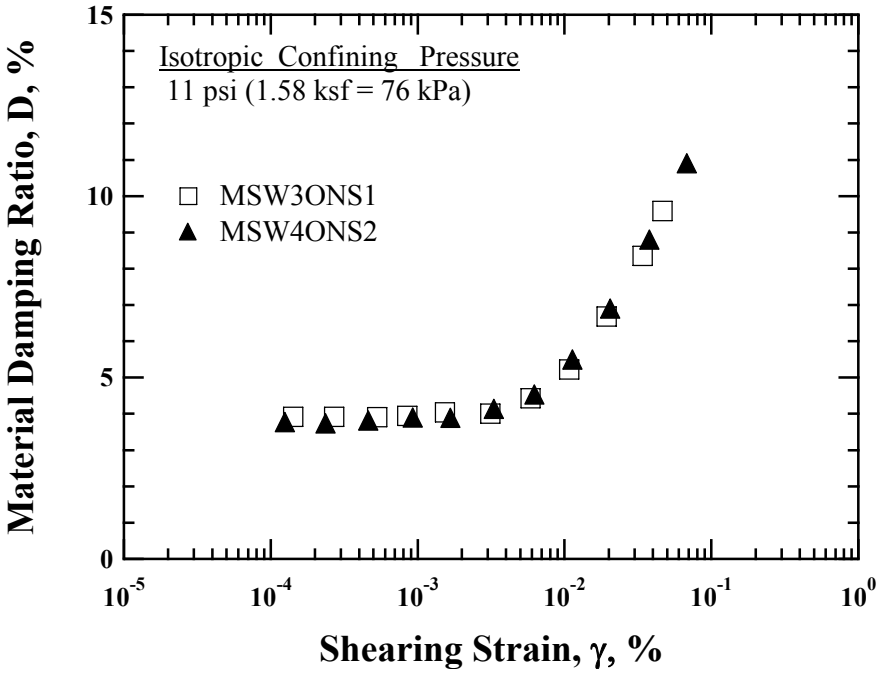

Figure 10.33 Comparison of the Variation in Material Damping Ratio with Shearing Strain from RC Tests of Specimens with Different Particle Sizes for 100 % Soil-Size Old MSW in the RCTS Device

Nonlinear measurements were performed at a confining pressure of 11 psi (76 kPa). The initial material properties of these specimens are given in Table 5.5.

The variation in G and G/G_{max} with shearing strain for Specimens MSW2ONL2 and MSW2ONL2 is presented in Figures 10.34 (a) and (b), respectively. As can be seen in Figure 10.34 (a), for both specimens, the values of G are constant below γ_t^e. However, G decreases with increasing shearing strain beyond γ_t^e. The values of γ_t^e for Specimens MSW2ONL2 and MSW4ONL1 are 0.0022 % and 0.0021 %, respectively. There is a difference in the shearing strains below γ_t^e largely due to the difference in their initial material properties and excitation frequency. Excitation frequency changes from 183 Hz to 208 Hz for Specimen MSW2ONL2 and from 236 Hz to 262 Hz for Specimen MSW4ONL1, respectively. Figure 10.34 (b) shows that normalized shear modulus for

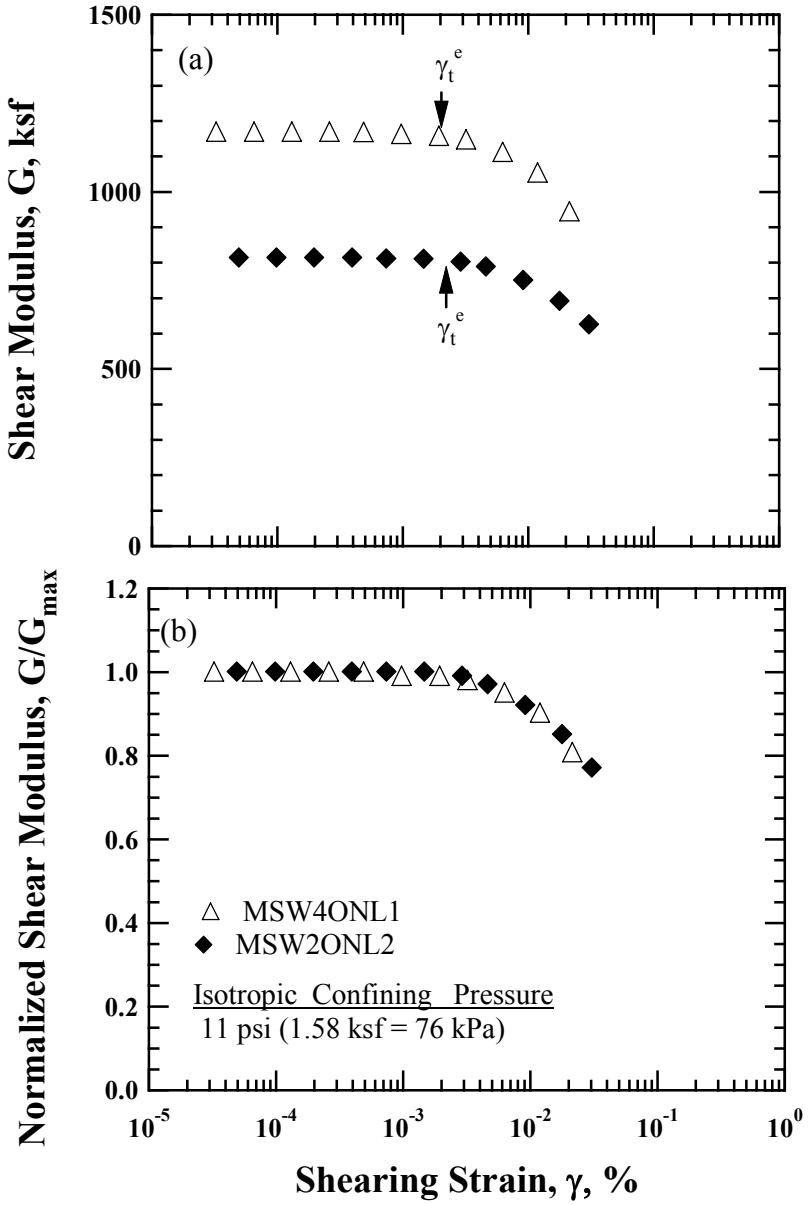

Figure 10.34 Comparison of the Variation in (a) Shear Modulus and (b) Normalized Shear Modulus with Shearing Strain of Specimens with Different Particle Sizes for 100 % Soil-Size Old MSW in the LSRC Device

both specimens exhibits almost the same, indicating that the nonlinear behavior for the same material type is barely affected by the particle size of specimen.

The variation in D with shearing strain for Specimens MSW2ONL2 and MSW4ONL1 is shown in Figure 10.35. Although there is a slight difference in the strain ranges below about 0.002 %, the values of D with shearing strain exhibit nearly the same regardless of the particle size of the specimens. As a result, like the test results measured in the RCTS device, the effect of particle size on the specimens passing the 3/8-in. (9.5-mm) sieve has some effect on the G – log γ curves, whereas the G/G_{max} – log γ and D – log γ curves are barely affected by the particle size of the specimen.

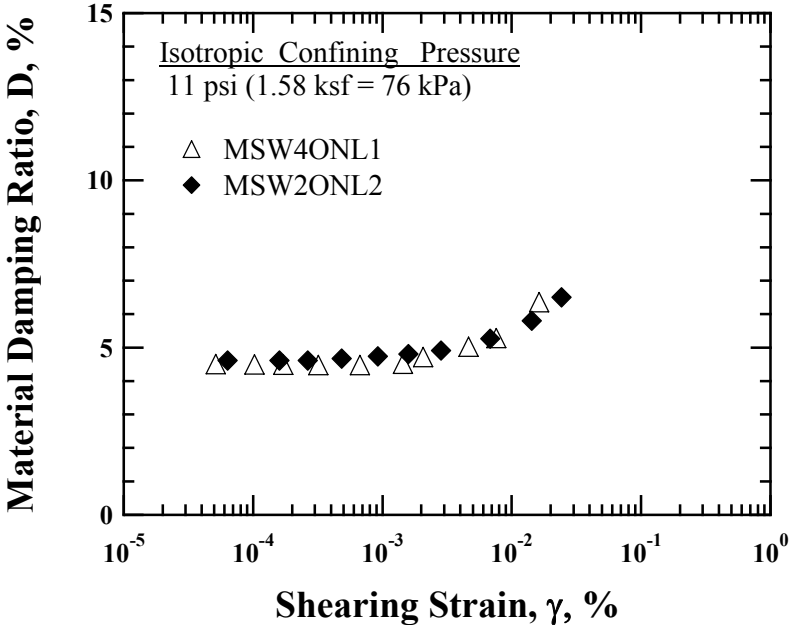

Figure 10.35 Comparison of the Variation in Material Damping Ratio with Shearing Strain from RC Tests of Specimens with Different Particle Sizes for 100 % Soil-Size Old MSW in the LSRC Device

10.5 RELATIONSHIP BETWEEN NORMALIZED SHEAR MODULUS AND MATERIAL DAMPING RATIO OF OLD MSW

An empirical relationship between normalized shear modulus, G/G_{max}, and modified material damping ratio, $D\text{-}D_{min}$, for RC and TS tests were derived by means of data from RCTS and LSRC tests for all Groups of old and mixed MSW. For the development of empirical relationship, RC data contained the data from small- and large-diameter RC tests in the RCTS and LSRC devices, whereas TS data only included the data from small-diameter TS tests in the RCTS device. $D\text{-}D_{min}$ represents a modified material damping ratio, which is obtained by subtracting the average value of D_{min} from the values of D. The entire data set was used from high-amplitude RCTS tests at confining pressure levels of 2.5 psi (17 kPa), 11 psi (76 kPa), and 40 psi (276 kPa) upon loading sequence.

The empirical relationship between G/G_{max} and $D\text{-}D_{min}$ are illustrated in Figure 10.36. It should be pointed out that the shearing strains for the normalized shear modulus and material damping ratio were not the same in the RC tests. In the small-strain ranges, the values of D calculated from a half-power bandwidth method were used for the generation of material damping curves with shearing strain, resulting in same shearing strains for material damping ratio as normalized shear modulus. However, shearing strains for material damping ratio at higher shearing strains were computed taking an average of the first three cycles. Thus, the empirical relationships were plotted using the values of $D\text{-}D_{min}$, which were directly corresponded to the values of G/G_{max} during high-amplitude RC tests.

The data from RC tests are represented by open circle symbols and the data from TS tests (1^{st} and 10^{th} cycles) are represented as solid triangle symbols. The data obtained from RCTS and LSRC tests were fitted using least-squares method as a form of

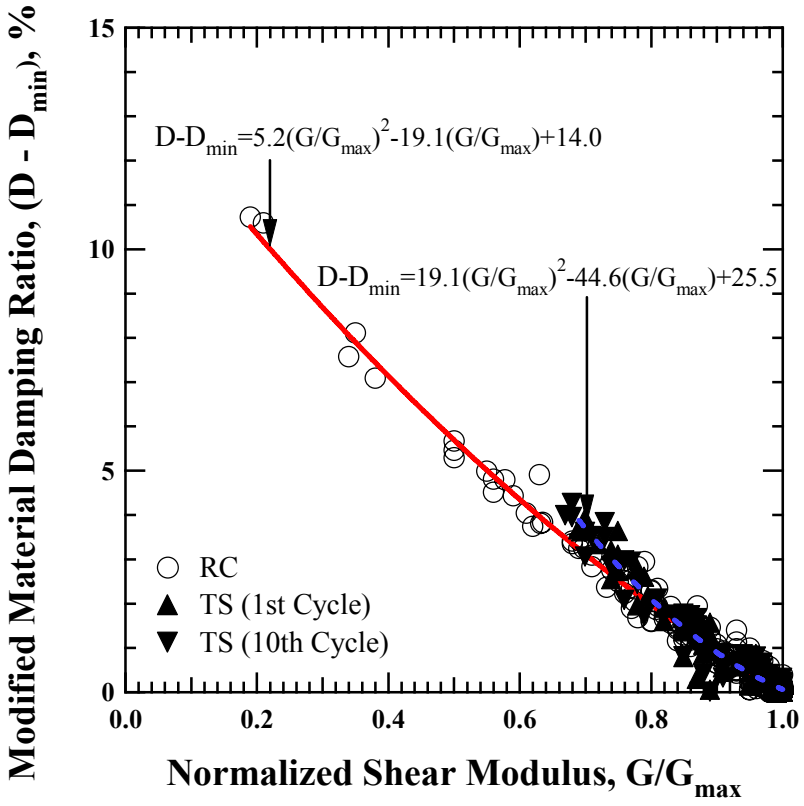

Figure 10.36 Plot of Normalized Shear Modulus with Modified Material Damping Ratio from RCTS and LSRC Tests for All Groups of Old and Mixed MSW

the second-order of polynomials and fitted curves are represented by the solid and dashed lines for RC and TS tests, respectively. These equations are given by:

$$D - D_{min} = 5.2(G/G_{max})^2 - 19.1(G/G_{max}) + 14.0 \quad \text{for RC tests} \qquad (10.1)$$

$$D - D_{min} = 19.1(G/G_{max})^2 - 44.6(G/G_{max}) + 25.5 \quad \text{for TS tests} \qquad (10.2)$$

where,

D_{min} is a material damping ratio at small-strain ranges,

D is a material damping ratio at any given shearing strains,

G_{max} is a shear modulus at small-strain ranges, and

G is a shear modulus at any given shearing strains.

As shown in Figure 10.36, the data from RC and TS show a good agreement down to the value in terms of G/G_{max} of 0.76, however, below this point, the difference between RC and TS data begins to increase, implying a fact that the effects of excitation frequency and number of loading cycles in material damping ratio becomes smaller as shearing strain increases. In other words, the material damping ratios from TS tests are approaching gradually to those from RC tests as shearing strain increases. Hwang (1997) found the empirical relationships between G/G_{max} and D from RCTS tests obtained from a majority of undisturbed specimens. He obtained linear relationships between normalized shear modulus and material damping ratio. Zhang et al., (2005) also found similar relationships between G/G_{max} and $D\text{-}D_{min}$ from RCTS test performed upon 78 specimens obtained in South Carolina. They suggested the relationships as forms of the second-order of polynomials, showing that the TS data plot above the RC data because of the fact that excitation frequency in TS tests is kept constant whereas in RC tests, excitation frequency decreases.

The important feature of the empirical relationships derived from measured data is that if someone knows the values of G/G_{max}, then, the values of D can be computed at higher shearing strain ranges with the knowledge of D_{min}. In order to evaluate the accuracy of derived equations, the values of measured $D\text{-}D_{min}$ and predicted $D\text{-}D_{min}$ are compared in Figures 10.37 (a) and (b) for RC and TS tests, respectively. As shown in figures, predicted equation for RC provides a fairly good agreement between predicted and measured values whereas, predicted equation for TS tests gives a tolerably good agreement with some scatter.

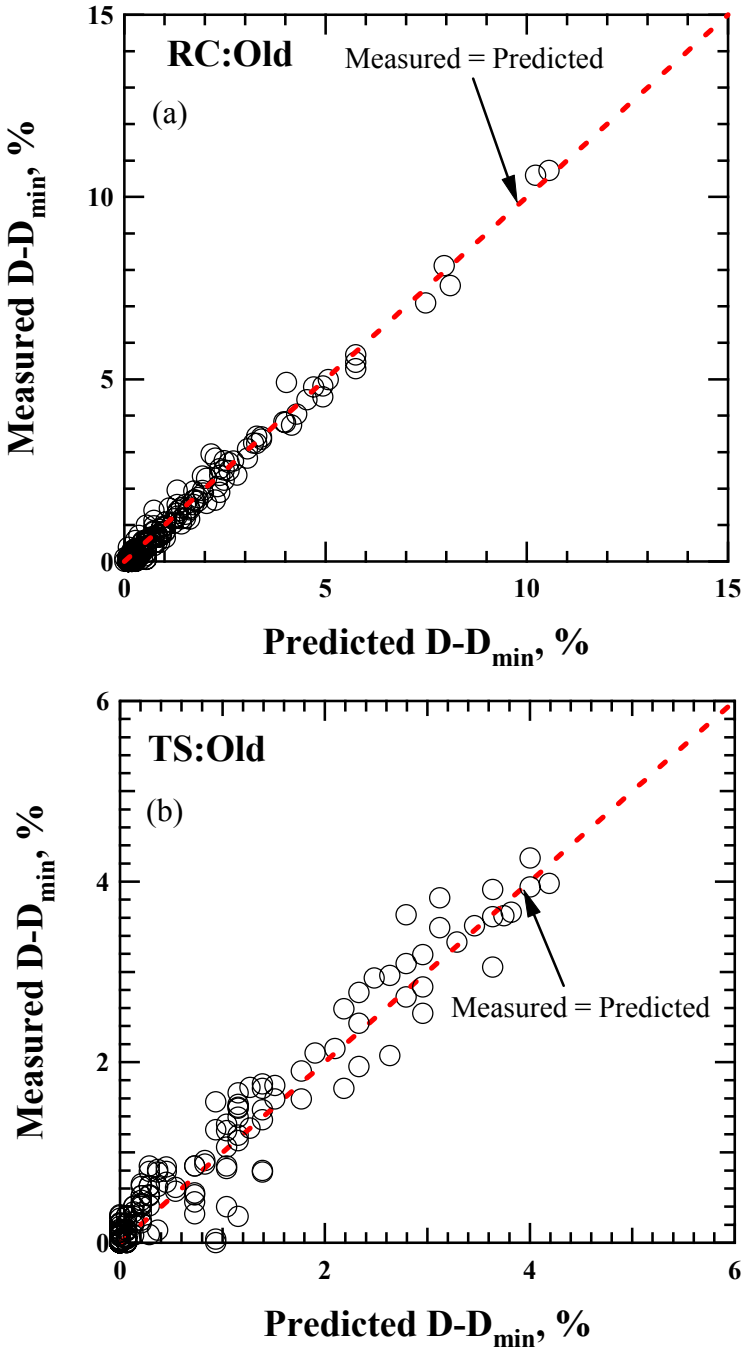

Figure 10.37 Comparison of the Values of Measured D-D_{min} and Predicted D-D_{min} from (a) RC Tests and (b) TS Tests for All Groups of Old MSW

10.6 COMPARISON OF NONLINEAR DYNAMIC PROPERTIES OF OLD MSW AND LOOSE SAND

The G – log γ, G/G_{max} – log γ, and D – log γ curves for old MSW are compared with this of loose sand in Figures 10.38, 10.39, and 10.40, respectively. The comparisons were made at a confining pressure of 11 psi (76 kPa). These nonlinear dynamic property curves were generated using equation, suggested by Menq (2003). The loose sand has a uniformity coefficient of 18 and void ratio of 0.4. Relative density of the loose sand is about 50 %. The values of G, G/G_{max}, and D for fresh MSW shown in the figures were corrected for frequency to f = 1 Hz. As seen in Figures 10.38, the value of G at small-strain range, the difference between loose sand and old MSW is approximately a factor of two. In terms of G/G_{max}, the G/G_{max} – log γ curve shifts to lower strains for the loose sand, indicating a more nonlinear behavior with shearing strain than old MSW. For material damping ratio, as shown in Figure 10.40, there is a large difference at small-strain range and is about factor of 3.3. D is small below shearing strain of 0.007 %, but becomes larger beyond this strain.

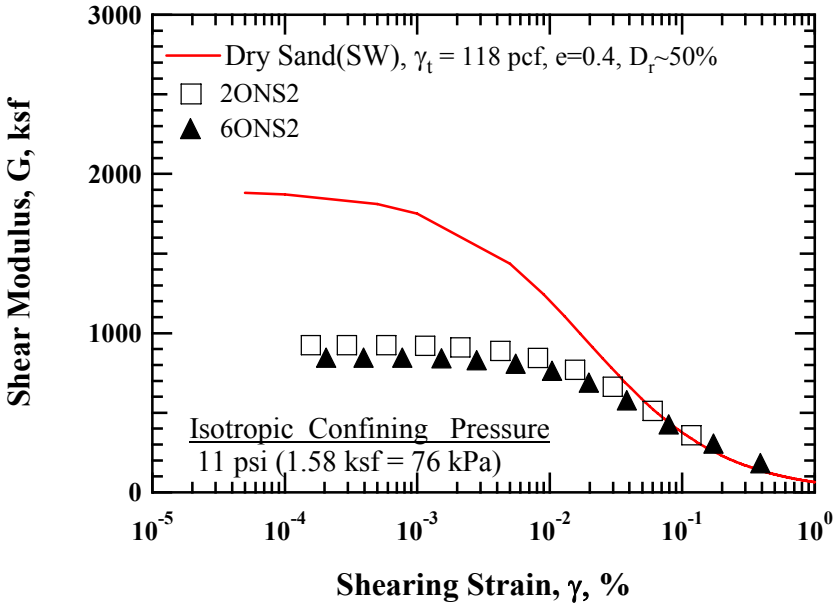

Figure 10.38 Comparison of the Variation in Shear Modulus with Shearing Strain at a Confining Pressure of 11 psi (76 kPa) for Old MSW and Loose Sand

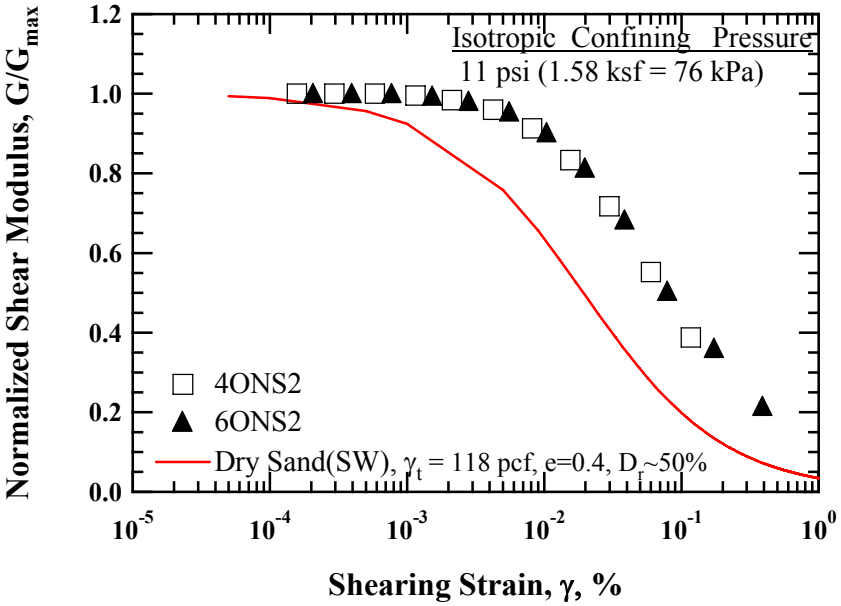

Figure 10.39 Comparison of the Variation in Normalized Shear Modulus with Shearing Strain at a Confining Pressure of 11 psi (76 kPa) for Old MSW and Loose Sand

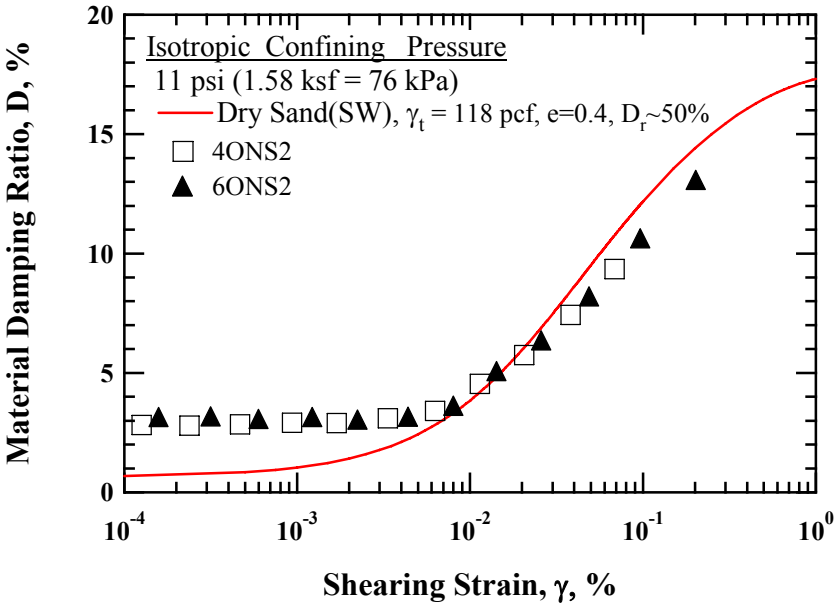

Figure 10.40 Comparison of the Variation in Material Damping Ratio with Shearing Strain at a Confining Pressure of 11 psi (76 kPa) for Old MSW and Loose Sand

10.7 SUMMARY

Test parameters affecting nonlinear dynamic properties, G and D, of old MSW are investigated in this chapter. These test parameters include: (1) shearing strain amplitude, (2) total isotropic confining pressure, (3) overconsolidation ratio, (4) number of loading cycles, and (5) excitation frequency. Each test parameters were studied and the influences on the nonlinear dynamic properties of old MSW were evaluated separately. Among these test parameters, very important parameters are shearing strain amplitude and total isotropic confining pressure; below γ_t^e, G and D are constant. However, beyond this, G and D vary dramatically with increasing shearing strain amplitudes; G decreases and D increases with increasing shearing strain. Absolute value of G increases significantly with increasing confining pressure. In terms of

G/G_{max}, the G/G_{max} – long γ curves shift to somewhat higher strains with increasing confining pressure. Other test parameters exhibit a small or some impact on G and D.

Additionally, material parameters affecting G and D are examined separately. These material parameters are: (1) waste composition, (2) water content, (3) total unit weight, and (4) particle size. Among these parameters, waste composition is the most important parameter; the G/G_{max} – log γ curves shift to higher strains as decreasing weight percentage of soil-size material in the MSW specimens. Other material parameters show small effects on G and D.

Empirical relationships between normalized shear modulus, G/G_{max}, and modified material damping ratio, $D\text{-}D_{min}$, are developed using the data obtained from RCTS and LSRC tests for old and mixed MSW specimens. For equation for RC tests, data from the specimens reconstituted with 100 %, 62 to 76 %, and 14 % soil-size material were used, whereas the data from specimens with 100 % soil-size material were used to develop the equation for TS tests. These equations were fitted using the least-squares method as a form of second-order of polynomial function. Comparisons in the data between measured and predicted by the Equations (10.1) and (10.2) are presented in Figures 10.37 (a) and (b) and gives a good agreement.

The G – log γ, G/G_{max} – log γ, and D – log γ curves of old MSW are compared with loose sand. There are large differences in absolute values of G and D at small-strain range. The loose sand exhibits more nonlinear behavior relatively when compared with old MSW; the G/G_{max} – log γ curve shifts lower strains.

CHAPTER 11: Nonlinear Behavior of Fresh MSW

11.1 INTRODUCTION

A series of RCTS and LSRC laboratory tests were performed on 2.8 in. and 6.0 in. diameter specimens to evaluate the dynamic properties of fresh MSW in the nonlinear strain ranges ($\gamma > 0.002$ %). Shear modulus (G) and material damping ratio (D) with shearing strain were measured for fresh MSW.

Test parameters affecting G and D for fresh MSW in the nonlinear strain ranges are investigated in this chapter. These parameters include: (1) shearing strain amplitude, γ, (2) total isotropic confining pressure, σ_o, (3) overconsolidation ratio (OCR), (4) number of loading cycles, N, and (5) excitation frequency, f. Other material parameters that influence the dynamic properties in the nonlinear strain range are studied as well. These material parameters are: (1) waste composition, (2) water content, (3) total unit weight, and (4) particle size. The test results and observations from the measurements are discussed and compared in the subsequent sections.

11.2 TEST PROCEDURES

11.2.1 Testing with the RCTS Device

Similar to nonlinear measurements for old MSW, high-amplitude RC (HARC) tests and high-amplitude TS (HATS) tests were performed for small-diameter specimens at their natural and hydrated conditions in accordance with predetermined confining pressures, as specified in Table 11.1. At first, low-amplitude RC (LARC) tests were performed to establish the baseline measurements of G_{max} and D_{min} for the purpose of comparison of those values after HARC and HATS tests had been conducted. Then, TS

Table 11.1 Isotropic Confining Pressures Used in High-Amplitude RCTS Tests for Small-Diameter 100% Soil-Size Fresh MSW Specimens in the RCTS Device

Specimen ID	Isotropic Confining Pressure	
	High-Amplitude RC Tests, psi (kPa)	High-Amplitude TS Tests, psi (kPa)
MSW1FNS1$^{\Delta}$	2.5, 11, 40 (17, 76, 276)	2.5, 11, 40 (17, 76, 276)
MSW1FHS1	2.5, 11 (17, 76)	2.5, 11 (17, 76)
MSW2FNS2$^{\triangle}$	2.5, 11, 40 (17, 76, 276)	2.5, 11, 40 (17, 76, 276)
MSW3FNS1	11 (76)	11 (76)
MSW4FNS2	11, 40 (76, 276)	11, 40 (76, 276)

Notes:

N denotes a natural condition.

H denotes a hydrated condition.

Δ1 denotes specimen reconstituted with material passed the 3/8-in. (9.5-mm) sieve.

⌂2 denotes specimen reconstituted with material passed the ¾-in. (19.1-mm) sieve in the specimen ID.

tests were performed with increasing shearing strain at a given frequency (typically 0.5 Hz). Another LARC tests were performed immediately after completion of HATS test to check any changes in the MSW skeleton due to HATS tests. After the HATS tests, each specimen was confined at the same confining pressure for an additional twelve to 24-hours in order to allow the specimen regain its original state in terms of G_{max} and D_{min}.

HARC tests were performed after the specimen had regained their original states that were checked by LARC tests. Likewise, LARC tests were also performed immediately after to monitor any change in MSW skeleton. The specimens required a resting period of either a half day to a full day to regain their original state before going to the next pressure level.

Once the LARC, HATS, and HARC tests are completed at a given confining

pressure, then RCTS tests continues to advance to next confining pressure.

It should be noted that the RCTS device was employed to investigate the test and material parameters with small-diameter specimens in the nonlinear strain ranges. These test parameters include: (1) shearing strain amplitude, (2) total isotropic confining pressure, (3) overconsolidation ratio, (4) number of loading cycles, and (5) excitation frequency. Material parameters investigated with the RCTS device are: (1) waste composition (only for 100% soil-size MSW material), (2) water content, (3) total unit weight, and (4) particle size.

11.2.2 Testing with the LSRC Device

High-amplitude RC tests were performed with large-diameter specimens at their natural conditions. These tests were performed at multiple confining pressures and the confining pressure levels are given in Table 10.2. Unlike the RCTS device, no high-amplitude torsional shear tests are available in the LSRC device. Thus, HARC tests are performed subsequently after the LARC tests.

Similarly, as shown in Figure 10.3, LARC tests are performed to establish the baseline measurements of G_{max} and D_{min} for the comparison of those values after the HARC tests have been performed.

HARC tests are conducted with increasing shearing strains and LARC tests are also performed immediately to check how much change in the MSW skeleton was induced due to the HARC tests. After the HARC tests, each specimen was confined at the same confining pressure for an additional twelve to 24-hours in an attempt to allow the specimen regain its original state in terms of G_{max} and D_{min}. Once the LARC and HARC tests are completed at a given confining pressure, then RC tests continue to go to next confining pressure.

Table 11.2 Isotropic Confining Pressures Used in High-Amplitude RC Tests for Large-Diameter 100 %, 76 %, and 62 % Soil-Sizes Fresh MSW Specimens in the LSRC Device

Specimen ID	Isotropic Confining Pressure
	High-Amplitude RC Tests, psi (kPa)
MSW1FNL2⌂	2.5, 11, 40, 11*, 2.5* (17, 76, 276, 76, 17)
MSW2FNL4□	2.5, 11, 40 (17, 76, 276)
MSW3FNL2	2.5, 11, 40, 11*, 2.5* (17, 76, 276, 76, 17)
MSW4FNL3◊	2.5, 11, 40, 11*, 2.5* (17, 76, 276, 76, 17)
MSW5FNL2	2.5, 11, 40, 11* (17, 76, 276, 76)
MSW6FNL4	2.5, 11, 40 (17, 76, 276)
MSW7FNL3	2.5, 11 (17, 76)
MSW8FNL4	2.5, 11, 40
MSW9FNL1Δ	2.5, 11, 40

Notes: * denotes unloading stage.

Δ1 denotes specimen reconstituted with material passed the 3/8-in. (9.5-mm) sieve.

⌂2 denotes specimen reconstituted with material passed the ¾-in. (19.1-mm) sieve.

◊3 denotes specimen reconstituted with paper, soft plastic, and wood.

□4 denotes specimen reconstituted with paper, soft plastic, wood, and gravel in the specimen ID.

As mentioned previous chapter, with a difficulty in assembling split mold around specimen, the effect of hydration on large-diameter specimens was not able to study. in addition, the effects of number of loading cycles and excitation frequency were not evaluated since the LSRC device could not perform the TS tests.

The LSRC device was employed to investigate the test and material parameters with large-diameter specimens in the nonlinear strain ranges. These test parameters

include: (1) shearing strain amplitude, (2) total isotropic confining pressure, and (3) overconsolidation ratio. Material parameters investigated with the LSRC device are: (1) waste composition (all groups of MSW material) and (2) particle size.

11.3 TEST PARAMETERS AFFECTING G AND D

11.3.1 Test Parameters Investigated

To investigate the effect of test parameters affecting G and D of MSW specimens in the nonlinear strains, both the RCTS and LSRC devices were employed. Test parameters investigated in the RCTS device include: (1) shearing strain amplitude, (2) total isotropic confining pressure, (3) overconsolidation ratio, (4) number of loading cycles, and (5) excitation frequency. However, in the LSRC device, test parameters investigated were: (1) shearing strain amplitude, (2) total isotropic confining pressure, and (3) overconsolidation ratio.

11.3.2 Shearing Strain Amplitude

The variation in G with shearing strain upon small- and large-diameter for fresh MSW specimens obtained from RCTS and LSRC tests at a confining pressure of 11 psi (76 kPa) is shown in Figure 11.1. This figure shows a typical variation in G with shearing strain for 100 % soil-size specimens that were reconstituted with material passed the 3/8-in. (9.5-mm) sieve measured in the RCTS and LSRC devices. Small-diameter specimens are represented by open symbols, whereas large-diameter specimen is represented by open symbol with an "x" in the symbol.

As discussed in Section 10.3.2, same definition on the γ_t^e was applied to fresh MSW specimens. As a result, the amplitudes of γ_t^e for Specimen MSW1FNS1, MSW3FNS1, and MSW9FNL1 are 0.002 %, 0.002 %, and 0.004 %, respectively.

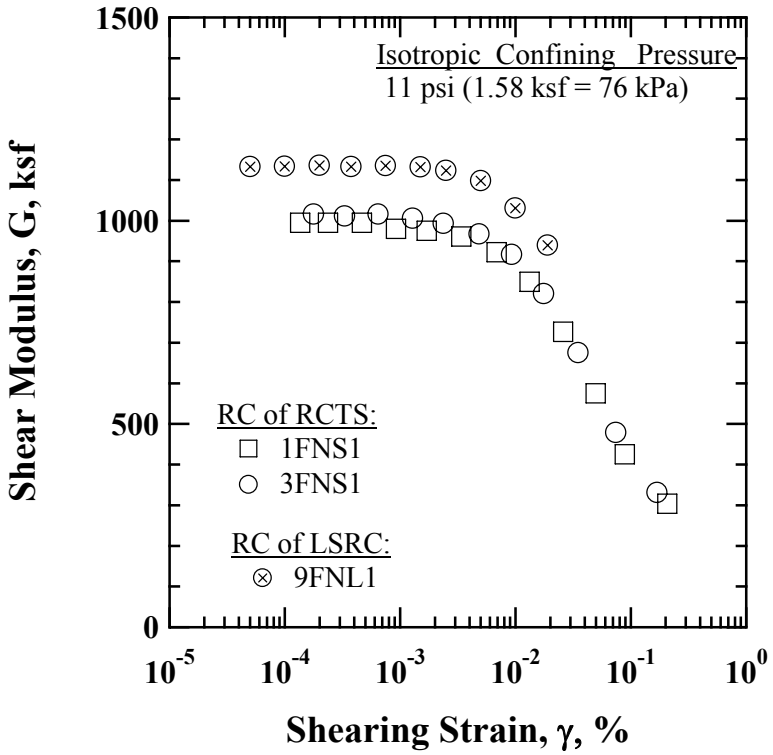

Figure 11.1 Comparison of the Variation in Shear Modulus with Shearing Strain for 100 % Soil-Size Fresh MSW Specimens Reconstituted with Material Passed the 3/8-in. (9.5-mm) Sieve in the RCTS and LSRC devices

Hence, G is constant below γ_t^e and equals to G_{max}. Beyond these shearing strains, G decreases with increasing shearing strain.

The variation in G with shearing strain for Specimen 3FNS1 obtained from RC and TS tests in the RCTS device is presented in Figure 11.2. RC data are denoted by open symbol and TS data are denoted by solid triangular symbols. The measurements were performed at a confining pressure of 11 psi (76 kPa). The values of γ_t^e for Specimen 3FNS1 of RC and TS tests are 0.002 % and 0.001 %, respectively. Thus, as seen in Figure 11.2, G is constant below γ_t^e and decreases with increasing shearing strain for both RC and TS tests. There is a difference between the absolute value of G_{max} in

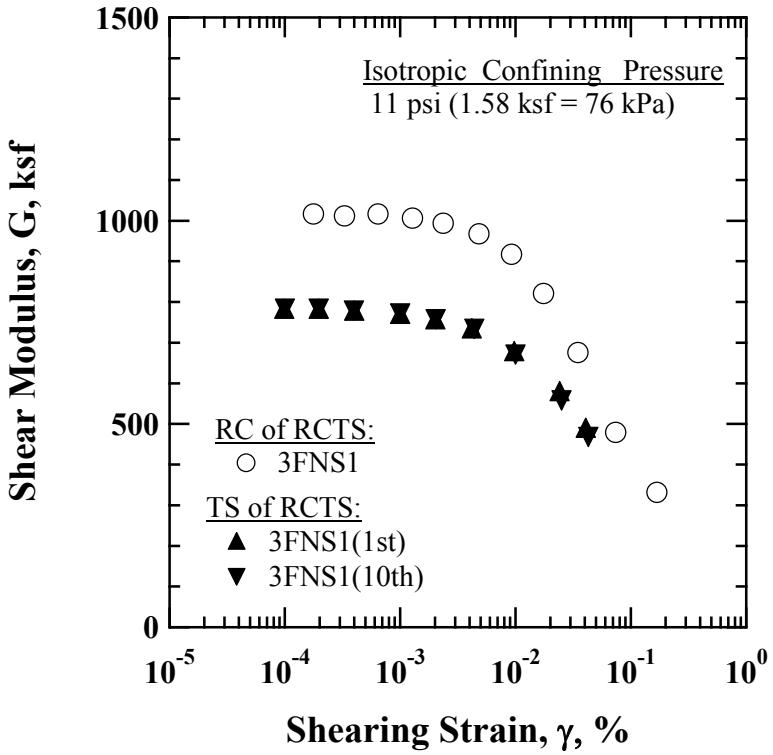

Figure 11.2 Comparison of the Variation in Shear Modulus with Shearing Strain for 100 % Soil-Size Specimen MSW3FNS1 Obtained from RC and TS Tests in the RCTS Device

the small-strain range in RC and TS tests due mainly to different excitation frequency. The excitation frequency of RC tests is relatively higher than TS tests. It is interesting to see that, similar to old MSW, the difference between RC and TS tests becomes smaller with increasing shearing strain, resulting in a decrease in frequency effect because of number of cycles.

A typical variation in G with shearing strain for small- and large-diameter fresh MSW specimens reconstituted with material passed the ¾-in. (19.1-mm) sieve measured in the RCTS and LSRC devices is shown in Figure 11.3. The measurements were performed at a confining pressure of 11 psi (76 kPa).

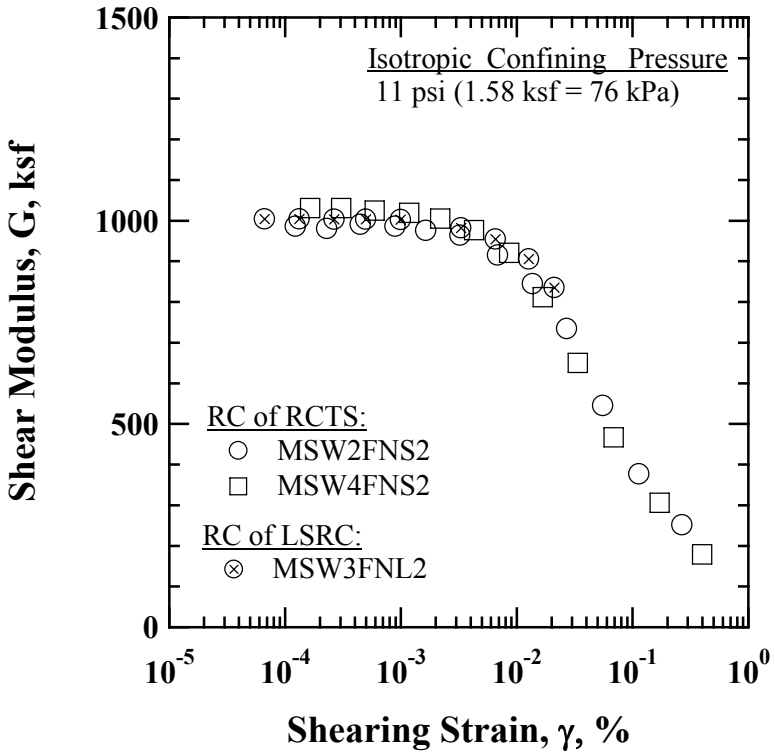

Figure 11.3 Comparison of the Variation in Shear Modulus with Shearing Strain for 100 % Soil-Size Fresh MSW Specimens Reconstituted with Material Passed the ¾-in. (19.1-mm) Sieve in the RCTS and LSRC devices

The values of γ_t^e for Specimens 2FNS2, 4FNS2, and 3FNL2 are equal to 0.003 %, 0.002 %, and 0.003 %, respectively. As seen in the figure, G is constant below these values, whereas G decreases significantly with increasing shearing strain.

A typical variation in D with shearing strain upon small- and large-diameter specimens for fresh MSW obtained from RCTS and LSRC tests is illustrated in Figure 11.4. Entire specimens were reconstituted with material passing the 3/8-in. (9.5-mm) sieve. The measurements were performed at a confining pressure of 11 psi (76 kPa). The values of γ_t^e for Specimens 1FNS1, 3FNS1, and 9FNL1 are 0.002 %, 0.002 %, and 0.004 %, respectively. As seen in the figure, the values of D is constant below γ_t^e, but

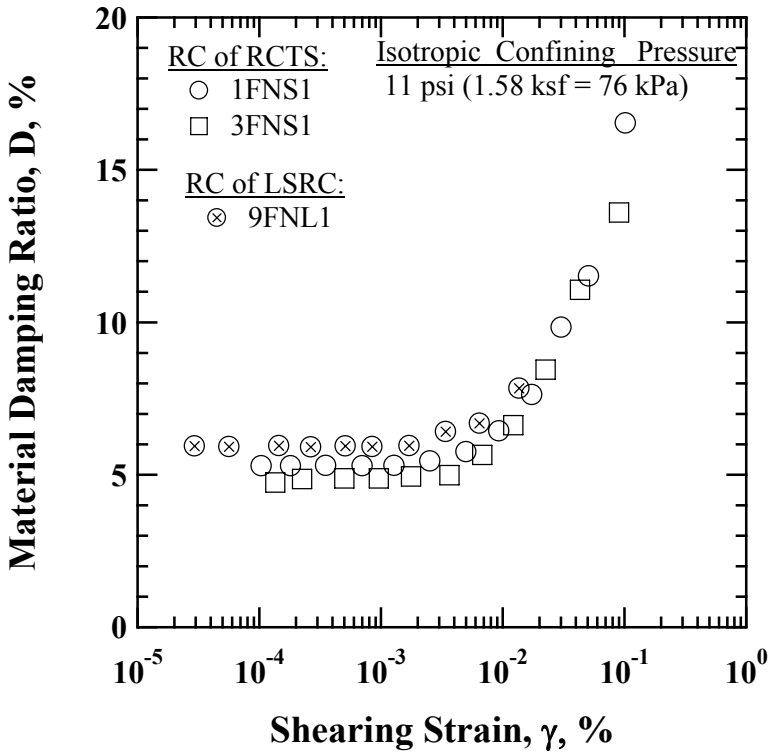

Figure 11.4 Comparison of the Variation in Material Damping Ratio with Shearing Strain for 100 % Soil-Size Fresh MSW Specimens Reconstituted with Material Passed the 3/8-in. (9.5-mm) Sieve in the RCTS and LSRC devices

increase significantly with increasing shearing strain for both small- and large-diameter specimens. There is a difference in D at small-strain range between small- and large-diameter specimens due to the excitation frequency.

The variation in D with shearing stain for 100 % soil-size fresh MSW Specimen 3FNS1 obtained from RC and TS tests is presented in Figure 11.5. The data from RC test are represented by open symbol and the data from TS test are represented by solid triangular symbols. The values of γ_t^e for Specimen 3FNS1 obtained from RC and TS tests are 0.002 % and 0.001 %, respectively. Similarly, D is constant these strains. However once the shearing strain exceeds these values, D starts to increases with

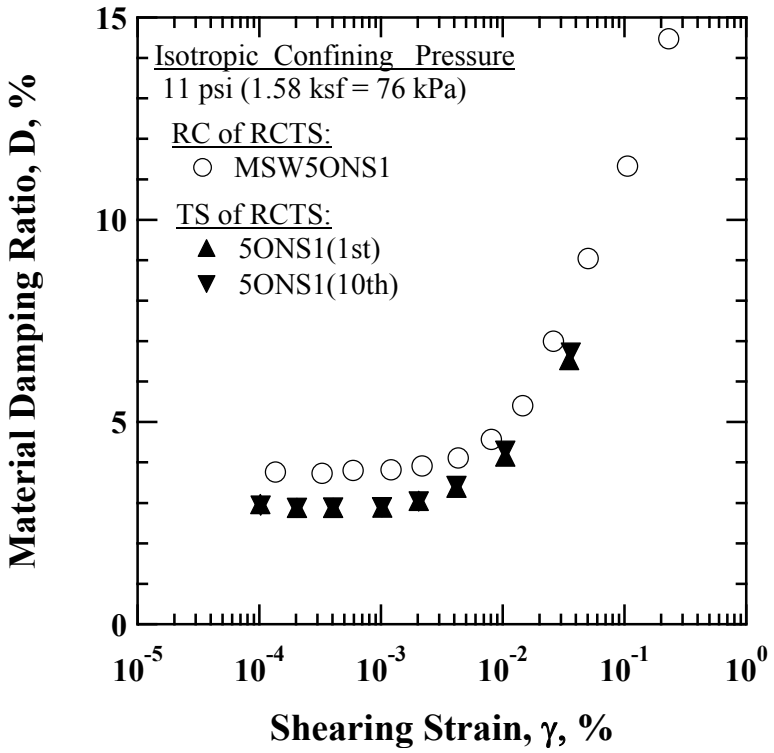

Figure 11.5 Comparison of the Variation in Material Damping Ratio with Shearing Strain for 100 % Soil-Size Specimen MSW3FNS1 Obtained from RC and TS Tests in the RCTS Device

increasing shearing strain. As can be seen, there is a difference in the values of D between RC and TS tests, resulting from a frequency effect. it is interesting to observe that the difference between RC and TS tests created by the frequency effect becomes smaller with increasing shearing strain mainly due to number of cycles.

A typical variation in D with shearing strain for 100 % soil-size Specimens 2FNS2, 4FNS2, 3FNL2, and 5FNL2 measured in the RCTS and LSRC devices is presented in Figure 11.6. Small-diameter specimens are represented by open symbols and large-diameter specimens are represented by open symbols with an "x" in the symbol. These specimens were constructed with material passing the ¾-in. (19.1-mm)

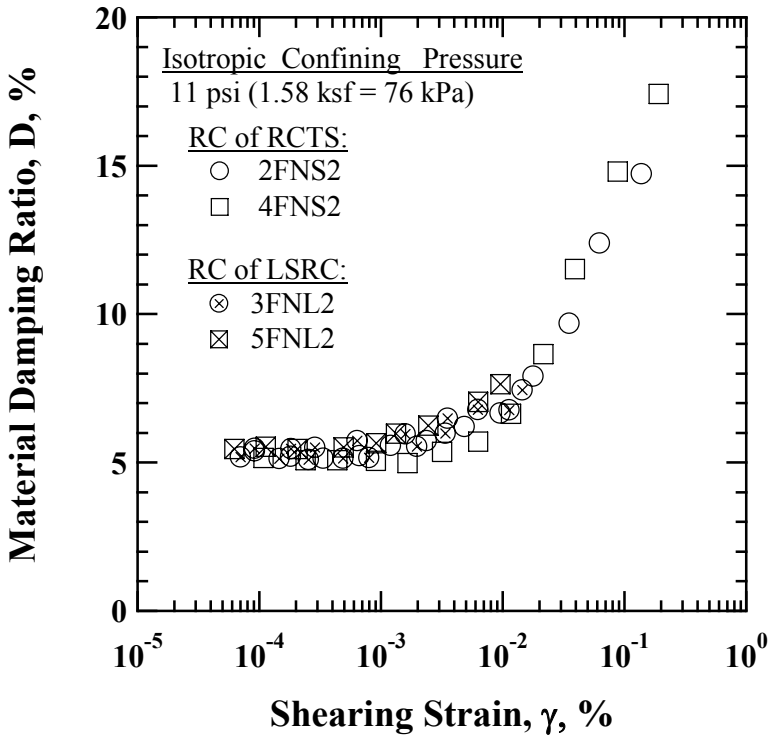

Figure 11.6 Comparison of the Variation in Material Damping Ratio with Shearing Strain for 100 % Soil-Size Fresh MSW Specimens Reconstituted with Material Passed the ¾-in. (19.1-mm) Sieve in the RCTS and LSRC devices

sieve. The values of γ_t^e for these specimens are 0.003 %, 0.002 %, 0.003 %, and 0.003 %, respectively. Again, D is constant below these values and starts to increase above these strains significantly. As seen in Figure 11.6, the variation in D with shearing strain for small- and large-diameter specimens is quite similar.

11.3.3 Total Isotropic Confining Pressure

A typical variation in G from RCTS tests with shearing strain at given confining pressures for Specimen MSW2FNS2 is shown in Figure 11.7. Open symbols indicate the data from RC tests and solid symbols indicate the data from TS tests. The absolute differences between RC and TS tests are due to frequency effect. As seen in Figure

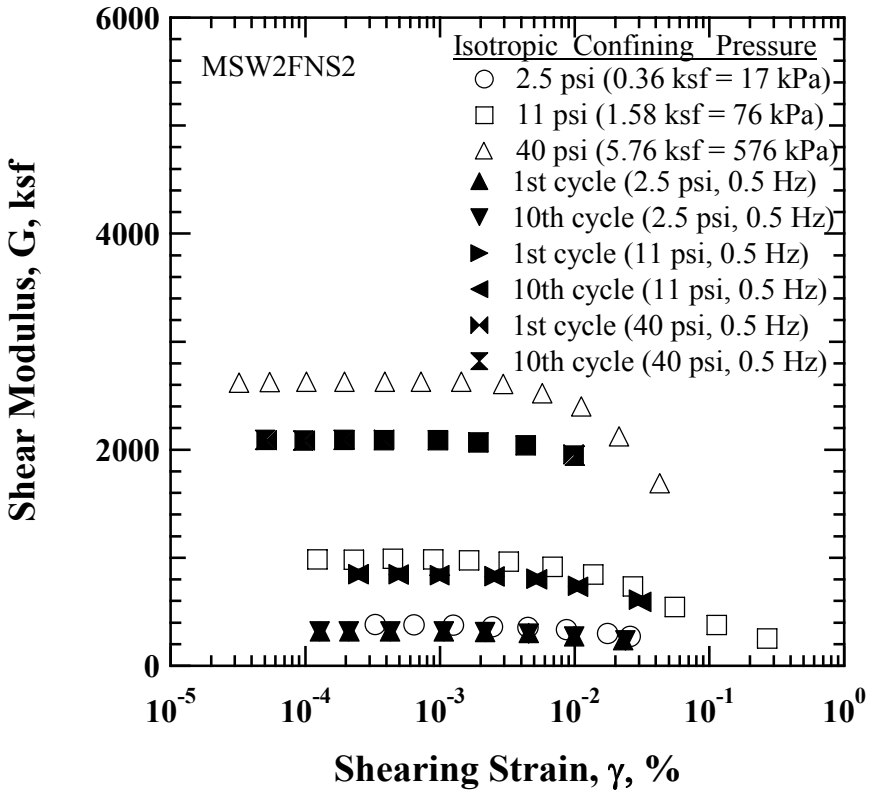

Figure 11.7 Comparison of the Variation in Shear Modulus with Shearing Strain and Isotropic Confining Pressures from RC tests for Specimen MSW2FNS2 Specimen (100 % Soil-Size Material)

11.7, the increase in G is significant with increasing confining pressure. The difference between RC and TS measurements produced by the frequency effect tends to disappear with increasing shearing strain. The values of γ_t^e, when nonlinear behavior begins to occur, increase with increasing confining pressure. As will be seen, this can be identified more clearly in the plot of normalized shear modulus with shearing strain, as discussed below.

The variation in G/G_{max} is presented in Figure 11.8. The G/G_{max} – log γ curves shift slightly to higher strains as confining pressure increases, indicating that nonlinear

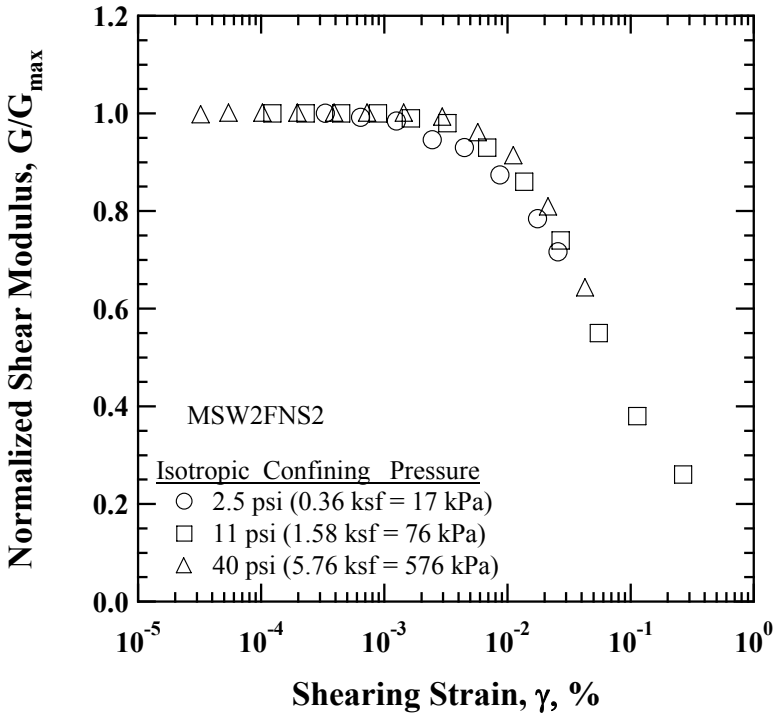

Figure 11.8 Comparison of the Variation in Normalized Shear Modulus with Shearing Strain and Isotropic Confining Pressures from RC tests for Specimen MSW2FNS2 Specimen (100 % Soil-Size Material)

behavior of fresh MSW becomes slightly more linear with increasing confining pressure.

As shown in Figure 11.8, the values of γ_t^e increase with increasing confining pressure and those values are given in Table 11.3. The amplitude of γ_t^e is defined as a shearing strain corresponding to G/G_{max} equal to 0.98. It should be noted that the values of γ_t^e corresponding to each confining pressure were interpolated with an assumption that the variation between data points around G/G_{max} equal to 0.98 is linear.

To investigate the effect of total isotropic confining pressure of other fresh MSW Groups (e.g., 100 %, 76 %, 62 %, and 14 % Groups), the values of elastic threshold shearing strain were calculated. The variation in γ_t^e with different weight percentage of soil-size material groups is shown in Figure 11.9.

Table 11.3 Values of Elastic Threshold Shearing Strain (γ_t^e) for G with Confining Pressures for Specimen MSW2FNS2 (100 % Soil-Size Material)

Confining Pressure, psi (kPa)	γ_t^e (%)
2.5 (17)	0.002
11 (76)	0.003
40 (276)	0.004

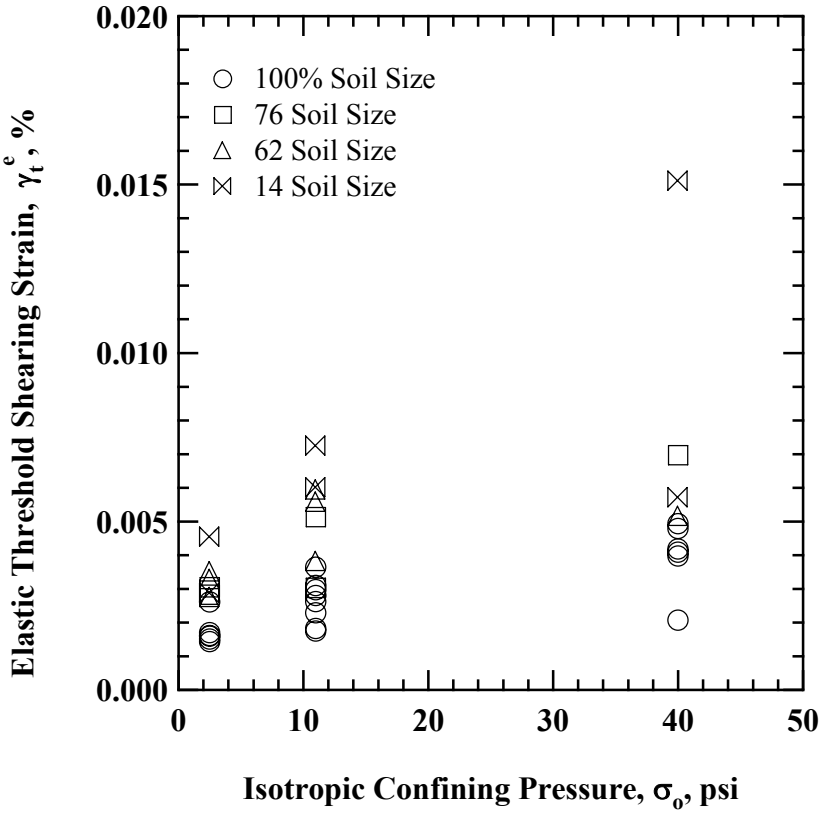

Figure 11.9 Comparison of the Variation in Elastic Threshold Shearing Strain with Isotropic Confining Pressures from RC tests for 100 %, 76 %, 62 %, and 14 % Soil-Size Fresh and Mixed MSW Groups

As seen in the figure, the amplitude of elastic threshold shearing strain increases with increasing confining pressure. Also, the values of γ_t^e increases with decreasing weight percentage of soil-size material, indicating that normalized shear modulus exhibits more elastic behavior with increasing confining pressure and decreasing weight percentage of soil-size material.

The variation in D obtained from RCTS tests with shearing strain is shown in Figure 11.10. The RC data are represented by open symbols and TS data are denoted by solid symbols. As shown in Figure 11.10, the values of D are constant in the range less than γ_t^e and equal to D_{min}. D_{min} values are not sensitive to the variation of confining pressure. In addition, D_{min} values exhibit also independent of the number of loading cycles measured in the TS tests at the first and tenth cycles. Beyond shearing strain larger than 0.006 %, D increases dramatically with increasing shearing strain. The effect of confining pressure is quite small; D moves downward slightly as confining pressure increases.

The amplitudes of γ_t^e for D were calculated for each confining pressure and those values are given in Table 11.4. As seen in Table 11.4, the amplitude of γ_t^e increases with increasing confining pressure

11.3.4 Overconsolidation Ratio

A set of high-amplitude RC tests in the loading and unloading sequences were performed to investigate the effect of OCR at a given confining pressure for 100 % soil-size fresh MSW. The variation in G and G/G_{max} with shearing strain at a confining pressure of 11 psi (76 kPa) for Specimen MSW4FNL3 is shown in Figures 11.11 (a) and (b), respectively. As shown in Figure 11.11 (a), G increases with an increase in the magnitude of OCR approximately by a factor of two. Substantial decrease in voids

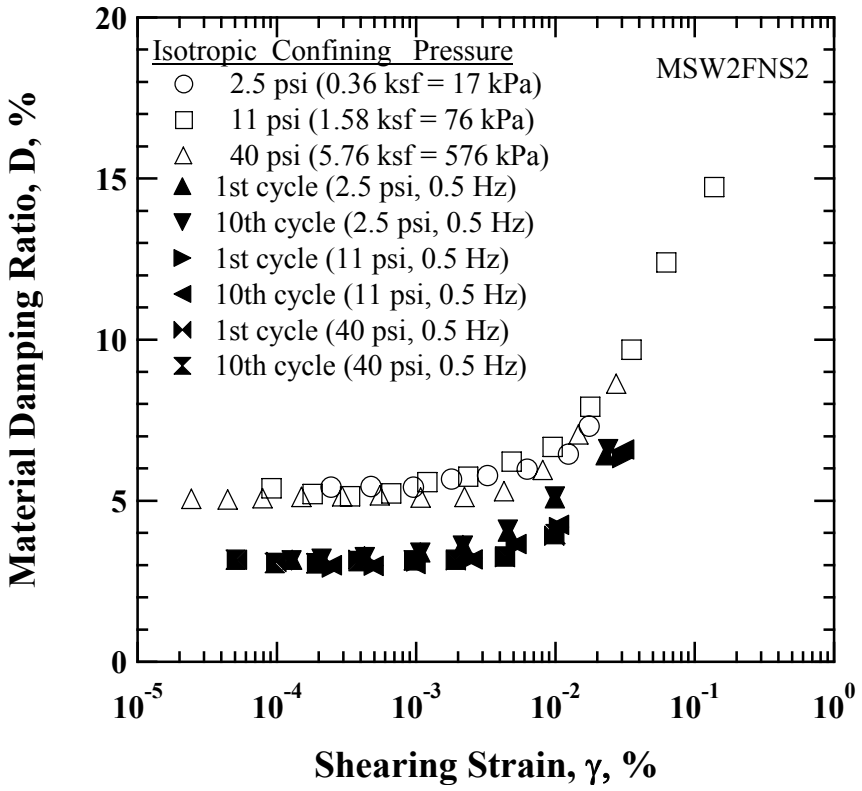

Figure 11.10 Comparison of the Variation in Material Damping Ratio with Shearing Strain and Isotropic Confining Pressures from RCTS tests for Specimen MSW2FNS2 (100 % Soil-Size Material)

Table 11.4 Values of Elastic Threshold Shearing Strain (γ_t^e) for D with Confining Pressures for Specimen MSW2FNS2 (100 % Soil-Size Material)

Confining Pressure, psi (kPa)	γ_t^e (%)
2.5	0.001
11	0.002
40	0.005

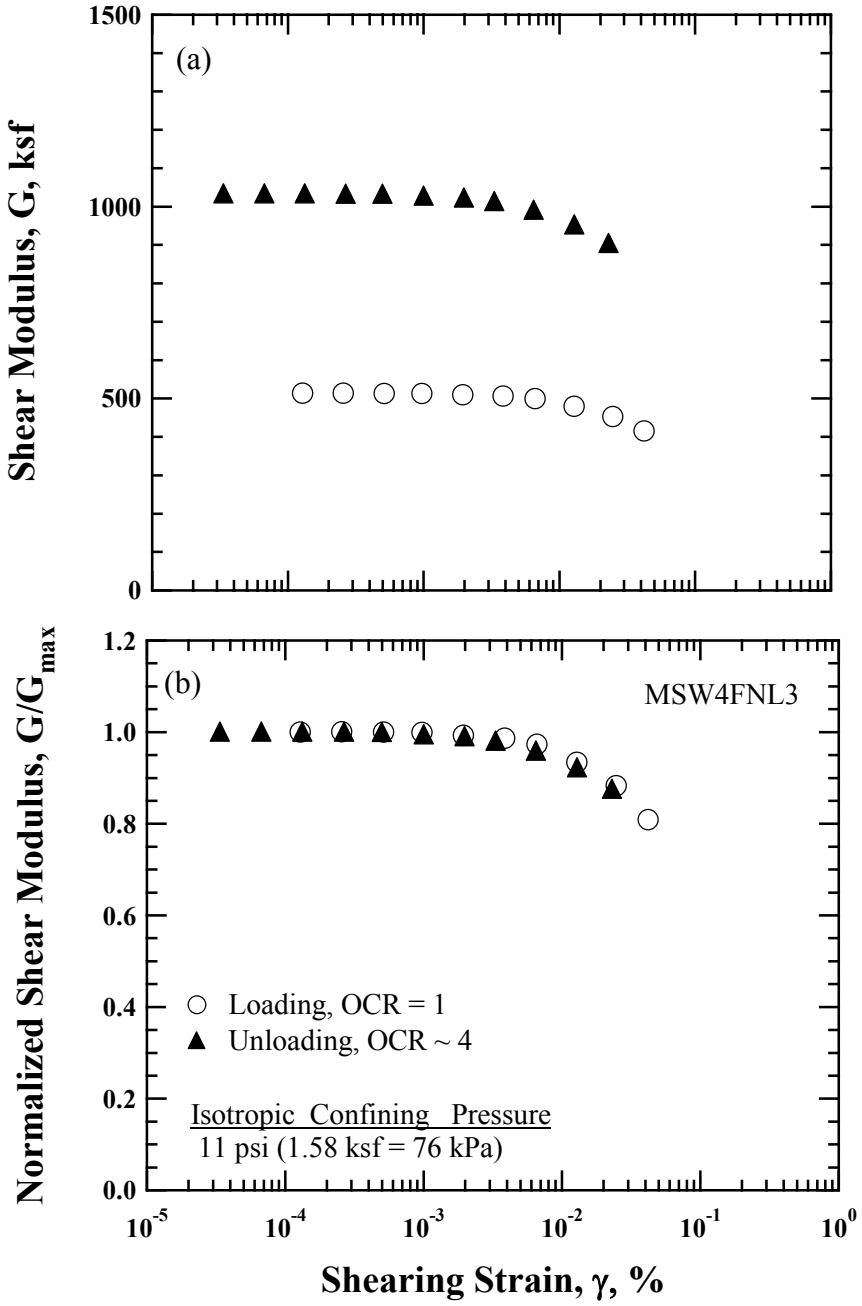

Figure 11.11 Comparison of the Variation in (a) Shear Modulus and (b) Normalized Shear Modulus with Shearing Strain upon Loading and Unloading Sequences from RC tests for Specimen MSW4FNL3 (100 % Soil-Size Material)

spaces can be attributed to such an increase in G. The effect of OCR on the fresh MSW is also evaluated in terms of G/G_{max} and it is plotted in Figure 11.11 (b). As seen in Figure 11.11 (b), the G/G_{max} – log γ curve corresponding to OCR of about four shifts slightly to lower shearing strains. Thus, the effect of OCR is very small on G/G_{max} – log γ relationship regardless of the magnitudes of OCR for fresh MSW.

The variation in D with shearing strain for Specimen MSW4FNL3 upon different magnitudes of OCR in loading and unloading sequences is presented in Figure 11.12. The values of D at small-strain range ($\gamma < 0.002$ %) are nearly the same, implying that the values of D_{min} are not affected by the change in stress history for fresh MSW. As a result, the influence of OCR on D is small.

11.3.5 Number of Loading Cycles

The variation in G with shearing strain and for 100 % soil-size Specimen MSW1NFS1 obtained from the RC and TS tests are shown in Figure 11.13. Open symbol indicates RC data and open and solid triangular symbols denote TS data. As shown in Figure 11.13, the values of G in the shearing strain ranges ($\gamma < 0.001$ %) are constant and those are not affected by the number of loading cycles in the RC and TS tests. The effect of the number of loading cycles appears to begin at shearing strain of about 0.03 %. It can be clearly identified in the plot of normalized shear modulus, G/G_{1st}, with the number of loading cycles, which is discussed below.

To quantify the effect of the number of loading cycles on G, the values of G at give loading cycles were normalized with one obtained from the first cycle from the TS test. The variation in normalized shear modulus, G/G_{1st}, is shown in Figure 11.14. The variation in G/G_{1st} was evaluated at shearing strain amplitudes of 0.0003 %, 0.003 %, 0.01 %, and 0.03 %. Also, the numbers of loading cycles were evaluated at the first, third,

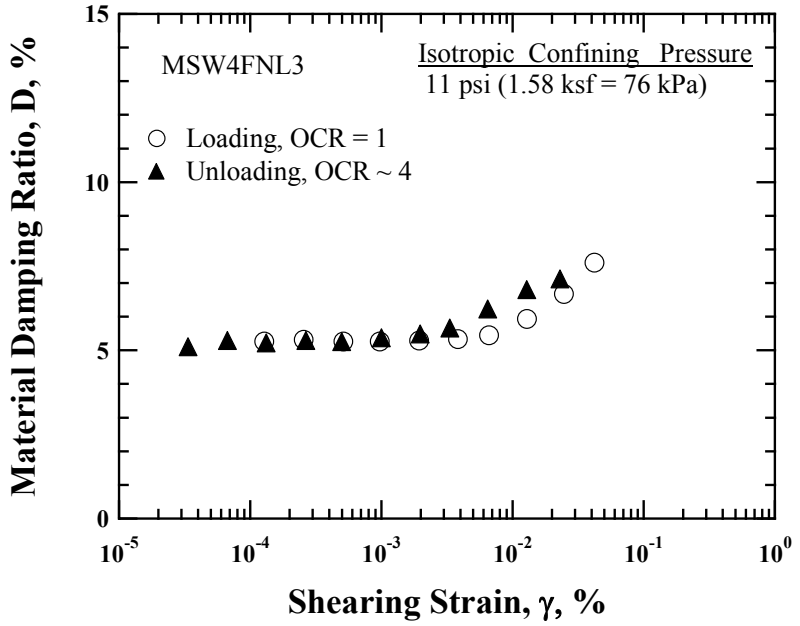

Figure 11.12 Comparison of the Variation in Material Damping Ratio with Shearing Strain upon Loading and Unloading Sequences from RC tests for Specimen MSW4FNL3 (100 % Soil-Size Material)

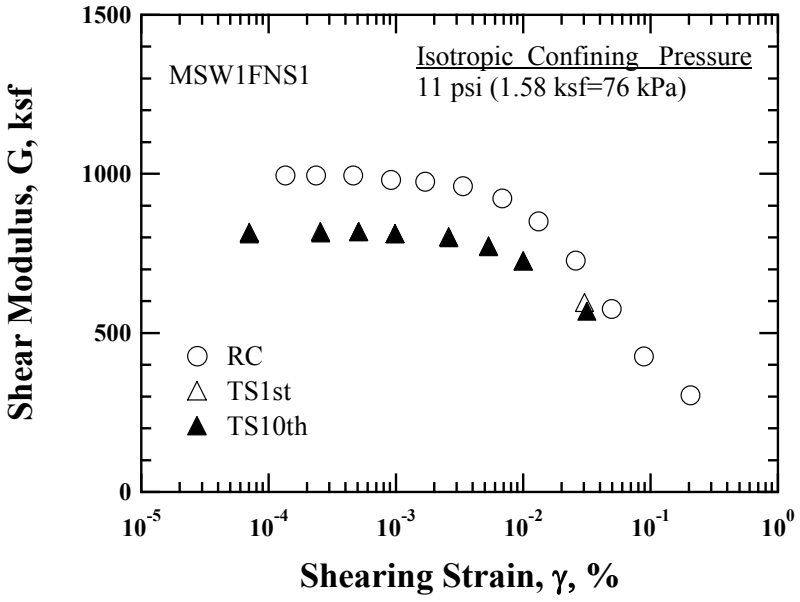

Figure 11.13 Comparison of the Variation in Shear Modulus with Shearing Strain from RCTS tests for Specimen MSW1FNS1 (100 % Soil-Size Material)

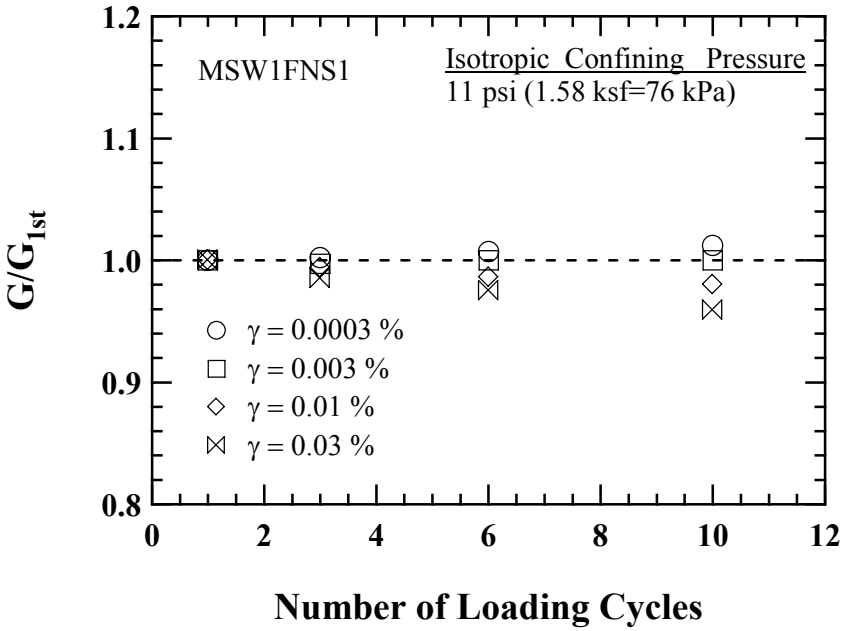

Figure 11.14 Variation in Normalized Shear Modulus, G/G_{1st}, with the Number of Loading Cycles from TS tests for Specimen MSW1FNS1 (100 % Soil-Size Material)

sixth, and tenth cycles. As can be seen in Figure 11.14, the effect of loading cycles begins obviously at a shearing strain of 0.01 %; the G/G_{1st} remains constant until shearing strain reaches 0.01 %. Shear modulus decrease gradually with increasing the number of loading cycles. The effect of the number of loading cycles starts to mobilize at a small number of cycles as shearing strain amplitude increase and it is negligible in the small-strain range less than 0.003 % (Lee et al., 2004).

The variation in D with shearing strain and the number of loading cycles for MSW1FNS1 is given in Figure 11.15. Similar to G, the values of D at shearing strains less than about 0.003 % are constant and are independent of the number of loading cycles in the RCTS tests. From the TS data, the effect of number of loading cycles begins to mobilize at shearing strain amplitude of about 0.03 %. That is, the value of D at the

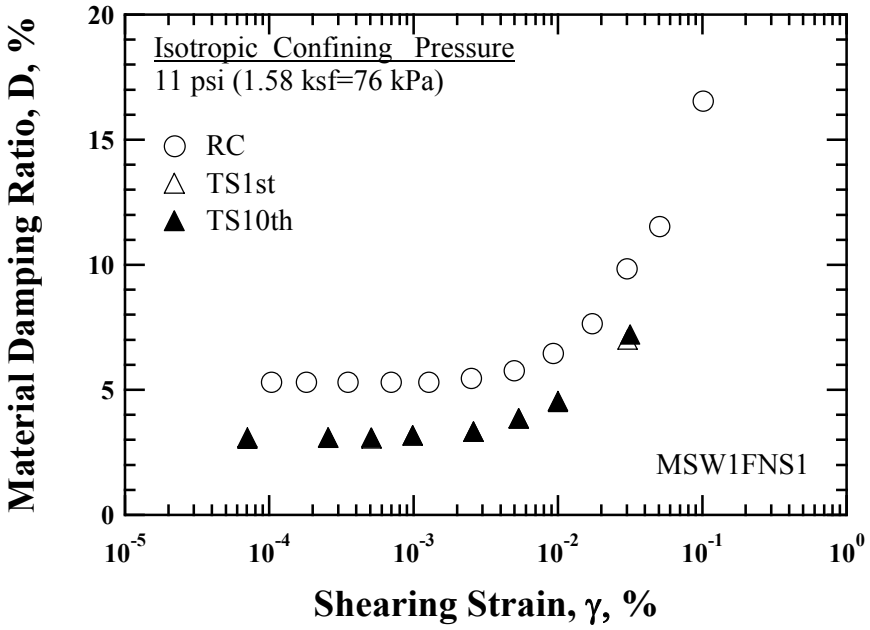

Figure 11.15 Comparison of the Variation in Material Damping Ratio with Shearing Strain from RCTS tests for Specimen MSW1FNS1 (100 % Soil-Size Material)

tenth cycle is larger than that at the first cycle.

To quantify the effect of the number of loading cycles on D, the values of D at given number of loading cycles was normalized with one at the first loading cycle. The variation in normalized material damping ratio, D/D_{1st}, with the number of loading cycles at different amplitudes of shearing strain is presented in Figure 11.16. As indicated in Figure 11.16, the values of D/D_{1st} remain almost constant until shearing strain reaches 0.01 % and the effect of the number of loading cycles begins to mobilize at a shearing strain of 0.03 %. In addition, the values of D/D_{1st} increase with increasing shearing strain. The effect of the number of loading cycles is negligible at strain range less than 0.01 %. This effect begins to mobilize at an intermediate number of cycles as shearing strain increase.

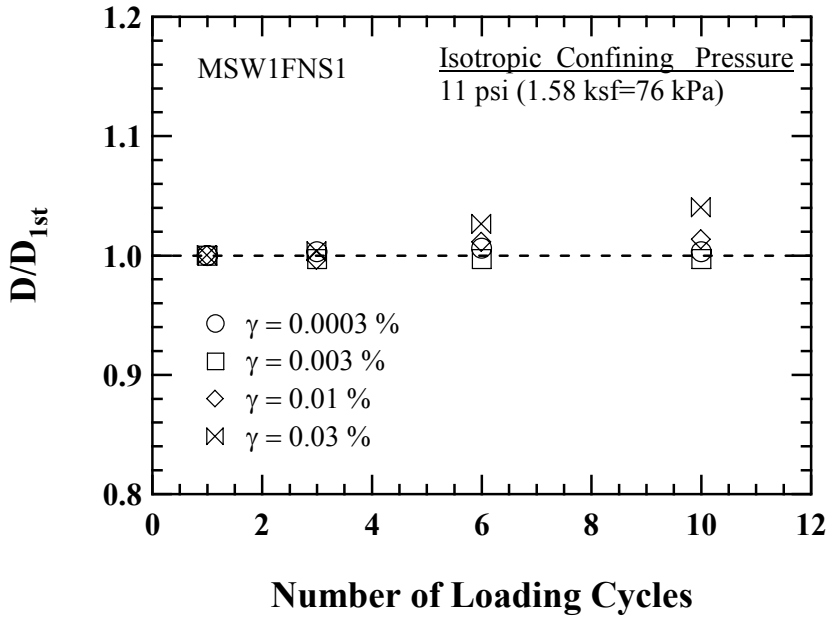

Figure 11.16 Variation in Normalized Material Damping Ratio, D/D_{1st}, with the Number of Loading Cycles from TS tests for Specimen MSW1FNS1 (100 % Soil-Size Material)

11.3.6 Excitation Frequency

In order to study the effect of excitation frequency on G and D in the nonlinear strain range, a series of RCTS and LSRC tests were performed on small- and large-diameter specimens. These specimens were Specimens MSW1FNS1, MSW2FNS2, MSW3FNS1, MSW4FNS2, MSW3FNL2, MSW5FNL2, and MSW9FNL1. The frequency variation tests were performed at a confining pressure of 11 psi (76 kPa). The variation in G with excitation frequency at given shearing strains of 0.01 % and 0.04 % is shown in Figure 11.17. The values of G measured from the LSRC test are indicated by "Fr-Fr". As seen in the figure, G – log f relationship increases linearly with increasing excitation frequency due to frequency effect; a faster application of loadings produces a higher strength of MSW specimens. G decreases with an increase in strain amplitude,

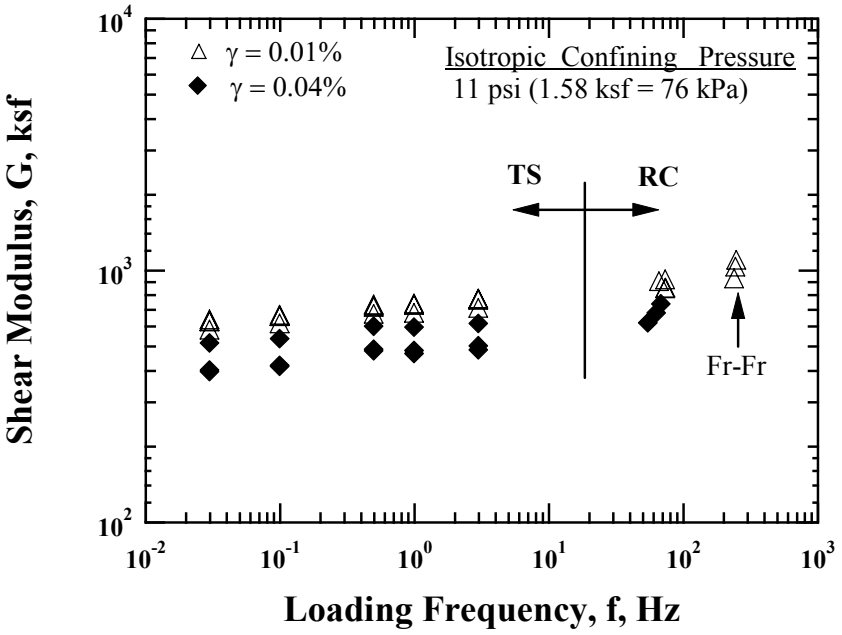

Figure 11.17 Variation in Shear Modulus with Excitation Frequency from the RCTS and LSRC Tests for 100 % Soil-Size Fresh MSW in the nonlinear strain range

implying the nonlinearity of MSW at higher shearing strains.

In order to quantify the effect of excitation frequency, the values of G were normalized with shear modulus obtained at a frequency of 1 Hz in the TS tests. It is necessary to note that no TS test was available for LSRC device such that the values of G obtained from the LSRC tests were normalized with averaged value of G from the TS tests measured at a frequency of 1 Hz. The variation in normalized shear modulus, $G/G_{f=1Hz}$, with excitation frequency is shown in Figure 11.18. The data were fitted using least-squares method and were represented by a dashed line. The equation is expressed by:

$$\frac{G}{G_{f=1Hz}} = 0.13 \times \log(\text{Frequency}) + 1.0 \qquad (11.1)$$

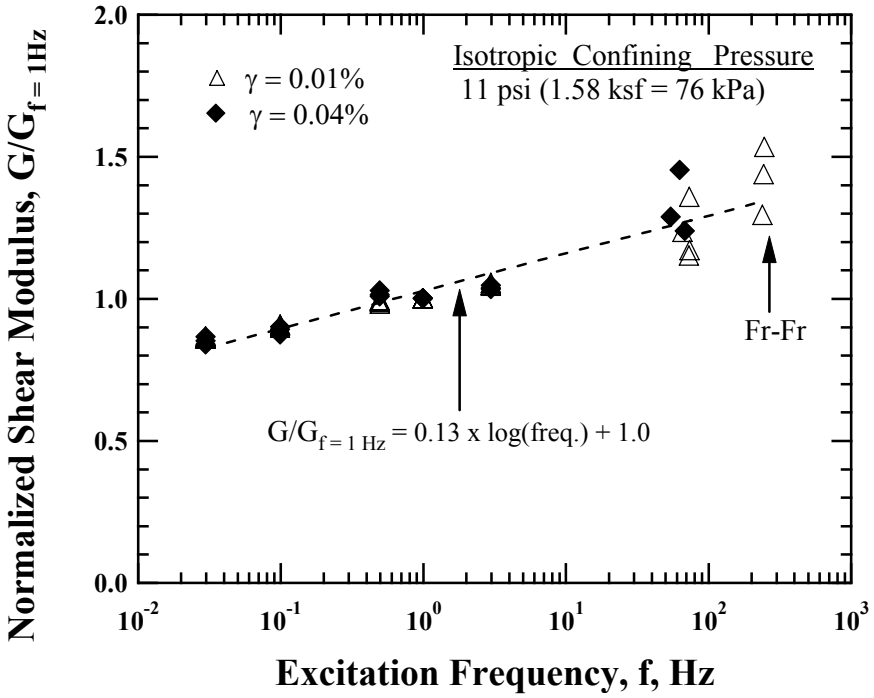

Figure 11.18 Variation in Normalized Shear Modulus with Excitation Frequency from the RCTS and LSRC Tests for 100 % Soil-Size Fresh MSW in the nonlinear strain range

where,

G is a shear modulus measured at a given frequencies, and

$G_{f=1Hz}$ is a shear modulus measured at a frequency of 1Hz.

As shown in Figure 11.18, the $G/G_{f=1Hz}$ – log f relationship increases linearly with increasing excitation frequency. It is interesting to note that the slope of the $G/G_{f=1Hz}$ – log f relationship is somewhat higher, when compared with the old MSW in the nonlinear strain range. This indicates that fresh MSW exhibits more viscous characteristic than the old MSW. The variation in G amounts to a factor of about 1.7 when the excitation frequency varies by approximately four orders of magnitude, from 0.03 Hz to 246 Hz,

thus, implying comparatively a small effect of excitation frequency on G. Based on this observation, it can be noted that variation in G with excitation frequency in the nonlinear strain range is slightly more pronounced that it is in the small-strain range.

The variation in D with excitation frequency for 100 % soil-size material fresh MSW specimens at different amplitudes of shearing strain is presented in Figure 11.19. The values of D measured from the LSRC tests are given and are denoted by "Fr-Fr". As seen in the figure, the values of D increases with decreasing excitation frequency in the strain range less than 1 Hz due to creep, whereas the values of D increase with increasing excitation frequency in the strain range larger than 1 Hz due to the frequency effect. As shearing strain amplitude increases, an increase in the values of D at lower strain ranges becomes larger.

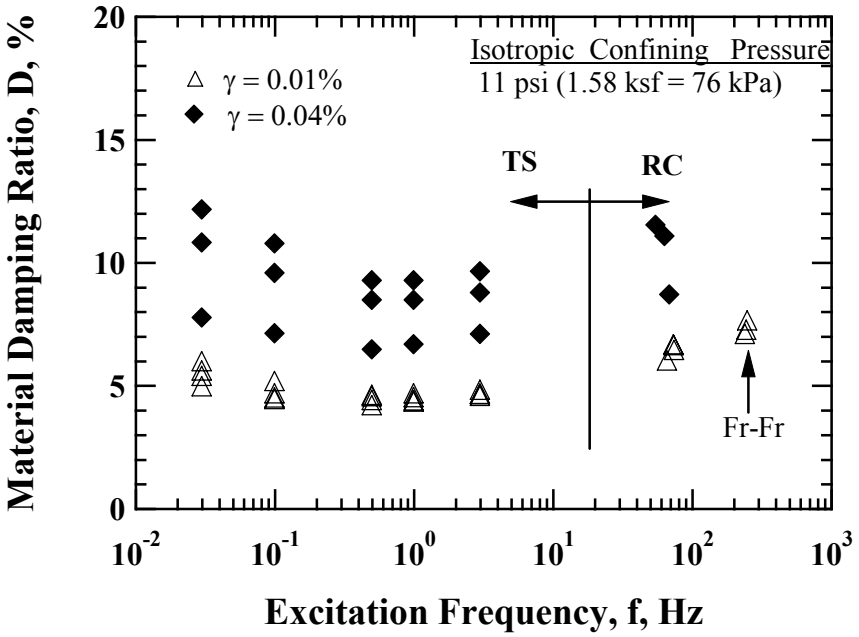

Figure 11.19 Variation in Material Damping Ratio with Excitation Frequency from the RCTS and LSRC Tests for 100 % Soil-Size Fresh MSW in the nonlinear strain range

To quantify the effect of excitation frequency on D, the values of D at given excitation frequencies were normalized with the value of D obtained at a frequency of 1 Hz. The variation in normalized material damping ratio with excitation frequency for 100 % soil-size fresh MSW specimens is shown in Figure 11.20. The values of D were fitted using least-squares method as a form of second-order of a polynomial function. This fitted line is represented by a dashed line. The equation is expressed by:

$$\frac{D}{D_{f=1Hz}} = 0.11 \times \log(\text{Frequency})^2 - 0.01 \times \log(\text{Frequency}) + 1.0 \qquad (11.2)$$

where,

D is a material damping ratio measured at a given frequencies, and

$D_{f=1Hz}$ is a material damping ratio measured at a frequency of 1Hz.

As shown in Figure 11.20, the values of normalized material damping ratio increase with decreasing excitation frequency in the strain range less than 1 Hz due to creep. The amount of increase in average is about a factor of 1.23 from the lowest frequency (0.03 Hz) to 1 Hz. On the other hand, the values of normalized material damping ratio increase with increasing excitation frequency due to the frequency effect. The increase in normalized material damping ratio in average amounts a factor of 1.64 from the excitation frequency of 1 Hz to 245 Hz. It is clear to observe the pattern, as mentioned previous section, that the increase in normalized material damping ratio is somewhat larger at lower excitation frequencies as shearing strain increases. However, as excitation frequency increases, the increase in normalized material damping ratio appears to be smaller at larger strain amplitude.

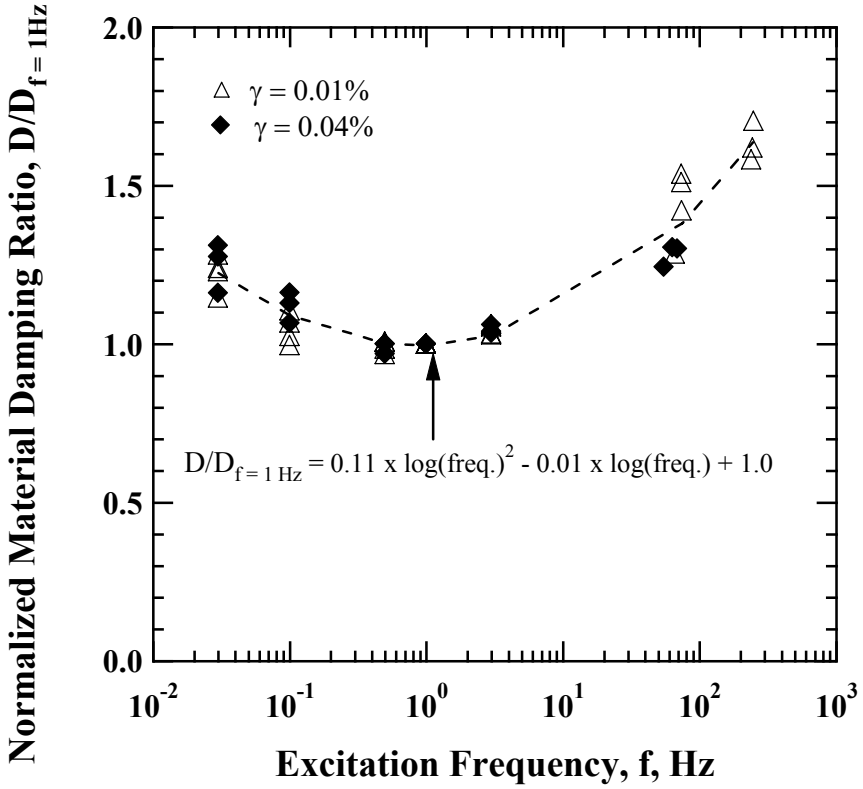

Figure 11.20 Variation in Normalized Material Damping Ratio with Excitation Frequency from the RCTS and LSRC Tests for 100 % Soil-Size Fresh MSW in the nonlinear strain range

11.4 MATERIAL PARAMETERS AFFECTING G AND D

11.4.1 Material Parameters Investigated

To investigate the effect of material parameters affecting G and D of MSW specimens in the nonlinear strains, both the RCTS and LSRC devices were employed. Material parameters investigated in the RCTS device include: (1) water content, (2) total unit weight, and (3) particle size. However, in the LSRC device, material parameters investigated were waste composition.

11.4.2 Waste Composition

Considering the nature of MSW, it is apparent that waste composition has an impact on the nonlinear dynamic behavior of fresh MSW. The variations in G and G/G_{max} with shearing strain of different weight percentages of soil-size material are shown in Figures 11.21 (a) and (b), respectively. Specimen MSW2ML4 was reconstituted with a mixture of the paper of the old and fresh MSW. The test result was compared at a confining pressure of 11 psi (76 kPa).

As shown in Figure 11.21 (a), G is constant and equal to G_{max} in the strain range less than about 0.002 %. As weight percentage of soil-size material decreases, G-log γ curves shift further to higher strains, which can be more easily identified in the G/G_{max}-log γ curves, as discussed in below. Figure 11.21 (b) shows that the G/G_{max}-log γ curves shift further to higher strains as weight percentage of soil-size material decreases, indicating that MSW specimen with the lowest weight percentage exhibits more elastic behavior. A majority of paper, wood and soft plastic in the MSW specimens lead to the mobilization of this elastic characteristic.

The variation in D with shearing strain upon the different weight percentages of soil-size material is presented in Figure 11.22. The values of D in the small-strain range ($\gamma <$ 0.005 %) are nearly the same regardless of the weight percentage of soil-size material. It is interesting to observe that substantial difference in absolute value in the variation of G does not exist in the variation in D at small-strain range, indicating that the variation of material damping ratio is independent of their initial conditions such as total unit weight, water content, and weight percentage of soil-size material. However, after shearing strain of about 0.005 %, the D - log γ curves begin to separate with different weight percentages of soil-size material. In other words, as weight percentage of soil-size material decreases, the D - log γ curves shift to higher strains.

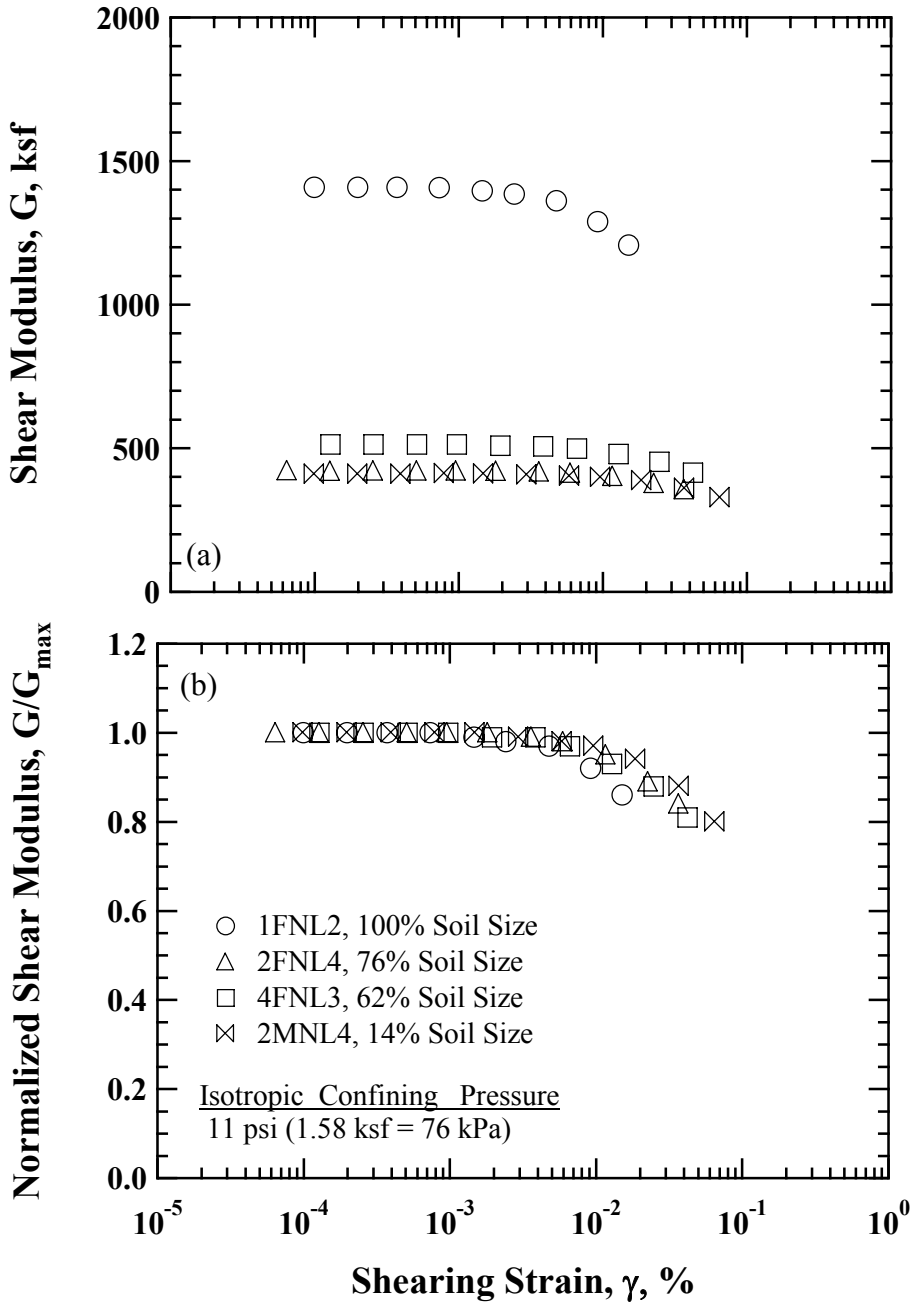

Figure 11.21 Comparison of the Variation in (a) Shear Modulus and (b) Normalized Shear Modulus with Shearing Strain from LSRC Tests upon Different Weight Percentages of Soil-Size Fresh and Mixed MSW Specimens

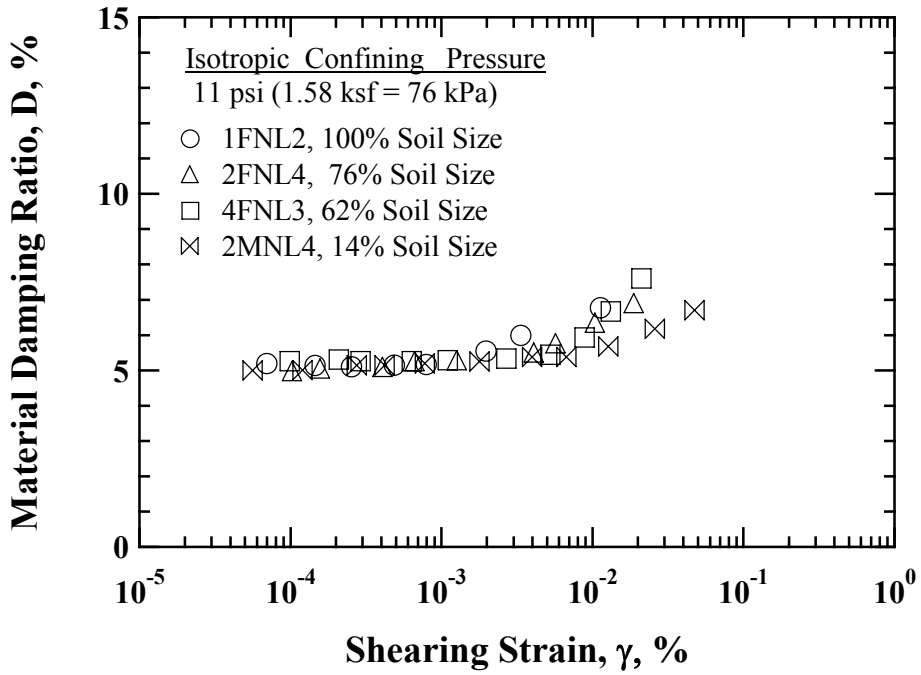

Figure 11.22 Comparison of the Variation in Material Damping Ratio with Shearing Strain from LSRC Tests upon Different Weight Percentages of Soil-Size Fresh and Mixed MSW Specimens

11.4.3 Water Content

A pair of specimens, MSW1FNS1 and MSW1FHS1, was prepared to examine the effect of water content on the nonlinear behavior of fresh MSW. High-amplitude RC tests were performed at its natural condition and hydrated conditions. The variations in G and G/G_{max} with shearing strain for 100 % soil-size material specimen at their natural and hydrated conditions are compared in Figures 11.23 (a) and (b), respectively. Comparison was made at a confining pressure of 11 psi (76 kPa). Natural condition is represented by open symbol and hydrated condition is represented by solid symbol.

As seen in Figure 11.23 (a), the difference in G results from a hydration process.

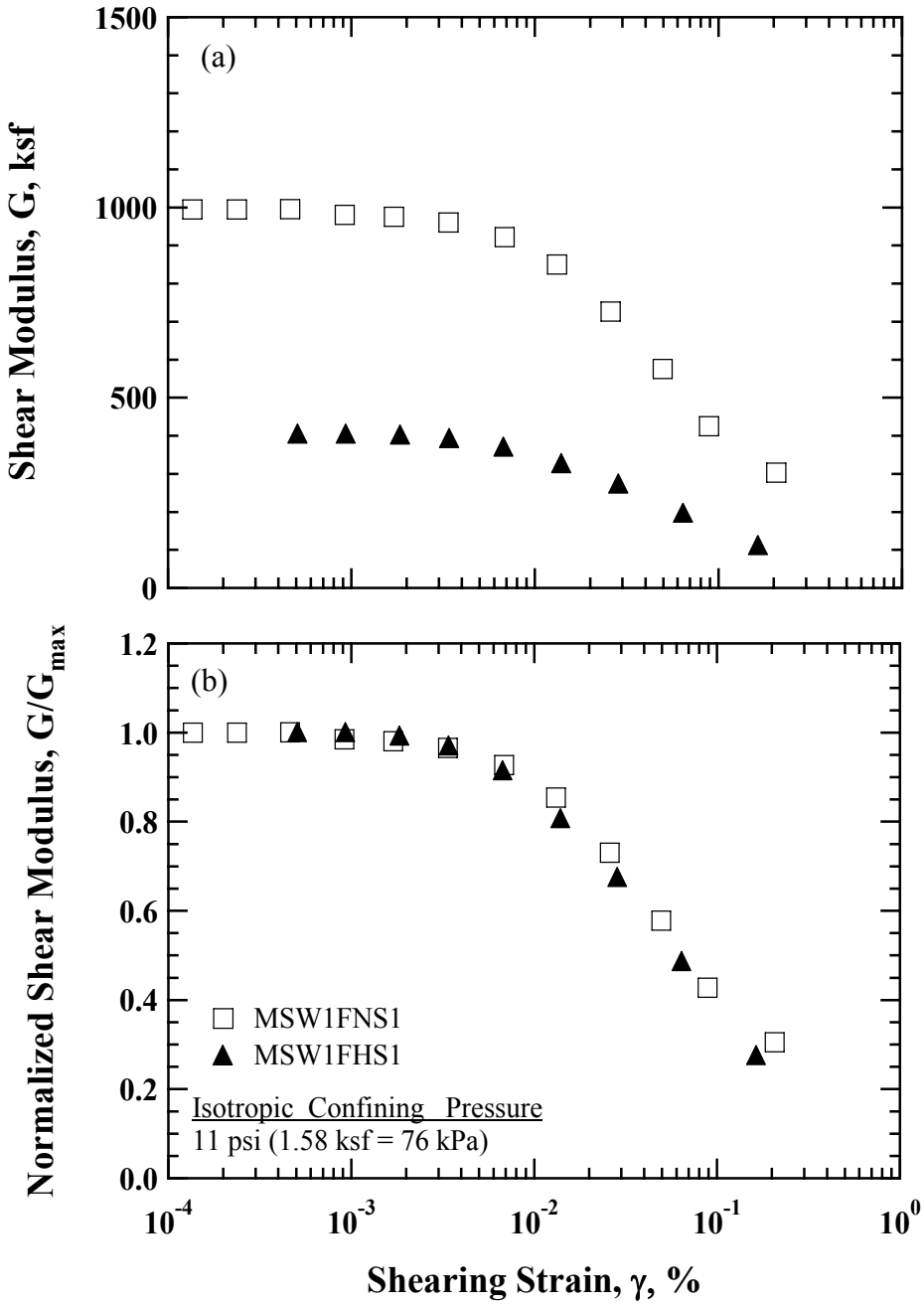

Figure 11.23 Comparison of the Variation in (a) Shear Modulus and (b) Normalized Shear Modulus with Shearing Strain from RC Tests of Specimens at Its Natural and Hydrated Conditions for Fresh MSW Specimens (100 % Soil-Size Material)

As shown in Figure 11.23 (b), the G/G_{max} - log γ curve measured at it hydrated condition is shifted slightly to lower strains. The reference strains, which are the amplitude of strain at normalized shear modulus equal to 0.5 from its natural and hydrated conditions, turned out to be 0.7 % and 0.6 %, respectively.

The variation in D with shearing strain for 100 % soil-size material specimen upon natural and hydrated conditions is presented in Figure 11.24. The values of D completely over shearing strains increased approximately by 20 % due to the hydration process. Energy dissipation caused by relative movements between MSW particles and added water results in an increase of material damping ratio.

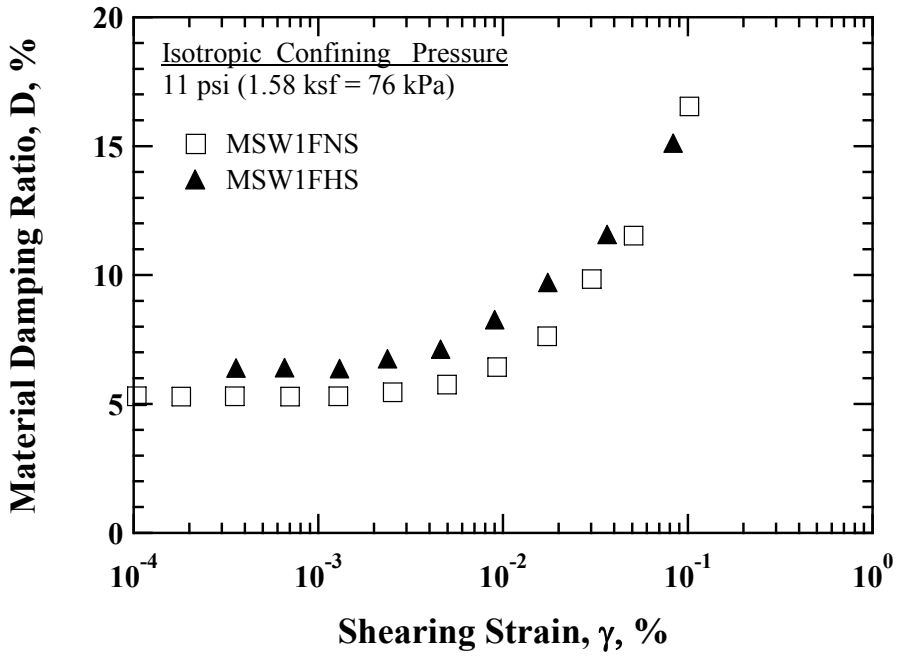

Figure 11.24 Comparison of the Variation in Material Damping Ratio with Shearing Strain from RC Tests upon Specimens at Its Natural and Hydrated Conditions for 100 % Soil-Size Fresh MSW Specimens

11.4.4 Total Unit Weight Variation for the Same Material Type

The variations in G and G/G_{max} with shearing strain with respect to different total unit weight for 100 % soil-size material are shown in Figures11.25 (a) and (b), respectively. The comparison was made at a confining pressure of 11 psi (76 kPa). Higher total unit weight specimen, MSW2FNS2, is denoted by open square symbol and lower total unit weight specimen, MSW4FNS2, is denoted by solid triangular symbol.

As seen in Figure 11.25 (a), it is of interest to observe that although two specimens had different unit weight at the moment of construction, absolute value of G for Specimen MSW4FNS2 is slightly higher than that for Specimen MSW2FNS2. It is probably because of randomly-oriented particles within the specimen during the placement of soil-size waste material. The values of G are constant in the strain range less than about 0.002 %, beyond this point, G decreases with increasing shearing strain for both specimens. Similarly, the G/G_{max} – log γ curve for the lower unit weight specimen shifts slightly to lower strains than that for the higher unit weight specimen, as shown in Figure 11.25 (b). The values of reference strain for Specimen MSW2FNS2 and Specimen MSW4FNS2 were equal to 0.06 % and 0.05 %, respectively.

The variation in D with shearing strain upon different total unit weight specimens is shown in Figure 11.26. The values of D at small-strain range are almost the same. However, as shearing strain increases, D – log γ curve for Specimen MSW2FNS2 shifts to slightly higher strains beyond a shearing strain of 0.02 %, as shown in Figure 11.26. Therefore, it can be concluded that the effects of the variation in total unit weight on the G – log γ, G/G_{max} – log γ, and D – log γ curves are very small for fresh MSW.

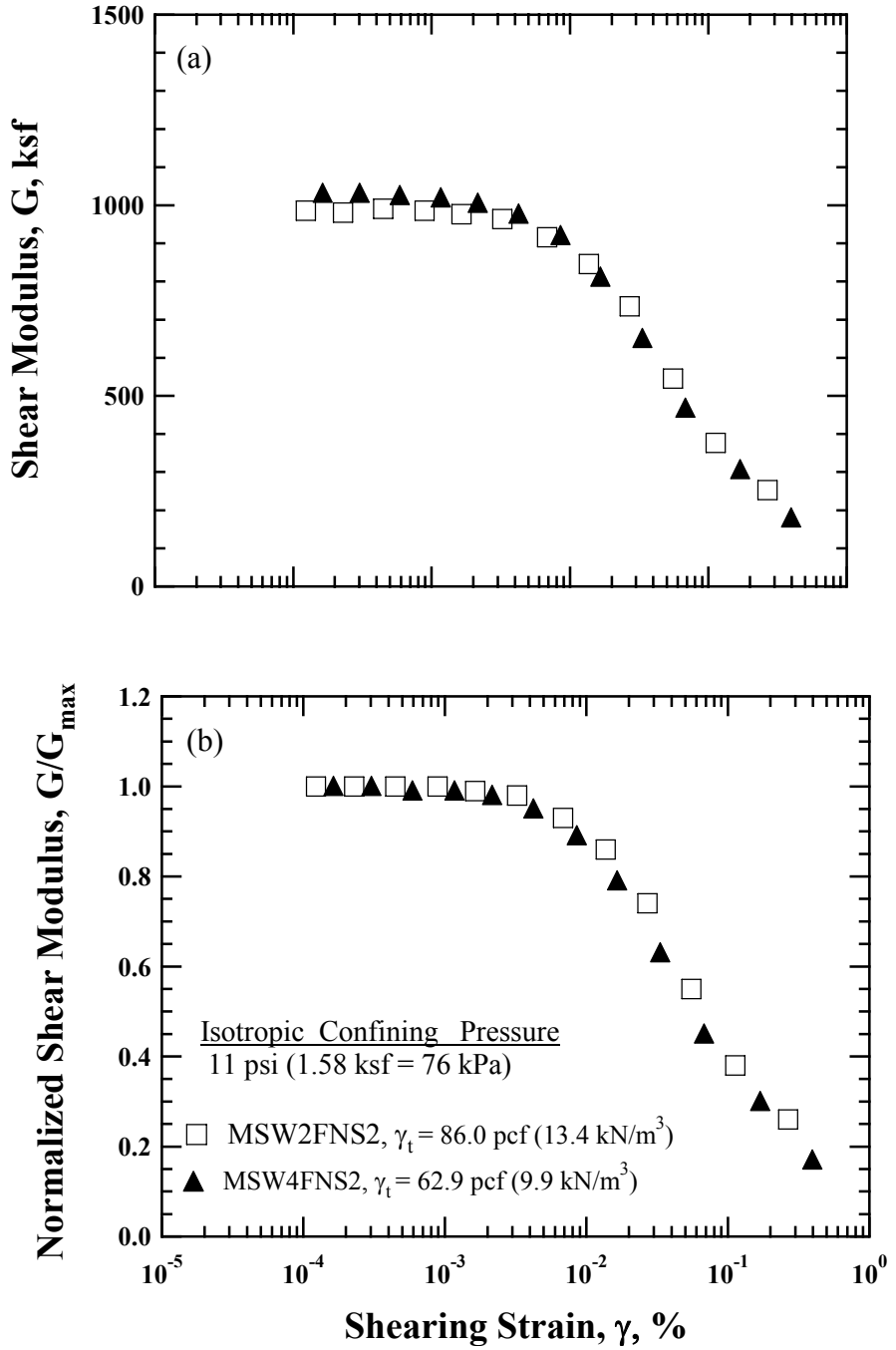

Figure 11.25 Comparison of the Variation in (a) Shear Modulus and (b) Normalized Shear Modulus with Shearing Strain from RC Tests of Specimens with Different Total Unit Weights for 100 % Soil-Size Fresh MSW Specimens

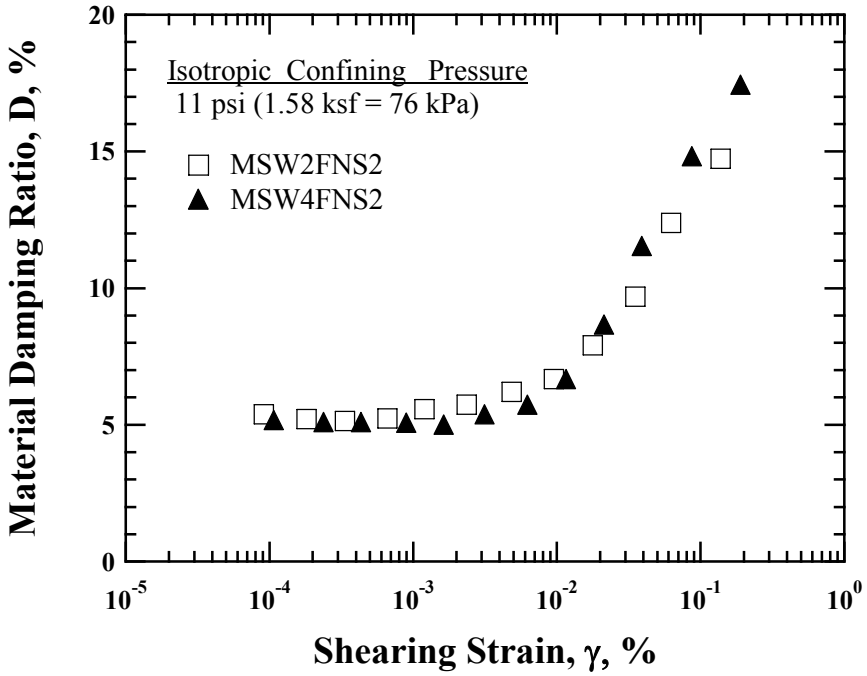

Figure 11.26 Comparison of the Variation in Material Damping Ratio with Shearing Strain from RC Tests of Specimens with Different Total Unit Weights for 100 % Soil-Size Fresh MSW Specimens

11.4.5 Particle Size

To investigate the effect of particle size on the nonlinear behavior of fresh MSW, a pairs of small-diameter specimens were prepared. These specimens are Specimens MSW1FNS1 and MSW2FNS2. Specimen MSW1FNS1 was reconstituted with material passing the 3/8-in. (9.5-mm) sieve and Specimen MSW2FNS2 was reconstituted with material passing the ¾-in. (19.1-mm) sieve.

The variations in G and G/G_{max} with shearing strain for 100 % soil-size fresh MSW specimens are presented in Figures 11.27 (a) and (b), respectively. As shown in Figure 11.27 (a), the variation in G is almost identical with shearing strains. G is constant below about 0.02 %. Once shearing strain exceeds this value, G decreases

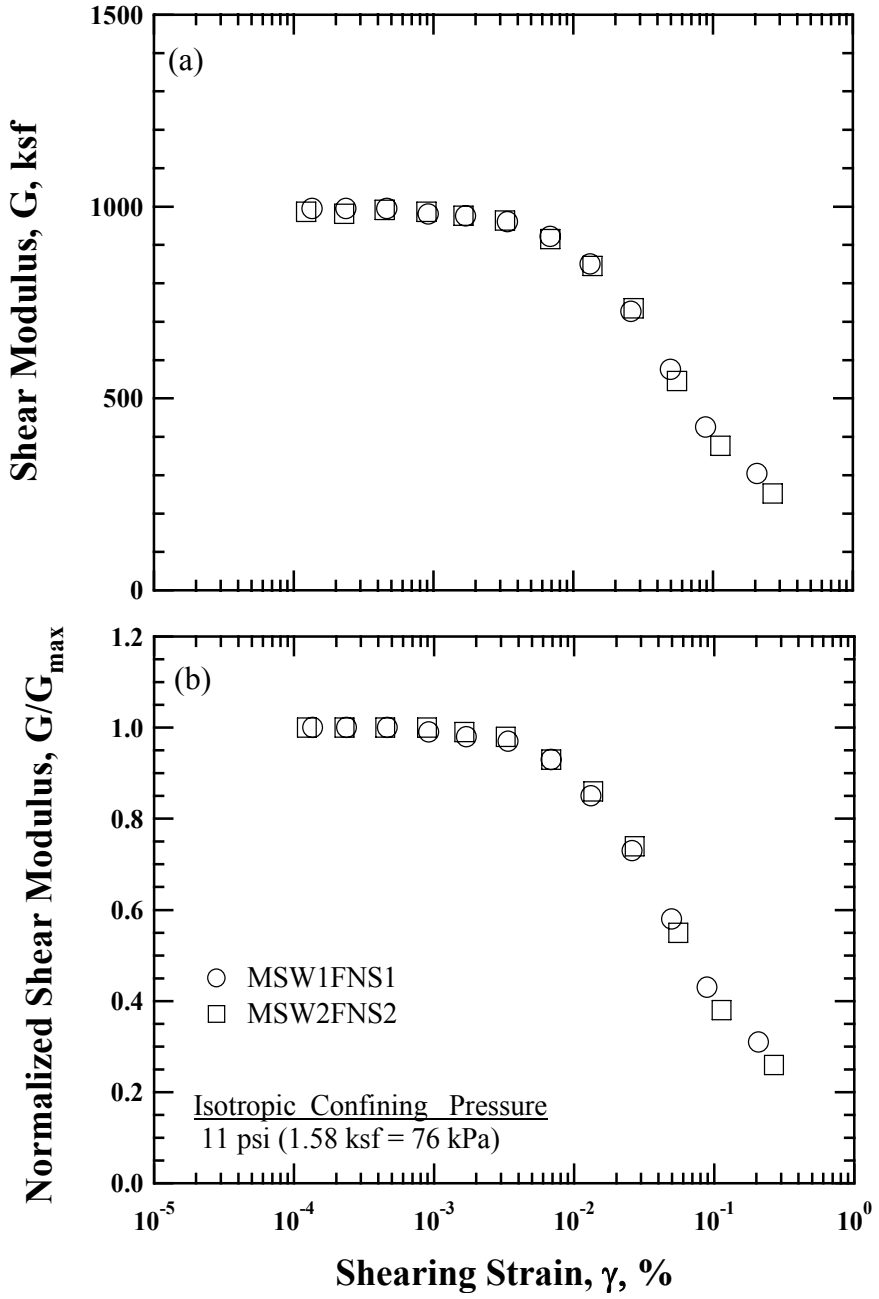

Figure 11.27 Comparison of the Variation in (a) Shear Modulus and (b) Normalized Shear Modulus with Shearing Strain from RC Tests of Specimens with the Different Particle Size of Fresh MSW Specimens (100 % Soil-Size Material)

significantly with increasing shearing strain. As seen in Figure 11.22 (b), the G/G_{max} – log γ curves are nearly the same for both specimens, indicating that the effect of particle size is very small for 100 % soil-size material specimens.

The variation in D with shearing strain for 100 % soil-size Specimen MSW1FNS1 and MSW2FNS is shown in Figure 11.28. As shown in Figure 11.28, the variation in D exhibits almost the same behavior regardless of the particle sizes. As a conclusion, the nonlinear behavior of fresh MSW for 100 % soil-size material does not affected by the particle size of specimens.

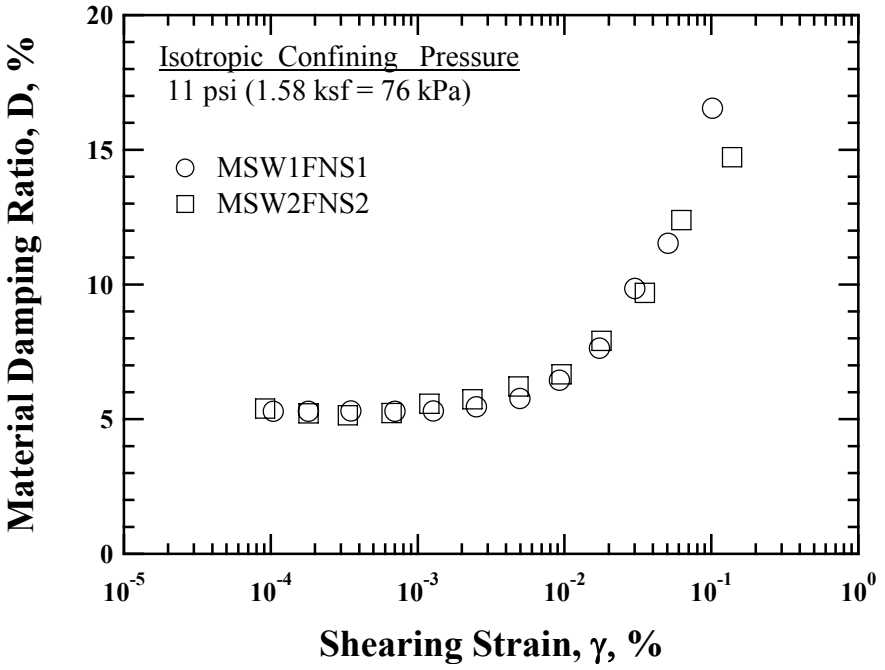

Figure 11.28 Comparison of the Variation in Material Damping Ratio with Shearing Strain from RC Tests upon Specimens with the Different Particle Size of Fresh MSW Specimens (100 % Soil-Size Material)

11.5 RELATIONSHIP BETWEEN NORMALIZED SHEAR MODULUS AND MATERIAL DAMPING RATIO OF FRESH MSW

Empirical relationships between normalized shear modulus (G/G_{max}) and modified material damping ratio ($D-D_{min}$) for the RC and TS tests were developed using data from a series of RCTS and LSRC tests for all groups of fresh MSW. TS data were only available from small-diameter RC tests, whereas RC data included both small- and large-diameter RC tests. $D-D_{min}$ was obtained by subtracting the average value of D_{min} at small-strain ranges from the entire measurements of D. An entire data set was selected from high-amplitude RC tests at confining pressure levels of 2.5 psi (17 kPa), 11 psi (76 kPa), and 40 psi (276 kPa) upon loading sequence.

The empirical relationship between G/G_{max} and $D-D_{min}$ is given in Figure 11.29. As discussed in Section 10.5, shearing strain for normalized shear modulus and material damping ratio are not identical in the RC tests. More detailed explanation is provided in Section 10.5. Although the values of shearing strain of normalized shear modulus and material damping ratio are different, these are plotted as a pair at given measurements during high-amplitude RC tests. The data obtained from the RCTS and LSRC tests were fitted using least-squares method as a form of second-order of a polynomial function. Fitted equations are represented by solid and dashed lines for the RC and TS tests, respectively. The equations are expressed by:

$$D - D_{min} = 8.2(G/G_{max})^2 - 23.9(G/G_{max}) + 15.8 \quad \text{for RC tests} \qquad (11.1)$$

$$D - D_{min} = 17.7(G/G_{max})^2 - 42.7(G/G_{max}) + 25.1 \quad \text{for TS tests} \qquad (11.2)$$

where,

D_{min} is a material damping ratio at small-strain ranges,

D is a material damping ratio at any given shearing strains,

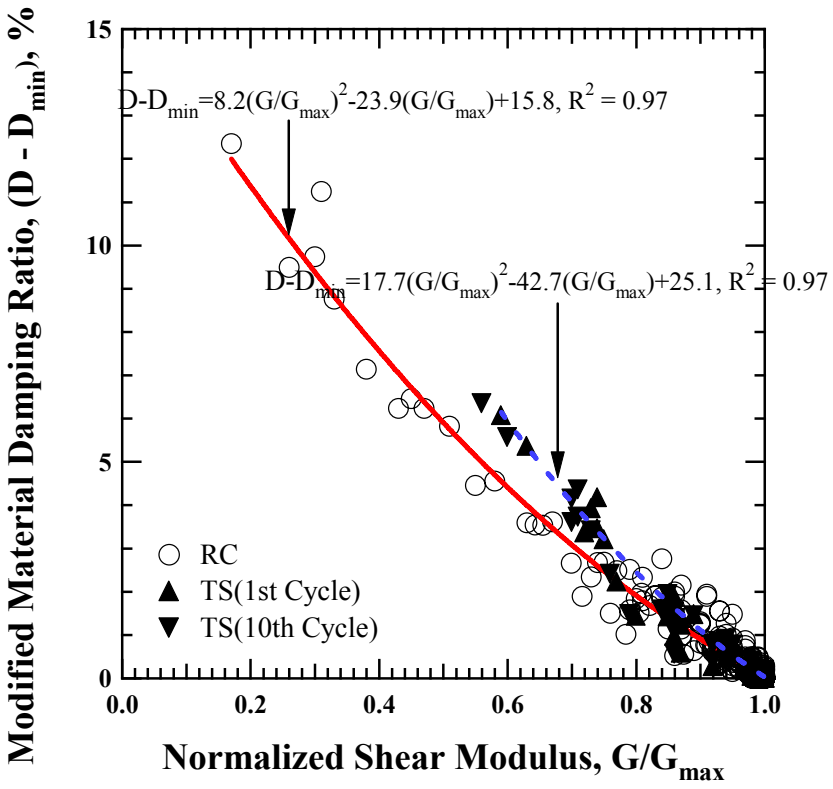

Figure 11.29 Plot of Normalized Shear Modulus with Modified Material Damping Ratio from RCTS and LSRC Tests for All Groups of Fresh and Mixed MSW Specimens

G_{max} is a shear modulus at small-strain ranges, and

G is a shear modulus at any given shearing strains.

As shown in Figure 11.29, similar to old MSW, relationship from the RC and TS tests shows a good agreement down to the value in terms of G/G_{max} of 0.76. However, beyond this point, the difference in relationship between RC and TS tests begins to increase, indicating that the frequency effect in material damping measurements from the RC and TS tests becomes smaller as shearing strain increases. The important feature of this empirical relationship is that at a given value of G/G_{max}, material damping ratio can

be predicted with knowledge of D_{min}. In order to evaluate how the predicted values match well with measured values, the values of measured D-D_{min} are compared with the values of D-D_{min} in Figures 11.30 (a) and (b) for the RC and TS tests, respectively. As shown in figures, the predicted values using equations for the RC and TS tests show a quite good agreement with measured values.

11.6 COMPARISON OF NONLINEAR DYNAMIC PROPERTIES OF OLD MSW AND LOOSE SAND

The G – log γ, G/G_{max} – log γ, and D – log γ curves for old MSW are compared with this of loose sand in Figures 11.30, 11.31, and 11.32, respectively. The comparisons were made at a confining pressure of 11 psi (76 kPa). These nonlinear dynamic property curves were generated using equation, suggested by Menq (2003). The loose sand has a uniformity coefficient of 18 and void ratio of 0.4. Relative density of the loose sand is about 50 %. The values of G, G/G_{max}, and D for fresh MSW shown in the figures were corrected for frequency to f = 1 Hz. As seen in Figures 11.30, the value of G at small-strain range, the difference between loose sand and old MSW is approximately a factor of 2.3. In terms of G/G_{max}, the G/G_{max} – log γ curve for the loose sand shifts to lower strains, indicating a more nonlinear behavior with shearing strain than fresh MSW. For material damping ratio, as shown in Figure 11.32, there is a large difference at small-strain range and is about factor of 3.9. D is small below shearing strain of 0.01 %, but becomes larger beyond the strain amplitude of 0.04 %.

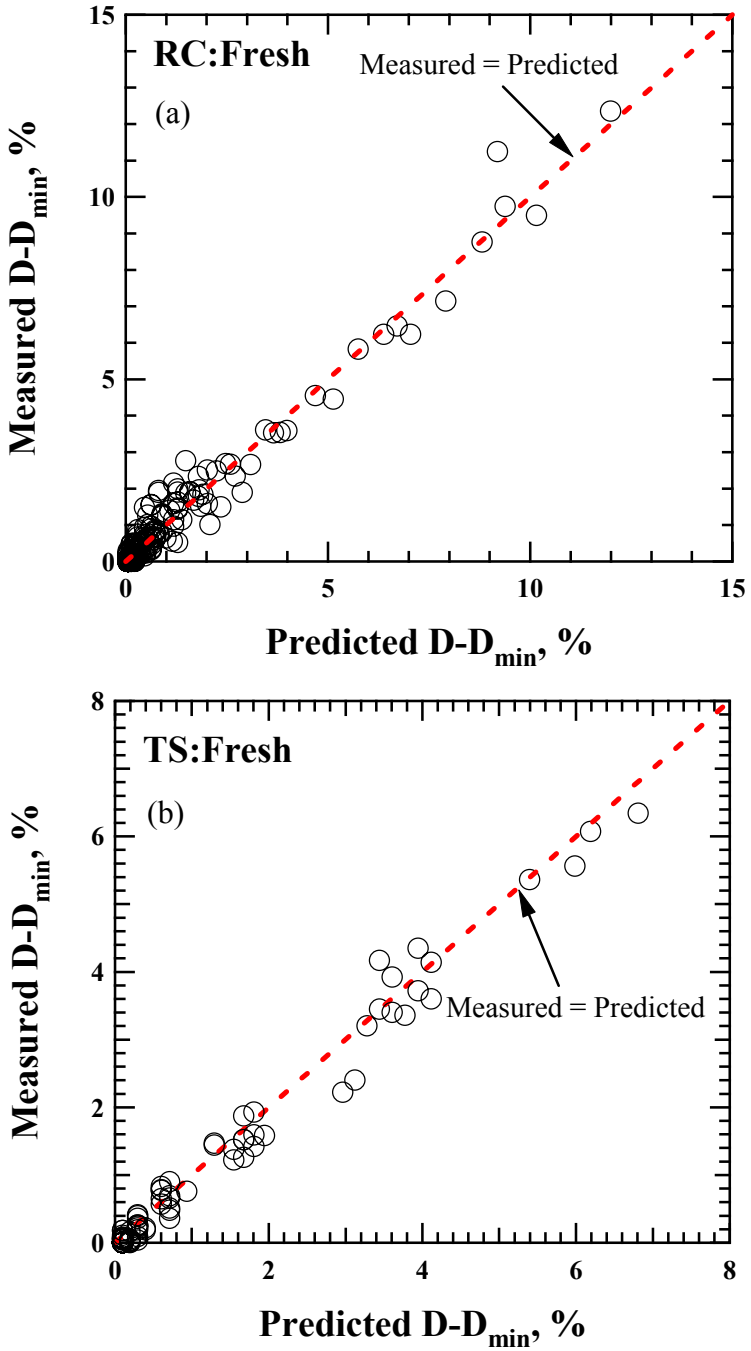

Figure 11.30 Comparison of the Values of Measured D-D_{min} and Predicted D-D_{min} from (a) RC Tests and (b) TS Tests for Fresh MSW Specimens

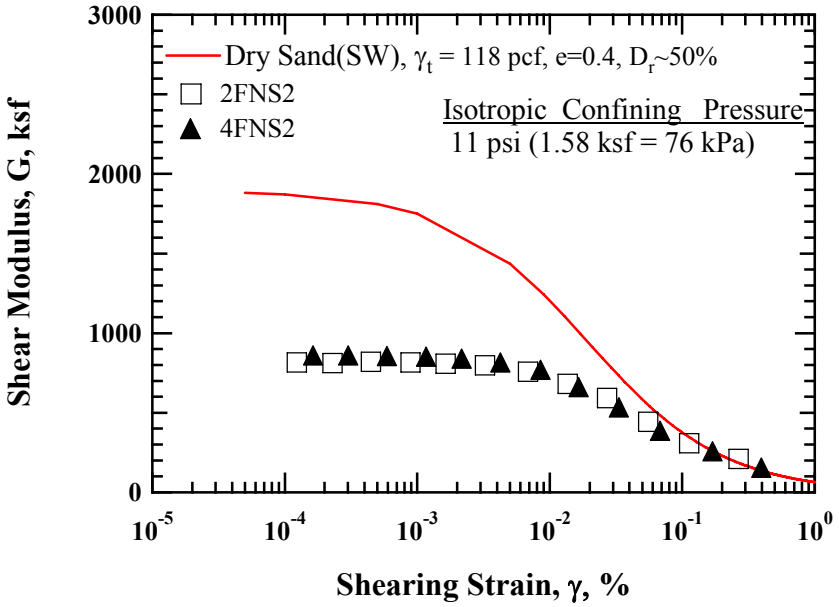

Figure 11.31 Comparison of the Variation in Shear Modulus with Shearing Strain at a Confining Pressure of 11 psi (76 kPa) for Fresh MSW and Loose Sand

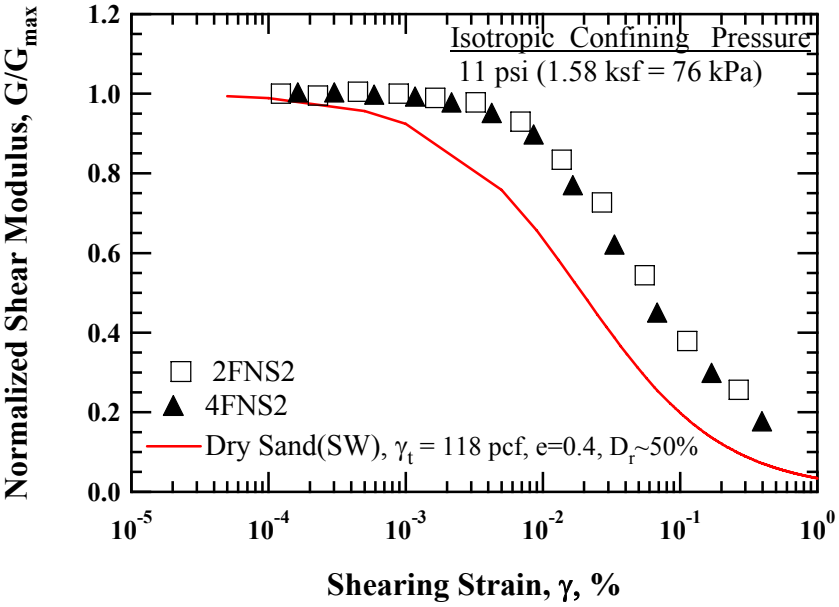

Figure 11.32 Comparison of the Variation in Normalized Shear Modulus with Shearing Strain at a Confining Pressure of 11 psi (76 kPa) for Fresh MSW and Loose Sand

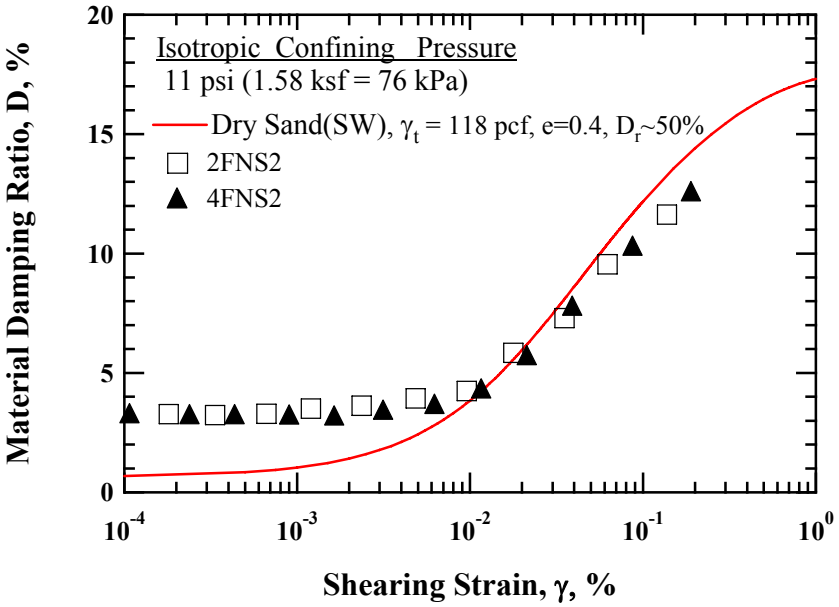

Figure 11.33 Comparison of the Variation in Material Damping Ratio with Shearing Strain at a Confining Pressure of 11 psi (76 kPa) for Fresh MSW and Loose Sand

11.7 SUMMARY

Test parameters affecting nonlinear behavior of fresh MSW are investigated in this chapter. These test parameters include: (1) strain amplitude, (2) confining pressure, (3) overconsolidation ratio, (4) number of loading cycles, and (5) excitation frequency. Each test parameters was studied and the influence of those parameters on G and D in the nonlinear strain range individually. Among these test parameters, very important parameters are strain amplitude and confining pressure; G and D considerably change with increasing strain amplitude and G varied significantly with increasing confining pressure. However, the effect of confining pressure was small on G/G_{max} and D. Other test parameters had a small or some impact on G and D.

In addition, material parameters were also investigated with respect to the influence of material parameters on G and D. Those material parameters are: (1) waste composition, (2) water content, (3) unit weight, and (4) particle size. Among these material parameters, waste composition had a great impact on G/G_{max} and D; the lower weight percentage of soil-size material exhibits more linear behavior. Other material parameters showed a small influence on G and D.

An empirical relationship between normalized shear modulus (G/G_{max}) and modified material damping ratio ($D-D_{min}$) was derived using the data from RCTS and LSRC tests for all groups of fresh and mixed MSW. The data were fitted using least-square method as a form of second order of polynomial function. Predicted values are compared with measured values in Figures 11.25 (a) and (b) and provide a fairly good agreement with measured values.

The G – log γ, G/G_{max} – log γ, and D – log γ curves of fresh MSW are compared with loose sand. There are large differences in absolute values of G and D at small-strain range. The loose sand exhibits more nonlinear behavior relatively when compared with fresh MSW; the G/G_{max} – log γ curve shifts lower strains.

CHAPTER 12: Comparison of the Nonlinear Behavior of Old and Fresh MSW

12.1 INTRODUCTION

In order to investigate the nonlinear dynamic behavior of old and fresh MSW, nonlinear dynamic properties, G, G/G_{max} and D, of old and fresh MSW were compared in this chapter on the basis of observations in Chapter Ten and in Chapter Eleven. The comparison of the variation in G and/or G/G_{max} and D with shearing strain was made at a confining pressure of 11 psi (76 kPa) for old and fresh MSW. The variation of G and D with excitation frequency was also made at a confining pressure of 11 psi (76 kPa) for both old and fresh MSW. Additionally, the variation of normalized shear modulus and material damping ratio at a frequency of 1 Hz was used to make a comparison for old and fresh MSW. A detailed description for the comparison of old and fresh MSW is provided and discussed in the subsequent sections.

12.2 VARIATION IN SHEAR MODULUS, NORMALIZED SHEAR MODULUS, AND MATERIAL DAMPING RATIO WITH SHEARING STRAIN AT A GIVEN CONFINING PRESSURE

In order to investigate the effect of waste age on the nonlinear behavior of MSW, two pairs of 100 % soil-size material specimens were prepared. Those specimens were MSW3ONS1, MSW4ONS2, MSW1FNS1, and MSW2FNS2 and were reconstituted using materials passed throughout 3/8-in. (9.5-mm) and ¾-in. (19.1-mm) sieves. Comparisons were made at a confining pressure of 11 psi (76 kPa) for the nonlinear measurements of old and fresh MSW. The variations in G and G/G_{max} with shearing strain are compared for old and fresh MSW in Figures 12.1 (a) and (b), respectively. Absolute difference of G at small-strain ranges between old and fresh MSW specimens

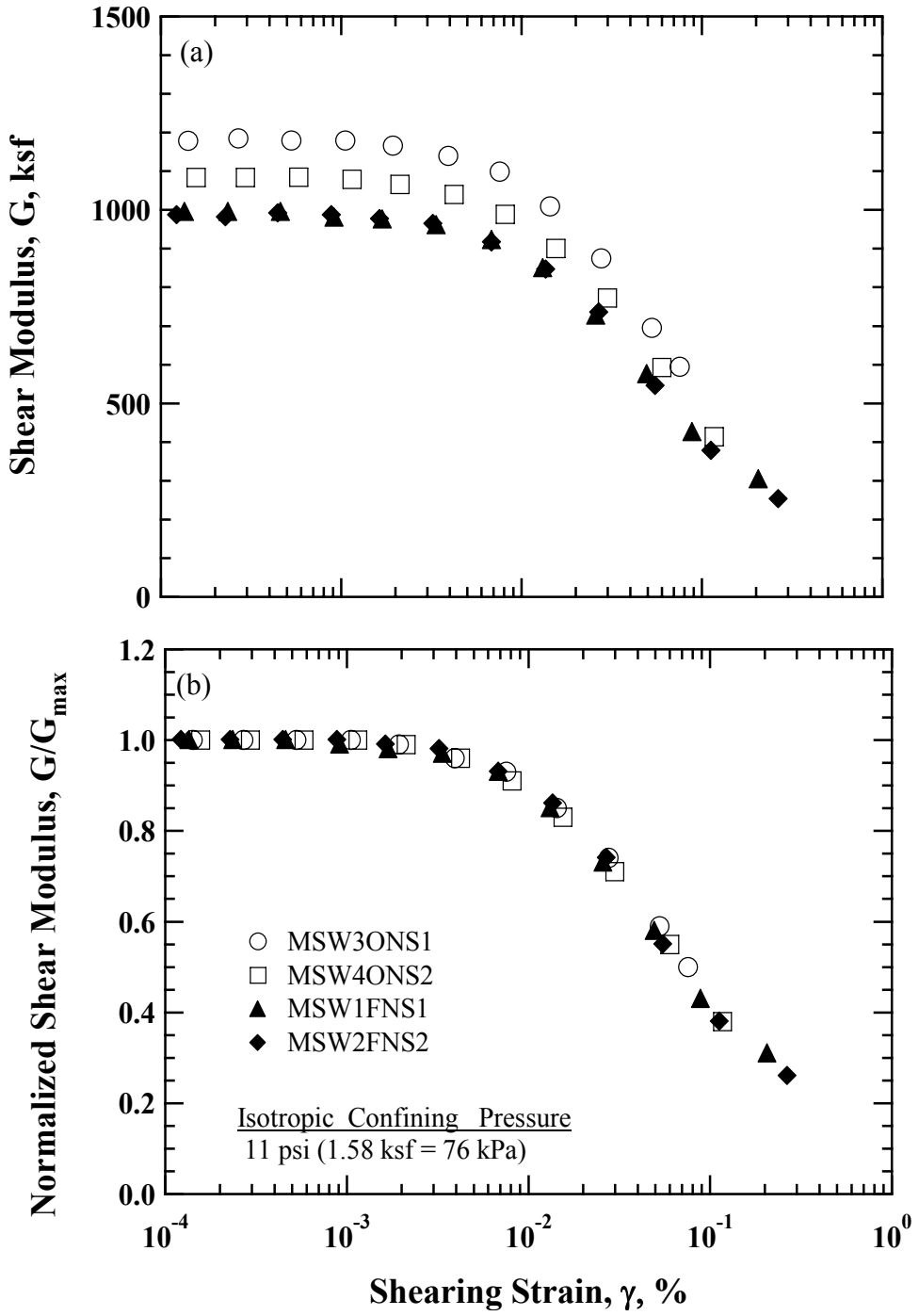

Figure 12.1 Comparison of the Variation in (a) Shear Modulus and (b) Normalized Shear Modulus with Shearing Strain from RC Tests for Old and Fresh MSW Specimens (100 % Soil-Size Material)

results from the difference of their initial material properties, as described in Table 5.3. Absolute difference of G at small-strain ranges is about 10 % or 20 % between old and fresh MSW. It is of interest to observe that the difference of G decreases as shearing strain increases, as shown in Figure 12.1 (a). Figure 12.1 (b) indicates that normalized shear modulus with shearing strain is identical regardless of waste age. Additionally, as discussed at previous two chapters about the effect of particle size, normalized shear modulus is not affected by the particle size of specimen.

The variation in D with shearing strain of old and fresh MSW is plotted in Figure 12.2. As illustrated in Figure 12.2, the variation in D for fresh MSW is located above that of old MSW over shearing strains. One possible explanation for this is that more viscous characteristic due to less degradation of fresh MSW can contribute to a higher material damping. The variation of the material damping ratio of old and fresh MSW appears to be maintained over shearing strain ranges. Absolute difference of D at small-strain ranges are approximately 40% between old and fresh MSW, which is considerable difference when compared with the difference of G. Similar to normalized shear modulus, as shown in Figure 12.2, the variation of material damping ratio with shearing strain does not affected by the particle size of specimen. Therefore, it can be drawn a conclusion that the influence of waste age is more pronounced on D than it is on G or G/G_{max}.

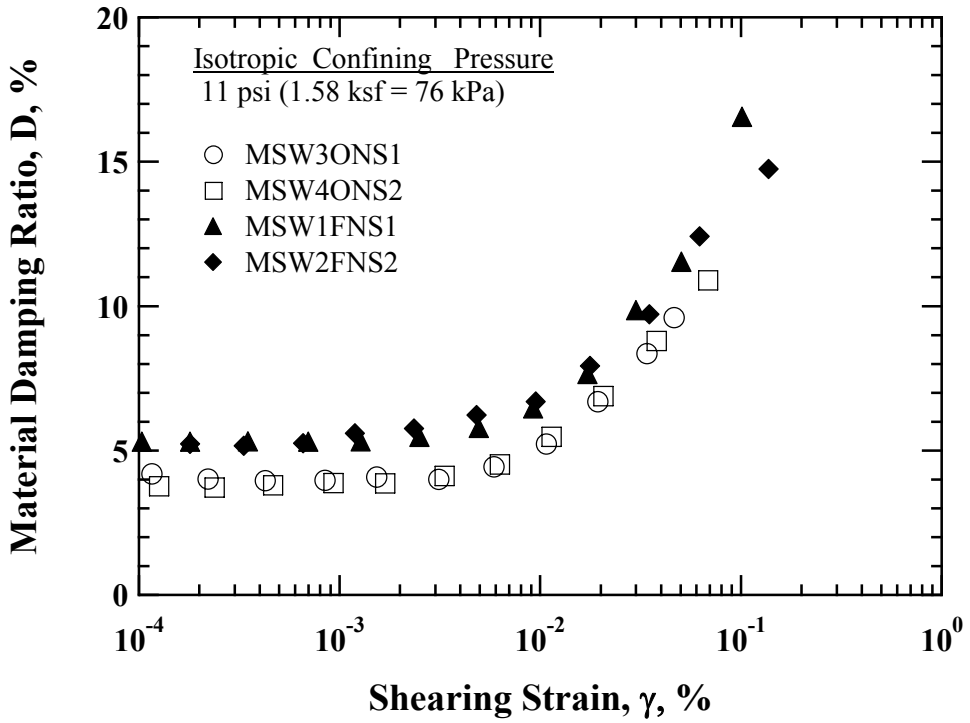

Figure 12.2 Comparison of the Variation in Material Damping Ratio with Shearing Strain from RC tests for Old and Fresh MSW Specimens (100 % Soil-Size Material)

12.3 VARIATION IN SHEAR MODULUS, NORMALIZED SHEAR MODULUS, AND MATERIAL DAMPING RATIO WITH SHEARING STRAIN AT A GIVEN EXCITATION FREQUENCY

The variations in normalized shear modulus with excitation frequency for old and fresh MSW are presented in Figures 12.3 (a) and (b), respectively. Data measured from LSRC tests were denoted as Fr-Fr in the figures. The values of G obtained from RCTS tests were normalized with G at a frequency of 1 Hz. Since no TS test was available in LSRC device, the values of G from LSRC tests were normalized with one averaged from TS tests. Data from RCTS and LSRC tests were fitted using least-squares method and the fitted lines are expressed by dashed lines.

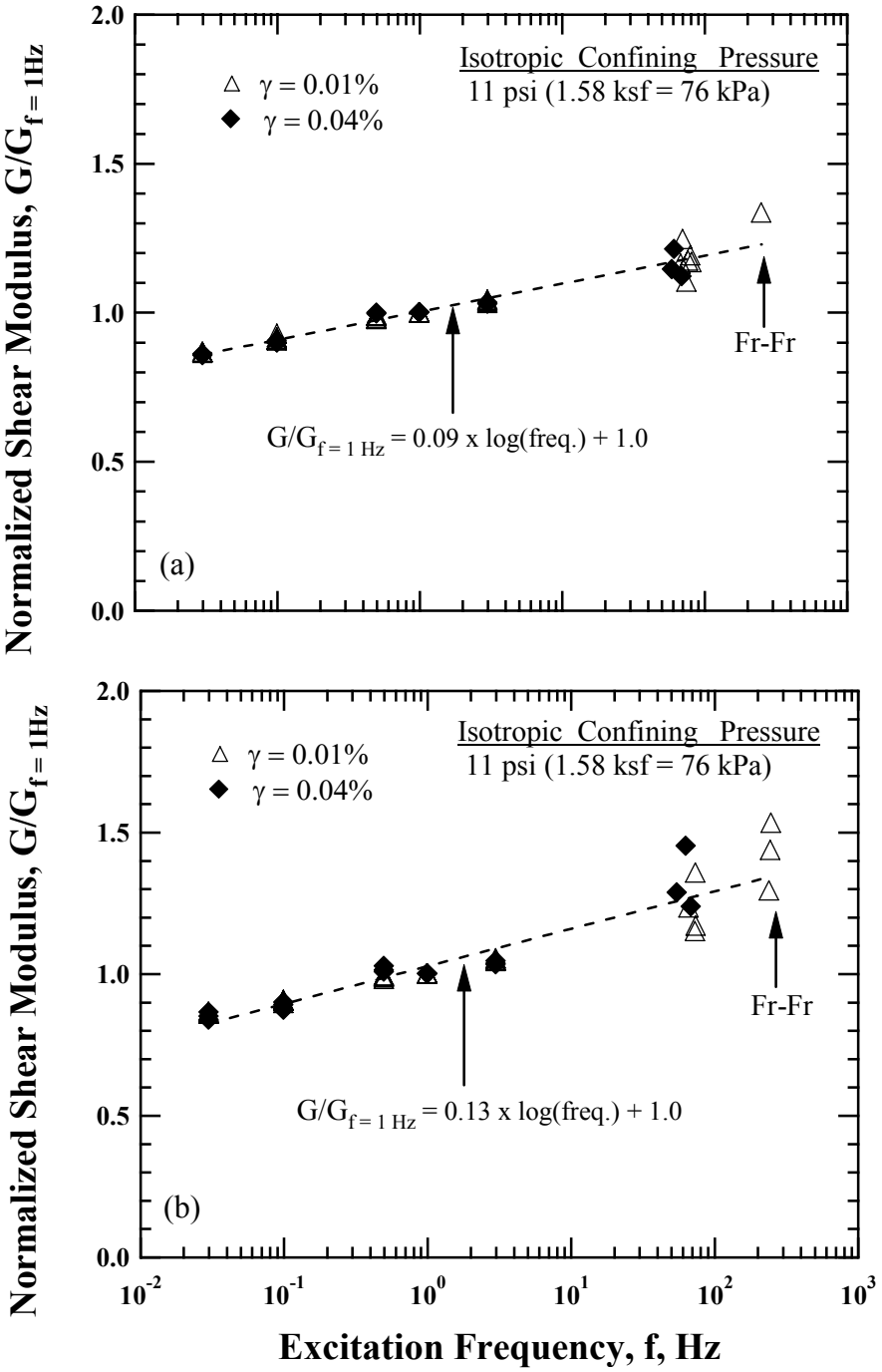

Figure 12.3 Comparison of the Variation in Normalized Shear Modulus with Shearing Strain from RC tests for (a) Old and (b) Fresh MSW Specimens (100 % Soil-Size Material)

The equations are given by:

$$\frac{G}{G_{f=1Hz}} = 0.09 \times \log(\text{Freq.}) + 1.0 \quad \text{for old MSW} \tag{12.1}$$

$$\frac{G}{G_{f=1Hz}} = 0.13 \times \log(\text{Freq.}) + 1.0 \quad \text{for fresh MSW} \tag{12.2}$$

where,

G is a shear modulus measured at a given frequencies, and

$G_{f=1Hz}$ is a shear modulus measured at a frequency of 1Hz.

As indicated in Figures 12.3 (a) and (b), normalized shear modulus varies linearly with increasing excitation frequency due to frequency effect for both old and fresh MSW. In addition, the variation of normalized shear modulus for old and fresh MSW does not affected by the amplitude of shearing strain. That is, the variation of normalized shear modulus at shearing strain amplitudes of 0.01 % and 0.04 % is similar. Fresh MSW exhibits comparatively somewhat higher order of increase rate than old MSW, implying that fresh MSW responds more sensitively to excitation frequency.

The variation in normalized material damping ratio with excitation frequency for old and fresh MSW is illustrated in Figures 12.4 (a) and (b), respectively. Data from the RCTS and LSRC tests were fitted using least-squares method as a form of second-order of polynomial function and the fitted lines are represented by dashed lines. The equation is expressed by:

$$\frac{D}{D_{f=1Hz}} = 0.08 \times \log(\text{Freq.})^2 - 0.04 \times \log(\text{Freq.}) + 1.0 \quad \text{for old MSW} \tag{12.3}$$

$$\frac{D}{D_{f=1Hz}} = 0.11 \times \log(\text{Freq.})^2 - 0.01 \times \log(\text{Freq.}) + 1.0 \quad \text{for fresh MSW} \quad (12.4)$$

where,

D is a material damping ratio measured at a given frequencies, and

$D_{f=1Hz}$ is a material damping ratio measured at a frequency of 1Hz.

As illustrated in the figures, both old and fresh MSW, normalized material damping ratio increases with decreasing excitation frequency due to creep behavior in the shearing strain ranges less than 1 Hz, while normalized shear modulus increases with an increase in excitation frequency due to frequency effect in the shearing strain ranges larger than 1 Hz. Similarly, normalized material damping ratio also is not affected by the amplitude of shearing strain. It is of interest to note that the variation of normalized material damping ratio with excitation frequency is fairly similar between old and fresh MSW in the ranges less than 1 Hz, however, the variation of normalized material damping ratio shows a remarkable difference in higher excitation frequencies. More viscous characteristic induced by less degradation may results in a higher material damping ratio for fresh MSW. As a result, the effect of waste age is more significant on normalized material damping ratio than on normalized shear modulus, especially in higher excitation frequencies for fresh MSW.

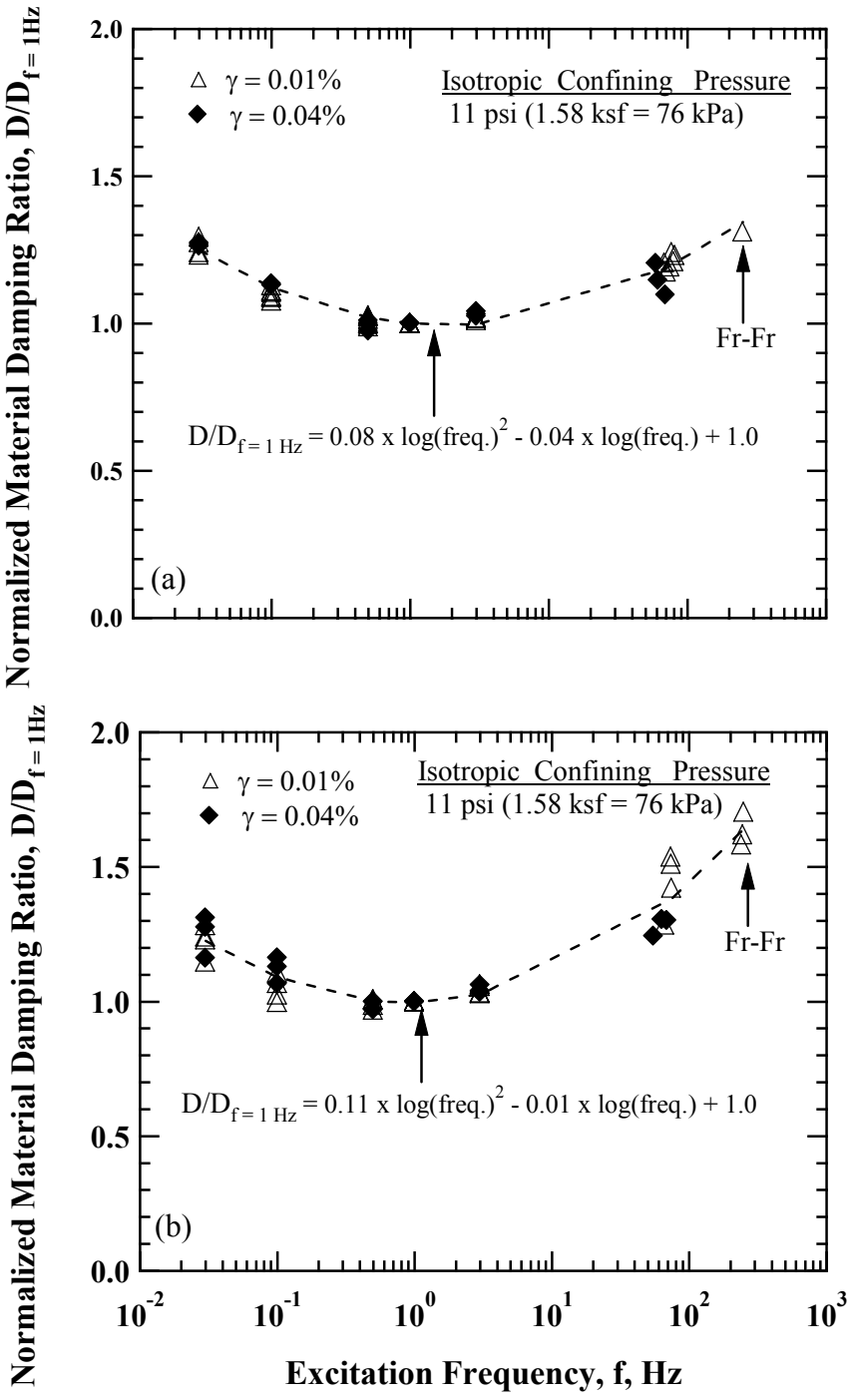

Figure 12.4 Comparison of the Variation in Normalized Material Damping Ratio with Shearing Strain from RC tests for (a) Old and (b) Fresh MSW Specimens (100 % Soil-Size Material)

12.4 SUMMARY

Nonlinear dynamic material properties, G and D, of old and fresh MSW are compared in this chapter. Comparisons were made on the variation in G, G/G_{max}, and D with shearing strain at a given confining pressure to evaluate how the age of waste affects on nonlinear behavior of MSW. As illustrated in Figure 12.1 (b), the variation in normalized shear modulus with shearing strain at a given confining pressure of 11 psi (76 kPa) is identical regardless of waste age and particle size. However, in case of the material damping ratio, the values of material damping for fresh MSW exhibits somewhat higher than those for old MSW over shearing stains. More viscous characteristic induce by less degradation may resulted in a higher material damping ratio for fresh MSW.

Another comparison was made on the normalized shear modulus and material damping ratio with excitation frequency for old and fresh MSW. As indicated in Figures 12.3 (a) and 12.3 (b), regardless of the age of waste, normalized shear modulus with excitation frequency increases linearly due to frequency effect. However, fresh MSW exhibits a somewhat higher increase rate when compared with old MSW. The variation in normalized material damping ratio with excitation frequency was quite similar with an exception at higher excitation frequencies; normalized material damping ratio increases as decreasing excitation frequency due to creep behavior, whereas normalized material damping ratio increases with increasing excitation frequency due to frequency effect. The variation of normalized material damping ratio is more pronounced in higher excitation frequencies for fresh MSW.

CHAPTER 13: Comparison of Shear Modulus Reduction and Material Damping Ratio Curves with UCB and Other Studies

13.1 INTRODUCTION

As part of this collaborative research project, a large number of laboratory tests were performed on MSW material retrieved from the Tri-Cities landfill in an effort to evaluate the dynamic properties of MSW. To accomplish this goal, UT employed 2.8-in. (71.1-mm) and 6.0-in. (152.4-mm) diameter RC devices and UCB used 12-in. (304.8-mm) diameter cyclic triaxial device. As a result, nonlinear shear modulus reduction and material damping curves for old and fresh MSW generated by UT are compared with similar curves generated by UCB in this chapter. The data measured by UT were fitted using a modified hyperbolic model, suggested by Darendeli (2001), in terms of normalized shear modulus. These data were also fitted using an adjusted "Masing behavior" model for material damping ratio as suggested by Darendeli (2001). In addition, other comparisons are made with other shear modulus reduction and material damping ratio curves previously used by researchers.

13.2 DATA FITTING USING A MODIFIED HYPERBOLIC MODEL

The old, fresh, and mixed MSW RC data measured in the RCTS and LSRC devices were used to evaluate and model the nonlinear dynamic behavior of old and fresh MSW in terms of the normalized shear modulus, G/G_{max}, and material damping ratio, D, variations with shearing strain amplitude. The data were fitted using a modified hyperbolic model, suggested by Darendeli (2001), for the generation of normalized shear modulus curves. The modified hyperbolic model is given by:

$$\frac{G}{G_{max}} = \frac{1}{1+\left(\frac{\gamma}{\gamma_r}\right)^a} \tag{13.1}$$

where,

G is a shear modulus at a given shearing strain,

G_{max} is the shear modulus at small strains,

γ is shearing strain at which G was measured,

a is a curvature coefficient, and

γ_r is a reference strain.

Reference strain, as shown in Equation (13.1), is the shearing strain at which normalized shear modulus is equal to 0.5 and is a function of PI, OCR, and mean effective confining pressure in Darendeli's model. The equation for reference strain for soil is given by:

$$\gamma_r = (0.0352 + 0.001 \times PI \times OCR^{0.3246}) \times \sigma_o^{'0.3483} \tag{13.2}$$

where,

PI is the plasticity index of soils,

OCR is the overconsolidation ratio, and

$\sigma_o^{'}$ is the mean effective confining pressure.

The reference strain, as defined above, is different from the one defined by Hardin and Drenevich (1972). They defined reference strain as a ratio of maximum shear stress to maximum shear modulus (maximum shear stress is the shear stress at failure and maximum shear modulus is the initial slope of hyperbolic curve). The curvature coefficient, a, as shown in Equation (13.1) determines an overall shape of the hyperbolic

curve. For example, as "a" increases, the change in the shape of the curve becomes more abrupt, while as "a" decreases, the change in the shape of the curve becomes smoother with increasing shearing strain.

13.2.1 G/G_{max} c log γ Relationships

The variation in normalized shear modulus with shearing strain for old, fresh, and mixed MSW with respect to different weight percentages of soil-size material is shown in Figure 13.1. All data shown in the figure were measured with RC tests in the RCTS and LSRC devices. The data are represented by open circular, triangular, and square symbols, which correspond to 100 %, 62 to 76 %, and 14 % soil-size MSW specimens, respectively. These fits were constructed for tests performed at a confining pressure of 11 psi (76 kPa).

As seen in Figure 13.1, the G/G_{max} – log γ curves shift to higher strains as the weight percentage of soil-size material decreases. For example, the lowest weight percentage of soil-size material exhibit more elastic behavior with shearing strain. An attempt was made to produce a best fit on the measured data using the modified hyperbolic model by changing the parameters, as presented in Equations (13.1) and (13.2). It should be noted that based on the observations in the linear and nonlinear strain ranges, 62 % and 76 % soil-size material groups were combined together. The different sets of parameters for each group are summarized in Table 13.1. It is interesting to note that the value of equivalent PI for a given group increases dramatically with decreasing weight percentage of soil-size material when fitting using a modified hyperbolic model. Reference strain also increases with decreasing weight percentage of soil-size material. The value of "a" was chosen as a value of 1.04 for the best fitting.

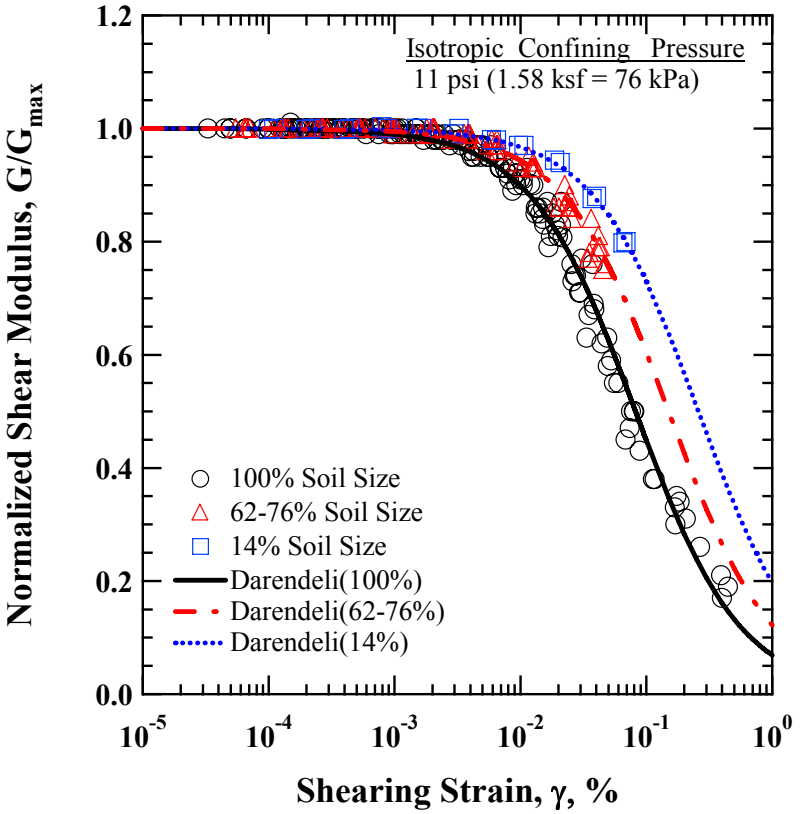

Figure 13.1 Comparison of the Fitted Relationships for the Variation in Normalized Shear Modulus with Shearing Strain from RC Tests in of Old, Fresh, and Mixed MSW Patterned After Darendeli's (2001) Model

Table 13.1 Summary of the Values of Modified Hyperbolic Parameters used for the Best Fit of Each Group of Normalized Shear Modulus Curves Patterned After Darendeli's (2001) Model

% Weight of Soil-Size Material	a	Equivalent PI	OCR	σ_o(atm)	γ_r (%)
100 %	1.04	55	1	0.75	0.082
62-76 %	1.04	130	1	0.75	0.150
14 %	1.04	250	1	0.75	0.259

13.2.2 D – log γ Relationships

Measured material damping ratio was fitted using the adjusted Masing behavior model proposed by Darendeli (2001). The adjusted "Masing behavior" equation is expressed by:

$$D = F \times D_{Masing} + D_{min} \tag{13.3}$$

where,

$D_{Masing} = c_1 D_{Masing,\ a=1.0} + c_2 D_{Masing,\ a=1.0}^{2} + c_3 D_{Masing,\ a=1.0}^{3}$,

$$D_{Masing,\ a=1.0} = \frac{1}{\pi}\left[4\frac{\gamma - \gamma_r \ln\left(\frac{\gamma+\gamma_r}{\gamma_r}\right)}{\frac{\gamma^2}{\gamma+\gamma_r}} - 2\right],$$

$c_1 = -1.1143a^2+1.8618a+0.2523$,

$c_2 = 0.0805a^2-0.0710a-0.0095$,

$c_3 = -0.0005a^2-0.0002a+0.0003$,

$$F = b\times\left(\frac{G}{G_{max}}\right)^{0.1},$$

b is a scaling coefficient (=0.6329-0.0057ln(N)),

D_{Masing} is a material damping ratio from Masing behavior, and

D_{min} is a material damping ratio at small-strain ranges.

One of the advantages of this equation is to take into account an overestimated material damping ratio measured at higher strains, usually larger than 0.01 %, by assuming the "Masing behavior".

The variation in material damping ratio with shearing strain for both old, fresh, and mixed MSW with respect to different weight percentages of soil-size material is presented in Figure 13.2. As shown in Figure 13.2, the values of D_{min} slightly increase

with decreasing weight percentage of soil-size material. However, the values of D_{min} of 62 to 76 % and 14 % of soil-size material specimens exhibit nearly the same. Since there is a great deal of overlap in the small-strain range, the data for each group are replotted in Figure 13.3. In addition, the data uncorrected for frequency as well as the data corrected for frequency are shown in Figure 13.3. The D-log γ curves shift to higher strains with a decrease in weight percentage of soil-size material, indicating that specimens with larger particles show a more linear characteristic.

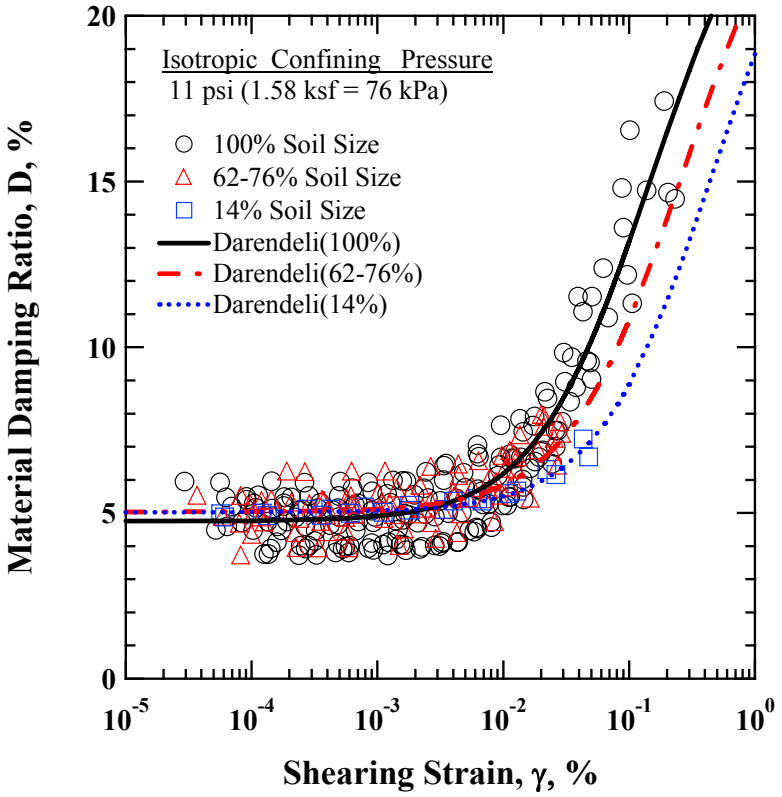

Figure 13.2 Comparison of the Fitted Relationships for the Variation in Material Damping Ratio with Shearing Strain from RC Tests of Old, Fresh, and Mixed MSW Patterned After Darendeli's (2001) Model

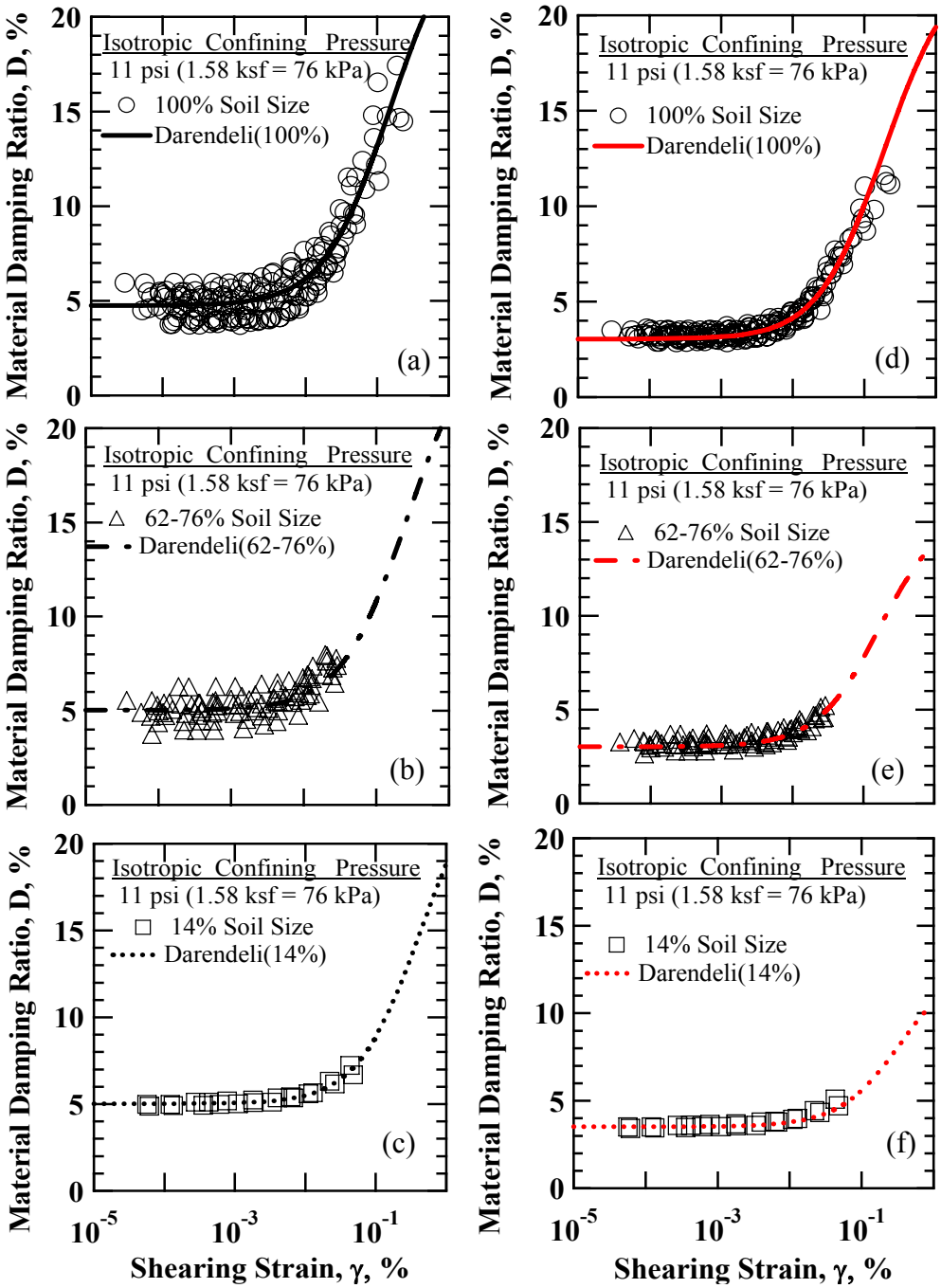

Figure 13.3 Comparison of the Fitted Relationships for the Variation in Material Damping Ratio with Shearing Strain from RC Tests of Old, Fresh, and Mixed MSW Patterned After Darendeli (2001): (a), (b), and (c) Uncorrected for f and (d), (e), and (f) Corrected for f

Similarly, an attempt was made for the best fit of the uncorrected measured material damping ratio using the adjusted Masing behavior model by changing the parameters. These parameters are presented in Table 13.2. In addition, the variations in material damping ratio corrected to f = 1 Hz were fitted by changing the parameters in conjunction with the variation in material damping ratio curves at higher shearing strains measured by UCB. These parameters are tabulated in Table 13.3. Like normalized shear modulus, the value of equivalent PI increases considerably with a decrease of the weight percentage of soil-size material. It should be noted that curvature coefficient decreased from the value of 1.04 to 0.92 for the best fitting for material damping ratio curves. However, a value of 1.04 can be used, with the result of slightly overestimating beyond the shearing strain of 0.01 %.

Table 13.2 Summary of the Values of the Adjusted Masing Behavior Model Parameters Used for Best Fit of Each Group of Uncorrected Material Damping Ratio Curves for Frequency

% Weight of Soil-Size Material	a	Equivalent PI	OCR	σ_o(atm)	D_{min}, (%)
100 %	0.92	55	1	0.75	4.75
62-76 %	0.92	130	1	0.75	5.03
14 %	0.92	250	1	0.75	5.02

Table 13.3 Summary of the Values of the Adjusted Masing Behavior Model Parameters Used for Best Fit of Each Group of Corrected Material Damping Ratio Curves for Frequency

% Weight of Soil-Size Material	a	Equivalent PI	OCR	σ_o(atm)	D_{min}, (%)
100 %	0.90	85	1	0.75	3.04
62-76 %	0.73	150	1	0.75	3.02
14 %	0.60	480	1	0.75	3.52

13.3 COMPARISON OF NONLINEAR SHEAR MODULUS REDUCTION AND MATERIAL DAMPING RATIO CURVES BETWEEN UT AND UCB

13.3.1 G_{max} Values

Absolute values of G_{max} measured by UT using the LSRC device and UCB using the cyclic triaxial device were compared. It is important to note that Zekkos (2005) used different Poisson's ratios for the estimation of shear modulus. Values of Poisson's ratio of 0.3 and 0.2 were used for 100 % and other lower weight percentages of soil-size MSW specimens, respectively. He estimated the shear modulus at shear strains as low as 0.0002 %.

The comparison in the absolute values of G_{max} for 100 % and 62 to 76 % soil-size old MSW with confining pressure measured by UT and UCB is shown in Figure 13.4. The values of G_{max} measured by UT are represented by open circle symbol, whereas the values of G_{max} estimated by UCB are represented by solid triangular symbol. It should be noted that excitation frequency of G_{max} for the 100 % soil-size specimen (UT) varies from 122 Hz to 349 Hz, while the values of G_{max} of UCB were measured at a frequency of 1 Hz. In the case of 62 % to 76 % soil-size old MSW specimens (UT), excitation

frequency varies from 143 Hz to 483 Hz. Therefore, to compare the absolute values of G_{max}, the excitation frequencies were corrected to 1 Hz using Equation (6.5) for the values measured by UT.

The values shown in the figure are obtained from old MSW specimens reconstituted with soil-size material passed the ¾-in. (19.1-mm) sieve. Estimated total unit weights of the specimens (denoted by symbols "*" and "+") at a confining pressure about 11 psi (76 kPa) are equal to 75.4 pcf (11.8 kN/m^3) and 86.6 pcf (13.6 kN/m^3) for UT and UCB measurements, respectively. It is interesting to see that, as seen in Figure 13.4, although taking the difference of total unit weight into consideration, the difference

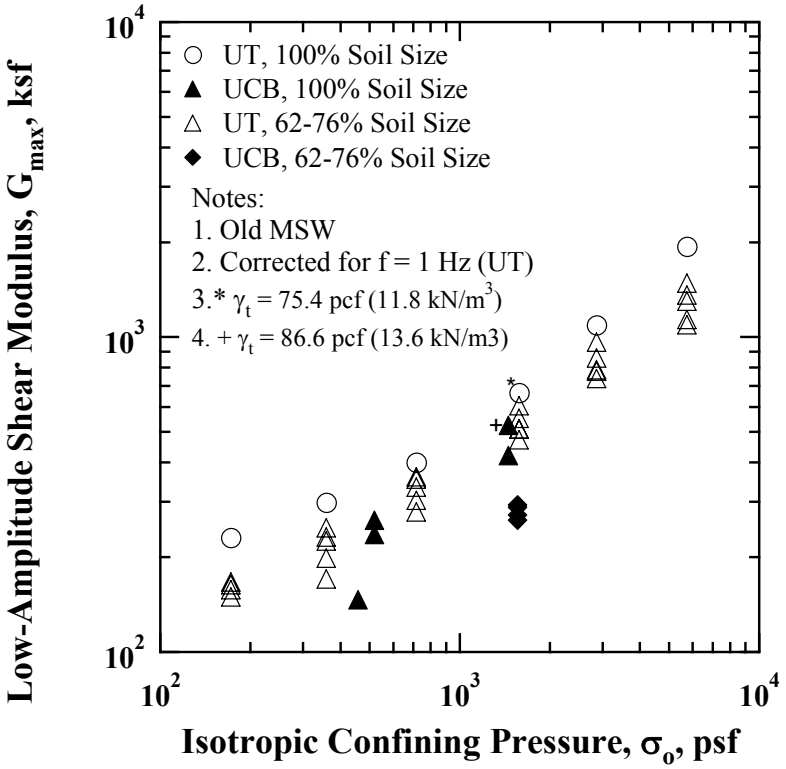

Figure 13.4 Comparison of the Variation in Low-Amplitude Shear Modulus with Isotropic Confining Pressure from RC and Cyclic Triaxial Tests of 100 % and 62 to 76 % Soil-Size Old MSW: UT and UCB

in G_{max} for the 100 % soil-size specimens is approximately 27 %.

For the 62 % to 76 % soil-size material, again, the values of G_{max} measured by UT were corrected for excitation frequency of 1 Hz using Equation (6.5), assuming that response with respect to excitation frequency will be similar. Average estimated total unit weights at a confining pressure of 11 psi (76 kPa) are 63.7 pcf (10.0 kN/m^3) and 68.4 pcf (10.8 kN/m^3) for UT and UCB specimens, respectively. As can be seen, the difference in G_{max} becomes more significant, resulting in about 87 %. It is interesting to observe that the values of G_{max} of 100 % soil-size material estimated by UCB are similar to the values of G_{max} of 62 % to 76 % soil-size material.

For fresh MSW, similar to old MSW, the values of G_{max} measured by UT were corrected to excitation frequency of 1 Hz using Equation (7.1). The comparison in absolute values of G_{max} for 100 % and 62 to 76 % soil-size fresh MSW with confining pressure measured by UT and UCB is shown in Figure 13.5. G_{max} values measured by UT are represented by open symbols, whereas G_{max} values measured by UCB are represented by solid symbols.

As seen in Figure 13.5, the values of G_{max} measured by UT still higher than that measured by UCB at a confining pressure of 11 psi (76 kPa). The difference is equal to about 42 % in average for the 100 % soil-size fresh MSW specimens. On the other hand, the difference in G_{max} of the 62 to 76 % soil-size fresh MSW specimens, as represented by triangular symbols, is about 44 % in average.

As a result, absolute values of G_{max} estimated by UCB for the same material group are generally lower than the values of G_{max} measured by UT.

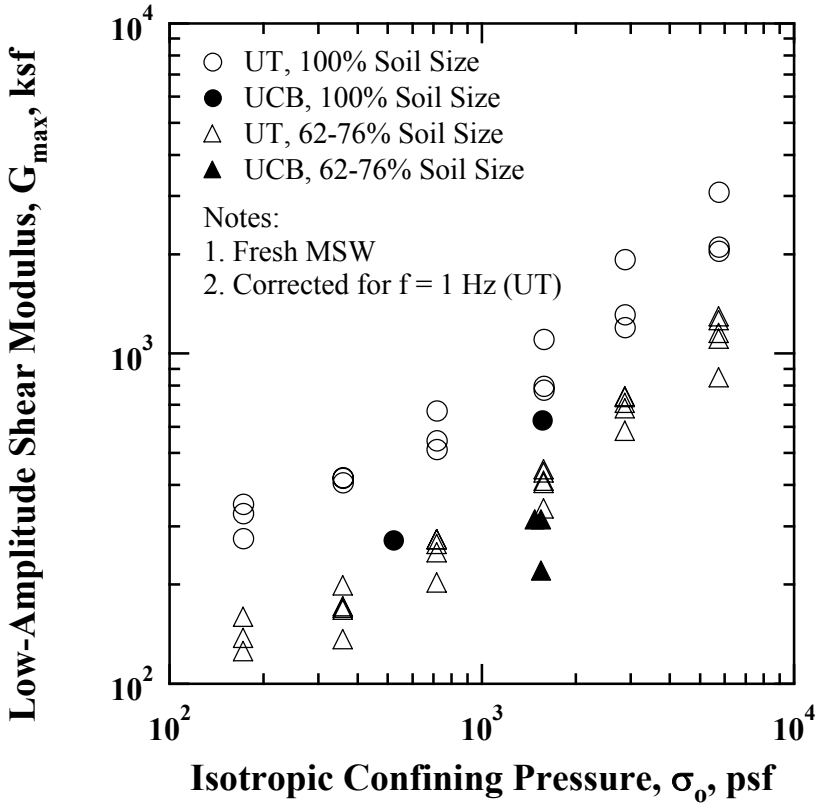

Figure 13.5 Comparison of the Variation in Low-Amplitude Shear Modulus with Isotropic Confining Pressure from RC and Cyclic Triaxial Tests of 100 % and 62 to 76 % Soil-Size Fresh MSW: UT and UCB

13.3.2 G/G_{max} – log γ Relationships

As part of the collaborative research project, nonlinear shear modulus reduction and material damping ratio curves were generated using different laboratory testing devices on MSW material retrieved from the Tri-Cities landfill. For the RC tests with the lowest weight percentage of soil-size material (14 %) mixed MSW specimens were generated by mixing the paper of old and fresh wastes. A comparison of the variation in normalized shear modulus curves with different weight percentages of soil-size material generated by UT and UCB is presented in Figure 13.6.

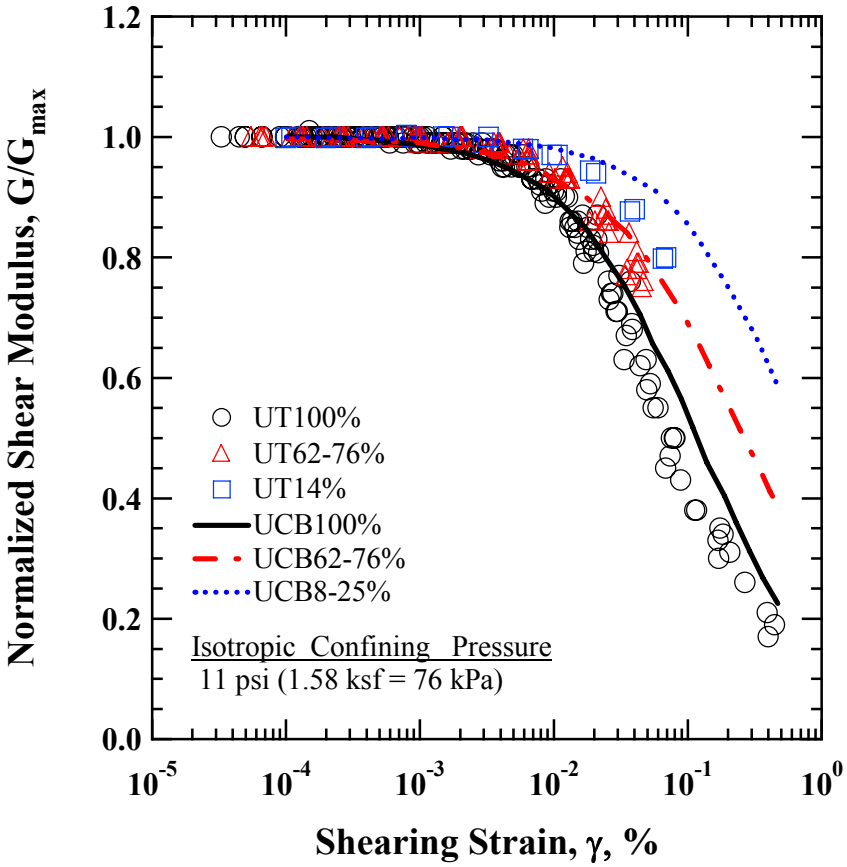

Figure 13.6 Comparison of the Variation in Normalized Shear Modulus with Shearing Strain for Different Weight Percentages of Soil-Size Material between UT and UCB Measurements

For 100 % soil-size material, the values of normalized shear modulus exhibit nearly the same pattern with shearing strain up to a strain of about 0.02 %. However, beyond this strain, the values of normalized shear modulus measured by UT are slightly below the curve generated by UCB. The UT values were measured with the RCTS device. Hence, the difference may be attributed to the difference in particle size combined with specimen size of the different testing methods, i.e., 3/8-in. (9.5-mm) and ¾-in. (19.1-mm) particle sizes and 2.8-in. (71.1-mm) and 12.0-in. (304.8-mm) diameters.

Another possible explanation is that, for the UCB data, the values of shear

modulus were not normalized with the correct G_{max} due to difficult making measurements at low shearing strain ranges ($\gamma < 0.0005$ %). This possible limitation in normalization of shear modulus would shift the normalized shear modulus curves to somewhat higher strains.

Similarly, the values of normalized shear modulus for 62 to 76 % of soil-size material give a fairly good agreement with shearing strain up to about 0.02 %. However, after this point, the values of normalized shear modulus measured by UT are below the curve proposed by UCB. Similarly, as discussed above, this difference may be possibly due to the effects of particle and/or specimen sizes. In fact, in terms of size of maximum particle size, UCB used larger particles in this case (3-in. (76.2-mm) for paper and plastic) and is likely more correct. Interestingly, in the lowest weight percentage of soil-size material, the difference in normalized shear modulus between UT and UCB becomes more significant. That is, the values of normalized shear modulus from UCB shift to much more higher strains than those measured by UT.

As a result, the variation in normalized shear modulus with shearing strain for old, fresh, and mixed MSW measured by UT and UCB provided reasonably good agreement for the specimens reconstituted with 100 % and 62 to 76 % of soil-size material, while the variation in normalized shear modulus for the lowest weight percentage of soil-size material specimens showed some difference.

13.3.3 D – log γ Relationships

For the purpose of comparison, excitation frequencies of measured data from resonant column tests by UT were corrected to a frequency of 1 Hz in accordance with the test results of frequency variation tests on material damping ratio, as provided in Sections 6.3.3, 7.3.3, 10.3.6, and 11.3.5. For reference, UCB performed a majority of

tests at an excitation frequency of 1 Hz. It should be noted that frequency variation tests were only available for small-diameter specimens with 100 % soil-size material specimens. Thus, for 62 to 76 % and 14 % soil-size material specimens, the characteristics of frequency variation on material damping ratio may be similar to that for 100 % soil-size material specimens.

With a frequency correction, a comparison of the variation in material damping ratio with different weight percentages of soil-size material generated by UT and UCB is presented in Figure 13.7. When corrected to an excitation frequency of 1 Hz, different correction factors were applied depending on the shearing strain; up to shearing strain 0.01 %, a correction factor was used from the frequency variation tests in the small-strain ranges, whereas after shearing strain of 0.01 %, another correction factor was used from the frequency variation tests in the nonlinear strain ranges for each MSW. For mixed MSW specimens, average value of old and fresh MSW in the small- and nonlinear strain ranges was used for the frequency corrections on material damping ratio. These correction factors are tabulated in Table 13.4.

Different pattern of behavior of material damping ratio at small-strain ranges is observed between UT and UCB, as shown in Figure13.7. Material damping ratio at small-strain range measure by UT exhibit almost the same regardless of the weight percentage of soil-size material, whereas the values of material damping ratio for specimens with lower weight percentage of soil-size material are higher than those with 100 % soil-size material specimens. Material damping ratio measurements for 100 % soil-size material specimens give a quite good agreement between UT and UCB. On the other hand, after strains above 0.01 %, material damping ratio measurements from UT follow the lines generated by UCB.

With a difference in material damping ratio measurements at small-strain range

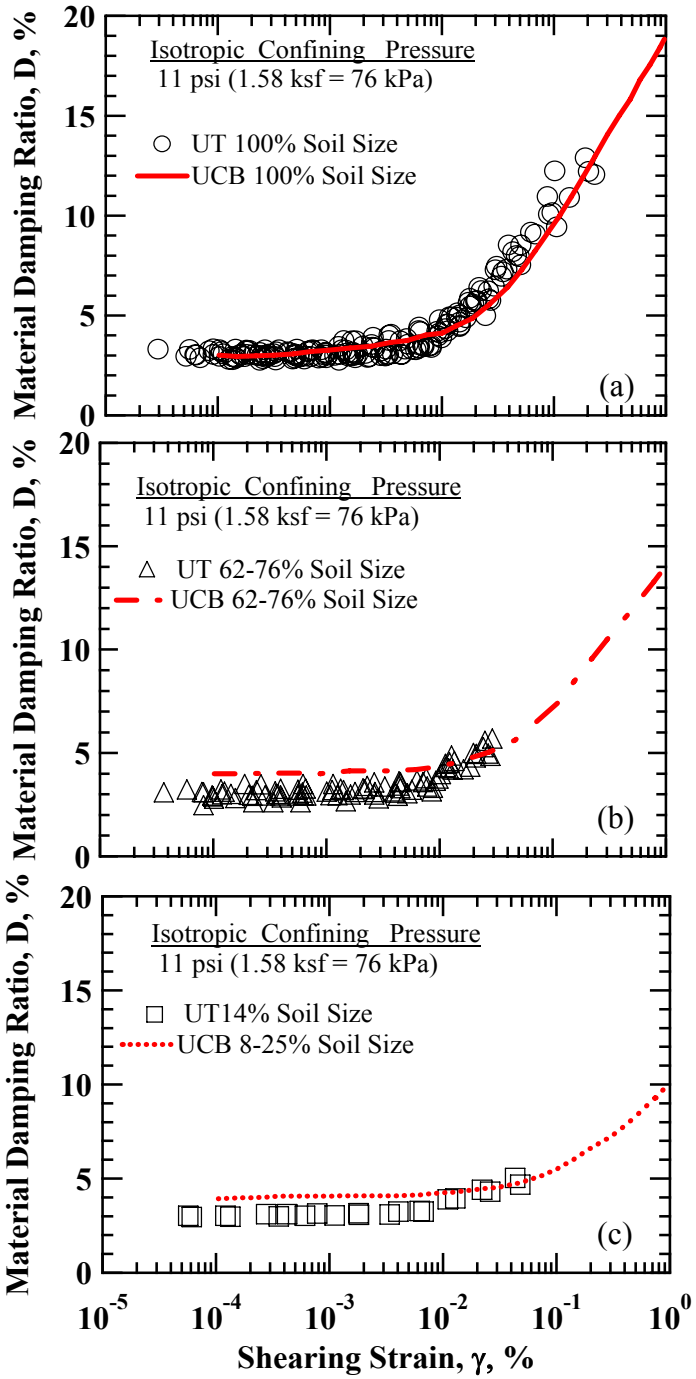

Figure 13.7 Comparison of the Variation in Material Damping Ratio with Shearing Strain upon Different Weight Percentages of Soil-Size Material between UT and UCB: (a) 100 %, (b) 62 to 76 %, and (c) 14% (8 to 25 %)

Table 13.4 A Summary of the Values of Factors Used for Frequency Corrections for Material Damping Ratio Curves with Different Weight Percentages of Soil-Size Material

% Weight of Soil-Size Material		Correction Factor					
		$\gamma < 0.01$ %			$\gamma > 0.01$ %		
		Old	Fresh	Mixed	Old	Fresh	Mixed
100 %	Small-Diameter	0.74	0.62	-	0.83	0.74	-
	Large-Diameter	0.66	0.56	-	0.77	0.63	-
62 – 76 % (Large-Diameter)		0.63	0.56	-	0.77	0.63	-
14 % (Large-Diameter)		-	-	0.61	-	-	0.7

between UT and UCB, the variation in material damping ratio gives a fairly good agreement in the intermediate strain ranges.

13.4 COMPARISON OF NONLINEAR SHEAR MODULUS REDUCTION AND MATERIAL DAMPING RATIO CURVES WITH OTHER STUDIES

The variation in normalized shear modulus with shearing strain measured by UT was compared with that proposed by other researchers. The comparison is presented in Figure 13.8. It should be noted that other reference nonlinear shear modulus reduction and material damping ratio curves, as presented in Figures 13.8, proposed by Kavazanjian et al. (1995), Idriss et al. (1995), and Augello et al. (1998), were derived from the recorded ground motions at the surface of the OII landfill using back-calculation analyses to evaluate the dynamic nonlinear properties of MSW.

For curves proposed by Singh and Murphy (1990), these curves were synthesized by combining the nonlinear shear modulus reduction and material damping curves of peat

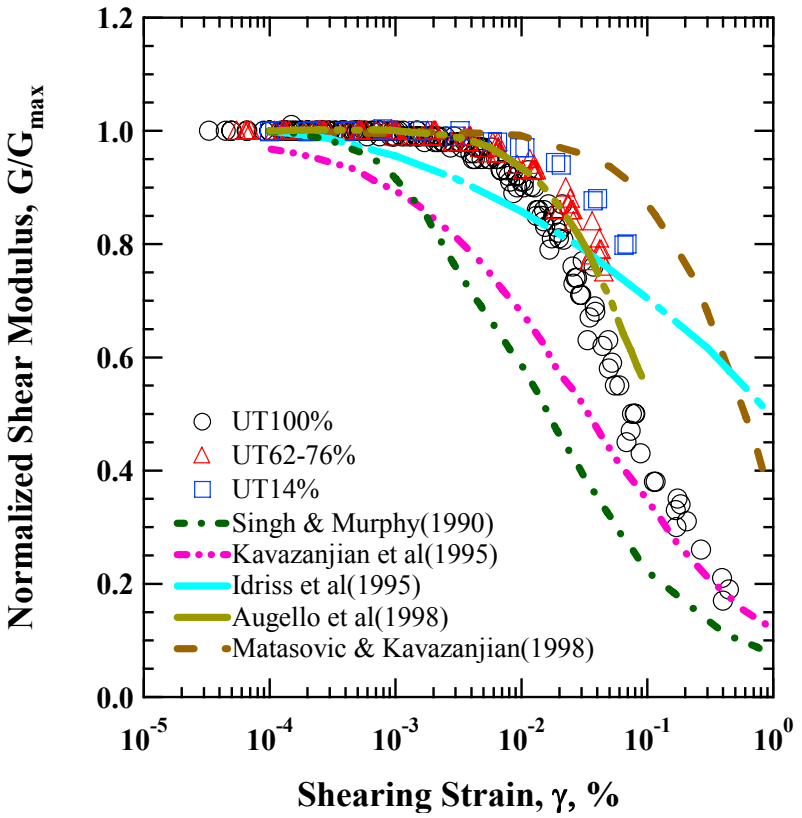

Figure 13.8 Comparison of the Variation in Normalized Shear Modulus with Shearing Strain with Other Studies

and clay. Matasovic and Kavazanjian (1998) combined the nonlinear shear modulus reduction and material damping ratio curves with the data from cyclic direct simple shear tests. As shown in Figure 13.8, nonlinear shear modulus reduction curves proposed by Kavazanjian et al. (1995) and Singh and Murphy (1990) exhibit considerable shear modulus reduction even below the shearing strain of 0.001 %. Another nonlinear shear modulus reduction curve suggested by Idriss et al. (1995) shows conversely a slow modulus reduction over shearing strain ranges. Augello et al (1998) provides a very similar shear modulus reduction curve to the curve created from 100 % soil-size material specimens by UT. The curve reported by Matasovic and Kavanzanjian (1998) forms an

upper bound in the variation of normalized shear modulus reduction curves.

Comparison of the variation in material damping ratio with shearing strain with other studies is given in Figure 13.9. As shown in Figure 13.9, material damping curve proposed by Augello et al.(1998) matches comparatively well with the variation of measured material damping ratio measured by UT exceeding the shearing strain of approximately 0.01%, however, below this strain ranges, significant difference exist. Some fractions of material damping ratio curves at small-strain range suggested by Kavazanjian et al. (1995), Idriss et al. (1995), and Matasovic and Kavazanjian (1998) were close to measured values.

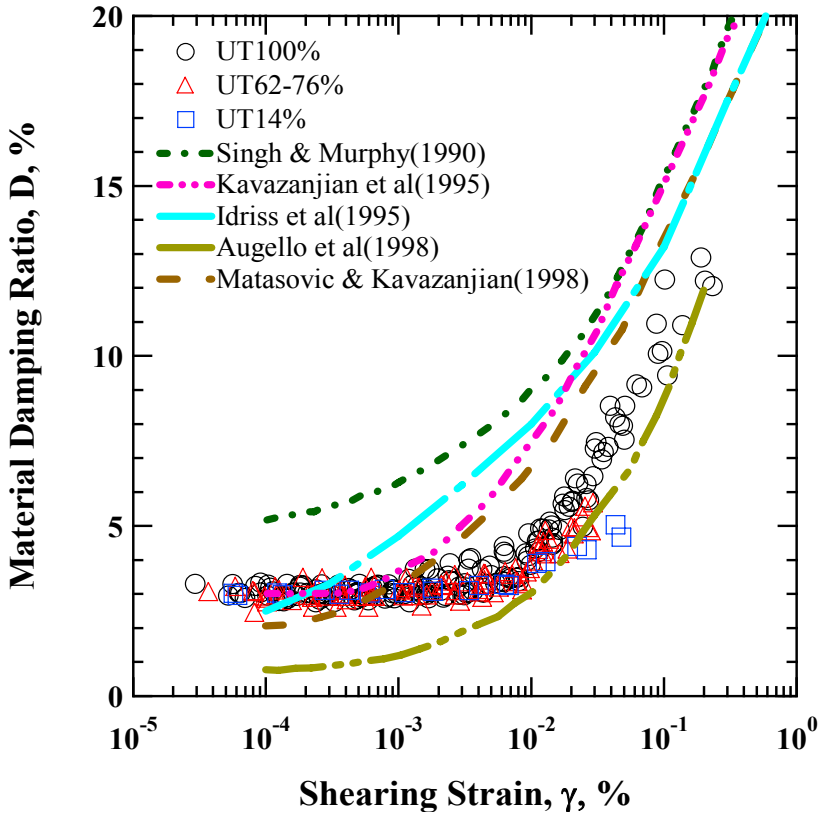

Figure 13.9 Comparison of the Variation in Material Damping Ratio with Shearing Strain with Other Studies

In general, other reference curves show their nonlinear behavior relatively earlier and overestimate the value of material damping ratio with shearing strain than one measured by UT.

In conclusion, there are a wide range of variations in nonlinear shear modulus reduction and material damping ratio curves. Thus, further study is required to identify the nonlinear characteristics of MSW.

13.4 SUMMARY

Nonlinear shear modulus reduction and material damping ratio curves generated by UT using small- and large-diameter RC devices are compared with those generated by UCB in this chapter. With a significant difference at the lowest weight percentage of soil-size material, nonlinear shear modulus reduction curves of other percentages of soil-size material exhibit comparatively close match. For material damping ratio curves, after the correction of excitation frequency to 1 Hz, those provided a fairly good agreement between UT and UCB in the intermediate strain ranges. However, there is a slight difference in the values of D_{min} between UT and UCB, except for the 100 % soil-size material specimens.

Another comparison of nonlinear shear modulus reduction and material damping curves are made with curves proposed by other researchers. As a reference, nonlinear shear modulus reduction and material damping curves were mostly derived from the recorded strong ground motions in the OII landfill throughout back-calculation analyses. A comparison shows a wide range of variations in nonlinear shear modulus reduction and material damping curves.

CHAPTER 14: Summary, Conclusions, and Recommendations

14.1 SUMMARY

Dynamic properties, shear modulus, G, and material damping ratio, D, of MSW were investigated using the RCTS and LSRC equipment at UT. MSW material was retrieved from Tri-Cities Landfill by personnel form the University of California at Berkeley under the direction of Professor Jonathan Bray (Zekkos, 2005). This landfill is located near Fremont, California, just north of San Jose and east of the San Francisco Bay. Material properties of the MSW, e.g., total unit weight, water content, and distribution of temperature with depth, were characterized in the field by UCB. Grain size distribution analyses of samples sent to UT by UCB personnel were performed by UT in the laboratory. The specimens were reconstituted in accordance with sample preparation procedure established by UCB. A total of 30 MSW specimens were constructed for the dynamic laboratory tests. Ten specimens were used for small-diameter RCTS tests and 20 specimens were used for large-diameter RC tests in the LSRC device. Initial characteristics of these specimens are tabulated in Tables 5.3, 5.5, and 5.7, respectively. For small-diameter specimens, three old MSW specimens and one fresh MSW specimen were tested at their natural and hydrated conditions. Large-diameter specimens were constructed according to the weight percentages presented in Table 5.6 and tested only at their natural conditions.

With a mixture of paper of old and fresh MSW, mixed MSW was generated for the purpose of investigating the dynamic properties in the nonlinear strain range at the lowest weight percentage of soil-size material(14 % soil-size material).

Test parameters affecting small-stain dynamic properties, G_{max} and D_{min}, of old

and fresh MSW were investigated using the RCTS and LSRC devices. These test parameters included (1) duration of confinement at a constant pressure, (2) total isotropic confining pressure, (3) excitation frequency, and (4) specimen size. In addition, material parameters affecting G_{max} and D_{min} of old and fresh MSW were studied. These material parameters included (1) waste composition, (2) water content, (3) total unit weight, and (4) particle size. The small-strain dynamic properties of MSW were also compared with the same properties of loose sands.

Total unit weights of old, fresh, and mixed MSW specimens were estimated during the RC tests. The values of estimated total unit weight were also compared with other total unit weight profiles measured at different MSW landfills.

An empirical relationship between estimated total unit weight and confining pressure including weight percentage of soil-size (material passing the ¾-in. (19.1-mm) sieve) material was developed using the measured RC data. A comparison between estimated total unit weight and predicted total unit weight using the derived equation was provided. Another empirical relationship between G_{max} and D_{min} was derived using measured RC data from old, fresh, and mixed MSW specimens.

Shear wave velocities measured in the laboratory from old, fresh, and mixed MSW specimens were compared with those obtained in the Tri-Cities landfill. A series of SASW tests were performed by UT personnel under the supervision of Dr. Stokoe at the Tri-Cities landfill. Additionally, shear wave velocities were also compared with in-situ V_s profiles measured at different MSW landfills.

Nonlinear dynamic properties of old and fresh MSW were expressed in terms of shear modulus, G, normalized shear modulus reduction, G/G_{max},, and material damping ratio, D, curves. Test parameters affecting G and D of old and fresh MSW in the nonlinear strain ranges were investigated using the RCTS and LSRC devices. These test

parameters included (1) shearing strain amplitude, (2) total isotropic confining pressure, (3) overconsolidation ratio, (4) number of loading cycles, and (5) excitation frequency. Material parameters that affect G and D included (1) waste composition, (2) water content, (3) total unit weight, and (4) particle size. A comparison was made regarding the variation of G, G/G_{max}, and D at a given confining pressure and excitation frequency. Also, the nonlinear dynamic properties of MSW were compared with the same properties of loose sands.

An empirical relationship was developed between G/G_{max} and modified material damping ratio ($D-D_{min}$) for old and fresh MSW. A comparison was made between measured $D-D_{min}$ and predicted $D-D_{min}$.

The variation in G/G_{max} – log γ and D – log γ curves were fitted using a modified hyperbolic model and an adjusted "Masing behavior" model (Darendeli, 2001), respectively. Representative curves of MSW at a given confining pressure were provided for the dynamic site response analysis of MSW landfills. As part of collaborative research project, G/G_{max} – log γ and D-log γ curves measured by UT were compared with those obtained by UCB. The comparison comprised of different weight percentages of soil-size material. Also, G/G_{max} – log γ and D – log γ curves were compared with those proposed previously by other researchers, which were mostly derived by back-calculation analyses using recorded ground motions in the OII landfill.

14.2 CONCLUSIONS

14.2.1 Small-Strain Dynamic Behavior of Old and Fresh MSW

Small-strain dynamic properties, G_{max}, and D_{min}, of MSW were investigated using RCTS and LSRC testing devices. The following conclusions were drawn:

1. For both old and fresh MSW, G_{max} increases with increasing duration of confinement, whereas D_{min} decreases with an increase in duration of confinement. The effect of duration of confinement at a constant pressure is more pronounced on G_{max} than it is on D_{min}. The effect of duration of confinement is quite important on G_{max} and D_{min}.

2. G_{max} increases significantly with increasing confining pressure while D_{min} decreases slightly as confining pressure increases regardless of the age of waste. The variation in G_{max} with confining pressure of MSW specimens consists of a bi-linear log G_{max} – log σ_o relationship. This bi-linear relationship is due to the compaction effort during specimen construction. The response of G_{max} of MSW with confining pressure is very similar for the 100 % soil-size material Group for old and fresh MSW. However, for 62 to 76 % soil-size material Groups, the response of fresh MSW is softer and exhibits more pressure dependency in the normally consolidated (NC) state. In contrast to G_{max}, D_{min} does not show a bi-linear relationship with confining pressure; D_{min} decreases only slightly with increasing confining pressure for old and fresh MSW. However, fresh MSW shows less pressure dependency. D_{min} tends to increase slightly with decreasing weight percentage of soil-size material. The effect of confining pressure is much less on D_{min} than G_{max}. The effect of total isotropic confining pressure on G_{max} is very important, but is only minor important to D_{min}.

3. G_{max} increases with increasing excitation frequency due to the frequency effect for old and fresh MSW. The rate of increase with excitation frequency is slightly higher for fresh MSW than old MSW. Hence, on the other hand, the Dmin – log f relationship is nonlinear. D_{min} increases with decreasing excitation frequencies below 0.5 Hz due to creep regardless of the age of MSW. D_{min} increases with increasing excitation

frequencies larger than 1 Hz due to the frequency effect for old MSW and larger than 0.5 Hz for fresh MSW. However, for old MSW, G_{max} is reasonably constant between 0.5 Hz to 1 Hz. The increase in D_{min} at higher excitation frequencies for fresh MSW is somewhat larger than old MSW. The effect of excitation frequency has a moderate impact on G_{max}, but large impact on D_{min} at higher frequencies.

4. For both old and fresh MSW, the variation in G_{max} on small- and large-diameter specimens after correcting for excitation frequency and total unit weight is approximately the same. The variation in D_{min} on small- and large-diameter specimens after correcting for excitation frequency is almost the same. As a result, the effects of specimen size on G_{max} and D_{min} is insignificant.

5. G_{max} depends on the weight percentage in the waste composition regardless of the age of MSW; G_{max} decreases as the weight percentage of soil-size material decreases. D_{min} appears to be nearly independent of weight percentage of soil-size material; D_{min} decreases only slightly with increasing confining pressure for old and fresh MSW. The effect of waste composition has a moderate impact on G_{max}, but a small impact on D_{min}.

6. The absolute value of G_{max} decreases and the absolute value of D_{min} increases by adding water regardless of the age of waste. Overconsolidation effects that have been established due to stress release during the unloading sequence are eliminated when the specimen is completely unload, and then hydrated. The effect of hydration has a small impact on G_{max} and D_{min}, with G_{max} decreasing slightly and D_{min} increases slightly.

7. For old and fresh MSW, the variation in G_{max} with γ_t for specimens with

different total unit weights for the same material type is slightly different in the normally consolidated state; G_{max} of a lower total unit specimen increases more rapidly because of the specimen's more compressible frame. The variation in D_{min} exhibits a similar behavior but decreasing with increasing σ_o after eliminating the effect of excitation frequency; D_{min} decreases rapidly at the beginning, but it remains nearly constant for old and fresh MSW. As a result, the effects of variation of total unit weight on G_{max} and D_{min} are small. (It is important to note that the waste composition does have a moderate impact on G_{max}, with G_{max} decreasing as weight percentage of soil-size material decreases as noted in item 5 above)

8. For old and fresh MSW, the variation in G_{max} for specimens reconstituted with material passing the 3/8-in. (9.5-mm) and ¾-in. (19.1-mm) sieves is nearly the same after correcting for excitation frequency and total unit weight. Thus, the effect of particle size on for particle < ¾-in. (19.1-mm) G_{max} is negligible. The variation in D_{min} for specimens reconstituted with material passing the 3/8-in. (9.5-mm) and ¾-in. (19.1-mm) sieves after removing the effect of excitation frequency is almost the same. Therefore, the effect of particle size on D_{min} is insignificant.

9. Shear wave velocities measured in the laboratory were compared with the V_s profiles measured at in-situ. The V_s profiles measured with 100 % soil-size material specimens show higher values, but the V_s profiles 62 to 76 % soil-size material specimens, which is a representative weight percentage of the Tri-Cities MSW landfill, give a good agreement with field measurements. On the other hand, the Vs profiles from the 14 % soil-size material specimens form a lower-bound.

10. small-strain dynamic properties of the MSW were compared with the same properties of loose sands. G_{max} values are somewhat lower than those of loose sands. However, the values of D_{min} are much larger than those of loose sands.

14.2.2 Nonlinear Dynamic Behavior of Old and Fresh MSW

Nonlinear behavior of MSW was studied using the RCTS and LSRC devices. The nonlinear behavior was described in terms of shear modulus, G, normalized shear modulus, G/G_{max}, and material damping ratio, D. The following results were drawn from this research.

1. For old and fresh MSW, G and D were constant and independent of shearing strain amplitude as strain less than the elastic threshold strain, γ_t^e. For instance, at σ_o = 11 psi (76 kPa), the values of γ_t^e 0.002 % for the 100 % soil-size material specimens. However, at shearing strains above γ_t^e, G and D show nonlinear behavior with increasing shearing strain; G decreases considerably with increasing shearing strain amplitude, whereas D increases significantly with increasing shearing strain amplitude. The effect of shearing strain amplitude on G and D is very important.

2. G – log γ curves dramatically shift to higher G values at the same γ values with increasing confining pressure for old and fresh MSW. In terms of normalized shear modulus, G/G_{max} – log γ curves shift only slightly to higher strains with increasing confining pressure regardless of the age of MSW. D – log γ curves move slightly downward with increasing confining pressure. The effect of total isotropic confining pressure on the G – log γ relationships is very important, whereas the effect of total isotropic confining pressure on G/G_{max} – log γ and D – log γ is small.

3. G – log γ curves increase with an increasing overconsolidation ratio due to a substantial decrease in voids spaces in the old and fresh MSW specimens. D – log γ curves increase with increasing overconsolidation ratio for old MSW. However, for fresh MSW, D – log γ curves are almost the same regardless of magnitudes of overconsolidation ratio. G/G_{max} – log γ curves were approximately the same regardless of the magnitudes of OCR for both old and fresh MSW. The effect of overconsolidation ratio has some impact on G, while the effect of overconsolidation ratio on G/G_{max} and D is small.

4. The effect of the number of loading cycles is negligible at strains less than about 0.001 % for the 100 % soil-size material old and fresh MSW. The effect of the number of loading cycles begins to have a small influence with number of loading cycles as shearing strain amplitude increase to 0.03 %. As a result, the effect of number of loading cycles is small on G and D for old and fresh MSW at these strain levels.

5. G generally increases with increasing excitation frequency due to frequency effect regardless of the age of waste. For old MSW, the pattern of increase in G with excitation frequency is identical regardless of the amplitudes of shearing strain. However, for fresh MSW, the rate of increase in G is slightly higher at higher strains than in small-strain range. Similar to small-strain behavior, D increases with decreasing excitation frequency due to creep below 1 Hz, while D increases with increasing excitation frequency due to frequency effect for both old and fresh MSW. The values of D at lower excitation frequencies become larger due to creep. The values of D at higher frequencies increase for both old and fresh MSW due to frequency effect. The effect of excitation frequency on G is moderate. However, the effect of excitation frequency has

a larger impact on D at higher frequencies.

6. G/G_{max} – log γ curves shift to higher strains with decreasing weight percentage of soil-size material for old and fresh MSW. Similarly, D-log γ curves move to higher strains as weight percentage of soil-size material decreases. The effect of waste composition on G/G_{max} – log γ curves and D-log γ curves is moderately important.

7. G – log γ curves shift slightly downward with increasing water content and G/G_{max} – log γ curves shift slightly to lower strains by adding water. D-log γ curves move slightly upward with increasing water content over the complete shearing strain range. The effect of water content has a small impact on G and D, whereas G/G_{max} is barely affected by water content.

8. The effect of the variation in unit weight for the same material type has a small impact on G – log γ curves for the 100 % soil-size material old and fresh MSW. However, G/G_{max} – log γ and D – log γ curves are nearly the same for a significant variation in thetotal unit weight of a given material type. The effect of variation in total unit weight on has small impact on G. However, G/G_{max} and D are nearly unaffected by the variation in total unit weight.

9. The effect of particle size has little impact on G – log γ curves for the 100 % soil-size material old MSW, whereas G – log γ curves for fresh MSW are almost the same. However, G/G_{max} – log γ and D – log γ curves are nearly the same with different particle sizes for old and fresh MSW. The effect of particle size is a very small.

14.2.3 Comparisons in G_{max} in the Small-Strain Range and G/G_{max} – log γ Curves and D – log γ Curves in the Nonlinear Strain Range between UT and UCB and Sands

As a part of collaborative research project, linear and nonlinear dynamic properties of MSW were investigated using the RCTS and LSRC device at UT and using a cyclic triaxial device at UCB. The following results are drawn from comparisons between these two sets of data.

1. Absolute values of G_{max} measured by UT in the small-strain range are higher than those estimated by UCB for the same material groups (e.g., 100 % and 62 to 76 % soil-size material groups) regardless of the age of MSW. The values of G_{max} of the 100 % and 62 to 76 % soil-size material specimens measured by UT are higher than about 27 % to 87 % for old MSW and are higher about 42 % to 44 % for fresh MSW specimens.

2. In terms of G/G_{max}, the variation in the G/G_{max} – log γ curves for the 100 % soil-size group is very similar. For the 62 to 76 % soil-size material group, the G/G_{max} – log γ curve from the UCB tests are somewhat more linear than UT. Furthermore, the one possible reason is that the UCB tests involved larger particles and their results may be more reflective of the behavior. However there is some difference in G/G_{max} – log γ curves for 14 % (8 to 25 %) soil-size material group is even more linear; G/G_{max} – log γ curve measured by UCB shifts to higher strains than UT.

3. After correcting frequency to f = 1 Hz on D – log γ curves measured by UT, although there is small difference in D_{min}, D – log γ curves of each group follow the D –

log γ curves measured by UCB.

4.

14.3 RECOMMENDATIONS

1. Additional TS tests with large-diameter MSW specimens with larger particles would allow evaluation of the effect of excitation frequency such that a more generalized relationship of the effect of excitation of frequency may be established.

2. The LSRC device should be modified so that higher strains can be generated and the nonlinear dynamic properties of MSW at shearing strains above 0.1 % can be measured. To fulfill this goal, the driving system needs to be modified.

3. Further investigation of the effect of water content is necessary using the LSRC device to obtain more representative conditions of in-situ MSW landfills.

References

Abrahamson, N. A., Somerville, P. G., and Cornell, C. A. (1990), "Uncertainty in Numerical Strong Ground Motion Predictions," Proceeding of 4th U.S. National Conference on Earthquake Engineering , EERI, El Centro, California, pp. 407-416.

Afifi, S .S. and Woods, R. D. (1971), "Long-Term Pressure Effects on Shear Modulus of Soils," Journal of the Soil Mechanics and Foundation Engineering Division, ASCE, Vol. 97, No. SM10, pp. 1445-1460.

Anderson, D. G. and Richart, F. E., Jr. (1976), "Effect of Shearing of Shear Modulus of Clays," Journal of Geotechnical Engineering, ASCE, Vol. 102, No. GT5, pp. 525-537.

Anderson, D.G. and Stokoe, K.H., II (1978), "Shear Modulus: Time-Dependent Soil Property," Dynamic Geotechnical Testing, ASTM STP 654, American Society for Testing and Materials, pp. 66-90.

Augello, A. J., Matasovic, N., Bray, J. D., Kavazanjian, E. Jr., and Seed, R. B. (1995), "Evaluation of Solid Waste Landfill Performance During the Northridge Earthquake," Earthquake Design and Performance of Solid Waste Landfills, ASCE Geotechnical Special Publication No. 54, pp. 17-50.

Augello, A. J., Bray, J. D., Abrahamson, N. A., Seed, R. B. (1998), "Dynamic Properties of Solid Waste Based on Back-Analysis of OII Landfill," Journal of Geotechnical and Geoenvironmental Engineering, Vol. 124, No. 3, March.

Bellotti, R., Ghionna, V. N., Jamiolkowski, M., and Robertson, P. K. (1998), "Design Parameters of Cohesionless Soils from In-Situ Tests," Specialty Session on In-Situ Testing of Soil Properties for Transportation Facilities, Sponsored by Committee A2L02-Soil and Rock Properties, National Research Council, Transportation Research Board, Washington, January, 1989.

Chen, Albert T. F., and Stokoe, K. H., "Interpretation of Strain-Dependent Modulus and Damping from Torsional Soil Tests,"Report No. USGS-GD-79-002, NTIS No. PB-

298479, U. S, Geological Survey, pp. 41-42.

Drnevich, V.P., Hall, J. R., Jr., and Richart, F. E., Jr. (1976), "Effect of Amplitude of Vibration on the Shear Modulus of Sand," Proceedings of International Symposium on Wave Propagation and Dynamic Properties of Earth Materials, Albuquerque, New Mexico, pp. 189-199.

Drnevich, V. P., and Richart, F. E. Jr. (1970), "Dynamic Prestraining of Dry Sand," Journal of the Soil Mechanics and Foundation Division, ASCE, Vol. 96, No. SM2, pp. 453-469.

Darendeli, B. M. (2001), "Develop of a new Family of Normalized Modulus Reduction and Material Damping Curves," Ph.D. Dissertation, The University of Texas at Austin.

Dobry R. and Vucetic M. (1987), "Dynamic Properties and Respond of Soft Clay Deposits," State of the Art Report, Proceedings of the International Symposium on Geotechnical Engineering of Soft Soils, Mexico City, August 13-14, Vol. 2, pp. 51-87.

Dugkeun Park (1998), "Evaluation of Dynamic Soil Properties: Strain Amplitude Effects on Shear Modulus and Damping Ratio," Ph.D. Dissertation, the University of Cornell. pp. 21-22.

Earth Technology Corporation, "Instability of Landfill Slope, Puente Hills, Livermore, CA" Report to DePaolia Equipment Company Inc., Livermore, CA 94550, July, 1988.

Gabr, M. A. and Valero, S. N., "Geotechnical Properties of Municipal Solid Waste," Vol. 18, No. 2, June 1995, pp. 241-251

GeoSyntec Consultants (1995), "Standard Operating Procedure OII-2," Solid Waste Sampling and Field Testing, Revision A, November.

Gere, J. M. (2001), "Mechanics of Materials," Brooks/Cole, 5th Edition, pp. 187-197.

Hardin, B. O. and Bkack, W. L. (1966), "Sand Stiffness Under Various Triaxial Stresses", Journal of the Soil Mechanics and Foundations Division, ASCE, Vol. 94, No. SM2, March, pp. 516-529.

Hardin, B. O. and Drnevich, V. P. (1972), "Shear Modulus and Damping in Soils: Measurements and Parameter Effect," Journal of Soil Mechanics and Foundation Division, ASCE, Vol. 98, No. SM6, June, pp. 603-624.

Hisham T. Eid, Timothy D. Stark, W. Douglas Evans, and Paul E. Sherry (2000), "Municipal Solid Waste Slope Failure. I: Waste and Foundation Soil Properties," Journal of Geotechnical and Geoenvrionmental Engineering, Vol. 136, No. 5, May, pp. 397-407.

Houston, W. N., Houston, S. L., Liu, J. W., Elsayed, A., Sanders, C. O. (1995), "In-Situ Testing Methods for Dynamic Properties of MSW Landfills," Earthquake Design and Performance of Solid Waste Landfills, ASCE Geotechnical Special Publication No. 54, pp. 73-82.

Hwang, Seon Keun (1997), "Dynamic Properties of Natural Soils," Ph.D. Dissertation, The University of Texas at Austin.

Ishihara, K. (1996), "Soil Behavior in Earthquake Geotechnics," Clarendon Press, Oxford, U.K.

Idriss, I. M., Fiegel, G., Hudson, M.B., Mundy, P. K., and Herzig, R. (1995), "Seismic Response of the Operating Industries Landfill," Earthquake Design and Performance of Solid Waste Landfills, M. K.Yegian and W. D. L. Finn, eds., ASCE Geotech. Spec. Publ., No. 54, ASCE, Reston, Va., pp. 83-118.

Iwasaki, T., Tatsuoka, F. and Takagi, Y. (1978), "Shear Moduli of Sands under Cyclic Torsional Shear Loading," Soils and Foundations, Vol, 18, No. 1, March, pp. 39-56.

Kavazanjian, E. Jr., Matasovic, N. (1995), "Seismic Analysis of Solid Waste Landfills", Proceedings of GeoEnvrionment, 2000, ASCE Geotechnical Special Publication, No. 46, Vol. 2, pp. 1066-1080.

Kavazanjian, E. Jr., Matasovic, N., Bonaparte, R., Schmertmann, G. R. (1995), "Evaluation of MSW Properties for Seismic Analysis," Proceedings of Geoenvironment 2000, ASCE Geotechnical Special Publication No. 46, Vol. 2, pp. 1126-1141.

Kavazanjian, E. Jr, Matasovic, N, Stokoe, K. H., and Bray, J. D. (1996), "In-Situ Shear

Wave Velocity of Solid Waste from Surface Wave Measurements," Proc., 2nd Int. Congr. On Envir. Geotechnics, 1, pp. 97-1102.

Kim, Dong Soo (1991), "Deformational Characteristics of Soils at Small Strains from Cyclic Tests," Ph.D. Dissertation, The University of Texas at Austin.

Kramer, S. L. (1996), "Geotechnical Earthquake Engineering," Prentice-Hall, New Jersey, pp. 653.

Ladd, R.S., "Preparing Test Specimen Using Undercompaction," Geotechnical Testing Journal, GRJODJ, Nol. 1, No. 1, Marcg 1978, pp. 16-23

Landva, A.O., Valsangkar, A.J., and Pelkey, S.G (2000), "Lateral Earth Pressure at Rest and Compressibility of Municipal Solid Waste," Canadian Geotechnical Journal, Volume 37, Number 6, December, pp. 1157-1165.

Lee, J.J, Stokoe, K. H., II, and Rathje, E. M. (2004), "Laboratory Data Report No. 1: Municipal Sold Waste, Combined Resonant Column and Torsional Shear Testing," Geotechnical Engineering Report GR04-2, The University of Texas at Austin.

Laird, J.P. (1994), "Linear and Nonlinear Dynamic Properties of Soils at High Confining Pressrues," M.S. Thesis, The University of Texas at Austin.

Lin, Y.C., Resenblad, B., and Stokoe, K.H. (2004), "Data Report on Shear Wave Velocity Profiles Determined by SASW Method at: Altamont Landfill, Redwood Landfill, and Tri-Cites Landfill," Geotechnical Engineering Report GR04-3, The University of Texas at Austin.

Lodde, P. F. (1982), "Shear Moduli and Material Damping of San Francisco Bay Mud," M.S. Thesis, The University of Texas at Austin.

Lo Presti, D.C.F., Jamiolkowski, M., Pallara, O. and Cavallaro, A. (1996), "Rate and Creep Effect on the Stiffness of Soils," Proceedings, Conference on Measuring and Modeling Time Dependent Soil Behavior, Held in Conjunction with the ASCE National Convention, November 10-14, Washington, D.C., pp. 166-180.

Lo Presti, D. C. F, and Pallara, O. (1997), "Damping Ratio of Soils from Laboratory and In-Situ Tests," Proceedings, 14th International Conference on Soil Mechanics and Foundation Engineering, Hamburg, Germany, 6-12, September, 1997.

Marcuson, W.R., III, and Wahls, H.E. (1978), "Effect of Time on Damping Ratio of Clays," Dynamic Geotechnical Testing, ASTM STP 654, American Society for Testing and Materials, pp. 126-147.

Matasovic, N., and Vucetic, M. (1993), "Cyclic Characterization of Liquefiable Sands," Journal of Geotechnical Engineering, Vol. 119, No. 11, November, pp. 1805-1822.

Matasovic, N., Kavazanjian, E. Jr., and Abourjeily, F. (1995), "Dynamic Properties of Solid Waste from Field Observations," Proc., 1st Int. Conf. on Earthquake Geotech. Engrg., 1, pp. 549-554.

Matasovic, N., Kavazanjian, E. Jr. (1998), "Cyclic Characterization of OII Landfill Solid Waste," Journal of Geotechnical and Geoenvironmental Engineering, Vol. 124, March, No. 3, pp. 197-210.

Menq, F. Y., Stokoe, K. H., Kavazanjian, E. Jr., (2001), "Dynamic Properties of Municipal Waste from Large-Scale Resonant Testing," Seventh International Waste Management and Landfill Symposium S. Margherita di Pula, Cagliari, Italy, 1-5 October 2001.

Menq, F. Y. (2003), "Dynamic Properties of Sandy and Gravelly Soils," Ph.D. Dissertation, The University of Texas at Austin.

Morochnik, V., Bardet, J. P., Hushmand, B. (1998), "Identification of Dynamic Properties of OII Landfill," Journal of Geotechnical and Geoenvironmental Engineering, Vol. 124, No. 3, March, pp. 186-222.

Ni, S.-H. (1987), "Dynamic Properties of Sand Under True Triaxial Stress States from Resonant Column/Torsional Shear Tests," Ph.D. Dissertation, The University of Texas at Austin.

Orr, W. R., and Finch, M. A. (1990), "Solid Waste Landfill Performance During the

Loma Prieta Earhquake," ASTM STP 1070, Geotechnics of Waste Fills – Theory and Practice, American Society for Testing Materials, pp. 22-30.

Repetto, P.C., Bray, J.D., Byrne, R.J. and Augello, A.J. (1993) "Seismic Design of Landfills", Progress in Geotechnical Engineering Practice, Central Pennsylvania Section, ASCE, April 12-14, Hershey, Pennsylvania.

Richart, J. E. Jr., Hall, J. R., Jr., and Woods, R. O. (1970), "Vibration of Soils and Foundations," Prentice-Hall Inc. Englewood Cliff, New Jersey, 27p.

Rix, G. J., Lai, C. G., Spang, A. W., Jr. (2000), "In-Situ Measurement of Damping Ratio Using Surface Waves," Journal of Geotechnical and Geoenvironmental Engineering, Vol. 126, No. 5, May, pp. 472-480.

Lin, Y.C, Rosenblad, B., Cox, B.R., Stokoe, K.H., and Rathje E.M., (2004), "Second Report on Shear Wave Velocity Profiles Determined at Five MSW Landfills from SASW Testing,"

Seed H.B. and Idriss I.M., (1970), "Analyses of Ground Motions at Union Bay, Seattle During Earthquakes and Distance Nuclear Blasts", Bulletin of the Seismological Society of America, Vol. 60, No. 1, pp. 125-136.

Seed, H. B. and Idriss, I. M. (1970), "Soil Moduli and Damping Factors for Dynamic Response Analysis," Report No. EERC 70-10, Earthquake Engineering Research Center, University of California, Berkeley, CA, Dec., 41p.

Seed, H. Bolton, and Idriss, I. M., (1992) "Seismic Analysis and Design of Waste Fills: Current Practice, "Proceedings of ASCE Specialty Conference on Stability and Performance of Slopes and Embankments – II, Berkeley, California June 28-July 1.

Sharma, H. D., Dukes, M. T., Olsen, D. M. (1990), "Field Measurements of Dynamic Moduli and Poisson's Ratio of Refuse and Underlying Soils at a Landfill Site, Geotechnics of Waste Fills – Theory and Practice, STP 1070, Landva and Knowles (ed.), ASTM, pp. 57-70.

Singh, S. and Murphy, B. (1990), "Evaluation of the Stability of Sanitary Landfills",

Geotechnics of Waste Fills – Theory and Practice, ASTM STP 1070, A. Landva and G.D. Knowles, eds., American Society of Testing and Materials, pp.240-258.

Silver, M. L. and Seed, H. B. (1971), "Deformational Characteristics of Sands under Cyclic Loading," Journal of the Soil Mechanics and Foundation Division, ASCE, Vol. 97, No. SM8, pp. 1081-1098.

Stokoe, K. H., II and Lodde, P. E. (1978), "Dynamic Response of San Francisco Bay Mud," Proceedings, Earthquake Engineering and Soil Dynamics Conference, ASCE, Vol. II, pp. 940-959.

Stoll, R.D. (1989), "Sediment Acoustics," Berlin, New York, Springer-Verlag, pp. 153.

U.S.Environmental Protection Agency. Municipal Solid Waste in The United States: 2003 Facts and Figures.

Vucetic, M. and Dobry, R.(1991), "Effect of Soil Plasticity on Cyclic Response," Journal of Geotechnical Engineering Division, ASCE, Vol. 117, No. 1, January, pp. 89-107.

Vucetic, M. (1994), "Cyclic Threshold Shear Strains in Soils," ASCE, Journal of Geotechnical Engineering, Vol. 120, No. 12, pp. 2208-2228.

Wenston, T. R. (1995), "Effect of Grain Size and Particle Distribution on the Stiffness and Damping of Granular Soils at Small-Strain," M.S. Thesis, The University of Texas at Austin, 229p.

White, J. E. (1983), "Underground Sound: Applications of Seismic Waves," Amsterdam, New York, pp. 253.

Zekkos, D. P. (2005), "Evaluation of Static and Dynamic Properties of Municipal Solid-Waste," Ph.D. The University of California at Berkeley.

Zhang, J., Andrus, R. D., Juang, C. H. (2005), "Normalized Shear Modulus and Material Damping Ratio Relationships," Journal of Geotechnical and Geoenvironmental Engineering, Vol. 131, No. 4, April 1, pp. 453-464.

Zornberg, J. G., Jernigan, B.L., Sanglerat, T. R., Cooley, B. H. (1999), "Retention of Free

Liquids in Landfill Undergoing Vertical Expansion, ASCE, Journal of Geotechnical and Geoenvironmental Engineering, July, Vol. 125, No. 7, pp. 583-594.

Vita

Jung Jae Lee was born in Kimje, Korea, on April 25th, 1973, the son of Gab No Lee and Kyu Woon Han. After graduating from Wan-San High School in Jeonju, Korea in 1992, he entered the Kyunghee University. He served military service from February, 1994, to April, 1996. He received the B.S. Degree in Civil Engineering in February, 1999 and the degree of Master in Civil Engineering in February, 2001. During his graduate studies at the Kyunghee University, he worked as graduate research assistant. Upon graduation, he worked in the Korea Railroad Research Institute from June, 2001, to May, 2002. He married Sun Young Im on November 18th, 2001. They have daughters, So Jeong Lee and Claire (So Min) Lee. In August 2002, he entered the Graduate School of The University of Texas at Austin.

Permanent address: 169 Shinjeong-ri, Youngji-myun
Kimje, 576-973, Jeonbuk, Korea

This dissertation was typed by Jung Jae Lee.